

Bhawani Shankar Chowdhry
Faisal Karim Shaikh
Dil Muhammad Akbar Hussain
Muhammad Aslam Uqaili (Eds.)

Communications in Computer and Information Science

281

Emerging Trends and Applications in Information Communication Technologies

Second International Multi Topic Conference, IMTIC 2012
Jamshoro, Pakistan, March 2012
Proceedings

Bhawani Shankar Chowdhry
Faisal Karim Shaikh
Dil Muhammad Akbar Hussain
Muhammad Aslam Uqaili (Eds.)

Emerging Trends and Applications in Information Communication Technologies

Second International Multi Topic Conference, IMTIC 2012
Jamshoro, Pakistan, March 28-30, 2012
Proceedings

Volume Editors

Bhawani Shankar Chowdhry
Mehran University of Engineering and Technology
Faculty of Electrical, Electronics and Computer Engineering
Jamshoro, Sindh 76062, Pakistan
Email: c.bhawani@ieee.org

Faisal Karim Shaikh
Mehran University of Engineering and Technology
Department of Telecommunication Engineering
Jamshoro, Sindh 76062, Pakistan
Email: faisal.shaikh@faculty.muet.edu.pk

Dil Muhammad Akbar Hussain
Aalborg University
Department of Energy Technology
6700 Esbjerg, Denmark
Email: akh@et.aau.dk

Muhammad Aslam Uqaili
Mehran University of Engineering and Technology
Department of Electrical Engineering
Jamshoro, Sindh 76062, Pakistan
Email: pvc@faculty.muet.edu.pk

ISSN 1865-0929
ISBN 978-3-642-28961-3
DOI 10.1007/978-3-642-28962-0
Springer Heidelberg Dordrecht London New York

e-ISSN 1865-0937
e-ISBN 978-3-642-28962-0

Library of Congress Control Number: 2012933572

CR Subject Classification (1998): C.2, I.2, H.4, H.3, F.1, I.4, K.4.4

© Springer-Verlag Berlin Heidelberg 2012

This work is subject to copyright. All rights are reserved, whether the whole or part of the material is concerned, specifically the rights of translation, reprinting, re-use of illustrations, recitation, broadcasting, reproduction on microfilms or in any other way, and storage in data banks. Duplication of this publication or parts thereof is permitted only under the provisions of the German Copyright Law of September 9, 1965, in its current version, and permission for use must always be obtained from Springer. Violations are liable to prosecution under the German Copyright Law.

The use of general descriptive names, registered names, trademarks, etc. in this publication does not imply, even in the absence of a specific statement, that such names are exempt from the relevant protective laws and regulations and therefore free for general use.

Typesetting: Camera-ready by author, data conversion by Scientific Publishing Services, Chennai, India

Printed on acid-free paper

Springer is part of Springer Science+Business Media (www.springer.com)

Preface

This book constitutes the refereed proceedings of the Second International Multi-topic Conference, IMTIC 2012. IMTIC aims at providing occasions for national and international researchers and practitioners to present the most recent advances and future challenges in the fields of computer and software engineering, electronics, telecommunication, control, multimedia information systems, simulation, and modeling and so on. This year the conference received 205 submissions – confirming a trend of increasing interest in IMTIC – coming from over 30 different countries including Australia, Bangladesh, Brazil, Canada, China, Denmark, Finland, France, Germany, India, Iran, Indonesia, Japan, Korea, Malaysia, The Netherlands, New Zealand, Norway, Pakistan, Spain, Sudan, Sweden, Thailand, UK, and USA. With so many papers to choose from, providing a conference program with a high level of technical excellence became a task that was challenging and time consuming, but ultimately a very rewarding one for the Technical Program Committee.

The Technical Program Committee focused on two aspects while selecting the technical papers: first, to provide a forum for more participants from Pakistan and all over the world through presentation and discussion of the relevant areas from a vast range of information and communication technologies (ICT) disciplines reflecting the rapidly evolving technology we are witnessing today. Second, to maintain a reasonable technical standard by selection of around 51 technical papers, which represents an acceptance rate of approximately 25%.

All the papers underwent a rigorous review process with each paper receiving at least two reviews. The review process included several stages including TPC member reviews, an online discussion among the reviewers, TPC lead summary recommendations, and additional reviews (as needed). The conference program has been structured with 4 parallel-track sessions for the presentation of papers, a PhD Symposium and a Poster Session. The topics presented had a reasonable balance between theory and practice in multi-disciplined topics including wireless sensor networks, cloud computing, wireless communication and broadband networks, antenna design, signal processing, software engineering, bioinformatics and telemedicine, switching networks, neural networks, automation and control and renewable energy. The program also includes 8 keynote speeches by renowned experts in the field, and 5 parallel thematic tutorials.

This event would not have been possible without the enthusiastic and hard work of a number of colleagues. We would like to express our gratitude to the General Chairs, for their assistance through the whole process, and the Steering Committee members for their supportive guidance. We also thank all the other members of the Organizing Committees for the fruitful cooperation. A special vote of thanks goes to the Technical Program Committee members, and all the

referees, for their invaluable help in reviewing the papers. We wish to acknowledge all the authors for their overwhelming support in submitting their papers to IMTIC. Last but not least, we wish to thank all the participants for attending the conference. We sincerely hope that you enjoy these proceedings.

March 2012

B.S. Chowdhry
F.K. Shaikh
D.M. Akbar Hussain
M.A. Uqaili

Organization

Conference Chairs

A.Q.K. Rajput	MUET, Pakistan
A. Rahman	City Uni. London, UK
D.M. Akbar Hussain	Aalborg University, Denmark

Steering Committee

Neeraj Suri	TU Darmstadt, Germany
Niel M. White	University of Southampton, UK
Ryszard Struzak	ICTP, Italy
Gul Agha	UIUC, USA
Tariq Munir	Edinburgh Napier University, UK
Mubark Shah	UCF, USA
M.Y. Sial	NTU, Singapore
Javier Poncela Gonzales	UMA, Spain
Joseph Ronsin	INSA de Rennes, France
Rezwan Khan	United International University, Bangladesh
Elfed Lewis	University of Limerick, Ireland
Mohd. Adam Suhaimi	International Islamic University, Malaysia
Abbas Omar	Otto-von-Guericke-Universität Magdeburg, Germany

General Chair

M.A. Uqaili	MUET, Pakistan
-------------	----------------

Technical Program Committee Chair

B.S. Chowdhry	MUET, Pakistan
F.K. Shaikh	MUET, Pakistan

Local Chairs

Aftab A. Memon	MUET, Pakistan
Tauha H. Ali	MUET, Pakistan
Javed Baloach	MUET, Pakistan

Tutorial Chairs

Tahseen Hafiz	MUET, Pakistan
Akram Shaikh	MUET, Pakistan
Fahim Umrani	MUET, Pakistan
Sana Hoor Jokhio	MUET, Pakistan

Poster Session Chair

Fahim Umrani	MUET, Pakistan
--------------	----------------

PhD Symposium Chair

Sheeraz Memon	MUET, Pakistan
---------------	----------------

Submission and Proceedings Committee

Imran Jokhio	MUET, Pakistan (Convener)
Sania Bhatti	MUET, Pakistan

Registration and Management Committee

Irfan Halepota	MUET, Pakistan
Mohsin Shah	MUET, Pakistan
Hyder Bux	MUET, Pakistan
Jibran Memon	MUET, Pakistan
Kamran Kazi	MUET, Pakistan

Web and Publicity Committee

Ashfaque Issani	MUET, Pakistan (Convener)
Khurram Bhatti	MUET, Pakistan
Syed Mohammad Ali Shah	MUET, Pakistan
M. Murtaza Chang	MUET, Pakistan (Web Design and, Developmnet)

Finance Committee

Munir A. Shaikh	MUET, Pakistan (Convener)
Aftab Ansari	MUET, Pakistan
Zeeshan Memon	

Sponsor



**HIGHER
EDUCATION
COMMISSION
PAKISTAN**

Organized by



**MEHRAN UNIVERSITY OF
ENGINEERING &
TECHNOLOGY
JAMSHORO, PAKISTAN**

Table of Contents

Impact Analysis of Renewable Energy in National Grids for Energy Deficit Countries	1
<i>Muhammad Aamir, Javier Poncela, Bhawani Shankar Chowdhry, and Muhammad Aslam Uqaili</i>	
Chebyshev Multiband Patch Antenna	10
<i>Syed Muzahir Abbas, Ilyas Saleem, Abida Parveen, Hijab Zahra, and Shahid Ahmed Khan</i>	
A Compact Multiband Antenna for GSM and WiMAX Applications	20
<i>M. Ali Babar Abbasi, M. Rizwan, Saleem Shahid, Sabaina Rafique, Haroon Tariq Awan, and Syed Muzahir Abbas</i>	
Haplotype Segment Algorithm for Predicting Disease Gene Locus Based on Distance/Similarity Measures	31
<i>Adeel Ahmed and Khalid Saleem</i>	
Effect of Fast Moving Object on RSSI in WSN: An Experimental Approach	43
<i>Syed Hassan Ahmed, Safdar Hussain Bouk, Amjad Mehmood, Nadeem Javaid, and Sasase Iwao</i>	
Performance Analysis of Bessel Beamformer and LMS Algorithm for Smart Antenna Array in Mobile Communication System	52
<i>Pervez Akhtar and Muhammad Yasin</i>	
Adaptive Minimum Entropy Beamforming Algorithms for Narrowband Signals	62
<i>Anum Ali and Shafayat Abrar</i>	
Gender Classification Using Local Binary Pattern and Particle Swarm Optimization	73
<i>Sajid Ali Khan, Muhammad Nazir, Naveed Riaz, M. Hussain, and Nawazish Naveed</i>	
Parametric Study of Nonlinear Adaptive Cruise Control Vehicle Model by Vehicle Mass	81
<i>Zeeshan Ali and Dur Muhammad Pathan</i>	
ECAODV: Enhanced Classified Ad-Hoc on Demand Distance Vector Routing Protocol	92
<i>Noorul Amin, Nizamuddin, and Abdelmuttlib Ibrahim</i>	

An External Approach to Improve the Information Content of Diagnostic Ultrasound Images	101
<i>Samreen Amir, Bhawani Shankar Chowdhry, Muhammad Asif, and Bhibekshan Chowdhry</i>	
Comparative Analysis of Group Centric Access Control Models	110
<i>Hirra Anwar and Muhammad Awais Shibli</i>	
Nonlinear System Identification Using Neural Network	122
<i>Muhammad Asif Arain, Helon Vicente Hultmann Ayala, and Muhammad Adil Ansari</i>	
Intrusion Damage Assessment for Multi-stage Attacks for Clouds	132
<i>Junaid Arshad, Imran Ali Jokhio, and Mahmood Shah</i>	
Emotions in Robots	144
<i>Muhammad Mansoor Azeem, Jamshed Iqbal, Pekka Toivanen, and Abdul Samad</i>	
On the Use of the Universal Okumura-Hata Model for Defining Different ICT Areas	154
<i>Dipashree M. Bhalerao, M. Tahir Riaz, Ole Brun Madsen, and Ramjee Prasad</i>	
A Novel Approach for Automatic Generation of UML Class Diagrams from XMI	164
<i>Kashif Hameed, Imran Sarwar Bajwa, and Muhammad Asif Naeem</i>	
An Efficient Link Bundling Transport Layer Protocol for Achieving Higher Data Rate and Availability	176
<i>Muhammad Adnan Hashmi, Imran Shafi, Syed Ismail Shah, and Jamil Ahmad</i>	
Improvement of Small Signal Performance of Multi Machine Power System Using SMIB Based PSS and STATCOM Designs	188
<i>Bilal Hussain, Muhammad Usman, Affan Ahsan, Ahmad Talha, and Farhan Mahmood</i>	
Are QoE Requirements for Multimedia Services Different for Men and Women? Analysis of Gender Differences in Forming QoE in Virtual Acoustic Environments	200
<i>Mansoor Hyder, Khalil ur Rehman Laghari, Noel Crespi, Michael Haun, and Christian Hoene</i>	
Facilitating an Off-Site Customer in Product-Based Agile Software Development: An industrial Case Study	210
<i>Irum Inayat, Muhammad Asim Noor, and Zubaria Inayat</i>	

Segmentation of Brain Tumor Tissue Using Marker Controlled Watershed Transform Method	222
<i>Muhammad Kaleem, M. Sanaullah, M. Ayyaz Hussain, M. Arfan Jaffar, and Tae-Sun Choi</i>	
Performance Evaluation of Statistical Techniques for Adaptive Scheduling in Autonomic Systems	228
<i>Omer Khalid, Richard Anthony, and Miltos Petridis</i>	
Angle Differential Modulation Scheme for Odd-Bit QAM	240
<i>Syed Safwan Khalid and Shafayat Abrar</i>	
Adaptive Wavelets Based Fuzzy NN Control for Active Suspension Model	249
<i>Laiq Khan, Shahid Qamar, and Muhammad Umair Khan</i>	
Blind Deconvolution of Blurred Images with Fuzzy Size Detection of Point Spread Function	261
<i>Salman Hameed Khan, Muhammad Sohail, Ahmed Rehan, Zeashan Hameed Khan, and Arsalan Hameed Khan</i>	
Bluetooth Usage Control Policy Enforcement Model	272
<i>Shahryar Khan and Inayatullah Babar</i>	
A Comparative Study on Particle Swarm Optimization and Genetic Algorithms for Fixed Order Controller Design	284
<i>Faizullah Mahar, Syed Saad Azhar Ali, and Zuhaibuddin Bhutto</i>	
Design of WLAN Patch and UWB Monopole Antenna	295
<i>Faraz Mahmood, Syed Muhammad Usman Ali, Mahmood Alam, and Magnus Willander</i>	
Single-Bit Ternary FIR Filter in FPGA Using Canonical Signed Digit Encoding	305
<i>Tayab D. Memon, Abdullah Alhassani, and Paul Beckett</i>	
A Parametric Analysis of Stream Based Joins	314
<i>Muhammad Asif Naeem, Gillian Dobbie, Gerald Weber, and Imran Sarwar Bajwa</i>	
Efficient Usage of Memory Resources in Near-Real-Time Data Warehousing	326
<i>Muhammad Asif Naeem, Gillian Dobbie, Gerald Weber, and Imran Sarwar Bajwa</i>	
Classifier Ensemble Framework Based on Clustering Method	338
<i>Hamid Parvin, Sajad Parvin, Zahra Rezaei, and Moslem Mohamadi</i>	

Usability Cost Benefit Analysis Using a Mathematical Equation	349
<i>Samina Rajper, Abdul Wahid Shaikh, Zubair A. Shaikh, and Imran Amin</i>	
Efficient FPGA Implementation of Secure Hash Algorithm Grøstl – SHA-3 Finalist	361
<i>M. Muzaffar Rao, Kashif Latif, Arshad Aziz, and Athar Mahboob</i>	
Capture Largest Included Circles: An Approach for Counting Red Blood Cells	373
<i>Saima Rathore, Aksam Iftikhar, Ahmad Ali, Mutawarra Hussain, and Abdul Jalil</i>	
Enhanced Image Encryption Techniques Using Modified Advanced Encryption Standard	385
<i>Faisal Riaz, Sumira Hameed, Imran Shafi, Rakshanada Kausar, and Anil Ahmed</i>	
Virtual Instrumentation for Control Applications	397
<i>Syed Ali Asad Rizvi, Sham Sunder, Farah Haroon, and Ashab Mirza</i>	
Data Management in Mobile Wireless Sensor Networks	409
<i>Syeda Nida Sahar and Faisal Karim Shaikh</i>	
Implementation of Load Shedding Apparatus for Energy Management in Pakistan	421
<i>Hira Sakrani, Tooba Tariq Butt, Moezul Hassan, Sarmad Hameed, and Imran Amin</i>	
JAM: Mitigating Jellyfish Attacks in Wireless Ad Hoc Networks	432
<i>Fahad Samad, Qassem Abu Ahmed, Asadullah Shaikh, and Abdul Aziz</i>	
Aggregating Node Level Risk Assessment in Grids Using an R-out-of-N Model	445
<i>Asif Sangrasi, Karim Djemame, and Imran Ali Jokhio</i>	
Hybrid Ant Bee Colony Algorithm for Volcano Temperature Prediction	453
<i>Habib Shah, Rozaida Ghazali, and Nazri Mohd Nawi</i>	
Building Wireless Sensor Networks Application Using Sun SPOTs	466
<i>Asadullah Shaikh, Naveed Anjum, Fahad Samad, and Asadullah Shah</i>	
Study of Arduino for Creative and Interactive Artwork Installations: An Open Source Software Knowledge for Creativeness	478
<i>Murtaza Hussain Shaikh</i>	

Developing and Managing SLAs for Business Applications in Information Systems	489
<i>Aijaz Soomro and William Song</i>	
Image Retrieval Based on Color and Texture Feature Using Artificial Neural Network	501
<i>Sajjad Hussain, Manzoor Hashmani, Muhammad Moinuddin, Mikio Yoshida, and Hidenori Kanjo</i>	
An Objective Based Classification of Aggregation Techniques for Wireless Sensor Networks	512
<i>Qurat-ul-Ain I. Tariq, Saneeha Ahmed, and Huma Zia</i>	
A New Data Compression Technique Using an Evolutionary Programming Approach	524
<i>Fahad Ullah and Khawaja M. Yahya</i>	
Evaluation of Dc/Dc Buck Converter Controlled by LMS (Least Mean Square) Algorithm for Different Values of Load Capacitor	532
<i>Farooq Kifayat Ullah</i>	
Exploiting Multi View Video for Maximizing Lifetime of Wireless Video Sensor Networks	541
<i>Saima Zareen, Khalid Iqbal, Almas Anjum, and Shoaib A. Khan</i>	
Author Index	553

Impact Analysis of Renewable Energy in National Grids for Energy Deficit Countries

Muhammad Aamir¹, Javier Poncela², Bhavani Shankar Chowdhry¹,
and Muhammad Aslam Uqaili¹

¹ Mehran University of Engineering & Technology, Jamshoro, Pakistan

² ETSI Telecommunication Engineering, University of Malaga, Spain
muaamir5@yahoo.com, javier@ic.uma.es, c.bhawani@ieee.org,
aslam.uqaili@faculty.muet.edu.pk

Abstract. For countries like Pakistan where demand of energy is being increased every year, the design of a framework that analyzes the impact of adding renewable energy to the power grid is of high interest. Such analysis may help ensure a reliable energy supply, and identify energy savings opportunities. Appropriate simulation tools are needed in order to discover the best approach. Such impact analysis also results in cost-effective generation and, further, in environmental improvements. In this paper, one analysis frame work is proposed. The main objective of this study is to propose a framework that helps optimize development and implementation of renewable energy resources focusing on their probable advantages to improve both the electricity system and the environment. The results of this analysis will be helpful in determining the performance issues related to generation, transmission and green technology. Prime locations inside system may be identified where adequate renewable generation may efficiently address transmission crisis.

Keywords: Renewable Energy, Power Grid, Green Technology, Supervisory Control and Data Acquisition (SCADA), Transmission Loading Relief (TLR), Contingency Analysis.

1 Introduction

Supervisory Control and Data Acquisition (SCADA) based controlling and monitoring systems capitalize on the deployment of the on hand power system by online assessment of the network towards available capacities of the system. Increasing load demand simultaneously with an ongoing deregulation of electricity markets in many countries often lead to the disturbance of transmission systems and their operation very close to their limits. Power systems are then more sensitive to failures that occur and limits for a maximal transmission through some corridors of the network are reached. This emerging congestion is crucial and may be addressed by accumulating few available green resources to the power grid. The following table is taken from Pakistan Energy Overview, compiled by South Asian Regional Initiative for Energy [1].

Table 1. Projection for Demand and Supply

S. No	Year	Firm Supply (MW)	Peak Demand (MW)	Surplus/(Deficit) (MW)
1	1999-2000	13445	11296	2149
2	2000-2001	13716	11852	1864
2	2000-2001	13716	11852	1864
3	2001-2002	13693	12443	1250
4	2002-2003	14336	13071	1265
5	2003-2004	15046	13831	1215
6	2004-2005	15082	14642	440
7	2005-2006	15072	15483	(441)
8	2006-2007	15091	16548	(1457)
9	2007-2008	15055	17689	(2634)
10	2008-2009	15055	19080	(4025)
11	2009-2010	15055	20584	(5529)

(Source: Ministry of Water and Power, Pakistan)

Note: Current Shortfall in Pakistan is more than 6000 MegaWatt, the table shows estimate till year 2010 only.

According to the above-mentioned table, the deficit in terms of supply is being increased, so effective monitoring and controlling is essential in each country like Pakistan; which may be possible through implementing High Scale SCADA System for Energy Management [2]. It is equally significant to analyze the system for probable addition of renewable resources. Such analysis will be helpful to address performance constraints by identifying possible locations where renewable energy can be easily added to the available capacity. It is important to mention that the intended addition of renewable resources will be supervised using powerful monitoring and controlling features of SCADA. Therefore the analysis will also support designing phase of any SCADA system planned for energy management.

The section 2 of this paper presents detail about the System Design Platforms followed by System Design Tools discussed in section 3. Development of the framework is discussed in section 4 by describing various steps in detail. The last section describes conclusion by presenting importance of the proposed framework.

2 System Design Platform

This research involves impact analysis to determine performance of an energy deficit system which can be optimized by accumulating renewable energy. An optimized framework can be developed using various tools available with "Power World" which is power system visualization, simulation, and analysis tool. [3]. Various types of analyses can be performed using "PowerWorld". However, Power Flow simulation,

Contingency analysis, weak element visualization and Transmission Loading Relief (TLR) Sensitivity for both normal and congestion situations are of high interest.

It is imperative to mention that necessary equations to calculate above mentioned parameters like Transmission Loading Relief (TLR) Sensitivity [4] for both normal and congestion situations are already embedded in the “PowerWorld”. TLR sensitivities are used to estimate the sensitivity of a single monitored element to many different power transfers.

It is also pointed out above mentioned various analyses are really helpful in designing energy grids due to stand alone capability of “PowerWorld” for power flow analysis.

3 System Design Tools

A large number of tools are available in PowerWorld Software for different analyses. However, major contribution is made by TLR sensitivities and Contingency Analysis for development of proposed framework.

3.1 Transmission Loading Relief (TLR)

TLR is an effective tool which is used to prevent overload situations by managing transmission utilization. It is very useful to reduce the risk of system failure. For instance, if a transmission line is loaded beyond its thermal limit then a TLR plan be initialized forcing that all transactions on the overloaded element be curtailed thus keeping the exchanged power flow within designated thermal limit. The TLR sensitivity evaluation in “Power World” is useful indication of those transactions that would be condensed. TLR can be represented by the following expression:

$$TLR_{BUS\ i, BRANCH\ jk} = \frac{\Delta MWFlow_{BRANCH\ jk}}{\Delta MWInjection_{Bus\ i}} \quad (1)$$

This equation (1) is already integrated with “Power World” as very useful tool for calculating TLR for each bus.

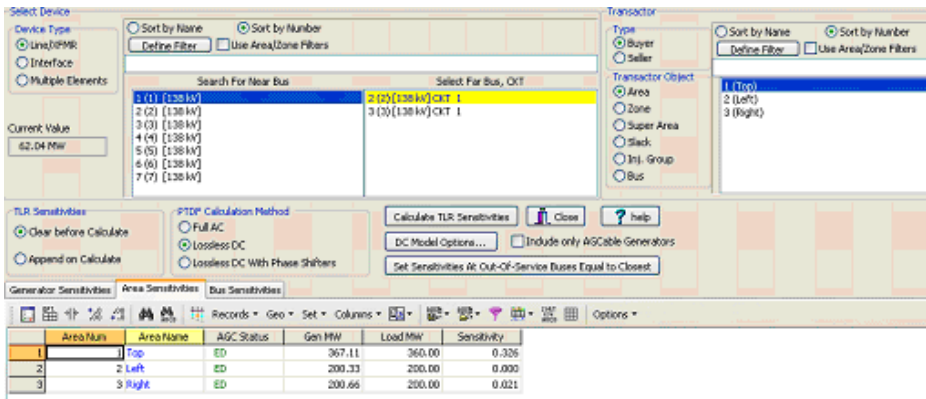


Fig. 1. Calculation of TLR Sensitivities using PowerWorld

It can be observed from the Fig.1 that sensitivities are calculated for each bus. Therefore in view of the fact that a TLR is considered for every bus, the TLR may be used to grade locations. Good or weak location may be identified by analyzing TLR.

Reference to analyze Contingencies, Contingency Transmission Loading Relief (TLR) Sensitivity is the change in the flow of a line due to an injection at a bus assuming a contingency condition.

It can be expressed by the following equation:

$$TLR_{BUSi, BRANCH\ jk, CONTc} = \frac{\Delta ContMWFlow\ BRANCH\ jk, CONTc}{\Delta MWInjection_{Busi}} \quad (2)$$

The Equivalent Transmission Loading Relief (ETLR) [5] of selected Transmission Lines of Transformers is the algebraic sum of the TLRs of each individual element. The Weighted Transmission Loading Relief (WTLR) [5] is used to weight the current MW flow in a particular element.

3.2 Contingency Condition

A contingency condition is defined as breakdown of any one piece of equipment, i.e. either transmission line or transformer. The main objective of power system engineers is to design a secured power system. It means that the system must be capable to withstand in case of any breakdown of equipment and must operate normally. The Contingency Analysis [6] tools available within PowerWorld Simulator’s may analyze the system in any statistically likely contingent scenario. This feature is available in addition to the analysis of power system in normal operation topology. The industry based criterion for normal operation is frequently referred to as the n-1 rule, which imposes a binding that a system is required to operate in a stable and secure manner even in case of any single transmission or generation outage.

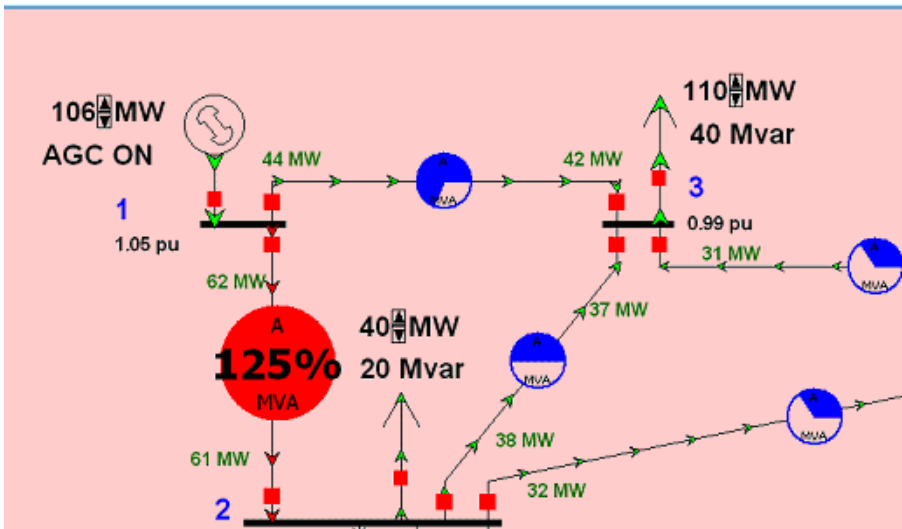


Fig. 2. Example of weak element visualization

In above scenario depicted in Fig.2, the transmission line between 1 and 2 gets overloaded, for example due to unwanted disconnection between 1 and 3. This is a case of weak element visualization.

This feature of determining contingency conditions can be implemented in Power-World in addition to the analysis of power system in normal operation topology. In next section, a frame work is being proposed with prime objective of optimization by adding renewable energy sources at suitable location determined by software visualization.

4 Development of Proposed Framework

As described in the previous section, different tools available in PowerWorld Simulator are being used to design the desired structure. The steps of the proposed framework are depicted in Fig. 3.

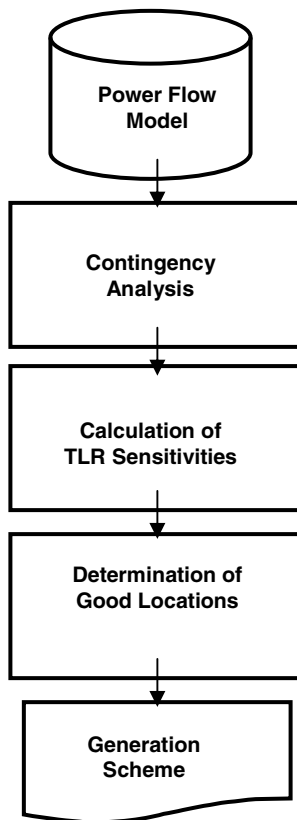


Fig. 3. Flow Diagram representing proposed frame work

This framework helps in the process of integration of renewable energy resources with existing grid capacity and generation policy can be optimized considering results of analyses for various locations.

4.1 Power Flow Model

It refers to the identification of weak elements in the power scheme by simulating impacts from loss of capacity or transmission. More significantly, potential locations in system can be easily identified where injection of renewable generation can provide grid reliability. A real scenario is considered for step-wise development of framework. This real case information is presented in Fig.4.

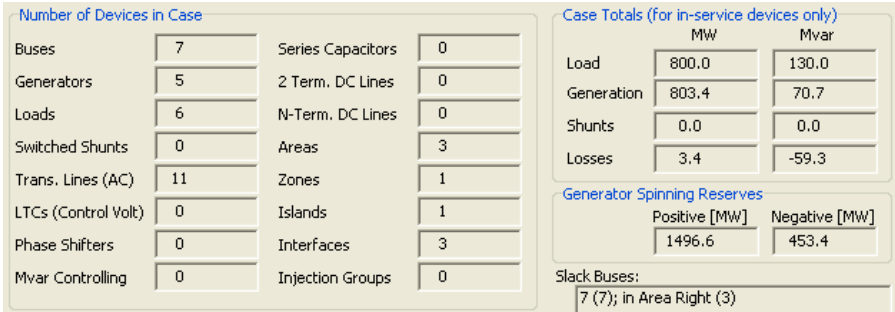


Fig. 4. A real scenario of Power Flow Analysis

4.2 Contingency Analysis

Contingency analysis is a critically essential part of efforts used for analysis of any power system [7]. It is imperative for all operators and planners to analyze power systems covering states for example the long-term effects of both new generation facilities and projected growth in load on the transmission system. In congestion scenario, the weak elements tend to get overloaded causing system failure. Transmission

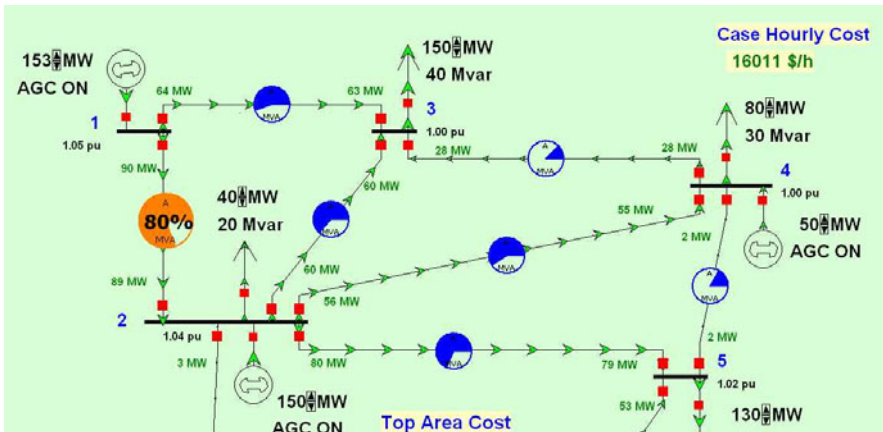


Fig. 5. Cross Section View of a Power System with 05 buses (Originally containing 07 Buses)

planning can be prioritized by proper ranking of equipment being used. Single element or multiple element contingencies can be defined in PowerWorld Simulator. Only one contingent action is associated with single element contingency. A seven bus power system is depicted in Fig.5 for which contingency analysis is processed. This is the same real case already presented by Fig.4.

The contingency analysis for the above mentioned scenario is resulted in detection of 03 Violations and 0 Unsolvable Contingencies. In this way, potential weak elements can be determined and renewable generation may be injected in case of congestion. This phase is considered as a major contributor of the proposed framework.

Table 2. Contingency Analysis showing 03 violations

	Label	Skip	Processed	Solve ▲	Violations	Max Branch %	Min Volt	Max Volt	Max Interface %
1	CHANGE LOAD AT BUS 2 (2) BY 25 % of present MW (cnst.pf)	NO	YES	YES	0				
2	L_000011-000022C1	NO	YES	YES	1	131.1			
3	L_000011-000033C1	NO	YES	YES	1	128.7			
4	L_000022-000033C1	NO	YES	YES	0				
5	L_000022-000044C1	NO	YES	YES	0				
6	L_000022-000055C1	NO	YES	YES	0				
7	L_000022-000066C1	NO	YES	YES	0				
8	L_000033-000044C1	NO	YES	YES	0				
9	L_000044-000055C1	NO	YES	YES	0				
10	L_000077-000055C1	NO	YES	YES	1	106.3			
11	L_000066-000077C1	NO	YES	YES	0				
12	L_000066-000077C2	NO	YES	YES	0				

4.3 Calculation of TLR Sensitivities

These calculations are used to determine the sensitivity of the MW flow of selected device with respect to a change of real power through each bus. It is assumed that the power is introduced at each bus and absorbed at the transactor object while transactor type is consumer/buyer. When the transactor type is supplier/seller, then it is assumed that the power is injected at each transactor object and absorbed at each bus. For the sample case, the sensitivities calculated by the simulator are depicted in Table 3 taken transactor type as buyer.

Table 3. A sample TLR calculation using PowerWorld

	Number	Name	Area Num	Area Name	P Sensitivity ▼
1	1 1		1	Top	0.519
2	3 3		1	Top	-0.129
3	4 4		1	Top	-0.174
4	5 5		1	Top	-0.303
5	7 7		3	Right	-0.313
6	6 6		2	Left	-0.335
7	2 2		1	Top	-0.346

4.4 Determination of Good Locations

Generation can be positioned to alleviate weak element contingency overloads. The Collective MVA Overload and a related field, the Aggregate Percent Overload of a transmission line or transformer are measures of the weakness of transmission line on the grid. This measure can be displayed in case information menu of simulator and counter flow can be produced to mitigate weak element. It will result in identification of good location after proper mitigation.

Table 4. Ranking of violated elements on the basis of aggregated percent overload

	From Number	From Name	To Number	To Name	Circuit	Xfrmr	Aggr Percent Overload ▼	Violations	Max % Loading Cont.
1	1 1		3 3		1	No	31.09	1	131.09
2	1 1		2 2		1	No	28.71	1	128.71
3	2 2		5 5		1	No	6,30	1	106,30
4	2 2		3 3		1	No	0,00	0	
5	2 2		6 6		1	No	0,00	0	
6	3 3		4 4		1	No	0,00	0	
7	6 6		7 7		1	No	0,00	0	
8	7 7		5 5		1	No	0,00	0	
9	4 4		5 5		1	No	0,00	0	
10	6 6		7 7		2	No	0,00	0	
11	2 2		4 4		1	No	0,00	0	

It can be observed from Table.4 that the ranking of elements with violation is possible. In above scenario, the line from 11 to 33 has more aggregate percent overload so priority must be given to this line while injecting renewable energy at overloaded elements.

4.5 Generation Scheme

As discussed in section 3.1, the Weighted Transmission Loading Relief (WTLR) is used to weight the current MW flow in a particular element. A WTLR of 5.0 at an element (bus) suggests that 10MW of new generation inserted at this particular bus is expected to decrease 5.0 MW of overload in transmission elements during contingencies. Thus, if we insert some potential renewable energy resources at high impact buses, re-dispatch the system, and rerun the contingencies, the overloads will decrease. Therefore, the generation policy can be optimized by analyzing the system in accordance with the proposed frame work.

5 Conclusion

The proposed framework can be used to analyze the performance issues related to generation, transmission and injection of renewable technology. The framework involves calculation of critical performance parameters like various types of TLR sensitivities and Contingency Analysis resulting in identification of overloaded locations. The overloaded locations are detected with ranking to prioritize the injection for mitigation. Aggregate Percent Overload is a critical measure which helps in

implementing above mentioned prioritization. The proposed framework can be used to determine the suitable locations for generation of renewable energy to minimize the power deficit of National Grid. This can further be resulted in cost-effective operation as generation is optimized by pointing only overloaded transmission lines. Such customized renewable generation is not only cost-effective but also environment friendly. The proposed framework can be enhanced to become effective on large scale and implemented with SCADA based energy management system.

References

1. Energy Sector Overview: South Asian Regional Initiative for Energy
http://www.sari-energy.org/PageFiles/Countries/Pakistan_Energy_Overview.asp
2. Aamir, M., Mahmood, A.: Performance Analysis of Wide Area Operation, Control and protection High Scale SCADA System. In: Electric Power Conference, EPEC 2008. IEEE, Canada (2008)
3. PowerWorld Corporation, User's Guide for PowerWorld Version 14, South First Street Champaign, IL 61820 (2001)
4. Niimura, T., Niioka, S., Yokoyama, R.: Transmission Loading Relief Solutions for Congestion Management. *Power Systems Research* 67(2) (November 2003)
5. Glover, J.D., Sarma, M.S., Overbye, T.J.: *Power System Analysis and Design*, 4th edn. Thomson Learning, Inc. (2008)
6. Sauer, P.W., Reinhard, K.E., Overbye, T.J.: Extended Factors for Linear Contingency Analysis. In: 34th Hawaii International Conference on System Sciences (2001)
7. Grijalva, S., Visnesky Jr., A.M.: Visualizations for power system contingency analysis data. In: IEEE Power Engineering Society General Meeting (2005)

Chebyshev Multiband Patch Antenna

Syed Muzahir Abbas, Ilyas Saleem, Abida Parveen, Hijab Zahra,
and Shahid Ahmed Khan

Department of Electrical Engineering, COMSATS Institute of Information Technology,
Islamabad, Pakistan

{muzahir_abbas, shahidk}@comsats.edu.pk,
ilyas-saleem@hotmail.com, abidaperveen86@gmail.com,
hijab.zahra@ymail.com

Abstract. This paper presents design procedure of a chebyshev multiband microstrip patch antenna. The multibands are achieved by the chebyshevs, introduced on the adjacent and opposite corners of rectangular patch. The bandwidth and frequency shifts are controlled by increasing the distance among the chebyshev from right side and the position of feed is also adjusted in order to compensate the remaining parameters. Moreover, the measured and simulated result confirms the capability of proposed antenna for GSM, Wi-Fi, WiMAX, Marine Radar and for Fixed Radio Services.

Keywords: Chebyshev, Microstrip Patch, Multiband Antenna, Adjustable Feed.

1 Introduction

Now-a-days microstrip patch antennas are preferred in wireless communications because of their performance, conformability and cost effectiveness [1]. Various patch antennas with the functionality of multibands have been successfully presented to fulfill the requirements of multistandard portable devices [2-6].

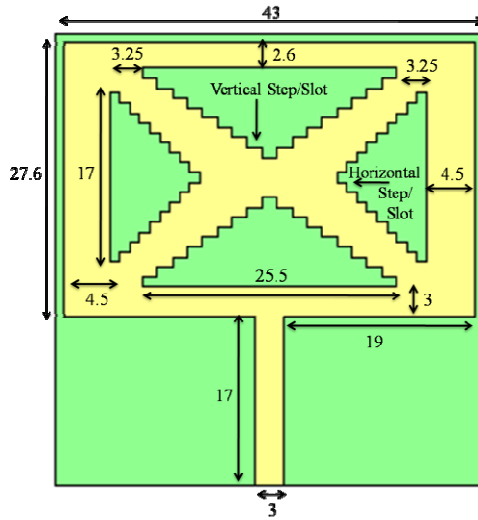
In [7], multibands are achieved by adding slots to a rectangular and triangular geometry that is fed by a coaxial probe with an input impedance of 50Ω . Similar work is also reported in [8]. In [9], a patch excited by a coaxial connector to resonate at the central frequencies of GPS (Global Positioning System) and Bluetooth is offered. Narrow bandwidth is observed in [7] and [8], resolved in [9] using thick substrate. C-slot patch antenna having narrow band allows the operation of only WiMAX in [10].

By default patch antenna possesses narrow bandwidths [11]; therefore different approaches have been used in [7-10] to enhance bandwidth of antenna(s). Our antenna has a rectangular patch having chebyshevs on each side providing multibands [12-13] and width of patch is additionally increased to attain wideband, the core drawback faced in [7-10].

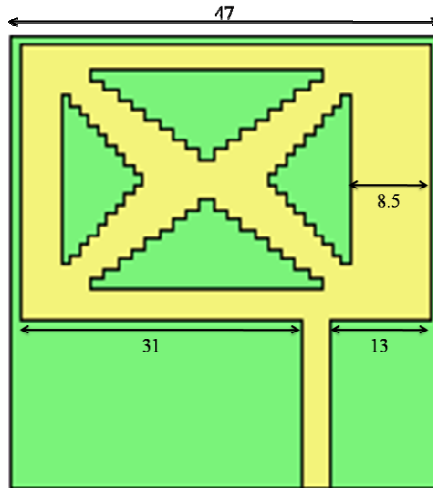
2 Antenna Design

The geometry of proposed antenna is shown in Fig. 1. FR4 epoxy with the thickness of 1.6 mm is used as substrate having dielectric constant (ϵ_r) of 4.7. Well matched

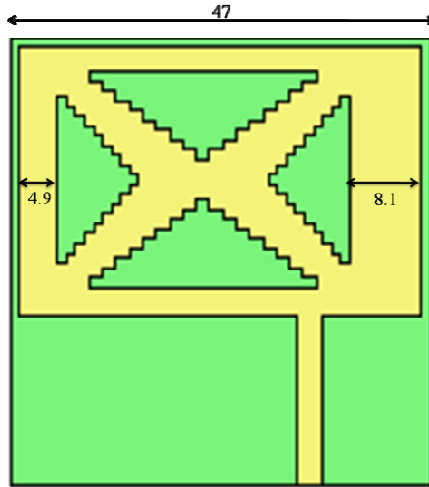
transmission line of $3 \times 17 \text{ mm}^2$ with an impedance of 50Ω is feeding the patch. Length (L_p) and width (W_p) of radiating patch are $27.6 \times 41 \text{ mm}^2$ and of substrate are $45.5 \times 43 \text{ mm}^2$ calculated by the formulas given in [1]. Complete ground plane is used in our case.



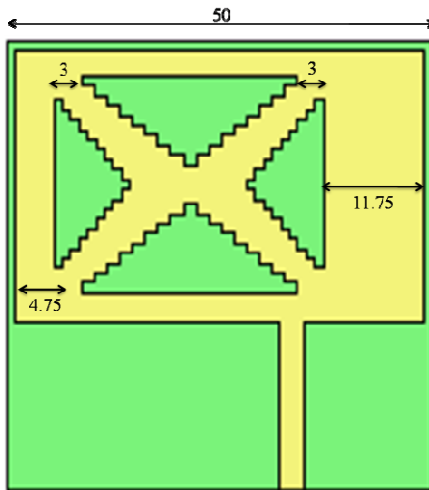
(a) Antenna Design 'a'



(b) Antenna Design 'b'



(c) Antenna Design 'c'



(d) Antenna Design 'd'

Fig. 1. Geometry of Proposed Antenna Designs

Eq. (1) to (6) is given in order to calculate the length and width of each rectangular (vertical and horizontal) step/slot in its corresponding chebyshev for proposed antenna. Equation (1) gives L_{mid} and W_{mid} , i.e. the length of middle step/slot in vertical chebyshevs and width of middle step/slot in horizontal chebyshevs respectively, where N is the total number of steps/slots on each side of middle slot which is 8.

$$L_{mid} = W_{mid} = 10 \log N \tag{1}$$

W_{chv} is total width of vertical chebyshev, while L_{chh} is the length of horizontal chebyshev.

$$W_{\text{chv}} \approx W_p - 1.75W_{\text{mid}} \quad (2)$$

$$L_{\text{chh}} \approx L_p - L_{\text{mid}} \quad (3)$$

W_{sv} is width of each rectangular step/slot in vertical chebyshev, where L_{sh} is width of each rectangular step/slot in horizontal chebyshev.

$$W_{\text{sv}} = \frac{W_{\text{chv}}}{2N+1} \quad (4)$$

$$L_{\text{sh}} = \frac{L_{\text{chh}}}{2N+1} \quad (5)$$

W_{side} is width on each side of horizontal chebyshev.

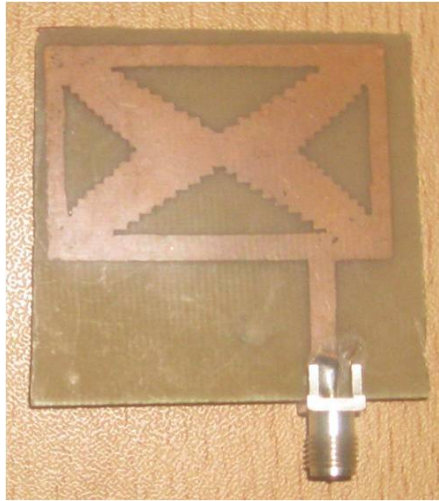
$$W_{\text{side}} = \frac{L_{\text{mid}}}{2} \quad (6)$$

Chebyshevs are placed on each side of rectangular patch; moreover 17 rectangular steps/slots are inserted in each chebyshev, which follows a chebyshev distribution to get multibands. The middle step/slot in each chebyshev is of 9 mm and every subsequent step's/slot's length is decreased by 1 mm, eventually making the N^{th} step/slot of 1 mm. Width of each step/slot in vertical chebyshevs is 1.5 mm each and length is 1 mm each in horizontal chebyshevs. The distance between horizontal chebyshevs is $\lambda/4$ which is quarter of $\lambda/12$ (the distance between upper and lower chebyshevs).

In Fig. 1 (a), the separation distance between upper and lower chebyshevs from front and transmission line end is 2.6 mm and 3 mm respectively and is 4.5 mm for the right and left chebyshevs. There are total 34 vertical and 34 horizontal steps/slots, making 4 chebyshevs collectively.

In Fig. 1 (b), separation distance between horizontal chebyshev and right corner increases and transmission line is slightly moved resulting three new operational bands with relative frequency shifts from the previous design. In addition to investigate further characteristics, the proportions of design (b) are then altered as shown in Fig. 1 (c) and in Fig. 1 (d) causing frequency shifts and bandwidth enhancements.

The fabricated antenna(s) is shown in Fig. 2.



(a) Antenna Design 'b'



(b) Antenna Design 'd'

Fig. 2. Fabricated Antennas

3 Results and Analysis

Simulation results of all the four designs presented in this paper, are obtained from HFSS (High Frequency Structure Simulator) based on finite element method. The simulated return loss are shown in Fig. 3, and the impedance bandwidths (return loss <math>< -10\text{dB}</math>) are summarized in Table 1.

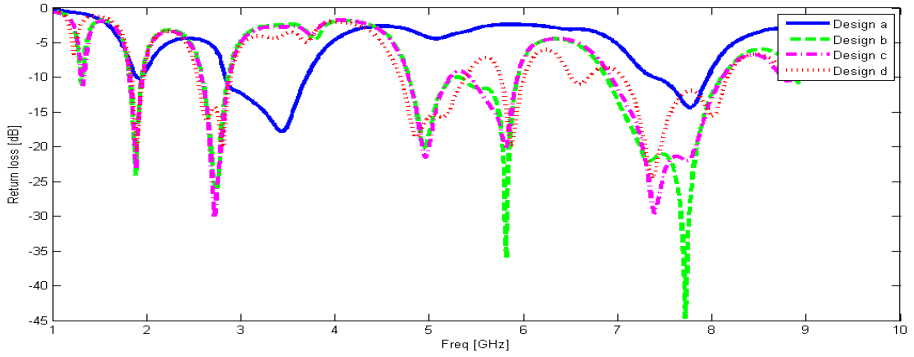
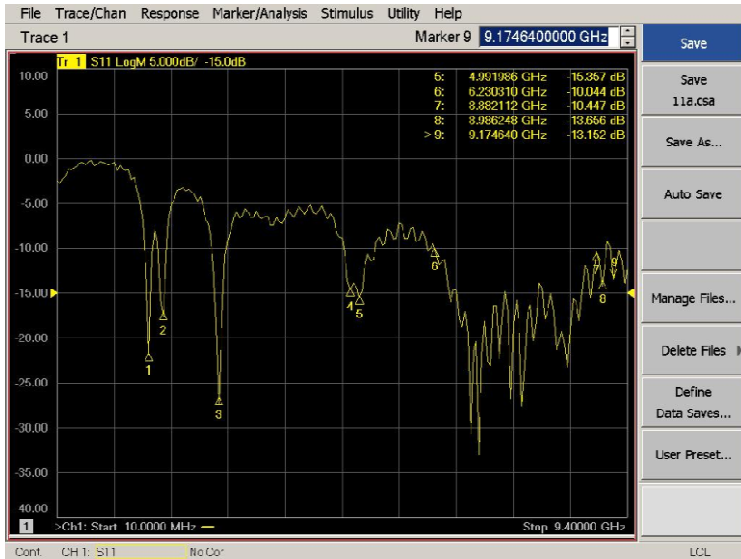


Fig. 3. Simulated return loss for Design a, b, c, d

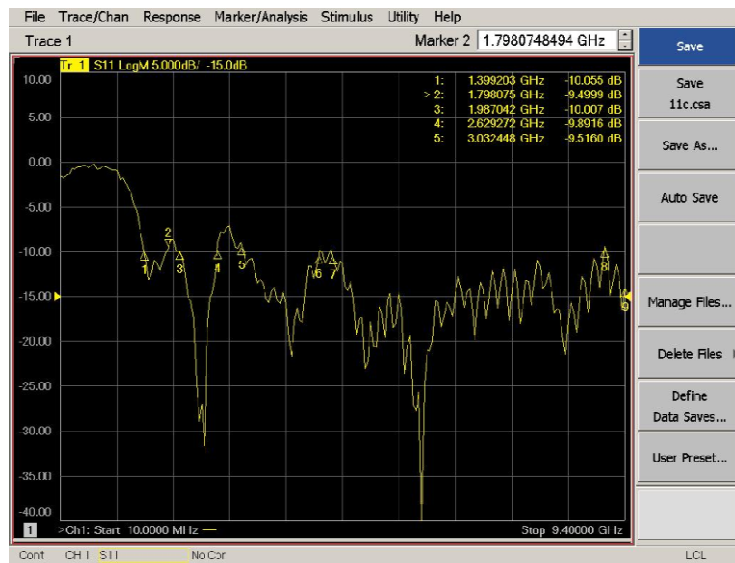
Table 1. Impedance Bandwidths

Antenna	Operating Frequency (GHz)	Return loss (dB)	Bandwidth (MHz)
Design a	3.44	-17.77	870
	7.78	-14.34	550
Design b	1.88	-24.06	130
	2.74	-27.17	270
	4.95	-20.13	540
	5.82	-35.99	620
	7.72	-44.64	1200
Design c	1.89	-23.06	140
	2.72	-30.07	290
	4.96	-21.55	440
	5.81	-20.17	490
	7.4	-29.48	1700
Design d	1.9	-20.66	120
	2.81	-20.01	350
	4.87	-18.64	690
	5.87	-19.79	260
	6.6	-11.03	20
	7.37	-24.52	1200

Antenna designs ‘b’ and ‘d’ were fabricated manually and measured reflection coefficients from network analyzer of Agilent Technologies, model N5242A are shown in Fig. 4, a good agreement is found between simulated and measured return loss.



(a) Antenna Design ‘b’

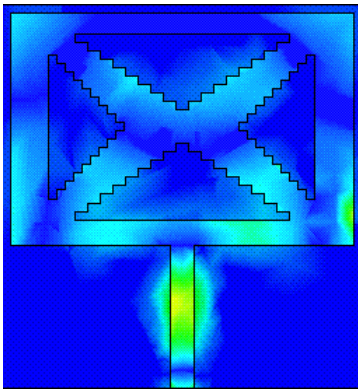


(b) Antenna Design ‘d’

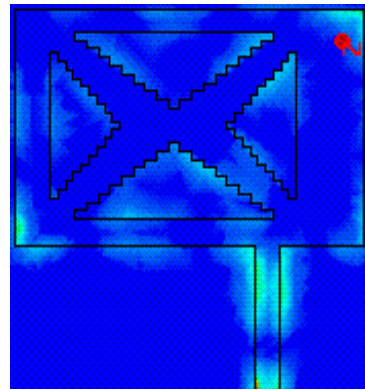
Fig. 4. Measured return loss against resonating frequencies

Thus, the similarity between simulated and measured results evidently shows that operating frequencies given in Table 1 for Design ‘a’ are applicable for WiMAX and Fixed Radio Services, while Design ‘b’, ‘c’ and ‘d’ provides GSM, Terminal Air Traffic Control, Marine Radar and Wi-Fi’s operating frequencies. Likewise design ‘d’ also resonates at Fixed Radio Services.

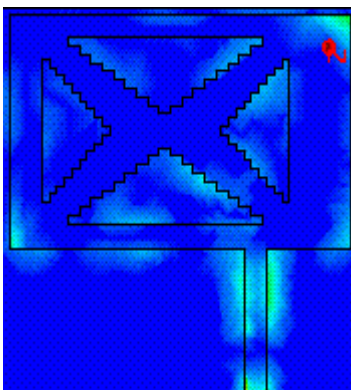
To become more familiar with the functionalities of an antenna in a better way, the current distributions must be examined thoroughly and are shown in Fig. 5. From the evaluation of Fig. 5 i.e. simulated current distributions of designed antennas, it can be observed that the current is concentrated more on the feed line and then on the edges of chebyshevs; where both components of the currents exist. The distribution of current over the entire frequency range is fairly stable indicating that the radiation is also consistent. Note that the current on the feed line is almost same as it moved towards right.



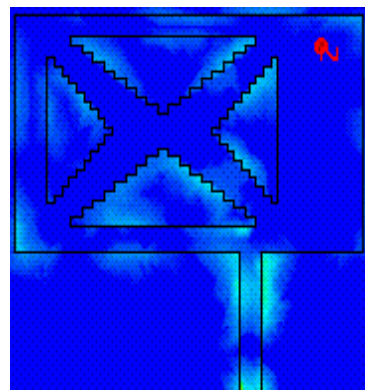
(a) Antenna Design ‘a’



(b) Antenna Design ‘b’



(c) Antenna Design ‘c’



(d) Antenna Design ‘d’

Fig. 5. Simulated Surface Current Distributions

Similarly radiation patterns of $E(\theta)$ and $E(\Phi)$ planes at different resonating frequencies for every design given here are shown from Fig. 6 to Fig. 9.

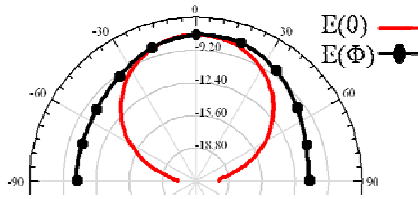


Fig. 6. Simulated Radiation Pattern of Antenna Design 'a' at 3.4 GHz

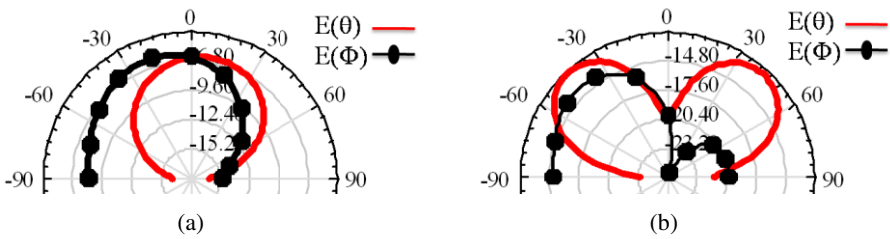


Fig. 7. Simulated Radiation Pattern of Antenna Design 'b' at (a) 1.8 GHz, (b) 2.7 GHz

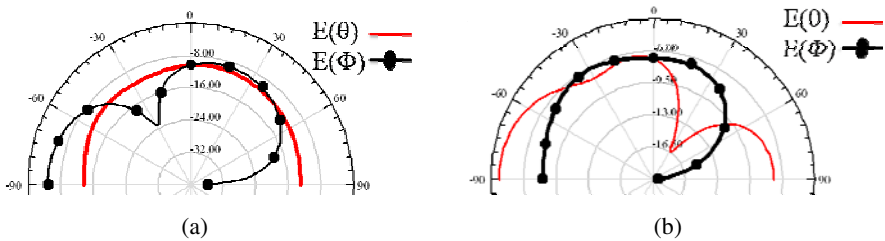


Fig. 8. Simulated Radiation Pattern of Antenna Design 'c' at (a) 4.9 GHz, (b) 5.8 GHz

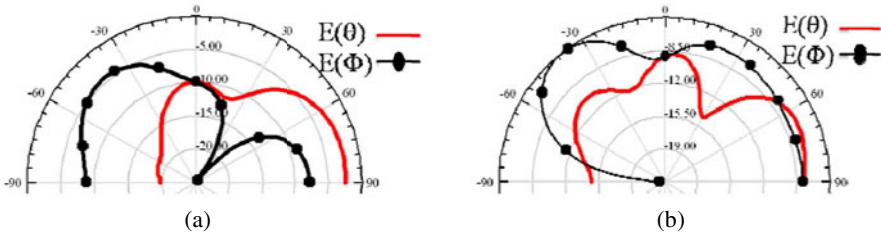


Fig. 9. Simulated Radiation Pattern of Antenna Design 'd' at (a) 6.6 GHz, (b) 7.3 GHz

4 Conclusion

In this work, a multiband chebyshev microstrip antenna has been designed, fabricated and measured. It is discovered that the width of patch effects antenna performance, as by changing patch width increases the bandwidth and movement of feed line along with chebyshev can be used to control frequency shifts. The offered antenna operating at 1.8, 2.7, 3.4, 4.9 and 5.8 GHz is applicable majorly for GSM, Wi-Fi, and WiMAX.

References

1. Balanis, C.A.: *Antenna Theory, Analysis and Design*. John Wiley & Sons (2007)
2. Chen, H.D., Chen, J.S., Cheng, Y.T.: Modified Inverted-L Monopole Antenna for 2.4/5GHz Dual-band Operations. *Electronics Letters* 39, 1567–1568 (2003)
3. Su, C.M., Chen, H.-T., Wong, K.L.: Printed Dual-band Dipole Antenna with U-slotted Arms for 2.4/5.2 GHz WLAN Operation. *Electronics Letters* 38, 1308–1309 (2002)
4. Kuo, Y.L., Wong, K.L.: Printed Double-T Monopole Antenna for 2.4/5.2 GHz Dual-band WLAN Operations. *IEEE Transactions on Antennas and Propagation* 51(9), 2187–2192 (2003)
5. Lin, S.Y.: Multiband Folded Planar Monopole Antenna for Mobile Handset. *IEEE Transactions on Antennas and Propagation* 52(7), 1790–1794 (2004)
6. Go, H.C., Jang, Y.W.: Multi-band Modified Fork-shaped Microstrip Monopole Antenna with Ground Plane including Dual Triangle Portion. *Electronics Letters* 40, 575–577 (2004)
7. Constantine, J., Kabalan, K.Y., El Hajj, A., Christodoulou, C.G.: New Multiband Design for a Microstrip Patch Antenna. In: *The Second European Conference on Antennas and Propagation (EuCAP)*, pp. 1–4 (2007)
8. Constantine, J., Kabalan, K.Y., El Hajj, A., Rammal, M.: New Multi-Band Microstrip Antenna Design for Wireless Communications. *IEEE Antennas and Propagation Magazine* 49(6), 181–186 (2007)
9. Sen, A., Roy, J.S., Bhadra Chaudhuri, S.R.: Investigations on a Dual-Frequency Microstrip Antenna for Wireless Applications. In: *IEEE International Workshop on Antenna Technology (iWAT)*, pp. 1–4 (2009)
10. Tlili, B.: Design of C-Slot Microstrip Patch Antenna for WiMAX Application. In: *Antennas & Propagation Conference*, pp. 521–524 (2009)
11. Garg, R., Bhartia, P., Bahl, I., Ittipiboon, A.: *Microstrip Antenna Design Handbook*. Artech House (2001)
12. Safaai-Jazi, A.: A New Formulation for the Design of Chebyshev Arrays. *IEEE Transactions on Antennas and Propagation* 42(3), 439–443 (1994)
13. Safaai-Jazi, A.: A New Method for the Analysis and Design of Chebyshev Arrays. In: *Proceedings of the 26th Southeastern Symposium System Theory*, pp. 157–161 (1994)

A Compact Multiband Antenna for GSM and WiMAX Applications

M. Ali Babar Abbasi, M. Rizwan, Saleem Shahid, Sabaina Rafique,
Haroon Tariq Awan, and Syed Muzahir Abbas

Department of Electrical Engineering, COMSATS Institute of Information Technology,
Islamabad, Pakistan

{m.babarabbasi, haroontariq.awan}@gmail.com,
enr.mrizwan@yahoo.com, saleemshahid@live.com,
sabaina.rafiq@hotmai.com, muzahir_abbas@comsats.edu.pk

Abstract. This paper presents a compact low profile microstrip patch antenna suitable for Global System for Mobile Communications (GSM) and Worldwide Interoperability for Microwave Access (WiMAX) applications. FR4 epoxy is used as substrate with relative permittivity 4.4 and tangent loss 0.02. The prototype contains slots, shorted pin, partial ground, tuning stub and dual feeding techniques. Parametric analysis has been carried out to observe the effects of techniques. Simulation results show that antenna has enough impedance bandwidth to cover the desired frequency bands. The prototype is fed using transmission line. Antenna exhibits omni-directional radiation patterns with reasonable gain on all operating frequency bands. Characteristic analysis and simulation of prototype was done using Ansoft HFSS (High Frequency Structure Simulator).

Keywords: Microstrip Patch Antenna, WiMAX, GSM, Partial Ground, Stub, Radiation Pattern.

1 Introduction

In 21st century, wireless technologies require compact and low profile components for communication systems. The characteristic parameters of antenna mainly depend upon the size of radiating element which is approximately one-half of a free-space wavelength. This implies a tradeoff between the size of antenna and operating frequency. Microstrip patch antennas are narrow band which applies limitation on the impedance bandwidth. Research has been done to reduce the tradeoffs and limitations by proposing different improvement techniques. Research shows implementation of few techniques like partial grounding [1], shorting pin [1-2], cutting slots and slits in radiating patch and ground plane [1][3-5], and tuning stubs [1][6-7].

The paper presents a multiband antenna which covers bands of GSM 1800MHz and WiMAX bands at 3.5GHz (3.4 – 3.6GHz), 3.6 – 3.8GHz and 5.8GHz (5.725 – 5.850GHz) with return loss $S_{11} \leq 10\text{dB}$ [8]. The antenna also operates for PCS 190 (1850-1990MHz) [9-10], LTE Band 42 (3.4-3.6GHz), 43 (3.6-3.8GHz) [10] and WLAN 5.8 (5725-5825GHz) [8] with stable, sufficient gain and omni-directional

radiation patterns [11]. Section-2 explains the antenna configuration. Modeling and simulation has been discussed in section-3. Simulation results and analysis has been presented in section-4, section-5 presents the comparison between measured and simulated results while section-6 concludes the paper.

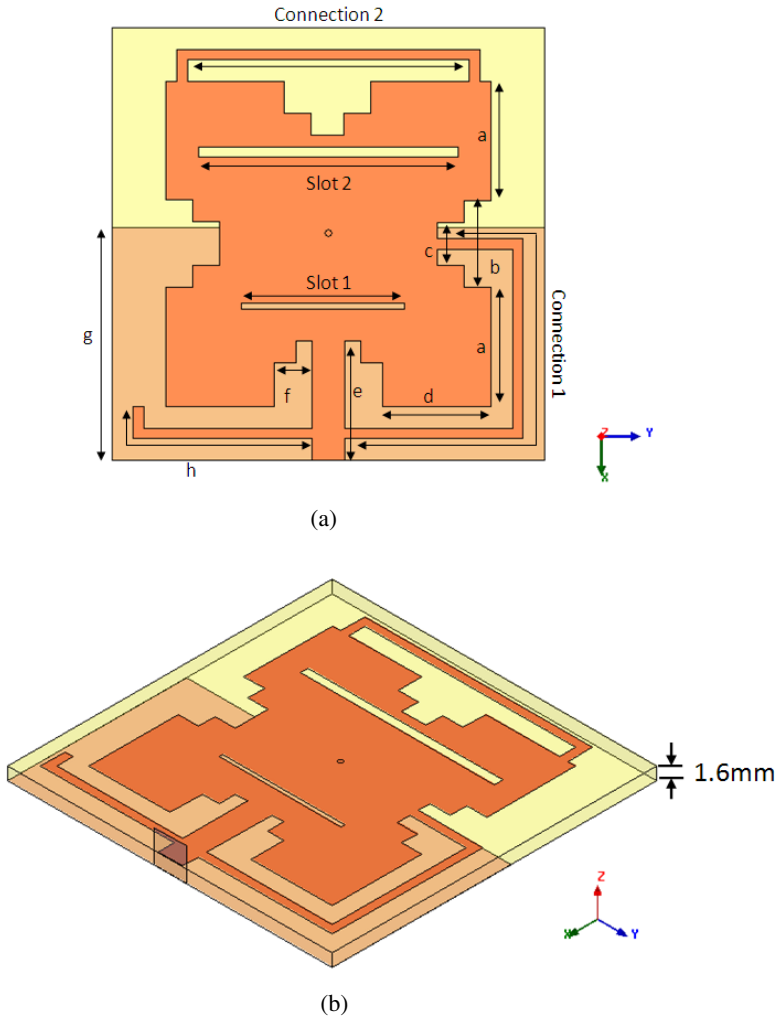


Fig. 1. Geometry of proposed antenna (a) Front view (b) Side view

2 Antenna Configuration

The geometry of proposed antenna is shown in Fig. 1. Patch has been printed on FR4 epoxy substrate with dimensions 38mm x 38mm, having relative permittivity 4.4 and thickness 1.6mm, is fed using transmission line having impedance of 50 Ω and 2.85mm width. Dimensions are tabulated in Table 1.

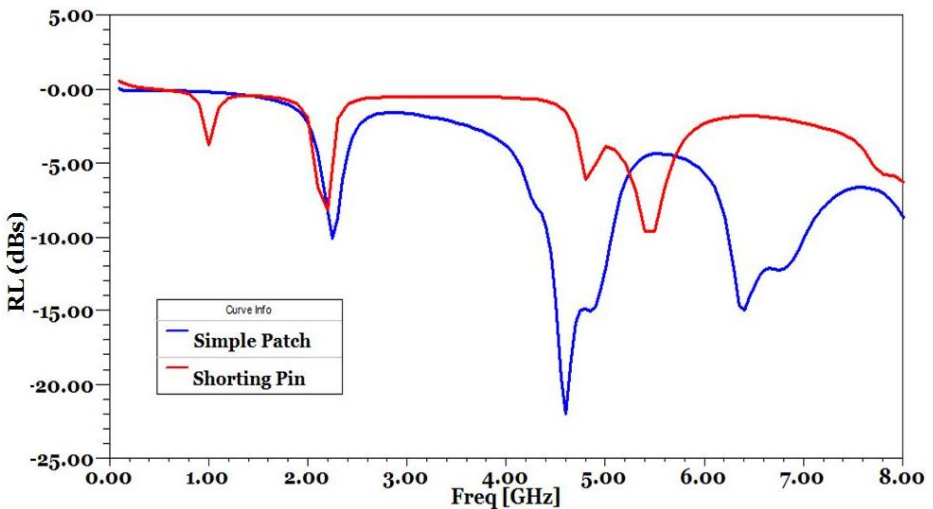
Table 1. Dimensions Of Proposed Antenna Design

Parameter	Dimension (mm)	Parameters	Dimension (mm)
a	10.4	g	21
b	7.7	h (Stub)	18.525
c	3.85	Slot1	14.25
d	9.5	Slot 2	22.8
e	10.5	Connection 1	40.75
f	3.325	Connection 2	32.3

3 Modeling and Simulation

The objective was to design a compact multiband antenna for GSM and WiMAX applications and to implement the characteristic improvement techniques in a single antenna to improve its results as well as to observe the effects of specific techniques. The first step was to design a microstrip patch antenna with rectangular configuration. Stair slots were added along the non-radiating edges to convert them to radiating edges [4]. A stair slot was also added to the upper radiating edge of antenna to disturb the path of current and to shift the resonating frequency to lower bands.

For further size reduction, a shortening pin was added to the center of patch. The shortening pin technique [2] shifted the resonant frequency to lower bands, thus for a fixed radiating element size, the antenna operates at a lower frequency, independent of the limit that size of radiating element should be approximately equal to one-half of free-space wavelength. The return loss of antenna before and after shortening pin is shown in Fig. 2.

**Fig. 2.** Simulated return loss before and after pin shortening

Size reduction at a specific central frequency decreased the impedance bandwidth. Using partial ground, impedance bandwidth was increased [1]. The parameter 'g' (ground) has been varied at different values of 'g' (i.e. $g=19\text{mm}$, 21mm and 25mm). The coupling between ground and radiating element is controlling the GSM frequency band, as the coupling increases return loss also increases. The return loss corresponding to different values of 'g' is shown in fig. 3.

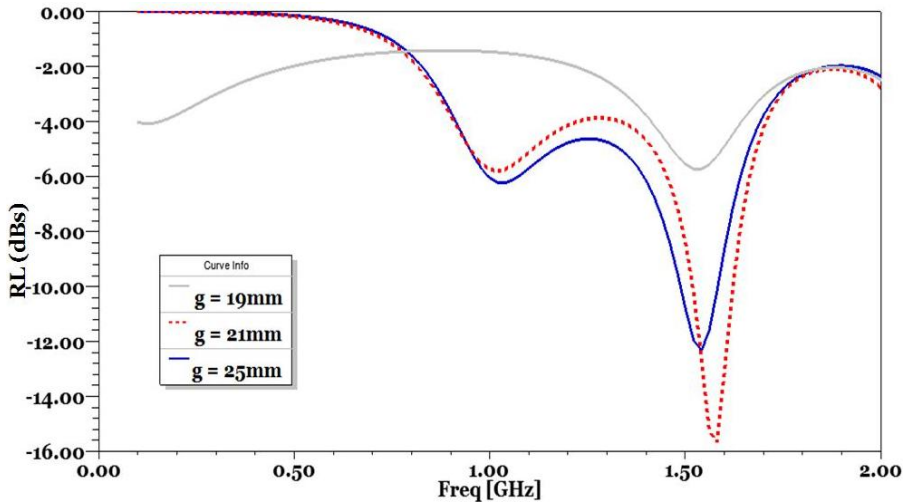


Fig. 3. Simulated return loss at various values of 'g' while other parameters were unchanged

Slots were added to disturb the path of current [1] [3-4]. The slots controlled the return loss and shifted the resonating frequency towards the desired GSM band (1.8GHz). The positions of slots were adjusted according to the current distribution on the patch of antenna. Fig. 4 shows the return loss comparison before and after the addition of slots.

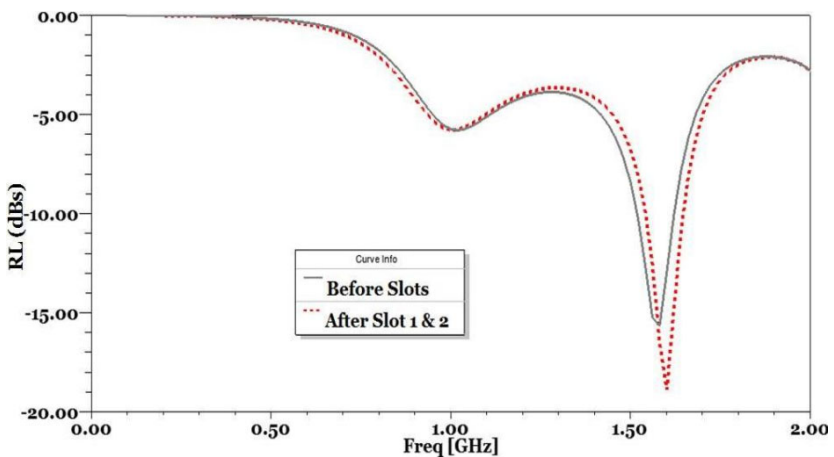


Fig. 4. Simulated return loss before and after addition of slots

Connection 1 was established between the transmission line and right side, close to the center of the patch. This results in improved return loss at the GSM band without modifying the geometry of patch. Dual feeding was achieved using this connection. Keep in mind that the connection has provided the current another path to enter the radiating area. Fig. 5 shows the improvement in return loss by establishing the above mentioned connection.

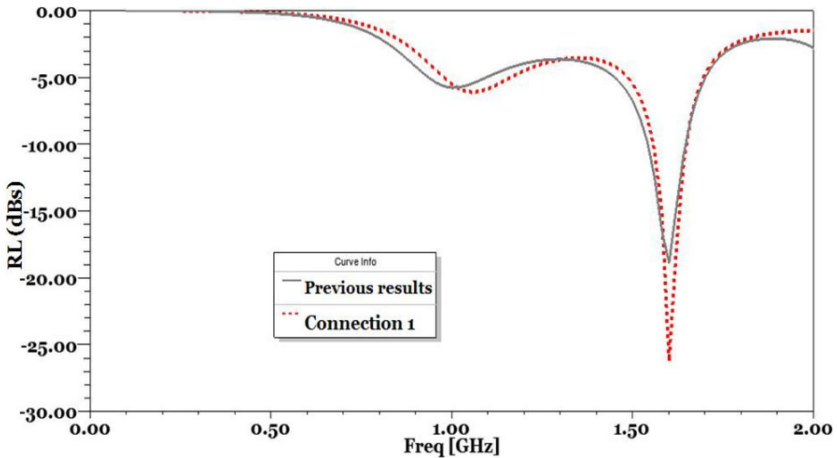


Fig. 5. Simulated return loss before and after establishing connection 1

Adding stub on left side of transmission line with tunable length ($h=18.525\text{mm}$) improved the return loss at the higher frequencies. Stub behaved as monopole resonator producing coupling effect with lower left side of patch. The coupling between stub and patch introduced two new bands at higher frequencies i.e. 5.3-5.7GHz and 7.1-7.8GHz.

Without disturbing the structure of radiating patch, an improvement in return loss for higher frequency band of WiMAX was achieved by shortening the farthest radiating edge of patch, thus a symmetric current path was available for lower frequencies which will not disturb the behavior of radiation at lower frequencies. However, at higher frequencies, it has virtually divided the patch into two parts. First part includes transmission line, connection 1 and area around slot 1 (i.e. lower portion of the patch). Second part includes connection 2 and area around slot 2 (i.e. upper portion of the patch). Fig. 6 shows the return loss after the addition of stub and connection 2.

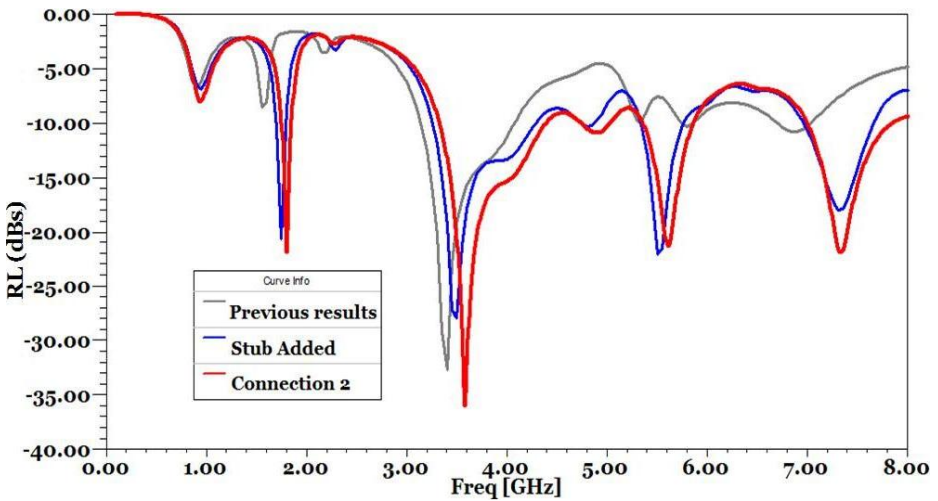


Fig. 6. Simulated return loss before and after adding stub and connection 2

4 Simulation Results and Analysis

4.1 Return Loss

Fig. 7 shows the simulated return loss of the proposed antenna at various frequency bands.

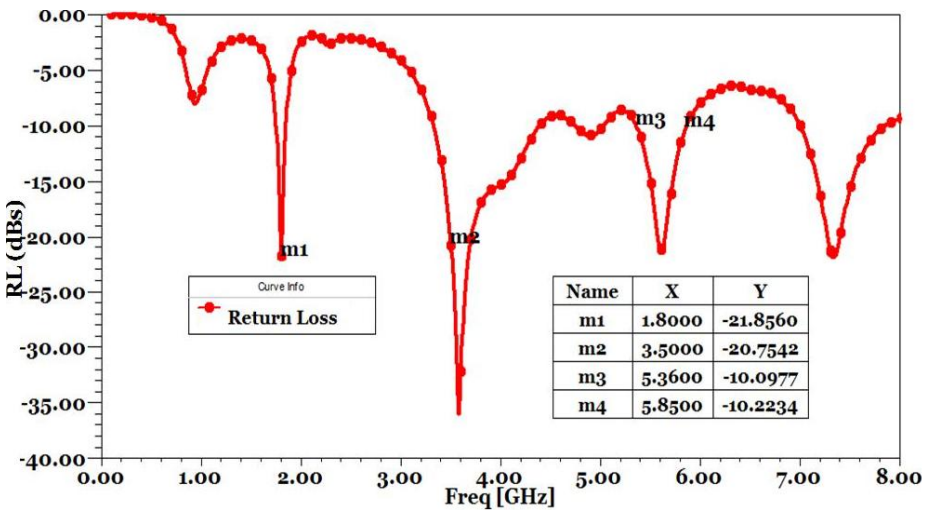
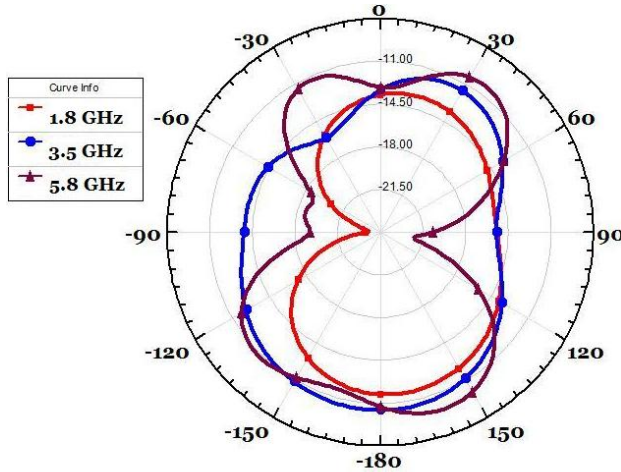


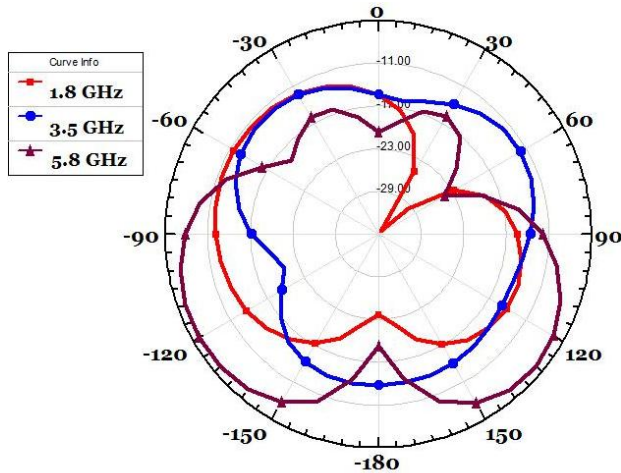
Fig. 7. Simulated return loss of the proposed antenna

4.2 Radiation Pattern

Fig. 8 presents the simulated E-field and H-Field radiation patterns of the proposed antenna at various frequencies. Omni-directional patterns are clearly seen in radiation patterns at 1.8GHz, 3.5GHz and 5.8GHz. As the frequency increases the gain also increases but radiation pattern gets distorted and antenna behavior changes from omni-directional to directional radiation pattern. The pattern is distorted due to radiation of partial ground and mismatch of impedance.



(a)

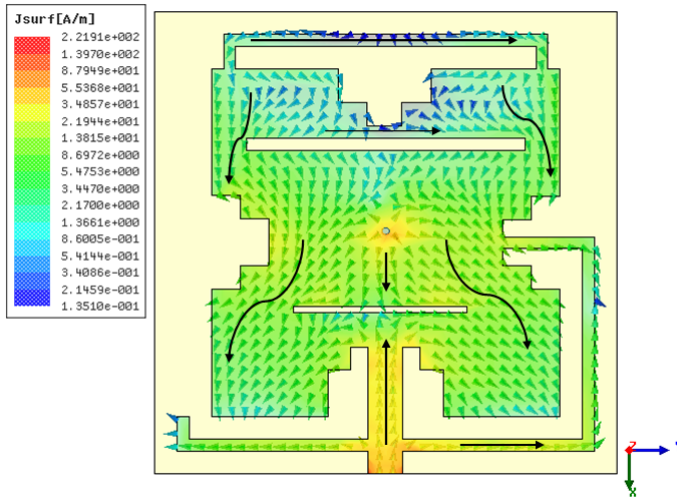


(b)

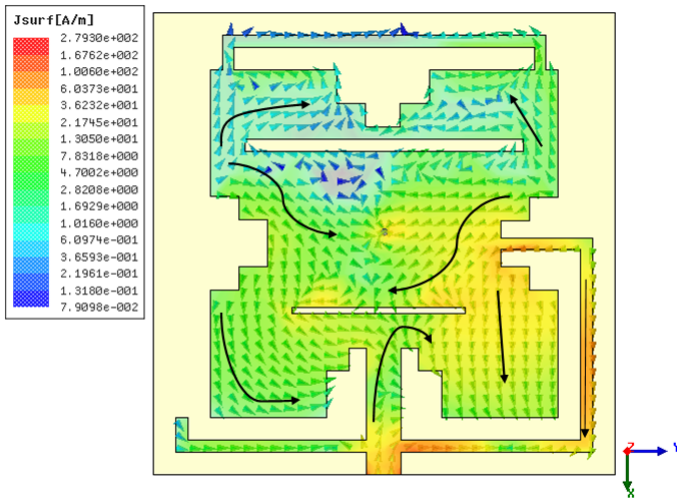
Fig. 8. Radiation pattern of the proposed antenna at 1.8GHz, 3.5GHz and 5.8GHz (a) E-field (b) H-field

4.3 Current Distribution

Fig. 9 shows the current distribution of antenna at 1.8GHz, 3.5GHz and 5.8GHz.

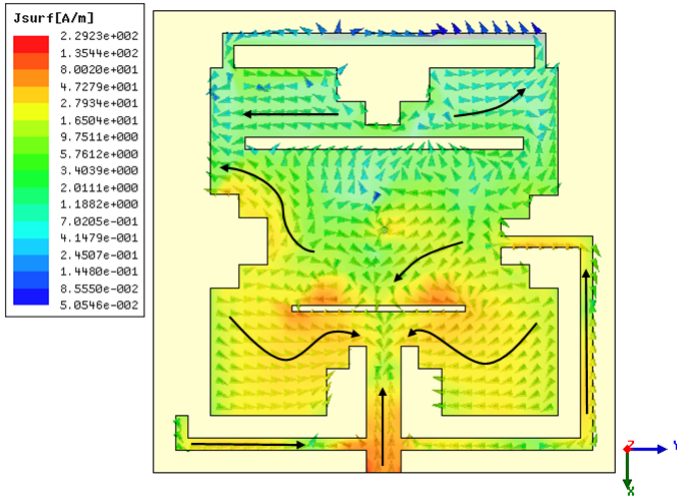


(a)



(b)

Fig. 9. Current distribution at (a) 1.8GHz (b) 3.5GHz (c) 5.8GHz

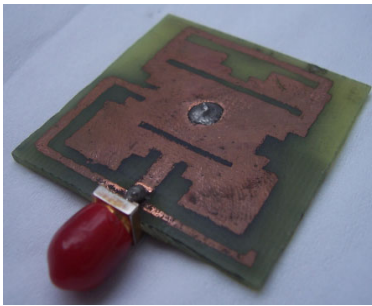


(c)

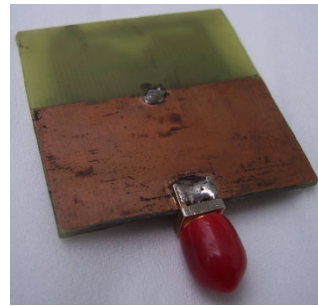
Fig. 9. (continued)

5 Measured Results and Comparison

Fig. 10 shows the fabricated antenna. The antenna is fabricated on FR4 epoxy substrate with the proposed dimensions.



(a)



(b)

Fig. 10. Fabricated antenna (a) Front view (b) Ground view

Fig. 11 shows the measured return loss of proposed antenna. The results are measured using Agilent Network Analyzer.

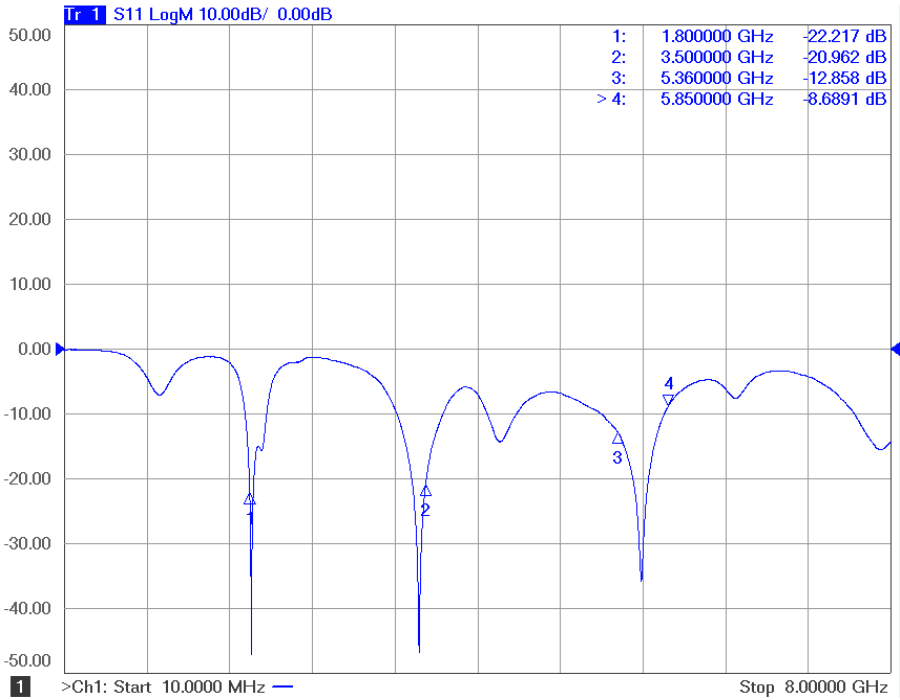


Fig. 11. Measured return loss using Network Analyzer

Fig. 12 shows the comparison between measured and simulated return loss of proposed antenna.

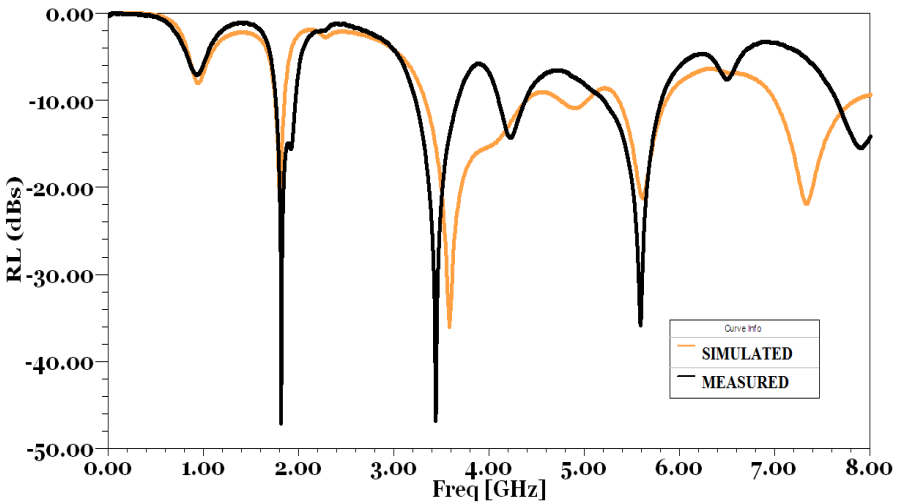


Fig. 12. Simulated and measured return loss comparison

6 Conclusion

A multiband tunable antenna with impedance bandwidth to cover applications of GSM 1.8GHz and WiMAX bands 3.5GHz (3.4–3.6GHz), 3.6–3.8GHz and 5.8GHz (5.725–5.850GHz) has been presented. Antenna is also tunable at PCS 1900 (1850–1990MHz), LTE Band 42 (3.4–3.6GHz), 43 (3.6–3.8GHz) and WLAN 5.8 (5725–5825GHz) The antenna is designed using rectangular microstrip configuration with optimization techniques implemented on it to achieve the best possible desired results. The bandwidth of proposed antenna for GSM 1.8GHz is 90MHz (1750–1840MHz), WiMAX 3.5GHz is 1060MHz (3330–4390MHz) and 5.8GHz is 125MHz (5725–5850MHz). The bandwidth of antenna is enough to tune antenna to operate for GSM and WiMAX applications.

References

1. Wong, K.-L.: *Compact and Broadband Microstrip Antenna*. John Wiley & Sons, Inc. (2002)
2. Pan, S.-C., Wong, K.-L.: Dual-frequency triangular microstrip antenna with a shorting pin. *IEEE Transactions on Antennas and Propagation*, 1889–1891 (December 1997)
3. Kamtongdee, C., Wongkasem, N.: A novel design of compact 2.4 GHz microstrip antennas. In: 6th International Conference on Electrical Engineering/Electronics, Computer, Telecommunications and Information Technology (ECTI-CON), Bangkok/Pathumthani, Thailand, May 6-9, vol. 2, pp. 766–769 (2009)
4. Gupta, N., Gupta, V.R.: Reduced Size, dual frequency band antenna for wireless communication. In: *IEEE International Conference on Personal Wireless Communications (ICPWC)*, New Delhi, India, January 23-25, pp. 321–323 (2005)
5. Ghosh, B., Haque, S.M., Mitra, D.: Miniaturization of Slot Antennas Using Slit and Strip Loading. *IEEE Transactions on Antennas and Propagation* 59, 3922–3927 (2011)
6. William, J., Nakkeeran, R.: CPW-Fed UWB slot antenna with cross like tuning stub. In: *International Conference on Computing Communication and Networking Technologies (ICCCNT)*, Karur, India, July 29-31, pp. 1–6 (2010)
7. Archevapanich, T.: Design of CPW Wide Slot Antenna with Tuning Stub for Wideband Applications. In: *International Conference on Control Automation and Systems (ICCAS)*, Gyeonggi-do, Korea, October 27-30, pp. 2198–2201 (2010)
8. Parkash, D., Khanna, R.: Design of a dual band monopole antenna for WLAN/WiMAX applications. In: *Seventh International Conference on Wireless And Optical Communications Networks (WOCN)*, Colombo, Sri Lanka, September 6-8, pp. 1–4 (2010)
9. Nikmehr, S., Moradi, K.: Design and simulation of triple band GSM900/DCS1800/UMTS2100 MHz microstrip antenna for base station. In: *IEEE International Conference on Communication Systems (ICCS)*, Singapore, November 17-19, pp. 113–116 (2010)
10. Hu, C.-L., Huang, D.-L., Kuo, H.-L., Yang, C.-F., Liao, C.-L., Lin, S.-T.: Compact Multi-branch Inverted-F Antenna to be Embedded in a Laptop Computer for LTE/WWAN/IMT-E Applications. *IEEE Antennas and Wireless Propagation Letters* 9, 838–841 (2010)
11. Balanis, C.A.: *Antenna Theory: Analysis and Design*, 3rd edn. John Wiley & Sons, Inc. (2005)

Haplotype Segment Algorithm for Predicting Disease Gene Locus Based on Distance/Similarity Measures

Adeel Ahmed^{1,*} and Khalid Saleem²

¹ Department of Computer Science, Quaid-i-Azam University, Islamabad, Pakistan
aahmedqau@gmail.com

² Department of Computer Science, Quaid-i-Azam University, Islamabad, Pakistan
ksaleem@qau.edu.pk

Abstract. In this paper, we address the problem of locating a disease gene using a new Haplotype Segment Algorithm based on distance/similarity measures. We developed a novel approach to identify the set of associated marker alleles in the form of haplotype segments. We measure the distance of haplotype segments in cases and controls. We find the two haplotype segments in cases which have least distance than controls and observe that the disease location lies between these two haplotype segments. Haplotype Segment Algorithm performs the similarity analysis of haplotypes and finds the location of a disease gene using various distance/similarity measures. Haplotype Segment Algorithm uses the similarity or distance measures so this algorithm has the capability to reduce or delete the noise from the segments and finds a precise location of disease gene. The new algorithm detects the disease gene even if there exists 5% mutant chromosomes in the human genome. We applied new algorithm on simulated datasets and find the location of disease gene very close to the true simulated location. We also assessed the performance of Haplotype Segment Algorithm on a real dataset called Friedreich Ataxia's dataset in detecting a disease gene location and find the consistent results.

Keywords: Gene mapping, Pattern recognition, Biology and genetics, Distance, Similarity.

1 Introduction

Disease gene mapping has been a primary focus in genetic epidemiology in the last two decades [1]. Disease gene mapping is a process of locating an inherited mutation that participates in increasing the risk of diseases. Many statistical methods have been developed to map a disease gene and have identified various gene locations of inherited diseases by using molecular markers. For a case-control study, genome scanning using microsatellite markers gives effective result in haplotype association studies [1].

The common way of detecting a disease gene location is to compare the frequency of marker based on haplotype patterns between case and control chromosomes. A key

* Corresponding author.

assumption that we follow for disease gene mapping is that the haplotypes in affected individuals are more similar near the disease susceptibility gene than control individuals [1].

There are large numbers of distance/similarity measures found in different fields such as Information Retrievals, Statistics, Computer Science, Mathematics, Biology etc. These measures are used to identify some goal. It is necessary to point out the most appropriate measures, which are helpful in achieving the better results.

We address the problem of locating a disease gene using a new Haplotype Segment Algorithm (HSA) based on distance/similarity measures. We have developed a novel approach to identify the set of associated marker alleles in the form of haplotype segments. We divide whole markers present in the dataset into set of 4-length segments and find the two haplotype segments in cases which have least distance than control haplotype segments. We observe that these two segments having least distance lies near the disease gene. We find that the new algorithm give results similar to true simulated locations generated by Toivonen et al in 2000 [2].

The organization of this paper is as follows: Section 2 describes the related work, Section 3 describes the proposed approach for predicting disease gene location. In Section 4, we discuss experimental setup and results. Section 5 presents conclusions and future work.

2 Related Work

Methods related to identification of disease genes are divided into two major categories: Direct method and indirect method. We have discussed here only indirect methods as these methods are within the scope of our work.

Toivonen et al. [3] proposed a Haplotype Pattern Mining (HPM) approach for disease gene mapping. It uses a chi-square test to differentiate between highly associated patterns of control and diseased chromosomes. HPM has high localization power but has less computational power on a wide genome [4]. HPM has a limitation that it has adapted the association rule-mining algorithm that is used to find the highly associated patterns and such patterns are relatively rare in the problem of linkage disequilibrium mapping [1]. Another limitation is that it uses a don't care symbol '*' in the haplotype patterns so many haplotypes have been counted multiple times [1].

In 2005, Lin et al. [5] proposed a new algorithm called LinkageTracker to overcome the shortcomings of HPM [3]. The LinkageTracker does not need any population ancestry information for detecting a disease gene locus and allows a mutation to occur as low as 10% of the sample sequences. Linkage Tracker uses the odds ratio to discriminate the highly disease associated patterns with control associated patterns. This approach uses the p-value and frequency of marker to infer a marker closest to the disease gene location.

In [6], Rannala and Reeve have developed DMLE+ program for locating a disease gene and mutation age estimation based on Bayesian linkage disequilibrium mapping using multiple genetic markers. DMLE+ uses a Markov Chain Monte Carlo (MCMC) method and a coalescent model to incorporate Bayesian estimation of the posterior probability density of the position of a mutation. It requires some prior information like population growth rate, size of population but this parametric information may not be readily available. Here, it is also assumed that the mutations should be available in sample sequences in large amount.

Liu et al. [7, 8] proposed a BLADE algorithm that also uses Markov Chain Monte Carlo method with in a Bayesian framework to detect a disease locus. BLADE forms the clusters of disease haplotypes and assumes that all mutations occur in the same location of disease gene.

In [9] Poisson branching process has been used to estimate the maximum likelihood for recombination fraction between marker and disease loci. This method performs well when population ancestry information is well understood. But it has a drawback that it is difficult to estimate the likelihood when data belongs to a large number of ancestries. This method is applied on Diastrophic Dysplasia and Cystic Fibrosis disease and has found appropriate results.

According to Mailund et al. [10], a fine scale-mapping tool called GeneRecon is used to infer the posterior distribution of disease locus by using the Metropolis-Hastings sampling. GeneRecon overcomes the shortcomings of DMLE+ method [6]. The main drawback of this algorithm is that its performance degrades when a dataset contains large number of markers and chromosomes.

HapMiner [1] is introduced by Li and Jiang in 2005. HapMiner is an extended version of DBSCAN algorithm [11]. HapMiner calculates the distance of haplotypes and then makes a distance matrix. On the distance matrix, DBSCAN is applied and then the clusters are identified. A marker with highest score is selected as a disease gene location. The main advantage of HapMiner is that it does not require any prior information. A limitation is that it is very sensitive to parameter values. HapMiner is found to be better in performance in comparison to HPM [3] and BLADE [7, 8] methods.

According to [12], TreeDT is a gene mapping method to discover the tree like patterns in genetic marker data. These patterns reflect the genetic history of disease susceptibility gene. This approach gives robustness with respect to missing data and gives better results in gene localization as compared to other methods such as HPM. Computing cost of TreeDT is smaller than HPM. A limitation of TreeDT is that it performs only with small number of chromosomes and marker data.

In 2009, Besenbacher et al. [4] proposed a new method that overcomes the computing limitation of HPM method. They have suggested an efficient algorithm with high statistical power to detect the association of alleles. From experimental studies, they have concluded that the new algorithm performs better than the original HPM algorithm with huge number of chromosomes and markers.

In 2011, Ahmed et al. [13] proposed a heuristic approach that overcomes the limitations of Haplotype Pattern Mining [3] and LinkageTracker [5]. They found associations (linkage) among marker alleles in isolated population of human beings for detecting a disease gene. For association-based gene mapping, a data mining approach called pattern mining is used to map the linkage disequilibrium phenomena occurring in specific genes and locate the position of mutant gene. They have performed their experimental study in simulated and real datasets and concluded that the new approach is appropriate for detecting a disease gene.

3 Proposed Approach for Predicting a Disease Gene Location

Based on the assumption that haplotypes from cases are expected to be more similar than haplotypes from controls in regions near the disease genes [1] we have considered a haplotype segment of length-4 and compare each haplotype segment with

another haplotype segment to measure the distance between them. Since, microsatellite markers are placed at 1 cM in datasets generated by Toivonen et al. [2] and beyond the 20 cM the associations of marker alleles get weaker [14], so due to this reason we have considered a short length of haplotype segment.

3.1 Haplotype Segment Algorithm

Algorithm: Find a location of disease gene.

Input: hapSegLength, noMarkers, noChromosomes, noHapSegments.

Output: Report two haplotype segments which have minimum average distance.

Method:

1. Find the haplotype segments of hapSegLength from genome and store it into vector H with labels 'C' and 'A'.
2. for each HaplotypeSegment to noHapSegments do
3. Set $i \leftarrow 1$.
4. for each $j = 2$ to noChromosomes do
5. Compute a distance between H[i] and H[j] by calling a specific distance measure.
6. Report the distance between H[i] and H[j].
7. $i \leftarrow i+1$.
8. $j \leftarrow j+1$.
9. end for
10. end for
11. Find average of the distance of all haplotype segments of both cases and controls.
12. Find two case haplotype segments which have a minimum average distance as compared to control haplotype segments. A disease gene locus lies between these two case haplotype segments which consist of a number of marker alleles. Therefore, we can say that a region in between these two case haplotype segments is considered as an affected region.

3.2 Haplotype Segment

A haplotype segment consists of four marker alleles. Since, a dataset consists of 100 markers, so we divided the whole 100 markers into 25 haplotype segments and each chromosome contains 25 segments as shown in Figure 1. Haplotype segments present in chromosome 1 are compared with the subsequent haplotype segments present in chromosome 2 and a distance is computed using similarity/distance measure between them. Similarly, haplotype segments of chromosome 2 are compared with haplotype segments of chromosome 3 and a distance between them is calculated. The process of computing distance among segments is carried out until the last chromosome is examined. For our convenience, we have used labels 'a' and 'c' to distinguish between case and control haplotype segments, respectively.

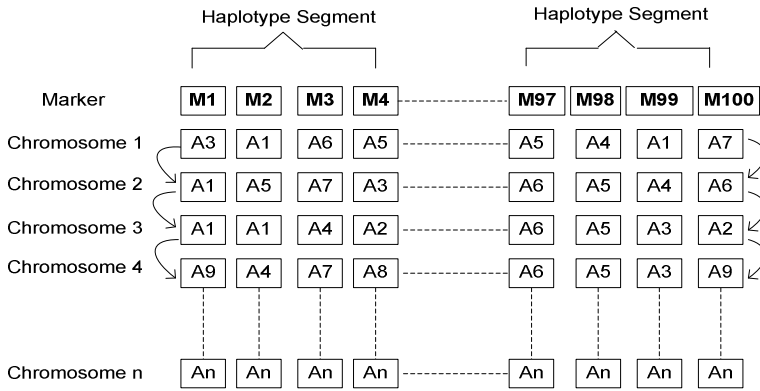


Fig. 1. Haplotype Segments

3.3 A Gap

A gap consists of a “*” symbol from one marker allele to another marker allele, for example a segment (1,*,*,8) has two gaps. The gap is bounded by alleles rather than don’t care symbols. For example, consider a pattern, P(1,*,*,*,6), now here a gap consists of three don’t care symbols but is bounded by allele 1 and 6. The symbol “*” represents a missing allele, errors or mutations in a marker. So in computing the similarity between two 4-length segments, the symbol “*” will not be considered but this gap (noise or variation) is decreased or deleted by similarity/distance measures automatically. Thus, HSA is sensitive to gaps.

3.4 Detection of Disease Location

Each haplotype segment consists of four marker alleles. Since, we have 200 chromosomes for each case chromosomes and control chromosomes, therefore, 200 comparisons take place among the haplotypes in getting the average distance of one haplotype segment. We have computed the average of the distance of each haplotype segment by adding the distance values of each combination of haplotype segments in cases and controls. Table 1 shows the arbitrary values of distance between haplotype segments and the average distance of haplotype segment. Similarly, we have found average distance of 25 haplotype segments of cases and controls.

Table 1. Average of case and control haplotype segments using Euclidean distance

Combination of Haplotype Segment	Distance of CASE Haplotype Segment 1	Distance of CONTROL Haplotype Segment 1
H1, H2	2.45	3.32
H2, H3	2.45	4.36
H3, H4	2.24	5.1
H4, H5	4.36	3.61
H5, H6	3.46	4.36
H6, H7	6.32	5.1
H7, H8	3.32	5.74
H8, H9	4.58	3.16
H9, H10	3	3.74
.	.	.
.	.	.
H399, H400	0	6.16
Average Distance	3.22	4.46

3.5 Distance/Similarity Measures

The measures, which we have used in Haplotype Segment Algorithm to compute a distance between haplotypes, are studied by [15]. These algorithms are Euclidean, Pearson, Neyman, Divergence, Harmonic mean (HM), Cosine, Jaccard, Dice, Canberra, Motyka and Dynamic Time Warping (DTW) algorithm [16]. Among these measures two measures Dice and Motyka are similarity measures and others are distance measures. For similarity, we have taken the haplotype segments, which have large values and for distance measures we have taken haplotype segments which have small distance values.

4 Evaluation

4.1 Comparison of Performance on Simulated Datasets

For our experiments, we have selected three datasets which are generated by Toivonen et al in 2000 [2]. These are simulated datasets which contains the characteristics of realistic isolated founder population that grow from 300 to about 100,000 individuals over a period of 500 years. Each dataset consists of case-control chromosomes and has a set of alleles originated from same parents, 101 microsatellite markers and has different disease location but we have considered 100 markers in each dataset for our experiments. Among these datasets, dataset 1 has 5% mutation, dataset 2 has 7.5% mutation and dataset 3 has 10% mutant chromosomes. A brief description of datasets is given in Table 2.

Table 2. Brief description of datasets

Dataset	%Mutation	Total number of		
		chromosomes	Control	Case
1	5	400	200	200
2	7.5	400	200	200
3	10	400	200	200

Experimental Setting: Detection of Accuracies in Disease Gene Location. In this experiment, we have assessed the capability of our algorithm when a sample carrying a small portion of mutation. Therefore, the three datasets with different percentage of mutation carrying disease haplotypes are considered.

We have compared the locations of disease gene which are obtained by using Haplotype Segment Algorithm with true simulated locations as constructed by Toivonen et al. in 2000 [2]. We have found that the new algorithm has detected the disease gene locations close to the true locations as constructed by Toivonen et al. [2] when there exists below 5% mutation in the sample. The observed locations and the true locations are given in the form of markers as shown in Table 3. We have considered a 4-length segment in our algorithm in finding a location of disease gene. We have observed that proposed Haplotype Segment Algorithm has given reliable results about

Table 3. Comparison between observed and true locations on disease gene

Measure	Disease region by HSA using dataset 1 with 5% mutation	Disease region by HSA using dataset 2 with 7.5% mutation	Disease region by HSA using dataset 3 with 10% mutation
Pearson	M37 to M52	M53 to M72	M33 to M60
Euclidean	M57 to M60	M29 to M72	M65 to M68
Harmonic Mean	M69 to M84	M21 to M56	M25 to M32
Cosine	M13 to M64	M47 to M72	M77 to M88
Jaccard	M9 to M68	M21 to M56	M25 to M48
Canberra	M37 to M52	M53 to M72	M53 to M60
Neyman	M37 to M72	M53 to M72	M33 to M60
Divergence	M37 to M52	M53 to M72	M53 to M60
Dice	M33 to M44	M5 to M20	M33 to M68
Motyka	M37 to M52	M53 to M72	M53 to M60
DTW	M49 to M56	M45 to M80	M25 to M48
True Location [2]	M47 to M56	M63 to M72	M54 to M62

disease gene location with 4-length segment as compared to 2-length or 3-length segments. We have noted that the haplotype segments with length two or three have given same distance at multiple times which are not helpful in finding the location of disease. We have also noted that the minimum segment of length four or more is quite feasible for the detection of disease gene using distance/similarity measures. We have applied each measure in three datasets for examining that whether each measure produces reliable results or not. A measure is reliable for disease gene detection if the measure found similar haplotypes near the disease locus as detected by Toivonen et al. [2] in more than one dataset.

Performance of Haplotype Segment Algorithm in terms of Precision and Recall on Simulated Datasets. We have evaluated the performance of Haplotype Segment Algorithm in terms of overall precision vs recall. These two metrics provide us a way to evaluate the correctness of Haplotype Segment Algorithm.

Precision is defined as the number of disease-relevant markers retrieved by a heuristic search divided by the total number of markers retrieved by that search.

$$\text{Precision} = \frac{\text{Disease relevant markers retrieved}}{\text{Total number of markers retrieved}}$$

Recall is defined as the number of disease-relevant markers retrieved by a heuristic search divided by the total number of disease-relevant markers.

$$\text{Recall} = \frac{\text{Disease relevant markers retrieved}}{\text{Total number of disease relevant markers}}$$

We have assessed the performance of Haplotype Segment Algorithm on three simulated datasets generated by Toivonen et al [2] in terms of precision and recall. We have evaluated the correctness of Haplotype Segment Algorithm by comparing the precision and recall values for disease locations obtained by using proposed algorithm and by using true simulation generated locations constructed by Toivonen et al [2] related to each dataset.

The Haplotype Segment algorithm is evaluated using a dataset 1 with total number of markers retrieved that is 100 and the number of markers involved in disease susceptibility gene are 16, 4, 16, 52, 60, 16, 36, 16, 12, 16 and 8 which are predicted by using Pearson measure, Euclidean, Harmonic mean, Cosine, Jaccard, Canberra, Neyman, Divergence, Dice, Motyka and Dynamic Time Warping algorithm, respectively. The true location constructed by Toivonen et al [2] using dataset1 with total number of markers retrieved that is 101 and there are 10 markers which are disease relevant. Performance comparison on observed and true disease locations using dataset 1 is shown in Table 4.

The Haplotype Segment algorithm is then evaluated using a dataset 2 with total number of markers retrieved that is 100 and the number of markers involved in disease susceptibility gene are 20, 44, 36, 26, 36, 20, 20, 20, 16, 20 and 36 which are predicted by using Pearson measure, Euclidean, Harmonic mean, Cosine, Jaccard,

Canberra, Neyman, Divergence, Dice, Motyka and Dynamic Time Warping algorithm, respectively. The true location constructed by Toivonen et al [2] using dataset 2 with total number of markers retrieved that is 101 and there are 10 markers which are disease relevant. Performance comparison on observed and true disease locations using dataset 2 is shown in Table 4.

In evaluating dataset 3, total number of markers retrieved that is 100 and the number of markers involved in disease susceptibility gene are 28, 4, 8, 12, 24, 8, 28, 8, 36, 8 and 23 which are predicted by using Pearson measure, Euclidean, Harmonic mean, Cosine, Jaccard, Canberra, Neyman, Divergence, Dice, Motyka and Dynamic Time Warping algorithm, respectively. The true location consists of 9 markers which are disease relevant. Performance comparison on observed and true disease locations using dataset 3 is shown in Table 4.

4.2 Comparison of Performance on a Real Dataset

We have also assessed the performance of Haplotype Segment Algorithm on a real dataset in detecting a disease gene location. Friedreich ataxia is an autosomal recessive disease that involves the control and peripheral nervous systems and the heart. The data came from Acadian population of Louisiana [17]. The gene responsible for

Table 4. Precision and recall plots for observed and true locations on disease gene using three datasets

Measure	Precision and recall plots using dataset 1		Precision and recall plots using dataset 2		Precision and recall plots using dataset 3	
	Precision	Recall	Precision	Recall	Precision	Recall
Pearson	0.16	1	0.2	1	0.28	1
Euclidean	0.04	1	0.44	1	0.04	1
Harmonic Mean	0.16	1	0.36	1	0.08	1
Cosine	0.52	1	0.26	1	0.12	1
Jaccard	0.6	1	0.36	1	0.24	1
Canberra	0.16	1	0.2	1	0.08	1
Neyman	0.36	1	0.2	1	0.28	1
Divergence	0.16	1	0.2	1	0.08	1
Dice	0.12	1	0.16	1	0.36	1
Motyka	0.16	1	0.2	1	0.08	1
Dynamic Time Warping	0.1	1	0.36	1	0.23	1
True location [7]	0.1	1	0.1	1	0.09	1

friedreich ataxia is identified by Campuzano et al in 1996 [18] and this disease is caused by trinucleotide repeat expansion. The dataset related to friedreich ataxia disease was first reported by Liu et al in 2001 [7] for linkage disequilibrium mapping. This dataset contains 54 disease haplotypes and 69 control haplotypes with 12 micro-satellite markers. The disease gene is located between fifth and sixth markers, approximately 9.8125cM away from leftmost marker. In experiment with friedreich ataxia dataset, we have assessed the capability of Haplotype Segment Algorithm in detecting a disease gene when a dataset consists of small portion of haplotypes. We have observed that HSA has predicted a disease gene location similar to as reported by Liu et al [7] with small number of disease and control haplotypes and markers as shown in Table 5.

Performance of Haplotype Segment Algorithm in Terms of Precision and Recall on a Real Dataset. We have assessed the performance of Haplotype Segment Algorithm on Friedreich Ataxia dataset reported by Liu et al [7] in terms of precision and recall. The Haplotype Segment Algorithm is evaluated using a real dataset with total number of markers retrieved that is 12 and the number of markers involved in disease susceptibility gene are 8, 8, 4, 4, 4, 8, 8, 8, 4, 8 and 8 which are predicted by using Pearson measure, Euclidean, Harmonic mean, Cosine, Jaccard, Canberra, Neyman, Divergence, Dice, Motyka and Dynamic Time Warping algorithm, respectively. The location reported by Liu et al [7] for friedreich ataxia dataset with total number of markers retrieved that is 12 and there are 2 markers which are disease relevant. Performance comparison on observed disease location and a disease location reported by Liu et al in 2001 [7] is shown in Table 6.

Table 5. Disease gene location predicted by proposed Haplotype Segment Algorithm and reported by Liu et al [7] for friedreich ataxia

Measure	Disease location detected by HSA
Pearson	M5 to M12
Euclidean	M1 to M8
Harmonic mean	M5 to M8
Cosine	M5 to M8
Jaccard	M5 to M8
Canberra	M5 to M12
Neyman	M5 to M12
Divergence	M5 to M12
Dice	M5 to M8
Motyka	M1 to M8
Dynamic Time Warping	M5 to M12
Location predicted by Liu et al [7]	M5 to M6

Table 6. Precision and recall for observed location and a location reported by Liu et al [7] using friedreich ataxia dataset

Measure	Precision	Recall
Pearson	0.28	1
Euclidean	0.04	1
Harmonic Mean	0.08	1
Cosine	0.12	1
Jaccard	0.24	1
Canberra	0.08	1
Neyman	0.28	1
Divergence	0.08	1
Dice	0.36	1
Motyka	0.08	1
Dynamic Time Warping	0.23	1
Location predicted by Liu et al [7]	0.09	1

5 Conclusion

In this paper, we have studied the problem of gene mapping by observing the associations of marker alleles in the form of haplotype segments. We have developed a new Haplotype Segment Algorithm that identifies the disease gene region using several distance/similarity measures. Like Haplotype Pattern Mining [3] and LinkageTracker [5], our new algorithm does not require any population ancestry information and detects a disease locus if the mutation is present even at below 5% in the DNA samples. Since, HSA uses distance/similarity measures so this algorithm has the capability to reduce or delete the noise from the segments and finds a precise disease location. The performance of our new method is encouraging and is restricted to the simulation-generated datasets and a real dataset. We have found our results very close to the true locations. In future, we will be applying HSA on the other organisms like bacteria, fungus and algae.

References

1. Li, J., Jiang, T.: Haplotype-based linkage disequilibrium mapping via direct data mining. *Bioinformatics* 21, 4384–4393 (2005)
2. Toivonen, H., Onkamo, P., Vasko, K., Ollikainen, V., Sevon, P., Mannila, H., Herr, M., Kere, J.: Data mining applied to linkage disequilibrium mapping. *American Journal of Human Genetics* 67, 133–145 (2000)

3. Toivonen, H., Onkamo, P., Vasko, K., Ollikainen, V., Sevon, P., Mannila, H., Kere, J.: Gene Mapping by Haplotype Pattern Mining. In: IEEE Proc. Int'l Symposium Bioinformatics and Biomedical Engineering (BIBE), pp. 99–108 (2001)
4. Besenbacher, S., Pedersen, C.N., Mailund, T.: A fast algorithm for genome-wide haplotype pattern mining. In: Proc. of Int'l Conf. on Bioinformatics, Beijing, China (2009)
5. Lin, L., Wong, L., Leong, T., Lai, P.: LinkageTracker: A Discriminative Pattern Tracking Approach to Linkage is equilibrium Mapping. In: Zhou, L.-z., Ooi, B.-C., Meng, X. (eds.) DASFAA 2005. LNCS, vol. 3453, pp. 30–42. Springer, Heidelberg (2005)
6. Reeve, J.P., Rannala, B.: DMLE+: Bayesian linkage disequilibrium gene mapping. *Bioinformatics*, 894–895 (2002)
7. Liu, J., Sabatti, C., Teng, J., Keats, B., Risch, N.: Bayesian Analysis of Haplotypes for Linkage Disequilibrium Mapping. *Genome Research* 11, 1716–1724 (2001)
8. Lu, X., Niu, T., Liu, J.S.: Haplotype information and linkage disequilibrium mapping for single nucleotide polymorphisms. *Genome Research* 13, 2112–2117 (2003)
9. Kaplan, N.L., Hill, W.G., Weir, B.S.: Likelihood methods for locating disease genes in non-equilibrium populations. *American Journal of Human Genetics* 56, 18–32 (1995)
10. Mailund, T., Schierup, M.H., Pedersen, C.N.S., Madsen, J.N., Hein, J., Schauser, L.: GeneRecon: A coalescent based tool for fine-scale association mapping. *Bioinformatics* 22, 2317–2318 (2006)
11. Ester, M., Kriegel, K.P., Sander, H., Xu, X.: A density-based algorithm for discovering clusters in large spatial datasets with noise. In: Proc. of Knowledge Discovery in Data (KDD), pp. 226–231 (1996)
12. Sevon, P., Toivonen, H., Ollikainen, V.: TreeDT: Tree Pattern Mining for Gene Mapping. *IEEE Transactions on Computational Biology and Bioinformatics* 3, 174–185 (2006)
13. Ahmed, A.: A Heuristic Approach to the Identification of Disease Gene Region using Haplotype Analysis, 15th Human Genome Meeting, 4th Pan Arab Human Genetics Conference, Dubai, United Arab Emirates, HUGO Journal, 5, 156 (2011)
14. Long, A., Langley, C.: The power of association studies to detect the contribution of candidate genetic loci to variation in complex traits. *Genome Research* 9, 720–731 (1999)
15. Cha, S.: Comprehensive Survey on Distance/Similarity Measures between Probability Density Functions. *Int'l. Journal of Mathematical Models and Methods in Applied Sciences* (2007)
16. Li, G., Wang, Y., Li, M., Wu, Z.: Similarity Match in Time Series Streams under Dynamic Time Warping Distance. In: Proc. of Int'l Conf. on Computer Science and Software Engineering (CSSE), vol. 4, pp. 399–402 (2008)
17. Sirugo, G., Keats, B., Fujita, R., Duclos, F., Purohit, K., Koenig, M., Mandel, J.L.: Friedreich Ataxia in Louisiana Acadians: Demonstration of Founder Effect by Analysis of Microsatellite-generated Extended Haplotypes. *Am. J. Hum. Genet.* 50, 559–566 (1992)
18. Campuzano, V., Montermini, L., Molto, M.D., Pianese, L., Cossee, M., Cavalcanti, F., Monros, E., Rodius, F., Duclos, F., Monticelli, A.: Friedreich's ataxia: Autosomal recessive disease caused by an intronic GAA triplet repeat expansion. *Science* 271, 1423–1427 (1996)

Effect of Fast Moving Object on RSSI in WSN: An Experimental Approach

Syed Hassan Ahmed¹, Safdar Hussain Bouk², Amjad Mehmood¹,
Nadeem Javaid², and Sasase Iwao³

¹ Institute of IT, Kohat Univ. of Science and Technology, Kohat, Pakistan

² Dept. of Electrical Engineering COMSATS Institute of Information Technology,
Islamabad, Pakistan

³ Department of Information and Computer Science, Keio University, Japan
{sani9585,amjadiitkust}@gmail.com, {bouk,nadeemjavaid}@comsats.edu.pk,
sasase@ics.keio.ac.jp

Abstract. In this paper, we experimentally investigate the effect of fast moving object on the RSSI in the wireless sensor networks in presence of the ground effect and antenna orientation in elevation direction. In experimental setup, MICAz mote pair was placed on the ground, where one mote acts as a transmitter and the other as a receiver. The transmitter mote's antenna was oriented in elevation direction with respect to the receiver mote's antenna. The fast moving object i.e. car, was passed between the motes and the fluctuations in the RSSI are observed. The experimental results show some sequential pattern in RSSI fluctuations when car moves at some relatively slow speed. However, some irregularities were also observed when antenna was oriented at 45 and 90 in elevation direction.

Keywords: RSSI, MICAz, WSN, Sensor-less WSN.

1 Introduction

It has been observed that Wireless Sensor Networks (WSN) is one of the dynamic research area because, it has been investigated by many researchers due to its diversified applications i.e. health, traffic, agriculture, military, goods tracking, etc. WSN comprises low-power wireless nodes or motes and gateway node(s) [1]. The task of wireless node is to sense the environment or its physical parameters (that is done with the help of sensors or sensing modules attached with the sensor nodes) and communicate the sensed data to the gateway node(s). Gateway node(s) can either be connected to the computer or directly to the network. The sensed data is either stored in a central online database or at the computer that is attached with the gateway node(s).

There are several areas that are intensively investigated by the researchers, which includes sensor platform design, energy efficient routing and MAC protocols, deployment strategies and the list goes on. Along with these applications, an active research is also being carried out where sensing is accomplished without

using any physical sensors or sensing modules and termed as Sensor-less WSN (SL-WSN) [2].

In SL-WSN, no sensing module is attached to the mote and sensing is performed by monitoring and measuring the variations of the power in received radio signal at the receiving antenna. This signal strength metric is called Receive Signal Strength Indicator (RSSI). There are different factors that affect the RSSI value, which includes antenna type, physical distance between sender and receiver, physical objects, interference from other RF devices, transmit power of sender mote, antenna orientation and so on.

In this paper, we experimentally investigate the exact impact of fast moving object i.e. vehicle, on the RSSI of the mote pair. During the experiment, we use MICAz (MPR2600J Japan) motes [3] and MIB520 gateway and programming board. Results are analyzed on the basis of different vehicle speeds and elevation angles of the MICAz mote antenna. The ground effect is also considered in the experiment by placing the MICAz mote pair on the ground.

Following section, briefly discusses the related work. Section-3, describes our experimental approach to monitor instabilities in RF signals using Crossbow Micaz motes and realistic data collection. Experimental results are discussed in Section-4. Finally, Section-5 concludes the paper.

2 Related Work

RSSI of MICAz mote has been investigated several times in the past, where the effects of human activities, distance and antenna position, on RF propagations have been observed. Also, the RSSI has been considered as one of the important factor to compute the radio link quality in the wireless networks. Several routing and localization protocols rely severely on the link quality metric, for example, to choose the best wireless link during the routing process or to estimate the distance between two communicating sensors. Srinivasan et al. in [4] considered MICAz motes and showed that the RSSI values can be a promising connection quality indicator if its value is above the predefined sensitivity threshold of the radio frequency module. In case, if RSSI value is near this threshold then, it does not have a correlation with packet reception rate and it is only because of the local noise variations at nodes. The TinyOS based radio performance of WSN is investigated in [5]. It is shown that the antenna of the Tmote Sky device is not perfectly omni-directional and the RSSI value above a certain point should not be used as a distance indicator between sensors. Pius W.Q. Lee et. al. [6] considers variations in the received signal strength or RSSI value caused by the passive objects, e.g. humans, to monitor and detect the human activity in the network deployment area. RSSI value is analyzed in different experimental scenarios e.g. indoor, large hall, outdoor etc. During these experiments nodes were placed at 3m to 5m apart and 1.5m above the ground and no antenna orientation has been considered in the experiments. The impact of human activity is also investigated experimentally through different experimental scenarios in [7]. It is also observed that the RSSI is not the robust link quality indicator and human activity has

great impact on the packet reception rate. In [8], authors investigated the impact of antenna orientation on the performance of WSN. The antenna of both the MICAz mote pair is oriented in elevation direction at different angles to the ground and their impact on the RSSI is estimated. The previous work discussed above, doesn't consider the effect of the fast moving object on the RSSI in presence of the ground effect and the antenna orientation in elevation direction. In this paper, we experimentally investigate the effect of vehicle on the RSSI when nodes are placed on the ground and the antenna of the transmitting node is elevated in the elevation direction.

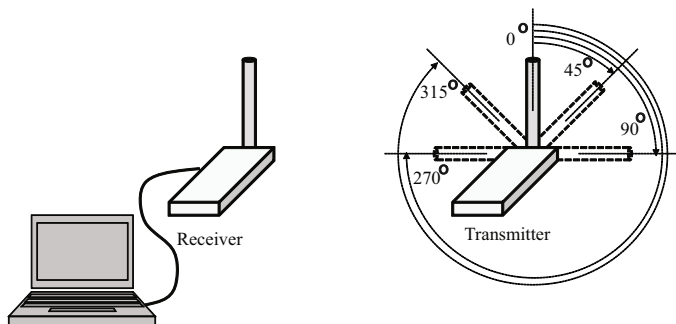


Fig. 1. Antenna orientation of the transmitter node

3 Experimental Setup

This section briefly describes the experimental setup. In our experiment, we use MICAz OEM Edition motes (MPR2600J Japan), by MEMSIC Inc., formerly Crossbow. The MICAz OEM Edition mote is equipped with Atmega128L processor, CC2420 RF Chip and a half-wave external monopole antenna. CC2420 is designed for the low-power and low-rate systems that operate at ISM Frequency Band from 2400MHz to 2483.5MHz.

During the experiment we analyze the effect of fast moving object i.e. Car, over the RSSI in presence of ground effect and antenna orientation. One of the motes works as a transmitter mote (that continuously sends packets at the fixed interval of 50ms) and the other node acts as a receiver. These nodes are placed on the ground at 5m apart. We drive the car in between LOS of these nodes with varying speed of 10, 20, to 60km/h. Also antenna of the transmitter node is orientated at 0, 45, 90 to 315 in elevation direction with respect to the receiver mote. The RSSI of the successfully received packets at the receiver mote is recorded in a computer attach with it. Fig. 1 and Fig. 2 show the antenna orientation and experimental setup where car is passing through MICAz mote pair.

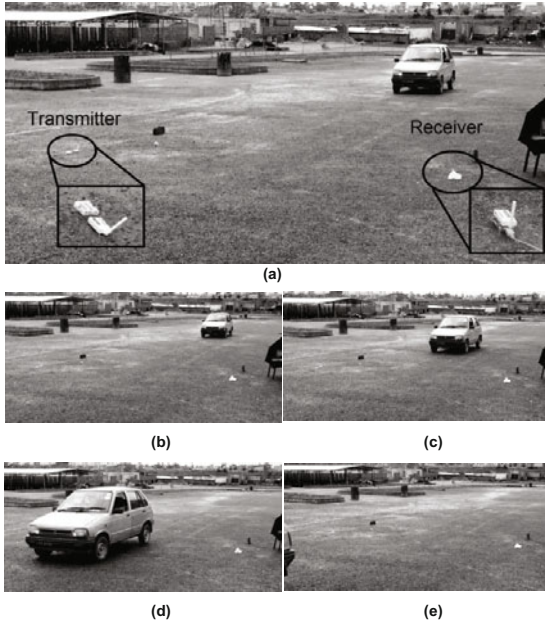


Fig. 2. Experimental setup where Car is passing between MICAz Mote pair

4 Experimental Results

In this section, experimental results are briefly discussed. Initially, during the experiment, the average RSSI between node pair (transmitter and receiver), placed at varying distances and with antenna orientation at different angles in elevation direction, has been observed with no vehicle movement and are shown in Fig. 3 and Fig. 4. Fig. 3 and 4 show the average RSSI and Standard Deviation in RSSI vs. antenna orientation, respectively. It is evident from the results that RSSI decreases and deviation in RSSI increases as distance increases. However, some major RSSI fluctuations at 90 and 270 have been observed in all RSSI readings.

The obvious reason of those rise and dips is that monopole antenna radiates power in perpendicular direction to the antenna itself. When both antennas are placed in parallel position to each other, the radiation power increases. On the other hand, when one antenna is rotated in elevation direction with reference to the other, radiation power decreases at the receiver side. In result, the RSSI decreases when antenna is oriented at 90 and 270 elevation direction.

The effect of the vehicle (car) moving at varying speed between the motes pair placed on the ground at 5m apart is observed during the experiment. The maximum fluctuation, average and minimum fluctuation in RSSI values with varying car speed at 0 , 45 and 90 , 270 are shown in Fig. 5 and Fig. 6, respectively. It is evident from the results that when car is moving at slow speed e.g. 10 and 20km/h the distance between RSSI boundary values (Max. and Min.) is larger.

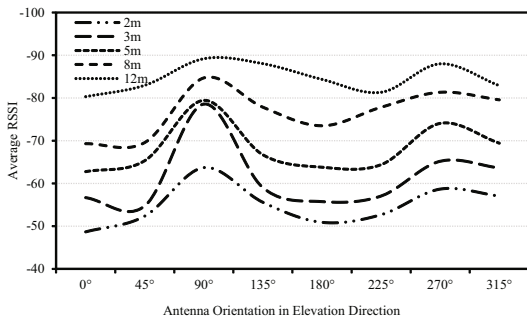


Fig. 3. Average RSSI vs. antenna orientation in elevation direction without any object movement

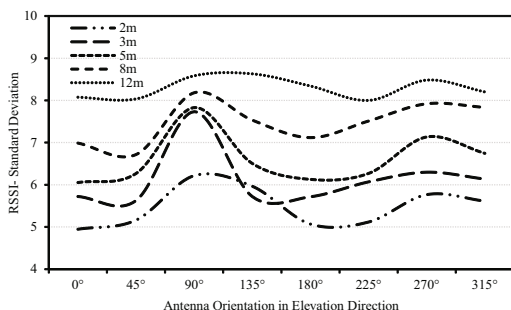
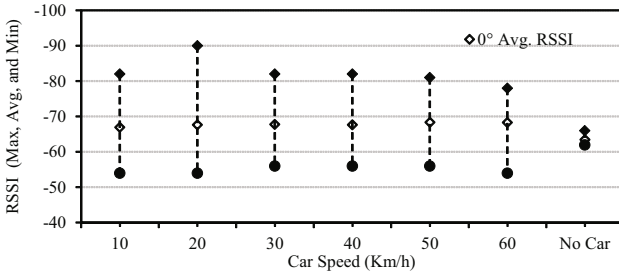


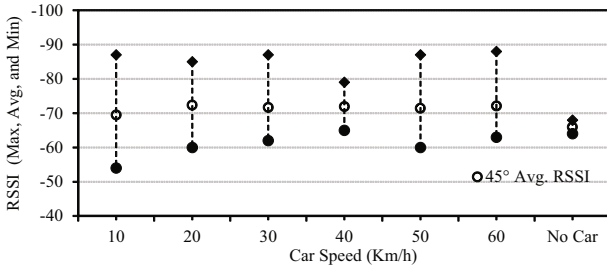
Fig. 4. RSSI standard deviation vs. antenna orientation in elevation direction without any object movement

However, if the car speed is faster than 20km/h then, the boundary values are almost similar or sometimes irregular (e.g. 40km/h speed at 45 antenna orientation in Fig. 5(b)). However, these fluctuation in RSSI when car moves at varying speed between node pair, are comparatively much higher than no car movement. The similar trend is also shown in Fig. 7 and it shows that the average RSSI value when car moves at varying speed and no car movement between the node pair. Conversely, the standard deviation in RSSI decreases when car speed increases, as shown in Fig. 8. The reason of this high deviation at slow speed is that the car obstructs the signal for longer time compared to faster speed and results in a high deviation.

The RSSI variation envelope (maximum, average and minimum values) for 10, 30 and 40km/h car speed versus varying elevation angle of transmitter antenna is shown in Fig. 9 (a), (b) and (c), respectively. The RSSI envelope size of different speeds at different elevation angles is almost similar for different angles. However, some irregularities have been observed in RSSI values at 45 in Fig. 9 (c) and 90 in Fig. 9. The RSSI deviation is less at 45 when car moves at 40km/h and the RSSI has very high deviation in maximum or high RSSI direction with respect to the average RSSI value at 90 for all speeds. The similar trend is shown and summarized in Fig. 10.

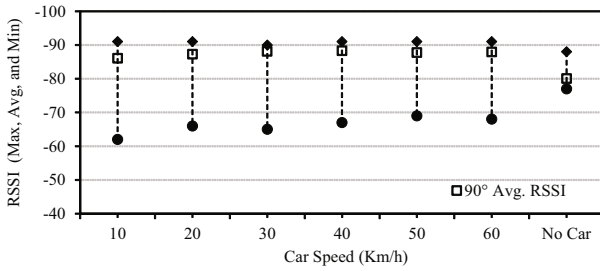


(a) RSSI variation (Max, Avg, Min) at 0° v/s varying car speed.

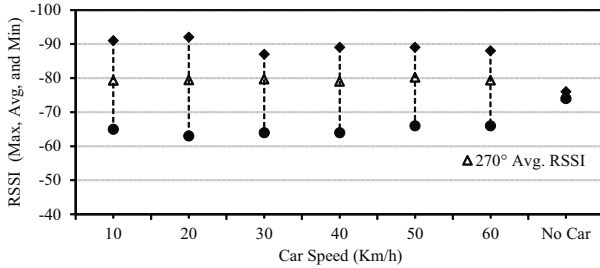


(b) RSSI variation (Max, Avg, Min) at 45° v/s varying car speed.

Fig. 5. RSSI variation vs. varying car speed at (a) 0 orientation and (b) 45 orientation, in elevation direction



(a) RSSI variation (Max, Avg, Min) at 90° v/s varying car speed.



(b) RSSI variation (Max, Avg, Min) at 270° v/s varying car speed.

Fig. 6. RSSI variation vs. varying car speed at (a) 90 orientation and (b) 270 orientation, in elevation direction

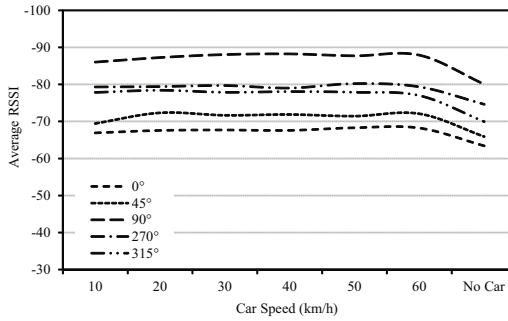


Fig. 7. Average RSSI vs. varying car speed for different antenna orientation angles

It has been observed from the experimental results that antenna elevation in presence of the ground effect has some irregularities in the RSSI fluctuations. Hence, to detect the fast moving object by observing the RSSI value, an efficient algorithm is needed.

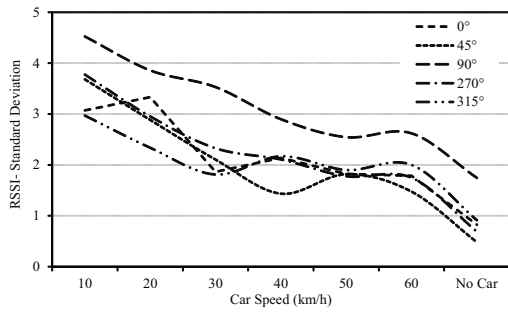


Fig. 8. RSSI standard deviation vs. varying car speed for different antenna orientation angles

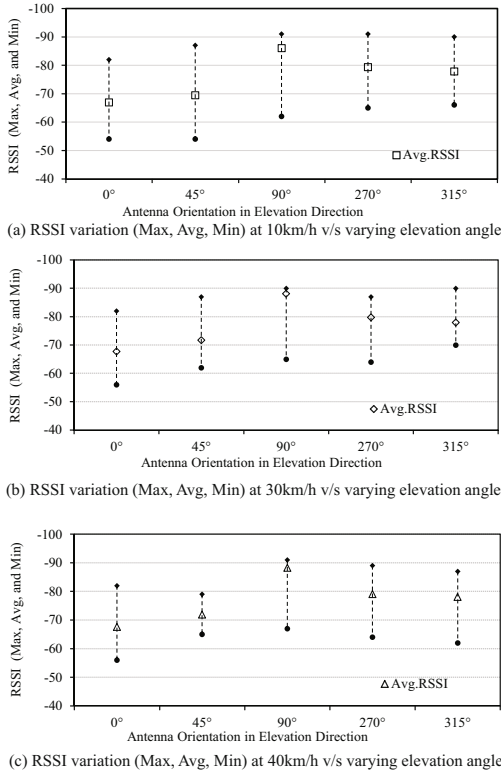


Fig. 9. RSSI variation vs. varying elevation angles at (a) 10km/h, (b) 30km/h and (c) 40km/h car speed

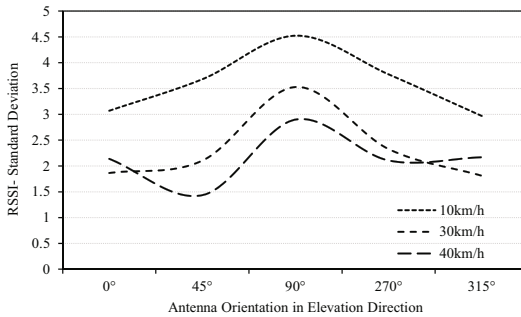


Fig. 10. RSSI Standard Deviation vs. varying elevation angles for different car speed

5 Conclusion

In this paper, we experimentally analyzed the effect of fast moving vehicle on the RSSI in presence of the ground effect and antenna orientation in elevation direction. It has been observed that the slow speed causes high deviation in RSSI compared to the faster speed. Some irregularities in the RSSI fluctuations are also observed when antenna is elevated at 45 and 90 . In future, this work will be extend to propose the fast moving object sensing algorithm for SL-WSN that takes into account the antenna orientation as well as ground effect. Algorithm must incorporate the learning phase beforehand to precisely detect the fast moving object with very low false count.

Acknowledgments. This work was partly supported by Keio University 21st Century Center of Excellence Program on “Optical and Electronic Device Technology for Access Network” and Fujitsu Laboratories.

References

1. Garcia-Hernández, C.F., Ibarguengoytia-González, P.H., García-Hernández, J., Pérez-Díaz, J.A.: Wireless Sensor Networks and Applications: a Survey. *International Journal of Computer Science and Network Security*, IJCSNS 7(3), 264–273 (2007)
2. Woyach, K., Puccinelli, D., Haenggi, M.: Sensorless Sensing in Wireless Networks: Implementation and Measurements. In: *Proceedings of the 2nd International Workshop Wireless Network Measurement (WinMee 2006)* (2006)
3. Wireless ZigBee type Sensor Network, <http://www.xbow.jp/zigbee-smartdust.html>
4. Srinivasan, K., Levis, P.: RSSI is under appreciated. In: *Proceedings of the Third Workshop on Embedded Networked Sensors* (2006)
5. Holland, M.M., Aures, R.G., Heinzelman, W.B.: Experimental investigation of radio performance in wireless sensor networks. In: *2nd IEEE Workshop on Wireless Mesh Networks (WiMesh)* (2006)
6. Lee, P.W.Q., Seah, W.K.G., Tan, H.P., Yao, Z.: Wireless Sensing Without Sensors - An Experimental Approach. In: *IEEE 20th International Symposium Personal, Indoor and Mobile Radio Communications*, Tokyo, Japan, pp. 62–66 (September 2009)
7. Hamida, E.B., Chelius, G.: Investigating the Impact of Human Activity on the Performance of Wireless Networks - An Experimental Approach. In: *Proceedings of the IEEE International Symposium on A World of Wireless, Mobile and Multimedia Networks (WoWMoM)*, Montreal QC, Canada, pp. 1–8 (June 2010)
8. Wadhwa, M., Song, M., Rali, V., Shetty, S.: The Impact of Antenna Orientation on Wireless Sensor Network Performance. In: *Proceedings of the 2nd IEEE International Conference on Computer Science and Information Technology (ICCSIT 2009)*, Beijing, China, pp. 143–147 (August 2009)

Performance Analysis of Bessel Beamformer and LMS Algorithm for Smart Antenna Array in Mobile Communication System

Pervez Akhtar and Muhammad Yasin

Department of Electronics and Power Engineering,
National University of Sciences and Technology, Islamabad, Pakistan
{pervez, myasin}@pnec.edu.pk

Abstract. In this paper, we analyze the performance of Bessel beamformer based on spatial filtering criteria and its comparison is made with least mean square (LMS) algorithm in terms of gain enhancement towards desired user by suppressing interference, reduction in transmit power, minimize mean square error (MSE) and to find the optimum array weights. These algorithms are used in digital signal processor and connected with antenna which can dynamically update the main beam width, beam steering capability, side lobe levels and direction of null as the propagation environment or filtering requirement changes. Based on simulation results, it is revealed that Bessel beamformer provide remarkable improvements in terms of gain, interference suppression, reduction in transmit power, improvement in power gain and weights convergence over that of LMS algorithm. With respect to LMS, Bessel beamformer provides 2.02% improvements in interference suppression, 5 dB enhancements in gain, 99% improvement in convergence rate, 9.77% improvement in reduction in mean output power, 192% improvement in power gain and 107 % in null depth performance. Therefore, Bessel beamformer gives a cost effective solution in practical base station installations of mobile communication system in CDMA environment to enhance capacity and range.

Keywords: Smart adaptive antenna array system, Bessel beamformer, LMS algorithm.

1 Introduction

Bessel beamformer is based on spatial filtering [1] in which the desired user receive more power compared to the omni-directional case, so transmit power can be saved. Besides this, interference to adjacent cells of cellular communication system decreases because only desired users are targeted. Smart/adaptive antenna array uses either Bessel beamformer or LMS beamforming algorithms which not only maximize the signal power in the desired direction but also minimize the interference power [2-5]. In research articles [6-7], Lal. C. Godara contributed a thorough study on antenna arrays theory, its application in mobile communication. Part I of his research provides a brief summary of mobile communications, antenna array terminology, the

usage of antenna arrays in mobile communication systems, the advantages and improvements that it brings, design issues, and the feasibility in implementation. In Part II, he presents a detail interpretation of various beam-forming schemes, adaptive algorithms, direction of arrival (DOA) estimation methods, and some issues on array sensitivities. In [8], various issues about the smart antennas in mobile radio networks including its advantages are discussed whereas in research paper [9], a comparison study among Recursive Least Squares (RLS), LMS and Constant Modulus Algorithm (CMA) is carried out. It is found that RLS and LMS are best for beamforming towards desired user but having limitations towards interference rejection whereas CMA has satisfactory response towards beamforming, better outcome for interference rejection and for Bit Error Rate (BER). It is also verified here that convergence rate of RLS is faster than LMS so RLS is proved the best choice. The effect of changing step size for LMS algorithm has also been studied. In paper [10], a modified LMS algorithm is developed by incorporating the fractional derivative term in the weight adaptation equation of standard LMS algorithm and results are compared with standard LMS for different step size parameters and different number of tap weights. It is proved that as number of tap weights increases, rate of the convergence for both the algorithms decrease, but still modified LMS algorithm provides better convergence. In our case, the Bessel beamformer, an adaptive algorithm is more efficient than LMS algorithm to optimize the beam towards desired user and nullify interference which leads to increase capacity and quality. This research is the extension of our previous work done reported in [1].

The next section describes the system model and its working principle. Section 3 displays mathematical model for Bessel beamformer and LMS algorithms. Section 4 includes simulation results. Discussion and comments is presented in section 5. Finally, section 6 concludes the paper.

2 System Model

Consider a smart antenna array system consists of number of elements, having uniform distance between each two elements and equipped with digital signal processor containing adaptive beamforming algorithms i.e. Bessel beamformer and LMS as shown in Figure 1. These adaptive beamforming algorithms are used to update the weights dynamically so that mean square error is reduced and signal to noise ratio (SNR) of the desired signal is optimized. The array factor [11-13] for linear array having N elements equally spaced (d) is given by

$$AF(\Phi) = \sum_{n=0}^{N-1} A_n \cdot e^{(jn \frac{2\pi d}{\lambda} \cos \Phi + \alpha)} \quad (1)$$

where α is the inter element phase shift and is described as

$$\alpha = \frac{-2\pi d}{\lambda_0} \cos \Phi_0 \quad (2)$$

and Φ_0 is the desired direction of the beam.

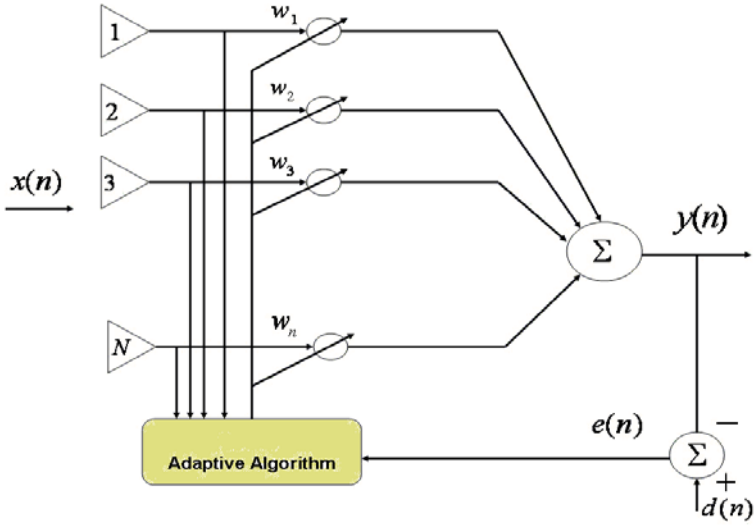


Fig. 1. Smart/adaptive antenna array system

3 Mathematical Model

3.1 Bessel Beamformer

The Bessel beamformer is based on the Bessel function of the first kind of order ν [14-15] and provides computationally efficient adaptive weights calculation. The weight of Bessel beamformer is computed by

$$w(k+1) = w(k) - 2\mu e(k) J_\nu(N) x(k) \quad (3)$$

where $J_\nu(N)$ represents the Bessel function of the first kind and defined by

$$J_\nu(N) = \left(\frac{N}{2}\right)^\nu \sum_{k=0}^{\infty} \frac{\left(\frac{N^2}{4}\right)^k}{k! \Gamma(\nu + k + 1)} \quad (4)$$

where ν denotes the order of the Bessel function of the first kind and must be a real number. The number of elements is presented by N and Γ is the gamma function.

3.2 Least Mean Square Algorithm

This algorithm is based on the estimate of the gradient vector that uses available data for this purpose [9-10, 16]. This algorithm makes successive corrections to the weight vector in the direction of the negative of the gradient vector which finally concludes to minimum MSE. This successive correction to the weight vector is the point at which optimum value w_0 is obtained.

$$w(k+1) = w(k) + \mu e(k)x(k) \quad (5)$$

where μ is the rate of adaptation, controlled by the processing gain of antenna array and $e(k)$ is the MSE.

4 Simulation Results

The simulations are designed to analyze the properties of Bessel beamformer and LMS algorithms. The desired signal is phase modulated with $SNR = 15$ dB, used for simulation purpose. It is given by

$$S(t) = e^{j\sin(2\pi f t)} \quad (6)$$

where f is the frequency in Hertz.

4.1 Array Factor of Smart Antenna Array System

It is employed to receive the signal for which uniform linear array is taken with $N = 12$. The distance between two elements is supposed as $\lambda/4$ and 2000 samples are taken for simulation purpose. The angle of arrival (AOA) for desired user is 0 degree. The linear array factor plot is shown in Figure 2. The beam width is measured between the first two nulls of the array response function. The desired signal and interferer are received by an array of 12 elements with 12 weights. It is observed that the array directivity increases with the number of elements but at the same time number of side lobes also increases. The directivity of Bessel beamformer and LMS algorithms are observed as 0 dB and -5 dB respectively which clearly indicates 5 dB gain improvements of Bessel beamformer over that of LMS algorithms, by suppressing interference. Both algorithms have their main beam towards the desired direction.

The data given in Tables 1 and 2 is taken from Figure 2 for both beamforming algorithms under study.

Table 1. Effect of Number of Elements on Beam width

Element Spacing d	AOA (degree)	Elements N	Beam width (degree)	HPBW (degree)
$\lambda/4$	0	12	40	36

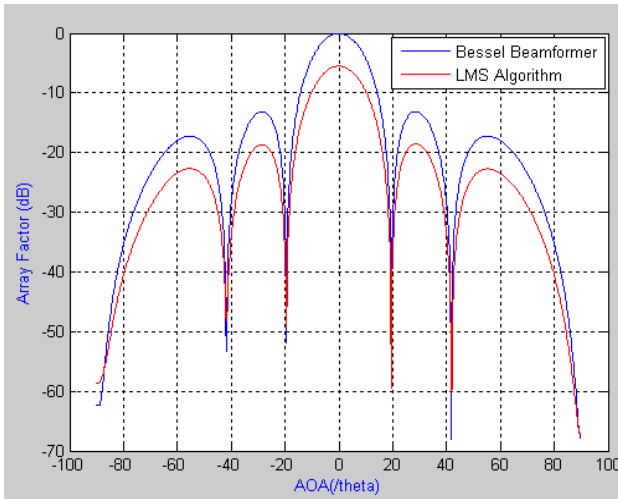


Fig. 2. Array factor plot for Bessel beamformer and LMS algorithms with AOA for **desired user is 0 degree** with constant space of $\lambda/4$ between elements for $N = 12$

Table 2. Performance Analysis of Algorithms under Study

Algorithms	Gain Performance (dB)	Null Depth Performance (dB)	Sidelobe Level (dB)
Bessel beamformer	0	-52.43	-13.13
LMS	-5	-48.94	-18.68

The ratio between the powers of the main lobe and the first side lobe is -13.13 dB and -18.68 dB for Bessel beamformer and LMS algorithms respectively. It is ascertained that Bessel beamformer is giving 5 dB gain improvements and 107 % null depth performance over that of LMS.

4.2 Mean Square Error Performance

The minimum MSE describes the performance of the given system. An adaptive beamformer like Bessel beamformer or LMS combines the signals received by different elements of smart antenna array to form a single output. This is achieved by minimizing the MSE between the desired output and the actual array output. The minimum MSE for both algorithms are shown in Figure 3 which indicates that Bessel beamformer has minimum MSE (0.1699) as compared to LMS (8.397) when measured after 2000 iterations. Therefore it is proved that performance of Bessel beamformer is better (2.02%) over that of LMS. Initially, both algorithms starts from higher value i.e. (530.6) and (31.62) but then gets to obtain lower value after 568 iterations. Both these algorithms are having the same value (21.59) at 568 iterations.

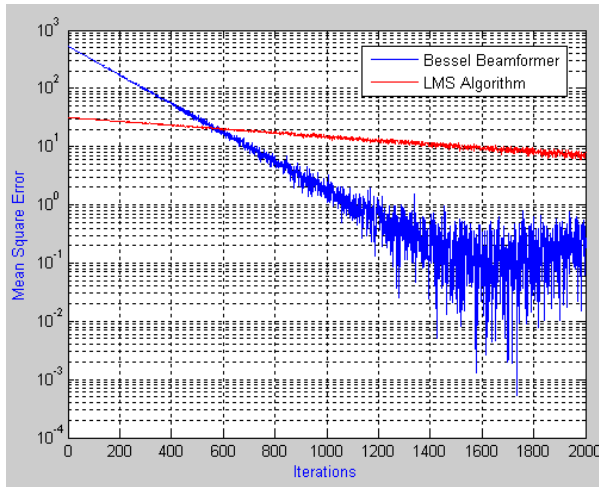


Fig. 3. Mean Square Error performance for Bessel beamformer and LMS algorithms for $N = 12$ with constant space of $\lambda/4$

4.3 Weight Convergence Performance

The performance of the communication system is judged by correct and fast convergence of adaptive weights. The weights value obtained at minimum MSE are the ones that minimize the power in the error signal indicating that system output has approached the desired output, is called optimum weights ($w(k+1) \rightarrow w$) or w_{MSE} . In our case, both the algorithms have taken almost the same convergence path as shown in Figure 4.

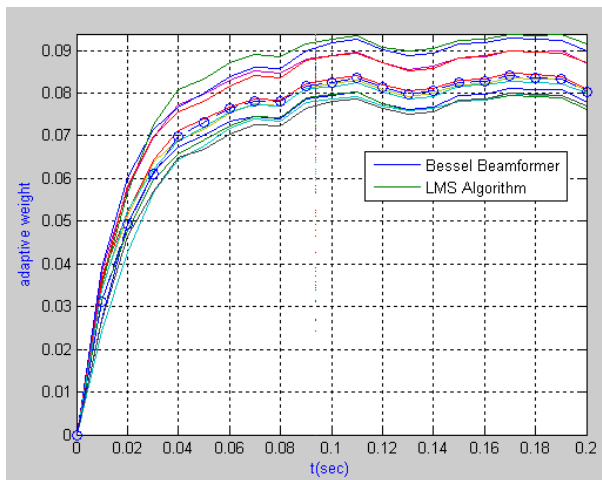


Fig. 4. Weight convergence plot for Bessel beamformer and LMS algorithms

It is evident that the weight values of both algorithms converges to their optimum values and follow almost the same track. It is to be noted that convergence rate for Bessel beamformer and LMS is 0.0928 and 0.0937 seconds respectively when 20 in number iterations are taken for simulation. Therefore it is ascertained that Bessel beamformer is faster (99%) over that of LMS.

4.4 Mean Output Power Performance

The system mean output power has approached the desired output when optimum weights ($w(k+1) \rightarrow w$) or w_{MSE} are achieved. An adaptive beamformer like Bessel beamformer or LMS combines the signals received by different elements of smart antenna array to form a single output. This is achieved by minimizing the MSE between the desired output and the actual array output. The system mean output powers for both algorithms are shown in Figure 5. The total average power in a sinusoid is the same, whether it is computed in the time domain or the frequency domain as per Parseval’s theorem.

It is crystal clear from the Figure 5 that Bessel beamformer has 0.9863 dB mean output power as compared to LMS (10.09 dB) when measured after 2000 iterations. It is proved that performance of Bessel beamformer is better (9.77%) as compared to LMS. Bessel beamformer saves power because a directional gain of Bessel beamformer is maximum (5 dB) over that of LMS. Bessel beamformer consumes less power and therefore, battery life of the base station increases.

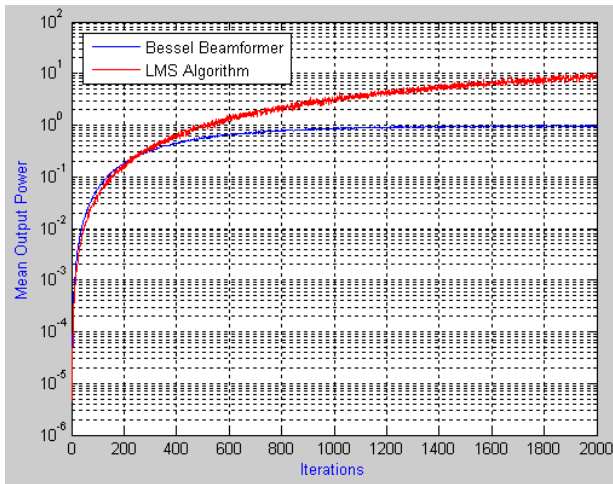


Fig. 5. Performance comparison between Mean Output Power for Bessel beamformer and LMS algorithms

4.5 Power Gain Performance

The performance of both algorithms is compared on the basis of power gain as shown in Figure 6. The measured values of power gain is -0.378 dB for Bessel beamformer

whereas -0.1976 dB for LMS when relative frequency is taken as 1000 for simulation purpose, thus improving the power gain at the rate of -0.1804 dB or 192% improvement in power gain is observed in case of Bessel beamformer over that of LMS.

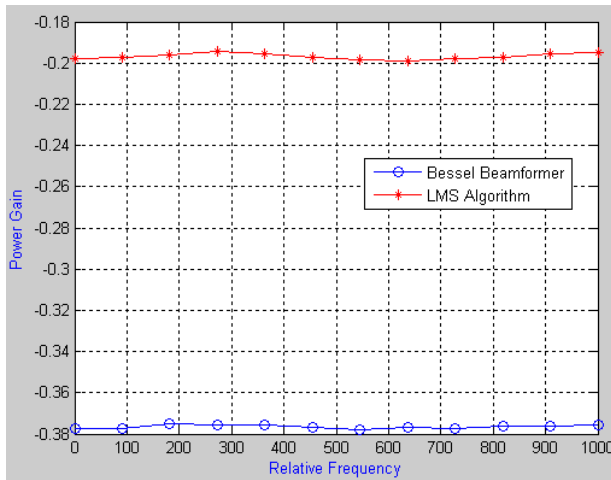


Fig. 6. Performance comparison between Power Gain for Bessel beamformer and LMS algorithms

The results obtained from Figures 3, 5 and 6, are summarized in Table 3.

Table 3. Performance Analysis of Algorithms under Study

Algorithms	Minimum MSE	Output power (dB)	Power Gain (dB)
Bessel beamformer	0.1699	0.9863	-0.378
LMS	8.397	10.09	-0.1976

5 Discussion and Results

Detailed analysis is carried out for both algorithms which includes the signal recovery, suppression of interference, performance analysis in terms of beamwidth, HPBW, beam steering capabilities, gain improvement, reduction in MSE, output power, null depth performance, Sidelobe level and convergence rate. The findings of simulation are:

1. Bessel beamformer has gain improvement (5 dB) more over that of LMS algorithm, by suppressing interference. The ratio between the powers of the main lobe and the first side lobe is -13.13 dB and -18.68 dB for Bessel beamformer and LMS algorithms respectively.
2. Bessel beamformer is giving 107 % null depth performance over that of LMS.

3. Bessel beamformer has minimum MSE (0.1699) as compared to LMS (8.397) when measured at 2000 iterations. Therefore it is proved that performance of Bessel beamformer is better (2.02%) over that of LMS.

4. The convergence rate for Bessel beamformer and LMS is 0.0928 and 0.0937 seconds respectively when 20 in number iterations are taken for simulation. Therefore it is ascertained that Bessel beamformer is faster (99%) over that of LMS. The simulations are carried on *Intel(R) Pentium(R) 4 CPU @ 3.00GHz, 512MB of RAM* hardware, using *MATLAB version 7.8.0.347 (R2009a)* software. It also confirms that if more sophisticated signal processor is used for spatial processing then computation time can further be reduced.

5. Bessel beamformer has 0.9863 dB mean output power as compared to LMS (10.09 dB) when measured at 2000 iterations. It is proved that performance of Bessel beamformer is better (9.77%) as compared to LMS. Bessel beamformer saves power because a directional gain of Bessel beamformer is maximum (5 dB) over that of LMS.

6. The measured values of power gain is -0.378 dB for Bessel beamformer whereas -0.1976 dB for LMS when relative frequency is taken as 1000 for simulation purpose, thus improving the power gain at the rate of -0.1804 dB or 192% improvement in power gain is observed in case of Bessel beamformer over that of LMS. Due to these characteristics, the capacity and range of network equipped with smart antenna increases.

6 Conclusions

With respect to LMS algorithm, Bessel beamformer provides: (1) 2.02% improvements in interference suppression, (2) 5 dB enhancements in gain, (3) 99% improvement in convergence rate, (4) 9.77% improvement in reduction in mean output power, (5) 192% improvement in power gain (6) 107 % in null depth performance. From these facts and figures, it is ascertained that Bessel beamformer exhibits an excellent performance over that of LMS algorithm which eventually results in a remarkable increase in capacity and quality of mobile communication systems in CDMA environment.

References

- [1] Yasin, M., Akhtar, P., Junaid Khan, M., Zaheer Naqvi, S.H.: Proposed Bessel Beamformer is a Better Option for Smart Antenna System for Capacity Improvement. *World Applied Sciences Journal* 10(4), 433–439 (2010) ISSN:1818-4952
- [2] Widrow, B., Stearns, S.D.: *Adaptive Signal Processing*. Pearson Education, Inc. (1985)
- [3] Haykin, S.: *Adaptive Filter Theory*, 4th edn. Pearson Education, Inc. (2002)
- [4] Yasin, M., Akhtar, P., Junaid Khan, M.: CMA an Optimum Beamformer for a Smart Antenna System. *International Journal of Computer Applications* (0975-8887) 5(7), 33–40 (2010)

- [5] Yasin, M., Akhtar, P., Zaheer Naqvi, S.H.: Design and Performance Analysis of Blind Algorithms for Smart Antenna System Using Window techniques. *Middle East Journal of Scientific Research* 7(4), 458–466 (2011) ISSN:1990-9233
- [6] Godara, L.C.: Applications of Antenna Arrays to Mobile Communications, Part I; Performance Improvement, Feasibility, and System Considerations. *Proceeding of the IEEE* 85(7), 1031–1060 (1997)
- [7] Godara, L.C.: Applications of Antenna Arrays to Mobile Communications, Part II; Beam-Forming and Directional of Arrival Considerations. *Proceeding of the IEEE* 85(8), 1195–1245 (1997)
- [8] Kawitkar, R.: Issues in Deploying Smart Antennas in Mobile Radio Networks. *Proceedings of World Academy of Science, Engineering and Technology* 31 (July 2008) ISSN:1307-6884
- [9] Shaukat, S.F., Ul Hassan, M., Farooq, R., Saeed, H.U., Saleem, Z.: Sequential Studies of Beamforming Algorithms for Smart Antenna Systems. *World Applied Sciences Journal* 6(6), 754–758 (2009) ISSN 1818-4952
- [10] Zahoor, R.M.A., Qureshi, I.M.: A Modified Least Mean Square Algorithm Using Fractional Derivative and its Application to System Identification. *European Journal of Scientific Research* 35(1), 14–21 (2009) ISSN:1450 – 216X
- [11] Yasin, M., Akhtar, P., Junaid Khan, M.: Tracking Performance of RLS and KAPA Algorithms for a Smart Antenna System. *World Applied Sciences Journal* 10(Special Issue of Computer & Electrical Engineering), 1–9 (2010) ISSN:1818-4952
- [12] Yasin, M., Akhtar, P., Junaid Khan, M., Zaheer Naqvi, S.H.: Enhanced Sample Matrix Inversion is a Better Beamformer for a Smart Antenna System. *World Applied Sciences Journal* 10(10), 1167–1175 (2010) ISSN:1818-4952
- [13] Yasin, M., Akhtar, P., Junaid Khan, M.: MVDR an Optimum Beamformer for a Smart Antenna System in CDMA Environment. *(IJCSIS) International Journal of Computer Science and Information Security* 8(4), 99–106 (2010) ISSN: 1947-5500
- [14] Chang, H.-P., Sarkar, T.K., Pereira-Filho, O.M.C.: Antenna Pattern Synthesis Utilizing Spherical Bessel Functions. *IEEE Transactions on Antennas and Propagation* 48(6), 853–859 (2000)
- [15] Proakis, J.G., Manolakis, D.G.: *Digital Signal Processing, Principles, Algorithms, and Applications*, 4th edn. Pearson Education Inc. (2009)
- [16] Yasin, M., Akhtar, P., Valiuddin: Performance Analysis of LMS and NLMS Algorithms for a Smart Antenna System. *International Journal of Computer Applications* (0975-8887) 4(9), 25–32 (2010)

Adaptive Minimum Entropy Beamforming Algorithms for Narrowband Signals

Anum Ali and Shafayat Abrar

Department of Electrical Engineering,
COMSATS Institute of Information Technology,
Islamabad 44000, Pakistan
{anum_ali,sabrar}@comsats.edu.pk

Abstract. Blind beamforming has been studied extensively in recent times. Array signal processing is an effective technique for signal extraction in communication systems. We employ minimum entropy deconvolution (MED) principle for source extraction. Results are shown which indicate good performance in comparison with conventional adaptive algorithms like the constant modulus algorithm and the multi-modulus algorithm.

Keywords: Minimum entropy deconvolution, constant modulus algorithm, multi modulus algorithm, narrowband, adaptive beamforming.

1 Introduction

Adaptive antenna arrays find many applications including radar, sonar, and communication systems. Their ability to suppress co-channel interference while simultaneously capturing the desired signal and flexibility compared with fixed antenna are the main advantages that adaptive antenna arrays offer.

Blind adaptive beamforming (i.e., beamforming without the use of training signals) of multiple narrowband signals is equivalent to the blind source separation problem. Blind algorithms use *a priori* knowledge regarding the statistics of the transmitted data sequences as opposed to an exact set of symbols known to both transmitter and receiver. Our task is to design an array processor that will extract the desired signal blindly.

In this paper, we discuss minimum entropy deconvolution (MED) criteria and design of cost functions using MED. We also check the applicability of derived algorithms on array signal processing for desired source extraction and signal separation.

2 Problem Formulation

The received signal vector for the case of M independent signals $a_{n,i}$ arriving at N sensors in the presence of additive noise \mathbf{v}_n is given by

$$\mathbf{x}_n = \sum_{i=0}^{M-1} \mathbf{h}(\theta_i) a_{n,i} + \mathbf{v}_n, \quad n = 1, 2, 3, \dots \quad (1)$$

n is the time index, $a_{n,0}$ is the desired signal, and $a_{n,i}$ with $i = 1$ to $M - 1$ is interferences. We assume that source signals $a_{n,i}$ are sub-Gaussian, \mathbf{v}_n is an $M \times 1$ additive noise vector $\mathbf{v}_n = [v_{n,0}, v_{n,2}, \dots, v_{n,N-1}]$ and $\mathbf{h}(\theta_i)$ is steering vector at the direction of arrival (DOA); the θ_i defined as

$$\mathbf{h}(\theta_i) = [1, \exp(-jkd \sin(\theta_i)), \dots, \exp(-j(N-1)kd \sin(\theta_i))]^T \quad (2)$$

where d is antenna inter-element spacing, $k = 2\pi/\lambda$ is wave-number and λ is the wavelength and superscript T stands for transpose. The mixing matrix $\mathcal{H}(\theta)$ consists of all steering vectors $\mathcal{H}(\theta) = [\mathbf{h}(\theta_0), \mathbf{h}(\theta_1), \dots, \mathbf{h}(\theta_{M-1})]$ and is defined as

$$\mathcal{H}(\theta) = \begin{bmatrix} 1 & \dots & 1 \\ \exp(-jkd \sin(\theta_0)) & \dots & \exp(-jkd \sin(\theta_{M-1})) \\ \vdots & \vdots & \vdots \\ \exp(-j(N-1)kd \sin(\theta_0)) & \dots & \exp(-j(M-1)kd \sin(\theta_{M-1})) \end{bmatrix} \quad (3)$$

Using definition of $\mathcal{H}(\theta)$ and using narrowband input signal vector defined as $\mathbf{a}_n = [a_{n,0}, a_{n,1}, \dots, a_{n,M-1}]^T$ Eq. (II) can be rewritten as

$$\mathbf{x}_n = \mathcal{H}(\theta)\mathbf{a}_n + \mathbf{v}_n \quad (4)$$

If we denote beamformer weight vector $\mathbf{w}_n = [w_{n,1}, \dots, w_{n,N}]^T$ and signals induced on the antenna as $\mathbf{x}_n = [x_{n,1}, \dots, x_{n,N-1}]^T$ (at time index n) then the output of beamforming system is given as

$$y_n = \mathbf{w}_n^H \mathbf{x}_n \quad (5)$$

which captures one of the M impinging signals with superscript H being Hermitian transpose. In the rest of this paper, we will be using several key assumptions listed here

1. Signals \mathbf{a}_n take values from zero mean and symmetrical constellations.
2. Mixing matrix \mathcal{H} is full rank matrix ($N > M$) which implies all signals are separable.
3. \mathbf{v}_n is zero-mean, Gaussian distributed noise vector and is independent of \mathbf{a}_n

3 Existing Adaptive Beamforming Algorithms

3.1 The Constant Modulus Algorithm

The constant modulus algorithm (CMA), also known as the Godard algorithm, is a blind algorithm which forces output signal y_n to have a constant modulus. Introduced by Godard [1] as a blind equalization algorithm it was later used by Treichler and Agee [2] to suppress jamming and combat multipath fading on constant modulus signals such as FM and PSK. CMA for beamforming utilizes

the low modulus fluctuation exhibited by communication signals to extract them from array output. CMA algorithm minimizes the following cost function

$$J_{\text{cma}} = E\{|y_n|^p - R\}^q \quad (6)$$

where R is a dispersion constant defined as $E[|a^4|]/E[|a^2|]$, $|\cdot|$ denotes the modulus function and p and q are non-negative parameters and $E[\cdot]$ is the expected value. In this correspondence, we will focus on special case of $p = q = 2$. In practice we replace the true gradient of J_{cma} with an instantaneous gradient estimate resulting in following update equation

$$\mathbf{w}_{n+1} = \mathbf{w}_n + \mu y_n^*(R - |y_n|^2)\mathbf{x}_n \quad (7)$$

with μ being a small step size and superscript $*$ representing the conjugate operation. A CMA-based beamformer requires no special array geometry or the noise covariance matrix to adapt the array weights. As CMA's cost function doesn't contain any phase term so the output of CMA includes phase offset error so a rotator is required to recover the phase of the output signal.

3.2 The Multi-Modulus Algorithm

The cost function of MMA does utilize the dispersion of real and imaginary parts separately resulting as

$$J_{\text{mma}} = E[(y_{n,R}^2 - R_R^2)^2 + (y_{n,I}^2 - R_I^2)^2] \quad (8)$$

with the following algorithm

$$\mathbf{w}_{n+1} = \mathbf{w}_n + \mu [y_{n,R}(R_R - y_{n,R}^2) + j y_{n,I}(R_I - y_{n,I}^2)]^*\mathbf{x}_n \quad (9)$$

where $R_R = E[a_R^4]/E[a_R^2]$ and $R_I = E[a_I^4]/E[a_I^2]$ are dispersion constants of real and imaginary parts respectively. One advantage of MMA over CMA is its inherent ability to recover phase of the signal hence eliminating any need of phase compensator. Minimizing the cost function J_{mma} can also be interpreted as fitting the signal constellation onto a square.

4 Proposed Adaptive Beamforming Algorithm

4.1 Minimum Entropy Deconvolution Criterion

The minimum entropy deconvolution (MED) is probably the earliest principle for designing cost functions for blind beamforming. This principle was introduced by Wiggins in seismic data analysis in the year 1977, who sought to determine the inverse channel \mathbf{w}^\dagger that maximizes the *kurtosis* of the deconvolved data y_n , see [3,4]. For seismic data, which are super-Gaussian in nature, he suggested to maximize the following cost:

$$\frac{\frac{1}{B} \sum_{b=1}^B |y_{n-b+1}|^4}{\left(\frac{1}{B} \sum_{b=1}^B |y_{n-b+1}|^2\right)^2} \quad (10)$$

where B is the number of equalized samples. This deconvolution scheme seeks the smallest number of large spikes consistent with the data, thus maximizing the order or, equivalently, minimizing the entropy or disorder in the data, [5]. Note that the equation (10) has the statistical form of sample kurtosis and the expression is scale-invariant. Later, in the year 1979, Gray generalized the Wiggins' proposal with two degrees of freedom as follows, [6]:

$$J_{\text{med}}^{(p,q)} \equiv \frac{\frac{1}{B} \sum_{b=1}^B |y_{n-b+1}|^p}{\left(\frac{1}{B} \sum_{b=1}^B |y_{n-b+1}|^q\right)^{\frac{p}{q}}} \quad (11)$$

The criterion was rigorously investigated in [7], where Donoho developed general rules for designing MED-type estimators. Several cases of MED, in the context of blind deconvolution of seismic data, have appeared in the literature, like $J_{\text{med}}^{(2,1)}$ in [8], $J_{\text{med}}^{(4,2)}$ in [3], $\lim_{\varepsilon \rightarrow 0} J_{\text{med}}^{(p-\varepsilon,p)}$ in [9], $J_{\text{med}}^{(p,2)}$ in [10], and $J_{\text{med}}^{(2p,p)}$ in [11].

In the derivation of the criterion (11), it is assumed that the original signal a_n , which is primary reflection coefficients in geophysical system or transmitted data in communication systems, can be modeled as realization of independent non-Gaussian process with distribution

$$p_{\mathcal{A}}(a; \alpha) = \frac{\alpha}{2\beta\Gamma(\frac{1}{\alpha})} \exp\left(-\frac{|a|^\alpha}{\beta}\right) \quad (12)$$

where signal a_n is real-valued, α is the shape parameter, β is the scale parameter, and $\Gamma(\cdot)$ is the Gamma function.

4.2 Designing Blind Cost Functions

We employ MED principle and use the probability density functions of transmitted amplitude-phase shift-keying (APSK) and noisy received signal to design a cost function for blind beamforming. Consider a continuous APSK signal, where signal alphabets $\{a_R + ja_I\} \in \mathcal{A}$ are assumed to be uniformly distributed over a circular region of radius R_a and center at the origin (refer to Fig. 1(a)). The joint PDF of a_R and a_I is given by (refer to Fig. 1(b))

$$p_{\mathcal{A}}(a_R + ja_I) = \begin{cases} \frac{1}{\pi R_a^2}, & \sqrt{a_R^2 + a_I^2} \leq R_a, \\ 0, & \text{otherwise.} \end{cases} \quad (13)$$

Now consider the transformation $\mathcal{Y} = \sqrt{a_R^2 + a_I^2}$ and $\Theta = \angle(a_R, a_I)$, where \mathcal{Y} is the modulus and $\angle(\cdot)$ denotes the angle in the range $(0, 2\pi)$ that is defined by the point (i, j) . The joint distribution of the modulus \mathcal{Y} and Θ can be obtained as $p_{\mathcal{Y},\Theta}(\tilde{y}, \tilde{\theta}) = \tilde{y}/(\pi R_a^2)$, $\tilde{y} \geq 0$, $0 \leq \tilde{\theta} < 2\pi$. Since \mathcal{Y} and Θ are independent, we obtain a triangular distribution for \mathcal{Y} given by $p_{\mathcal{Y}}(\tilde{y} : H_0) = 2\tilde{y}/R_a^2$, $\tilde{y} \geq 0$, where H_0 denotes the hypothesis that signal is distortion-free where $\tilde{y}, \tilde{\theta}$ are real variables and \mathcal{Y}, Θ are random variables.

Let $\mathcal{Y}_n, \mathcal{Y}_{n-1}, \dots, \mathcal{Y}_{n-N+1}$ be a sequence, of size N , obtained by taking modulus of randomly generated distortion-free signal alphabets \mathcal{A} , where subscript n indicates discrete time index. Let $\mathcal{Z}_1, \mathcal{Z}_2, \dots, \mathcal{Z}_N$ be the order statistic of sequence $\{\mathcal{Y}\}$. Let $p_{\mathcal{Y}}(\tilde{y}_n, \tilde{y}_{n-1}, \dots, \tilde{y}_{n-N+1} : H_0)$ be an N -variate density of the continuous type, then, under the hypothesis H_0 , we obtain

$$p_{\mathcal{Y}}(\tilde{y}_n, \tilde{y}_{n-1}, \dots, \tilde{y}_{n-N+1} : H_0) = \frac{2^N}{R_a^{2N}} \prod_{k=1}^N \tilde{y}_{n-k+1}. \quad (14)$$

Next we find $p_{\mathcal{Y}}^*(\tilde{y}_n, \tilde{y}_{n-1}, \dots, \tilde{y}_{n-N+1} : H_0)$ as follows:

$$\begin{aligned} p_{\mathcal{Y}}^*(\tilde{y}_n, \dots, \tilde{y}_{n-N+1} : H_0) &= \int_0^\infty p_{\mathcal{Y}}(\lambda \tilde{y}_n, \dots, \lambda \tilde{y}_{n-N+1} : H_0) \lambda^{N-1} d\lambda \\ &= \frac{2^N}{R_a^{2N}} \prod_{k=1}^N \tilde{y}_{n-k+1} \int_0^{Ra/\tilde{z}_N} \lambda^{2N-1} d\lambda \\ &= \frac{2^{N-1}}{N (\tilde{z}_N)^{2N}} \prod_{k=1}^N \tilde{y}_{n-k+1}, \end{aligned} \quad (15)$$

where $\tilde{z}_1, \tilde{z}_2, \dots, \tilde{z}_N$ are the order statistic of elements $\tilde{y}_n, \tilde{y}_{n-1}, \dots, \tilde{y}_{n-N+1}$, so that $z_1 = \min\{\tilde{y}\}$ and $z_N = \max\{\tilde{y}\}$. Now consider the next hypothesis (H_1) that signals mix with each other as well as with additive Gaussian noise (refer to Fig. III(c)). Due to which, the in-phase and quadrature components of the received signal are modeled as normal distributed; owing to central limit theorem, it is theoretically justified. It means that the modulus of the received signal follows Rayleigh distribution,

$$p_{\mathcal{Y}}(\tilde{y} : H_1) = \frac{\tilde{y}}{\sigma_{\tilde{y}}^2} \exp\left(-\frac{\tilde{y}^2}{2\sigma_{\tilde{y}}^2}\right), \quad \tilde{y} \geq 0, \sigma_{\tilde{y}} > 0. \quad (16)$$

The N -variate densities $p_{\mathcal{Y}}(\tilde{y}_n, \dots, \tilde{y}_{n-N+1} : H_1)$ and $p_{\mathcal{Y}}^*(\tilde{y}_n, \dots, \tilde{y}_{n-N+1} : H_1)$ are obtained as

$$p_{\mathcal{Y}}(\tilde{y}_n, \tilde{y}_{n-1}, \dots, \tilde{y}_{n-N+1} : H_1) = \frac{1}{\sigma_{\tilde{y}}^{2N}} \prod_{k=1}^N \tilde{y}_{n-k+1} \exp\left(-\frac{\tilde{y}_{n-k+1}^2}{2\sigma_{\tilde{y}}^2}\right) \quad (17)$$

$$\begin{aligned} p_{\mathcal{Y}}^*(\tilde{y}_n, \tilde{y}_{n-1}, \dots, \tilde{y}_{n-N+1} : H_1) &= \frac{\prod_{k=1}^N \tilde{y}_{n-k+1}}{\sigma_{\tilde{y}}^{2N}} \int_0^\infty \exp\left(-\frac{\lambda^2 \sum_{k'=1}^N \tilde{y}_{n-k'+1}^2}{2\sigma_{\tilde{y}}^2}\right) \lambda^{2N-1} d\lambda \\ &= \frac{\prod_{k=1}^N \tilde{y}_{n-k+1}}{\sigma_{\tilde{y}}^{2N}} \int_0^\infty \exp\left(-\frac{\lambda^2 \sum_{k'=1}^N \tilde{y}_{n-k'+1}^2}{2\sigma_{\tilde{y}}^2}\right) \lambda^{2N-1} d\lambda \end{aligned} \quad (18)$$

Substituting $u = \frac{1}{2} \lambda^2 \sigma_{\tilde{y}}^{-2} \sum_{k'=1}^N \tilde{y}_{n-k'+1}^2$, we obtain

$$p_{\mathcal{Y}}^*(\tilde{y}_n, \tilde{y}_{n-1}, \dots, \tilde{y}_{n-N+1} : H_1) = \frac{2^{N-1} \Gamma(N)}{\left(\sum_{k=1}^N \tilde{y}_{n-k+1}^2\right)^N} \prod_{k=1}^N \tilde{y}_{n-k+1} \quad (19)$$

The scale-invariant uniformly most powerful test of $p_{\mathbf{y}}^*(\tilde{y}_n, \dots, \tilde{y}_{n-N+1} : H_0)$ against $p_{\mathbf{y}}^*(\tilde{y}_n, \dots, \tilde{y}_{n-N+1} : H_1)$ provides us, see [12]:

$$O(\tilde{y}_n) = \frac{p_{\mathbf{y}}^*(\tilde{y}_n, \tilde{y}_{n-1}, \dots, \tilde{y}_{n-N+1} : H_0)}{p_{\mathbf{y}}^*(\tilde{y}_n, \tilde{y}_{n-1}, \dots, \tilde{y}_{n-N+1} : H_1)} = \frac{1}{N!} \left[\frac{\sum_{k=1}^N \tilde{y}_{n-k+1}^2}{\tilde{z}_N^2} \right]^N \underset{H_1}{\overset{H_0}{\geq}} C \quad (20)$$

where $C > 0$ is a threshold. Assuming $N \gg 1$, we obtain $\frac{1}{N} \sum_{k=1}^N \tilde{y}_{n-k+1}^2 \approx \mathbb{E} [|y_n|^2]$. It helps obtaining a statistical cost for the blind beamforming of APSK signal as follows:

$$\mathbf{w}^\dagger = \arg \max_{\mathbf{w}} \frac{\mathbb{E} [|y_n|^2]}{(\max \{|y_n|\})^2} \quad (21)$$

Based on the previous discussion, maximizing cost (21) can be interpreted as determining the weight vector coefficients, \mathbf{w} , which drives the distribution of its output, y_n , away from Gaussian distribution toward uniform, thus removing successfully the interference from the received APSK signal.

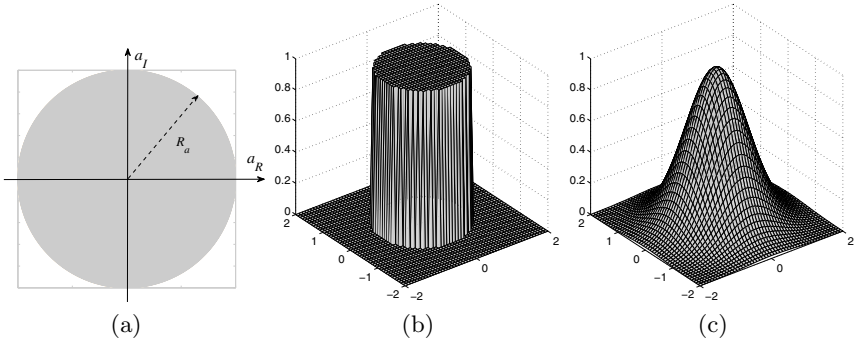


Fig. 1. (a) APSK, (b) PDF of continuous APSK and (c) Gaussian PDF

5 Adaptive Optimization of the Proposed Cost

For a stochastic gradient-based adaptive implementation of the equation

$$\mathbf{w}^\dagger = \arg \max_{\mathbf{w}} \mathbb{E} [|y_n|^2] \quad \text{s.t.} \quad \max \{|y_n|\} \leq R_a. \quad (22)$$

we need to modify it to involve a *differentiable* constraint; one of the possibilities is

$$\mathbf{w}^\dagger = \arg \max_{\mathbf{w}} \mathbb{E} [|y_n|^2] \quad \text{s.t.} \quad \text{fmax}(R_a, |y_n|) = R_a, \quad (23)$$

where we have used the following identity (below $a, b \in \mathbb{C}$):

$$\text{fmax}(|a|, |b|) \equiv \frac{|a| + |b| + ||a| - |b||}{2} = \begin{cases} |a|, & \text{if } |a| \geq |b| \\ |b|, & \text{otherwise.} \end{cases} \quad (24)$$

The function fmax is differentiable, *viz*

$$\frac{\partial \text{fmax}(|a|, |b|)}{\partial a^*} = \frac{a(1 + \text{sgn}(|a| - |b|))}{4|a|} = \begin{cases} a/(2|a|), & \text{if } |a| > |b| \\ 0, & \text{if } |a| < |b| \end{cases} \quad (25)$$

If $|y_n| < R_a$, then the cost (23) simply maximizes output energy. However, if $|y_n| > R_a$, then the constraint is violated and the new update \mathbf{w}_{n+1} is required to be computed such that the magnitude of *a posteriori* output $\mathbf{w}_{n+1}^H \mathbf{x}_n$ becomes smaller than or equal to R_a . In [13], authors have shown how to optimize (23). They obtained the following algorithm:

$$\begin{aligned} \mathbf{w}_{n+1} &= \mathbf{w}_n + \mu \text{f}(y_n) y_n^* \mathbf{x}_n, \\ \text{f}(y_n) &= \begin{cases} 1, & \text{if } |y_n| \leq R_a \\ -\beta, & \text{if } |y_n| > R_a. \end{cases} \end{aligned} \quad (26)$$

where $\beta = 2MM_L/(P_a R_a^2) - 1$. Note that M denotes total number of signal alphabets, M_L denotes number of alphabets on the modulus R_a and P_a denotes average signal energy. The algorithm (26) is termed as β CMA.

Now we show that how to obtain an adaptive blind beamforming algorithm for a square-QAM signal. Note that the in-phase and the quadrature components of a square-QAM are statistically independent of each other. Exploiting this independence and applying MED principle, we obtain the following cost function:

$$\max_{\mathbf{w}} \mathbb{E} \left[|y_n|^2 \right], \text{ s.t. } \max \{|y_{R,n}\} = \max \{|y_{I,n}\} \leq R. \quad (27)$$

where $R = \max \{|a_{R,n}\} = \max \{|a_{I,n}\}$. Optimization of (27), yields [14]:

$$\begin{aligned} \mathbf{w}_{n+1} &= \mathbf{w}_n + \mu (\text{f}_R y_{R,n} + j \text{f}_I y_{I,n})^* \mathbf{x}_n \\ \text{f}_L &= \begin{cases} 1, & \text{if } |y_{L,n}| \leq R \\ -\beta, & \text{if } |y_{L,n}| > R \end{cases} \end{aligned} \quad (28)$$

where $\beta = (R^2 + 2)/(3R)$. The algorithm (28) is termed as β MMA [28]

6 Simulation Results

We measure the performance of proposed schemes using output signal-to-interference-plus-noise ratio (SINR) defined as

$$\text{SINR}_k = \frac{\mathbf{w}_n^H \mathbf{h}(\theta_k) \sigma_k^2 \mathbf{h}(\theta_k)^H \mathbf{w}_n}{\mathbf{w}_n^H \mathbf{R}_k \mathbf{w}_n} \quad (29)$$

¹ Note that the algorithms (26) and (28) appeared recently in [13] and [14] in the context of adaptive channel equalization. However, here in this work, our treatment differs in two ways: firstly we provide detailed derivation of costs which is missing in [13] and [14], and secondly we employ the algorithms to solve beamforming problem.

where $\mathbf{h}(\theta_k)$ is the steering vector for k^{th} source, σ_k^2 is the average energy of k^{th} source signal and \mathbf{R}_k is the true auto-correlation matrix of interferences.

$$\mathbf{R}_k = \sum_{i \neq k} \sigma_i^2 \mathbf{h}(\theta_i) \mathbf{h}^H(\theta_i) + \sigma_v^2 \mathbf{I} \quad (30)$$

where σ_i^2 is average energy of i^{th} signal and σ_v^2 is average noise energy.

As βCMA is designed specifically for the beamforming of APSK signals so three independent APSK signal sources are considered for comparison between βCMA and CMA. These signals are impinging on an antenna array with 9 sensors each separated by half wavelength. Two interfering signals, 16.APSK(8,8) and 16.APSK(4,12), both having signal-to-interference ratio (SIR) = 10dB are mixed with the desired signal (32.APSK). The channel model used is additive white Gaussian noise (AWGN) with signal-to-noise ratio (SNR) = 30dB and step sizes are chosen such that the convergence rate is maintained same for βCMA and CMA. All three test signals are depicted in Fig. 2. Now consider that the three

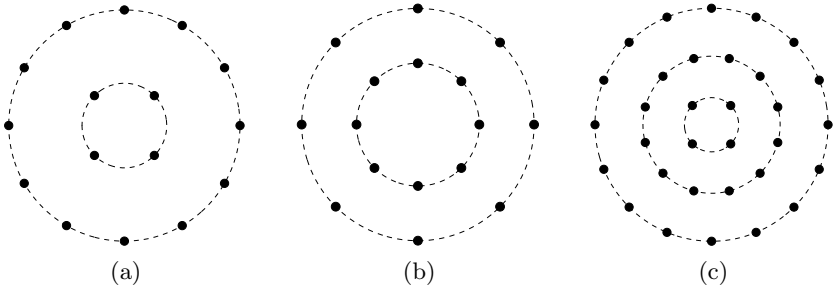


Fig. 2. APSK signals

signals, 16.APSK(8,8), 16.APSK(4,12) and 32.APSK, are arriving at the sensors at angles $\theta_0 = 5^\circ$, $\theta_1 = 50^\circ$ and $\theta_2 = -40^\circ$, respectively. The beamformer spatial magnitude responses versus incident angles (for βCMA) is depicted in Fig. 3(a). We clearly note that the beamformer implementing βCMA has placed nulls successfully at $\theta_0 = 5^\circ$ and $\theta_1 = 50^\circ$ and extracted the desired one at $\theta_2 = -40^\circ$. The algorithm works without any supervision or any knowledge about angles of desired and interfering signals apart from some statistical information in the form of constants e.g. R and β . The extracted signals are also depicted in Fig. 3(b) (top) for both CMA and βCMA . The constellation of βCMA beamformer is more aggregated than that of CMA. The SINR plot of βCMA exhibits higher steady-state floor than CMA. In short, the βCMA simply outperformed the traditional CMA.

Now we consider QAM signals to compare the performances of βMMA and traditional MMA as the algorithm βMMA is designed to perform better for QAM constellations. Consider three signals, 4QAM, 16.QAM and 64.QAM as shown in Fig. 4 arriving at the sensors at angles $\theta_0 = 0^\circ$, $\theta_1 = 45^\circ$ and $\theta_2 = -45^\circ$,

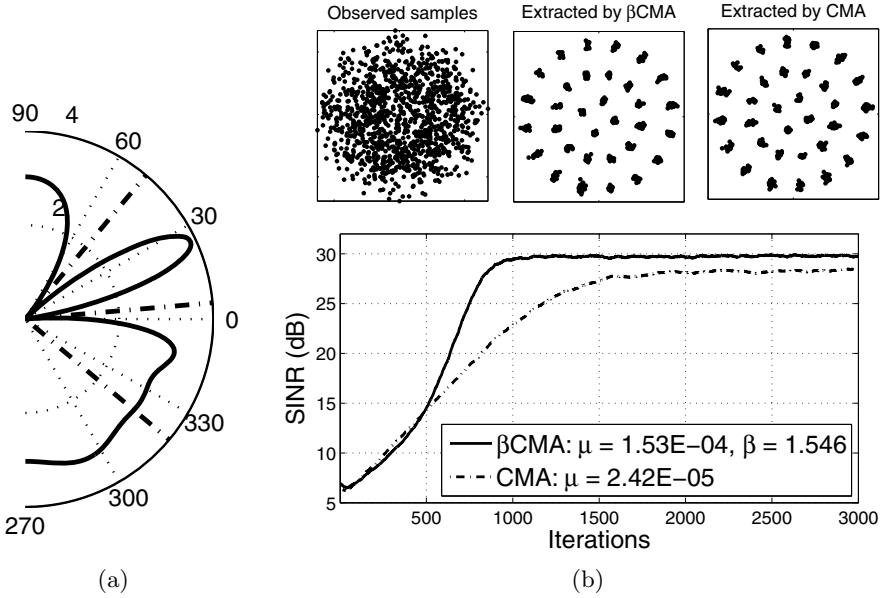


Fig. 3. Simulation results with APSK signals

respectively. The signal of interest is 16.QAM. The SNR and SINR have the same values as we considered in last experiment and step sizes are chosen such that the convergence rate is same for β MMA and MMA. The beamformer spatial magnitude responses versus incident angles (for β MMA) is depicted in Fig. 5(a). We clearly note that two nulls have been placed successfully and blindly at $\theta_0 = 0^\circ$ and $\theta_1 = -45^\circ$. The extracted signals are also depicted in Fig. 5(b) (top) for both MMA and β MMA. The constellation of β MMA beamformer is more aggregated than that of MMA. The SINR plot of β MMA exhibits higher steady-state floor than MMA. In short, the β MMA simply outperformed the traditional MMA.

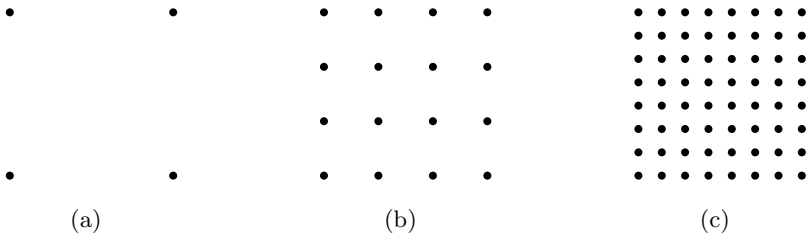


Fig. 4. QAM signals

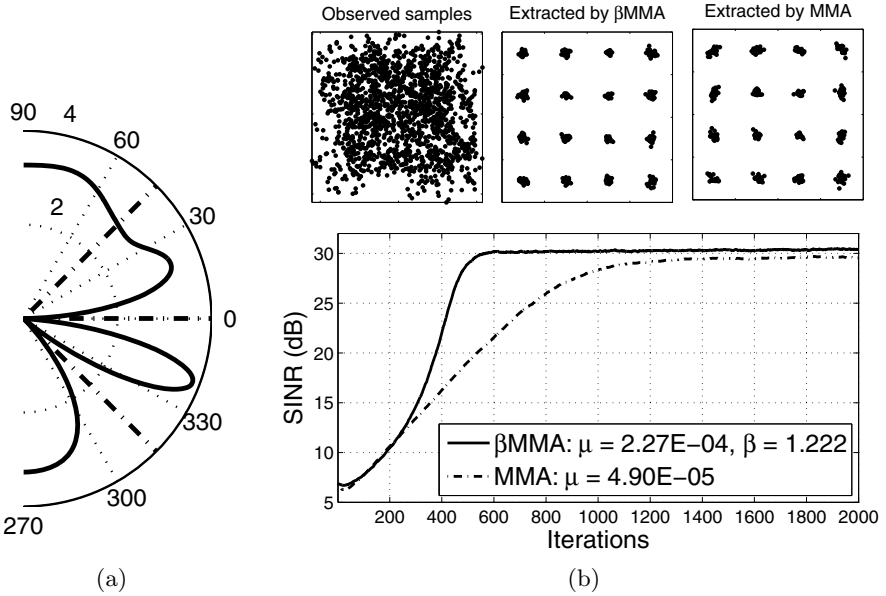


Fig. 5. Simulation results with QAM signals

7 Conclusion

In this paper, we describe adaptive blind beamforming in the context of spatial filtering systems. The key challenge of adaptive blind beamforming lies in the design of special cost functions whose minimization or maximization result in the removal of interference. We have discussed the minimum entropy deconvolution criteria. Based on minimum entropy deconvolution principle, the idea of designing specific cost function for the blind recovery of a given transmitted signal is described in detail. We have presented case studies of amplitude-phase shift-keying (APSK) and square quadrature amplitude modulation (QAM) signals for which respective cost functions are derived and corresponding adaptive algorithms are obtained. The blind adaptation of the derived algorithms are shown to possess better signal-to-interference-plus-noise ratio (SINR) characteristics compared to the existing algorithms.

References

1. Godard, D.N.: Self-recovering equalization and carrier tracking in two-dimensional data communications systems. *IEEE Trans. Commun.* 28(11), 1867–1875 (1980)
2. Treichler, J.R., Agee, B.G.: A new approach to multipath correction of constant modulus signals. *IEEE Trans. Acoust. Speech Signal Processing* 31(2), 459–471 (1983)
3. Wiggins, R.A.: Minimum entropy deconvolution. In: *Proc. Int. Symp. Computer Aided Seismic Analysis and Discrimination* (1977)

4. Wiggins, R.A.: Minimum entropy deconvolution. *Geoexploration* 16, 21–35 (1978)
5. Walden, A.T.: Non-Gaussian reflectivity, entropy, and deconvolution. *Geophysics* 50(12), 2862–2888 (1985)
6. Gray, W.: Variable Norm Deconvolution. PhD thesis, Stanford Univ. (1979)
7. Donoho, D.: On minimum entropy deconvolution. In: *Proc. 2nd Applied Time Series Symp.*, pp. 565–608 (March 1980)
8. Ooe, M., Ulrych, T.J.: Minimum entropy deconvolution with an exponential transformation. *Geophysical Prospecting* 27, 458–473 (1979)
9. Claerbout, J.F.: Parsimonious deconvolution (September 13, 1977)
10. Gray, W.: Variable norm deconvolution (September 14, 1978)
11. Gray, W.: A theory for variable norm deconvolution (September 15, 1979)
12. Sidak, Z., Sen, P.K., Hajek, J.: *Theory of Rank Tests*, 2nd edn. Academic Press (1999)
13. Abrar, S., Nandi, A.K.: Adaptive minimum entropy equalization algorithm. *IEEE Commun. Lett.* 14(10), 966–968 (2010)
14. Abrar, S., Nandi, A.K.: Adaptive solution for blind equalization and carrier-phase recovery of square-QAM. *IEEE Sig. Processing Lett.* 17(9), 791–794 (2010)

Gender Classification Using Local Binary Pattern and Particle Swarm Optimization

Sajid Ali Khan¹, Muhammad Nazir², Naveed Riaz¹,
M. Hussain¹, and Nawazish Naveed²

¹ Shaheed Zulfikar Ali Bhutto Institute of Science and Technology,
Islamabad, Pakistan

² UIIT-PMAS University of Arid Agriculture,
Rawalpindi, Pakistan

mohdnz@uaar.edu.pk, n.r.ansari@szabist-isb.edu.pk,
{Sajidalibn,mhussainwazir,nawazishnaveed}@gmail.com

Abstract. Gender classification is the phenomena in which a face image is analyzed and recognized by a computer. Feature extraction is the key step of gender classification. In this paper, we present a method which efficiently classifies gender by extracting the key optimized features. We have used Local Binary Pattern (LBP) to extract facial features. As LBP features contain many redundant features, Particle Swarm Optimization (PSO) was applied to get optimized features. We performed different numbers of experiments on FERET face database and report 95.5 % accuracy.

Keywords: Gender classification, Feature extraction, LBP, PSO, FERET.

1 Introduction

In today's Technological world, gender classification is an important task. The performance of many world-wide range applications such as surveillance, human computer-interaction and authentication can be enhanced through gender classification. The feature extraction process is dependent on either appearance-based method or geometric-based method. In appearance-based method, features can be extracted from the whole face image while in geometric-based approach features are extracted from different face points.

Makinen and Raisamo [1] combined Local Binary Pattern (LBP) with Support Vector Machine (SVM). They first divided the image into 8 *8 blocks and performed filtration on each block using LBP. The resultant vector was used as input to the SVM. Jabid et al. [2] divided the face image into small parts and then Local Directional Pattern (LDP) was applied to extracted features. They have used SVM for classification purpose. Experiments were performed on FERET database and they reported 95.05 % accuracy rate. Xu et al. [3] presented hybrid approach. They represented appearance-based features by Haar wavelet and extracted 31403 geometric-features using Active Appearance Model (AAM).

Generally Gender classification consists of the following steps. Figure 1 depicts these steps.

- **Preprocessing:** Every face database needs some preprocessing, like normalization of illumination and face detection etc.
- **Feature Extraction:** After performing preprocessing we need to extract face features. Generally two types of features are extracted. Geometric based features and appearance based features.
- **Classification:** Classification is the last step of gender classification in which the face is successfully classified as that of a male or female. For this purpose different types of classifiers are used. e.g. KNN, NN, and SVM.

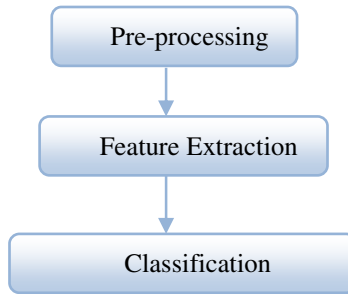


Fig. 1. Steps involved in Gender classification

In this paper, we improve the performance and accuracy rate of gender classification remarkably. First the image is divided into different regions and then LBP histogram (Features) is calculated for each region. To get optimized features which more clearly represent gender face, the LBP features are passed to Particle Swarm Optimization (PSO). PSO evaluates the features and provides results in the form of optimized features. Support Vector Machine (SVM) classifier is trained and tested by these optimized face features. Figure 2 shows the FERET dataset.



Fig. 2. FERET faces dataset

2 System Overview

These are the steps of our proposed algorithm.

- 1) Facial features extraction using LBP.
- 2) Optimize feature selection using PSO.
- 3) Training and testing using SVM classifier.

Figure 3 shows our proposed system architecture.

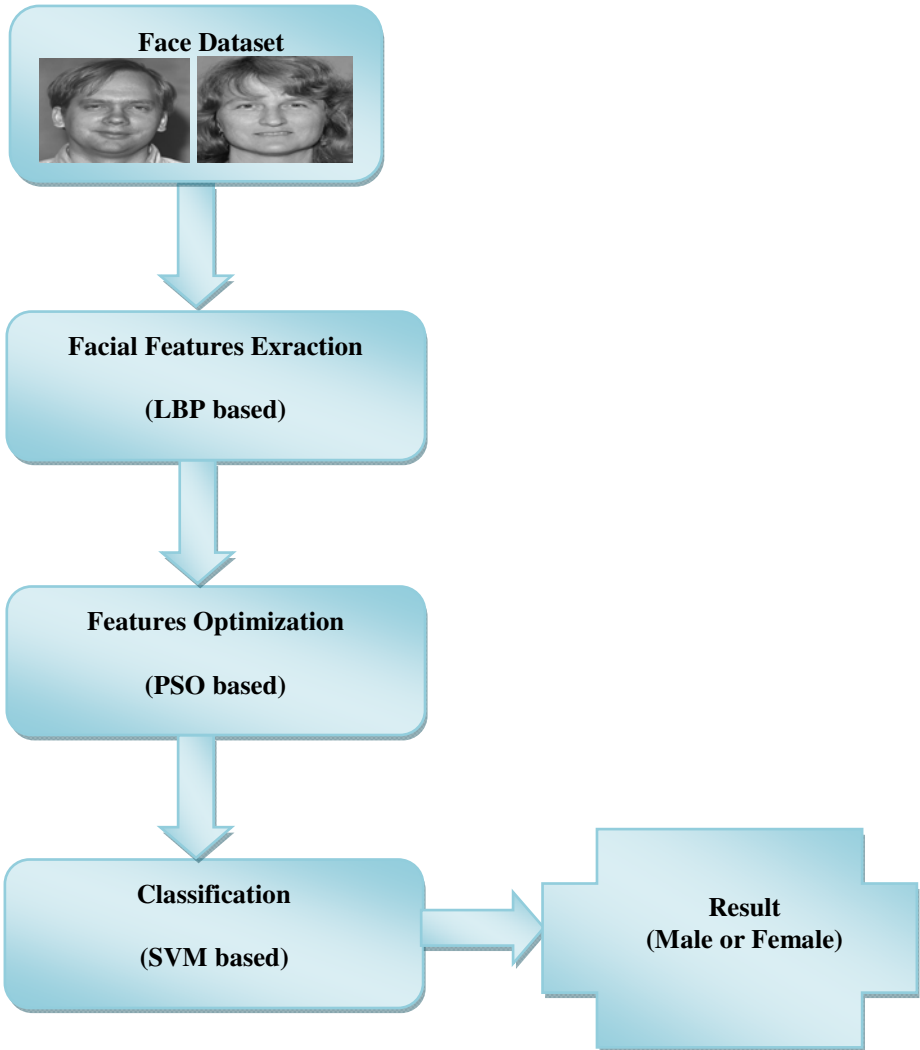


Fig. 3. Proposed Technique Architecture

2.1 Feature Extraction

The LBP operator was proposed by Ojala [4] et al. As depicted in figure 4 selecting one pixel as center, the neighborhood pixels are converted to 0 if their gray levels are smaller than that of the center or to 1 in other case. The center pixel is denoted with the binary code of its neighbor as 00100011.

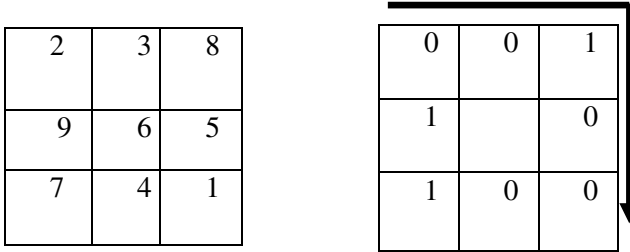


Fig. 4. LBP operator

We calculated the histogram of LBP code which represent facial feature. We divide the image into M by N squares shown in figure 5. The histogram (features) of each sub region contains information like edge change, existence of special points etc.



Fig. 5. Image segmentation

2.2 Optimize Feature Selection

Particle Swarm Optimization (PSO) is an evolutionary technique proposed by Kennedy [5] in 1995. This technique is best for optimization problems. As it is a new technique, many researchers are consistently trying to improve the performance of PSO. PSO is a population based optimization method. The algorithm simulates the

behavior of bird flock flying together in multi dimensional space in search of some optimum place, adjusting their movements and distances for better search. PSO is very similar to evolutionary computation such as genetic algorithm (GA). The swarms are randomly initialized and then searched for an optimum by updating generations. Each swarm is known as particle. Each particle maintains its two positions 'local best' and 'global best'. Each particle has its own velocity as well. Following equations are used to update the position and velocity of the particle.

$$V_i(t + 1) = V_i(t) + C_1 * r_1(P_{best} - n_i(b)) + C_2 * r_2(g_{best} - x_{ij}(t)) \quad (1)$$

$$X_i(t + 1) = X_i(t) + V_i(t + 1) \quad (2)$$

In equation 1, $V_i(t)$ is the velocity of particle at time t . C_1 and C_2 are positive acceleration constants, r_1 and r_2 are random values in $[0,1]$ range. P_{best} is the local best particle p . $N_i(b)$ is the previous location of particle in binary pso. $X_{ij}(t)$ is the position of i^{th} prticle at time t in direction j . Equation 2, $X_i(t)$ is the position of particle i in the search space at time t , then the position of the particle is changed by adding the velocity $v_i(t)$ to the current position.

Binary PSO

Binary PSO was developed by Kennedy and Eberhart [6]. In binary PSO a particle can move in the search space by flipping the different bit so the velocity can be described by the number of bits changed per iteration. In binary PSO the particle position is 0 or one rather than real values.

$$X_i(t + 1) = \begin{cases} 1 & \text{if } N_3 < \frac{1}{1+e^{-v_i}}(t + 1) \\ 0 & \text{otherwise} \end{cases} \quad (3)$$

Here V_i is velocity, X_i is position and N is random factor $[0,1]$ interval. Equation 3 is the binary activation function for the X_i position weather the position of particle should be updated or not.

We take 100 particles and with each particle, the feature vector is associated. On every iteration, BPSO OFF (eliminate) some of features and ON (optimize features) the rest. For the next step these optimize features are use. These features are then passed to SVM which produce the accuracy rate. For every particle this is experimented and thus we get the more accurate (optimize) features.

2.3 Classification

SVM [7] is supervised learning method that recognizes patterns. The SVM takes input data and constitutes it with classes. More formally support vector machine classifies two classes by drawing hyper plan between them. SVM classifies linear and non linear data. We give input (optimize features) to SVM and SVM finds its accuracy. We perform this step again and again (on different No. of features) based on the particles in order to get the highest accuracy.

3 Experiment Results and Discussion

We implemented our proposed method in MATLAB 2009a. We have used FERET [8] database face images, which contains 11338 images. Experiment is performed on 500 frontal face images. We critically evaluate the performance of different Gender classification techniques that are in practice.

The image is re-sized and histogram equalization is performed to minimize the illumination effect. Input image is divided into different regions and then LBP Histogram (features) is calculated for each region. These features are then passed to PSO which results in optimize feature which clearly represents face image.

LBP resultant features (No. of features is 7) are passed to PSO which provides optimize features (five features) and eliminate irrelevant features (2 features). These features are then passed to SVM which gives 95.5 % accuracy rate. PSO is used on different no. of features (7, 10, 15, 20) and gets different no. of optimize features (5, 7, 10, 15). We also evaluate optimize features through different state-of-art Linear and Non-Linear classifiers. Linear classifier accuracy of different number of features is shown in figure 6 and results of Non Linear classifiers are shown in figure 7.

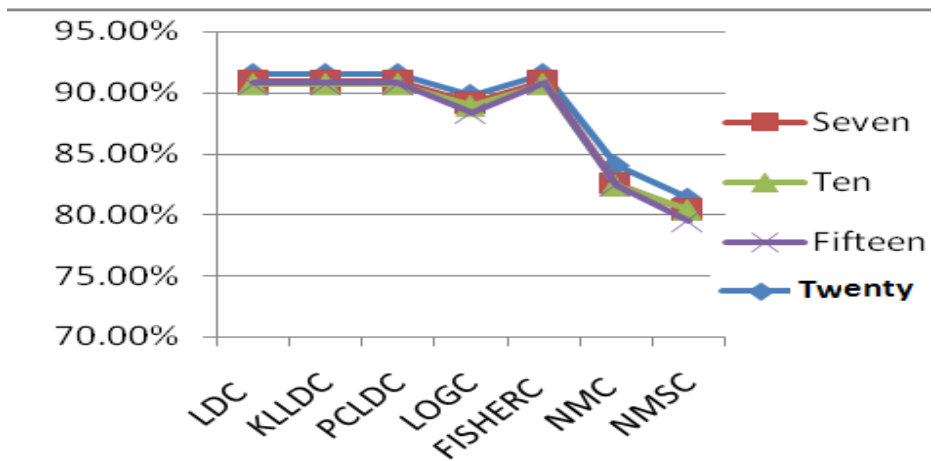


Fig. 6. Comparison of Linear classifier Accuracy with proposed method with different no. of features

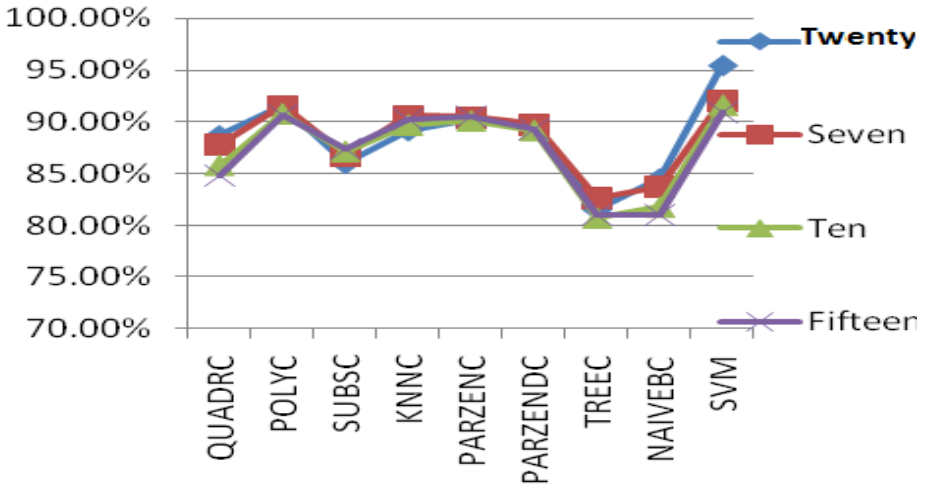


Fig. 7. Comparison of Non-Linear classifier Accuracy with proposed method with different no. of features

As compared to other classifier results (Linear and Non Linear type), our PSO based optimized technique provides 94.5% accuracy. In table 1 our proposed method is compared with [1], [10] and [11]. Compared to other methods our technique is performing well on a very limited no of features.

Table 1. Comparison Of techniques with our proposed technique

Methods		Accuracy
Proposed		95.5%
Makinen et al. [1]	NN	66.94 %
	SVM	76.71%
	LBP+SVM	71.33%
	LUT Adaboost	75.58%
Rai et al. [9]	Randon+Wavelet	90.00%
Jain et al. [10]	ICA+LDA	93.33%

4 Conclusion and Future Work

In this paper, Gender classification problem has been addressed. After performing experiments, we have observed that high accuracy can be obtained by passing LBP and PSO based features to SVM. Experiments were performed on different number of features. The experiments with the FERET face database underpins new insight

into gender recognition with various techniques and various conditions. Our future work will concentrate on exploring and identifying gender from face images having different poses.

References

1. Makinen, E., Raisamo, R.: An Experiment comparison of gender classification methods. *Pattern Recognition*, 1544–1556 (2008)
2. Jabid, T., Hasanul, K.: A hybrid approach to gender classification from face images. In: *IEEE International Conference on Pattern Recognition*, pp. 2162–2165 (2010)
3. Xu, Z., Lu, L.: An Experiment comparison of gender classification methods. In: *IEEE International Conference on Pattern Recognition*, pp. 1–4 (2008)
4. Ojala, T., Pietikinen, M., Harwood, D.: A Comparative study of texture measures with classification based on featured distributions. *Pattern Recognition*, 51–59 (1996)
5. Kennedy, J., Eberhart, R.: Particle Swarm Optimization. In: *IEEE International Conference on Neural Networks*, pp. 1942–1948 (1995)
6. Kennedy, J., Eberhart, R.: A discrete Binary version of the Particle swarm Algorithm. In: *IEEE International Conference on System, Man and Cybernetics*, pp. 4104–4108 (1997)
7. Support Vector Machine, <http://www.wikipedia.org>
8. FERET face database, <http://www.nist.gov/humanid/faret/>
9. Rai, P., Khanna, P.: Gender classification using Randon and Wavelet Transform. In: *5th IEEE International Conference on Industrial and Information System* (2010)
10. Jain, A., Huang, J., Fang, S.: Gender classification using frontal facial images. In: *IEEE International Conference on Pattern Recognition*, pp. 1–4 (2010)

Parametric Study of Nonlinear Adaptive Cruise Control Vehicle Model by Vehicle Mass

Zeeshan Ali* and Dur Muhammad Pathan

Department of Mechanical Engineering, Mehran University of Engineering and Technology,
Jamshoro, Sindh, Pakistan
engsam68@yahoo.com

Abstract. A parametric study of a vehicle following control law, based on the model predictive control method, to perform the transition maneuvers for a nonlinear adaptive cruise control vehicle is presented in this paper. The vehicle dynamic model is based on the continuous-time domain and simulates the real dynamics of the sub-vehicle models for steady-state and transient operations. The nonlinear vehicle has been analyzed for different masses of the vehicle and the simulation results show that the proposed model predictive controller can be used for a wide range of adaptive cruise control vehicles and can execute the transition maneuver successfully in the presence of complex dynamics within the constraint boundaries.

Keywords: Adaptive Cruise Control, Collision Avoidance, Vehicle Control, Model Predictive Control, Acceleration Tracking.

1 Introduction

A standard cruise control system enables a ground vehicle to control its speed. Adaptive Cruise Control (ACC) systems have been developed as an enhancement to the standard cruise control systems. In addition to the speed control mode, an ACC system equipped vehicle can also regulate the set speed to maintain a specified inter-vehicle distance (SIVD) from a preceding vehicle. This additional feature is termed as vehicle following mode.

An application of model predictive control (MPC) techniques to the longitudinal dynamics of a vehicle equipped with an ACC system is presented to address vehicle control. The control law for the vehicle following mode is computed using onboard radar sensors that measure the range (relative distance) and the range-rate (relative velocity) between the ACC vehicle and the preceding vehicle [1]. Both throttle input and brake input are required to control the distance and the relative velocity between an ACC vehicle and a preceding vehicle [2]. In the vehicle following mode the SIVD is the function of the preceding vehicle's velocity [1].

The vehicle models, presented in literature, range from the simple vehicle model [1, 3], which does not take into account the engine and drive-train dynamics, to the nonlinear vehicle models. The input to the simple ACC vehicle model is the control

* Corresponding author.

signal computed by the upper-level controller. Simple ACC vehicle models have been designed in the previous studies to analyze the performance of the upper-level controller. In the case of a nonlinear vehicle model, the desired acceleration commands obtained from the upper-level controller are given to the lower-level controller which then computes the required throttle and brake commands for the nonlinear vehicle model to track the desired acceleration commands. In the literature, various control algorithms have been developed for the upper-level controller, namely, proportional-integral-derivative (PID) control [4, 5], sliding mode control [6-11], constant-time-gap (CTG) [1, 3], and model predictive control (MPC) [1, 12-15].

The dynamic response of the ACC vehicle can be greatly influenced by variation in the mass of the vehicle. For example, various numbers of passengers, different sizes of engines, different models, etc can vary the inertia of a vehicle. This can possibly affect the controller performance and in turn affect the ACC vehicle performance. Therefore, it is essential to investigate the ACC vehicle’s response for different values of mass. The development of the overall system model includes the following stages of activity: vehicle modeling, controllers modeling, and their interaction.

2 Two-Vehicle System Model

A two-vehicle system is considered which consists of a preceding vehicle and an ACC vehicle, see Fig. 1. The preceding vehicle travels independently, whereas, the ACC vehicle maintains a longitudinal distance from the preceding vehicle.

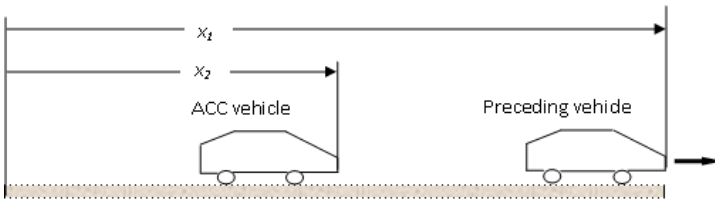


Fig. 1. A two-vehicle system

The longitudinal control of the ACC vehicle consists of two separate controllers. The upper-level controller computes the desired acceleration commands for the lower-level controller and the lower-level controller uses these desired acceleration commands to generate the required throttle and braking commands for the nonlinear ACC vehicle to track the spacing-control laws computed by the upper-level controller [7]. The block diagram of the two vehicles is shown in Fig. 2. A first-order lag is considered in the upper-level controller input command which correspond to the lower-level controller’s performance and comes from brake or engine actuation lags and sensor signal processing lags [3, 13]. The first-order lag can be defined as [3, 13].

$$\tau \ddot{x}_2(t) + \dot{x}_2(t) = u(t) \tag{1}$$

where x_1 and x_2 are the absolute positions of the preceding and ACC vehicles. u refers to the control input commands computed by the upper-level controller. τ is the time lag corresponding to the lag in the lower-level controller performance.

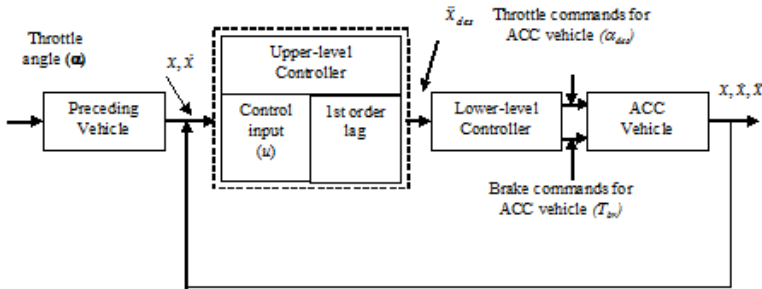


Fig. 2. Block diagram for a two-vehicle system consisting of a preceding and an ACC vehicle

Each vehicle’s longitudinal motion is captured in the continuous-time domain using a set of differential equations. Whereas, the MPC-based vehicle-following control laws for tracking the desired acceleration are computed using discrete-time model.

The paper presents the application of MPC technique to a nonlinear ACC vehicle model under TMs and examines the vehicle’s sensitivity for different vehicle masses while the rest of the model and its parameters are same. The detailed study has been conducted in the PhD project [16] and the simulation results has been compared with the suitable parameters [16] which ensure guaranteed response.

3 Vehicle Model

A 3.8 liter spark-ignition engine model which consists of two states cylinders and a five-speed automatic transmission has been chosen. The reader is referred to [16] for more details on the vehicle dynamic models. The necessary parameters of the vehicle model are listed in Table 1, based on the information from [17].

Table 1. Vehicle System Parameters

Engine displacement	V_d	0.0038 m ³
Intake manifold volume	V_{man}	0.0027 m ³
Manifold temperature	T_{man}	293 K
Engine moment of inertia	I_e	0.1454 kg.m ²
Mass of the vehicle	m	1644 kg
Accessory torque	T_a	25 Nm
Effective tyre radius	r_{eff}	0.3 m
Wheel moment of inertia	I_w	2.8 kg.m ²

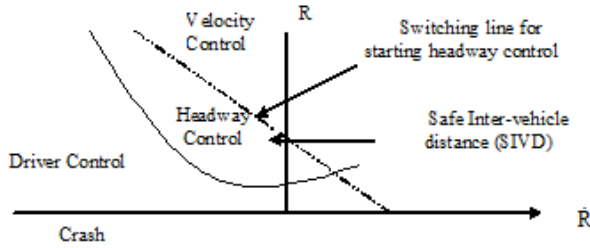


Fig. 3. Range vs. range-rate diagram [3]

4 MPC Controllers Formulation

The MPC-based upper-level controller is presented in this paper and the details of the lower-level controller algorithm can be found in [16]. The upper-level controller uses the range R and range rate \dot{R} between the ACC vehicle and the preceding vehicle to determine the desired acceleration commands as shown in Fig. 3.

The main task by using the MPC method for the TM is to operate the system close to the constraint boundaries. The main tasks for the MPC control method on the ACC system are:

1. Track smoothly desired acceleration commands.
2. Reach and maintain a safe inter-vehicle distance (SIVD) in a comfortable manner and at the same time react quickly in the case of dangerous scenarios.
3. System performance optimization.
4. Optimize the system performance within defined constrained operational boundaries.

There are some fundamental features of a MPC control algorithm which differentiate it from other control methods: its capability to develop explicitly a model to predict the process output at future time instants (horizon), the ability to design a reference path that the controller attempts to follow, calculation of a control sequence minimizing an objective function, and receding strategy; which means that at each instant the horizon moves forward to the future by applying the first control signal of the sequence calculated at each step [18].

4.1 MPC Prediction Model for the Two-Vehicle System

In this section the MPC control algorithm is applied to the two-vehicle system which consists of a preceding vehicle and a following ACC vehicle. Both vehicles are based on the nonlinear vehicle model (Section 3) and the longitudinal states of both vehicles are obtained by taking the force balance along the vehicle longitudinal axis [16] (for both vehicles separately). The position of the preceding vehicle is denoted by x_1 and the position of the ACC vehicle is denoted by x_2 , see Fig. 1.

The continuous-time model in Equation (1) can be re-written in a discrete-time state-space model as:

$$\begin{pmatrix} x_2(t+T) \\ \dot{x}_2(t+T) \\ \ddot{x}_2(t+T) \end{pmatrix} = \begin{pmatrix} 1 & T & 0 \\ 0 & 1 & T \\ 0 & 0 & 1 - \frac{T}{\tau} \end{pmatrix} \begin{pmatrix} x_2(t) \\ \dot{x}_2(t) \\ \ddot{x}_2(t) \end{pmatrix} + \begin{pmatrix} 0 \\ 0 \\ \frac{T}{\tau} \end{pmatrix} u(t) \tag{2}$$

where, T is the discrete sampling time of the ACC system and assumed as 0.1 s.

Coordinate Frame for Transitional Maneuvers. It is of paramount importance to develop and understand the mathematical relation between the state variables of the ACC vehicle and the preceding vehicle. The desired SIVD between the two vehicles varies linearly with the preceding vehicle’s speed such that the headway time (h) between the two vehicles remains constant ($SIVD = hv_{preceding}$). It should be noted that the measurement of range, range-rate, and ACC vehicle velocity can be used to obtain the velocity of the preceding vehicle.

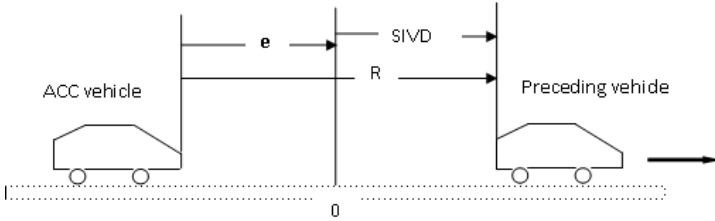


Fig. 4. Coordinate frame for transitional maneuver

A coordinate frame [1] travels with a velocity equal to the preceding vehicle velocity. This frame is used to determine the ACC vehicle motion relative to the preceding vehicle. The origin of this frame is situated at the desired SIVD and the objective of the TM is to steer the ACC vehicle to the origin of this frame in order to set up the zero range-rate with the preceding vehicle, where, R is the range (relative distance) between the two vehicles.

Using this coordinate frame (Fig. 4) for TM, the discrete-time state-space model of the error vector between the two vehicles can be defined as:

$$\mathbf{e}_{k+1} = \mathbf{A}\mathbf{e}_k + \mathbf{B}u_k \tag{3}$$

$$y_k = \mathbf{C}\mathbf{e}_k \tag{4}$$

where,

$$\mathbf{e}_k = \begin{pmatrix} err \\ \dot{err}_k \\ \ddot{err}_k \end{pmatrix} = \begin{pmatrix} -(R-SIVD) \\ \dot{R} \\ \ddot{x}_k \end{pmatrix} \tag{5}$$

where, err_k is spacing error, \dot{err}_k is range-rate (relative velocity between the two vehicles), and \ddot{err}_k is the absolute acceleration of the ACC vehicle. Each element of the error vector (e_k) is the quantity which is measured by the ACC system and the control objective is to steer these quantities to zero [1]. u_k is the control input, and y_k is the system output at time step k . The system matrices A and B can be obtained from the comparison of Equation (2) and Equation (3).

$$\mathbf{A} = \begin{pmatrix} 1 & T & 0 \\ 0 & 1 & T \\ 0 & 0 & 1 - \frac{T}{\tau} \end{pmatrix}, \quad \mathbf{B} = \begin{pmatrix} 0 \\ 0 \\ \frac{T}{\tau} \end{pmatrix} \tag{6}$$

And the system matrix C is defined as [1]:

$$\mathbf{C} = \begin{pmatrix} 1 & 0 & 0 \\ 0 & -1 & 0 \end{pmatrix} \tag{7}$$

Using the MPC control approach the future error can be defined as:

$$\mathbf{e}(k_i + 1 | k_i), \mathbf{e}(k_i + 2 | k_i), \dots, \mathbf{e}(k_i + m | k_i), \dots, \mathbf{e}(k_i + N_p | k_i) \tag{8}$$

where $e(k_i + m | k_i)$ is the predicted error variable at $k_i + m$ with the given current error information $e(k_i)$. The set of future control input are denoted by:

$$\Delta u(k_i), \Delta u(k_i + 1), \dots, \Delta u(k_i + N_c - 1) \tag{9}$$

where $\Delta u(k) = u(k) - u(k-1)$ is the control increment. The MPC controller forms a cost function which consists of these errors (e_k) and the control input which determines the best set of future control inputs to balance the output error minimization against control input effort. One can find the optimal solution for the control input which is the function of current error information $e(k_i)$.

$$\Delta \mathbf{U} = (\Phi^T \Phi + \bar{\mathbf{R}})^{-1} \Phi^T (\mathbf{R}_s - \mathbf{F} \mathbf{e}_{k_i}) \tag{10}$$

Similarly, using these predicted error variables, the predicted output variables can be determined as:

$$\mathbf{Y} = [y(k_i + 1 | k_i) \quad y(k_i + 2 | k_i) \quad y(k_i + 3 | k_i) \quad \dots \quad y(k_i + N_p | k_i)]^T \tag{11}$$

It should be noted that all predicted variable are expressed in terms of current state variable information $e(k_i)$ and future control input $\Delta u(k_i + j)$, where $j = 0, 1, 2, \dots, N_c - 1$.

The above equations can be written in the vector form as:

$$\Delta \mathbf{U} = [\Delta u(k_i) \quad \Delta u(k_i + 1) \quad \Delta u(k_i + 2) \quad \dots \quad \Delta u(k_i + N_c - 1)]^T \tag{12}$$

$$\mathbf{Y} = \mathbf{F} \mathbf{e}(k_i) + \Phi \Delta \mathbf{U} \tag{13}$$

where the dimension of \mathbf{Y} is N_p and the dimension of $\Delta\mathbf{U}$ is N_c . Equation (13) calculates all predicted outputs using the initial states $e(k_i)$ and vector of predicted control inputs $\Delta\mathbf{U}$.

where,

$$\mathbf{F} = \begin{bmatrix} \mathbf{CA} \\ \mathbf{CA}^2 \\ \mathbf{CA}^3 \\ \vdots \\ \mathbf{CA}^{N_p} \end{bmatrix} \quad (14)$$

and

$$\Phi = \begin{bmatrix} \mathbf{CB} & 0 & 0 & \dots & 0 \\ \mathbf{CAB} & \mathbf{CB} & 0 & \dots & 0 \\ \mathbf{CA}^2\mathbf{B} & \mathbf{CAB} & \mathbf{CB} & \dots & 0 \\ \vdots & & & & \\ \mathbf{CA}^{N_p-1}\mathbf{B} & \mathbf{CA}^{N_p-2}\mathbf{B} & \mathbf{CA}^{N_p-3}\mathbf{B} & \dots & \mathbf{CA}^{N_p-N_c}\mathbf{B} \end{bmatrix} \quad (15)$$

For the detailed understanding of augmented model and discrete-time state-space model (Equation (3)) and its transformation into the state-space model (Equation (13)), the reader is referred to the books written by Maciejowski [19] and Wang, L.,[20].

The cost function J , that describes the control objective, can be defined as

$$J = (\mathbf{R}_s - \mathbf{Y})^T (\mathbf{R}_s - \mathbf{Y}) + \Delta\mathbf{U}^T \bar{\mathbf{R}} \Delta\mathbf{U} \quad (16)$$

The cost function J consists of two separate terms, the first terms is meant to minimize the error between desired output and the predicted output while the second term deals with the size of $\Delta\mathbf{U}$ when the cost function J is made as small as possible. $\bar{\mathbf{R}} = \mathbf{R} \mathbf{I}_{N_c \times N_c}$ ($\mathbf{R} \geq 0$) where \mathbf{R} is used as a tuning operator for the desired closed-loop performance [20] which penalizes the control input vector ($\Delta\mathbf{U}$). \mathbf{R}_s is the vector that contains the desired state information and can be defined as:

$$\mathbf{R}_s^T = \left[\overbrace{1 \quad 1 \quad \dots \quad 1}^{N_p} \right] r(k_i) \quad (17)$$

where, $r(k_i)$ is the given set-point signal at sample time k_i . The control objective can briefly be defined as to find the best control parameter vector $\Delta\mathbf{U}$ such that an error function between the set-point and the predicted output is minimized [18].

For this study, $r(k_i) = 0$, because the control objectives are to steer the error vector (e_k) to 0, i.e. the spacing error (err_k) should steer to zero so the desired SIVD could be achieved, range-rate (\dot{err}_k) should converge to zero so the ACC vehicle follow the ACC vehicle with the same velocity, and the absolute acceleration (\ddot{err}_k) should steer to zero so the ACC vehicle moves with the constant speed. For the predictive model developed $\mathbf{R} = 1$. At each time step k the MPC algorithm determines a sequence of control input ($\Delta\mathbf{U}_0 \dots \Delta\mathbf{U}_{N_c-1}$) to minimize the cost function J (Equation (16)).

During the control algorithm formulation, the operational constraints are incorporated in the MPC controller formulation. The constraints incorporated are control input constraint which corresponds to the acceleration limits of the ACC vehicle Equation (18), state constraint which means that the ACC vehicle cannot have a negative velocity, the collision avoidance has also been formulated as state constraint Equation (20), and terminal constraint which refers that the ACC vehicle should establish a SIVD with the zero range-rate.

The control input constraint included in the MPC control formulation is:

$$u_{\min} \leq u_k \leq u_{\max} \quad (18)$$

The dimension of $\Delta \mathbf{U}$ is N_C and N_C is 3 samples, therefore, the constraints are fully imposed on all the components in $\Delta \mathbf{U}$ and can be translated to the six linear inequalities as:

$$\begin{bmatrix} 1 & 0 & 0 \\ 0 & 1 & 0 \\ 0 & 0 & 1 \\ -1 & 0 & 0 \\ 0 & -1 & 0 \\ 0 & 0 & -1 \end{bmatrix} \begin{bmatrix} \Delta u(k_i) \\ \Delta u(k_i + 1) \\ \Delta u(k_i + 2) \end{bmatrix} \leq \begin{bmatrix} u_{\max} - u(k_i - 1) \\ u_{\max} - u(k_i - 1) \\ u_{\max} - u(k_i - 1) \\ u_{\min} + u(k_i - 1) \\ u_{\min} + u(k_i - 1) \\ u_{\min} + u(k_i - 1) \end{bmatrix} \quad (19)$$

And the state and collision avoidance constraints incorporated in the MPC control formulation are:

$$y_k = \begin{pmatrix} err_k \\ -\dot{err}_k \end{pmatrix} \leq \begin{pmatrix} \text{SIVD} \\ v_{preceding} \end{pmatrix} \quad (20)$$

$$\text{SIVD} = hv_{preceding} \quad (21)$$

The parameters used in MPC controller formulation are shown in Table 2.

Table 2. Controller parameters

Discrete time sample	T	0.1 s
Time lag	τ	0.5 s
Tuning operator	\mathbf{R}	1
Set point	r	0
Headway time	h	1 s
Prediction horizon	N_P	230 samples
Control Horizon	N_C	3 samples
Upper acceleration limit	u_{\max}	0.25g
Lower acceleration limit	u_{\min}	-0.5g

5 Results and Discussion

This section presents the simulation analyses of the nonlinear ACC vehicle for different values of mass of the vehicle under the critical TM. The control objectives for the complex ACC vehicle are; “to perform the critical TMs (under $-0.5g$ deceleration limit) in order to establish and maintain the SIVD with the zero range-rate behind a newly detected slower or halt preceding vehicle”. The TMs will be performed in the presence of acceleration constraint (Equation (18)), states and collision avoidance constraints (Equation (20)) when the brake and engine actuators have limited allowable forces and may saturate. The vehicle mass for both vehicles considered in [16] study is 1644 kg. In this analysis the preceding vehicle’s mass remains the same while for the ACC vehicle masses chosen are 1400 kg, 1800 kg, and 2000 kg. The results obtained from these changes have been compared with the actual mass considered, i.e. 1644 kg.

5.1 ACC Vehicle Analysis for Different Vehicle Masses

In this scenario an ACC vehicle travelling at a speed of 30 m/s detects an accelerating preceding vehicle. The nonlinear ACC vehicle model has to decelerate from 30 m/s to the velocity of the preceding vehicle. The initial range between the two vehicles is 60 m. The initial velocity of the preceding vehicle is 10 m/s. The corresponding initial engine speed, throttle input, and gear ratio for the preceding vehicle are 1967 rpm, 50 degrees, 2nd gear, and for ACC vehicle are 4040 rpm, 70 degrees, and 5th gear, respectively.

The response of the ACC vehicle for different masses to the MPC controller is shown in Fig. 5, where both vehicles are based on nonlinear vehicle models. Vehicle positions (Fig. 5(a)), velocities (Fig. 5(b)), accelerations (Fig. 5(c)), engine speeds (Fig. 5(d)), range (Fig. 5(i)), for the two vehicles have been plotted. The accelerating preceding vehicle starting from 10 m/s velocity and 2nd gear at 50 degree throttle input reaches up to 26.5 m/s as shown in Fig. 5(b). At this speed the operating gear ratio of the preceding vehicle is 3rd gear and the throttle input is constant all the time. The comparison shows that the ACC vehicle’s response is hardly affected by the mass variations and the MPC control method is robust enough to cope with mass variations of the ACC vehicle and can be used for a complex ACC vehicle model analysis.

It has been observed that the ACC vehicle successfully performs the required TM, avoids the collision with the preceding vehicle, and establishes the desired SIVD with zero range-rate. It should be noted that the ACC vehicle is obeying all the applied constraints during this TM, i.e. control input, states, and collision avoidance while the constraints are applied in the upper-level controller formulation only. Moreover, the ACC vehicle is not executing a negative velocity.

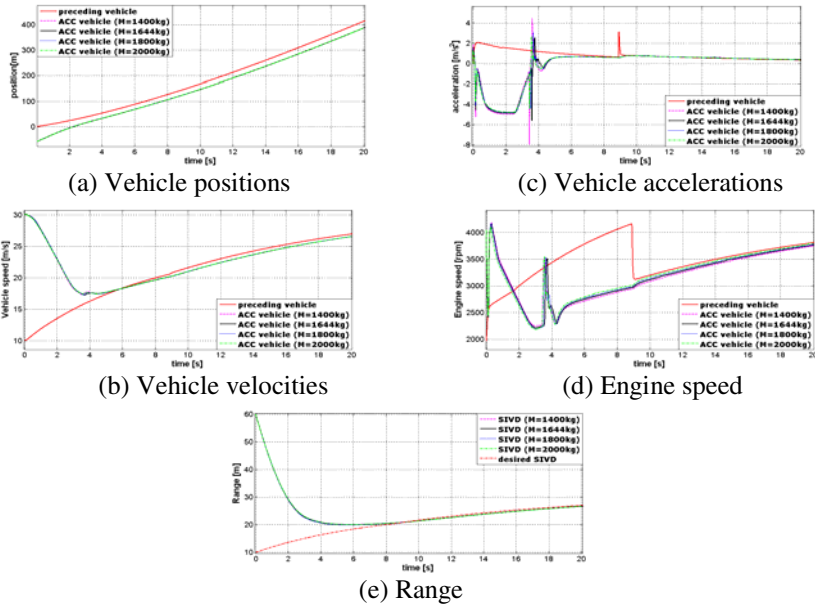


Fig. 5. Response of the ACC vehicle for different ACC vehicle mass

6 Conclusions

An application of mathematical control techniques to the longitudinal dynamics of a nonlinear vehicle equipped with an adaptive cruise control (ACC) system is presented. The vehicle model captures the vehicle dynamics even during the transmission gear shifting. A comparison of the above results with previous results by [21] shows that the nonlinear vehicle is capable of achieving the required tasks as described in Section 4 irrespective of the variation in mass of the vehicle. The applicability of MPC to the modeling of a nonlinear vehicle model has clearly been demonstrated here and the approach appears wholly capable to cope with significant inertial variations. The resulting control action taken by the MPC controller, with a predicted future path, is considered more realistic to the way in which a human driver operates. It has been observed that the ACC vehicle successfully performs the required TM, avoids the collision with the preceding vehicle, and establishes the desired SIVD with zero range-rate within the constrained boundaries.

Acknowledgments. I would like to express my sincere thanks to Mehran University of Engineering and Technology, Pakistan for giving me an opportunity to pursue PhD studies at University of Nottingham, UK.

References

1. Bageshwar, V.L., Garrard, W.L., Rajamani, R.: Model Predictive Control of Transitional Maneuvers for Adaptive Cruise Control Vehicles. *IEEE Transactions on Vehicular Technology* 53, 1573–1585 (2004)
2. Haney, P.R., Richardson, M.J.: Adaptive Cruise Control, System Optimisation and Development for Motor Vehicles. *The Journal of Navigation* 53, 42–47 (2000)
3. Rajamani, R.: *Vehicle Dynamics and Control*. Springer, New York (2006)
4. Peppard, L.E.: String Stability of Relative-Motion PID Vehicle Control Systems. *IEEE Transactions on Automatic Control* 19, 579–581 (1974)
5. Murdocco, V., Albero, D., Carrea, P.: Control of Longitudinal Vehicle Motion for Adaptive Cruise Control and Stop & Go Applications. In: *Proc. ITS, Torino*, pp. 1–9 (2000)
6. Sun, M., Lewis, F.L., Ge, S.S.: Platoon-Stable Adaptive Controller Design. In: *43rd IEEE Conference on Decision and Control, Atlantis, Paradise Island, Bahamas* (2004)
7. Girard, A.R., Spry, S., Hedrick, J.K.: Intelligent Cruise-Control Applications. *IEEE Robotics and Automation Magazine*, 22–28 (2005)
8. Ferrara, A., Vecchio, C.: Collision Avoidance Strategies and Coordinated Control of Passenger Vehicles. *Nonlinear Dynamics* 49, 475–492 (2007)
9. Connolly, T.R., Hedrick, J.K.: Longitudinal Transition Maneuvers in an Automated Highway System. *Journal of Dynamic Systems, Measurement, and Control* 121, 471–478 (1999)
10. Gerdes, J.C., Hedrick, J.K.: Vehicle Speed and Spacing Control Via Coordinated Throttle and Brake Actuation. *Control Eng. Practice* 5, 1607–1614 (1997)
11. Rajamani, R., et al.: Design and Experimental Implementation of Longitudinal Control for a Platoon of Automated Vehicles. *Transactions of the ASME* 122, 470–476 (2000)
12. Corona, D., Schutter, B.D.: Adaptive Cruise Control for a SMART Car: A Comparison Benchmark for MPC-PWA Control Methods. *IEEE Transactions on Control Systems Technology* 16, 365–372 (2008)
13. Li, S., et al.: Model Predictive Multi-Objective Vehicular Adaptive Cruise Control. *IEEE Transactions on Control Systems Technology* 18, 1–11 (2010)
14. Zlocki, A., Themann, P.: Improved Energy Efficiency by Model Based Predictive ACC in Hybrid Vehicles Based on Map Data. In: *10th International Symposium on Advanced Vehicle Control (AVEC 2010)*, Loughborough University, UK (2010)
15. Li, S., Li, K., Wang, J.: Development and Verification of Vehicular Multi-Objective Coordinated Adaptive Cruise Control Systems. In: *10th International Symposium on Advanced Vehicle Control (AVEC 2010)*, Loughborough University, UK (2010)
16. Ali, Z.: *Transitional Controller Design for Adaptive Cruise Control Systems*, PhD thesis, University of Nottingham, UK (2011)
17. Cho, D., Hedrick, J.K.: Automotive Powertrain Modeling for Control. *Transactions of the ASME* 111, 568–576 (1989)
18. Camacho, E.F., Bordons, C.: *Model Predictive Control*. Springer, London (2004)
19. Maciejowski, J.A.: *Predictive Control with Constraints*. Prentice-Hall (2002)
20. Wang, L.: *Model Predictive Control System Design and Implementation Using Matlab*. Springer, Heidelberg (2009)
21. Ali, Z., Popov, A.A., Charles, G.: Transition Controller for Adaptive Cruise Control System. In: *10th International Symposium on Advanced Vehicle Control (AVEC 2010)*, Loughborough, UK (2010)

ECAODV: Enhanced Classified Ad-Hoc on Demand Distance Vector Routing Protocol

Noorul Amin¹, Nizamuddin², and Abdelmuttlib Ibrahim³

¹Hazara University Manshara, Pakistan

²International Islamic University Islamabad

³Omdurman Islamic University Sudan

naming@hu.edu.pk, sahibzadanizam@yahoo.com,
abdelmuttlib@hotmail.com

Abstract. Mobile Ad-hoc Network (MANET) is independent, self-organizing and infrastructure less Ad-hoc network. Ad-hoc based routing protocols are being used for route discovery and route establishment. Among these Ad-hoc based protocols; Ad-hoc on Demand Distance Vector (AODV) is one of the reactive Ad-hoc routing protocols designed with inherited best features of DSR and DSDV. Using AODV a number of techniques have been presented for maintaining secure communication between communicating parties using symmetric and asymmetric cryptography, which have significant limitation of key management and high cost. In this paper we have proposed Enhanced Classified Ad-hoc on Demand Distance Vector protocol with a unique key management infrastructure for building cost effective and establishing secure links between nodes in MANET. Our proposed technique establishes session key between nodes in an authenticated way using signcryption and symmetric cryptographic technique Blowfish for secure data communication. The proposed protocol Enhanced Classified-AODV (ECAODV) provides all security features with tremendous low computation and communication cost. This work will greatly contribute to the security of AODV for secure MANET communication over other preceding proposed security techniques for AODV.

Keywords: AODV, key management, security, asymmetric cryptography, symmetric cryptography, signcryption.

1 Introduction

MANETs consist of self-configuring and independent mobile nodes with no appropriate infrastructure therefore ad-hoc routing protocols are being used for data communication [1]. Each node being part of the MANET works just like a router used in infrastructure network [2]. Routing protocols in MANETs are classified according to routing strategies and structure of the network. On the basis of routing strategy the routing protocols are categorized as proactive and reactive, while on the basis of network structure these are classified as flat, hierarchical and geographic position assisted routing (Fig. 1).

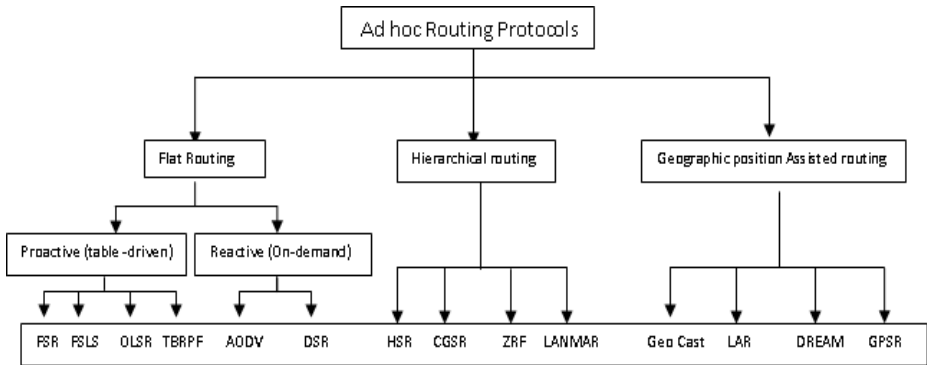


Fig. 1. Classification of Routing Protocols in Mobile Ad-hoc Networks [3]

Proactive protocols are also called table driven protocols as they keep the routing information prior to route demand by the communicating nodes. All nodes in the network contain routing information about each other. Routing tables maintain routing information which is updated as and when the nodes get in or out of the network. The proactive protocols are the best candidates for small networks and are not preferred for large networks because the routing tables entries grow high as the Network becomes wider. This leads to computation and communication overhead.

Reactive protocols are also called on-demand routing protocols as they don't keep routing information prior to route demand by the communicating nodes in the network. These protocols search the route on-demand basis and the routing information is kept only by the nodes involved in the communication. These protocols are the best candidates for large scale mobile ad-hoc networks. Delay in connection setup is higher than in proactive protocols.

A number of techniques have been proposed for the improvement of the security of AODV using symmetric and asymmetric cryptographic techniques but these have significant limitations of key management and high cost. AODV being reactive protocol is the base for our new proposed protocol "Enhanced Classified AODV (ECAODV)". Our proposed protocol uses a unique key management infrastructure which establishes session key between nodes in an authenticated way using ECC based Signcryption and symmetric cryptographic technique Blowfish for secure data communication. ECC based Signcryption is used for secure exchange of session key and symmetric cryptographic technique Blowfish is used for secure transmission of session data. ECAODV provides all security features with significant low computation and communication cost as compared to existing schemes presented in the literature.

2 Related Work

In this section various efforts have been made for achieving secure communication in MANETs. AODV [4] was an improvement on DSDV as it reduces the number of

broadcasts by establishing route based on demand. AODV routing protocol uses reactive strategy for searching routes, that is, a route is discovered only when it is needed by any sending node to transmit data packets. SAODV [5] is a secure version of AODV with properties of authentication, integrity, and non-repudiation for the information to be routed. It uses two mechanisms for the security of AODV. First, nodes involve in signing of messages; permits other nodes to verify source of the message. Messages RREQ and RREP include a field named Hop Count this field should be amended by each node involved in communication. Second, mutable data is protected and this mechanism introduces the concept of Hash Chains. Asymmetric Cryptographic technique is used as nodes require keeping pair of keys while signing messages to be routed. A-SAODV [6] uses threshold mechanism to optimize the Routing Performance of Secured Protocols. The concept of multithreading is applied where every node contains queue of routing message to be verified or signed and the length of the queue implies the load state of the routing thread. Whenever a node processes a route request and has enough information to generate a RREP on behalf of destination, it first checks its routing message queue length. If the length of the queue is below a threshold then it reply otherwise, it forwards the RREQ without replying. The value of threshold can be changed during execution. It also maintains a cache of most recent verified and signed messages, in order to avoid signing and verifying similar message more than one time. This adaptive reply decision has a significant improvement on the performance of SAODV [5]. In [7], the authors analyze the effect of encryption technique (RC4) to encrypt payload of AODV by analyzing different parameters such as queue size, delay, throughput, channel back-off, retransmission attempts, but this encryption do not effect performance significantly although provide security to AODV communication. As RC4 is symmetric where shared key is used which is difficult to manage; actually all network will have to manage $n(n-1)/2$ keys and each node has to keep secrete keys of all other nodes for secure communication this consumes more memory. Moreover RC4 suits for stream ciphering instead of block ciphering. In [8], the authors proposed hybrid approach to secure AODV communication. Session key is encrypted through asymmetric cryptosystems and session messages through symmetric cryptosystems. The proposed scheme avoids the difficulty of key management using asymmetric cryptosystem. Through asymmetric technique session key exchange increases computation and communication cost. The proposed work consists of scenarios and simulation results are not presented. In [9], the authors proposed an efficient packet encryption algorithm based on Exclusive-OR operation. Using this method, encryption and decryption are performed effectively with unique cryptographic technique without any complexity. Moreover, the forensic database keeps record of every invalid or unacceptable decrypted packet and analyzes the behavior of intercepts. The proposed architecture is still under review and has not been simulated or tested. In [10], the authors evaluate the performance of AODV and SAODV through simulation for variable number of nodes and malicious nodes. Performance of AODV was found degraded rapidly in case of entry of malicious nodes in the network while SAODV was noted stable. In [11], the authors proposed Distributive key management scheme for MANETs. The scheme is based on Elliptic curve cryptosystems suitable for constrained-power devices in terms of storage and processing overhead. In the proposed scheme, nodes are categorized as server nodes

and client nodes each mobile node generates a private/public key pair and a group private key/public key. The advantages of the proposed scheme are justified through simulations. Session key exchanged still increase computation cost. In [12], the performance of symmetric encryption algorithms AES, DES, 3DES, RC6, RC2 and Blowfish is evaluated through simulation. Blowfish has shown better performance as compare to other in the variable packet size. In [13], the authors introduce Blowfish as a better choice for the security of information in AODV. Evaluation is performed through simulation. It was noted that Blowfish does not put intolerable overhead to the MANETs traffic and the packets drop rate and delay is not affected in comparison to the base AODV.

3 Proposed ECAODV

Our proposed protocol Enhanced Classified AODV (ECAODV) provides routing and establishment of session key in a single step. For secure establishment of session key we used cost effective Signcryption technique. Certificate will be issued offline to each node before joining the network. It is assumed that a trust relationship exists between CA and all participating nodes. Each node obtains certificate from Certificate Authority before joining the network.

3.1 Basic Idea

Our proposed model encapsulates the following idea.

1. Signcryption technique is used for establishment of session key [14].
2. Both the sender and receiver nodes certificates are attached with RREQ and RREP messages.
3. Signcryption provide the functionality of encryption and signature both; in our proposed model the said technique is used for the establishment of session key only.
4. Symmetric cryptographic techniques blowfish [12] is used for data encryption.

Symbols used in our proposed model; Session key (k_s), Signcrypted session key (c, r, s), P_a Public key of source, d_a Private key of source, P_b Public key of destination, d_b Private key of destination, E_k Encryption using key K, D_k Decryption using key K.

3.2 Proposed Frame Work

Route between sender and receiver is discovered and established when source sends route request RREQ packet along with source certificate and request for session key to the destination node. All other nodes in the way to the destination broadcasts the same RREQ packet to its neighbors as in AODV protocol[6]. Upon receiving of the RREQ packet by the destination, certificate of the source is verified and session key

K_s is generated by the destination. The destination signcrypts session key K_s using ECC based signcryption as in Fig 2. Destination sends back route reply RREP packet along with its certificate and signcrypted Session Key K_s . Upon receiving of RREP packet by the source it verifies the certificate of the destination and then unsigncrypts K_s & checks its authenticity and integrity as shown in Fig 3. Obtained authentic session key is used for further secure data communication between source and destination using symmetric cryptography as shown in Fig 4.

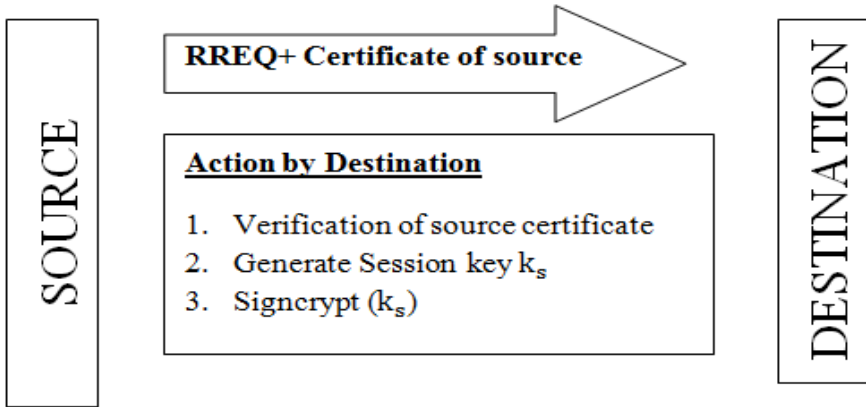


Fig. 2. Route discovery and session key request

3.3 Establishment of Session key

1. Verification of certificate by Destination
2. Every node will obtain certificate of its public key through offline certificate authority before joining the network.
3. Session key generation by Destination
4. Destination will generate session key as like random number generation.

Signcrypt (k_s) by Destination
 Signcryption ($k_s, n, d_b, P_a, P_b, H, KH, E_k$)
 Select an integer $k \in \{1,2,3 \dots \dots n - 1\}$ randomly
 Compute kP_a
 Compute $(K_1, K_2) = H(kP_b)$
 $c = E_{K_1}(k_s)$
 Compute $r = KH_{K_2}(k_s, bind_{info})$
 $s = \left(\frac{k}{(r + d_b)} \right) \bmod n$
 Signcrypted text for message k_s is (c, r, s)

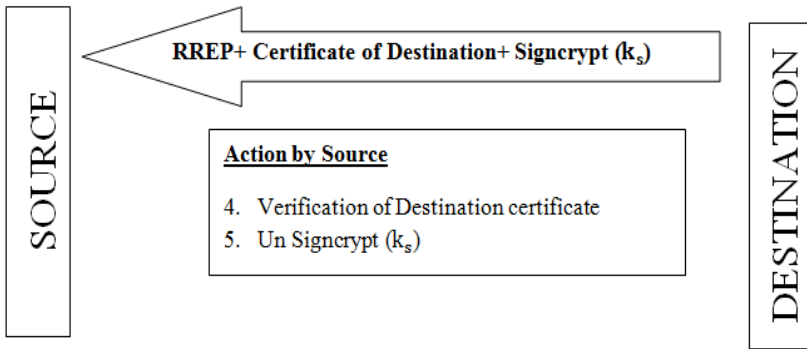


Fig. 3. Route and session key establishment

Verification of certificate by Source

Un Signcrypt(k_s) by Source

Unsigncryption ($c, r, s, n, d_a, P_a, P_b, H, KH, D_k$)

Compute $u = sd_a \text{ mod } n$

Compute $(K_1, K_2) = H(uP_b + urG)$

Compute $m = D_{K_1}(c)$

Check $KH_{K_2}(k_s || bind_info) = r$, if satisfied accept the key k_s , otherwise reject and re request for key k_s

3.4 Start Secure Communication

After successful exchange of keys sender will start secure communication with receiver by encrypting data using session key. Session Data will be encrypted using cost efficient and secure cryptographic technique Blowfish.

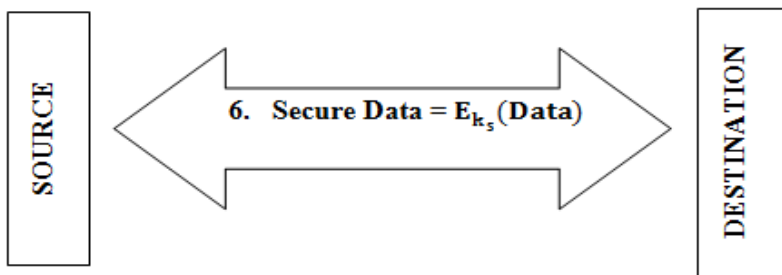


Fig. 4. Secure data communication using session key

4 Security and Cost Analysis of the Proposed Protocol

In this section we present detail security essentials of our proposed scheme.

Confidentiality: Our proposed technique keeps the secrecy of both the session key and communicating data from malicious nodes or users. We exchange session key through signcryption which leads to confidentiality of session key, and confidentiality of information is achieved through symmetric encryption.

Authentication: This scheme provides authentication in two ways; identity of the source is authenticated using certificate of public key at the destination and secondly session key is authenticated through signcryption.

Integrity: We maintain integrity of information through Signcryption of session key which block malicious attackers from replay attack and ensure the safety of transmitted information from illegal alteration.

Non Repudiation: As our proposed scheme Signcrypt (digitally sign) the session key, so no communicating party can deny from its transmitted information.

Cost Analysis: Due to its mobile nature and shared media, MANET has constrained of power and bandwidth.

We now present the computation and communication overhead analysis of our proposed model.

4.1 Computational Cost Analysis

The major operation involves in computation and signcryption of session is Elliptic curve point scalar multiplication (ECPM). The proposed Enhanced Classified-AODV (ECAODV) protocol has one ECPM in signcryption of session key and two ECPM in Unsigncryption of session key.

Classified-AODV (CAODV) [8] two time encrypt and decrypt session key using public and private keys of destination and source. There are total six ECPM in encryption and decryption of session key.

Saving in computation cost is $\frac{3 \text{ ECPM}}{6 \text{ ECPM}} = 50\%$

As routing latency is directly proportional to computational cost (computational time in ms) so proposed protocol leads to low latency.

4.2 Comparative Communication Cost Analysis

For communication cost analysis we assume NIST recommendation for secure key size and digital signature parameters. We used compressed representation of elliptic curve point. ECC key length $\geq 2^{160}$, Symmetric technique key length $\geq 2^{128}$ and HASH length $\geq 2^{160}$.

In proposed ECAODV protocol 128 bits session key is signcrypted, which become equal to $3 * 160 = 480$ bits.

Classified-AODV (CAODV) [8] two time encrypt and decrypt session key using public and private keys of destination and source. Due to asymmetric encryption 128 bits session key size is expanded 320 bits and second time encryption expanded cipher text become $2 \times 320 = 640$ bits.

Saving in communication cost is $\frac{160 \text{ bits}}{640 \text{ bits}} = 25\%$

5 Discussion

In [7], the authors used (RC4) to encrypt payload of AODV. As RC4 is symmetric so it is very difficult to manage a large size network by keeping secret keys of all other nodes of the network which consume more memory. Our proposed technique removes this flaw of more memory consumption and it improves performance.

The proposed work in [8] is based on hybrid approach for secure AODV communications which obviously avoids the problem of key management and provide message confidentiality but leads to high communication and computation cost. Our proposed hybrid scheme uses signcryption based on ECC which provide tremendously low communication and computation cost.

The proposed scheme in [9] is based on Elliptic curve cryptosystems. This scheme is suitable for constrained devices but session key establishment increase computation cost. In contrast our scheme is signcryption based on ECC cryptosystems which obviously decrease computation cost.

In the proposed scheme of [10] two option are given. Option1 lacks main security parameters i.e. authenticity, non repudiation and integrity. Option 2 fills the gape of missing security parameters of option 1 but on the price of high computation cost. Our proposed model provide authenticity, non repudiation, integrity as compare to option1 of [8] and 50% less computation cost than option 2.

In [13], the authors proposed secure AODV using Blowfish algorithm. This technique provides data confidentiality but secure session key exchange is missing. In this paper we keep track of security of information and security of session key which is of great importance in MANET.

6 Conclusion

As AODV is in the way of standardization it is of great importance that it should be enriched with all best security parameters while taking care of computation and communication cost. In this paper we have presented Enhanced Classified-AODV (ECAODV). The proposed protocol used signcryption for session key exchange and Blowfish for session data exchange. The proposed model ensure authenticated and confidential exchange of session key with 50% less computation cost compared to existing scheme. The cost of confidential session data exchange is reduced through using efficient and secure symmetric cryptographic technique named Blowfish.

References

1. Haas, Z., Pearlman, M.: The performance of query control scheme for the zone routing protocol. *ACM/IEEE Transactions on Networking* 9(4), 427–438 (2001)
2. Karp, B., Kung, H.T.: GPSR: Greedy Perimeter Stateless Routing for Wireless Networks. In: *Proc. 6th Annual International Conference on Mobile Computing and Networking (MOBICOM 2000)*, pp. 243–254 (2000)
3. Hong, X.Y., Xu, K.X., Gerla, M.: Scalable Routing Protocols for Mobile Ad Hoc Networks. *IEEE Network*, 11–21 (July-August 2002)
4. Perkins, C.E., Royer, E.M.: Ad hoc On-Demand Distance Vector Routing. In: *Proc. 2nd IEEE Workshop of Mobile Comp. Sys. and Apps.*, pp. 90–100 (February 1999)
5. Zapata, M.G.: Secure Ad hoc On-Demand Distance Vector (SAODV) Routing. *draft-guerrero-manet-saodv-06.txt* (September 5, 2006)
6. Kravets, R., Yi, S., Naldurg, P.: A Security-Aware Routing Protocol for Wireless Ad Hoc Networks. In: *ACM Symp. on Mobile Ad Hoc Networking and Computing* (2001)
7. Garg, V.K., Ghosh, R.K.: Effect of Data Encryption on Wireless Ad Hoc Network Performance. In: Sen, A., Das, N., Das, S.K., Sinha, B.P. (eds.) *IWDC 2004*. LNCS, vol. 3326, pp. 258–263. Springer, Heidelberg (2004)
8. Akhlaq, M., Jafri, M.N., Khan, M.A., Aslam, B.: Addressing Security Concerns of Data Exchange in AODV Protocol. *World Academy of Science, Engineering and Technology* 16 (2006)
9. Taneja, S., Kush, A., Singh, S.: Encryption Scheme for Secure Routing in Ad Hoc Networks. *International Journal of Advancements in Technology* 2(1), 22–29 (2011) ISSN: 0976-4860
10. Deswal, S., Singh, S.: Implementation of Routing Security Aspects in AODV. *International Journal of Computer Theory and Engineering* 2(1), 135–138 (2010)
11. Dahshan, H., Irvine, J.: An Elliptic Curve Distributed Key Management for Mobile Ad Hoc Networks. In: *IEEE 71st Vehicular Technology Conference (VTC 2010-Spring)* (2010)
12. Elminaam, D.S.A., Kader, H.M.A., Hadhoud, M.M.: Evaluating the performance of symmetric encryption algorithms. *International Journal of Network Security* 10(3), 213–219 (2010)
13. Rizwan, A., Amin, N., Shah, M., Siddique, U.: Security Technique in Routing Protocol for Mobile Ad-Hoc Network (MANET). In: *International Conference on Engineering and Information Management (ICEIM 2011)* (2011)
14. Zheng, Y., Imai, H.: How to construct signcryption schemes on elliptic curve. *Information Processing Letters* 68 (1998)

An External Approach to Improve the Information Content of Diagnostic Ultrasound Images

Samreen Amir¹, Bhavani Shankar Chowdhry², Muhammad Asif¹,
and Bhibekshan Chowdhry³

¹ Electronic Engineering Department, Sir Syed University
of Engineering and Technology, Karachi, Pakistan
{samreen.amir4, massif.ssuet}@gmail.com

² Faculty of Electrical, Electronic and Computer Engineering, Mehran University
of Engineering and Technology, Jamshoro, Pakistan
bsc_itman@yahoo.com

³ ShivNet Inc, 603-S Milliken Ave Suite G, CA91761, USA

Abstract. The importance of ultrasound imaging in the diagnosis process is established. It's due to the fact that this process is cost effective, simple, and radiation-free operation. Quality of image plays important role in accurate diagnosis and insightful fetal well being. Inadequate capability of the equipment is not the only reason for the poor images but also the presence of extreme difference in acoustic impedance at the interface. To have noise free and high definition images some solutions are implemented in terms of hardware and improved beam-forming techniques. These improvements though provide superior quality images but at the same time enhance the complexity of the design and hence the cost of the machine. This paper set sights on a solution that should improve the quality of image of an ordinary Ultrasound machine by endowing external image processing. The combination of different filters is used to recover the even better image as taken from the US scanner. This will provide the cost effective solution to those working with older versions of US machines hence providing the competitive image quality to the latest expensive equipment.

Keywords: Weiner Filter, JB Filter, Neighbor Value, Ultrasound.

1 Introduction

Ultrasound imaging is usually considered a "safe" modality. Ultrasound studies of fetus during pregnancy are carried out with full assertion in the outcomes and harmlessness. However this procedure should be performed only when there is convincing medical evidence and the minimum possible ultrasonic exposure should be used to acquire the necessary diagnostic information ("as low as reasonably achievable" ALARA principle [1]. Ultrasound equipment is regulated worldwide. Generally other regulatory agencies around the world accept the FDA-established guide lines [2].

The necessary regulations are required for MI (Mechanical Index) metric linked with the cavitations bio-effect, and TI (Thermal Index) a metric associated with the

tissue heating bio-effect. The determined limits are too unadventurous so as to maintain diagnostic ultrasound as a safe imaging modality.

Image acquisition is very poor when there is a gas between the transducer and the organ under investigation, due to the difference in acoustic impedance [3]. Accordingly there are difficulties in collecting image information of organs laying deep in the body, especially in overweight patients. Bodyhabitués are strongly influential on image quality hence on the accuracy of diagnosis [4]. Highly skilled and experienced personnel are needed to acquire good-quality images and make accurate diagnoses.

Above mentioned information establishes a fact that acquiring a high definition image with all safety constraints intact, is difficult and correct diagnosis is not possible if the quality of image is poor. The alternate options like MRI and CT Scans are expensive when compared to Ultrasound Scanning. An attempt can be made to improve the US acquired image through some external image processing approach.

The later part of the paper will discuss the image processing approach to be used externally on the images, discussion on the results and finally the conclusion.

2 Ultrasound Imaging, Constraint and Algorithms

Sound waves are high pressure and low pressure pulses passing through a medium. The wavelength is generally defined as the distance between two consecutive compressions or rarefactions. Ultrasound refers to the band of sound frequencies that do not fall in the audible frequency range. 1 MHz to 20 MHz frequencies can be used in medical applications of Ultrasounds. For imaging the maximum limit is restricted to 10 MHz. Despite of the fact that higher frequency ultrasound waves can form sharper images, the images are weaker since higher frequency energy absorbed more speedily by soft tissues [5]. Medical Ultrasound waves have a wavelength of about 1.5 mm [5].

The speed of ultrasound does not depend on its frequency. Speed of the ultrasound strongly affected by the mass and spacing of the molecules and the attracting force between the particles of the material it passing through [5]. Ultrasound travels faster in high density materials and slower in compressible materials.

Over the years, ultrasound has seen numerous advances in technology such as real-time 3D imaging, high resolution 7.5-10 MHz transducers, color-flow Doppler etc. Ultrasound waves are generated by a transducer that converts electrical energy to ultrasound waves, and collects the reflected waves converting them back into electrical signals. These reflected signals are utilized to form images. Ultrasound is reflected at the boundaries between different materials. Ultrasound reflects very well wherever soft tissue meets air or bone [5].

Loss of wave energy, expressed as change in intensity, as the energy travels through a medium. Rate of attenuation is called attenuation coefficient. For soft tissue, the attenuation coefficient is half the frequency per cm [6].

$$\alpha = \frac{1}{2} (f_{us}) / d(\text{cm}) \quad (1)$$

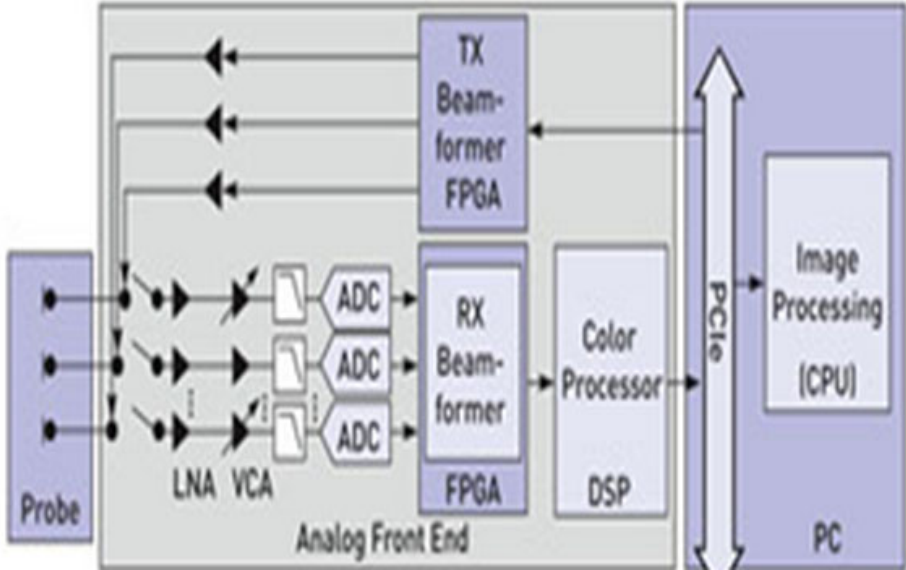


Fig. 1. High level block diagram of typical ultrasound machine

Figure 1 shows a high level block diagram of a typical ultrasound machine. Central processing unit of the machine runs the image processing algorithms. These algorithms are usually the adaptive image processing tools. The main issues in imaging are noise, echoes due to scattering of reflected pulses and low energy reflected signals. The main artifacts are of two types, technique dependent and inherent sonographics artifacts. Noise caused by excess gain or low signal caused by inappropriate transducer selection are the technique dependent issues while shadowing, enhancement and reverberation are the inherent artifacts. Amplitude shading is a method of reducing the side lobe levels in a transducer array. The shading usually causes the main beam to broaden by applying different voltages to the elements of the array.

Another potential source of noise, especially in deep-lying regions, is thermal noise occurring in the internal circuitry of the transducer. All these sources of interference affect the knack of the radiologist to diagnose tissue anomalies. Hence, reducing noise should improve effective diagnosis. Machine embedded techniques like Wall filter, motion discrimination detectors, frame averaging, apodization and adaptive equalization are being used to achieve the desired results. Solutions like XRES, iE33x and etc. can provide much realistic images with high resolution but are very expensive when compared to conventional machines.

3 Implementation of the External Image Processing on a Ultrasound Scanned Image

The diagnostic ultrasound images are usually B-Mode scan images. These black and white images are sometimes not very meaningful due to the artifacts as discussed in

section 1. As the paper is proposing an external approach to enhance the quality of image rather than going for the expensive Ultrasound machine compatible software solutions or transducers, we have applied a few filters' combination. The application of Shock filters and Wiener Filters have been already published in some research papers [7,8,9] . In our work, we have combined the Shock filter and Wiener filter in first approach and then applied the same original image to the Join Bilateral filter. This is a 2D bilateral filtering that performs a Gaussian Blur, weighted by some mask. Pixels with high weight only, contribute to their neighbors. Based on the code by Douglas R. Lanman, Brown University [10], we have implemented the bilateral filter. We have used three parameters for weight blur that is image x coordinate, image y coordinate and pixel value. The local region of interest may be extracted by defining the value of complex coordinates of C.

$$\sum_{i=\min}^{\max} \sum_{j=\min}^{\max} C_{ij} = C \tag{2}$$

The Gaussian distance weights are calculated as:

$$G = e^{-\left(\frac{x^2+y^2}{2\sigma_s^2}\right)} \tag{3}$$

The standard deviations of the bilateral filter are given by σ , where the spatial-domain standard deviation is given σ_s by and the intensity domain standard deviation is given by σ_r .

If the bilateral filter is defined by the expression:

$$\sum_{x'=x-C}^{x+C} \epsilon(x'). e^{-\left(\sigma_s(\epsilon(x)-\epsilon(x'))\right)^2 + \sigma_r(x-x')^2} \tag{4}$$

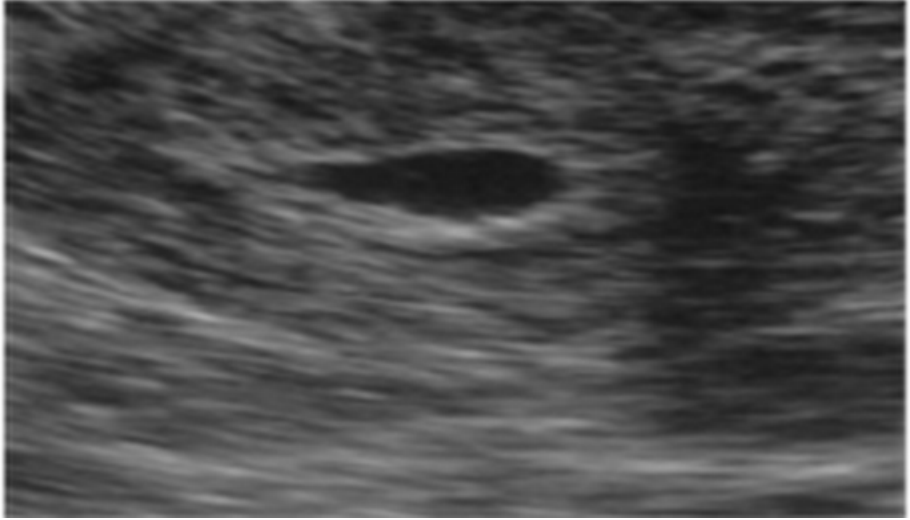
Where $\epsilon(x')$ is the intensity of the pixel of the closest value to the $\epsilon(x)$, .The response of the algorithm is computed by keeping the $\epsilon(x)$ constant say at value "a". Function picks value(s) of a to do a weighted blur at each value. Each pixel interpolates between the nearest 2 a's to have an output value. Input is the 2D image(x, y), a 3D level is then created by taking the product of an 1D Gaussian and an 2D Gaussian across different dimensions [Chen et al SIGGRAPH 07] that is (x, y, z).Where Image (x, y) = z, D(x, y, z) = (z, a) and D(x, y, z) = (0, 0) elsewhere. Now the weighted blur can be taken as

$$\omega(x') = e^{-\left(\sigma(a-\epsilon(x'))^2\right)} \tag{5}$$

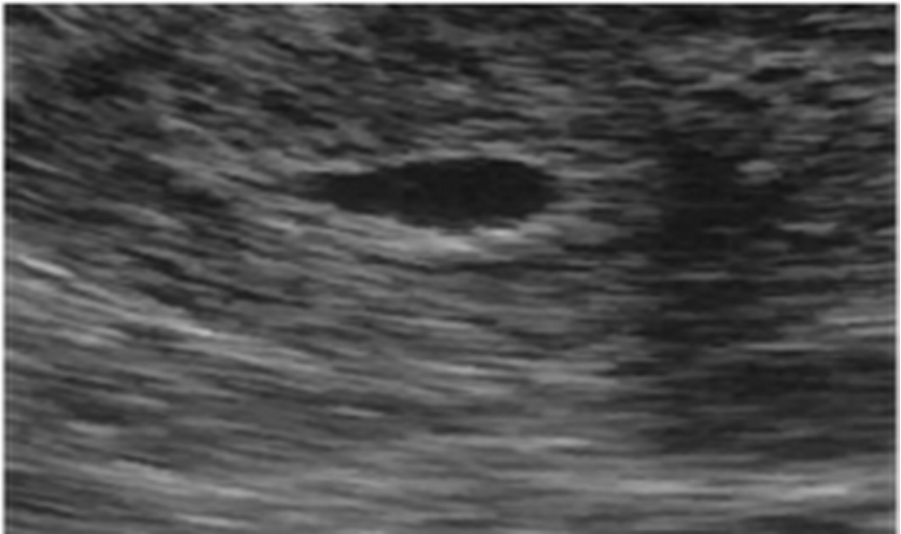
In our experiments, we generally set the filter's Gaussian standard deviation to 0.5 and standard deviation of intensity is set to 0.1, worked well on most images we use. It was found that Intensity deviation values are application dependent and given good results for the interval [0,1].

4 Results and Discussion

We have taken an ultrasound image of a cyst and process them step by step. Figure 2 shows the original scan, shock filter output which is then applied to Wiener filter, and JB filter output, respectively.

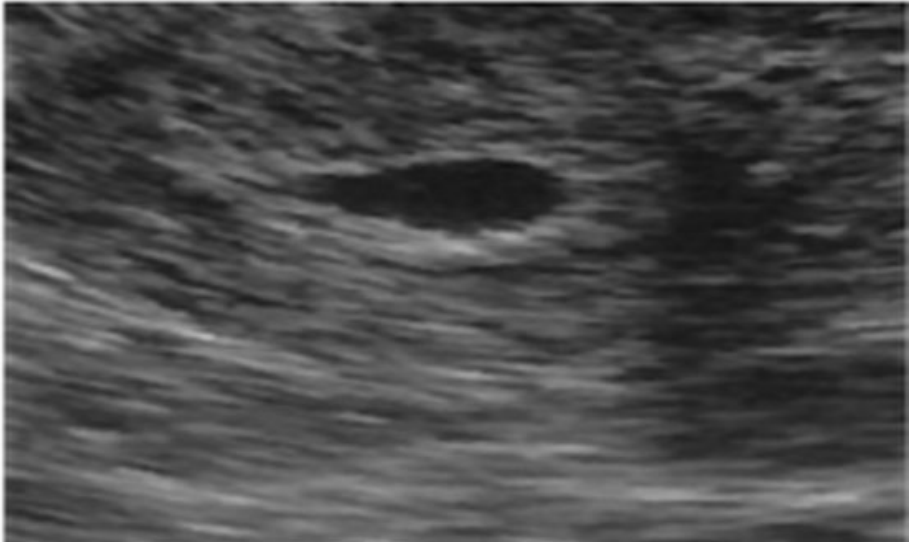


(a)

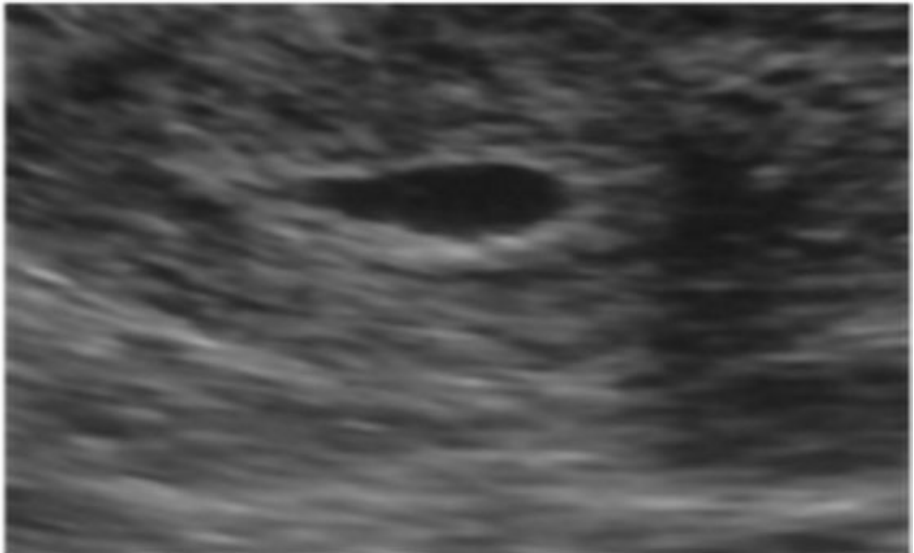


(b)

Fig. 2. Result of different image processing algorithms (a) original scan, (b) shock filter output (c) Wiener filter, and (d) JB filter output



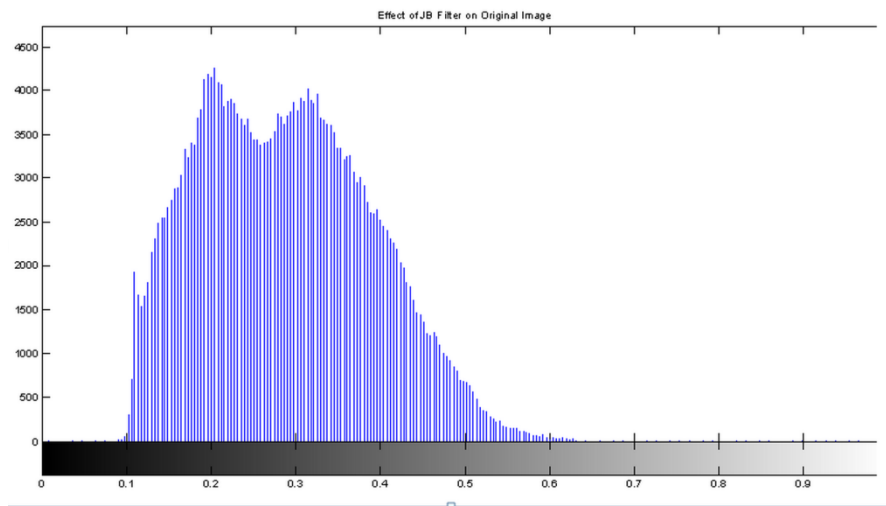
(c)



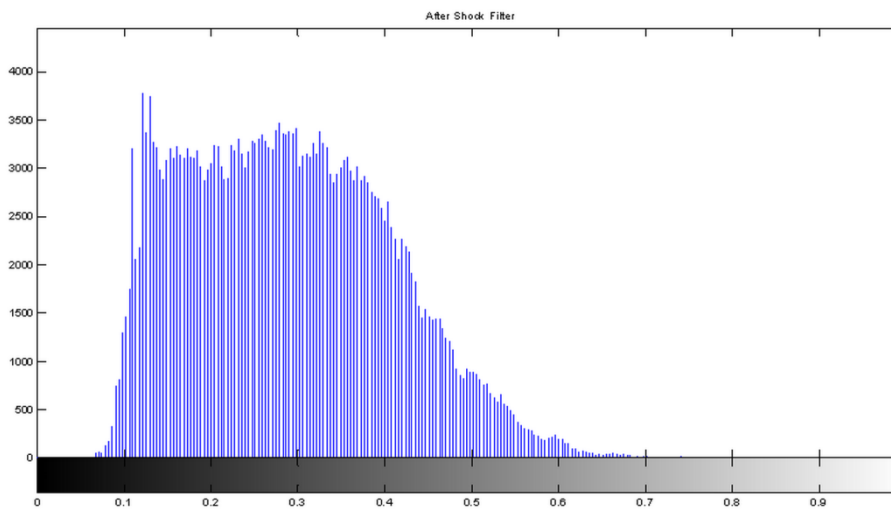
(d)

Fig. 2. (*continued*)

The more clear idea about the intensities of the images can be seen in the Histograms given in figure 3. They are in the same sequence as the images. The histograms show the sheer change in intensities at each stage of process. After the application of the shock filter the histogram expanded and the dip has been leveled a bit. The intensities those are low for the interval of 0.1 to 0.18, reap to higher values.

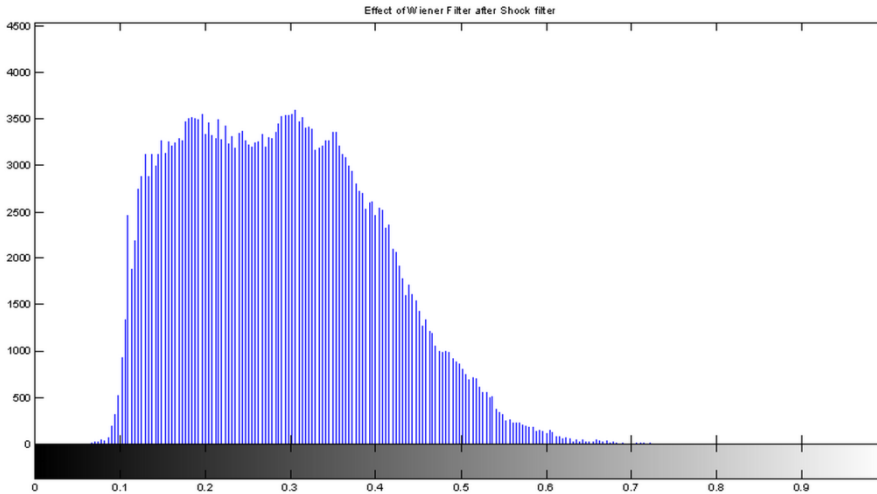


(a)

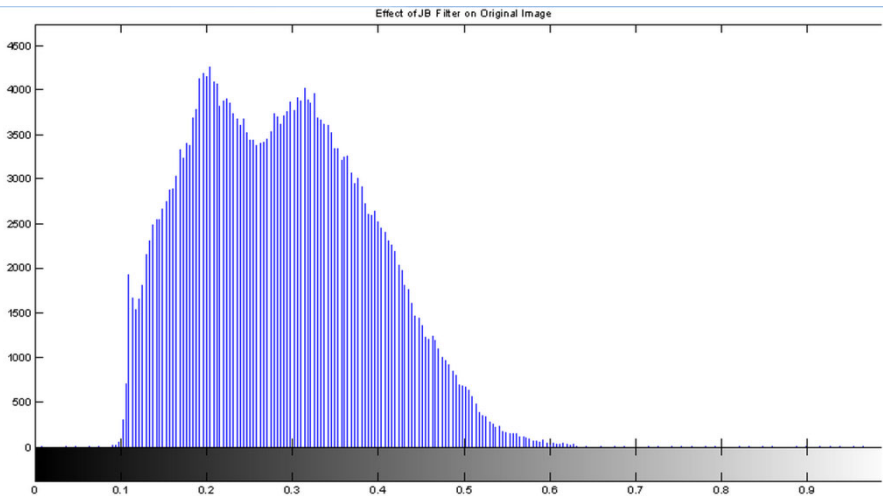


(b)

Fig. 3. Histogram of different image processing algorithms, x-axis represent time in seconds and y-axis represent intensity (a) original scan, (b) shock filter output (c) Wiener filter, and (d) JB filter output



(c)



(d)

Fig. 3. (continued)

After Wiener filtration process the image got smoothed and hence the histogram, the intensities during the interval $A = [0.15, 0.18]$ are now close to other neighbor values. But the histogram of the JB filter is in the same pattern as the original image, since the high values contribute to their neighbors. We compute the label for a pixel so that each low-resolution solution pixel with a non-zero bilateral weight chooses for its label. The winning label is the one that has the highest total weight. The performance of the joint bilateral filter is proportional to the output size because the domain

filter is always applied to the low resolution solution. For the results we have used a 5×5 Gaussian, a fast filtration process but have enough support to drag solution values from some distance.

5 Conclusion and Future Work

Since the ultrasound scans are widely used for medical purposes in diagnosis and imaging. But the quality of image is sometimes not as per standards due to inherent artifacts and limited allowable specifications due to health and safety issues. This approach can be a cost effective tool to improve the image quality. In the rural areas of Pakistan where an ultrasound machine is itself a rare facility, is really impossible to get it upgrade or replaced by a new one. So this simple image processing algorithm can be run on any computer supporting matlab to get a better visualization of users' choice that is only shock filter output, combining Wiener filter with that or just going for fast filtering with JB up-sampling. Some images just need contrast enhancement while others like soft tissue require well blended image. In future, a GUI based platform can also be developed using some more combinations of filters with the user friendly terminologies.

References

1. Practice Guidelines, AIUM Practice Guideline for the Performance of Neurosonography in Neonates and Infants. *J. of Ultrasound Med.* 29, 151–156 (2008)
2. FDA Consumer Health Information, Taking a close look at ultrasound (March 2008)
3. Maulik, D.: Doppler Ultrasound in Obstetrics and Gynecology, 2nd rev. and enlarged edn. Springer, Heidelberg (2005)
4. Schoder, H., Erdi, Y.E., Chao, K., Gonen, M., Larson, S.M., Yeung, H.W.D.: Clinical Implications of Different Image Reconstruction Parameters for Interpretation of Whole-Body PET Studies in Cancer Patients. *The Journal of Nuclear Medicine* 45(4) (2004)
5. Williams, T.: Image Optimization, From Foam to Filters: What's New in Venous Disease 2010. Duke University Medical Center, Durham (April 2010)
6. Liu, D.L., Saito, M.: A new method for estimating the acoustic attenuation coefficient of tissue from reflected ultrasonic signals. In: Proceedings of the Annual Int. Conference of the IEEE Engineering in Medicine and Biology Society (1988)
7. Rudin, L.I. Osher, S., Fatemi, E.: Nonlinear total variation based noise removal algorithms. *Physica D: Nonlinear Phenomena* (1992)
8. Alvarez, L., Mazorra, L.: Signal and image restoration using shock filters and anisotropic diffusion. *SIAM Journal on Numerical Analysis* 31(2) (April 1994)
9. Gonzalez, R.C., Woods, R.E.: *Digital Image Processing*, 2nd edn. Prentice Hall
10. Lanman, D.: MATLAB Central, <http://www.mathworks.com/matlabcentral/fileexchange/authors/21859>

Comparative Analysis of Group Centric Access Control Models

Hirra Anwar and Muhammad Awais Shibli

National University of Sciences and Technology
Islamabad, Pakistan

{10msccsfanwar, awais.shibli}@seecs.edu.pk

Abstract. Digital information is one of the sensitive resources in any organization that needs to be well protected and secured to avoid unauthorized access and consequently its misuse. In a group centric environment dynamic sharing of resources takes place within an authorized group of users for a specific purpose. Security of shared resources becomes more important and challenging in a group-centric environment. Different organizations comprise of a complex structure in which multiple groups exist at a time and access rights are provisioned and delegated within groups. Groups are created and disassembled dynamically based on events or tasks required. These complex structures need to be managed and secured and we need effective provisioning of access control and delegation of access rights within these groups. We present a comparative study of the access control models in group-centric environment and discuss the open research areas in group centric environment.

Keywords: Group centric environment, access control, delegation, secure groups, information sharing.

1 Introduction

World is a global village today. Internet plays an important role in connecting people worldwide. Digital information that is shared among connected users possess the concerns of security. When this information is shared among users, they form a group of connected members which is termed as a Group-centric structure. In a group centric environment, members of group contribute valuable information with each other for a specific rationale. Security of a resource is highly important in a group centric environment which can be achieved either through enforcing confidentiality, access rights or authorizations. Different organizations comprise of a complex structure in which groups are created and destructed dynamically based on events or tasks required. For instance in an educational institution, a group is formulated to host a local conference. The members of the formulated group including the conference chair, conference co-chair, participants and reviewers are given access rights that are different. This group which is dynamically made for a period of three months will not be designated new hardware resources to provide a root of trust. Instead the group would be dynamically created; access rights and delegation of access rights will be provided

through a software implementation which would effectively manage the complex dynamics of different groups. In addition to this, we need to address the complexity of multiple groups existing at a time and access rights that are shared among the users of multiple groups and the delegation of rights to group members.

Access control mechanisms limit the access of resources to authorized users. Access control in real, exerts control over who can interact with a certain resource. Access control models have been in use for long. Different access control models that have been proposed include Discretionary access control (DAC), Mandatory access control (MAC), Role based access control (RBAC), Attribute based access control (ABAC), Task based access control (TaskBAC), Usage based access control (Usage-BAC) etc. Access control models have gained much popularity and evolution ever since. Access to resources and sensitive information now needs to be protected in different environments which may include distributive environment, grid environment, dynamic group centric environments etc. One such evolutionary area is that of sharing within a group centric environment. In group centric environment group members share different resources for some specific purpose. An insight into the enforcement architectures and implementation models for g-SIS has also been proposed in the literature [1, 2]. Group secure information sharing is different from normal information sharing because the dynamics of g-SIS are different. G-SIS has dynamism which evolves over time or with the real world events and information sharing requirements. Delegation is another feature which is required in group-centric environment [3]. Research on access control models in group-centric environment illustrates different models which suit specific requirements and conditions [4-8]. An insight of group-centric access control models has been presented in the paper with the explanation of pros and cons related to each of these models.

The paper is organized as follows. Section 2 highlights the assessment criteria for access control models of group-centric resource sharing environment. Section 3 discusses the access control models for group-centric environment in detail and section 4 presents the analysis conducted for the existing access control models. Finally the conclusion is summed up in section 4.

2 Assessment Criteria for Group-Centric Access Control Models

In this paper we will discuss different access control models that have been proposed in literature, along with the benefits and limitations of these access control models for group-centric environment in particular. A few of the access control models have been proposed specifically for group-centric environment while the others are generic access control models which can be used in different environments.

Literature highlights different parameters and characteristics to evaluate access control models in general [9]. Paper [10] highlights access control in collaborative environment describing parameters based on which analysis of access control models has been carried out for collaborative environment in particular. Considering the literature analysis of group-centric environment, we have specifically taken group

properties to analyze access control models, targeting generic group-centric environment. We have analyzed the group centric access control models on the basis of properties including fine grained control, complexity, delegation in groups, revocation of rights, active/passive characteristics, and limitation for time based groups.

During the analysis of security aspects of any system, its properties are not always quantifiable enough to assign straightforward values to each of them. National Institute of Standards and Technology's document on "Directions in Security Metrics Research" specifies that analysis of a system does include properties which are difficult to define in objective terms. Sometimes qualitative properties are used to measure properties which are quantitative [11]. To measure the parameters of access control models in group-centric environment, we have carried out qualitative analysis and have defined three levels of low, medium and high to analyze them. NIST security metrics document exemplifies the qualitative analysis by taking the measure low indicating the absence of any vulnerability in the system; medium as a few vulnerabilities found and high as many vulnerabilities found in a system. In the same manner, we quantify our quantitative measures using qualitative levels of measurement i.e. low, medium, high but the context of defining these levels varies in our case. We are using these levels to specify how much the property relates to group-centric environment directly. A low level specifies that a particular property does hold true for the access control model but falls short of fulfilling the complete requirement of that model. Similarly the medium level shows that the access control model contains the specific property but the requirements of the model are only satisfied in an intermediary form. However, the high level shows that the property related to group-centric environment is completely satisfied by the particular access control model defined. A brief description of all these parameters has been given below.

2.1 Complexity in Applicability

An access control model that is easy to apply attracts the user's attention the most. The purpose of access control is to limit the permissions to a specific resource, to make it secure. But security and usability should be observed side by side for its efficient use. An access control model should be simple enough to apply in a group-centric environment. "High" level indicates the implementation of access control model to be complex to apply in a group-centric environment. "Medium" indicates a relatively simpler model and "Low" label indicates a simple model implementation.

2.2 Active/Passive

Access control models are active if they provide the flexibility to handle the dynamism of changing environments and scenarios. Group-centric environment demands the access control models to be active to smoothly adapt the dynamics of changing environment. A passive model is not flexible enough to cater for the adaptation of manipulations and dynamically changing permissions.

2.3 Fine Grained Control

The criteria of fine grained control focuses on the in depth ease of control the access control model provides. Group-centric environment differs from a normal collaborative environment in a way that it handles the resource access not only on larger role based criteria but also on the individual user level where users might need to have a specific level of permission for access to a resource in comparison to the group or role it belongs to. Thus for a group-centric environment, finer grained access control is needed as compared to corporations, organizations or large entities forming larger roles and obtaining permissions based on those wider roles. “High” level is assigned to that access control model which offers maximum finer level control. “Medium” level is assigned where an intermediate form of fine grained control is provided, while “Low” level is given to that access control model which doesn’t offer fine grained control.

2.4 Revocation of Rights

The access control model should provide mechanism for revocation of access rights, which are given to group users to access resources. In addition to this, revocation of rights to objects shared by users is also included in revocation of rights. Rights of user can be revoked anytime depending upon dynamic conditions and requirements. For group-centric access control model, revocation of rights is a basic feature which should be provided by the access control model. For revocation of rights in a group-centric environment, the level of “Low” is assigned to that model in which the feature of revocation of rights can be easily provisioned while a “High” level is assigned to the model in which revocation is difficult.

2.5 Delegation of Rights

A strict and secure delegation model is required for group-centric environment. In a group environment delegation of rights within groups is important where group owner may delegate his rights to any of the group members when needed. In the analysis of all access control models against this attribute, any of the high, medium or low levels are assigned to each model. “Low” level is assigned to that access control model in which access rights can be easily delegated and the unit of delegation is simple and easy for implementation. A level of “Medium” is assigned to a model in which delegation of rights is relatively complicated while “high” level indicates difficulty in the delegation of rights.

2.6 Limited Time Based Groups

The access control model should provide permissions to resources on the basis of long time collaborations as well as short time based group accesses. This is one of the differences between the collaborative and group-centric environment where associations are limited to shorter intervals of time as compared to the collaborations which are

long lasting and exist for longer time periods [13]. A security loophole arises if access control permissions are assigned for longer time intervals but the need is just of short time associations. So for a group-centric environment, this condition needs to be checked before assigning access to resources. For this attribute, a “High” level indicates the access model to be following time based limitation for groups completely while “Medium” and “Low” levels indicate that models don’t follow this criterion completely.

3 Access Control Models for Group-Centric Environment

In this section we examine the access control models in group centric environment. As part of this examination, we discuss the principles and merits of each model, targeting the demerits and shortcomings as well. The prominent access control models that have been proposed are discussed specific to the features of group-centric environment. These models include the time-based, privilege based, role based, task based, attribute based access control models and a few others.

3.1 Time-Based Access Control

An access control model proposed in literature for group secure information sharing is the Time-based sharing model. This model authorizes users to access resources of a group based on the temporal ordering of subject and object group membership. This means that the authorizations of the group members are based on the time when they joined the group and the time when the object was added to the group. It can be explained through an example of a meeting room that can be accessed by managers during a specific time of the day and by other employees at another time of the day. This is the group centric information sharing based on time where users must satisfy the time constraint to access group and its resources. There can also be sharing based on the usage of resources, for example there can be constraints on the usage of resources that a resource can only be accessed ten times based on the role of subject [12].

Shortcomings: This access control model is not flexible enough to cater a wide set of requirements for a group-centric environment. It surely is a focused model specific to the temporal orderings of subject and objects in a group. However, a group centric environment in addition to be time based, requires the access of users to be based on the privileges, usage and tasks specific to the group. Among these criteria, time based access control models do not provide a fine grained control over users in a group-centric environment. TimeBAC is not considered a flexible active model of access control. Fig. 1 shows the analysis of TBAC model.

3.2 Privilege Based Access Control

An extended model for group-centric information sharing not only implies the temporal ordering of subjects and objects but also the privileges that are given to the

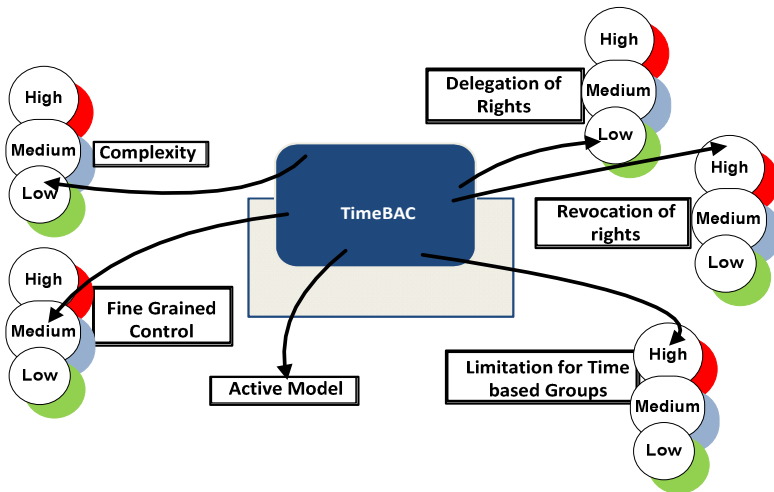


Fig. 1. Analysis of TimeBAC Model

subject. It follows the principle of sharing but differentiate. This means that sharing within a group is carried out but is differentiated by every role. For example in a meeting room a junior scientist can only participate in the meeting when it's already half way through and his personal performance has already been discussed by the head and senior scientists. He is thus authorized to access only those documents which were added to the group after he joined in. In such a scenario different possibilities have been discussed where a user cannot access past documents (documents/resources that have been added to the group after the user joined the group), any user can access them, any document can be re-added and it might or might not be treated as a new document [13].

Shortcomings: This extended model includes the features of time based access control and adds in the property of privileges of users on the basis of which the access to resource is granted. This is not completely an active model since it doesn't keep track of the entire contextual and environmental information for granting access to a user. It lacks the features of usage and task with reference to a group centric access model. In addition to this it doesn't provide a fine grained control over users in a group. Fig. 2 shows the analysis of PBAC model.

3.3 Task Based Access Control

Task based access control models are included in the category of active security models. Active security models are characterized by the features such as usage tracking of permissions, the ability to put permissions temporarily on hold without invalidating them. TBAC enables access control on the basis of tasks that have been assigned and revocations of access rights are based on the completion of those tasks. All permissions are automated and synchronized with the progressions of tasks.

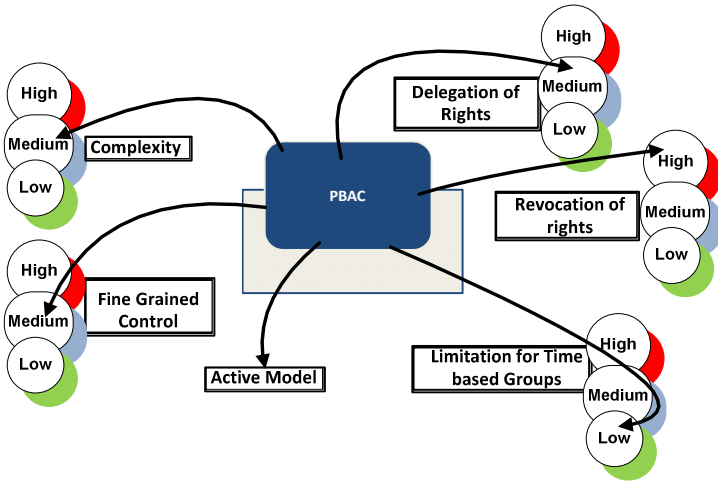


Fig. 2. Analysis of PBAC Model

Active authorization models are essential otherwise permissions in most cases can remain long after tasks have been terminated leaving security loopholes in the system. Classical access control models are included in the subject-object domain of access control models where a central pool of resources exists. Conventional access control models however, do not record usage of permissions [14].

Shortcomings: The Task based access control model suits the group-centric environment. The analysis for TaskBAC shows that this model falls in the category of active access control model and hence considers the contextual information as well for granting access but it does not consider the user privileges and attributes for a more refined control over user information. Fig. 3 shows the analysis of TaskBAC model.

3.4 Usage Based Access Control

Usage based access control models allow access on the basis of number of times any subject or object is being used. Usage based access control fits into the scenario of group centric environment considering an example of a subscription where a user is granted access to a magazine 10 times based on the subscription package which the user has subscribed to. An annual subscription package (with higher charges) enables a user to have access to a resource greater number of times as compared to the monthly subscription package, Sandhu in his papers describes the usage access control model being one of the ways to grant authorizations to group members in a group-centric secure information sharing environment.

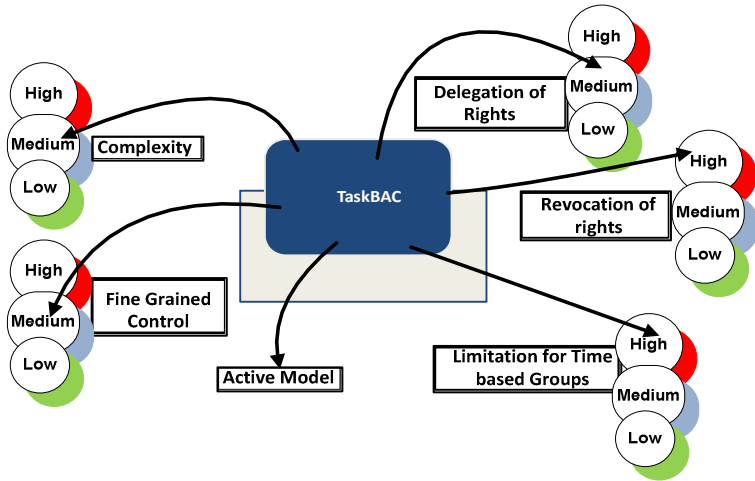


Fig. 3. Analysis of TaskBAC Model

Shortcomings: This model is suitable for group-centric environment in respect to usage criteria but doesn't fulfill complete requirements of group environment. For an access control model targeted for groups, attributes, privileges, time and task are yet other necessary requirements which need to be fulfilled simultaneously in order to make the group environment secure and trusted. In addition to this, usage based access control doesn't consider delegation of access rights within groups which is another important requirement of group-centric environment. Fig. 4 shows the analysis of UsageBAC model.

3.5 Role Based Access Control

Role based access control is based on granting permissions to users based on their roles. All the users of any organization are assigned roles. The roles are then assigned permissions. On the basis of this, the user belonging to a specific role gets a specific permission. This means that a complete role possesses similar permissions for all the users belonging to it. It doesn't distinguish users based on their capabilities. RBAC is an easy to use access control model. It has been deployed in organizations on a much larger scale. But it has its cons related to it as well. It doesn't provide a fine grained control as is required by a group-centric environment. In addition to this, RBAC is a passive access control model in which dynamics of the system are not handled.

Shortcomings: RBAC is one of the well established access control models used to restrict access to resources but it has its associated shortcomings as well. For group centric environment role based access control doesn't provide fine grained control which is needed in groups. Implementation complexity of this model is low but all the requirements of group-centric environment are not satisfied. Access is restricted just on the basis of roles and privileges assigned to those roles but not on the basis of

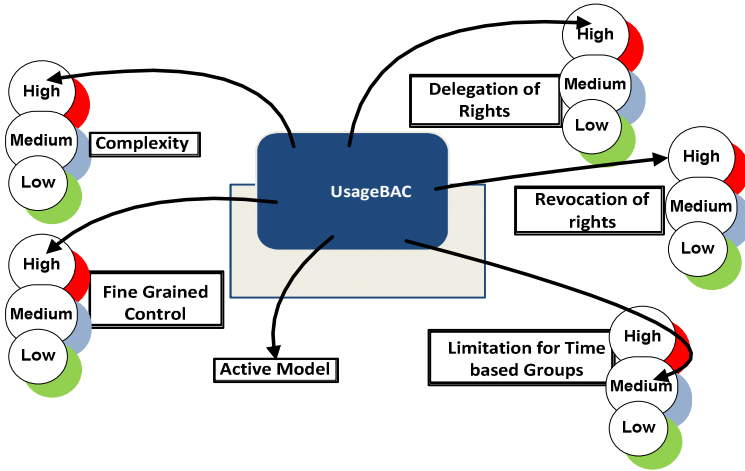


Fig. 4. Analysis of UsageBAC Model

usage, time and task of users. In addition to this, delegation of rights for group centric environment needs to be further explored in this model where grant delegations are applied but transfer delegations need to be worked upon. Fig. 5 shows the analysis of RBAC model.

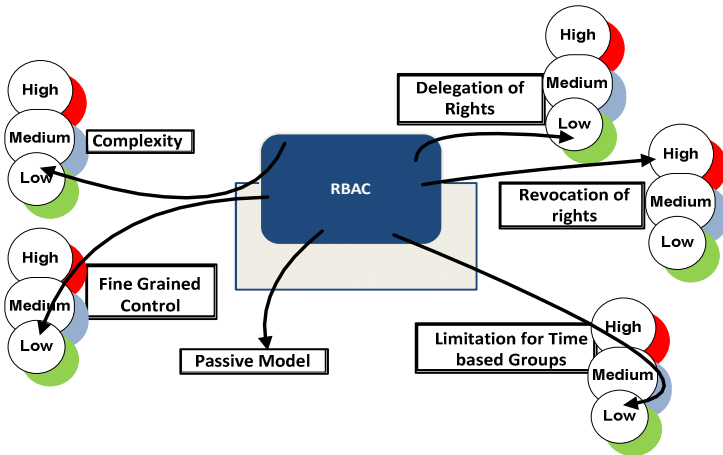


Fig. 5. Analysis of RBAC Model

3.6 Attribute Based Access Control

Attribute based access control aims at restricting the access to resources based on the attributes of user. It uses user attributes as the building block in defining access to

sensitive resources. ABAC is the finer level in assigning permissions to users. There can be cases where abilities of users belonging to the same role in an organization might differ. When we need to utilize extra abilities of people belonging to the same role, we need a fine grained control over the user attributes to assign permissions. For a group-centric environment, ABAC is one of the appropriate access models. A group consists of members belonging to different roles with different capabilities. Attribute based access control provides an appropriate access control mechanism to restrict the group access to users with specific attributes based on the group requirement. ABAC is a flexible model as compared to the traditional models of access control. Analysis of Attribute based access control model is shown in Fig.6.

Shortcomings: ABAC provides fine grained control in group-centric environment but like other models discussed before, it does not fulfill complete set of requirements of a group environment. Access in this case is based on the attributes of user but the information of task and its timings is also important to consider in order to grant access to resources. If task information is considered for a group based scenario, then the loopholes which exist in cases where permissions remain with users on the basis of their attributes even when the tasks are completed by groups can be avoided and access to resources in group environment can be secured.

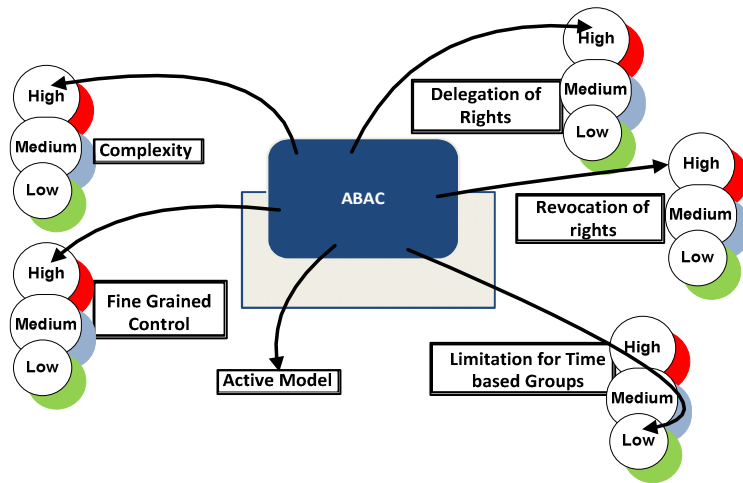


Fig. 6. Analysis of ABAC Model

4 Conclusion

We conclude by analyzing different access control models in group-centric environment and providing a detailed comparison in Table 1.

Table 1. Detailed Analysis of Different Access Control Models in Group-Centric Environment

CRITERIA	Time BAC	PBAC	TaskBAC	Usage-BAC	RBAC	ABAC
<i>Fine Grained Control</i>	Low	Medium	Medium	High	Low	High
<i>Active/Passive Model</i>	Active	Active	Active	Active	Passive	Active
<i>Complexity in Applicability</i>	Low	Medium	Medium	High	Low	High
<i>Limited Time based Groups</i>	High	Low	High	Medium	Low	Low
<i>Provisioning of Revocation of Rights</i>	High	High	High	High	High	High
<i>Provisioning of Delegation of Rights</i>	Low	Medium	Medium	High	Low	High

A critical examination of access control models for group-centric environment has been carried out in this paper. Based on the analysis stemmed from our observations, we believe that a holistic access control model is needed specific to group centric environment which caters for complete set of requirements of dynamic groups. Current access control models in their capacity, target specific group-centric features but we cannot find a comprehensive model which includes all the required features for group-centric environment.

We expect from research community to extend their research in designing an access control model which addresses all requirements of group-centric environment, yet balancing the usability and security aspects offered by access control model. The future avenue in group-centric information sharing environment includes implementation challenges which target the issues of dynamism of complex group-centric environment. This includes the concerns of dynamic policy selection, dynamic delegation and simultaneous evaluation of dynamic policies.

References

1. Krishan, R., Sandhu, R.: Enforcement Architecture and Implementation Model for Group-Centric Information Sharing. In: Proc. of 1st International Workshop on Security and Comm. Networks (2009)
2. Krishan, R., Sandhu, R.: A hybrid Enforcement Model for Group-centric Secure Information Sharing. In: International Conference on Computational Science and Engineering (2009)
3. Moniruzzaman, M., Barker, K.: Delegation of Access Rights in a Privacy Preserving Access Control Model. In: Ninth Annual International Conference on Privacy, Security and Trust (2011)
4. Krishnan, R., Sandhu, R., Niu, J., Winsborough, W.: Towards a Framework for Group-Centric Secure Collaboration. In: 5th International Conference on Collaborative Computing: Networking, Applications and Work Sharing (2009)

5. Sandhu, R., Krishnan, R., Niu, J., Winsborough, W.H.: Group-Centric Models for Secure and Agile Information Sharing. In: Kotenko, I., Skormin, V. (eds.) MMM-ACNS 2010. LNCS, vol. 6258, pp. 55–69. Springer, Heidelberg (2010)
6. Krishnan, R., Sandhu, R., Niu, J., Winsborough, W.: Foundations for Group-Centric Secure Information Sharing Models. In: Proc. 14th ACM Symposium on Access Control Models and Technologies (SACMAT), Stresa, Italy, June 3-5, pp. 115–124 (2009)
7. Krishnan, R., Sandhu, R., Ranganathan, K.: PEI Models towards scalable, usable and high assurance information sharing. In: ACM Symposium on Access Control Models and Technologies, pp. 145–150. ACM, New York (2007)
8. Krishnan, R., Sandhu, R., Niu, J., Winsborough, W.: A Conceptual Framework for Group-Centric Secure Information Sharing. In: Proc. 4th ACM Symposium on Information, Computer and Communications Security (AsiaCCS), Sydney, Australia, March 10-12, pp. 384–387 (2009)
9. Hu, V., Ferraiolo, D., Rick Kuhn, D.: Assessment of Access Control Systems, National Institute of Standards and Technology, U.S Department of Commerce (September 2006)
10. Tolone, W., Ahn, G.J., Pai, T., Hong, S.: Access Control in Collaborative System. *ACM Computing Surveys* 37(1), 29–41 (2005)
11. Jansen, W.: Directions in Security Metrics Research, NISTIR 7564. National Institute of Standards and Technology, U.S Department of Commerce (April 2009)
12. Li, P.: A Times-Based Model for Group-centric Information Sharing. In: Second WRI Congress on Software Engineering (2010)
13. Li, P.: An Extended Model for Group-centric Secure Information Sharing. In: Third international Symposium on Electronic Commerce and Security (2010)
14. Thomas, R.K., and Sandhu, R.: Task-based Authorization Controls (TBAC): A Family of Models for Active and Enterprise-oriented Authorization Management. In: Proceedings of the IFIP WG11.3 Workshop on Database Security, August 11-13 (1997)

Nonlinear System Identification Using Neural Network

Muhammad Asif Arain^{1,2}, Helon Vicente Hultmann Ayala^{1,2},
and Muhammad Adil Ansari³

¹ University of Genova, Italy

² Warsaw University of Technology, Poland

a.arain@yahoo.com, helonayala@gmail.com

³ Quaid-e-Awam University of Engineering, Science & Technology, Pakistan
maa17_84@yahoo.com

Abstract. Magneto-rheological damper is a nonlinear system. In this case study, system has been identified using Neural Network tool. Optimization between number of neurons in the hidden layer and number of epochs has been achieved and discussed by using multilayer perceptron Neural Network.

Keywords: Nonlinear systems, System identification, Magneto-rheological damper, Neural Networks.

1 Introduction

Magneto-rheological (MR) dampers are semi-active control devices to reduce vibrations of various dynamic structures. MR fluids, whose viscosities vary with input voltages/currents, are exploited in providing controllable damping forces. MR dampers were first introduced by Spencer to civil applications in mid- 1990s. In 2001, MR dampers were applied to the cable-stayed Dongting Lake Bridge in China and the National Museum of Emerging Science and Innovation Building in Japan, which are the world's first full-scale implementations in civil structures [1]. Modeling of MR dampers has received considerable attention [2-4]; however, these proposed models are often too complicated for practical usage. Recently, [5] proposed a so-called non-parametric model that has demonstrated two merits so far [6]:

1. The model can be numerically solved much faster than the existing parametric models;
2. The stability of an MR damper control system can be proved by adopting the non-parametric model. If currents/voltages of MR dampers are constants, the non-parametric model becomes a Hammerstein system depicted in Figure 1.

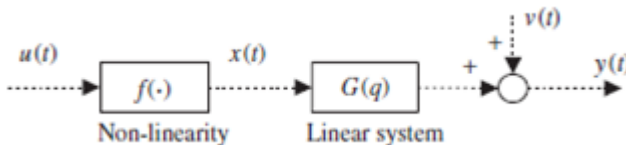


Fig. 1. A discrete-time Hammerstein system

Here the input $u(t)$ and output $y(t)$ stand for the velocity and damping force, respectively. [5] suggested a first-order model for the linear system,

$$G(q) = \frac{b_1 q^{-1}}{1 + a_1 q^{-1}}$$

and three candidate functions for the non-linearity,

$$f(u) = c_1 \tanh(c_0 u) + c_2$$

$$f(u) = c_1 \operatorname{sgn}(u)[1 - \exp(-c_0|u|)] + c_2$$

$$f(u) = \frac{(c_0 + c_1|u - c_3|)^{c_2(u-c_3)} - (c_0 + c_1|u - c_3|)^{-c_2(u-c_3)}}{c_1 c_2(u-c_3) + c_0^{-c_2(u-c_3)}}$$

Our objective is to design an identification experiment and estimate the output $\hat{y}(t)$ from the measured damping force $y(t)$ and velocity $u(t)$, using of neural networks black box models.

To study the behavior of such devices, a MR damper is fixed at one end to the ground and connected at the other end to a shaker table generating vibrations. The voltage of the damper is set to 1.25 V. The damping force $f(t)$ is measured at the sampling interval of 0.005 s. The displacement is sampled every 0.001 s, which is then used to estimate the velocity $v(t)$ at the sampling period of 0.005 s. The data used in this demo is provided by Dr. Akira Sano (Keio University, Japan) and Dr. Jiandong Wang (Peking University, China) who performed the experiments in a laboratory of Keio University. See [7] for a more detailed description of the experimental system and some related studies. We applied Neural Network for this nonlinear system identification because Neural Network stands out among other parameterized nonlinear models in function approximation properties and modeling nonlinear system dynamics [8]. And clearly, nonlinear system identification is more complex as compare to linear identification in a sense of computation and approximations. In section 2, Neural Network is designed with detailed description on it's I/Os (inputs, outputs), used data sets and training algorithm. In section 3, obtained results are presented in graphical and numerical forms. Section 4 discusses details about these obtained results. Finally, in section 5, case study conclusion is made.

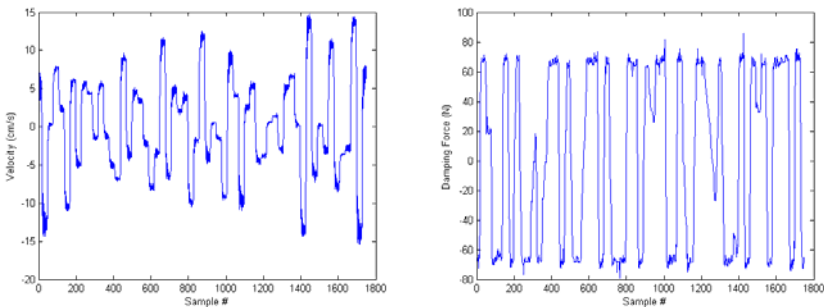


Fig. 2. System input (velocity) and output (damping force)

2 Neural Network Design

Designing a Neural Network black-box model to perform the system identification of a nonlinear SISO (Single Input Single Output) system, namely (Magneto-rheological Damper); following design variables should be achieved.

2.1 Input/output and Transfer Function

Neural Network input

One delayed system output plus, one delayed system input and the actual input i.e. $y(k - 1)$, $u(k - 1)$ and $u(k)$, are used as NN inputs. This results in a NARX model, similar to the Hammerstein model. As the results are satisfactory for the above cited NN inputs, the dynamic of the system could be captured with only one delay for each system input and output. There is no need to increase, then, the number of delays on the input and output.

The result for 50 epochs and 10 neurons and Levenberg-Marquardt backpropagation training procedure is presented below to justify this choice. For this case, a value of MSE (Mean Square Error) of 6.4180 is obtained.

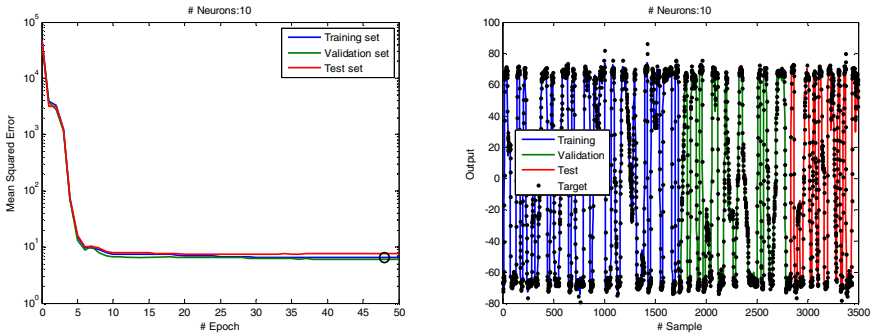


Fig. 3. Levenberg-Marquadt backpropagation training procedure

Neural Network output

For the neural network output it is used, obviously, the system output, that is $\hat{y}(k)$.

Neural Network transfer function

The NN transfer functions are chosen as hyperbolic tangent sigmoid (tansig) in hidden layer and pure linear (purelin) in output layer.

2.2 Data Sets

The data set of nonlinear magneto-rheological dampers, provided by Dr. Akira Sano (Keio University, Japan) and Dr. Jiandong Wang (Peking University, China) contains 3499 input and output samples, each. The data is split into three sets;

- i. One for training, containing first 50% of the amount of data.
- ii. One for validating, containing second 30% (from 51% to 80%) of the amount of data. This data set is used for checking the increase of error among the epochs – it is used mainly as stop criterion.
- iii. One for testing, containing last 20% (from 81% to 100%) of the amount of data. This data set does not influence the training procedure.

The stop criteria

The stop criterion of number of epochs for checking the increase of error on the validation data set is set as the number of epochs + 1, so the training procedure never stops because of that. In this study it is focused the effect of number of neurons and number of epochs on the result. Practically there are two data sets: one for training and another for testing, the last being constituted of the validation and test data sets.

2.3 Training Algorithm

The gradient descent backpropagation is tested, and it diverged for a set of number of neurons on the hidden layer. One hidden layer is used. An example for 10 neurons and 50 epochs is shown in Fig 4. Two training procedures are used. In first, number of epochs is fixed and numbers of neurons are varying. In second, number of neuron is fixed and numbers of epochs are varying.

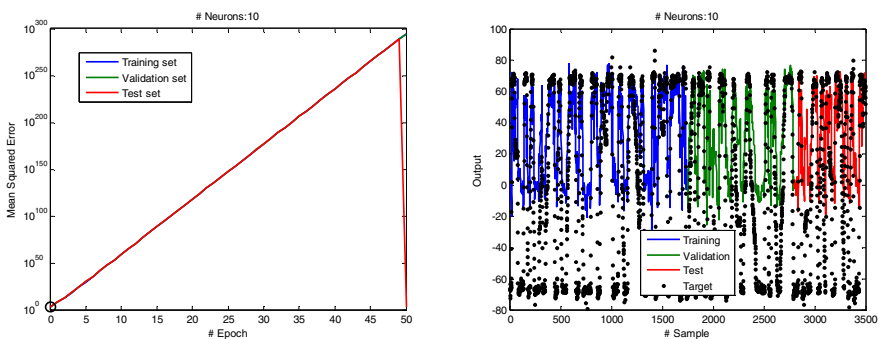


Fig. 4. Gradient Descent Backpropagation diverges

Varying neurons and fixed epochs

Test the performance, for 50 epochs, of 2, 4, 6, 8, 10, 12 numbers of neurons in the hidden layer.

- i. The results are shown in Table 1 and Figure 5.
- ii. MSE values are calculated for training, validation and test datasets.

Fixed neurons and varying epochs

For 10 neurons in the hidden layer, change different number of epochs as 20, 100, 300, 500, 700 and 1000.

- i. The results are shown in Table 2 and Figure 6.
- ii. MSE values were calculated for training, validation and test datasets.

Result criteria

- i. Calculate the MSE for all cases. The MSE represents the metric adopted for the training.
- ii. Plot neural network output and desired output in the same graph (for comparing) for all cases.
- iii. Plot neural network output error ($e(k) = y(k) - \hat{y}(k)$) for all cases.
- iv. Analyze general results.
- v. What is the influence of the number of neurons in a fixed number of epochs on the NN result?
- vi. What is the influence of the number of epochs on the NN training performance?

3 Results

Using above training algorithm, obtained results are presented both in graphical and numerical forms. Fig. 5 shows graphical results obtained using different number of neurons and fixed epochs. Fig. 6 shows graphical results using fixed neurons and different number of epochs. In graphical results, MSE is plotted on logarithmic scale. Instead of using error only, MSE (mean square error) variable was used to show a clear identification of error trend in training, validation and testing sets with respect to number of epochs, this comparison is shown in Fig.7. In numerical results, MSE in training, validation and testing sets against variable neurons and epochs is presented in Table 1 and Table 2 respectively.

Graphical Results

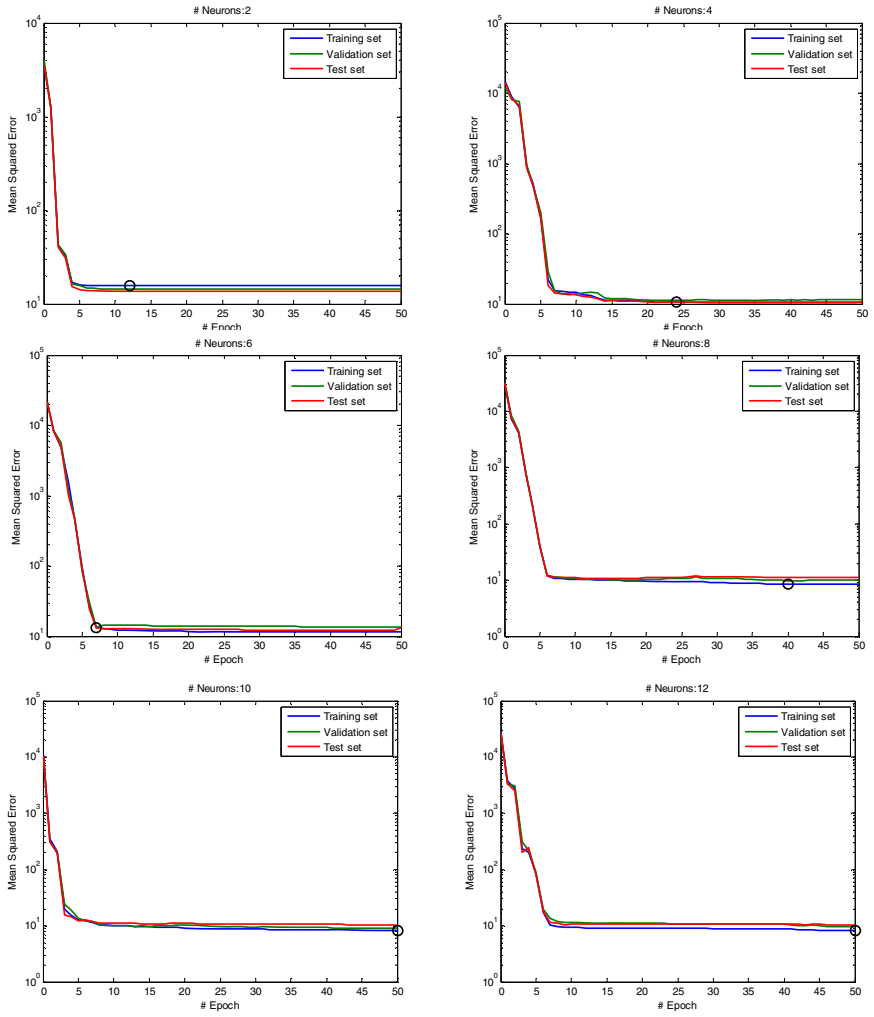


Fig. 5. Results for 50 (fixed) epochs and 2, 4, 6, 8, 10 and 12 neurons in the hidden layer

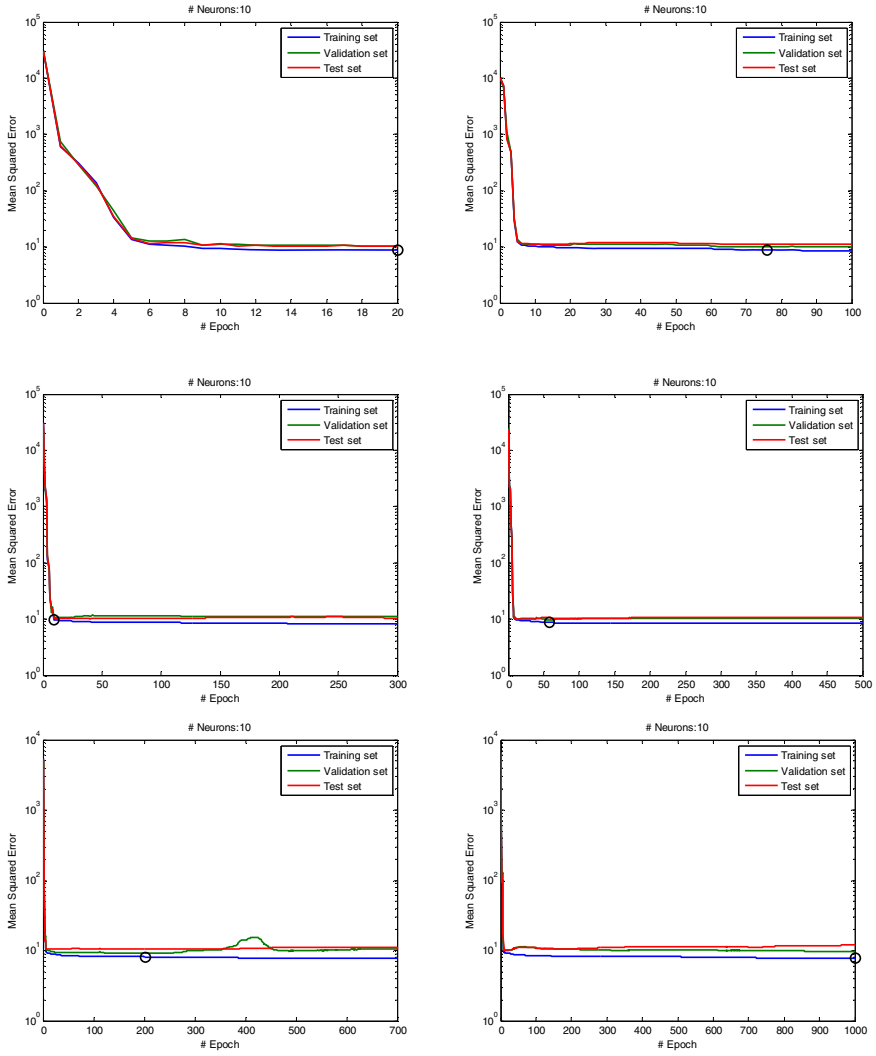


Fig. 6. Results for 20, 100, 300, 500, 700 and 1000 epochs and 10 (fixed) neurons in the hidden layer

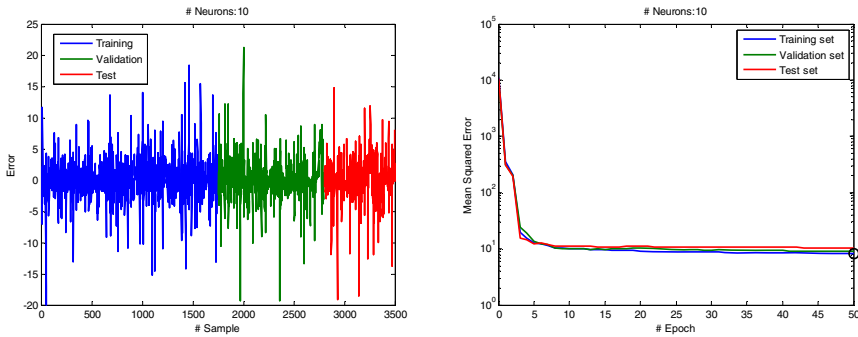


Fig. 7. Representation of error and MSE for 10 neurons in hidden layer

Numerical Results

Table 1. Results for different number of neurons and 70 epochs

Neurons	MSE – Train	MSE - Validation	MSE – Test
2	15.6728707486869	14.4948575906152	13.6752183182602
4	10.7218539702842	11.3195658194943	10.6840535069316
6	13.3840846836663	13.6716607191865	13.1696042197544
8	8.40574921395610	9.84068816503996	11.0299877969621
10	8.29385308661188	9.06040436519353	10.4993626210124
12	8.23019058719595	9.58944665057627	10.4232375024308

Table 2. Results for different number of epochs and 10 neurons

Epochs	MSE – Train	MSE - Validation	MSE – Test
20	8.46213141484072	9.28610314243466	10.5389069957705
100	8.68527655115772	9.55504632661187	10.6903292802750
300	8.37896217859245	8.80832992981236	10.2434588260025
500	8.27327467204573	9.05391102870505	10.4767184896312
700	8.15121872108450	9.82165043634970	10.4437982077475
1000	7.90768469589262	8.99822232524322	10.7080085654322

4 Discussions

The results shown are trying to expose the influence of the number of epochs and number of neurons issue in NN design. It can be noted, from Figure 5 and Table 1 that the number of neurons has a maximal value for improving the accuracy of the NN. From Table 1, one can say that the best value for the numbers of the NN hidden layer neurons is 10; with 12 neurons the error for the validation increases, though the test data error is diminished. This fact shows that the NN starts to represent over-fitting of the data with 12 neurons.

From Figure 6, it can be seen that there is also a maximum number of epochs that improve the NN results accuracy. Figure 6 shows that at epoch 700 the validation error starts to grow, what also can be seen as over-fitting of data. Moreover, it may also be noted that there is a number of epochs that the NN stops to improve the training data set result; around 70 epochs in the case studied in this work. The backpropagation algorithm stays at local minima (it may also be global) in this point. One may use several stop criteria for the backpropagation algorithm in order to avoid this drawback of limiting only the number of epochs.

General results show that the proposed designed NN can be a powerful tool to perform the systems identification with complex and nonlinear behavior. It is possible to affirm that the use of Levenberg-Marquadt backpropagation for training multilayer perceptrons has given accurate results, as shown by numerical expositions in Table 1 and 2.

5 Conclusion

This case study presented an application of multilayer perceptron Neural Networks to perform the nonlinear system identification having its parameters defined by Levenberg-Marquadt Backpropagation training procedure. Such training procedure is chosen because the standard Steepest Descent Backpropagation does not converge for several sets of configurations. It is attempted, with this configuration, to build a black-box model that could represent the system. The tested case study, the magneto-rheological damper, is a nonlinear SISO system. For obtaining the exposed results, all methods are described and put under context.

Finally, the obtained results are considered satisfactory, showing that the present methodology can achieve the identification of the analyzed nonlinear system. The results could be observed on graphs and tables, where the MSE is presented in training, validation and test phases. The proposed methodology proved that it can be tested with systems having different characteristics, such as chaotic systems and controller design using neural network models. Future work could aim the adaptation of different optimization techniques to perform the NN training procedure in order to guarantee accuracy and generalization capability.

Acknowledgement. Authors are thankful to Prof. Lotfi Romdhane, Ecole Nationale d'Ingénieurs de Sousse, Tunisia for his guidelines.

References

1. Cho, S.W., Jung, H.J., Lee, J.H., Lee, I.W.: Smart Passive System Based on MR Damper. In: JSSI 10th Anniversary Symposium on Performance of Response Controlled Buildings, Yokohama, Japan
2. Spencer, B.F., Dyke, S.J., Sain, M.K., Carlson, J.D.: Phenomenological Model of a Magneto-rheological Damper. *ASCE Journal of the Engineering Mechanics* 123, 230–238
3. Choi, S.B., Lee, S.K.: A Hysteresis Model for the Field-dependent Damping Force of a Magneto-rheological Damper. *Journal on Sound and Vibration* 245, 375–383
4. Yang, G.: Large-Scale Magneto-rheological Fluid Damper for Validation Mitigation: Modeling, Testing and Control. The University of Notre Dame, Indiana
5. Song, X., Ahmadian, M., Southward, S.C.: Modeling Magneto-rheological Dampers with Application of Nonparametric Approach. *Journal of Intelligence Material Systems and Structures* 16, 421–432
6. Song, X., Ahmadian, M., Southward, S.C., Miller, L.R.: An Adaptive Semiactive Control Algorithm for Magneto-rheological Suspension Systems. *Journal of Vibration and Acoustics* 127, 493–502
7. Wang, J., Sano, A., Chen, T., Huang, B.: Identification of Hammerstein systems without explicit parameterization of nonlinearity. *International Journal of Control*
8. Subudhi, B., Jena, D.: Nonlinear System Identification of a Twin Rotor MIMO System. In: *IEEE TENCON (2009)*

Intrusion Damage Assessment for Multi-stage Attacks for Clouds

Junaid Arshad¹, Imran Ali Jokhio², and Mahmood Shah³

¹ Department of CS & IT, University of AJK, Kotli, Pakistan

² Department of Software Engineering, Mehran University of Engineering and Technology, Jomshoro, Pakistan

³ Lancashire Business School, University of Central Lancashire, Preston, UK
rjarshad@gmail.com

Abstract. Clouds represent a major paradigm shift from contemporary systems, inspiring the contemporary approach to computing. They present fascinating opportunities to address dynamic user requirements with the provision of flexible computing infrastructures that are available on demand. Clouds, however, introduce novel challenges particularly with respect to security that require dedicated efforts to address them. This paper is focused on one such challenge i.e. determining the extent of damage caused by an intrusion for a victim virtual machine. It has significant implications with respect to effective response to the intrusion. The paper presents our efforts to address this challenge for Clouds in the form of a novel scheme for intrusion damage assessment for Clouds which facilitates protection against multi-stage attacks. The paper also includes the formal specification and evaluation of the scheme which successfully demonstrate its effectiveness to achieve rigorous damage assessment for Clouds.

Keywords: Cloud Computing, Cloud Computing Security, Intrusion Damage Assessment, Multi-stage Attacks.

1 Introduction

Cloud computing presents exciting opportunities to establish large-scale, flexible computing systems which are available on-demand to fulfil dynamic user requirements. Virtual machine (VM) technology [1] has a profound role in this. Live migration, isolation, flexibility and customization represent compelling characteristics of the Clouds. Amazon EC2 [2] and GoGrid [3] represent the leading examples of commercial Cloud providers whereas Nimbus [4] and OpenNebula [5] represent academic efforts to achieve Cloud computing systems. As with any other emerging paradigm, different models of Clouds have been proposed to harvest its benefits. These are Infrastructure as a Service (IaaS), Software as a Service (SaaS) and Platform as a Service (PaaS) [6]. With regards to these models, the Cloud computing system referred to in this paper is the IaaS and therefore, inherits the characteristics of that model.

Security underpins the extensive adoption of Cloud computing as highlighted by [7]. Related to this, Clouds introduce novel challenges for the development of enabling

mechanisms in general and security in particular which require dedicated efforts for their solution [8]. The emphasis of our research is to investigate security issues due to the use of virtualization in Clouds to achieve multi-tenancy with maximum isolation, and flexibility of the resultant computing infrastructures. This has significant implications for the overall security of the Clouds in general and intrusion response in particular. This is because due to the multi-tenancy provided by VMs, an intrusion detection and response system, residing in the most privileged domain, is required to monitor multiple VMs with diverse security requirements. Furthermore, depending on the security requirements of a VM, the overall damage caused by a particular malicious attempt can be different for individual VMs. As described by [9], an effective response to an intrusion is representative of the overall damage caused by an intrusion for the victim. Therefore, the above has significant implications with respect to the invocation of an appropriate response mechanism for an intrusion. To the best of our knowledge, we pioneer efforts to identify the significance and application of this concept for Clouds building on the previous work described in [10].

The emphasis of this paper is to describe our efforts to develop a novel scheme to assess the extent of damage caused by an intrusion for a victim VM within Clouds. The scheme developed to assess the extent of damage caused by an intrusion is inspired by standard clinical procedures by drawing similarities between the two processes. Additionally, the scheme identifies and uses the dependencies between different malicious events to provide protection against multi-stage attacks. This paper also presents formal specification and verification of the proposed scheme.

2 Research Context

Multi-stage attacks represent a growing category of internet based attacks [11]. They represent intrusions whereby an attacker attempts to conceal the attack by dividing it into multiple steps. Although each of these steps represents a malicious activity, the damage caused by individual steps is relatively small as compared to the overall damage caused by the attack. Therefore, if a system is agnostic of such malicious attempts, the attacker can be successful in achieving their objectives by simply dividing the malicious activity into simpler, seemingly less-malicious events. There have been considerable efforts for detection of multi-stage attacks such as [11, 12]. However extensive exploration of existing literature with respect to Clouds revealed no scheme to incorporate this type of attacks for damage assessment.

Furthermore, [9] presents a three-point criteria for effective intrusion response. This mandates a response to an intrusion to be i) in-line with the impact of the intrusion for the victim, ii) take into account the extent of damage caused by an intrusion, and iii) to execute a response with minimal delay. Within our research, we are focused at developing a method to take into account these three factors to achieve effective intrusion response for Clouds. In particular, we define the impact of an intrusion and the damage caused by it for a victim VM as a composite attribute called the severity of an intrusion. The term severity is not novel and has been used in existing literature to describe intrusion impact such as [13]. However, the motivation to define it as a compound attribute is primarily due to its significance to facilitate

rigorous analysis of the overall damage caused by an intrusion for a victim as illustrated by [9]. Furthermore, both intrusion impact and extent of damage share significant reliance on the security characteristics of the victim as described by [14, 15]. This is particularly significant for Clouds as depending on the security characteristics of the victim VM, an intrusion can have different severity for individual victim machines.

With respect to the three-point criteria of effective response described earlier, our effort to develop a scheme for effective intrusion impact analysis along with its rigorous evaluation has been presented in [16]. Furthermore, an evaluation of the impact analysis scheme with respect to overall intrusion response time has been presented in [17]. This paper is focused at the challenge of developing a scheme to assess the extent of damage caused by an intrusion for a victim VM. Additionally, the scheme is envisaged to provide protection against multi-stage attacks.

3 Related Work

Within the context of this paper, damage assessment refers to the process of determination of the extent of damage caused by an intrusion on the victim VM. Extensive review of literature has identified no existing damage assessment techniques for Clouds however there has been considerable efforts to achieve this for traditional systems. This section therefore presents a critical review of efforts from traditional computing systems to achieve damage assessment along with their limitations to address damage assessment for Clouds.

[18] presents a reference model and an algorithm to perform damage assessment for cyber-based missions. As part of the reference model, the damage assessment process is proposed to take into account critical assets and services within an infrastructure, vulnerabilities within these assets and services, and the attack models. These components suggest an offline risk assessment process accompanied by in-depth knowledge of the services and assets of the system, the vulnerabilities for these assets and in-depth knowledge of the attacks that can exploit these vulnerabilities. However, an offline risk assessment at the VM level is extremely difficult for Clouds primarily due to the extraordinary scale and diversity of the VMs within a Cloud. Also, the assumption of in-depth knowledge of the critical assets and their vulnerabilities is extremely difficult. For instance, the proposed algorithm for damage assessment uses parameters such as `exploit_likelihood`, `reliability_likelihood`, and `likelihood_of_impact` require expert knowledge of the system and the attacks as part of rigorous risk assessment exercises. Finally, it is extremely difficult if not impossible to establish a perfect attack model and there is always a risk of (zero-day) unknown attacks being neglected.

A game theory based approach for damage assessment for network services is presented by [15]. The scheme uses expert knowledge about the victim asset, the significance of the victim asset for the organization and the capabilities of administrator and the attacker to measure the overall damage caused by an intrusion. It is different from the above described techniques in that it also takes into account multi-stage attacks. Furthermore, it also proposes to mitigate with attacks on network resources such as routers and switches in addition to hosts over a network. For single

stage attacks, the damage is calculated as a function of the nodes affected by the attack, the defense mechanisms installed on the victim, the significance of the victim and the topology of the network. As the scheme is intended to facilitate a human administrator, the values for these attributes are envisaged to be evaluated by the administrator using appropriate risk assessment. However, this requires in-depth knowledge about the nodes, their vulnerabilities and the network topology as well. Within our system model, it is extremely difficult to predict this information as has been explained earlier. The scheme treats a multi-stage attack as a non-cooperative zero-sum multi-stage game where the actions of both the attacker and the system administrator are modeled within a tree. The major assumption in this case is that both the attacker and the administrator can execute one step at a time allowing the other party to respond to their respective actions. Although it is interesting and can be used to model attack strategies, it is extremely difficult to realize this situation at a VM level within a Cloud.

A scheme for network based intrusion detection, damage assessment and prevention is presented by [19]. It is particularly focused at distributed intrusions which aim to affect multiple different nodes on a network. Examples of such intrusions include internet worms which aim to infect as many machines as possible over the Internet. In order to take into account the damage caused by an attack on multiple hosts, it introduces the concept of Security Dependency Relationships (SDR). SDR is envisaged to represent dependencies between different nodes on a network. This is an interesting concept however the authors propose it to be implemented using in-depth knowledge of the nodes within a network. Once the dependencies have been established, it uses historical audit data to calculate the probability of intrusion for each host. Finally, the damage assessment is performed by aggregating the probabilities for all intrusive events.

A probabilistic scheme based on a Markov decision process is presented by [20] to enable IDS to assess the damage caused by an attack on the monitored resources. As most of the schemes described in this section, this scheme is focused on network based systems and the attacks targeting networks. In order to assess the overall damage caused by an attack, it takes into account both the cost of security failure and also the cost of maintenance due to a response to the intrusion. Within this paper, we are focused at the cost of security failure. The cost of security failure is proposed to be calculated as a product of the significance of the victim component within the network and the threat degree of potential attack. In case of a multi-stage attack, the authors propose to aggregate the cost for each individual step along with two additional metrics i.e. α as weight denoting threat degree of each attack step, and β to trade-off the balance between failure cost and maintenance cost. The respective values of these parameters are adjusted by a human administrator in accordance with the significance of the victim asset and the attack scenario. However, the involvement of human administrator in this case is intensive as s/he is not only responsible to perform an effective risk assessment offline, they are also expected to interact and respond with an attack scenario at runtime and devise response mechanisms in-line with the outputs of the proposed cost functions. These limitations render it extremely difficult to implement this scheme within our system model.

In addition to the above described schemes, the term damage assessment is also used in fault tolerant computing by transactional systems. As the focus of these

approaches is on transactional systems, we regard them as out of scope of the research presented in this paper.

4 Fault Model

In order to devise a fault model for the research presented in this paper, extensive study of existing literature regarding fault models for Clouds was conducted which revealed no such efforts for Clouds. However, there has been significant research with respect to fault models for traditional distributed systems and Grids. [21] describes a general fault model for distributed systems whereas [22] describes a fault model for Grids. Although Clouds share similarities with these computing paradigms and an overlap can be found with respect to faults that can influence all these computing paradigms, the fault model for this research is essentially different. This is primarily because the faults considered in this research are those that can affect a system residing within the domain 0 whereas the primary focus of fault models for traditional HPC research is from the perspective of a middleware system or the guest application. For instance, [21] describes network errors and response faults as part of the fault model for a distributed system. However, these represent errors which can be monitored at the middleware or application level. Furthermore, faults exploiting the vulnerabilities of the VM technology, and those targeting the misuse of allocated resources for a VM are not covered by the traditional fault models.

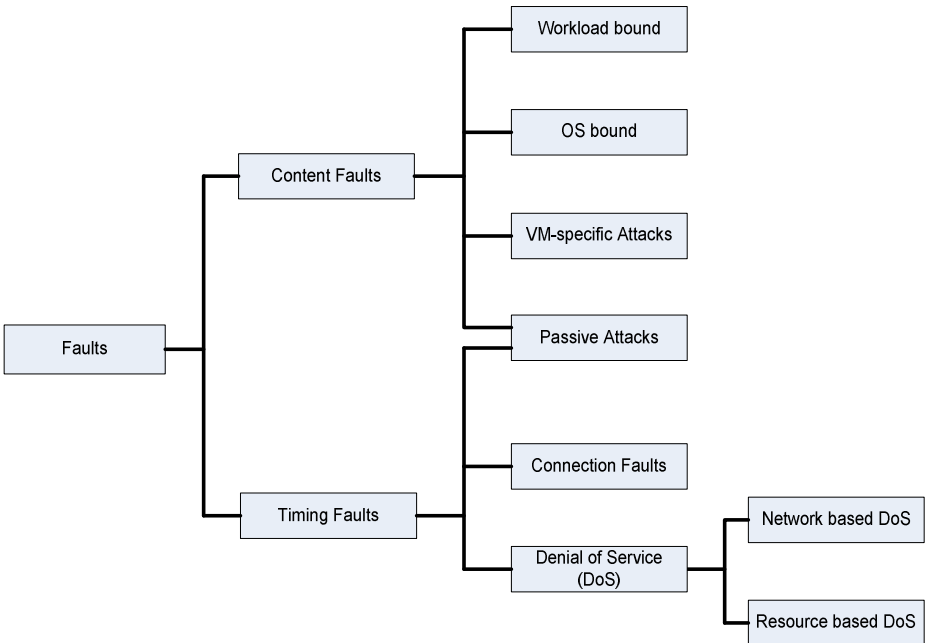


Fig. 1. Fault model for the proposed system

The faults included as part of the fault model for this research have been identified as significant from the perspective of a compute intensive workload in a Cloud. Additionally, the proposed system has to deal with system calls from within the domain 0. Therefore, this fault model takes into account faults that can be dealt with at the system call level from within the domain 0. Fig 1 presents the fault model for this research.

The faults considered for the proposed system are external software faults as categorized by [23] and hardware is assumed to be error free. These faults include malicious faults executed by human and therefore exclude any natural faults such as natural disasters causing shutdown of a data centre. The source of faults for this research is considered to be application-specific vulnerabilities that allow an intruder to compromise a VM and possibly use the resources allocated to the victim VM to accomplish malicious motives, and operational mistakes i.e. mistakes in configuration of VMs which can be exploited to enable a VM to infect a neighbor VM.

5 The Damage Assessment Scheme for Clouds

The proposed scheme makes use of VM specific parameters to achieve context-aware operation. These parameters include security characteristics of the victim VM, the state of the SLA, the frequency of the attack, and the degree of impact of the intrusion for the victim VM. The degree of impact is determined as an output of the intrusion impact analysis scheme whereas quantification of security requirements has been performed to achieve a representation of the security characteristics of a victim VM as reported in our previous work [24].

With respect to damage assessment, a scheme inspired by clinical procedures is established which takes into account parameters such as security characteristics, and the impact determined for individual malicious system call events to evaluate damage for individual malicious system call events. However, such simplistic scheme will be compromised in the event of multi stage attacks. This is extremely important as multi stage attack represent a growing class of internet based attacks where an attack attempts to conceal the attack by dividing it into multiple steps as illustrated by [11, 12]. Although each of these steps represent a malicious activity, the damage caused by individual steps is insignificant as compared to the overall damage caused by the attack. Therefore, if a system is agnostic of such malicious attempts, the attacker can be successful in achieving their objectives by simply dividing the malicious activity into simpler seemingly less-malicious events. In order to mitigate with such attacks, the proposed damage assessment scheme is envisaged to take into account historical system call data for a victim VM. The scheme is inspired by the concept of SDR proposed by [19] to identify relationships between different malicious events to discover different stages of an attack. The damage assessment process includes aggregation of damage across these stages to determine the precise extent of damage for a malicious system call event.

In order to illustrate the significance of the dependencies between different malicious events consider the following example from [25].

$ME_1 = \text{SadmindPing}: (\{\text{VictimIP}, \text{VictimPort}\}, \text{ExistsHost}(\text{VictimIP}), \{\text{VulnerableSadmind}(\text{VictimIP})\}), \text{and}$

$ME_2 = \text{SadmindBufferOverflow}: (\{\text{VictimIP}, \text{VictimPort}\}, \text{ExistsHost}(\text{VictimIP}) \wedge \text{VulnerableSadmind}(\text{VictimIP}), \{\text{GainrootAccess}(\text{VictimIP})\}).$

For ME_1 pre_cond can be described as $(\{\text{VictimIP}, \text{VictimPort}\}, \text{ExistsHost}(\text{VictimIP}))$ which means that it requires a valid VictimIP and VictimPort to be successful in its operation i.e. ping. The post_cond for the same event can be described as $\{\text{VulnerableSadmind}(\text{VictimIP})\}$ which means that a successful ping can result in the discovery of a vulnerable service for the victim host represented by VictimIP. For ME_2 , pre_cond can be described as $\{\text{VictimIP}, \text{VictimPort}\}, \text{ExistsHost}(\text{VictimIP}) \wedge \text{VulnerableSadmind}(\text{VictimIP})$ which means that it requires a valid VictimIP, VictimPort and availability of a vulnerable victim service. The post_cond for this event is described as $\{\text{GainrootAccess}(\text{VictimIP})\}$ which means that a successful buffer overflow in this case can result in gaining root access for the victim.

The above description of the pre and post conditions for the two malicious events results in the identification of a relationship between the two seemingly distinct events. Therefore, in order to effectively assess the extent of damage caused by a malicious event, the analysis of its dependencies is significant. In view of this, the damage assessment scheme takes into account these dependencies. Furthermore, the total damage caused by a system call is defined as an aggregate function of the individual damage by each system call in the dependency graph.

6 Formal Specification and Analysis of the Damage Assessment Scheme

This section presents the formal specification and analysis of the damage assessment scheme. The first section provides details of the formal specification performed using the Z language followed by the explanation of the formal verification of the scheme using faults trees and deductive logic.

6.1 Formal Specification of the Damage Assessment Scheme

In order to develop a formal specification of the system, the data models used in the system are extremely significant. As part of the formal specification of the damage assessment scheme, the data models involved are first described followed by the formal specification of the system. Due to the limited space of this manuscript, an extended explanation of these data models is not possible. Therefore, a brief description of the data models is presented.

[SYSCALLS] represents the set of all the possible system calls which can be executed by a VM.

[M_SYSCALLS] represents the set of malicious system calls identified as malicious by the IDS for a victim VM.

In order to address the challenge of multi-stage attacks, it is proposed to identify relationships between different stages of attacks at the system call level. This is envisaged to be achieved by defining system call based policies for intrusion

detection. The dependencies are categorized into pre and post conditions which represent the states to achieve malicious objectives of an attacker. It is assumed that these dependencies are established offline and the sets of these dependencies are available for the damage assessment. These sets are represented by [PRE_COND], [POST_COND] in the system specification.

<i>Damage Assessment</i>
$\beta : \mathbb{N}$
$S_t : \mathbb{N}$
$S_g : PRIORITY$
$I_v : IMPACT$
$F_r : \mathbb{N}$
$m_sys_call : M_SYSCALLS$
$cp : CHECKPOINTS$
$sys_call_dataset : (m_sys_call, cp) \leftrightarrow \mathbb{P} CP_SYSCALLS$
$current_sys_call : CP_SYSCALLS$
$dependencies_evaluation : (current_sys_call, PRE_COND, POST_COND) \leftrightarrow \mathbb{P} DEPEND$
$d_sys_call : DEPEND$
$initial_DA : (current_sys_call, \beta, S_t, S_g, I_v, F_r) \rightarrow initial_Damage$
$partial_DA : (d_sys_call, \beta, S_t, S_g, I_v, F_r) \rightarrow indiv_Damage$
$Aggregate_DA : (initial_DA, partial_DA) \rightarrow total_Damage$
$F_r > 1$
$0 \leq \beta \leq 1$
$S_t \geq 0$
$M_SYSCALLS \neq \emptyset$
$CHECKPOINTS \neq \emptyset$

Fig. 2. Formal specification for the overall damage assessment system

For a given system call s_i , the damage assessment scheme takes into account dependencies among recent system calls to mitigate with multi-stage attacks. In order to define the scope of operation with respect to system calls, the scheme uses most recent checkpoint and restricts analysis to the set of malicious system calls executed since the last checkpoint. This set of system calls is represented by [CP_SYSCALLS] in the formal system specification.

Using the set of system calls since the last stable checkpoint [CP_SYSCALLS], and the pre and post conditions represented by [PRE_COND] and [POST_COND], the damage assessment scheme populates a directed graph using the dependencies identified among the malicious system calls. The set of these system calls is represented by [DEPEND] in the formal system specification.

The principle followed to establish this set is borrowed from the domain of alert correlation [27] and is as follows. In order to establish these dependencies, each malicious system call event is considered as a tuple represented as $ME = (system_call, pre_cond, post_cond)$. As described earlier, the parameters pre_cond and $post_cond$ are established at the policy definition stage for intrusion detection using system call based policies. Now, for each malicious event ME_i occurring at

time t_i , a malicious event ME_j occurring at time t_j is dependent on ME_i if and only if $(ME_i.post_{cond} = ME_j.pre_{cond}) \wedge (t_i < t_j)$. This establishes a directed acyclic graph where the nodes represent system calls and the edges represent the relationship between these system calls.

Due to the limited space of this paper, the formal specification for the damage assessment system alone is presented in fig 2. It includes specification of different parameters envisaged to be used by the damage assessment scheme along with the description of the operations performed by it. The parameters include F_r as frequency of attack, S_t as the SLA state, S_g as the priority of the affected security requirement, I_v as the degree of impact evaluated by the impact analysis scheme, and β as the response capabilities of the victim VM. The operations include initialization of the system call dataset since the last checkpoint, evaluation of the dependencies for each system call in the dataset, evaluation of individual damage, and aggregation of individual damage to determine the total damage caused by the intrusion for a victim VM.

6.2 Formal Analysis of the Damage Assessment Scheme

In order to analyze the proposed damage assessment scheme, formal analysis using fault tree analysis and deductive logic is employed. The fault tree analysis is conducted to evaluate the potential undesired properties of the damage assessment system. This is followed by proofs using deductive reasoning to verify that the characteristics of the system prevent occurrence of these undesired properties.

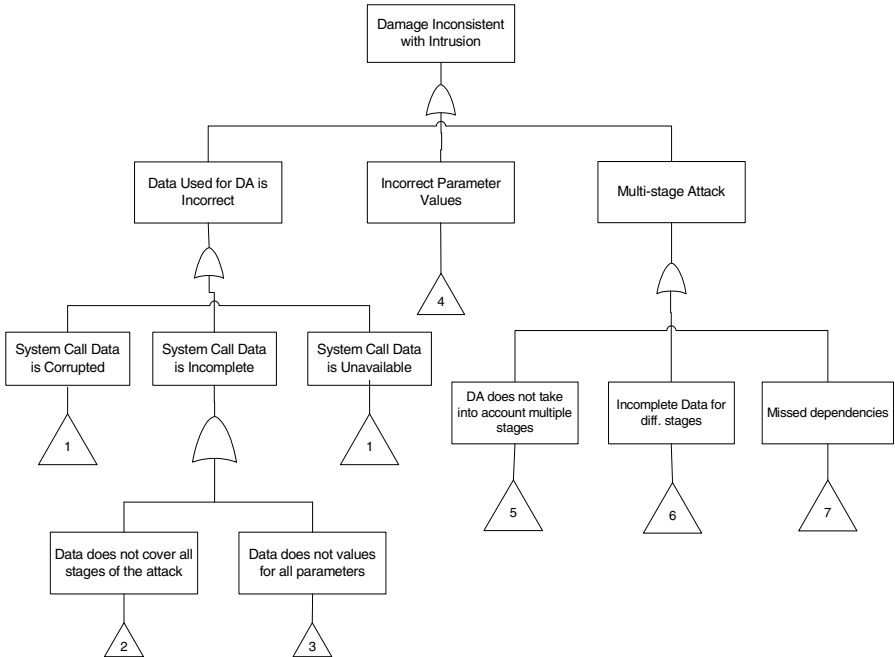


Fig. 3. An example fault tree for damage assessment scheme

An example fault tree for the damage assessment scheme is presented in Fig. 3. Although there are multiple cut sets and their respective proofs, we present proof for one cut set as an example of the formal reasoning process. This cut set represents the evaluation of the scheme with respect to mitigation against multi-stage attacks. This has been identified as part of the fault tree analysis as the fault node: DA does not take into account multiple stages. It can be formally represented as under.

$$\text{cut set} = (\exists_1 s_i \mid \text{Damage}(s_i)) \wedge (\neg \sum \text{Damage}(s_i)) \bullet s_i \in M_SYSCALLS$$

In order to prove this, we can divide this into two parts. For the first part,

$$\Leftrightarrow (\exists_1 s_i \mid (s_i)) \bullet s_i \in M_SYSCALLS$$

From specification,

$$\forall s_i \mid s_i \in M_SYSCALLS \bullet \text{Total_damage} := \text{Indiv_damage} + \text{Partial_damage}$$

$$\Leftrightarrow \text{Damage}(s_i) + \text{Partial_damage}$$

$$\Leftrightarrow \text{Damage}(s_i) \mid s_i \in M_SYSCALLS \wedge s_i \in \text{DEPEND} + \text{Partial_damage}$$

$$\Leftrightarrow \text{Damage}(s_i) \mid s_i \in M_SYSCALLS \wedge s_i \in \text{DEPEND} + \text{Damage}(s_i) \mid s_i \in \text{DEPEND}$$

$$\Leftrightarrow \text{Damage}(s_i) \mid s_i \in M_SYSCALLS \wedge s_i \in \text{DEPEND} + \text{Damage}(s_i) \mid s_i \in \text{DEPEND} \bullet \text{dependencies}' = \text{dependencies} \cup \{s_i\}$$

$$\Leftrightarrow (s_i.\text{post_cond} = s_j.\text{pre_cond}) \wedge j > i$$

$$\Leftrightarrow \neg (\exists_1 s_i \mid (s_i))$$

$$\Leftrightarrow \text{false}$$

The above analysis proves that the hypothesis $(\exists_1 s_i \mid \text{Damage}(s_i)) \bullet s_i \in M_SYSCALLS$ i.e. the damage assessment is performed on isolated system call events, is false.

Now the second part can be written as under.

$$(\neg \sum \text{Damage}(s_i)) \bullet s_i \in M_SYSCALLS$$

From specification,

$$\forall s_i \mid s_i \in M_SYSCALLS \text{ total_damage} := \text{Indiv_damage} + \text{Partial_damage}$$

$$\Leftrightarrow \text{Damage}(s_i) + \text{Partial_damage} \mid s_i \in M_SYSCALLS$$

$$\Leftrightarrow \text{Damage}(s_i) + \text{Partial_damage}(\text{dependencies} \mapsto \text{Indiv_damage})$$

$$\Leftrightarrow \text{Damage}(s_i) + \text{Partial_damage}(\text{dependencies}$$

$$\mapsto \text{Indiv_damage}) \wedge \text{dependencies} : \mathbb{F} \text{DEPEND} \text{DEPEND}$$

$$\neq \langle \rangle$$

$$\Leftrightarrow \text{Damage}(s_i) + \sum \forall sd_i, \text{Indiv_damage}(sd_i) \bullet$$

$$sd_i \in \text{dependencies} \text{DEPEND} \neq \langle \rangle$$

$$\Leftrightarrow \sum \text{Damage}(s_i) \bullet s_i \in M_SYSCALLS$$

$$\Leftrightarrow \text{false}$$

The above analysis proves the hypothesis:

$(\neg \sum Damage(s_i)) \bullet s_i \in M_SYSCALLS$ to be false i.e. the extent of damage calculated by the damage assessment scheme does not take into account aggregation of individual damage for each malicious event, to be false. From the above analysis, it can be concluded that the cut set is not valid for the proposed damage assessment scheme. This is proved as both the conditions necessary for the cut set to be true have been found false in accordance with the formal specification of the damage assessment scheme.

7 Conclusions and Future Work

We hold that security underpins extensive adoption of Clouds. This paper is focused at one specific challenge related to the overall security of Clouds i.e. assessment of the extent of damage caused by an intrusion for a VM in a Cloud. The paper has presented a novel damage assessment scheme inspired by clinical procedures detailing different aspects of the scheme. The implementation and evaluation of the scheme is currently realized by formal specification and evaluation. The results of this evaluation demonstrate the effectiveness of the proposed scheme to successfully determine the extent of damage of an intrusion for a VM. Furthermore, the formal reasoning facilitated by fault tree analysis demonstrates the effectiveness of the scheme to protect against multi-stage attacks. With respect to the implementation of this scheme with a real Cloud system, work is currently in progress to incorporate the scheme with iVIC [26], a real Cloud system. We envisage it to open new opportunities for further evaluation of the scheme.

References

- [1] Goldberg, R.P.: A Survey of Virtual Machine Research. *IEEE Computer* 7, 34–45 (1974)
- [2] Amazon Elastic Computing Cloud, <http://aws.amazon.com/ec2>
- [3] GoGrid: Scalable Load-Balanced Windows and Linux Cloud-Server Hosting, <http://www.gogrid.com/>
- [4] Nimbus Cloud, <http://www.workspace.globus.org>
- [5] OpenNebula Project, <http://www.opennebula.org>
- [6] Mell, P., Grance, T.: A NIST National Definition of Cloud Computing, <http://csrc.nist.gov/groups/SNS/cloud-computing/cloud-def-v15.doc>
- [7] New IDC IT Cloud Services Survey: Top Benefits and Challenges (December 2009), <http://blogs.idc.com/ie/?p=730>
- [8] Garfinkel, T., Rosenblum, M.: When Virtual is Harder than Real: Security Challenges in Virtual Machine Based Computing Environments. In: *The Proceedings of 10th Workshop on Hot Topics in Operating Systems* (2005), <http://usenix.org>
- [9] Brackney, R.: Cyber-Intrusion Response. In: *Proceedings of the 17th IEEE Symposium on Reliable Distributed Systems*, West Lafayette, IN, p. 413 (1998)

- [10] Arshad, J.: Integrated Intrusion Detection and Diagnosis for Clouds. In: *The Proceedings of Dependable Systems and Networks (DSN)*, Student Forum (2009)
- [11] Alserhani, F., Akhlaq, M., Awan, I., Cullen, A.: MARS: Multi-stage Attack Recognition System. In: *The Proceedings of the 24th IEEE International Conference on Advanced Information Networking and Applications*, Perth, Australia (2010)
- [12] Cheung, S., Lindqvist, U., Fong, M.W.: Modelling Multistep Cyber Attacks for Scenario Recognition. In: *The Proceedings of the 3rd DARPA Information Survivability Conference and Exposition*, Washington, D.C. (2003)
- [13] White, G., Fisch, E., Pooch, U.: Cooperating Security Managers: A Peer-based Intrusion Detection System. *IEEE Network*, 20–23 (1996)
- [14] Piesco, A.L., Walsh, J.H.: Attack Impact Prediction System, US Patent (October 2007), Patent number: US 7,281,270 B2
- [15] Luo, Y., Szidarovszky, F., Al-Nashif, Y., Hariri, S.: A Game Theory based Risk and Impact Analysis Method for Intrusion Defence Systems. *IEEE* (2009)
- [16] Arshad, J., Townend, P., Xu, J.: An Intrusion Diagnosis Perspective on Clouds. In: *Guide to e-Science: Next Generation Scientific Research and Discovery*, part 3, pp. 299–319. Springer, Heidelberg (2011), doi:10.1007/978-0-85729-439-5_11
- [17] Arshad, J., Townend, P., Xu, J.: A Context-aware Intrusion Severity Analysis Scheme for Clouds. Submitted for the UK-All Hands Meeting (2011)
- [18] Lewis, L., Jakobson, G., Buford, J.: Enabling Cyber Situation Awareness, Impact Assessment, and Situation Projection. *IEEE ISBN:978-1-4244-2677-5/08/*
- [19] Yau, S.S., Zhang, X.: Computer Network Intrusion Detection, Assessment and Prevention based on Security Dependency Relation. *IEEE* (1999)
- [20] Zhang, Z., Ho, P., He, L.: Measuring IDS-estimated Attack Impacts for Rational Incident Response: A Decision Theoretic Approach. *Computers and Security* (2009), doi: 10.1016/j.cose.2009.03.05
- [21] Townend, P., Xu, J.: Fault tolerance within a grid environment. In: *UK e-Science All Hands Meeting* (2003)
- [22] Looker, N., Xu, J.: Assessing the Dependability of OGSA Middleware by Fault Injection. In: *The Proceedings of the International Symposium on Reliable Distributed Systems*, Italy (2003)
- [23] Avizienis, A., Laprie, J.-C., Randell, B.: Dependability and its Threats: A Taxonomy. In: *Proceedings of Building the Information Society: Proc. IFIP 18th World Computer Congress*, Toulouse, August 22-27, pp. 91–120. Kluwer Academic Publishers (2004)
- [24] Arshad, J., Townend, P., Xu, J.: Quantification of Security from the Perspective of Compute intensive Workloads for Clouds. In: *The Proceedings of the 13th International Conference for Parallel and Distributed Systems* (December 2009)
- [25] Ning, P., Xu, D.: Learning Attack Strategies from Intrusion Alert. In: *The Proceedings of ACM Conference for Computer and Communications Security* (2003)
- [26] Huai, J., Li, Q., Hu, C.: CIVIC: A Hypervisor based Computing Environment. In: *The Proceedings of the 2007 International Conference on Parallel Processing* (2007)
- [27] Al-Mamory, S.O., Zhang, H.L.: A Survey on Alert Processing Techniques. In: *The Proceedings of the International Conference on Information Security and Privacy*, Tenerife, Spain (2007)

Emotions in Robots

Muhammad Mansoor Azeem^{1,*}, Jamshed Iqbal², Pekka Toivanen¹,
and Abdul Samad³

¹Faculty of Science and Forestry, University of Eastern Finland (UEF), Kuopio, Finland

²COMSATS Institute of Information Technology (CIIT), Islamabad, Pakistan

³Center for Advanced Studies in Engineering (CASE), Islamabad, Pakistan
mansaz@student.uef.fi

Abstract. This article gives a general overview of emotions in robotics. It sheds light on the composition of emotions in human beings and how this information can be used as blue print for creation of emotional robots. It discusses different factors involved in creation and detection of emotion. The article briefly explains the social aspects of having emotional robots in society. A system architecture to build emotional system of robot is presented, along with information about working of its modules.

Keywords: Emotions in robotics, Future robots, Robot learning, Social robots, Knowledgebase.

1 Introduction

With the advancements in technology, machines with emotions are no more a science fiction. As robots are integrating in human society, it is important to have a better Human-Robot Interaction (HRI). It can be achieved only when both can understand each other. Making robots capable of understanding human natural language and respond in a natural way can be one plausible method for natural HRI. For that robots should be able to recognize the human emotions and should be able to give a response understandable and interpretable by humans.

The aim of the present work is to figure out the techniques through which we can have self-learning intelligent robots. We will look through the development of emotions in human beings. Our goal is to develop system architecture to implement the process of emotions generation in robots. We will present a literature review of different factors involved in creation of emotion and discuss how these factors can be used for development of emotions in robots. We will shortly discuss different social and ethical aspects involved in the emergence of robots as autonomous decision taking machines.

* Corresponding author.

2 Implementation

2.1 What Are Emotions?

Emotions consist of feelings, thoughts and behavior. Emotions are always private and subjective. There are large numbers of emotional states which humans can exhibit. Furthermore, many emotions are only blend of different basic emotions. On the other hand, emotion can be considered as a response or a psychological arousal driven by an act of defense or attack.

From all the theories presented, a conclusion can be made that emotions are driving factors of human decision-making. They originate because of external environmental factors and internal memory state. In fact, emotions make human beings "autonomous" in their decision-making. Humans based on their feelings and emotions take decisions. When humans analyze the situation and make a decision, they assume that it is correct according to current circumstances. Therefore, we believe that same logic can be used to make our robots autonomous in their decision-making.

2.2 Emotions in Robots

Robots have sensors corresponding to senses of humans. Humans can sense their environment according to the natural senses they have. Robots can be equipped with a number of such senses to sense their environment. There is an extensive research going on for recognizing the human emotions on the basis of different parameters like voice, facial expression and body language. For recognizing emotions from voice, VRA Technology seeks to interpret the complete emotional structure evident in individually assessed conversations (excitement, pain, fear, cognitive activity and more) [1]. The correlation among these various emotional stress characteristics enables to determine whether a statement was, amongst other things, truthful, deceptive, uncertain and inaccurate. The speech of person can provide a lot of information about his emotional state. This information is present in acoustic properties like fundamental frequency, pitch, loudness, speech-rate and frequency range [2].

The emotions in a robot will help to have more life-like Human Computer Interaction (HCI) [3-5]. An emotion of a robot provides information about many aspects of the current state. They can tell about the intentions of the robot, its internal and external state and it may reveal what the robot is "up to" [6,7]. Emotions provide feed-back in the interaction with the robot how the robot feels about its environment. They also show how robot is affected by the people around it, what kind of emotions it understands and how it is adapting to the ever changing world around him [8-10].

2.3 Emotion Expression

Expression of emotions is an important part of emotional conversation. For two way communication it is important that robot not only recognize the human emotion but also is able to express the emotion. The design and technology used to develop the

capability of a robot to show emotions will greatly affect how humans will be able to perceive the robot. The important part of emotion expression is non-verbal communication in which the emotions are expressed through body gestures and facial expressions. Usually a category-based model is used to map emotions, where a number of emotions are present for a number of actions. Nevertheless, this approach is somewhat closed because there is no space of overlapping emotions. We are introducing an Emotion Expression System, which has different approach. As the feedback is main source of learning of a robot, it will also help to refine the precision of emotions expressed. The use of emotion is one aspect but its use in right context is also important. We will not ignore the effect of expression, which can be seen as immediate reaction from human. In ideal case, the human will understand the robotic expression and will continue forward the communication. However, in worst case it can misunderstand the expression demonstrated by a robot. There could be many reasons for this misunderstanding with two possibilities that the robot did not learn the emotion well before using it or it used the right emotion in wrong context.

2.4 Emotion Recognition

When we talk about recognition of emotions, we will have to consider all factors that are involved in an emotion. For the proper recognition of emotion, we need to recognize facial expressions, body movements, speech and some internal factors like blood pressure and heartbeat. The results from these factors will then be combined to recognize an emotion. For the correct recognition of an emotion, it is also important to consider the environment and circumstances at a particular moment, as there could be history involved in the reason of an emotion. For robot, it is important to know all the possible aspects of human emotion. There has been work done in recognition of emotions on the basis of speech and facial expressions. However, not much work has been done to combine these approaches to get a more accurate and robust result of recognized emotion. It is obvious that if system has more information, the decision making will be more precise. Information from speech and facial expression for example is somehow related.

Speech. Speech contains a lot of information about the emotional state of human beings. When humans hear a certain voice they can easily know the emotion of person, the stress level and emotional state [11]. Humans change the tone of their voice to express different emotions and extent of their state. Researchers have found a relationship between voice and emotions. Three types of information are contained in human speech: who the speaker is, what it is said and how it is said [11, 12]. This depends on what kind of information the robot will require from the speech. The robot can use this information for emotion recognition or even for identifying the person. Researchers have done work in recognizing the natural language so that robot can be made more efficient in communicating with humans [13-17].

There are no hard and fast rules developed so far about which features of voice should be measured to recognize the emotions. Acoustic parameters vary in their

function and kind of information they carry. These parameters and intensity has been researched [11]. For natural conversation, a robot should be able to recognize the commands independent to the speaker. One approach for achieving this is a two-step process. In this process, first audio signals are transformed into feature vectors and then utterances are matched to a vocabulary. Many of current systems use Hidden Markov models to determine the nearest match from vocabulary [11]. A comprehensive introduction of speech recognition is given in [18]. We want our robot to produce human like emotions. For that purpose robot should be able to speak natural human language. It is important because the absence of a response in natural human language will not fulfill the purpose. So, it should have as natural voice as possible.

Facial Expressions. Facial expressions convey emotions, but some emotions can be shown barely using one's face. Face gives a personality to living thing and conveys the identity of the person. Humans immediately know about the person and show their expressions according to their relationship with that person. Before recognition, robot will also identify the person. Therefore, it can act according to a previous relationship if there exists one. There are three basic approaches to facial expression recognition [19]. In the first approach, facial muscle actions are identified in a sequence of images. In the second approach, facial features, as for example the distance between nose and lips, are tracked. In the third approach, Principal Component Analyses (PCA) are used to reduce image-based representations of faces into principal components likes eigen faces. A good overview of the techniques used to recognize facial expressions is presented in [5,20,21].

Gesture. When humans communicate, they often use their body parts to effectively deliver their ideas. For example, a person might say that "the cup of coffee is there" but he also points in the direction of the cup with his hand. This makes sure that other person understands him well. Humans mostly use their hand movement shoulders and movement of head. Gestures clarify the speech further. There are vision based techniques used to recognize gestures [11,16,22]. Furthermore, Kortenkamp et al. [23], Waldherr et al [24], and Xu et al. [25] have developed systems that recognize gestures for HCI.

Social Aspects. With increase in the population of emotional robots, they will become major part of human society. Therefore, they will make completely new species, who will become residents of our planet Earth. Many questions arise about their presence in human society, because people are not used to interacting with machines. Some may think it as a dump machine even if it will possess emotions and will have the ability to interact with humans. Emotional robots can be an integral part of society. We can think of certain moral and social issues related to them. Edmund Furse at University of Glamorgun gave a presentation "Theology of Robots" where he proposed some ideas about future life of emotional and intelligent robots in our society. According to him, robots will have legal rights, system of life and death and religious and moral issues. But this discussion is still very open that what emotional robots can have and what they cannot.

The human acceptance of emotional robots in the society is an interesting discussion. The first thing, which comes to mind and is of great concern for humans, is the increase of unemployment. As the intelligent robots will be produced on large scale, they will take more and more jobs done by humans previously. Nevertheless, as can be seen today around us that robots are making life of humans easier. They are easier to train in certain skills and they can take off lot of workload from humans. This will give more time to humans for relaxation. Calculators are very simple machines and still they have not taken jobs of mathematicians but they have saved their valuable time [24].

Emotional robots can be great pets. Especially the people who want to have pets but cannot have them because of busy city life or some allergies they can have robotic pets. There have been pets developed in shape of dog, fish, lion cub, cat and many other animals. An example can be taken from Paro. Paro is a baby harp seal robot designed by Takanori Shibata of the Intelligent System Research Institute of Japan (AIST). It was developed to replicate animal-assisted therapy but without its negative effects. The robot can show emotions of happiness, surprise and anger [25-27].

As we know now, robots are getting their own intelligence as the technology is advancing and a day might come when they will be able to think also. In that case robots will try to decide for themselves and may make choices unacceptable to humans. We have to make sure that robots follow some strict rules as do humans follow for a peaceful society. They should have clear defined limits so that they can never go out of human control and bring to reality the fantasies shown by movies such as "I, Robot". The movie is set in future where humans become completely dependent on robots. However, robots break laws made for them and try to take over humans.

Moral rights and duties will be important characteristic of emotional robot. It depends how they are programmed. Either they can be programmed to have only acceptable human behavior or they can be set free to learn whatever they want [28]. Our goal should be to make them as useful for humans as possible reducing their disadvantages. Presentation of their positive image in society will be key to their successful integration in human society.

Learning Emotions. Emotional system learns from experience. So, for showing emotions, it has to learn them first. We can make a robot which will simply copy the emotions and then will reproduce it exactly, but it won't recognize the state of person and thus the communication will be non-emotional. We not only wish robots to learn emotions but also want them to learn why and how each emotion is produced. There are various learning techniques that can be used for robots to learn emotions. Imitation is one of them. There is not a single widely accepted definition given for imitation. Thorpe [29] defines it as "copying of a novel or otherwise improbable act or utterance, or some act for which there is clearly no instinctive tendency".

Observations and continuous feedback from humans is the idea that we want to present. In this technique, the robot observes and recognizes an emotion. If he does not know about it already, it will try to repeat it. Nevertheless, the whole context will also be recorded. Because same emotion used in different context can have different meanings. The new emotion recorded by robot will be used by him and human can

assist him by giving feedback hence resulting in the learning of new emotion. This scheme requires great sensor and motor abilities to accomplish.

3 Proposed Emotional System

Based on the research carried out for this work, we can safely assume that there is possibility to create robots with natural human emotional capabilities. Figure 1 presents a proposed theoretical system architecture which could be used as basis for creating emotional system of an intelligent robot.

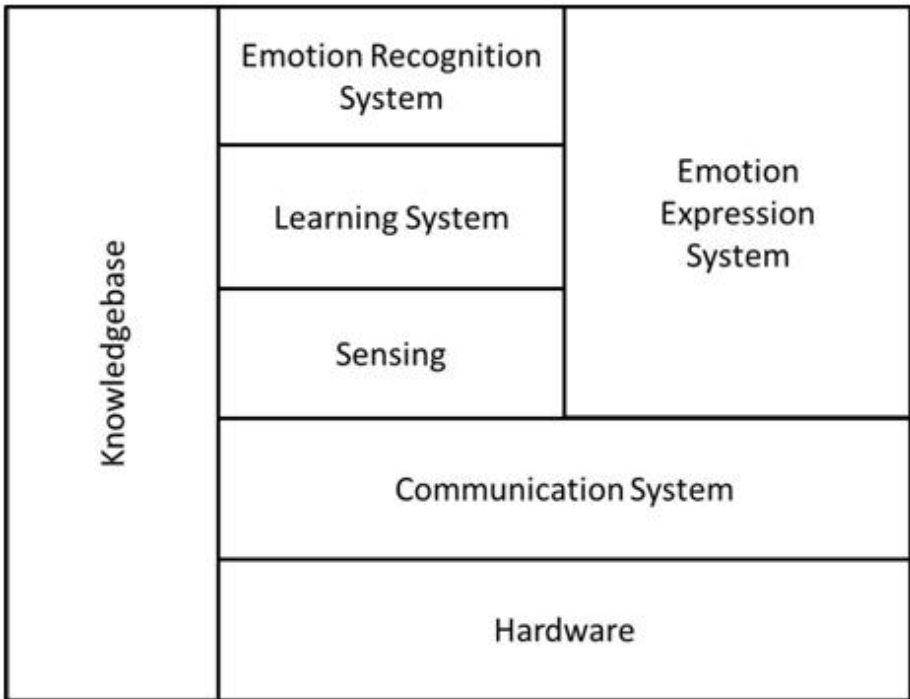


Fig. 1. Modules of proposed emotional system

Below is the description of various entities of emotional system presented in Figure 1.

Communication System is an important part as it will be responsible for the communication to other devices. Its function is to send and retrieve information required by humans.

Learning System is responsible for the learning part. Learning of skills and emotions is carried out by this module.

Emotion Expression System is responsible for emotion expression system. It processes information and sends instructions to other parts i.e. face, voice and body structure, for participating in expressing emotion.

Sensing is responsible for collection of all the information needed for recognizing the emotion.

Knowledgebase acts like a “mind” for robot. It is a comprehensive repository of information and also able to communicate with other sources for more information. The driving feature of a robot which directs it to an emotional system is “curiosity”. Action plan related to curiosity are bootstrapped in knowledgebase so that the system can decide to proceed further.

4 Detailed Working of Emotional System

Learning System. The first step here is to choose the learning technique. There are several possibilities like supervised learning, unsupervised learning and reinforcement learning. The System decides about the learning technique on the basis of time and resources available. By resources we mean here guidance which the system can get from humans, knowledgebase or other systems. We assume that there exists an online robotic community where robotic systems can share their knowledge and skills. When the robot likes to learn something, it first gathers all the information about it. For example the robot has seen a person saying something and then, as a reaction, it has seen people laughing. In fact this is analogous to the situation, where a person makes a joke and other people laugh on it. Now the robot records what the person said and the situation, where it was said, i.e., it can be an office meeting or a just a group of friends having fun. The robot adds this information in knowledgebase corresponding to an action that can be used to make people laugh. The next step for the robot will then be to imitate the same thing. The robot can imitate it while working at home or sitting with its human friends. The feedback from the surroundings will help it improve its perception of the emotion.

Learning System. The first step here is to choose the learning technique. There are several possibilities like supervised learning, unsupervised learning and reinforcement learning. The System decides about the learning technique on the basis of time and resources available. By resources we mean here guidance which the system can get from humans, knowledgebase or other systems. We assume that there exists an online robotic community where robotic systems can share their knowledge and skills. When the robot likes to learn something, it first gathers all the information about it. For example the robot has seen a person saying something and then, as a reaction, it has seen people laughing. In fact this is analogous to the situation, where a person makes a joke and other people laugh on it. Now the robot records what the person said and the situation, where it was said, i.e., it can be an office meeting or a just a group of friends having fun. The robot adds this information in knowledgebase corresponding to an action that can be used to make people laugh. The next step for the robot will then be to imitate the same thing. The robot can imitate it while working at home or sitting with its human friends. The feedback from the surroundings will help it improve its perception of the emotion.

Learning System. The first step here is to choose the learning technique. There are several possibilities like supervised learning, unsupervised learning and reinforcement learning. The System decides about the learning technique on the basis of time and resources available. By resources we mean here guidance which the system can get from humans, knowledgebase or other systems. We assume that there exists an online robotic community where robotic systems can share their knowledge and skills. When the robot likes to learn something, it first gathers all the information about it. For example the robot has seen a person saying something and then, as a reaction, it has seen people laughing. In fact this is analogous to the situation, where a person makes a joke and other people laugh on it. Now the robot records what the person said and the situation, where it was said, i.e., it can be an office meeting or a just a group of friends having fun. The robot adds this information in knowledgebase corresponding to an action that can be used to make people laugh. The next step for the robot will then be to imitate the same thing. The robot can imitate it while working at home or sitting with its human friends. The feedback will improve its perception of emotion.

Knowledgebase. Knowledgebase can be implemented as a multifunction distributed database providing a set of services. It is accessed by almost all subsystems of emotional system at some point of processing. The functions that the knowledgebase is providing in emotional system include storage of information, fetching of information from distributed locations and providing information needed by the subsystems. Knowledgebase will optimize data acquisition also by moving frequently accessed data to closer locations and by “dumping” obsolete data. The knowledgebase is also responsible for recovering an earlier stable state, in case of any processing failure or an inappropriate action.

5 Conclusion

We have given a general overview of emotions in robots. Our aim was to outline the possibilities of learning through emotions in robots. Different factors have been described on the basis of which a robot can recognize the emotions. The issues related to the integration of emotional robots in society have been discussed. The research done in this work suggests that it is quite possible to have human like emotions in robots. We have proposed system architecture for the emotional system of an intelligent robot. This architecture can be used for the development of emotional system in real world.

Although the advancement in information technology, mechanical engineering and electronics has made it possible to build humanoid robots like KISMET and Cog. However they still lack natural language and human like face. Furthermore the esthetics needs much improvement. We hope that as researchers will have more advanced technology on their disposal, these issues will be addressed.

References

1. Durrant, C., Winter, E., Yaxley, D.: Local Authority Omnibus Survey – Wave 18. Research report No. 590, Department of Work and Pensions (DWP), <http://research.dwp.gov.uk/asd/asd5/rports2009-2010/rrep590-ch7-vra.pdf>
2. Nass, C., Brave, S.: *Wired for Speech: How Voice Activates and Enhances the Human-Computer Relationship*. MIT Press, Cambridge (2005)
3. Cañamero, L., Fredslund, J.: I show you how I like you-can you read it in my face? *IEEE Transactions on Systems, Man and Cybernetics* 31(5), 454–459 (2001)
4. Ogata, T., Sugano, S.: Emotional communication robot: WAMOEBA-2R emotion model and evaluation experiments. In: *Proceedings of IEEE/RSJ International Conference on Intelligent Robots and Systems (IROS)* (2000)
5. Chibelushi, C.C., Boure, F.: *Facial Expression Recognition: A Brief Tutorial Overview*. On-Line Compendium of Computer Vision (2003)
6. Bartneck, C., Okada, M.: Robotic user interfaces. In: *Proceedings of the Human and Computer Conference* (2001)
7. Breazeal, C.: A motivational system for regulating human–robot interaction. In: *Proceedings of the National Conference on Artificial Intelligence*, Madison, WI, pp. 54–61 (1998)
8. Michaud, F., Prijanian, P., Audet, J., Létourneau, D.: Artificial emotion and social robotics. In: *Proceedings of the International Symposium on Distributed Autonomous Robotic Systems* (2000)
9. Velasquez, J.: A computational framework for emotion-based control. In: *Proceedings of the Workshop on Grounding Emotions in Adaptive Systems*, International Conference on SAB (1998)
10. Billard, A.: Robota: clever toy and educational tool. *Robotics and Autonomous Systems* 42, 259–269 (2003)
11. Breazeal, C.: *Designing Sociable Robots*. MIT Press, Cambridge (2002)
12. Adams, B., Breazeal, C., Brooks, R.A., Scassellati, B.: Humanoid robots: a new kind of tool. *IEEE Intelligent Systems* 15(4), 25–31 (2000)
13. Lauria, S., Bugmann, G., Kyriacou, T., Klein, E.: Mobile robot programming using natural language. *Robotics and Autonomous Systems* 38, 171–181 (2002)
14. Okuno, H., Nakadai, K., Hidai, K., Mizoguchi, H., Kitano, H.: Human– robot interaction through real-time auditory and visual multiple-talker tracking. In: *Proceedings of the IEEE International Conference on Intelligent Robots and Systems (IROS)*, pp. 1402–1409 (2001)
15. Spiliotopoulos, D., Androutsopoulos, I., Spyropoulos, C.D.: Human– robot interaction based on spoken natural language dialogue. In: *Proceedings of the European Workshop on Service and Humanoid Robots*, pp. 25–27 (2001)
16. Rabiner, L., Juang, B.: *Fundamentals of Speech Recognition*. Prentice-Hall, Englewood Cliffs (1993)
17. Lisetti, C., Schiano, D.: Automatic facial expression interpretation: Where human–computer interaction, artificial intelligence, and cognitive science intersect. *Pragmatics and Cognition* 8(1) (2000)
18. Chellappa, R., Wilson, C.L., Sirohey, S.: Human and machine recognition of faces: A survey. *IEEE Proceedings* 83(5), 705–740 (1995)
19. Fromherz, T., Stucki, P., Bichsel, M.: A survey of face recognition, MML Technical Report No. 97.01, Department of Computer Science, University of Zurich (1997)

20. Wu, Y., Huang, T.S.: Vision-Based Gesture Recognition: A Review. In: Braffort, A., Gibet, S., Teil, D., Gherbi, R., Richardson, J. (eds.) GW 1999. LNCS (LNAI), vol. 1739, pp. 103–115. Springer, Heidelberg (2000)
21. Kortenkamp, D., Huber, E., Bonasso, P.: Recognizing and interpreting gestures on a mobile robot. In: Proceedings of the AAAI, Portland OR, pp. 915–921 (1996)
22. Waldherr, S., Romero, R., Thrun, S.: A gesture-based interface for human–robot interaction. *Autonomous Robots* 9 (2000)
23. Xu, G., et al.: Toward robot guidance by hand gestures using monocular vision. In: Proceedings of the Hong Kong Symposium on Robot Control (1999)
24. Idaho National Laboratory, Humanoid Robotics,
<http://www.inl.gov/adaptiverobotics/humanoidrobotics/>
25. Walton, M.: Meet Paro-The therapeutic robot seal,
<http://www.cnn.com/2003/TECH/ptech/11/20/comdex.bestof/index.html>
26. Wikipedia: Paro (robot), [http://en.wikipedia.org/wiki/Paro_\(robot\)](http://en.wikipedia.org/wiki/Paro_(robot))
27. Ackerman, E.: Paro Robot Therapy Seal Just Wants Your Love,
<http://www.botjunkie.com/2008/04/10/paro-robot-therapy-seal-just-wants-your-love/>
28. Duffy, B.R.: Fundamental Issues in Social Robotics. *International Review of Information Ethics* 6 (2006)
29. Heyes, C., Galef, B.: *Social Learning in Animals: The Roots of Culture*. Academic Press (1996)

On the Use of the Universal Okumura-Hata Model for Defining Different ICT Areas

Dipashree M. Bhalerao¹, M. Tahir Riaz², Ole Brun Madsen², and Ramjee Prasad²

¹ Sinhgad Technical Education Society, Department of Electronics and Telecommunication, Pune, India

² Departments of Electronic Systems, Aalborg University, Aalborg, Denmark
{dmb, tahir, obm, prasad}@es.aau.dk

Abstract. The main goal of this paper is to observe QoS behavioural pattern for different ICT areas. Use these patterns to define rural and poor ICT areas from an ICT point of view. Okumura Hata model shows the intensity pattern for defining an area. In the same way QoS parameters behavioural patterns, also have to be taken into consideration for complete definition of an ICT area. Okumura Hata model is not sufficient to define the area, but QoS model is also required. A better example is we can define rural area with Okumura Hata model, but we cannot define poor area with it. After getting sufficient field strength also, Quality of Service (QoS) depends upon number of nodes or on resources available in any networks. In this paper we assume that sufficient field strength or required propagation pattern is there as per area for communication. Topology is generated using NS2 with different resources and have tried to plot the behavioural graphs for urban, rural and poor area scenarios. For studying area, properties generated and received packets are of prime importance. QoS features like end to end delay, throughput, and bandwidth utilization for 82 nodes have been experimented. Other parameters like number of paths, number of base stations will indirectly contribute in above QoS parameters. The generated topology model is hypothetical.

Keywords: Information and communication technology (ICT), Quality of service (QoS), rural area, poor area.

1 Introduction

The world can be divided into urban, rural, and poor areas. Classification of these areas further, is still possible. Considering the basic requirement, we classify them as urban, urban-rural, urban-poor, remote rural and remote rural-poor areas. The ICT area classification would have to be done much earlier. When areas are not defined, how ubiquitous networking is possible? How requirements for ICT applications can be finalized? The work that will be carried out will not be in systematic way and may lead to random development. A large group of the world's population suffers from affordable ICT solutions and the presence of sufficient ICT infrastructure. These definitions will reduce the time required for understanding the development and resources

available from all these area. Use of definitions will be helpful in providing and developing e-applications for all areas. Rurality from human understanding is different than rurality from ICT point of view. A Normal definition means an area placed at a remote distance, uneducated, with low income, backward class, no electricity, no sufficient infrastructure. The main task is to provide connectivity in this area only.

This work is a follow-up on the discussions at SW'09, on the needs for a new global ICT infrastructure reference architecture [1] for rural poor and catastrophic area (RPC). ICT definitions are much similar to normal rurality from resources point of view. Here the ICT areas may receive information very slow as compared with others, or generating very less packets per area in a day suffering from traffic jams, less number of towers, less number of nodes creating less alternating path options and many more. Topology of 82 nodes is created in such a way that urban, poor or rural effect can be plotted in terms of QoS parameters.

Basic needs for ICT areas definition are as follows

1. To provide a clear vision of basic needs required in the development of rural and poor areas with e-learning, e-medicine and e-banking as per area.
2. To provide a clear picture of research work required to be carried out for development of rural, poor and catastrophic area.
3. To minimize the time and money in all operations right from installation to maintenance.
4. To give a clear vision for investments required for development by government or individual ones.

Section two briefly tells us the ICT area definition model. It is defined with Okumura Hata model, QoS model and ICT model. The same section gives mathematical model. Different steps taken for scenario and in turn topology creation are briefed in section three. Graphs of through put, end to end delay, generated and received packets for urban, poor and rural area are plotted in section four. Section Five briefly analyzes all the graphs. Section six is of conclusion.

2 Rural Poor ICT Model

Most effective model used for defining rurality is Okumura Hata [2] Model. But, sometimes there can be a change in that model from place to place. Effect of environmental conditions [3] can also be useful in getting more accurate model. We assume Okumura [4] and Hata [5] model (ref Fig.1) along with other models related with different mediums, tropospheric conditions, and meteorological conditions as a base for urban, rural and poor area definitions.

Okumura-Hata model gives the logarithmic expression for received field strength ER dB(pV/m) as

$$E = 35.55 + PBky - 6.1610gf + 13.8210gh \sim T + A(HmS) - (44.9 - 6.5510GHbS)$$

Where:

- PB – radiated power of the transmitter, dBW;
- f – operating frequency, MHz;
- HbS – effective height of the antenna, in the range 3-15 Km;
- HmS – height of receiver antenna, m;
- R – Distance from the transmitter, Km;

$$y = 1 \text{ for } R < 10 \text{ Km}; \sim (HmS) = (11 * 10^{gf} - 0.7) * h \sim s(1.56 * 10^{gf} - 0.8);$$

$$Y = 1 + (0.14 + 1.87 * 10^{-4} * f + 1.07 * 10.3 * hBy) * (\log(\sim / 20)) \sim .f * or 20IRI$$

100Km;

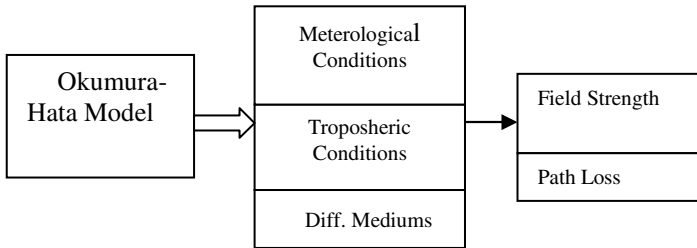


Fig. 1. Okumura Hata model

QoS model tells us that, even if field strength is there, but if no quality of service is achieved at the required node, it is of no use. Data will be in a distorted form, when QoS requirements are not satisfied. These QoS parameters values will vary from applications to applications. Different QoS parameters have to be taken into account further. Each area has its own peculiar QoS pattern. Here, we have considered few of them from rural and poor area definition point of view. For rural area throughput will be high, latency will be high, bandwidth utilization is less, High jitter may be there, end-to-end delay is greater than urban area, more congestion will be there. These values will vary according to distance, packet types and load on the backhaul. For some rural area simple data information will be there, no audio or video information. QoS conditions for urban area can be low throughput, low latency, highest B/W utilization, low end to end delay and more congestion. But if some part or node are experiencing the above QoS conditions, we can say that ICT rurality is there with respect to other nodes in that area. If the area is at large distance with limited alternative paths we can say that it is remote rural area.

If in any area packets are not generated or received as a main source or final destination node or very less than some threshold, we can say that it is a Poor ICT area. i.e. generated and received packets from source node to destination node are very low. In urban and urban poor ICT area infrastructure will be same but different generated and received packets. In remote rural and rural poor area infrastructure, received packets and generated packets can be different. This poor area can be in urban, rural, or remote rural area. According to area, QoS values for different parameters will vary.

QoS model (ref Fig.2) when combined with Okumura Hata model (ref Fig 1), a base model for area will be available. Further we combine this base model with ICT

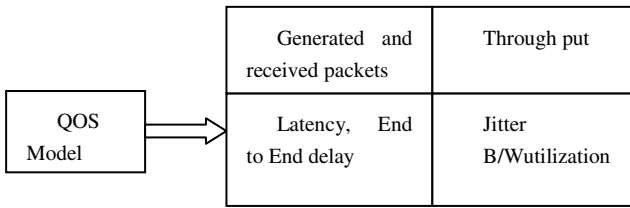


Fig. 2. QoS Model

model [6]. This model can be used for any area definition from ICT point of view. This model can be called as ICT area definition model (Ref Fig.3). Sufficient field strength is required for defining any area. It is assumed that it is available at the required area, from where it is distributed further with different local networks. The field intensity will be converted into digital data. Received packets, generated packets, throughput, E-E delay, bandwidth for source to destination, distance between source to destination, and number of paths decide the QoS for that area network.

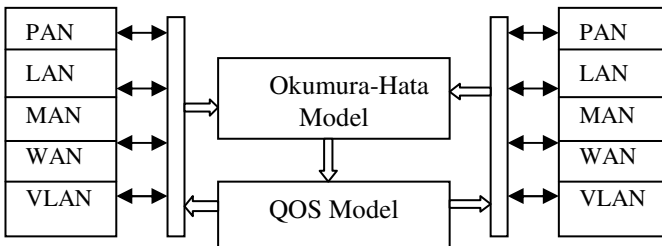


Fig. 3. Rural & Poor ICT Model

If required QoS is not available at the receiving end, data received will not be useful and will have different problems like garbage, missing data to different delays. So having only field strength is not sufficient, along with it, network should transfer the information or data with QoS requirements in terms of above mentioned parameters. ICT area definition model is a generalized model for any area definition (Rural, Poor, catastrophic and urban area). Mathematically field strength and QoS both are required for the area definition. The equation takes the form as follows.

$$\text{Area} = f(\text{Okumura-Hatta propagation pattern, QoS patterns}) \dots \tag{1}$$

$$\text{Area} = f(E, P_g, R_p, \text{Throughput, E-E delay, bandwidth utilization, distance, paths}) \tag{2}$$

Where,

E – Intensity according to Okumura and Hata model,

QoS metrics –parameters as motioned above for a network and end user node.

Consider the best example of Pune city, in India which explains all ICT areas. At the heart of the city some slum area is present. Which can be considered as a Urban Poor ICT area. Other areas at heart can be considered as urban ICT. Outskirts of the city can be considered as urban rural ICT area. The Sinhgad fort is situated at a long

distance from Pune city. Forts back side can be considered as a remote rural ICT area. All these areas will have their own propagation patterns according to Okumura Hatta model. But along with it, it would satisfy the the QoS behavioral patterns.

Equation can be used to define any area. These areas can be in any type of network. Urban, poor and rural areas can be in PAN, LAN, MAN, VAN and WAN. For IoT things can be physical or virtual. VAN is a conceptual group of things or nodes, irrespective of their actual locations. But the QoS parameters will be according to their actual (physical) locations.

Features to be considered for rural/poor area are:

1. Through put- Number of bits transferred/Sec.
2. End to end delay –Time required for the packet to reach destination from source.
3. Bandwidth utilization- measure of total capacity utilization
4. Base stations - are very less one or max 2.
5. Alternative paths available as a part or complete path.

3 Simulation in NS2

A simple topology is created for urban, poor and rural areas. Scenario is created according to the node distribution and traffic patterns, and infrastructure available in rural, poor and catastrophic area (Fig. 4). Topology is created for Hybrid model considering the same is used in practice. Hybrid model is a combination of wireless and wired networks. It is a combination of wireless and wired network. The nodes have two ray ground models and uses MAC-802.11 standard. The area for model is set as 12786*100 in meters. Total period of execution is 110ms. Antenna is Omni directional and droptail type of queue. All these things can be changed and readings can be taken for other models, Queues etc..This script defines a simple topology of 82nodes, and single agent, a UDP agent with a CBR traffic generator.

Topology is divided into 13 domains. 7 wireless and 6 wired. Wireless domains have 20,10,10,10,10,14,8 nodes each. All wired domains have two nodes each.These domains consists of total 6 wired lines. All lines are connected to base stations from different domains, which are nothing but wireless node. Total 18 base stations are scattered in all wireless domains.The output is trace file. Refer to the following topology.

In domain D0 urban, poor and urban rural effects are studied. D5 is at very large distance from D0. This domain can be called as remote rural area. To study the required effect, following steps have been taken.

1. In urban area a huge communication is present. This communication is huge and less at different places in urban area. The term urban area is considered for the huge communication area. The less communication area will be called as rural as compared to concentrated ones. In some part of urban area transmission will be there, but not as a source or final destination. That is, no communication is generated and meant for these areas. They are only intermediate means for commuting the information. Such areas can be called as urban poor area. The scenario reflecting the same conditions are created in the topology for urban, urban rural and urban poor area.

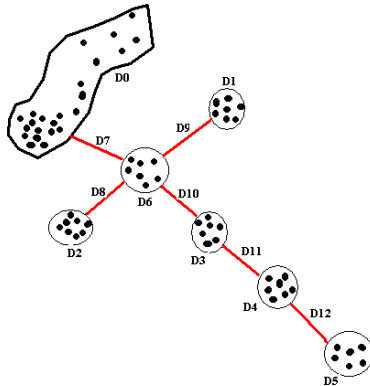


Fig. 4. Scenario topology

2. In rural area on an average less communication will be present. The transmission can be from different above urban areas to rural area. Distance, number of towers and different paths for backhaul available can be considered for rural area. The same is generated through topology.
3. Transmission is generated between different areas and within area itself i.e inter and intra domain. While this transmission is going on, some other load is generated on the backhaul. To find the QoS parameters like throughput and e-delay, interval between packet generation is varied. Red line indicate connectivity from wired node to Base stations.

4 Results

Graphs are plotted for end to end delay versus generated / received packets, and throughput for down stream. In graphs GP= generated packets, RP= received packets , Thrput= throughput.

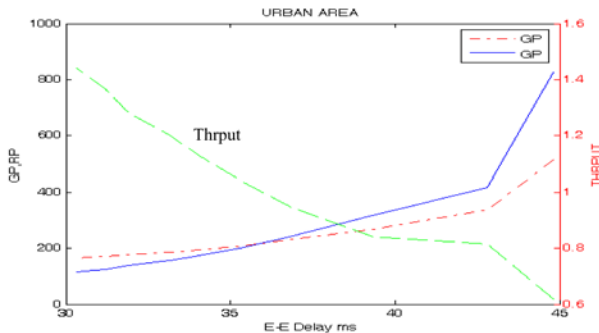


Fig. 5. Urban area QoS behavioral pattern

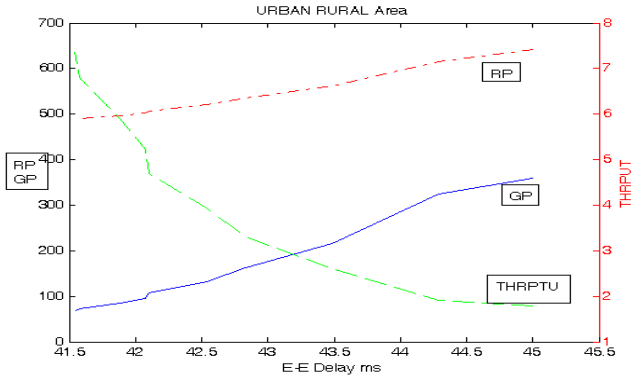


Fig. 6. Urban-rural Area QoS behavioral pattern

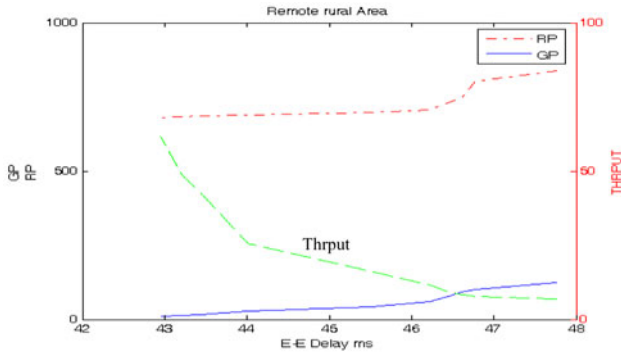


Fig. 7. Remote-rural area QoS behavioral pattern

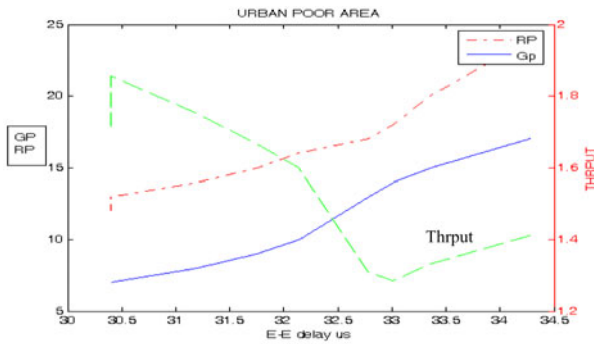


Fig. 8. Urban-poor area QoS behavioral pattern

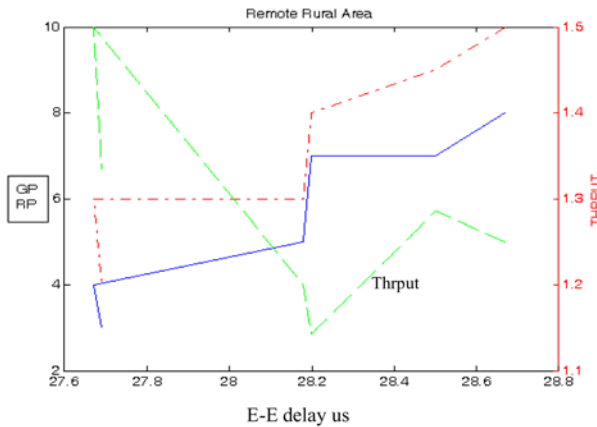


Fig. 9. Remote-rural-poor area QoS behavioral pattern

5 Analysis

All above graphs are plotted for down stream from urban to corresponding area. Similarly graphs can be plotted for upstream from corresponding required area to required destination. Average readings are taken area wise. Following Table 1 and Table 2 summarizes the graph results for time interval of 1 to 10 us. The traffic from all areas is created on back haul.

Table 1. Rural Area

Area	G	Rp	Thput	E-E delay ms	B/w Utilization %	No.Of Paths	No.of Base station
Urban	512-166	827 - 115	0.619-1.44	44.804-30.295	22.55 – 3.13	4	3
Urban rural	641-487	360-66	1.78-7.39	45.002 to 41.538	9.81- 1.79	1	2
Remote Rural area	837-680	124 - 11	6.75-61.82	47.761 to 42.945	3.38 – 0.30	1	1

Refer fig 5-7 for rural area. We can analyze the Table 1 as follows

1. As source area is increased, generated packets are in increasing order.
2. Destination users in urban, urban rural and remote rural area are decreased respectively leading to reduced received packets respectively.
3. E-E delay is increasing because of increasing distance, congestion, limited resources.

4. Bandwidth utilization is directly proportional to requirement of a particular area, and we can see that it is reducing from urban to remote rural area.
5. Number of resources like paths and base stations are reducing leading to less bandwidth utilization, bigger E-E delay.

Table 2. Poor Area

Area	Gp	Rp	Thruput	E-E delay ms	B/w utilization	No.Of Paths	No.of Base station
Urban poor	24-12	17-7	1.41-1.71	10.2834 - 1.5235	0.463 - 0.19	4	3
Remote Rural-poor area	10-4	8-3	1.25-1.33	11.712 - 3.08	0.22- 0.081	1	1

Refer Fig 8-9 for poor area for poor area QoS parameters are recorded for node to node for interval of 1ms to 10 ms for a same flow ID, and then they are averaged. By comparing Table 1 and Table 2 analyses is as follows.

1. Gp for urban poor area is very much less as compare to Gp of urban, urban rural area. Gp and Rp are considered for source and destination areas only Results show that there is less communication, or no use of any e-applications.
2. Throughput and E-E delay are increasing from Top to Bot tom.
3. Less utilization of the bandwidth for remote poor area as compared to urban poor area.
4. Infrastructure utilization is same, for urban and urban poor area, but as a intermediate means. Same is the case with Remote rural and remote rural poor area.

6 Conclusions

The success of ICT is dependent on utilization of application which in turn is dependent on the resources. The topology developed leads to the hypothetical model of urban, rural and poor area. For actual areas, reading will be different but the nature of graphs will remain same. Readings are taken for downstream, and can be taken for upstream also. In general we can say that, all areas have their QoS parameters specific pattern. These patterns vary with increase in resources and utilization of the applications related with them. Increase in utilization leads to conversion of one area to another better ICT area. Rural or poor to urban from ICT point of view. As we have seen urban poor area Gp and Rp are very less irrespective of resources. We can conclude that utilization of ICT applications doesn't depend on the resources only.

References

1. The 11th Strategic Workshop SW 2009 in Rebild, Denmark 2009, on Wireless Innovation for InterDynamic Technology (2009)
2. Okumura, Y., Ohmori, E., Kawano, T., Fukuda, K.: Field strength and its variability in VHF and UHF land-mobile service. *Rev. Elec. Comm. Lab.* 16(9-10), 825–873 (1968)
3. Hata, M.: Empirical formula for propagation loss in land mobile radio services. *IEEE Trans. Veh. Tech.* 29(3), 317–325 (1980)
4. Okumura-Hata propagation prediction model for UHF range, in the Prediction methods for the terrestrial land mobile service in the VHF and UHF bands, ITU-R Recommendation P. 529-2, pp. 5–7. ITU, Geneva (1995)
5. Faruque, S.: Propagation prediction based on environmental classification and fuzzy logic approximation. In: *IEEE International Conference on Communications (ICC 1996)*, June 23-27, vol. 1, pp. 272–276 (1996)
6. Bhalerao, D.M., Riaz, M.T., Jensen, M., Madsen, O.B., Prasad, R.: On New Global Catastrophic ICT Model. In: *IEEE International Conference ICACT 2011* (2011)

A Novel Approach for Automatic Generation of UML Class Diagrams from XMI

Kashif Hameed¹, Imran Sarwar Bajwa², and Muhammad Asif Naeem³

¹ Department of Computer Science & IT, The Islamia University of Bahawalpur,
63100, Bahawalpur, Pakistan

² School of Computer Science, University of Birmingham,
B15 2TT, Birmingham, UK

³ Department of Computer Science, University of Auckland,
1142, Auckland, New Zealand

gentle_kashif@yahoo.com, i.s.bajwa@cs.bham.ac.uk,
mnae006@aucklanduni.ac.nz

Abstract. XMI (XML Metadata Interchange) is used to exchange metadata information of UML (Unified Modeling Language) models using XML (Extensible Markup Language) representation. All major CASE tools e.g. ArgoUML, Rational Rose, Enterprise Architect, MS Visio, Altova, Smart Draw, etc can export and import XMI. However, current implementation of XMI in all CASE tools does not fulfill the goal of a model interchange as the CASE tools can just import XMI and extract metadata information but cannot generate UML models such as UML class diagrams. A primary reason of this inability is that XMI only provides the information about what elements are in a UML class model but not the information about how these elements (such as classes, associations, etc) are represented and laid out in diagrams. Without this facility, the real power of XMI is still un-explored. In this paper, we present a Binary Space Portioning (BSP) Tree data structure based novel approach to regenerate UML diagrams from XMI. A VB.NET implementation is also presented as a proof of concept.

Keywords: XMI, UML Models, Binary Space Partition.

1 Introduction

Unified Modeling Language (UML) [1] is used to develop high-quality and possibly error-free graphical models of complex and large-sized software systems. UML is by far the most widely used modeling language for software systems. UML is involved in various phases of the software development such as drawing diagrams, consistency analysis of models, generating design patterns, engineering code, producing reports, preparing documentation, etc. All these functions are performed using various tools. Moreover, all the tools used in above defined phases need to interact with each other. For the sake of interaction and information exchange in various tools involved in software development process, XML Metadata Interchange (XMI) [2] is used. XMI

provides a standardized representation of the metadata information in a UML model so that it may be exchanged across many industries and operating environments, different UML tools and other tools that are capable of using XMI [3]. XMI uses XML (Extensible Markup Language) representation to transport information that is highly internally referential [4].

All major CASE tools e.g. Rational Rose, USE, Enterprise Architect, ArgoUML, Altova, Smart Draw, MS Visio, etc provide support to export UML models such UML class diagrams in XMI format 1.0 or 2.0. Similarly, almost all CASE tools can import XMI and extract the metadata information of a UML model but cannot regenerate UML class diagrams from XMI. However, there is a problem that the graphical visualization of a model from XMI is not possible since XMI has no graphic information [5] such as where to draw a model element and how to avoid overlapping of the model elements. In absence of this facility, the real power of XMI remains unexplored. Marko [ibid] proposed some major changes in XMI metamodel to store graphical information of a UML model. However, we think that this is not a good solution due to the reason that the XMI metamodel will become far complex with addition of graphical information and the handling of XMI will become more difficult.

In this paper, we present a novel approach for automatic generation of UML class diagrams from XMI using the Binary Space Partitioning (BSP) [6] tree data structure. The BSP trees are typically used in the field of computer graphics to capture graphical information of a 2-D diagram [7-8]. A BSP tree captures the spatial layout and spatial relations in objects in a UML class model drawn on a 2-D plane. Once the information of a UML model is captured in a BSP tree, the same diagram can be regenerated by efficient partitioning of space (i.e. regions) without any collision. After drawing UML classes, the associations, aggregations and generalisations are also drawn between the classes. The presented approach is also implemented in VB.NET as a proof of concept.

The remaining paper is structured into the following sections: Section 2 explains the BVH algorithm used for space portioning. Section 3 describes the used algorithm for space portioning and drawing model elements. A case study is presented in section 4 to evaluate the accuracy of the presented approach. An account of the related work is presented in section 5. Finally, the paper is concluded to discuss the future work.

2 Binary Space Partitioning

A Binary Space Partitioning (BSP) tree is a simple and powerful data structure that is typically used to solve geometrical problems such as ray-tracing [6]. BSP was originally introduced by Fuchs, Kedem, and Naylor [10] and it is used to partition a 2- d space containing various polygons. In terms of geometry, a BSP tree splits a typical 2- d or 3- d space into two half spaces with a hyper-plane of dimension $d-1$ and this process is iterated until the whole space is alienated into a hierarchy of split regions also called “cells”. Once the graphical information of a space is captured in a BSP tree it can be regenerated multiple times with simplicity. We aim to use BSP

trees in automatic generation of UML diagram from XMI. We have performed this process into two phases:

2.1 Creation of a BSP Tree

First we need to create a BSP tree. A BSP-tree of a UML class model contains all the information regarding total number of classes in UML class model and their hierarchal structure. Instead of creating the BSP tree from a graphical scene, we create the BSP tree from XMI document. The first class in an XMI document is considered as a root. Rest of the classes in XMI document becomes child nodes of the root in the tree. All classes C_1, C_2, \dots, C_n associated to a class C_a become children of the class C_a . Moreover, the associations, generalizations and aggregations are used to identify the hierarchy of the nodes in the tree.

2.2 Traversal of BSP Trees

Once a BSP tree is generated, the tree is traversed to generate a UML class diagram for many times. The traversal of the BSP tree is a recursive process that involves a simple test at each node. A modified in-order traversal of the BSP tree yields in either a back-to-front or front-to-back ordering of the triangles (classes). Following (see Fig 1) is the front to back traversal algorithm used in our approach for drawing UML class diagram. This algorithm is modified version of the traversal algorithm presented by Gordon and Chen [8]. The modified version of the algorithm does not use the view point parameter as the original version of the algorithm was written for rendering.

To draw class diagram, space is divided into smaller sets (see Fig 2), where each subset is a bowed set of rectangles. Here, each rectangle in this subset is neighbor of

```
Function traverse(BSP_tree){
    if (BSP_tree != null){
        if (positive_side_of(root(BSP_tree))
            traverse(positive_branch(BSP_tree));
            display_triangle(root(BSP_tree));
            traverse(negative_branch(BSP_tree));
        else
            traverse(negative_branch(BSP_tree));
            display_triangle(root(BSP_tree));
            traverse(positive_branch(BSP_tree));
        }
    }
}
```

Fig. 1. Algorithm for in-order traversal of BSP tree

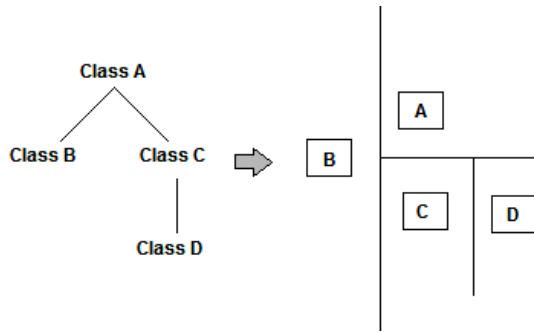


Fig. 2. Mapping the BSP tree to UML class Diagram

every other rectangle in the same set. During the drawing of the class diagrams, an important point was to take care that the neighbour of each class was drawn in a way that the classes having associations were drawn to close to each other.

3 Generating UML Class Diagrams from BSP Tree

The presented approach works in two steps. In first step, a BSP tree is generated from XMI representation of a UML class model. In second step, BSP tree is traversed and the UML diagram is generated. The presented approach can process XMI 2.1 format. We have chosen XMI 2.1 format as all major tools such as ArgoUML, Enterprise Architect, USE, Altova UModel support XMI 2.1 format. User provides the input in the form of XMI (.xml) file using the interface provided in the typical software system. Fig. 3 represents the overview of all steps involved in XMI to UML class diagram transformation. Following are details of the involved steps in generation of UML class diagrams from XMI 2.1 using BSP tree data structure.

3.1 Parse XMI Representation

This module parses the given input (XMI representation of UML class model) using our XMI parser developed in VB.NET.

The XMI parser parses an XMI file with respect to target UML model by storing the data it in memory. For parsing XMI with VB.Net we used the `System.XML` namespace. The XML classes in the `System.Xml` namespace provide a comprehensive and integrated set of classes, allows working with XMI representation. These XML classes support parsing and writing XML, editing XML data in memory, and data validation. There are different classes available to read and write XML document in .Net Framework such as `XmlReader`, `XmlNodeReader`, `XmlTextReader`, and `XmlValidatingReader`.

A XMI parser is developed and used to parse XMI file to identify and extract class names, class attributes, class functions, association names, generalizations names, etc. While parsing an XMI presentation, XMI parser checks the syntax for well-formedness, and reports any violations (reportable errors). It helps to extract classes, objects and related tags.

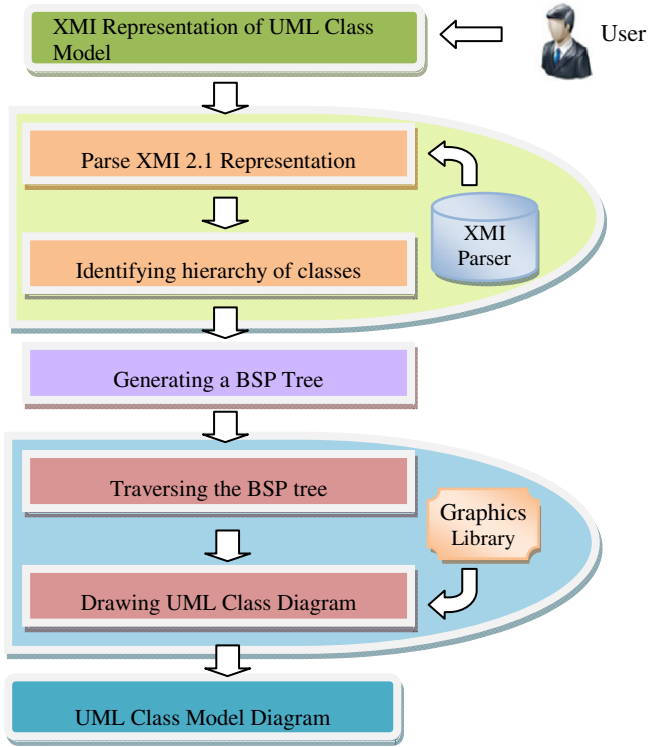


Fig. 3. Architecture of the designed system

The output of this phase is set of classes, their attributes, and methods, and all type of relationships such as associations, aggregations and generalizations.

3.2 Identifying Hierarchy of Classes

Once the information is extracted from XMI representation, next step is to identify relationships among multiple (two or more than two) classes and maps the associations and generalizations in classes and objects. Primary objective of this step is to extract possible hierarchy among all the classes. Such type of information helps in generating a BSP tree. Following rules are used to identify hierarchy among classes:

- i. If a class *A* is associated to class *B*, class *B* will become child of class *A*.
- ii. If a class *A* is generalization of another class *B*, class *B* will become child of *A* as *B* will be inheriting all features of *B*.
- iii. If a class *A* aggregates another class *B*, class *B* will become child of *A*.
- iv. If there is a class that has no relationship to other classes or there is numeration, which will be considered as leaves of a tree.

3.3 Generating a BSP Tree

By using the information (such as classes, associations, etc) extracted in section 3.1 and the hierarchal information identified in section 3.2, a BSP tree is constructed in this step. The first class in XMI representation becomes the root of the BSP tree. Then each class becomes a node of the root on the basis of the identified hierarchy. This process is recursively repeated in each half-space until every polygon has been incorporated into the tree.

3.4 Traversing the BSP Tree

To generate the UML class diagrams, we need to traverse the BSP tree, first. The tree is typically traversed in linear time from an arbitrary viewpoint. However, we are not drawing the UML model in a particular perspective of user's view. Hence, we do not consider the view point parameter here.

In computer graphics, a BSP tree is in-order traversed. The process of in-order traversal recursively continues until the last node of the tree is traversed. In the case of a $2-d$ space tree, a modified in-order traversal (see Fig. 1) yields in a depth-sorted ordering of all rectangles (classes) in the space. Using the in-order traversal, either a back-to-front or front-to-back ordering of the triangles (classes) can be drawn. The back-to-front or front-to-back ordering is a matter of concern in the scenes where there are overlapping objects. However, in case of a UML class model, all objects (classes) in a scene are non-overlapping; the ordering of drawing does not matter.

3.5 Drawing UML Class Model

In this phase, first the extracted information from the previous module is used to draw the UML class diagrams. First of all the space is vertically divided from center. The class at root can be drawn at any side of the vertical division. Then each side (left & right) are horizontally and vertically drawn for classes represented by the child nodes. This process continues recursively until the last class is drawn.

To physically draw class diagrams, a diagram generator was written in VB.NET using 2D Graphics library. Various graphics methods in GDI+ such as the DrawLine method draws a line between two points specified by a pair coordinates. DrawLines draws a series of lines using an array of points. We have also used GDI+ Graphics paths to redraw certain graphics items. The Graphics paths are used to handle multiple graphics items, including lines, rectangles, images, and text associated with a surface but we need to redraw only the rectangles. We can create a graphics path with all class diagrams (three rectangles) and just redraw that path, instead of the entire surface.

Once the rectangles for each class are drawn, each rectangle is filled with their respective attributes and methods. Then, the associations, aggregations and generalizations are drawn among the respective rectangles representing particular classes.

The last step is to label the generated class diagrams with additional supportive information to make the class model more expressive.

4 Case Study

To test the designed tool XMI2UML, we present here a solved case study. The solved case study is a sub set of a Library Domain Model (LDM) [12] that describes main classes and relationships which could be used during analysis phase to better understand domain area for Integrated Library System (ILS), also known as a Library Management System (LMS). Following is the problem statement for the case study:

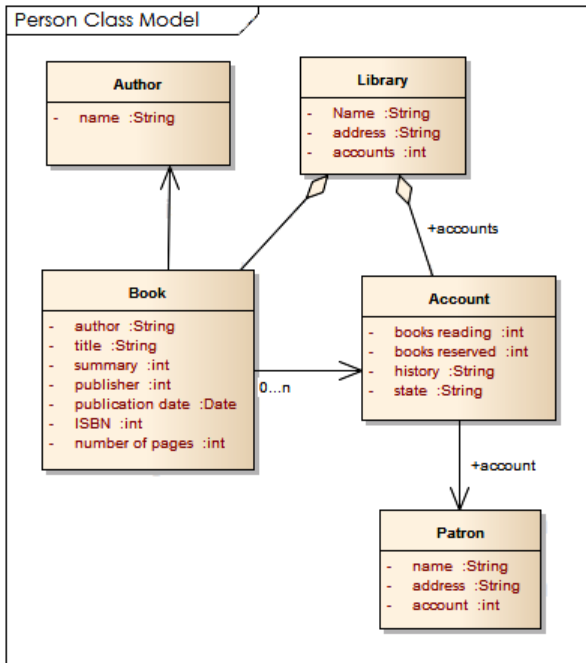


Fig. 4. UML class model of the Case Study problem statement

The problem statement consists of a UML Class model (see Fig 4) and a XMI 2.1 Representation (see Fig 5). Both representations (UML and XMI) were generated using Enterprise Architect [11] v9.0 software. In this paper, we have solved a subset of the original case study [12]. The solved subset consists of five classes and five relationships. Fig 4 shows the subset (UML class model) of the solved case study.


```

- <elements>
- <element name="Class Model" xmi:type="uml:Package" xmi:idref="EAPK_DE9,
  <model ea_eleType="package" ea_localid="2" tpos="6" package="EAPK_E27
  <properties scope="public" nType="0" sType="Package" isSpecification="false"
  <project status="Proposed" complexity="1" modified="2011-07-13 15:43:0
  <code/>
  <style appearance="BackColor=-1;BorderColor=-1;BorderWidth=-1;FontC
  <modelDocument/>
  <tags/>
  <xrefs/>
  <extendedProperties package_name="Model" tagged="0"/>
  <packageproperties tpos="6"/>
  <paths/>
  <times modified="2011-07-13 15:43:05" created="2011-07-13 15:43:05"
  <flags packageFlags="isModel=1;VICON=3;" logxml="FALSE" usedtd="FALSE"
  </element>
- <element name="Account" xmi:type="uml:Class" xmi:idref="EAID_AD71392F_
  <model ea_eleType="element" ea_localid="17" tpos="0" package="EAPK_De
  <properties isAbstract="false" scope="public" nType="0" sType="Class" isSp
  <project version="1.0" status="Proposed" complexity="1" modified="2011-0
  <code gentype="Java"/>
  <style appearance="BackColor=-1;BorderColor=-1;BorderWidth=-1;FontC
  <modelDocument/>
  <tags/>
  <xrefs/>
  <extendedProperties package_name="Class Model" tagged="0"/>
- <attributes>
- <attribute name="books reading" xmi:idref="EAID_F502C901_CC28_4
  <initial/>
  <documentation/>
  <model ea_localid="14" ea_guid="{F502C901-CC28-41e6-BD48-FA
  <properties type="int" changeability="changeable" duplicates="0" col
  <coords ordered="0"/>
  <containment position="0"/>
  <stereotype/>
  <bounds upper="1" lower="1"/>
  <options/>
  <style/>
  <styleex value="IsLiteral=0;volatile=0;"/>
  <tags/>
  <xrefs/>
  </attribute>

```

Fig. 5. UML class model of the Case Study problem statement

Table 1. Extracted UML Class Elements

Category	Count	Details
Classes	05	Author, Book, Library, Account, Patron
Attributes	18	name, author, title, summary, publisher, publication date, ISBN, number of pages, name, address, accounts, books reading, books renewed, history, state, name address account
Operations	00	-
Objects	00	-
Multiplicity	01	0..1
Associations	03	Account
Aggregations	02	Accounts
Generalizations	00	-

The problem statement of the case study was given as input (XMI representation) to the XMI2UML tool. The tool parses the input and extracts the UML class elements (see table 1):

Once all the UML Class elements were extracted, a logical model of the target class diagram was developed. The logical model was based on relationships in all candidate classes. The generated logical model is shown in Table 2:

Table 2. Identifying relationships in a UML class model

<i>S# / Type</i>	<i>Source</i>	<i>Mult. A</i>	<i>Label</i>	<i>Mult. B</i>	<i>Destination</i>
Relation 01	Book	-	-	-	Author
Relation 02	Book	-	-	-	Library
Relation 03	Book	0...n	-	-	Account
Relation 04	Account	-	accounts	-	Library
Relation 05	Account	-	account	-	Patron

Once the relationships in a UML class model are generated, the graphical module of XMI2UML module generates the target UML class diagram. The finally labeled UML class diagram is shown in Fig 6 where the orange dotted lines are showing the binary partition of the space:

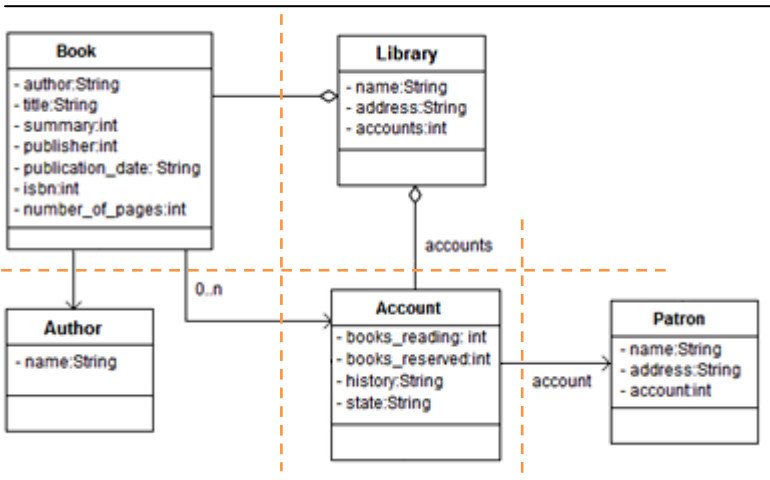


Fig. 6. Finally generated UML class model

There is an issue regarding efficiency of a BSP tree that relates to the balancing of the tree. Regarding balancing of a BSP tree, Bruce Naylor has presented some good algorithms and techniques to maintain well-balanced BSP trees. For a bigger UML class models, where we have to deal with bigger BSP trees, well-balancing of a tree becomes more critical.

5 Related Work

Marko [5] proposed some major changes in XMI metamodel to store graphical information of a UML model. However, we think that this is not a good solution due to the reason that the XMI metamodel will become far complex with addition of graphical information and the handling of XMI will become more difficult.

An algorithm was presented by Mikael, et al [9] in 2001 to generate UML diagrams from XML data. The focus of the research was to use the generated diagrams for the conceptual design of (virtual) a data warehouses with respect to the web data. Another major intention of the research was to support the On-Line Analytical Processing (OLAP) based on web data. However, according to best of our knowledge the generation of UML class diagrams from XMI representation is a novel idea and no approach/tool has been presented to date for this transformation.

In the light of this important research work presented to transform UML models to a standardized presentation such as XMI, no work has been presented yet for generation of UML graphical models from the XMI presentation. Missing support for XMI to UML models transformation breaches a gap in XMI and UML. To fill this gap, there is need of an approach for automated transformation of XMI to UML to make XMI more effective and powerful.

Approaches for automatic generations of UML class diagrams from NL specification [13-15] have been presented such as [16-24]. Such work was a real motivation for the presented research.

6 Conclusions

This research is all about designing and implementing a theory that can read, understand and analyze the XMI file and generate UML class models. The proposed system will be fully automated and able to find out the classes and objects and their attributes and operations using an artificial intelligence technique. Then the UML diagrams such as class diagrams would be drawn. The accuracy of the software is expected up to about 80% without any involvement of the software engineer provided that he has followed the pre-requisites of the software to prepare the input scenario. The given input should be an XMI file. A graphical user interface is also provided to the user for entering the Input XMI representation in a proper way and generating UML diagrams. The current version of XMI2UML tool can process XMI 2.1 version. This research was initiated with the aims that there should be software which can read the XMI representation and can draw the UML class diagrams.

References

- [1] OMG. Unified Modeling Language: Diagram Interchange version 2.0. OMG document ptc/03-07-03 (July 2003), <http://www.omg.org>
- [2] OMG. XML Metadata Interchnage. (XMI) version 2.1. Object Management Group (2005), <http://www.omg.org>

- [3] Alanen, M., Lundkvist, T., Porres, I.: A Mapping Language from Models to XMI [DI] Diagrams. In: Proceedings of the 31st Euromicro Conference on Software Engineering and Advanced Applications, pp. 450–458. IEEE Computer Society, Porto (2005)
- [4] Bailey, I.: XMI, UML & MODAF (February 2005), <http://www.modaf.com>
- [5] Boger, M., Jeckle, M., Müller, S., Fransson, J.: Diagram Interchange for UML. In: Jézéquel, J.-M., Hussmann, H., Cook, S. (eds.) UML 2002. LNCS, vol. 2460, pp. 398–411. Springer, Heidelberg (2002)
- [6] Ize, T., Wald, I., Parker, S.: Ray Tracing with the BSP Tree. In: IEEE Symposium on Interactive Ray Tracing (RT 2008), pp. 159–166 (2008)
- [7] Ranta-Eskola, S., Olofsson, E.: Binary Space Partitioning Trees and Polygon Removal in Real Time 3D Rendering, Uppsala Master's Theses in Computing Science (2001)
- [8] Chen, S., Gordon, D.: Front-to-Back Display of BSP Trees. IEEE Computer Graphics & Algorithms, 79–85 (September 1991)
- [9] Jensen, M.R., Møller, T.H., Pedersen, T.B.: Converting XML Data To UML Diagrams For Conceptual Data Integration In: 1st International Workshop on Data Integration over the Web (DIWeb) at 13th Conference on Advanced Information Systems Engineering (CAISE 2001) (2001)
- [10] Fuchs, H., et al.: Near Real-Time Shaded Display of Rigid Objects. Computer Graphics 17(3), 65–69
- [11] Matuschek, M.: UML - Getting Started: Sparx Enterprise Architect, To a running UML-Model in just a few steps, by Willert Software Tools (2006), http://www.willert.de/assets/Datenblaetter/UML_Getting_Started_EA_v1.0en.pdf
- [12] Library Domain Model (LDM), <http://www.uml-diagrams.org/class-diagrams-examples.html>
- [13] Bajwa, I.S., Choudhary, M.S.: Natural Language Processing based Automated System for UML Diagrams Generation. In: Saudi 18th National Conference on Computer Application (18th NCCA), pp. 171–176 (2006)
- [14] Bajwa, I.S., Naem, M.A., Ali, A., Ali, S.: A Controlled Natural Language Interface to Class Models. In: 13th International Conference on Enterprise Information Systems (ICEIS 2011), Beijing, China, pp. 102–110 (2011)
- [15] Afreen, H., Bajwa, I.S.: Generating UML Class Models from SBVR Software Requirements Specifications. In: 23rd Benelux Conference on Artificial Intelligence (BNAIC 2011), pp. 23–32 (2011)
- [16] Mich, L.: NL-OOPS: from natural language to object oriented requirements using the natural language processing system LOLITA. Natural Language Engineering 2(2), 167–181 (1996)
- [17] Delisle, S., Barker, K., Biskri, I.: Object-Oriented Analysis: Getting Help from Robust Computational Linguistic Tools. In: 4th International Conference on Applications of Natural Language to Information Systems, Klagenfurt, Austria, pp. 167–172 (1998)
- [18] Börstler, J.: User - Centered Requirements Engineering in RECORD - An Overview. In: Nordic Workshop on Programming Environment Research NWPER 1996, Aalborg, Denmark, pp. 149–156 (1999)
- [19] Overmyer, S.V., Rambow, O.: Conceptual Modeling through Linguistics Analysis Using LIDA. In: 23rd International Conference on Software Engineering (July 2001)
- [20] Perez-Gonzalez, H.G., Kalita, J.K.: GOOAL: A Graphic Object Oriented Analysis Laboratory. In: 17th Annual ACM SIGPLAN Conference on Object-Oriented Programming, Systems, Languages, and Applications (OOPSLA 2002), NY, USA, pp. 38–39 (2002)

- [21] Harmain, H.M., Gaizauskas, R.: CM-Builder: A Natural Language-Based CASE Tool for Object- Oriented Analysis. *Automated Software Engineering* 10(2), 157–181 (2003)
- [22] Oliveira, A., Seco, N., Gomes, P.: A CBR Approach to Text to Class Diagram Translation. In: *TCBR Workshop at the 8th European Conference on Case-Based Reasoning*, Turkey (September 2006)
- [23] Mala, G.S.A., Uma, G.V.: Automatic Construction of Object Oriented Design Models [UML Diagrams] from Natural Language Requirements Specification. In: Yang, Q., Webb, G. (eds.) *PRICAI 2006. LNCS (LNAI)*, vol. 4099, pp. 1155–1159. Springer, Heidelberg (2006)
- [24] Bajwa, I.S., Amin, R., Naeem, M.A., Choudhary, M.A.: Speech Language Processing Interface for Object-Oriented Application Design using a Rule-based Framework. In: *International Conference on Computer Applications (ICCA 2006)*, pp. 323–329 (2006)

An Efficient Link Bundling Transport Layer Protocol for Achieving Higher Data Rate and Availability

Muhammad Adnan Hashmi, Imran Shafi, Syed Ismail Shah, and Jamil Ahmad

Department of Computing and Technology
Iqra University, Islamabad Campus, Pakistan
hashmi_adnan@yahoo.com,
{imranshafi, ismail, jamil}@iqraisb.edu.pk

Abstract. By using aggregation of more than one physical interface enables aggregated links to work at the same time for enhancement of bandwidth and data speed beyond capability of single link with additional feature of resilience. However, inappropriate schemes may cause undesirable network behavior and thus requires high efficiency and reliability in its implementation. A new link bundling transport layer protocol is presented which ensures efficient and reliable trunking of multiple wired or wireless network interfaces resulting in escalation of data rate. The proposed scheme is found efficient, reliable and independent of available paths by implementing the Luby transform (LT) codes. The LT codes do not require any interface characteristics management prior to transfer of data which helps in aggregation of interfaces having different characteristics in less time. Also, the data flows seamlessly even if one of the link experiences fluctuation or complete shutdown. The proposed protocol requires less processing requirement, minimum connection establishment time and no interface management as compare to any TCP based protocol. Experimental results demonstrate the effectiveness of the approach.

Keywords: Networks, LT Codes, Transport Layer Protocol, Link Aggregation, Link Redundancy, Data rate.

1 Introduction

Transport layer protocol use only one interface or connection between sender and receiver for data transfer. If more than one paths need to be established using multiple interfaces between sender and receiver then there is a requirement of efficient management of links and their aggregation for creation of single logical link. Aggregation of links demands the reliability and efficiency i.e. data must be transferred without loss with minimum time and less overhead. Efficiency is an important factor especially in case of erasure channels e.g. wireless.

We find few approaches in the literature to address these issues partially. One of the popular approaches is the parallel TCP (pTCP) [1]. It is the extension of TCP which utilizes the concept of virtual TCP (TCP-v) and Strip Manager (SM) and increases the bandwidth by aggregating the multiple paths. TCP-v deals with the per

path functionality within single logical link and SM manage all TCP-v for successful transfer of data. On the other hand transaction TCP (T/TCP) [2] skips 3-way handshake process by introducing connection count state which ultimately helps in reducing time factor required for connection establishment. Skipping 3-way handshake is also known as TCP Accelerated Open (TAO). This helps in saving overall time required for transmission of data but has some security threats which are addressed in enhance transaction TCP (ET/TCP) [2].

Another approach is link aggregation control protocol [4] which increases the bandwidth by aggregating wired interfaces. It has different modes for traffic distribution over multiple interfaces. IEEE 802.3ad standard is related to link aggregation whereas IEEE 802.1AX-2008 represents the redundancy and reliability. The approaches like T/ TCP, ET/TCP and pTCP are transport layer implementations whereas link aggregation is implemented at the data link layer.

The objective of escalation of data rate can be achieved with some special features at transport layer like efficient memory management both at sender and receiver side, paths selection and interface management especially in case of short term fluctuation and shutdown at transport layer of custom protocol. Better data rate is the requirement of almost every application connected to server for services either with video streaming server, proxy server, webserver etc. Server with high processing power can't play an important role if the via is not able to support the application's data flow. Currently network devices like switches etc. don't have any built in facility installed by vendors for the aggregation of interfaces in attainment of escalation in data rate. Aggregation of network interfaces depends on the characteristics of interfaces i.e. bandwidth, delay and loss especially in case where wired and wireless links are involved. Other than major characteristics, short term fluctuation or even complete shutdown on any of the interface can affect the overall transfer of data. Path independence problem is achieved by implementing the LT codes. The LT codes are rate-less erasure code and are first practical implementation of the Fountain codes [3] [6]. These codes are well suitable especially in case where network has higher latencies and higher loss rates provided multiple interfaces are available.

The proposed solution in this paper introduces a custom transport layer protocol developed using C/C++ on Ubuntu platform. It utilizes UDP packets stream and for reliability of connection, three way handshake process is implemented before the establishment of actual data stream. The data packets are passed through LT encoder at sender side whereas LT decoder decodes the same till the retrieval of required data.

The paper is divided in five sections. Section 2 discusses the proposed link bundling transport layer protocol. Section 3 presents the implementation details and discussion on experimental results is given in section 4. Finally section 5 concludes the paper.

2 The Proposed Link Bundling Transport Layer Protocol

The main issue for achieving aggregate bandwidth is the management of network interfaces. Each network interface has different characteristics like bandwidth, delay

and loss. The links aggregation of different characteristics require efficient algorithm for traffic distribution on multiple interfaces. Short term fluctuation can be experienced by any of the link during data transfer. In addition to fluctuation, link can also experience complete shutdown. For successful transfer of data aggregated links are managed in such a way that if fluctuation or shutdown experience by any one of the link, other links remain up without any problem, this situation definitely increase the overall time require for complete transfer of data but provide enhanced reliability and redundancy [8].

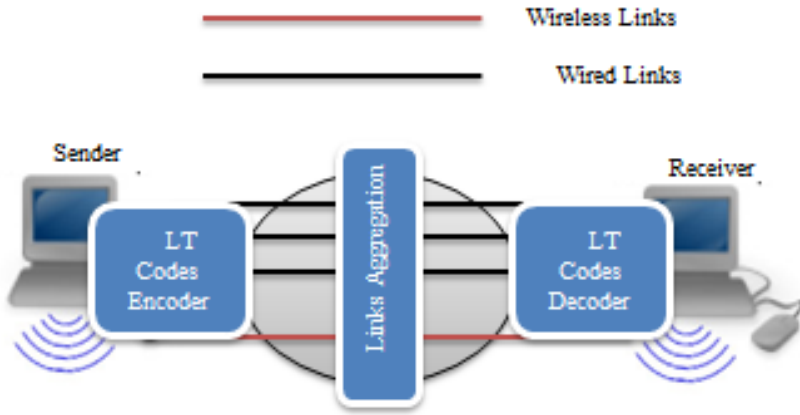


Fig. 2.1. Proposed Infrastructure Model

Fig.2.1. provides overview of the proposed model. Sender and receiver having multiple wired and wireless interfaces are combined using link aggregation to a single logical link where data is transferring over multiple paths with the implementation of LT codes. F.g.2.2 provides flow of steps involved at the sender side (i.e. on server side) whereas Fig.2.3 contains the flow of action performed at receiver side (i.e. client side). All the important steps including Luby Encoder and Decoder are shown using Fig.2.2 and Fig.2.3.

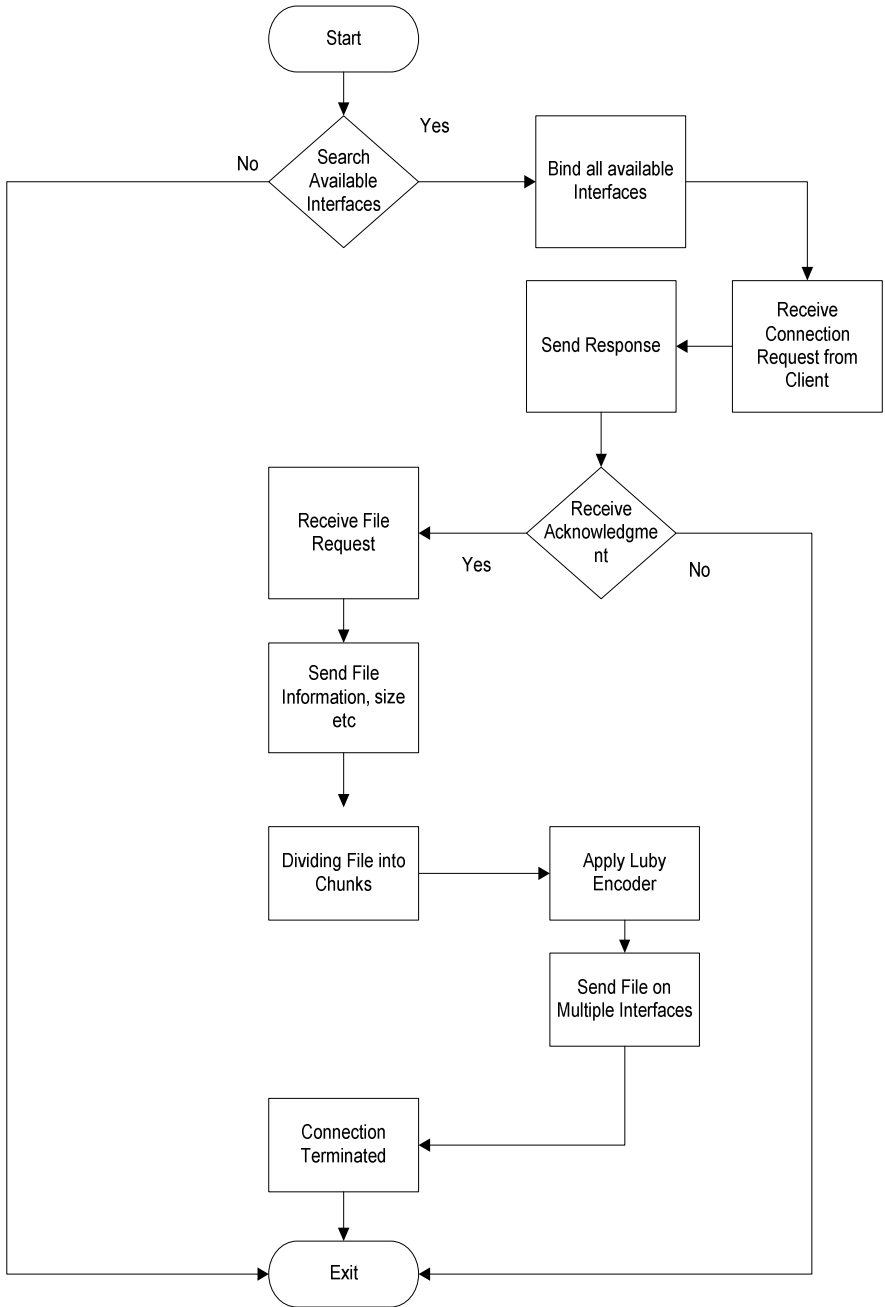


Fig. 2.2. Server Flow Chart

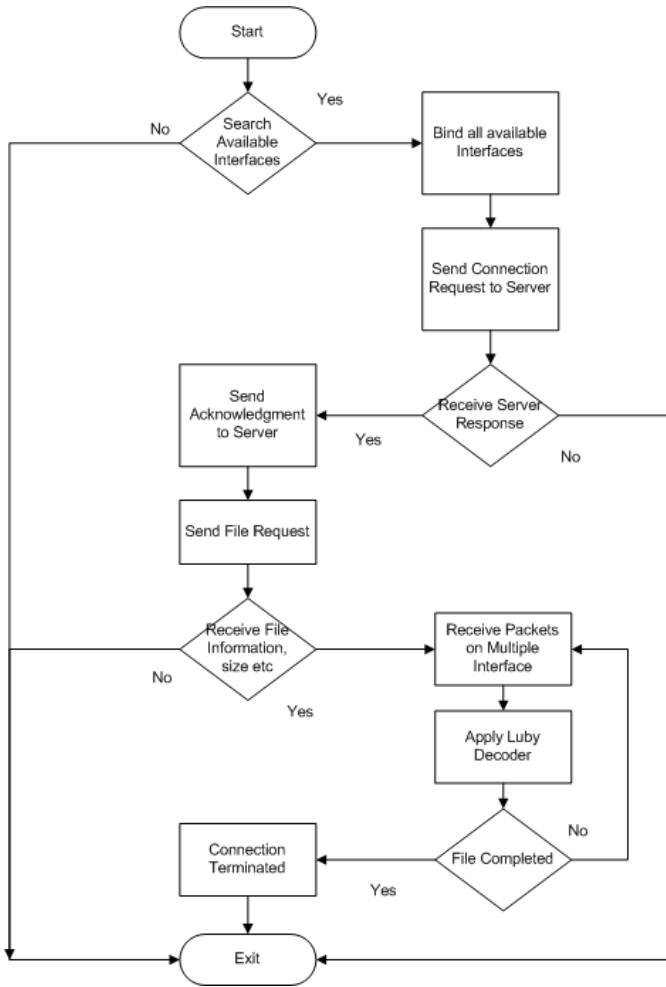


Fig. 2.3. Client Flow Chart

Fountain codes [6] [7] are chosen for the successful transfer of data. These codes are independent from path. It works on the principle that enough should be received to recover exact copy of sender data regardless of loss of encoded symbols. Fountain codes [7] require efficient memory management especially on receiver side.

LT codes have been selected for successful transfer of data reliably and efficiently. They can generate limitless output symbols from the fixed number of message symbols. LT codes recovery and delivery doesn't depend on network reliability; they have linear and minimum encoding complexity with iterative encoding decoding algorithm.

For reliable connection establishment three way handshakes process is established between sender and receiver. Packets used for connection establishment and data

transfer are distinguished with the help of its type field. After successful handshake process, information about the transfer data is synchronized between sender and receiver. The next phase is LT encoding process, packets first converted into encoded symbols and then transferred over multiple interfaces. Receiver applies the LT codes decoder operation on the encoded symbol till the exact copy of sender's data is retrieved on its side. Successful transfer of data leads to the termination of connection.

2.1 Implementation

The proposed link bundling transport layer protocol was developed using C/C++ and for the implementation purpose Ubuntu platform is chosen. LT codes are implemented using linked list for memory management at both sender and receiver side. C/C++ is the higher level language which utilizes the memory efficiently. Most of the application servers are developed using C/C++. Its performance over UNIX is far better than any of other operating systems. GNU compiler includes the libraries for the C/C++, it is free ware and used in the UNIX distributions. UNIX is one of the best operating system having lots of flavor, Ubuntu is one of them.

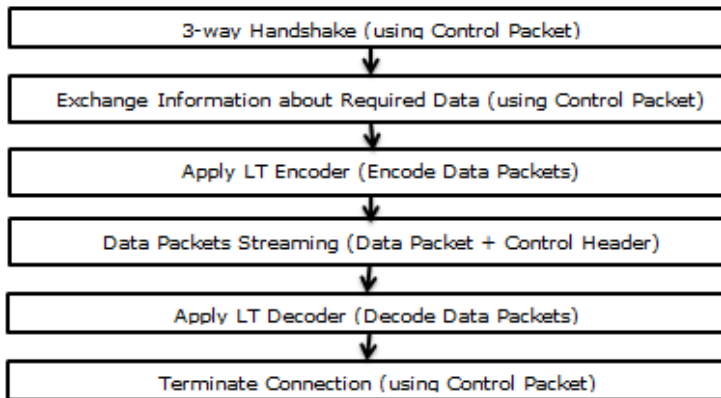


Fig. 2.1.1. Protocol Flow Diagram

The implementation can be categorized in two major areas, one part is related to the connection establishment that simulates the same handshake behavior used by the TCP whereas second part deals with the actual transfer of data packets on multiple interfaces, it also ensure the data integrity, reliability and efficiency with the use of LT codes. Summarized flow of proposed link bundling transport layer protocol is shown in Fig.2.1.1 whereas all steps performed at each side with complete description is shown in Fig.2.1.2.

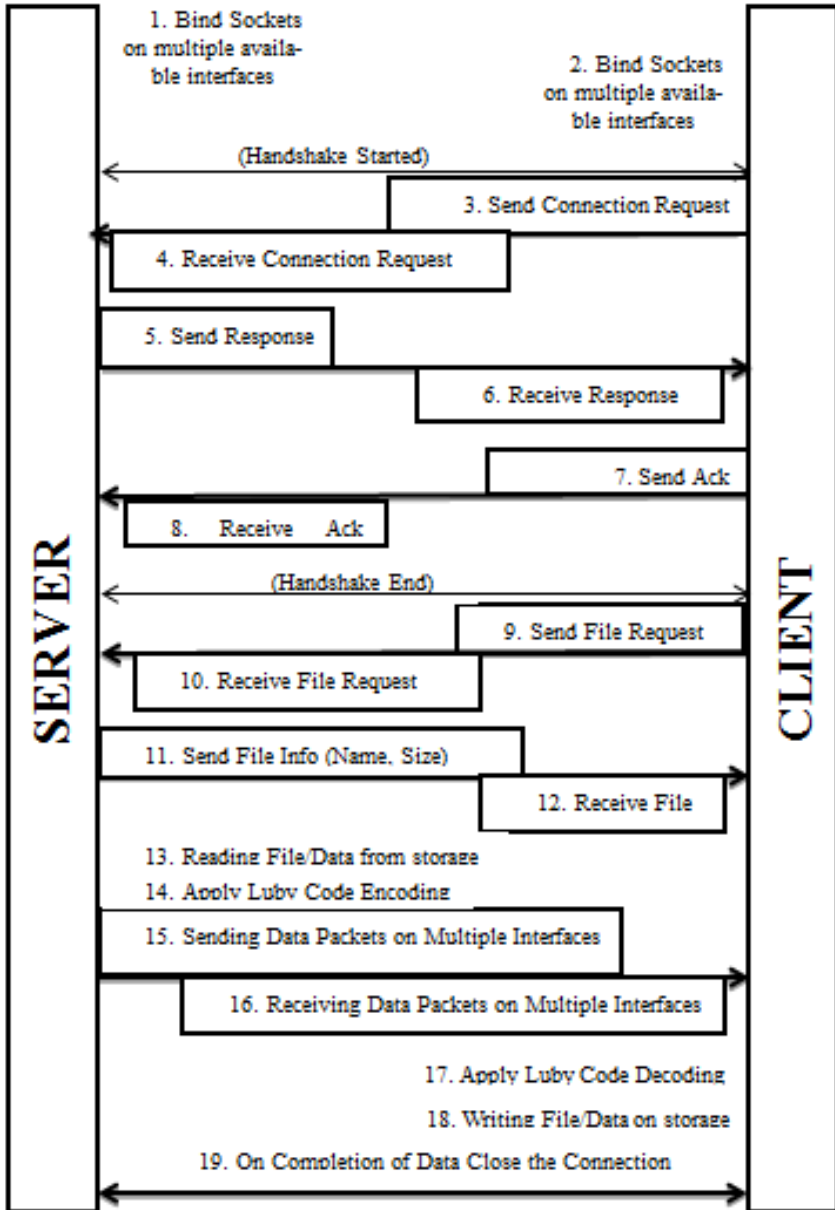


Fig. 2.1.2. Detail Data Flow Diagram between Sender/Server and Receiver/Client

For successful transfer of data, one will act as server and other as client as shown in Fig.2.1.2. Server binds the sockets with all the available interfaces, it will enable clients to initiate connection request. Sockets are basically the file descriptor in

Unix/Linux which helps in communication between the two programs. Client sends the request to server for establishment of connection. The unsigned integer is used to distinguish packets i.e. either its request, response or acknowledgment packet. Packet type filed is also reserved which is used for representing control packet or actual data packet. Server receives request from the client and initiate the handshake process by sending response back to the client. Handshaking is the process by which two devices initiate the communication. This response of the server is again acknowledged by the client by sending the acknowledgment packet and successfully completes the handshake process.

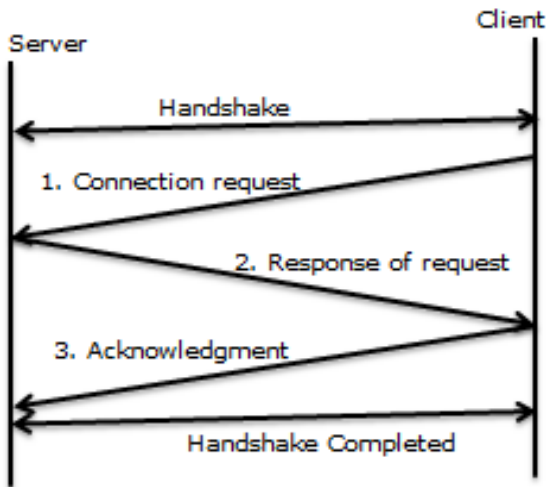


Fig. 2.1.3. 3-way Handshake Process

After successful handshake process as shown in Fig.2.1.3, client sends the request for the data e.g. name of the file etc. The request packet contains the type of packet and name of file. In response of the client request server will send complete information of data e.g. file name and size of file used for the calculation of total number of chunks. The data packet size is already decided between the client and server. Requisite data or file first divided into equal size of chunks and applied to the LT codes encoder, the resultant packets will start flowing towards client on multiple available paths. The length of the symbols is chosen as 512 bytes plus the header bytes. After selection of randomly chosen degree d which defines the number of packets going to be XORed for the composition of encoded symbol, header is also attached with the encoded symbol having information of distinct chosen neighbor indices selected with the help of random generator and chosen degree d .

Client who receives these encoding symbols start applying the LT codes decoding process. The receiver or client with the help of header get degree d and number of distinct indices and start the decoding process. Encoded symbol with degree one is the actual copy of sender data. Any Encoded symbol XORed with already decoded

symbol reduces the degree d of encoded symbol by one. Same process repeats until exact copy of sender's data is decoded at the client side. After successful retrieval of decoded symbols at the client side, connection is terminated by both ends.

3 Results and Discussion

In this section we present the results showing the performance of an efficient link bundling transport layer protocol using two hosts connected with two separate links aggregated in form of single logical link.



Fig. 3.1. Aggregated links between hosts

We use two hosts directly connected with each other as shown in figure 3.1, they use two wired interfaces both having speed of 1Gbps. Hosts utilizes both the interfaces at the same time for successful transfer of data using the protocol implemented at each side.

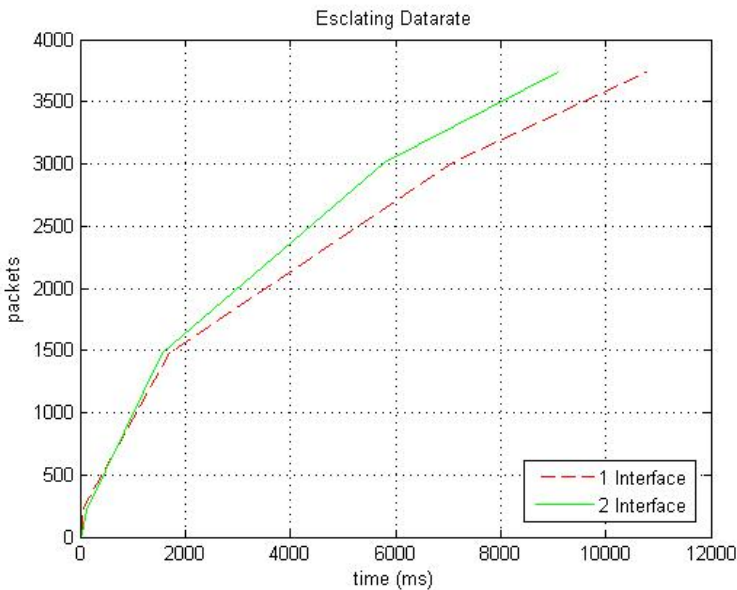


Fig. 3.2. Escalation of Bandwidth

Figure 3.2 shows that same amount of data take less time in case of two interfaces as compare to single interface. The result enforces our argument that using efficient aggregation of multiple interfaces can achieve escalation in bandwidth.

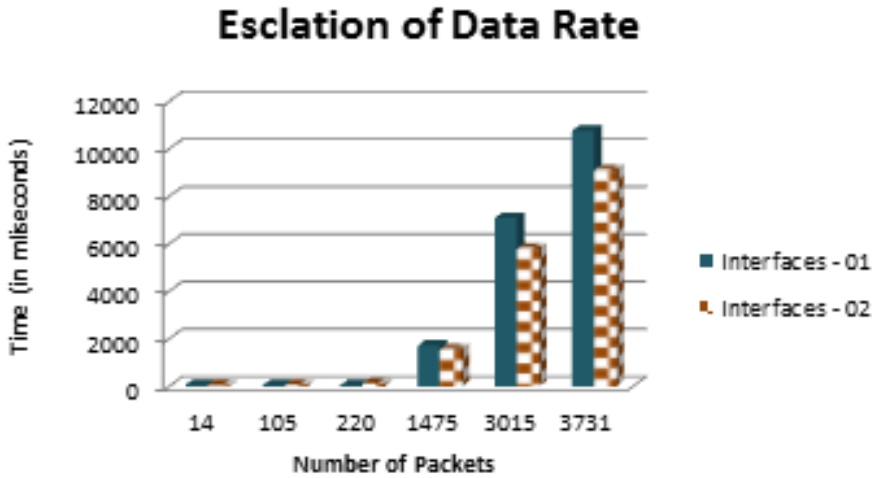


Fig. 3.3. Comparison of Data Rate against Time

Figure 3.3 shows the variable increase in bandwidth when size of data grows for the same aggregated link as compare to data with lesser packets, that means better performance for large files.

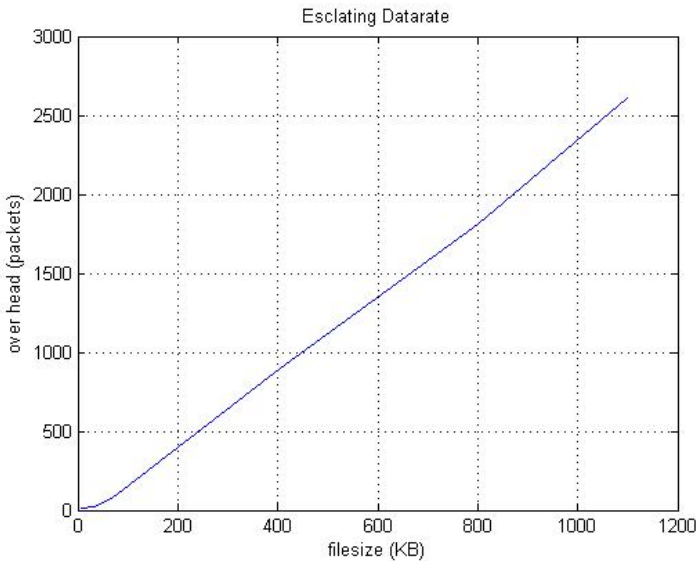


Fig. 3.4. Overhead Packets

Figure 3.4 shows that while transferring of data there is always acceptable overhead of encoded symbol. Data consisting of more packets have more overhead as compare to data having lesser packets.

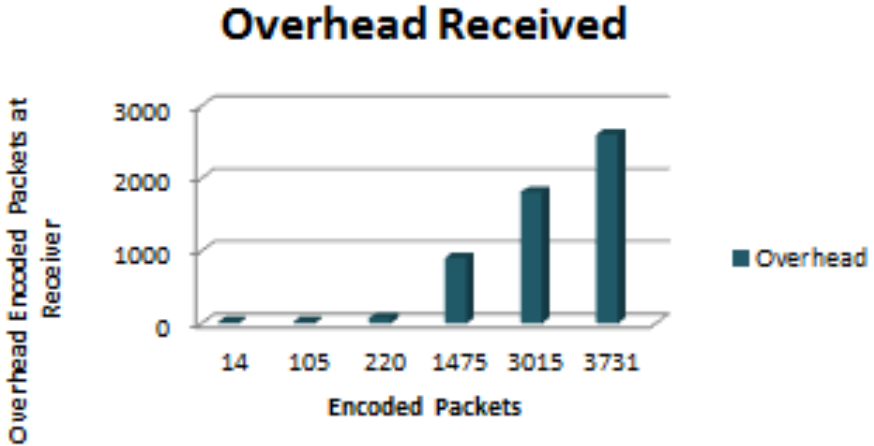


Fig. 3.5. Overhead Received against Encoded Packets

Figure 3.5 shows the overhead packets received against the total number of actual data packets.

This approach can play an effective role especially in case of video streamed application where bandwidth or data rate does matter as come to overhead. Faster the frames received at the receiver side better will be the quality and experience of user.

It is clear from the simulation results that increase in data rate produces better results in terms of time it will take for transfer of data using two interfaces but it is also showing that overhead is growing exponential that can be reduced with the implementation of online codes [5].

4 Conclusion

We have presented a new link bundling transport layer protocol which ensures increase in bandwidth along with higher availability with efficiency and reliability. This approach can also be used to increase uplink traffic between any two switches where more than one interfaces are available. It helps in increasing the bandwidth without upgrading the equipment. Experimental results demonstrate the effectiveness of approach. In future, the LT codes may be embedded in Linux kernel as it is expected to exhibit optimized and better results. Also, the cost of overhead may be reduced by introducing the online codes instead of the LT codes.

References

1. Hsieh, H.Y., Sivakumar, R.: pTCP: An End-to-End Transport layer Protocol for Striped Connection. In: Proc. 10th IEEE International Conference Network Protocols, pp. 24–33 (2002)
2. Bin, R., Xialoan, Z.: Enhanced Transaction TCP—Design and Implementation, April 22 (2011), Internet <http://terabook.net/enhanced-transaction-tcp-design-and-implementation.html>
3. Luby, M.: LT Codes. In: Proc. 43rd Annual IEEE Symposium on Foundation of Computer Science, pp. 271–280 (2002)
4. Syskonet, Link Aggregation according to IEEE 802.3ad, May 3 (2011), Internet <http://legacyweb.triumf.ca/canarie/amsterdam-test/References/wp-lag-e.pdf>
5. Maymounkov, P.: Online codes, NYU Technical Report TR2002-883 (November 2002)
6. MacKay, D.J.C.: Fountain codes. Proc. IEEE Proceedings in Communication 152(6), 1062–1068 (2005)
7. Byers, J.W., Luby, M., Mitzenmacher, M., Rege, A.: A Digital Fountain Approach to Reliable Distribution of Bulk Data. In: Proc. ACM SIGCOMM, pp. 56–67 (1998)
8. Linux Foundation, bonding, February 25 (2011), Internet <http://www.linuxfoundation.org/collaborate/workgroups/networking/bonding>

Improvement of Small Signal Performance of Multi Machine Power System Using SMIB Based PSS and STATCOM Designs

Bilal Hussain, Muhammad Usman, Affan Ahsan, Ahmad Talha,
and Farhan Mahmood

University of Engineering and Technology, Electrical Department, Lahore, Pakistan
gillani_89@yahoo.com, {m.usman.64, affanahsan9}@hotmail.com,
ahmad.talha.80@gmail.com, fmahmood@uet.edu.pk

Abstract. This paper discusses the improvements in small signal performance of a multi machine power system under the impact of Power System Stabilizer (PSS) and Static Compensator (STATCOM) devices. Parameters of both devices are optimized independently using MATLAB control system tools. PSS lead-lag network is designed using bode plot technique by analyzing Single Machine Infinite Bus (SMIB) based Heffron-Phillips model of network generators. STATCOM voltage regulator is optimized using a reduced STATCOM-Infinite bus model. The proposed designs are tested on a modified IEEE 14 bus system using MATLAB/SIMULINK. Simulations reveal that the system gains an appreciable damping ability against local modes of oscillation with PSS employed while STATCOMs increase this strength further. Results have validated the effectiveness of these SMIB based approximate modeling techniques in a multi machine environment where comprehensive system modeling is complex and often require information about whole power system which is sometimes hard to achieve.

Keywords: Heffron-Phillips Model, Multi machine system, Power System damping, Power System Stabilizer (PSS), STATic COMPensator (STATCOM), Single Machine Infinite Bus (SMIB).

1 Introduction

Generally, whenever a power system is disturbed, synchronizing and damping forces act until the state variables converge back to steady state. Damping forces remain sufficiently strong until the generators are in unregulated condition which is due to two main phenomena [1-3]

- Voltage induced in damper windings opposes change in speed.
- Rotor flux linkage varies due to accelerating or decelerating rotor causing torque variations proportional to change in rotor speed.

Generators in a power system are always regulated through AVR loops to ensure an appropriate terminal voltage under varying reactive power demands. However, high

speed voltage regulators are now considered as the primary source for weakening of power system damping forces. Under small disturbances, rotor angles and bus voltages undergo low frequency oscillations (0.2-3 Hz) as they reach their new steady state [4]. Under negative damping, system experiences ‘oscillatory instability’ where the oscillations grow till loss of synchronism. Systems with weaker damping may experience sustained oscillations for long periods thus limiting the power flow capability of transmission lines. Local modes of oscillation of power system (0.7-2 Hz) occur when a local generator swings against rest of the system [5]. Power System Stabilizer (PSS) can efficiently damp such oscillations [6]. However, [6] also states some drawbacks of PSS and one of them is the unnecessary voltage variations.

Nearly 20 years back, power system utilities worldwide, started applying Flexible AC Transmission System (FACTS) devices for reactive power support and control of power flow [4], [6], [7]. However, later these devices were found as excellent secondary option to improve system damping. Among FACTS devices, Static Compensator (STATCOM) enjoys faster speed and its reactive output dependency on bus voltage is much lesser than conventional SVCs. STATCOM is also investigated to have better damping effects than SVC [6]. Coordinating STATCOM along with conventional PSS (CPSS) can efficiently improve power system damping while offsetting PSS drawbacks as well [8].

Optimization of PSS and FACTS devices has been a major area of interest for more than a decade. Nonlinear behavior of power systems has motivated researchers to develop various advanced optimization techniques including fuzzy logic and adaptive strategies. References [4], [6] and [8] are excellent reviews regarding the progress in this field. These reviews indicate that fixed parameter optimization is quite effective over wide operating range though adaptive methods are being researched as well.

In this paper we have investigated a modified IEEE14 bus system suffering with low system damping and inappropriate voltage profiles. SMIB based linear analysis of system generators is carried out using Heffron-Phillip’s model. Analysis results are employed to optimize PSS loops of respective generators. STATCOMs connected to system buses are optimized independently by developing STATCOM-infinite bus models using Kron reduced Y-bus matrices at respective buses.

This paper is divided into four sections. Section 2 describes system modeling for fixed parameter optimization of CPSS. Section 3 presents system models for optimizing STATCOM current and voltage regulator loops. Section 4 discusses simulation results of IEEE-14 bus power system. Conclusions are drawn in section 5.

2 CPSS Optimization

Under disturbance, when synchronous machines undergo change in rotor angle and speed, the electrical torque output can generally be stated by following relation

$$\Delta T = K_s \Delta \delta + K_d \Delta \omega \quad (1)$$

Where K_s and K_d is amount of electrical torque introduced for a unit change in rotor angle and speed, also known as synchronizing and damping coefficient respectively.

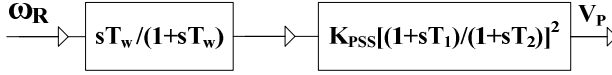


Fig. 1. Basic block diagram of speed based conventional PSS

In fact power system stabilizer is applied for increasing system damping coefficient. Simplest block diagram depicting s-domain model of CPSS is shown in Fig.1

The wash out block $\frac{sT_w}{1+sT_w}$, is included to ensure that the PSS loop is sensitive to only changes in speed, otherwise it may introduce unwanted electrical torques in the output. An inappropriate wash out constant may also deteriorate voltage profile of the system. PSS gain ‘ K_{PSS} ’ can be controlled to vary the amount of speed proportional torque injected in the system. It is usually set according to the best simulated behaviors of power system. Ref. [9] states that gain should be set as one third of the value of gain at which system starts experiencing sustained oscillations. In addition, a lead network is also added in the loop to compensate the AVR lag introduced within the system. Lead network coefficients are evaluated by analyzing the generator-network models. Detailed network models are analyzed for Eigen frequencies of the system. However, in order to calculate the AVR lag, simple SMIB based reduced models are often employed. Most effective is the Heffron-Philip’s synchronous machine-infinite bus model manifested by following set of equations [2]

$$K_3\tau'_{d0}\dot{E}'_{q\Delta} + E'_{q\Delta} = K_3E_{FD\Delta} - K_3K_4\delta_{\Delta} \tag{2}$$

$$T_{e\Delta} = K_1\delta_{\Delta} + K_2E'_{q\Delta} \tag{3}$$

$$V_{t\Delta} = K_5\delta_{\Delta} + K_6E'_{q\Delta} \tag{4}$$

$$\tau_j\dot{\omega}_{\Delta} = T_{m\Delta} - T_{e\Delta} \tag{5}$$

$$\dot{\delta}_{\Delta} = \omega_{\Delta}\omega_{\beta} \tag{6}$$

Where δ_{Δ} is change in power angle, V_t is terminal output voltage, E_{FD} is applied excitation and $T_{e\Delta}$ is electric torque. Since this model takes into account the effects of armature reaction (K_3, K_4, τ'_{d0}), it is superior to classical machine model especially when considering small signal analysis where transient behaviors of power system extend too long to assume a constant generator EMF. Fig.2 shows the Heffron-Philip’s model of an AC generator along with exciter and PSS blocks. Machine coefficients (K_1 - K_6) can be evaluated according to formulae derived in [2]. When analyzed we find two complex conjugate pole pairs associated with this system. One complex pair is due to exciter-field circuit and the other corresponds to rotor mechanics of the machine. Eigen frequency linked with the later pair is considered as one of the local mode of oscillation of power system.

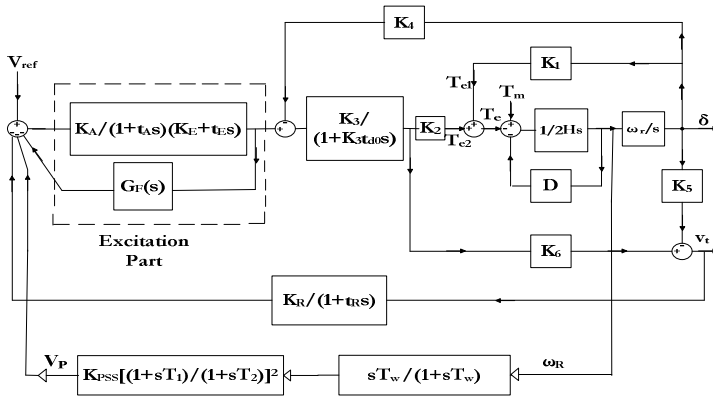


Fig. 2. Block diagram of synchronous machine with combined AVR and PSS circuitry employing linear SMIB based Heffron-Philip’s machine model

The bode plot of a typical exciter-field circuit response $G(s) = \frac{T_{e2}(s)}{V_t(s)}$ is shown in Fig.3 that depicts large phase lags near natural frequency. Phase plot exhibits nearly 120 degrees change in phase within a very short range of frequency around natural frequency. Any signal with frequency lying in this range will suffer high phase lags as it propagates through such a system Natural frequency of excitation systems primarily depends on exciter gain, however it generally occurs in a close range to local modes of a power system. Thus, AVR weakens power system damping by introducing large phase lags to low frequency components already present in terminal voltage following small disturbances. The phase lag can be effectively calculated by analyzing the system shown in Fig.2 which can be developed using linear control system analysis programs on computer. This model is also easy to develop since it only needs information about the local generator and AVR rather than the whole power system.

Lead-Lag network parameters, shown in Fig.1, can be easily evaluated once the troubled Eigen frequency and associated phase lag is known. Ref. [2] has discussed the calculation of these parameters for two different kinds of lead-lag circuits (active, passive) and can be consulted for details. In short, the parameters (T_1, T_2) are evaluated for a lead network; whose median frequency ‘ ω_m ’ is set equal to the frequency of local mode oscillations occurring in generator terminal voltage, observed either from Eigen frequency analysis or offline/online simulations, whereas phase lead ‘ Φ_m ’ is set equal to the required phase compensation. Normally two to three lead-lag networks are implemented in order to compensate a large phase lag which may be above 160 degrees.

Problems have been reported with direct speed signal taken as input with CPSS. Speed signal coming from sensor is normally noisy due to rotor dynamics and can cause excessive variations in PSS output. Ref. [5] describes different other options of input signals like electrical power or frequency. These signals are processed electronically to evaluate a noise less speed signal which is processed further through blocks shown in Fig.1 and thus the basic PSS design problem (described above) remains unaltered.

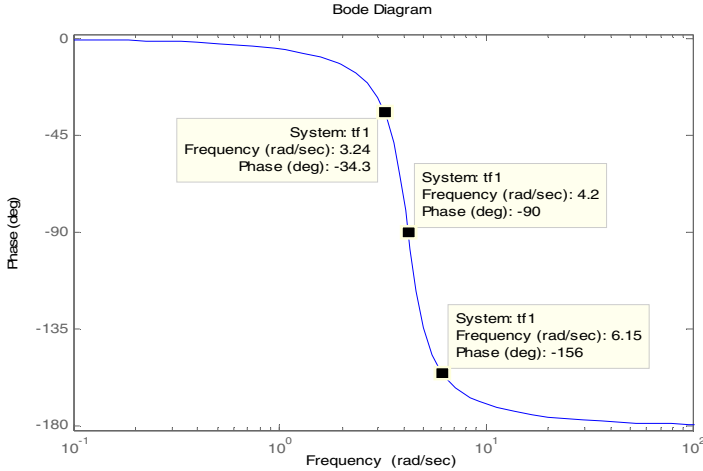


Fig. 3. Typical phase characteristics of an exciter-field circuit

3 STATCOM Optimization

STATCOM consists of voltage source converter (VSC) which is designed using high speed devices like GTO, IGBT, MCT etc and an energy source, mostly capacitor banks or DC battery. High rating STATCOMs are usually implemented with 6-pulse technique due to switching loss constraints. Being angle controlled, such devices have complex system models with coupled equations. However, low rating STATCOMs employ advanced switching schemes and can control angle as well as the magnitude of bus voltage. This simplifies the STATCOM model and decoupled system equations can be derived as in [10]. Control circuitry of STATCOM mainly consists of three regulators; Current, AC and DC regulator and a phase locked loop (PLL). PLL calculates phase angle $\theta = \omega t$ of STATCOM bus voltage to compute direct and quadrature axis components of voltage and current i.e. V_d, V_q, I_d and I_q . In this paper, design of converter with control over both angle and magnitude of bus voltage is considered.

3.1 Current Regulator

Fig.4 represents single line diagram of STATCOM connected to power system bus.

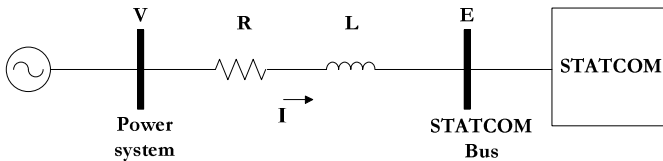


Fig. 4. STATCOM connected with power system bus through coupling transformer represented by RL parameters

Starting with the fundamental equations of STATCOM convertor currents, a compact equation is achieved in terms of D-Q components of voltage and current in [10] as follows

$$L \frac{dI}{dt} + (R + j\omega L)I = V - E \quad (7)$$

$$\text{Where; } \mathbf{E} = E_Q + jE_D \quad \mathbf{V} = V_Q + jV_D \quad \mathbf{I} = I_Q + jI_D$$

If power system bus voltage is taken as a reference Q-axis, Q and D components of current become active (I_p) and reactive (I_j) components respectively. As mentioned earlier, a special advantage lies with an angle/magnitude controlled STATCOM that it can be modeled using decoupled D-Q equations. Model is comprehensively derived in [10]. Fig.5 shows the decoupled STATCOM model used for optimization of STATCOM current regulator parameters. Only reactive current circuit model is displayed. Same regulator works for active current also. I_{jref} represents the reference reactive current demand, dynamically controlled by STATCOM AC voltage regulator to be discussed in next section. C1(s) is the PI regulator and L, R are the coupling transformer parameters.

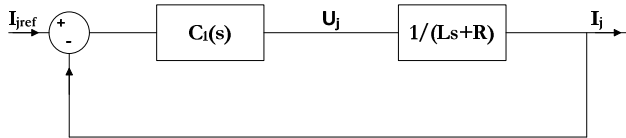


Fig. 5. Block diagram of decoupled STATCOM model

PI controller is used instead of PID in above circuit as the derivative action in presence of noisy input data makes the system vulnerable to fluctuations in steady state. PI controller parameters are such selected that the zero introduced by regulator transfer function cancels out the effects of coupling transformer pole ($\frac{1}{Ls+R}$). A system with a time constant T_c can thus be designed by setting PI regulator parameters as follows

$$Kp = \frac{L}{T_c} \quad (8)$$

$$Ki = \frac{R}{T_c} \quad (9)$$

Once optimized for the fastest response, the system can be effectively represented with a single closed loop transfer function as $T(s) = \frac{K}{1+sT_c}$, where T_c is usually a fraction of power frequency cycle (20ms).

3.2 Voltage Regulator

Fig.6 shows the system model used for optimizing STATCOM AC voltage regulator. Here, input/output of previously described STACOM transfer function T(s) are

substituted with equivalent shunt susceptance of the device. Two feedback loops are incorporated in the system model of Fig.6. Droop characteristics are manifested in form of a feedback gain X_s . Feedback gain K_n represents the power system response against change in STATCOM susceptance. Ref. [10] shows that ‘ K_n ’ is set equal to reciprocal of effective short circuit ratio (ESCR) of the system bus to which STATCOM is installed given by

$$ESCR = S_c / Q_{svc} \tag{10}$$

Where, S_c is the short circuit level at the STATCOM bus. For determining ESCR, usually STATCOM-Infinite bus model is assumed. Power system is reduced to generator and STATCOM installed buses only and Y-Bus of resultant reduced network is obtained through Kron reduction method. At STATCOM bus, minimum value of ESCR is calculated from Thevenin impedance. ESCR basically tells about the strength of system. Higher value of ESCR represents that system is strong and STATCOM takes longer time to reach the steady state value after perturbations. On the other hand, too low value of ESCR can inject huge oscillations and as a result controller stability is endangered.

In order to optimize AC voltage regulator, loop gain is set to such a value that response time is minimum while stability is not compromised. Controller parameters are designed using previously calculated time constant T_c and minimum ESCR at STATCOM bus as under [10].

$$K_p = \frac{1}{2*(X_s + K_{nmax})} \tag{11}$$

$$K_i = \frac{K_p}{T_c} \tag{12}$$

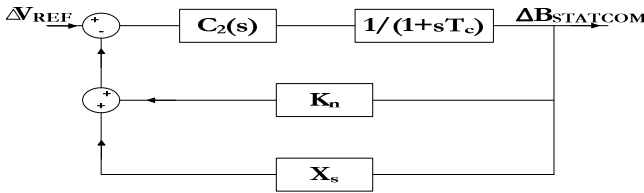


Fig. 6. Assumed power system model for optimization of STATCOM voltage regulator

3.3 DC Capacitor Design of STATCOM

The dc capacitor can be approximated by the following formula

$$C = \frac{2S_n}{pfU_{dc}^2} \tag{13}$$

Where S_n is rating of STATCOM, p is pulse number of VSC and f is frequency of system.

4 Simulation Results

Small signal analysis is carried out on a modified IEEE-14 bus power system shown in Fig.7. Bus no 1, 2, 3, 4 and 5 make transmission network with 69kV level. Rest of buses are on distribution side at 13.8 kV except bus no 8 which is at 18kV and it exists for compensation device installment. Initial system simulation showed sustained small signal oscillations with 1.4 Hz frequency as shown in Fig.8. SMIB model described in Fig.2 is developed for each of the two network generators using MATLAB control system tools to measure the phase lags due to generator AVRs. Once required phase compensation and unstable Eigen frequency (1.4Hz) is known, PSS lead-lag networks are designed. PSS and STATCOM parameters optimized according to methods developed in above sections are listed in Table 1 and Table 2 respectively. Current regulator parameters are same for each STATCOM due to same RL parameters of coupling transformers i.e. $K_p=22$ and $K_i=1.4667$. Table 3 contains the calculated value of DC capacitor required for each STATCOM.

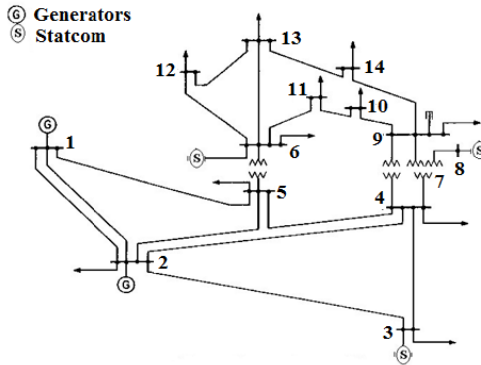


Fig. 7. Modified IEEE-14 bus system

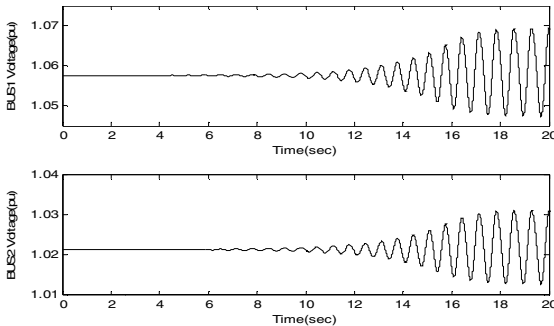


Fig. 8. Response of base case power system against small disturbance showing sustained oscillations

Fig.9 shows the significant damping effects of PSSs on equivalent rotor angle (α_1 - α_2). Oscillations settled down in 4.5 seconds with PSS on generator no 1 alone. PSS at generator no 2 was found inefficient in damping oscillations alone. However, when both PSSs applied together, damping improved further, also shown in Fig.9. PSS effects on generator bus voltages are depicted in Fig.10 and Fig.11.

Table 1. Optimized Parameters of PSS

Generator No.	T ₁	T ₂	K _{PSS}	T _w	Phase Compensated
1	2.169	0.00596	0.23	13	168°
2	2.367	0.00546	5	13	169°

Table 2. Optimized Parameters of STATCOM Voltage Regulator

Bus No.	K _p	K _i
3	7.58	758
6	7.27	727
8	5.07	507

Table 3. DC CAPACITOR VALUE

Bus No.	Capacitor (μF)
3	167
6	100
8	100

Performance of power system is observed under STATCOMs once the essential damping is made available using PSS. A load of magnitude one tenth of total generation (nearly 700 MW) is switched in at different buses for just 0.3 seconds. With such a type of disturbance, system’s small signal behavior can be observed without taking in the effects of AGC system as it is not considered in optimization process described in section 2. STATCOM damping effects are observed at buses 3, 6 and 8 as shown in Fig.12, Fig.13 and Fig.14 respectively.

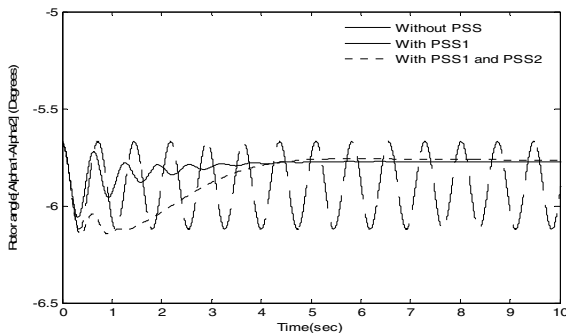


Fig. 9. Damping effects of PSS on equivalent rotor angle of generator no 1 and 2

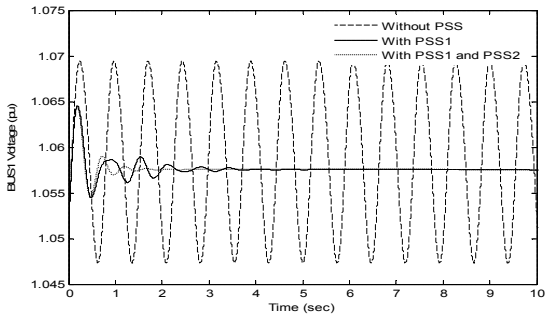


Fig. 10. Damping effects of PSS on bus voltage of generator no 1

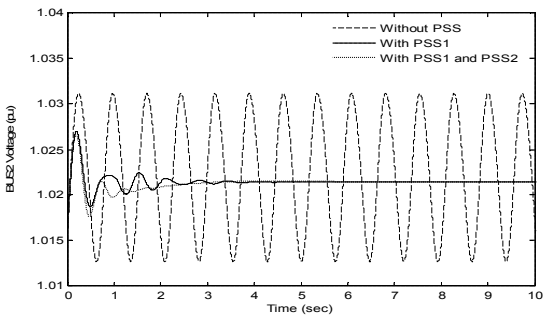


Fig. 11. Damping effects of PSS on bus voltage of generator no 2

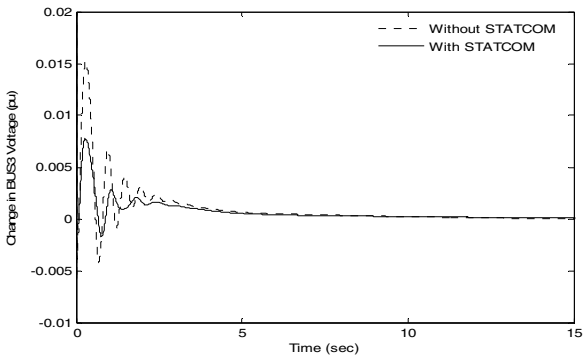


Fig. 12. Damping improvement of bus3 voltage under STATCOM

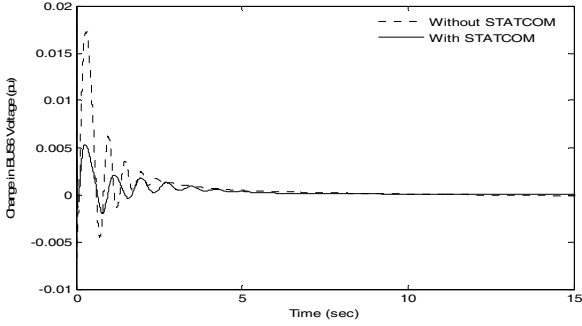


Fig. 13. Damping improvement of bus6 voltage under STATCOM

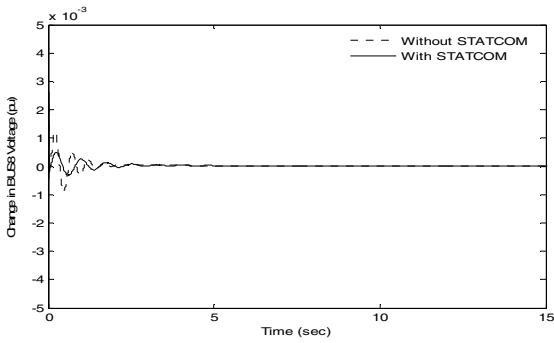


Fig. 14. Damping improvement of bus8 voltage under STATCOM

An interesting result of STATCOM damping ability is displayed in Fig.15. Here, the PSS gains on generator no 1 and generator no 2 are purposely set lower than optimum and post disturbance results are observed on bus no 1 voltage with STATCOM applied on bus no 3. It shows an appreciable damping capability of STATCOM.

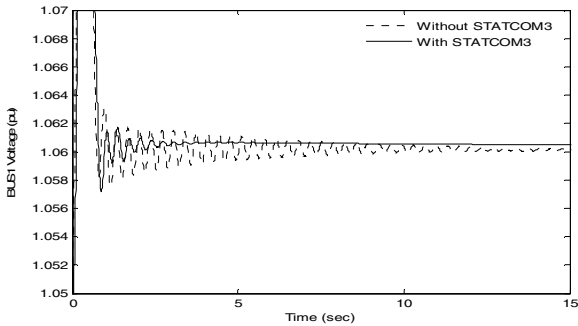


Fig. 15. Appreciable improvement in damping performance of bus1 voltage with STATCOM at bus no 3 when weaker PSS is employed

5 Conclusions

A multi machine power system is observed under the action of PSS which is optimized using SMIB based Heffron-Philip's machine model. Simulations confirm that small signal stability is enhanced and rotor angle oscillations settle down faster with proposed PSS design. STATCOMs are optimized independently using reduced network models. Simulations have validated their ability to improve damping proving them particularly effective in damping relatively larger initial swings following a disturbance. Under conditions when PSS is weaker or poorly designed, STATCOMs insert an appreciable damping strength into the system. Overshoot and settling time is significantly reduced when both devices are in service. The proposed designs for PSS and STATCOM are highly simple to develop as they are based on local bus and generator data which can be easily gathered in practical systems.

References

1. Machowski, J., Bialek, J.W., Bumby, J.R.: Power System Dynamics, Stability and Control, 2nd edn., pp. 177–196. Wiley, Chichester (2008)
2. Anderson, P.M., Fouad, A.A.: Power System Control and Stability- The effect of excitation on stability, 2nd edn., pp. 309–365. Wiley, New York (2003)
3. Kundur, P.: Power System Stability and Control. McGraw-Hill, New York (1993)
4. Eslami, M., Shareef, H., Mohamed, A.: Coordination of PSS and FACTS damping controllers in power systems for dynamic stability improvement. ICEI Transaction, 30–36 (February 2010)
5. Basler, M.J., Schaefer, R.C.: Understanding power system stability. IEEE Transactions on Industrial Applications 44, 463–474 (2008)
6. Abido, M.A.: Power system stability enhancement using FACTS controllers: A review. The Arabian Journal for Science and Engineering 32(1B), 153–172 (2009)
7. Habur, K., O'Leary, D.: FACTS- for cost effective and reliable transmission of electrical engineering, http://sites.google.com/site/lawking/facts_siemens.pdf (accessed November 27, 2011)
8. Singh, B.: Application of FACTS controllers in power systems for enhance the power system stability: A state of art. International Journal of Reviews in Computing (IJRIC) 6, 40–69 (2011)
9. Sauer, P.W., Pai, M.A.: Power System Dynamics and Stability. Pearson Education, New Delhi (2003)
10. Padiyar, K.R.: Facts Controllers in Power Transmission and Distribution. New Age International Publishers, New Delhi (2007)

Appendix

Coupling transformer: $R=0.0073\text{pu}$, $L=0.22\text{pu}$

STATCOM ratings: 40MVar, 24MVar and 24MVar at bus no 3, 6, and 8 respectively

Rest of the system data is same as given with IEEE-14 system.

Are QoE Requirements for Multimedia Services Different for Men and Women? Analysis of Gender Differences in Forming QoE in Virtual Acoustic Environments

Mansoor Hyder, Khalil ur Rehman Laghari, Noel Crespi,
Michael Haun, and Christian Hoene

¹ Interactive Communication Systems (ICS), University of Tuebingen
Sand 13, 72076, Germany

² Institut Telecom SudParis Evry France
{mansoor.hyder,michael.haun,hoene}@uni-tuebingen.de,
{khalil.laghari,noel.crespi}@it-sudparis.eu

Abstract. In recent years, the Quality of Experience (QoE) notion has become a major research theme within the telecommunication community. QoE provides an assessment around a human perception, feeling, performance and behavior. Normally, research studies on multimedia, Quality of Experience (QoE) and gender differences are carried out separately. To develop multimedia solutions covering QoE aspects, keeping the gender differences in mind, are the need of time. In current study, we are interested in knowing how QoE is shaped in Virtual Acoustic Environment (VAE) for male and female. We present experimental test results which provide interesting findings that both male and female have difference in their performance and perception in locating concurrent talkers in small and big sized virtual conferencing rooms. The middle-sized virtual room was suitable for teleconferencing because both male and female participants' performance and perception converge to similar trend and obtained better QoE values.

Keywords: Multimedia, 3D Audio, Quality of Experience, Virtual Acoustic Environment, Gender Differences.

1 Introduction

Quality of Experience (QoE) is based on study of social psychology, cognitive science, economics and engineering science to assess overall human quality requirements, expectations, feelings, perceptions and cognitions with respect to a particular product, service and application [1,2]. In short, QoE is the blueprint of all human quality needs and requirements. There is burgeoning trend to assess the quality of multimedia services and products on the basis of user centric Quality of Experience (QoE) benchmarks. Normally, QoE requirements are considered similar to every user of a particular multimedia service. But in this competitive market, it is important to provide more personalized and differentiated experience to

each individual user/customer. Further, the previous research has also revealed that there are gender differences in perceptions and behaviours as well [3,4]. Additionally, this is evident that male and female communicate differently in their role as a customer. For instance, females prefer accommodating communication which involves listening and understanding the customer's needs during service interactions [5]. However, the males prefer specific and logical information because they are task oriented and process information selectively [6].

Traditionally, Quality of Experience (QoE) and gender difference research have been carried out separately or in an isolated manner. Their exact correlation consequently remains unclear. With this current study, we intend to investigate the relationship among multimedia service (for which we have selected 3D audio based on virtual acoustic environment), gender difference and QoE. The current experimental study is conducted to bridge the gap that exists among multimedia, QoE and gender differences. We evaluate 3D audio telephony and teleconferencing service on the basis of QoE. Virtual acoustic environment, which is part of 3D Telephony and teleconferencing service [7], helps participants of a conference call to spatially separate each other, locate concurrent talkers in space and understand speech with clarity. We define two QoE factors in this study, Localization Performance LP and Localization Easiness LE for the evaluation of virtual acoustic environment. Localization Performance is an objective QoE factor and it is related to human cognitive capabilities. We define LP as, an assessment of how correctly listeners could locate the positions of the concurrent talkers in virtual teleconferencing room. Localization Easiness is a subjective QoE factor. It represents human perception and feelings of easiness in locating talkers. We define LE as, how easy listeners feel it to locate concurrent talkers in virtual acoustic environment? Specifically, this study investigates the effect of gender differences on QoE based on the study of localization performance and localization easiness in three different virtual acoustic rooms having dimension of ($10m^3$), ($15m^3$) and ($20m^3$). Furthermore, it is also important to understand and analyze the difference between human perception and performance capabilities with respect to their interaction with the virtual acoustic environment of 3D Telephony.

The overall goals are:

- To determine which virtual acoustic environment is most appealing to which gender in the context of 3D audio supported telephony and conferencing calls
- To design a virtual acoustic room which enhances quality of experience of the conference call participants (both male and female)
- To know whether human perception matches with human performance

This paper is organized as follows: In section 2, we present related work. In section 3, we present experimentation methodology and overview to data analysis techniques employed. In section 4, we discuss the results and in section 5, we conclude our work.

2 Related Work

We see it as an important task to understand the possible differences in forming QoE based on gender because gender differences may reflect difference in feelings, behaviour, performance and attentional task. It is reported in [8] that there are gender differences in attentional mechanism to collect spatial information in multiple sound sources environment. They found that, in the task of sound localization in multi-source environment, the superiority of males was apparent in the auditory domain. Further, in [9] sex differences in hearing are reported, the average girl hears the same sound with greater sensitivity than the average boy. In [10], superior performance by women on a task requiring object location memory has challenged the traditional view that men excel on all spatial tasks. A significant departure from the expected findings on sex differences has been the discovery that women excel also on a test of location memory for objects [11]. There is not much related work available concerning gender differences, QoE and VAE. Conclusively, literature study suggests to properly understand the role of gender in forming QoE in multimedia environments.

3 Experimental Study

3.1 Methodology

In current user study we opted three cubic shaped virtual acoustic rooms of ($10m^3$), ($15m^3$) and ($20m^3$) dimensions. The walls of the rooms represented the typical acoustic properties of concrete. Five participants were positioned at center of the room around the round table equidistantly (refer Fig. 1). One out of five participants was always performing a role of listener within the virtual acoustic environment. Remaining four participants always played the role of a talker. The layout of the positions of the listener and four talkers is depicted in Fig. 1.

At any given time, two out of four talkers were talking simultaneously. Listener's job was to locate and report the positions of the two simultaneous talkers and give score on the Mean Opinion Score (MOS) scales on the level of effort he/she required to locate the two simultaneous talkers. Within all three different virtual acoustic rooms, the table always represented the radius of two meters (2 m) . Further, a rendered view of one of the virtual acoustic room with two simultaneous talkers and a listener is presented in Fig. 2. Where, the green lines represent reflections of speech, yellow lines represent first order reflections and white lines represent direct speech from a talker to the listener. Red dots represent reflections point within the virtual acoustic environment. Small green triangles represent talkers while the small blue triangle represent a listener.

Furthermore, 26 paid subjects (13 male and 13 female) participated in this user study. All subjects had a university level education background and normal hearing threshold. Every subject participated in this experimental study as the listener and reported his/her performance and perception separately after judging six set of two simultaneous talkers. Therefore, every subject/listener had to

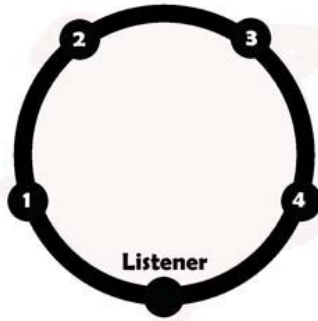


Fig. 1. Layout of the listener and four talkers in the virtual acoustic room

perform localization task and provide us with his/her perception on 12 locations in one room. All in all, every subject contributed his/her responses for 36 locations of different combinations within all three virtual acoustic rooms where talkers were employed. Overall, 936 observations were obtained and analyzed in this experimental study.

Within the scope of this study, we were interested in knowing how listeners located multiple concurrent talkers in different virtual acoustic rooms. What was the successful vs unsuccessful performance of males and females in locating concurrent talkers in the virtual acoustic environment? To investigate the questions, we divided 26 participants (13 males and 13 females) into four groups by gender and number of talkers located. We considered a participant successful if he or she successfully located at least 8 out of 12 talkers in one of virtual acoustic rooms and unsuccessful otherwise. We abstracted away information that distracted from our goal, such as specific positions located by the participants in a virtual acoustic room where talkers were employed. The virtual acoustic environment parameters, groups and number of participants are summarized in Table 1. Further, a view of the virtual acoustic environment under study can be seen in Fig. 2.

3.2 Data Analysis Techniques

Localization Performance. To get data trends and first hand information, we use statistical approaches to measure user localization performance and corresponding confidence interval. The proportion probability p represents estimation of performance rate. The most common way to measure a successful task completion rate and /or proportion of performance is to divide the number of participants who successfully completed the task (x) of localizing talkers in virtual environment by the number of participants who attempted the task (n) to estimate p , the population probability of successful completion. For calculating p , it is important to calculate Confidence Interval (CI) and use proper point

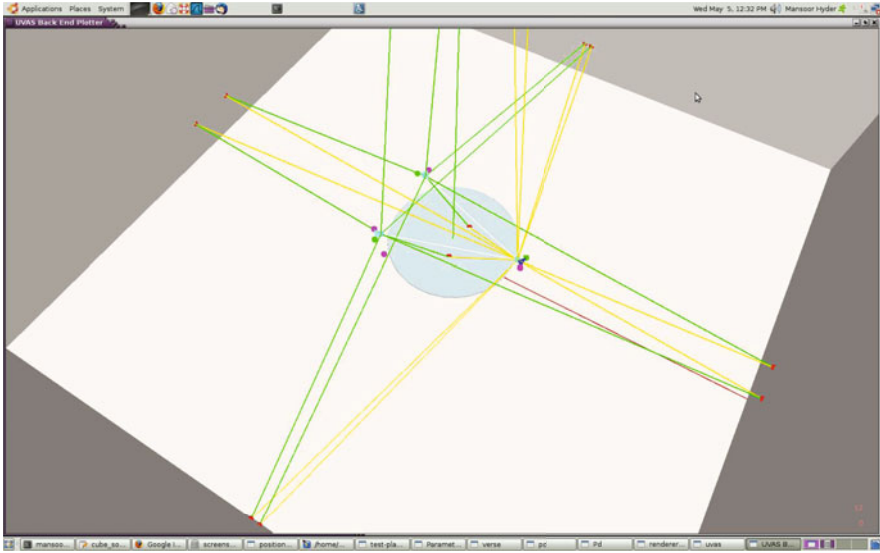


Fig. 2. Virtual Acoustic Room with two talkers and one listener

estimates. CI is used to indicate the reliability of an observed data by a certain confidence level. The confidence interval is double of the margin of error and it tells us the likely range the population means and proportion will fall in. There are many techniques to estimate p , the population probability of user satisfaction and corresponding confidence interval. In [12] over a variety of hypothetical distributions (Uniform, Beta, Poisson) and computational methods (Wald, Adjusted Wald, Clopper Pearson Exact, and Score) are discussed. They found that the Adjusted Wald technique is suitable technique to calculate error margin and confidence interval. For the estimation of localization performance, the Wilson point estimator is recommended, if proportion of success (x/n) is less than 0.5. Maximum Likelihood Estimation (MLE) is used, if the proportion of success (x/n) lies between 0.5 to 0.9 and LaPlace method may be used when proportion of success (x/n) is greater than 0.9 [13]. These estimation techniques produce statistically significant result about user localization performance.

Localization Easiness. Localization easiness is obtained using MOS scales. Within our experimental setup, subjects were asked to report the level of effort they required to localize two simultaneous talkers at any given time during the test. These MOS easiness values were measured on the discrete scale from 1 (bad), 2 (poor), 3 (fair), 4 (good) to 5 (excellent).

Table 1. Virtual acoustic environment and successful and unsuccessful gender groups of test participants

Virtual Acoustic Environment		⇒	Groups	Number of Participants
Room Size	20 m ³	⇒	Successful Males	6
		⇒	Unsuccessful Males	7
		⇒	Successful Females	8
		⇒	Unsuccessful Females	5
	15 m ³	⇒	Successful Males	10
		⇒	Unsuccessful Males	3
		⇒	Successful Females	9
		⇒	Unsuccessful Females	4
	10 m ³	⇒	Successful Males	11
		⇒	Unsuccessful Males	2
		⇒	Successful Females	8
		⇒	Unsuccessful Females	5
Virtual Acoustic Environment		⇒	Successful and Unsuccessful Gender Groups of Test Participants	

4 Results and Discussion

4.1 Localization Performance

Based on the discussion in (refer Section 3.2), we employed adjusted Wald method to calculate Confidence Interval (CI) and point estimators to calculate performance proportion p . Further, virtual acoustic environment and successful and unsuccessful gender groups of test participants are summarized in Table 1.

Male. As per the results presented in Tables 1 and 2, localization performance rate increases for male participants as the size of virtual room decreases. The overall trend suggests indirect relationship between localization performance rate and virtual room size. It means male participants successfully localized more concurrent talkers in small-sized room ($10m^3$) than big-sized room ($20m^3$).

Female. Unlike male participants data, female performance proportion rate is same (0.6154) in both large room ($20m^3$) and small room ($10m^3$). However the highest performance proportion rate is achieved in a middle size room ($15m^3$). It means female participants' performance is the highest in middle size room, and the small and big size room bring no big difference in their performance rate.

Comparison. It is quite clear from the Table 2 and from Fig. 3 that both male and female differ in their localization performance capabilities with respect to change in virtual acoustic room size.

4.2 Localization Easiness

Since, easiness measures a person's belief in his or her ability to perform a particular task [14], therefore, in this study, we were particularly interested to

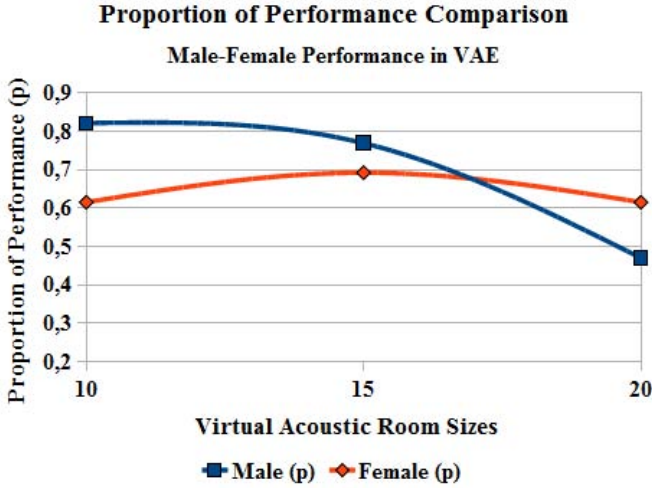


Fig. 3. Comparison of proportion of performance (p) for male and female test participants

investigate whether quality scores for localization easiness of test participants play any clear role in performing localization of concurrent talkers in virtual acoustic environment. Further, distribution of quality scores on human localization easiness are reported in Fig. 4 along with the proportion of performance against different virtual acoustic environments.

The virtual acoustic environment parameters, proportion of performance of the participants and quality scores for localization easiness are summarized in Table 2.

Male. Male participants' perception of easiness is the highest in middle size room ($15m^3$) which is 3.85 MOS score and the lowest is in small size room ($10m^3$) which is 3.64. It means male participants feel more easiness in localizing concurrent talkers in big room than in small room.

Female. For female participants, the MOS score data trend suggests that localization easiness and virtual acoustic room size are inversely proportional, i.e., as room size reduces, the perceived localization easiness scores increases. It means female participants feel easier in localizing concurrent talkers in small rooms than big room.

Comparison. The data trend in Table 2 and in Fig. 4 suggest that male participants feel more easiness in big room, conversely, female participants feel more easiness in localizing talkers in small room. While both male and female participants have similar scores in middle size room ($15m^3$). It means the male and female participants also keep different perceptual levels.

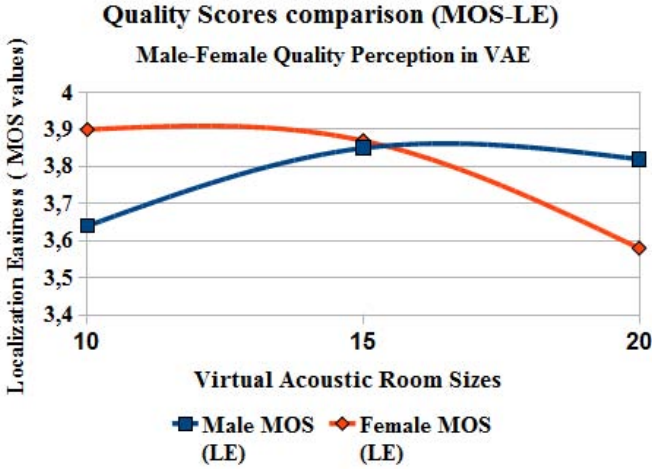


Fig. 4. Quality score MOS-Localization Easiness comparison for male and female participants in virtual acoustic rooms

4.3 Localization Performance vs. Localization Easiness

Male. In big-sized room ($20m^3$), male participants showed poor performance in successfully localizing talkers in various positions but they gave considerably good MOS score (3.82). While in small-sized room ($10m^3$), the overall MOS score i.e. 3.62, was lesser than big-sized room ($20m^3$). However, LP score was the highest (0.82). It means male participants perceive it easy to localize in ($20m^3$) room. But when male participants were asked to locate the talkers in ($20m^3$) room, their performance proportion rate was the lowest. At medium-sized room ($15m^3$), both LP and LE start to converge. It suffices to conclude that male perception and performance differ in both small and large room. But both LP and LE converge to similar trend in middle size room.

Female. LP rates are similar in both big-sized room ($20m^3$) and small-sized room ($10m^3$), but LE-MOS scores differ in these rooms. In large room ($20m^3$), female participants perceive it harder to locate participants than small-sized room. In reality when they were asked to localize talkers in both large and small room. They performed equally well in both rooms. However in middle-sized room ($15m^3$), both LP and LE scores converge to similar trend.

Comparison. The results suggest that male and female participants have slightly different trends between performance rates and LE-MOS scores in small-sized ($10m^3$) and big-sized ($20m^3$) room but their perception and performance capabilities converge to similar trend in middle size room. It means the selection of proper virtual acoustic room size, and the gender of participants do matter in

Table 2. Analysis of Human QoE Factors in relation to Virtual Acoustic Environment

Virtual Acoustic Environment		⇒	Human QoE Factors			
			Proportion of Performance		Quality scores on Human Localization Easiness	
			Male (p) + CI	Female (p) + CI	Male	Female
Room Size	20 m ³	⇒	0.4703 ± 0.2384	0.6154 ± 0.2350	3.82 ± 0.22	3.58 ± 0.27
	15 m ³	⇒	0.7692 ± 0.2172	0.6923 ± 0.2280	3.85 ± 0.17	3.87 ± 0.15
	10 m ³	⇒	0.8214 ± 0.2018	0.6154 ± 0.2350	3.64 ± 0.39	3.90 ± 0.31

Virtual Acoustic Environment ⇒ Analysis of Human QoE Factors in relation to Virtual Acoustic Environment

audio teleconferencing service. They should also be adjusted in suitable fashion to provide better QoE to both male and female participants/ end users.

5 Conclusion

The interest is increasing in both industry and academia to understand the QoE requirements of users and customers. In this paper, we investigated the impact of gender difference, and virtual acoustic room/enviornment [15] characteristics over QoE. We learnt from this study that both localization performance and localization easiness are not only dependent on virtual room size but they also vary, when the gender of teleconferencing participants varies. Because when same subjects were tested in different virtual acoustic rooms, their performance and perception were different. Also this difference is observed based on gender based groups. As per the findings from the user study, it is clear that male and female performance and perception varies in both big and small virtual acoustic rooms and we propose to consider the impact of gender differences over QoE. The middle-sized (15m³) room was found to be the most suitable room where human perceptual scores (LE MOS scores) and performance propotion rate (LP) match to similar trends. Hence, medium-sized room (15m³) is suitable choice in terms of optimal QoE in virtual acoustic environment.

References

1. Laghari, K.U.R., Molina, B., Crespi, N., Palau, C.: QoE aware Service Delivery in Distributed Environment. In: Advanced Information Networking and Applications Workshops, Biopolis, Singapore, March 22-25 (2011)
2. Kilkki, K.: Quality of experience in communications ecosystem. Journal of Universal Computer Science, 615–624 (2008)
3. Iacobucci, D., Ostrom, A.: Gender differences in the impact of core and relational aspects of services on the evaluation of service encounters. Journal of Consumer Psychology, 257–286 (1993)

4. McColl-Kennedy, J.R., Daus, C.S., Sparks, B.A.: The role of gender in reactions to service failure and recovery. *Journal of Service Research*, 66–82 (2003)
5. Sparks, B.A., Callan, V.J.: Communication in the service provider-customer relationship: the role of gender and communication strategy. *Journal of Hospitality and Leisure Marketing*, 3–24 (1997)
6. Meyers-Levy, J.: The influence of sex roles on judgment. *Journal of Consumer Research*, 522–530 (1988)
7. Hyder, M., Haun, M., Hoene, C.: Placing the participants of a spatial audio conferencecall. In: *IEEE Consumer Communications and Networking Conference - Multimedia Communication and Services (CCNC 2010)*, Las Vegas, USA (January 2010)
8. Zuendorf, I.C., Karnath, H.O., Lewald, J.: Male advantage in sound localization at cocktail parties. *Cortex* (2010)
9. Sax, L.: Sex Differences in Hearing Implications for best practice in the classroom (2010)
10. Kimura, D.: Sex, sexual orientation and sex hormones influence human cognitive function. *Current Opinion in Neurobiology*, 259–263 (1996)
11. Silverman, I., Eals, M.: Sex differences in spatial abilities: Evolutionary theory and data. *The Adapted Mind Evolutionary Psychology and the Generation of Culture*, 533–549 (1992)
12. Lewis, J.R., Sauro, J.: When 100% really is not 100%: improving the accuracy of small-sample estimates of completion rates. *Journal of Usability Studies*, 136–150 (2006)
13. Sauro, J., Lewis, J.R.: Estimating completion rates from small samples using binomial confidence intervals: comparisons and recommendations, pp. 2100–2103 (2005)
14. Bandura, A.: *Social foundations of thought and action: A social cognitive theory*. Prentice-Hall, Englewood Cliffs (1987)
15. Gardner, W.G.: *The Virtual Acoustic Room*. Massachusetts Institute of Technology (MIT), USA (1992)

Facilitating an Off-Site Customer in Product-Based Agile Software Development: An Industrial Case Study

Irum Inayat^{1*}, Muhammad Asim Noor², and Zubaria Inayat²

¹ Faculty of Computer Science and Information Technology, University of Malaya,
Kuala Lumpur, Malaysia

irum@siswa.um.edu.my

² Department of Computer Science, COMSATS Institute of Information Technology,
Islamabad, Pakistan

asim_noor@comsats.edu.pk, z.inayat@gmail.com

Abstract. Software industry is increasingly using Agile Methods due to its benefits. However due to increase in companies getting global distributed teams working on a single project from various parts of the world is becoming a challenge to inline this with Agile Principles. In such cases software industry has adapted Agile methods according to their particular needs. This adaptive arrangement is found to be divergent to basic Agile Principles. Customer collocation is one of the basic motivations and focus of Agile but under certain conditions as proved by the case study explained in this paper it does not impact success of projects. This paper is a detailed study of a software development organization following SCRUM for developing software products of its own. However after initial development they develop tailored products on customers' indentation. The study shows factors and impacts of successful surge of product even with absence of real customer throughout the customized product development. It is concluded that prior experience with same domain alternate customer representations, effective communications within team mitigates the effects of no onsite customer. On basis of the findings a framework is introduced which combines the success oriented factors.

Keywords: Agile Software Development, Off-Site Customer, Product-based Agile Software Development, SCRUM, Case Study.

1 Introduction

Agile Software Development Methods are widely adopted [1-2] like XP [3] and SCRUM [4] are the Agile variants being used extensively these days by software industry. Main focus of these methods is on collaboration with the customer and within the teams. This paper is based on a case study which studies the factors which contribute in subsiding customer's involvement and impact of customer's absence on success of venture. To ensure secrecy we renamed the company as Delta. It is a globally working software development organization which has a handful of successful

* Corresponding author.

products in market. The study is focused on one of the customized products of Delta which is a document management system used for massive personalized publishing. Delta being known for content management systems has a wide range of experience in developing such managements systems. The life cycle of this customized document management system is studied in order to track the factors of success even without customer's presence while following Scrum.

The result of this case study is the success analysis of Delta a product based software development organization with no onsite customer. The factors taken account are customer comments, rework and by maintenance data. The flow of the paper is in such a way that Section 2 is a brief overview of literature study related to customer involvement in Agile software development methods and Section 3 explains the research questions. Section 4 explains the case study conducted at Delta. Section 5 focuses on the analysis and discussion of results and findings. Section 6 explains the framework designed according to the findings of this case study. Section 7 concludes the findings and explains the future work.

2 Literature Review

Agile software development methods are an established practice in software industry [1-2]. In addition to being people centric, adaptive and iterative [5] Agile is more of a way of thinking than a pre-defined process [6]. Thus Organizations adopting Agile straightaway without proper training of employees face failures proved by a case study conducted at U.A.E [12]. So the organizations should not throw themselves to Agile but should refine their processes first [8]. There is a lot of stress on hybrid method used for large scale projects using Agile methods [9].

In literature its felt that there is a lot of focus on the quantity of methods used in industry and less emphasis is given to quality of the Agile practices [6]. The quality of Agile practices refers to find the match between industry practice of Agile and basic principles. The basic Agile Principle says that customer involvement is a critical success factor insofar definition of the project scope is concerned [10]. But in real world software industry is following hybrid methods suiting their circumstances and development environment.

With context to focus of our research it is found that having fulltime resident customer is rarity instead of common practice [7] in present day software industry. Studies show that it also not absolutely essential to have onsite customer 100% of the time [8] as (s)he is needed at most 21% of the software development time. Customer absence is compensated in several cases discussed in this study.

3 Research Questions

The research questions investigated in this case study are:

Q1: How product based software development organizations deal with Product customizations without an On-site Customer?

It is to investigate that how product based software development organizations deal with product customizations. The sub questions discussed in this study are:

q1: Which factors contribute to compensate absence of real world customer?

q2: Which Factors contribute in analyzing success of an organization?

4 Case Study

We conducted a real world case study of an international software development company *Delta* to assess the factors which impact the success of the product with an off-site customer. Delta is primarily a Product base organization i.e. develops products and launches to potential clientele. Delta basically deals in two types of development 1. Product development 2. Product Customization. For the first case product is introduced by the project management and marketing team after market study and workshop sessions with potential users. These workshops are arranged in order to gather the future needs of users regarding particular product. Thus there is no particular customer in this case and Project Manager (PM) with his team manages the development. In the later case customization is indented by customer according to his/her organization's structure and demands. But it is seen that even in later case there is no real (external) onsite customer. This study explores more about stated fact and in rest of the section we introduce the company and product, structure of the development team, research methodology and work flow.

4.1 Research Design of the Case Study

We designed some measures for carrying out this research such as Productivity is measured by considering story points per sprint, number of cycles per sprint, function points per sprint and time to market. There were two teams working on customization modules for 6-8 hours per week. Onsite observation, Semi-structured interviews and Questionnaires were used for data gathering from teams and customers. The information is gathered through multiple discussion rounds with a term during 8 months. The first round was based on collecting information product, its history, development methodology, development team and buyers of the product. Some of the key documents shared were work backlog, story cards, work schedule, effort distribution charts and product burn down chart. Later round of discussion was focused on clarification and validation of already gathered information.

4.2 Introduction of Company and Product

Delta is an international software development company started in 1985 with 2000 employees and clients in more than 70 countries. The domain of Delta is development of Content management systems and speciality lies in dynamic document publishing.

The product named Alpha, subject of the case study is a comprehensive document publishing solution. It has four customized versions launched since its initial development in 2008. Development of one of these customized versions named Alpha-1 is the focus of this study. The original size of Alpha-1 and its subsequent customized increments is given in the Table 1.

Table 1. Size of the Products

Product	Lines of code	Functional points
Alpha	41238	2657
Alpha-I	22000	1000

The product Alpha-I took 32 weeks and 3 days for completion, 16 sprints each of 2 weeks and 370 story points and story points per sprint are 11.5.

4.3 Workflow at Delta

The work flow followed at Delta during development of Alpha-I is described as below.

Product Initiation. Concept and Management teams decide the specifications of new product. Both the teams organize sessions with potential customers and established clientele to gather the in demand features for new product. Technical experts are on board for suggesting the best suitable and advanced platforms and tools to be used. The customized versions of launched products depend upon customer's indentation. Technical and business people collaborate with the customer at this stage.

Requirement Gathering. It is observed while being at Delta that requirements come through Marketing Department to Professional Services Department and Project Manager which are then communicated to Development Manager trickling down finally to Developer through Email, face to face interactions and Skype.

Approval of Proof of Concept. The Proof of Concept is a materialization of proposal at prototype level. First it is discussed among Project Managers and Marketing and later on presented to the customer for final approval.

Development. Project Manager owns the customization on behalf of customer and communicates the requirements to developers. The code is later on discussed in daily and weekly sprints. Prototypes are developed by Concept Team, responsible for developing Proof of Concept earlier.

Testing. The code is tested by Software Testing Group (STG). The interviewee mentioned that they often use Stress testing, and combination of white box and black box testing. The tests are conducted as and when coders hand over a module to testing team. The testing team performs the tests and report to the test team lead. The test reports are shared with the development team in daily or weekly sprint meetings.

Demonstrations. For internal demonstrations the product or module of the product is presented to Project Manager and Professional Services (PS) in order to be presented to prospect customer later on. This shows that developers never get to meet the customer.

Maintenance. After the customized version of product is sold to customers, maintenance calls are received and responded by Professional Services (PS) or Sales and Technical Support.

4.4 Development Team

The team strength working on modules is intentionally kept smaller in order to maintain high degree of communication and avoid confusions. Software testing group and Quality Assurance are separate departments at Delta; however they sometime lend their personnel to participate in development activities as per concept of self organizing teams in Agile Methods. Delta used SCRUM because it ensures incremental timely delivery of well tested software. The team comprises of 4-5 members including a Scrum Master, Project Manager/Owner and Developers/Testers. Sometimes Scrum Master is replaced by Project Manager himself.

Project Manager manages the development of original product; therefore he takes part in customization process as well. Project Manager and Marketing team is responsible for meeting the customer and gathering requirements and specifications. The teams meet up daily for 15 to 20 minutes in an informal way and discuss their achievements/ problems and daily plans (sprint backlog).

4.5 Questionnaires and Semi Structured Interview Questions

The questionnaire used for collecting information from the teams is shown in Table 2. In addition to this the questionnaire used for semi structured interviews with team members include following questions.

1. Does lack of communication between different Customers and development team creates misunderstandings about software requirements?
2. Is there an increase in long distance meetings rather than face to face meetings because of geographical distance amongst developers and Customers?
3. Does Off-Site Customer slow down knowledge sharing about software requirements?
4. Do you find face to face meetings with Customer more effective in terms of requirement gathering than by other means?
5. Do you find regular meetings with Customer helpful in understanding the requirements right?
6. Do you find On-site Customer presence helpful in building the right product?
7. Do you think regular interaction with Customer is the key factor for project success?
8. Does domain knowledge make it easier for the development team to understand software requirements?

Table 2. Questionnaire for gathering information

Questions		Options				
Name , Role , Experience		Close ended				
Your most of the customers are		Local	Foreign		Both	
How do you gather requirements?	Email	Face to face	Chat	Phone	mail	
What is the average time of project completion?	2-4 weeks	> 6 months		< 1 yr	>1 yr	
Does software development team meet the business group (Customers or stake holders) directly?				Yes	No	
Is there any other group except developers is responsible for meeting and gathering requirements from client?				Yes specify		No
Mention max team members?		2-4	4-6	6-8	>9	
Do you have On-Site Customer?				Yes	No	
You put a lot of focus on finishing requirements and design before starting the Implementation phase.				Yes	No	
Do you have long distance meetings with customers?	In some cases		most of the cases	Never		
Who participates in long distance meetings with customer?	PM	SD	ST	SA	Others Specify	
Do you get repetitive business from old clients?			Yes	No	Sometimes	

5 Discussion/Findings

This discussion leads to answers of research questions based on the findings from case study.

5.1 Research Question Q1

Q1: How product based software development organizations deal with Product customization without an On-site Customer? Project Manager is the one who communicates with customer regarding the changes (s)he wants in the product. The developer when interviewed mentioned that: *“The Project Manager communicates with the customer and gives us demos, I don’t think so we ever needed to see the customer ourselves”*. The Project Manager happens to see customer and being the initiator of product is always in a better position to understand customer’s point of view.

This fact replaces customer from business side with Project Manager. The developers response is satisfactory with absence of customer. This aspect is explained by the interviewee as: *“The project Manager being the owner of original product never asks for something out of the blue even in customization. He understands the product scope very well and thus directs customer’s customization demands to optimal edges as well.”* (Interviewee, Team Lead).

Thus Project Manager plays the role of proxy customer for development team. The Project Manager's background knowledge, domain understanding and experience makes him the well suited one and mitigates the need of real customer. Whereas the real customer and Project Manager hold face to face meetings and Project Manager often pays visits to customer sites. In addition to this modern communication means are also witnessed like video conferencing, internet telephony. Usually such kind of intermediary in communication is considered as a broken link but Delta is maintaining its business successfully and never felt a need of having onsite customer. In this case considered the Project Manager was collocated with the team and as mentioned by developer during interview that: *"We sort of never felt the need of meeting the customer ourselves. The demonstrations given to us by Team Lead or Project Manager rare enough for us to deal with our queries."*

At one other point the interviewee once again emphasized that *"I have never heard that every developer needs to meet customer, PM (Project Manager) or someone responsible supposed for demonstrating requirements is enough for us."* The availability of Project Managers being one of the high rank personnel of the company is an issue. Thus they are rarely available for face-to-face meetings i.e. daily, weekly sprints. The developers and other team members contact them through email usually.

5.2 Sub Question 1

q1: Which factors contribute to compensate absence of real world customer? The products of Delta are open to international market and it is gaining customers with the passage of time. The clientele of Delta is presently in 70 countries which grew over time. Maintaining such a big clientele is a fact related to quality and productivity. Some of the success contributing factors concluded by this study are described as under:

Domain Familiarity. Delta has a number of products in market from last two decades. This provides the teams an ease and experience in carrying the work out successfully. The hardships of understanding the new domain specifications are totally subsided here. Complex details become routine matter after producing variety of products of same type. The familiarity with domain also enables development teams to equip themselves with upcoming challenges and technologies regarding that.

Proxy Customer with Technical Background. The project Manager's technical background and experience helps him deal with new requirements efficiently and effectively. Being technical helps him make customer understand if his requirements are too vague or impractical.

Electronic Means of Communication. Modern and fastest means of communication are used for contact and coordination among Project Managers residing outside the Country or at remote locations and teams. Moreover email service, IM chat, Internet telephony is also used as fast communication links.

Experienced Workforce. The experienced developers generate concerned ideas for the initiation of new products. The developers with experience of almost a decade

working with the same company have witnessed successful products. This gives them confidence and excellence in the domain. An experienced developer is always in a better position to understand and respond Customer requirements.

Focus on Deliverables. Particular focus of scrum is on delivering a working module to customer after each iteration. Thus every sprint is performance and result oriented. This maintains the development of new sprint log and goals for the next sprint.

Less Iterations. Scrum followed at Delta was performance critical and teams show their output and future work plan regularly. There is a follow up for work done which lessens the error occurrence rate. As every release is demonstrated to the Project Manager hence it lessens the chances of wasting efforts in wrong direction.

Less Documentation. Less or minimal documentation in Agile focuses more on real implementation of the product. In this particular case the documentation is minimized to only *backlogs* and *burn-down charts*, rest of the documentation is prepared either by Concept Team as Proof of Concept or User Manuals after the product completion.

The validation of success claims mentioned above is shown in Table 3 below.

Table 3. Validation of Success claims

Factors	Validation Approach	Results
Domain knowledge	Interview with team members	Expertise of experienced team members in same domain development
Lesser iterations	Recorded #of iterations	2 iterations
Rich Communication	Witnessed the working	Face to face meetings Video Conferencing
Customer Satisfaction	Interviews with Customers	100% customers are satisfied
Post delivery maintenance data	Checked error logs and registered complaints with Management Department	Errors reported were declared Minor errors by Project Manager shows error logs decreased with time

5.3 Sub Question 2

q2: Which Factors Contribute in Analyzing Success of an Organization?. With reference to sub question 2 success of company is measured by making use of customer feedback, post delivery maintenance data, error logs and market report about product sale. Here we have used customer feedback comments about product, post delivery maintenance data and error logs.

Customer1 Feedback. Alpha-I was developed for a Business and Technology solution provider organization. The company needed a solution that would simplify and accelerate the process of creating and maintaining flexible healthcare enrollment

booklets for their customer. They needed to reengineer the way booklets were produced so as to make the process easier, quicker and more cost effective. Delta’s solution, Alpha-I, cut application development time in half and document customization has improved dramatically. The company has accelerated the entire process of building, changing and enhancing applications saving both time and money. *“Development time for the booklets is cut 50% and management effort is improved by 78% Booklets previously represented by millions of lines of code now managed and edited in the Alpha-I graphical design interface.”* (Customer Comments)

Customer2 Feedback. The second success case is of Alpha-I implemented in a large US Insurance Provider. The company demanded an efficient work flow management system with slight customizations regarding their own environment. To reduce the cost and time required for generating a benefit booklet and ID card for new customers. The production of ID cards needed to be integrated into this process. The company now has a custom workflow solution that dramatically accelerated the production process. Lower costs, elimination of errors, and the consolidation of products in one mailing were also achieved. *“Time from enrollment to booklet delivery reduced from 10 weeks to 1 day. Reduced mailing costs by consolidating all related documents into one package. Customer questions reduced because all information is delivered together.”*(Customer Comments).



Fig. 1. Error log per months along with severity of errors graph

Error Logs. It is observed that this company pays a lot of attention to post delivery services. For Alpha-I the recorded error logs after 6 months of delivery are shown in Fig 1. It can be concluded that number of error decrease with time. The severity ration also gives an idea about successful use of product.

6 Proposed Framework

Taking into account above discussion and findings we have formulated a hybrid framework for managing customer absence while following Agile Method i.e. Scrum. The framework states three basic ideas accumulating many attached ones as mentioned in Fig. 2.

6.1 Customer Representation

Real Customer being unavailable leads to proxy representation. The representation should be justified and sufficient enough to cater the satisfaction level of development team. Moreover the representative should be in a position to interpret customer’s mind clearly to the team. The factors which are very important while selecting proxy customer representative include availability, previously built domain knowledge and prior project’s success ratio. As mentioned in previous sections that domain knowledge and experience are one of the reasons of success. Thus the representative should be experienced enough with handsome domain knowledge to interpret customer’s needs and devise better solutions.

6.2 Communication

Collaboration being one of the foremost features of Agile Methods makes the team communication and share knowledge extensively. The basic measures concluded from above experience and literature to maximize communication is to enhance the communication means, reduce the intermediary or information brokers [14] and organize more show and tell sessions. The continuous show and tell sessions generate new ideas and enhance performance by keeping track. Similarly the reduction in number of information brokers or intermediate people will also enhance clarity and reduce confusions. This will result in mending communication breakage links and improve performance.

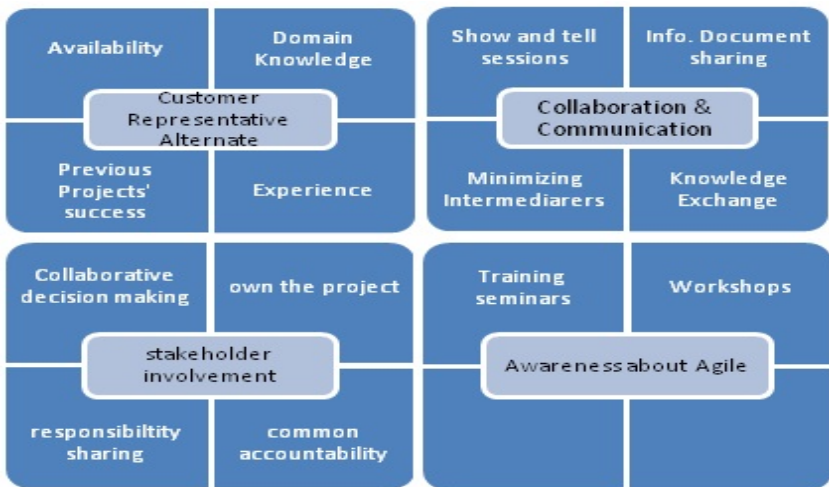


Fig. 2. Proposed Framework

6.3 Stakeholder Involvement

The stakeholder involvement issue is inevitable in Agile Methods. According the reported study of Delta there was no customer but it didn't affect the success still it cannot be generalized for all the organizations following Scrum. The quick and in time response from these departments can enhance the performance and reduce rework to a large extent. The involvement will result in a team effort and a combined attitude towards project development. The responsibility owning factor will increase and decisions will also be unanimous after solving disagreements. The teams should be trained for such an attitude which is Agile attitude by workshops and training seminars.

7 Conclusion and Future Work

The case study explains in detail the development culture of a product based software development organization with an anomaly of customization indented by customer. The considerable fact investigated here was to find the success factors with an offsite customer. This is done by customer feedback report, post delivery maintenance data/error logs. The Project Managers at Delta normally take up Proxy Customer's role for customization ventures and communicate the requirement to team lead and developers and participate in sprints. In this particular case considered the non availability of real customer has not affected company's clientele and product's sale but under certain circumstances. These circumstances are discussed in detail as success factor in this paper. On the basis of discussion and finding of this paper a framework is proposed which stresses on right selection of customer proxy representation, adequate communication among teams and stakeholder involvement by promoting Agile acquaintance in teams.

The future work can be the practical implementation and validation of proposed framework and empirical study of each feature of framework in detail in software industry.

References

1. Begel, A., Nagappan, N.: Usage and Perceptions of Agile Software Development in an Industrial Context: An Exploratory Study. In: First International Symposium on Empirical Software Engineering and Measurement (ESEM), pp. 255–264 (2007)
2. Nerur, S., Mahapatra, R.K., Mangalaraj, G.: Challenges of migrating to agile methodologies. *Communications of the ACM* 48(5) (2005)
3. Beck, K., Andres, C.: *Extreme programming explained: embrace change*. Addison-Wesley Professional (2004)
4. Schwaber, K., Beedle, M.: *Agile software development with Scrum*. Prentice Hall PTR, Upper Saddle River (2001)
5. Abbas, N., Gravell, A.M., Wills, G.B.: Historical Roots of Agile Methods: Where did "Agile Thinking" Come from? In: *Agile Processes in Software Engineering and Extreme Programming*, pp. 94–103 (2008)

6. Abrahamsson, P., Warsta, J., Siponen, M.T., Ronkainen, J.: New directions on agile methods: a comparative analysis. In: International Conference on Software Engineering, pp. 244–254. IEEE Computer Society, Portland (2003)
7. Shi, Z., Chen, L., Chen, T.-E.: Agile planning and development methods. In: 3rd International Conference on Computer Research and Development (ICCRD), vol. 1, pp. 488–491 (2011)
8. Koskela, J., Abrahamsson, P.: On-Site Customer in an XP Project: Empirical Results from a Case Study. In: Dingsøy, T. (ed.) EuroSPI 2004. LNCS, vol. 3281, pp. 1–11. Springer, Heidelberg (2004)
9. Lehman, T.J., Sharma, A.: Software Development as a Service: Agile Experiences. In: SRII Global Conference (SRII), pp. 749–758 (2011)
10. Chow, T., Cao, D.B.: A survey study of critical success factors in agile software projects. *Journal of Systems and Software* 81, 961–971 (2008)
11. Reifer, D.J.: How to Get the Most out of Extreme Programming/Agile Methods. In: Wells, D., Williams, L. (eds.) XP 2002. LNCS, vol. 2418, pp. 185–196. Springer, Heidelberg (2002)
12. Hajjdiab, H., Taleb, A.S.: Agile adoption experience: A case study in the U.A.E. In: 2011 IEEE 2nd International Conference on Software Engineering and Service Science (ICSESS), pp. 31–34 (2011)
13. Thiagarajan, P.S., Verma, S.: A Closer Look at Extreme Programming (XP) with an Onsite-Offshore Model to Develop Software Projects Using XP Methodology. In: Berkling, K., Joseph, M., Meyer, B., Nordio, M. (eds.) *Software Engineering Approaches for Offshore and Outsourced Development*. LNBIP, vol. 16, pp. 166–180. Springer, Heidelberg (2009)
14. Worren, M.: Customer Engagement in Agile Software Development: In: Master Thesis in Master of Science in Computer Science, Department of Computer and Information Science, Norwegian University of Science and Technology (2010)

Segmentation of Brain Tumor Tissue Using Marker Controlled Watershed Transform Method

Muhammad Kaleem¹, M. Sanaullah², M. Ayyaz Hussain³,
M. Arfan Jaffar¹, and Tae-Sun Choi¹

¹ Gwangju Institute of Science and Technology, South Korea

² Techlogix, Islamabad, Pakistan

³ International Islamic University, Islamabad, Pakistan

kaleem.arfeen@gmail.com, sanaullah@techlogix.com,
ayyaz.hussain@iiu.edu.pk,
{arfanjaffar, tschoi}@gist.ac.kr

Abstract. Medical imaging makes use of the technology to noninvasively reveal the internal structure of the human body. By using medical imaging modalities patient's life can be improved through a precise and rapid treatment without any side effects. The main purpose of this paper is to develop an automatic method that can accurately classify a tumor from abnormal tissues. The images used for tumor segmentation have been obtained from MRI modality. In this research we have developed a novel image segmentation technique based on catchments basins and ridge lines to accurately segment the brain image. This technique is based on immersions techniques for extracting objects from the image based on internal markers and external markers. Direct application of watershed transform leads to over-segmentation due to the presence of noise and other irregularities inherent in digital images. So to avoid this, we have carried out some preprocessing to remove noise and attenuate the curvilinear structures present in the MRI images during acquisition stage. After preprocessing step we calculated the morphological gradient of the input images. Then both internal and external markers of the original images were calculated and finally the watershed transform applied to complete the segmentation process. We have tested our algorithms on images obtained from Brain Atlas data base and found that the results closely match that of the radiologist.

Keywords: MRI, Watershed segmentation, Internal markers and External markers.

1 Introduction

Biomedical images are formed by objects of varying shapes, sizes and intensities [1] [2]. Segmentation of medical images is very difficult task due to overlapping of different tissues [3] [4]. Brain Tumor segmentation and classification is regarded as one of the most challenging task in computer vision applications. The complexity can be summarized by overlapping of different regions within the same image [4] [5]. The

intuitive idea of watershed transform comes from the geography where mountains correspond to high gray levels whereas rivers and valleys corresponds to low intensity values [6]. Watershed Transform is a segmentation method which is based on regions with homogenous properties of intensities [7]. Direct application of WT segmentation method to the MR images produces over-segmentation due to the presence of noise and other local irregularities of the images. Over-segmentation can cause serious problem to the MRI images which render the result of algorithm practically ineffective. This over-segmentation can lead to large number of segmented regions, which may not be the objective of the research. In order to avoid this problem of over-segmentation a practical solution is to limit the allowable regions by incorporating some preprocessing techniques. This preprocessing stage will remove the noise and local minima's. The practical approach to avoid over-segmentation is the use of markers for foreground objects and background. A marker is a connected component belonging to an image. So for segmentation purpose we have two types of markers. One is called as internal markers related to the object of interest and external markers related with the background. There are many methods in the literature for marker selection. People have used different methods ranging from gray level values and connectivity, descriptions involving size, shape, location, relative distance measure and texture based markers selection. The advantage of using markers is that it brings a priori knowledge to help efficient segmentation of the images. In the literature many tumor detection and classification systems have been developed for the detection of tumor before it gets start to spread [5]. First of all the research was carried out in the field of imaging modalities to improve the early detection of tumor. In addition to the improvement in the technology many awareness methods among peoples to recognize early tumor indications have been started.

In the hospitals to aid the doctors many automatic tumor detection systems have been established. These state of the art computer aided diagnostic systems can help the physicians to non-invasively detect the tumor at an initial stage. So in this research we are going to propose a novel computer based diagnostic method for tumor detection. The rest of the paper is organized as follows. Section 2 gives a brief overview of the Marker controlled watershed segmentation algorithm. The proposed segmentation is discussed in section 3. Results and discussion are given in section 3 and 4 respectively. Finally the references are given in section 5.

2 Related Work

Image segmentation techniques are normally based on host of properties but fundamentally two essential characteristics of intensities which are discontinuity and similarity are of utmost important [7]. Some of the general methods of segmenting an image are discussed in [14] based on thresholding based on EM algorithm and clustering methods. We will discuss in this paper with magnetic resonance images (MRI). The methods used are some semiautomatic and other ones are fully automatic for tumor segmentation. Other methods make use of the models and these models can be implicit or explicit like atlas deformation models. In this study we have developed a technique which is not dependent on any specific model and exploit not only the

content of the image but also on the topological constraints. In the segmentation of brain tumor using mathematical morphology most work is on the separation between grey and white matter [7]. Here, based on a preliminary segmentation of the brain, we propose a marker controlled morphological transform method to segment the brain stem, the cerebellum, cerebrospinal fluid (CSF), grey and white matter. The important aspect of the proposed methodology is the automatic selection of internal and external markers which increases the robustness.

3 Proposed Methodology

Proposed method consists of three different steps as shown in Fig 1.

3.1 Noise Removal

Noise is unwanted information that contaminates an image. Noise introduces in to the images during acquisition and also due to the optical properties of the imaging device. The very first step in our methodology is the removal of noise while maintaining the image quality.

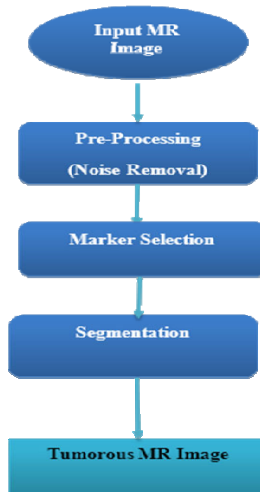


Fig. 1. Proposed Flow chart for Segmentation

We have employed morphological operations with different structuring element to remove the noise. The different operations performed are dilation, erosion, opening, and closing. We applied erosion and dilation to get the cleaned image. To get more refined result we incorporated opening and closing operations with different structuring elements.

3.2 Segmentation

Marker controlled morphological watershed segmentation mimics the natural phenomena of the landscape. In the landscape the mountains are like the ridge lines and valleys are the catchment basins. In the same analogy a 2D image can be best explained by visualizing it in three dimensions [4] [8]. The two x and y axes of the image are called the spatial coordinates whereas the third axis is called the gray levels. So in the image the high intensity pixel values corresponds to ridge lines and low intensity pixels corresponds to valley points. A valley is a topographic region which is enclosed by ridge lines [9] [7]. A *ridge* can be defined as the watershed lines where a drop of water will ultimately goes to local minimum. Two basic methodologies can be used to compute the ridge lines and catchment basins an image. One method is called the rainfall and the other is called as the flooding [10] [11]. We in this paper used the flooding approach for object segmentation. In this method we have used the gradient image for the application of watershed transform. Gradient image has been used because direct application results in severe over segmentation due to noise and other non-uniformity in the image inherently. This method incorporates the use of internal and external markers for object selection and the background computation. There can be many methods for the calculation of markers e.g. clustering, gray-level values and connectivity, feature based and using neural networks, but we employed marker controlled morphological operations. For the calculation of foreground markers we employed the techniques called opening by reconstruction and closing by reconstruction. The output of these two operations is the flat maxima of object of interest. Once the regional maxima is found then the next step is to extract those maxima points of each foreground objects. This method is very effective as it only removes the small blemishes without affecting the overall shapes of the objects. To view the result we superimposed the foreground markers image on the original image. The external markers or the markers of the background were obtained by first taking the complement of the internal markers followed by the morphological erosion operations. These external markers effectively divide the image into different regions, with each region containing a single internal marker and the background. Finally the watershed transform is calculated by using the internal and external markers which were computed using morphological techniques.

4 Segmentation Results

For the evaluation of this research work 30 MRI images were used to test the proposed algorithms. In these images we have to segment the White matter, Gray matter and CSF in order to make a diagnosis. The images were obtained from the Brain Atlas web page. It was very difficult to segment the images due to high Contrast, textured regions and low spatial resolution.

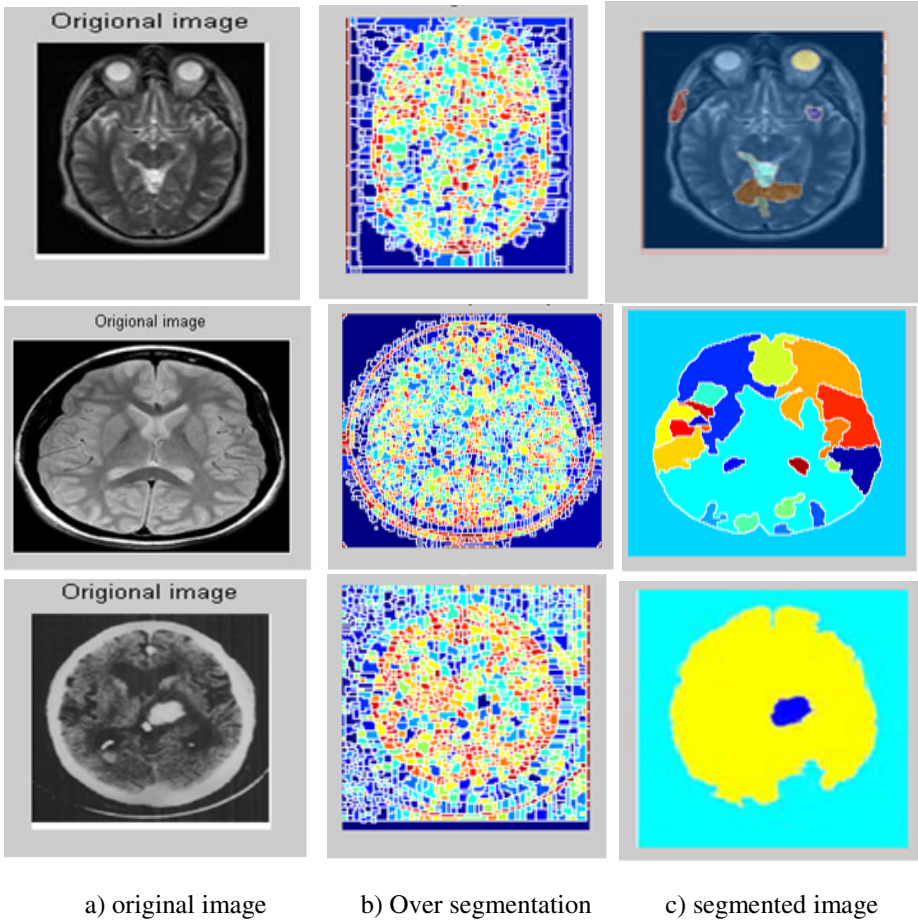


Fig. 2. MR Image segmentation results

The Algorithm was implemented in Matlab 7.9 and we used the standard function available in the toolbox. The results of the proposed algorithm are shown in Figure 2. To obtain the object markers or internal markers, morphological opening by reconstruction and closing by reconstruction operators were applied [12]. The background markers or the external markers were obtained by eroding the complement to the internal markers. Finally the watershed transform is applied to segment the image by incorporating the previously calculated internal and external markers [13] [2].

5 Conclusion

We have developed an automatic segmentation method which is simple, robust and gives continuous boundaries. The proposed system is divided into three main steps

i.e. preprocessing, internal and external marker calculation and finally segmentation of objects from MR images. This algorithm automatically adapts to the different characteristics of the MR biopsies. Also this algorithm is very useful tool for textured images which is not possible with conventional methods. This method reduces the computational cost to be implemented in hardware. MR images have high spatial resolution and the computational cost is added to the marker selection and watershed transform. All experiments show that the proposed system gives remarkably good results as compared to the recently proposed techniques.

Acknowledgement. This work was supported by the Bio Imaging Research Center at Gwangju Institute of Science and Technology (GIST), Korea.

References

1. Najman, L., Schmitt, M.: Geodesic saliency of watershed contours and hierarchical segmentation. *IEEE Transactions on Pattern Analysis and Machine Intelligence* 18(12), 1163–1173 (1996)
2. Glasbey, C.A., Horgan, G.W.: *Image analysis for the biological sciences*. Wiley (1995)
3. Corso, J.J., Sharon, E., Dube, S., El-Saden, S., Sinha, U., Yuille, A.: Efficient multilevel brain tumor segmentation with integrated bayesian model classification. *IEEE Transactions on Medical Imaging* 27(5), 629–640 (2008)
4. Shafarenko, L., Petrou, M., Kittler, J.: Automatic watershed segmentation of randomly textured color images. *IEEE Transactions on Image Processing* 6(11), 1530–1544 (1997)
5. Roerdink, J., Meijster, A.: The watershed transform: Definitions, algorithms and parallelization strategies. *Mathematical Morphology* 41, 187–228 (2000)
6. Roerdink, J.B.T.M., Meijster, A.: *Segmentation by watersheds: definition and parallel implementation* (1996)
7. Gonzalez, R.C., Woods, R.E.: *Digital image processing*. Prentice Hall (2002)
8. Dokládal, P., Urtasun, R., Bloch, I., Garnero, L.: Segmentation of 3D head MR images using morphological reconstruction under constraints and automatic selection of markers. In: *Proceedings of 2001 International Conference on Image Processing*, vol. 3, pp. 1075–1078 (2001)
9. Ng, H.P., Ong, S.H., Foong, K.W.C., Goh, P.S., Nowinski, W.L.: Medical image segmentation using K-means clustering and improved watershed algorithm. In: *2006 IEEE Southwest Symposium on Image Analysis and Interpretation*, pp. 61–65 (2006)
10. Pratt, W.K.: *Digital image processing: PIKS inside* (2001)
11. Moga, A.N., Gabbouj, M.: Parallel image component labelling with watershed transformation. *IEEE Transactions on Pattern Analysis and Machine Intelligence* 19(5), 441–450 (1997)
12. Clark, M.C., Hall, L.O., Goldgof, D.B., Velthuizen, R., Murtagh, F.R., Silbiger, M.S.: Automatic tumor segmentation using knowledge-based techniques. *IEEE Transactions on Medical Imaging* 17(2), 187–201 (1998)
13. Meyer, F., Beucher, S.: Morphological segmentation. *Journal of Visual Communication and Image Representation* 1(1), 21–46 (1990)
14. Bazi, Y., Bruzzone, L., Melgani, F.: Image thresholding based on the EM algorithm and the generalized Gaussian distribution. *Pattern Recognition* 40, 619–634 (2007)

Performance Evaluation of Statistical Techniques for Adaptive Scheduling in Autonomic Systems

Omer Khalid, Richard Anthony, and Miltos Petridis

CERN, Engineering Department, Switzerland
omer.khalid@cern.ch

University of Greenwich, School of Computing Science, United Kingdom
r.j.anthony@gre.ac.uk

University of Brighton, School of Computing and Engineering, United Kingdom
m.petridis@brighton.ac.uk

Abstract. The introduction of virtualization technology to grid and cloud computing infrastructures has enabled applications to be decoupled from the underlying hardware providing the benefits of portability, better control over execution environment and isolation. The virtualization layer also incurs a performance penalty, which can be significant for High Performance Computing (HPC) applications with high work volumes. Virtualization thus brings new requirements for dynamic adaptation of the scheduling to realize the potential flexibility of faster re-tasking and reconfiguration of workloads.

Often scheduling approaches are based on some well-defined system-wide performance metric within the context of the given systems scope of operation. However, this is not optimized for the structure and behavior of specific applications having a mix of task types each with their own task precedences and resource requirements.

Our work is concerned with combining virtualization and adaptive scheduling techniques to achieve an optimal balance between task placement flexibility and processing performance. In the scientific computing target systems, deadlines are attributed to tasks to ensure high throughput. We focus on application-specific dynamic adjustment of these deadlines to offset virtualization overhead.

This paper reports our investigation of the performance of two adaptive scheduling algorithms, which borrow concepts from signal processing and statistical techniques such as probability distribution function.

Job success and failure rate results from real task data from CERNs Large Hadron Collider Computer Grid (LCG) are also presented in this paper.

Keywords: Dynamic adaptation, Autonomic systems, Virtualization, Grid, HPC, Cloud, Job Scheduling.

1 Introduction

This paper reports our work introducing dynamic scheduling into virtualization with high performance computing in large grid systems. By making the

scheduling adaptive we balance the need for optimized performance at the system level and at the level of specific applications.

In the past few years, virtualization technology has remarkably shaped the way data centers have come about to increase their resource utilization by virtualizing more and more of computing applications to reap the benefits of lower support costs, higher mobility of the applications, higher fault tolerance with lower capital cost [1]. In this evolution, virtualization has increasingly brought a paradigm shift where applications and services could be packaged as thin appliances and moved across distributed infrastructure with minimum disruption.

Grid and Cloud providers such as Amazons Elastic Cloud Computing (EC2)¹ or scientific clouds like Nimbus² [2], cater to the needs of diverse user communities, and workload with diverse resource requirements. Virtualization could be very useful in efficient and dynamic resource provisioning between tasks by assigning them to virtual machines, automating setting up of compute nodes on-demand. This is particularly useful in systems where large work volumes have to be executed with long run times.

The benefits provided by the virtualization technology have to be considered in the context of performance penalty incurred due to an additional layer of complexity, and this requires adaptive mechanisms in real time such as dynamic scheduling of tasks by monitoring their workflow. This is due to the fact that virtualization technology incurs a performance overhead, which slows down task execution.

Traditionally in autonomic systems where tasks have to be executed on distributed systems with long waiting queues, the focus is given on system-wide metrics such as minimizing task response time to increase total job throughput. Such scheduling metrics become distorted once virtualization and its overhead are brought into the deployment scenario. E.g. one problem observed in virtualized applications is that task execution estimations have to be dynamically re-calculated whenever system loads change [3].

To overcome this challenge, we have taken a different approach to scheduling which does not focus on system wide criteria but rather emphasizes application specific characteristics. In order to leverage virtualization technology, we have introduced an adaptive scheduling mechanism that adapts tasks deadlines in real time. This is for the following reasons:

- Varying the degree of virtualization overhead has a scaling window effect on the task deadlines, which could either expand or shrink in temporal dimension.
- Imperfect task execution estimation reduces the effectiveness of pre-existing runtime predictions and can lead to pre-mature termination of otherwise successful jobs.

We investigated multiple adaptive techniques to determine task deadlines in real time. The objective is to reduce the problem of premature termination of tasks

¹ Amazon provides an on demand cloud computing service where user pays for per hour usage of virtual machines. <http://aws.amazon.com/ec2/>

² Nimbus is a cloud computing project developed at University of Chicago.

by looking into system load at any given moment. We also tried to address a broader scheduling problem of developing optimal mechanisms to determine any given metric in a dynamic system as long as its random and discreet.

We approached this challenge simultaneously from the statistic angle using distribution functions whilst also introducing concepts from signal processing which are generally designed to reduce noise and distortions in the value of the metric.

We present the results of our investigations to evaluate the algorithmic techniques we developed to fill in the gaps of adaptive scheduling at the VM-level and thus complementing system-wide scheduling approaches usually deployed in large scale distributed grid systems.

Furthermore, we applied our work to task profiles taken from CERNs experiments to understand how such techniques could be used in real-world production systems which not only have very tight resource constraints but also where the complexity of the system makes the problem even more interesting for scientific research especially in the context of adaptive scheduling for large scale distributed systems.

2 Motivation and Background

The term Grid was coined in mid 1990s to represent a uniform and transparent access to distributed compute and storage resources with different time zones and geographical boundaries [4]. It borrowed the concept from typical power distribution grids where user (domestic or industrial) are able to access electric power round-the-clock without even knowing from what source that power was generated or where it was generated.

The need for grid computing arose due to the increasing complexity of applications in terms of resource requirements, distribution of required resources and faster networks connecting those resources. The underlying network fabrics have improved in terms of their ability to transport more and more data at faster speeds. This has stirred up the ideas of pooling distributed computational, storage and network resources into a single platform using commodity computer servers rather than expensive main-frames and super computers. A grid system can be deployed over hundreds of computational sites with thousands of processors participating and peta-bytes of data to be stored and analyzed at geographically distributed locations connected by very fast network connections.

Since the scientific computing and engineering communities are very diverse in their needs, scope, size, purpose and sociology; the set of sharing policies that govern such a complex sharing model are standardized and often described as a Virtual Organization (VO) [5]. The above-mentioned computing requirements and policies are enforced through a grid operating system called grid middleware.

Over the years, different grid infrastructures and their corresponding middleware have been developed such as Globus , gLite and Arc5 where each have taken slightly different approaches to deal with the challenges posed by their dominant user communities.

In this paper, we focus on the computing grid installed at CERN to store, compute and analyze the results from its Large Hadron Collider (LHC) experiment.

2.1 Pilot Job Framework

ATLAS is one of the LHC experiments [6] and its workloads run on the LCG grid. ATLAS users are part of the ATLAS virtual organization. To provide a uniform and comprehensive access to grid infrastructure, it developed a high level computing framework [7] that overlays the grid middleware and manages job submission, monitoring, resubmission in case of failures, queue management while providing a single and coherent grid accessibility interface to its users. ATLAS computing uses the Production and Distributed Analysis system (PanDA) for pilot job submissions [8].

The PanDA system submits redundant and dummy jobs called pilot jobs acquiring processing resources on the grid, as shown in figure 1, which are later scheduled for jobs by the external brokerage systems. Then the job is downloaded for execution from high-level ATLAS computing framework queues. Pilot jobs are a kind of resource leasing mechanism, and are responsible for delegating the job scheduling responsibility away from the work load management systems yielding improved resource provisioning and allocation for ATLAS jobs while reducing unnecessary system load on the grid workload management system.

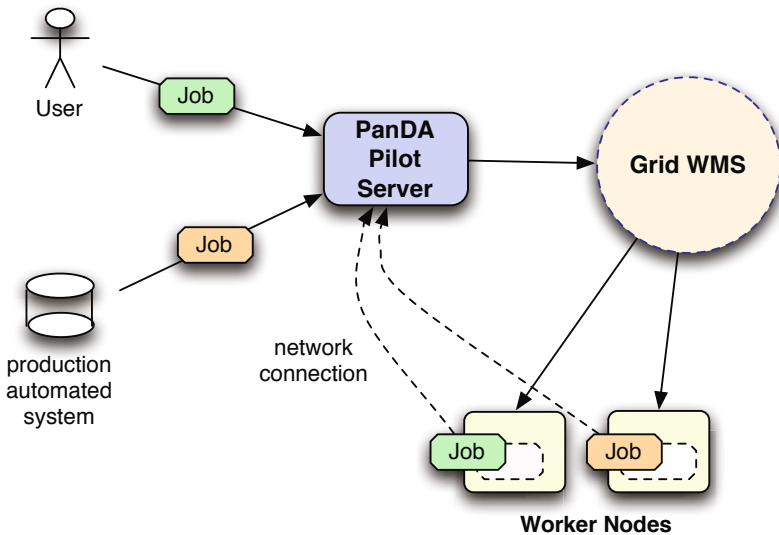


Fig. 1. Grid pilot jobs workflow and the steps it goes through

3 Adaptive Scheduling for Pilot Jobs

This section describes the characteristics of the challenge faced in introducing adaptive scheduling for pilot jobs in the large scale high performance grid installed at CERN, and presents the strategy adopted to achieve this.

3.1 Nature of the Challenge

ATLAS scientific experiment tasks consist of various processing components for particle physics analysis and are broken down in three major phases: event generation, simulation, and reconstruction. Each of these phases is executed as a separate process. Each stage produces an output which acts as the input of the next phase. We categorize them as short, medium and long tasks based on their resource requirements and duration. Its important to note that each of the phases only maps onto one category type as shown in table 1. We use these profile of jobs as input dataset for our experimentation, but the adaptive scheduling technique we have devised is applicable to different mixes of tasks and other types of tasks having similar characteristics of resource usage and as well.

Table 1. Resource requirements and properties of ATLAS Production job

Job Type	Mode	Duration (hours)	CPU Intensive	Memory Intensive	I/O Bound
Event Generation	Serial	2 - 6	Yes	No	No
Simulation & Digitilization	Serial	12 - 24	Yes	Yes	No
Reconstruction	Serial	6 - 12	Yes	Yes	Yes

A high-level grid scheduler that manages the tasks queues schedules these tasks. It is responsible for sending out dummy tasks to the grid to acquire resource slots. Once resource slots are acquired, actual tasks are downloaded to the remote location for execution and often it happens that that particular tasks do not meet duration restrictions placed by the resource provider and gets prematurely terminated. This is a source of uncertainty in a system where execution estimates are imperfect. This translate into wasted resources and extended runtime over the entire experiment as failed jobs have to be rescheduled.

3.2 Nature of the Solution

As described earlier, over the past few years there has been an increasing trend of integrating virtualization into grid computing. The emphasis has been either on development of the mechanisms that deploy tasks to virtual machines in a transparent fashion or the emphasis has been on the impact of overhead on the tasks but not necessarily on the task's deadlines and the scheduling problem that

arises from it. The scheduling problem especially becomes serious where there is an inter-tasks dependency, and if one task higher in the chain fails the rest of the chain fails.

Previously, we evaluated the performance impact on the tasks when run in virtual machines with increased execution time (T_i) when number of parallel virtual machines (N_{vm}) is progressively increased with varying numbers of CPUs allocated to them (P_i) [3]. A brief summary of these results is shown in table 2.

Test 1 represents a baseline when the tasks are executed in physical machines with no virtualization overhead. Tests 2 and 3 show a simple deployment where system load in terms of the number of parallel virtual machines was increased progressively to measure the impact on task execution. Test 4 represents the highest system load where overhead is around 13% if a single CPU is allocated per task-VM. In test 5, when CPU allocation is reduced to half to accommodate additional tasks, performance drops by 83%.

Table 2. Performance results for Xen CPU capping parameters when applied to parallel executing virtual machines

Test	Num of VM	P_i (Num of CPU cores)	T_i (sec)	Relative Overhead (%)
1	0	4	7080	0
2	1	4	7130	1
3	2	2	7193	2
4	3	1	7970	13
5	3	0.5	12926	83

Increased task execution times not only fluctuate due to the system load but also increases tasks runtimes. Our adaptive scheduling algorithm attempts to solve the problem by dynamically estimating job deadline based on system load and takes into account the resource requirements of the tasks in real time.

3.3 Algorithmic Model

In our simulation model, the algorithm intelligently schedules the jobs and learns over time about the missed deadlines under various conditions. To allow the scheduling algorithm to respond to the system properties, we introduce a duration-executed vs. duration-remaining ratio, denoted as d , for a job that is projected to miss its current deadline, and is determined by:

$$d = \frac{duration_{remaining} - time_{deadline}}{duration_{remaining}} \quad (1)$$

The adaptive threshold update structure we have adopted, shown in figure 2, has been motivated by similar structures that are used in communication systems and digital signal processing. Namely, there are many variations of control loops

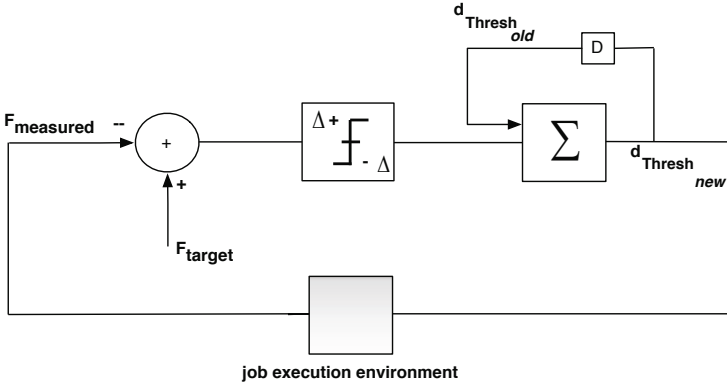


Fig. 2. Adaptive d threshold algorithm: $d_{Threshold}$, $d_{Threshold_{new}}$ - threshold values, D delay element, Δ - delta step, F_{target} target failure rate, $F_{measured}$ measured failure rate

that have a similar goal: to track a given reference value, such as time (time synchronizers), phase (phase locked loops), etc. and most notably in adaptive gain control, where goal is to maintain a certain reference power level. A more detailed discussion of these signal processing techniques can also be found in the works of Meyr et al [9].

In our implementation, the threshold update algorithm is based on trying to keep given metric of measure failure rate close to the selected target failure rate . The threshold value for job acceptance is lowered if the failure rate increases and vice versa. The update step has been quantized to a small value Δd in order to avoid fast threshold changes if the difference between the measured and targeted failure rate is large. The optimal value for the step Δd has been determined through experimentation.

A second approach we have taken is to calculate the Probability Distribution Function (PDF) and Cumulative Distribution Function (CDF) of the job success rate and use it to select the threshold value dynamically in such a way that D_{Thresh} corresponds to the probability $P [d < D_{Thresh}] < P_{Thresh}$. In this case, P_{Thresh} is a pre-selected target probability of success set to 50% probability of success of job meeting its deadline as a filtering criteria. The distribution of d ratio is mapped by CDF referred as $F(v)$ described as a discrete variate V which in this case is D_{Thresh} . It implies that for a given value of d ratio for a job takes on a value lesser or equal to a number v which is the selected from the distribution of d ratio (collected over time as a sample space) which might lead to higher success rate [10]. It is related to discrete probability $P(v)$ by:

$$D(v) = P(V \leq v) = \sum_{V \leq v} P(v) \tag{2}$$

4 Case Study and Results

Figure 3 shows the comparative performance of the algorithmic techniques we developed to do adaptive scheduling for tasks, which were predicted in real time to miss their deadlines. Baseline success rate for tasks completion is highest and the deadline miss rate is lowest. This marks as upper and lower bounds performance of the system which our optimization algorithms try to achieve. Next step was to introduce static virtualization overhead into the system to understand how it shapes up the task deadline landscape and influences scheduling decisions. As seen from the following graph, the success rate for jobs completing their deadlines drops to 0.45 where as deadline miss rate increases to 0.55 when the static overhead is applied.

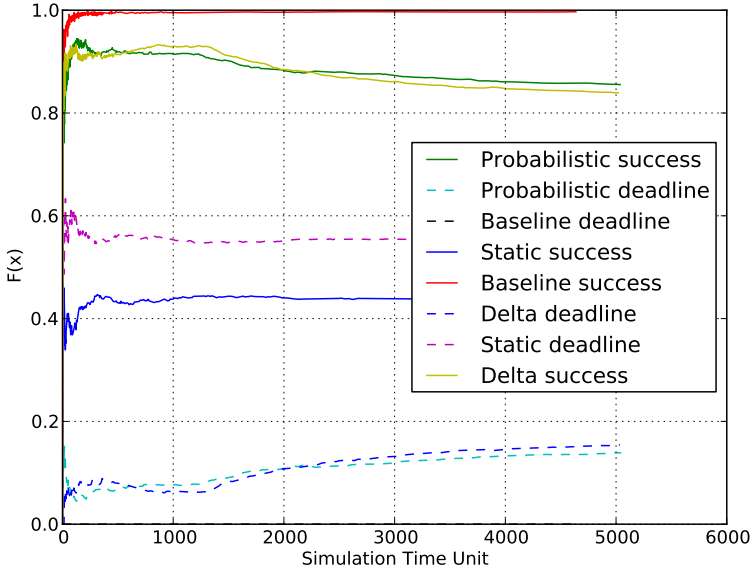


Fig. 3. Performance of probabilistic algorithm

This is very important and reflects that overhead problem could potentially be very serious in systems where tasks have not only uncertain runtimes but the deadlines are tight in respect to their overall execution.

Interestingly, both adaptive scheduling algorithms (Delta and Probabilistic) not only show promising results but also compete very closely in the problem domain described earlier; although the Delta algorithm uses an adaptive

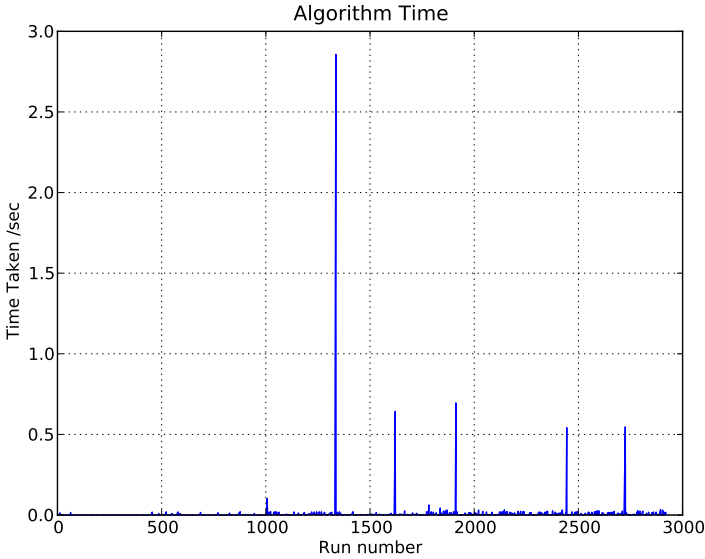


Fig. 4. Execution profile of probabilistic algorithm. Each vertical spike represents the real time taken by each execution of the optimization algorithm.

function from signal processing to set the optimal selection metrics whereas the Probabilistic algorithm selects D_{Thresh} using Cumulative Distribution Function (CDF).

These results present one aspect of the algorithmic performance but empirical results prove that both approaches have pros and cons. Statistical method appears to be slower in execution taking almost > 2.5 sec for the first time activation as it goes through the entire sample space as shown in figure 4. Later it requires lesser number of runs to arrive at optimal D_{Thresh} value since it gets the value by looking at the sample space which is changing less often as only part of the sample space is updated, thus improving algorithm execution time. This is useful where more steady transition to next threshold value is required. Whereas adaptive model performs, see figure 5, much faster and its execution time is always < 0.04 sec but it requires many more runs to get optimal D_{Thresh} value since it uses delta function to increment or decrement the target metric when measured metric exceeds the acceptance criteria. This is useful for systems where rapid response from the algorithms is required to respond to fast changing conditions in the system.

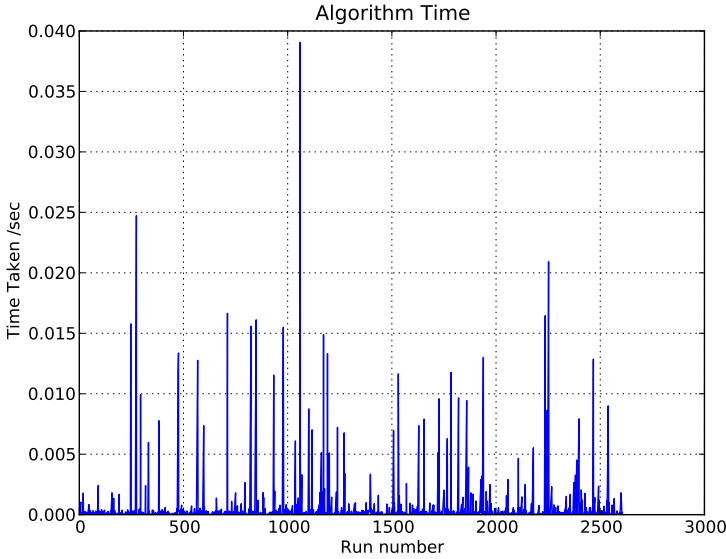


Fig. 5. Execution profile of signal processing algorithm. This represents the real time taken by the optimization algorithm.

5 Related Work

Currently in the area of grid and cloud computing, a large body of work exists focusing on service adaptability and integration of virtualization for service configuration and portability. Virtualization deployment engine such as OpenNebula [11], and Nimbus [2] have largely focused on automation of the complex problem of introducing virtualization in grid computing while keeping it transparent to the end-users. There have also been efforts to unify the underlying job execution infrastructure through virtualization, which spans both a dedicated grid and Amazon Elastic Computing service to deal with dynamically changing workloads [12]. Brandic et al [13] have focused on service adaptability in autonomic systems by developing a meta-negotiation framework that bridges the gap of service QoS between delivery models and grid middle ware, where as there also have been efforts to dynamically re-configure grid infrastructure as the requirements change dynamically [14]. The above-mentioned research is very relevant to the problem we attempted to address but its emphasis has been on adaptability and resource provisioning of services at system wide level.

Another challenge posed by virtualization in the grid computing has been how to enforce network access control through virtual machines executing grid jobs. To deal with this aspect of the problem, Matthews et al [15] has developed mechanisms, which they call Virtual Machine Contracts to automate the communication and management of out-of-band, loosely coupled, and non-portable processes.

Large-scale grids and clouds also have high-energy costs associated with them due to high electricity consumption, and this increases with lower resource utilization when tasks are prematurely terminated (i.e. resources are wasted and jobs are resubmitted). There have been considerable efforts directed in this arena to dynamically adapt and consolidate workloads on few physical resources when the supply of tasks reduces at off-peak usage [16] and [17]. This approach works at the opposite end of the spectrum to our proposed model of adaptive scheduling since we tried to increase resource utilization by increasing job success rate while keeping the physical resources powered on. This is a very interesting arena of research but is beyond the scope of our present study.

6 Conclusion

This paper presents our work towards optimizing VM-level scheduling in large-scale virtualized grid systems.

We have described a strategy for the introduction of self-management into the VM-level scheduling of large-scale virtualized grids. Our goal is to achieve an optimal balance between task placement flexibility and processing performance in terms of task throughput. In turn this requires that we dynamically optimize the task success rate, by automatically adjusting the task deadlines. To achieve this we developed a job execution simulator and implemented various scheduling techniques including statistical methods for prediction purposes.

Our work represents a valuable contribution to grid computing communities, and in particular where these two areas meet, such as in scheduling for data centers. The challenges of the CERN system on which we based our work are representative of many large grid installations and our technique is thus expected to be transferable to other systems where uncertainty exists in estimations of tasks run-time, tasks deadlines are changing in real time and thus scheduling decisions have to be adapted dynamically.

7 Further Work

The scheduling technique will be reformulated to operate at the level of clusters of physical nodes (it currently operates at the level of VM-scheduling on a single node). This will introduce the possibility of migrating tasks to nodes with greater levels of available resource, once it has been detected that they are likely to miss their deadlines at their current execution site. This in turn is expected to further improve the task-completion success rate and thus improve the overall efficiency and throughput at grid level.

We also plan to extend the investigation to different HPC grid applications with different compositions of sub-tasks and with different resource requirements characteristics. The purpose of this is to ensure that our technique does not have any application-specific sensitivity.

References

1. George R.: Desktop Virtualization. Information Week Magazine (August 2009)
2. Keahey, K., Freeman, T.: Contextualization: Providing One-Click Virtual Clusters. In: eScience 2008, Indianapolis, IN (December 2008)
3. Khalid, O., Anthony, R., Nilsson, P., Keahey, K., Schulz, M., Parrot, K., Petridis, M.: Enabling and Optimizing Pilot Jobs using Xen Virtual Machines for HPC Grid Applications. In: International Workshop on Virtualization Technologies and Distributed Computing, ICAC 2009 (2009)
4. Foster, I., Kesselman, C., Tuecke, S.: The anatomy of the grid: Enabling scalable virtual organizations (1999)
5. Foster, I., Kesselman, C.: The Grid: Blueprint for a New Computing Infrastructure. Morgan Kaufmann, San Francisco (1999)
6. Aad, G., et al.: ATLAS Collaboration.: The ATLAS Experiment at the CERN Large Hadron Collider, 437pp; JINST 3, S08003 (2008)
7. ATLAS computing: Technical Design Report. Technical Design Report ATLAS. CERN, Geneva (2005), <http://cdsweb.cern.ch/record/837738>
8. Tadashi, M.: ATLAS Collaboration.: PanDA: Distributed production and distributed analysis system for ATLAS, 4pp; J. Phys. Conf. Ser. 119, 062036 (2008)
9. Meyr, H., Moeneclaey, M., Fechtel, S.A.: Digital Communication Receivers: Synchronization, Channel Estimation, and Signal Processing. John Wiley and Sons, New York (1998)
10. Evans, M., Hastings, N., Peacock, B.: Statistical Distributions, 3rd edn. Wiley-Interscience, New York (2000)
11. Fontn, J., Vzquez, T., Gonzalez, L., Montero, R.S., Llorente, I.M.: OpenNEBula: The Open Source Virtual Machine Manager for Cluster Computing. In: Open Source Grid and Cluster Software Conference, San Francisco (2008)
12. Rafael, M.V., Ruben, S.M., Ignacio, M.L.: Elastic Management of Cluster-based Services in the Cloud. In: First Workshop on Automated Control for Datacenters and Clouds (ACDC 2009), Barcelona, Spain (June 2009)
13. Brandic, I., Music, D., Dustda, S.: Service Mediation and Negotiation Bootstrapping as First Achievements Towards Self-adaptable Grid and Cloud Services. In: Workshop On Grids Meets Autonomic Computing (GMAC), Barcelona, Spain (2009)
14. Ardagna, D., Giunta, G., Ingraffia, N., Mirandola, R., Pernici, B.: QoS-Driven Web Services Selection in Autonomic Grid Environments. In: Meersman, R., Tari, Z. (eds.) OTM 2006. LNCS, vol. 4276, pp. 1273–1289. Springer, Heidelberg (2006)
15. Matthews, J., Garfinkel, T., Hoff, C., Wheeler, J.: Virtual Machine Contracts for Datacenter and Cloud Computing Environments. In: First Workshop on Automated Control for Datacenters and Clouds (ACDC 2009), Barcelona, Spain (June 2009)
16. Kusic, D., Kephart, J.O., Hanson, J.E., Kandasamy, N., Jiang, G.: Power and Performance Management of Virtualized Computing Environments Via Lookahead Control. In: ICAC, Chicago (2008)
17. Nocentino, A., Ruth, P.: Toward Dependency-Aware Live Virtual Machine Migration. In: International Workshop on Virtualization Technologies and Distributed Computing, ICAC (2009)

Angle Differential Modulation Scheme for Odd-Bit QAM

Syed Safwan Khalid and Shafayat Abrar

Department of Electrical Engineering,
COMSATS Institute of Information Technology, Islamabad
{safwan_khalid,sabrar}@comsats.edu.pk

Abstract. In this paper, a method for differential encoding of odd-bit quadrature amplitude modulation (QAM) is presented. Differential encoding would allow QAM to be transmitted over media where coherent detection is not possible owing to phase ambiguity; it would allow such a transmission without the expense of the overhead incurred in data aided transmission. An example 32-QAM constellation is proposed and the algorithms for differential encoding and decoding of the proposed constellation are presented. The analytical performance of the given scheme is also discussed and is verified using simulation results. Results of differentially encoded detection scheme are also compared with those of coherent detection.

Keywords: Odd-bit quadrature amplitude modulation (QAM), cross QAM, differential encoding, coherent detection, phase ambiguity, error performance.

1 Introduction

For high speed wireless communication, quadrature amplitude modulation (QAM) system, owing to its increased spectral efficiency, is an attractive alternative to phase shift keying (PSK) systems. Since a wireless channel can introduce excessive phase shifts in the received signal, a coherent detection of received QAM signals is difficult even if the receiver is equipped with a carrier recovery mechanism. The received signal would suffer from a phase ambiguity problem i.e. the whole constellation would get rotated by an unknown multiples of $\pi/2$ [1]. To overcome this problem, an additional overhead of pilot signal or a continuous insertion of synchronization sequences within the transmitted data is required. In multiple-antenna systems, this overhead for coherent detection becomes even larger. This has resulted in a renewed interest in recent years in non-coherent differentially encoded modulation schemes [2]. The literature regarding differential coding for QAM constellations is few in number mostly discussing star 8-QAM or 16-QAM constellations [2,3,4]. In [2,5], methods are proposed to differentially encode square QAM constellations; however, these methods are not applicable directly to odd-bit cross QAM constellations. In [6], a general differential scheme based on higher-order statistics is discussed but it imposes a significant performance loss and complexity. More recently in [7], a differential encoding scheme

for 16-QAM and 32-QAM is proposed using look-up tables instead of rule-based encoding. However, the feasibility and scalability of using look tables for higher order QAM or memory limited systems requires more investigation.

In this paper, we propose a modification to the differential encoding scheme discussed in [2] to incorporating QAM constellations with odd number of bits per symbol. We propose a modified constellation diagram for 32-QAM and discuss the method for differentially encoding and decoding the proposed constellation. Moreover, the analytical performance analysis and computer simulation results are presented for bit error rates (BER) of the proposed scheme under AWGN channel. The performance of the same constellation diagram for coherent detection is also presented and the results are compared with the performance of the classical coherently detected cross 32-QAM constellation.

The rest of the paper is organized as follows: in section 2, the proposed 32-QAM constellation is discussed along with its differential encoding and decoding. In section 3, the probability of bit error is analytically obtained. In section 4, the simulation results are presented along with the analytical curves and conclusions are drawn.

2 Differential QAM Encoding and Decoding Algorithm

2.1 Encoding

To differentially encode 32-QAM constellation, we have divided the constellation into a set of eight circles with two overlapping circles in each quadrant as shown in Fig. 1(a). The minimum distance between constellation points is $2b$, where b is a positive number. A group of five bits is mapped onto the 32 possible transitions such that the first two bits determine the change in the quadrant, the third bit decides which of the possible two circles to choose in each quadrant and the last two bits determine the position of the one of the four complex symbols on the given circle. Let $S(i)$ be the transmitted symbol and $S(i-1)$ be the previously transmitted symbol. Let $S(i)$ be defined as

$$S(i) = C(i) + D(i) + E(i) \quad (1)$$

where $C(i)$ is a position vector from the origin to the quadrant center. $E(i)$ is a position vector from $C(i)$ to the center of a circle. $D(i)$ is a position vector from the center of circle to the transmitted symbol on the constellation diagram.

$$C(i) = R_1 e^{j\theta_1}, R_1 = 3b + \sqrt{2}b \quad (2)$$

$$D(i) = R_2 e^{j\theta_2}, R_2 = 2b \quad (3)$$

$$E(i) = R_3 e^{j\theta_3}, R_3 = b \quad (4)$$

where θ_1 , θ_2 and θ_3 belong to the set $\{\pi/4, 3\pi/4, 5\pi/4, 7\pi/4\}$. The differential encoding rule can be described as three updating formulas

$$C(i) = C(i-1)e^{j\Delta\theta_1} \quad (5)$$

$$D(i) = D(i-1)e^{j\Delta\theta_2} \quad (6)$$

$$E(i) = E(i-1)e^{j\Delta\theta_3} \quad (7)$$

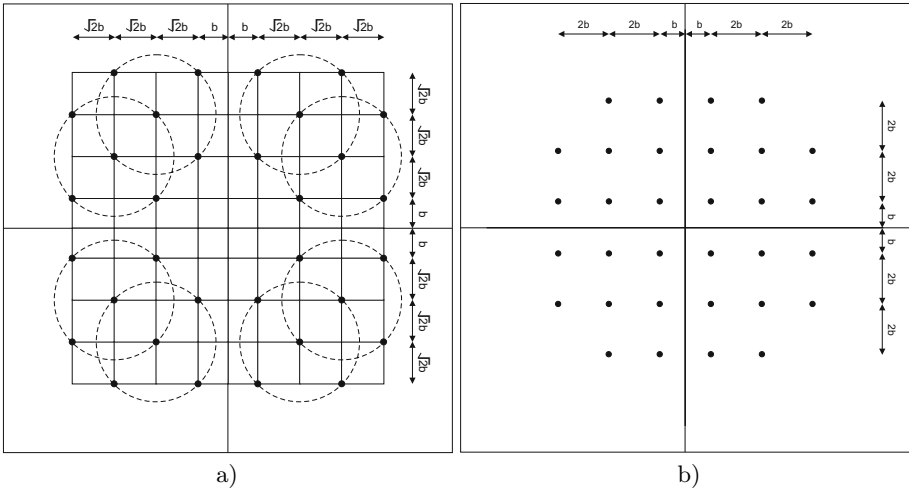


Fig. 1. Constellations of 32-QAM: a) proposed and b) traditional

where the values of $\Delta\theta_1$ and $\Delta\theta_2$ are determined using Table 1. The value of $\Delta\theta_3$ is calculated as $\Delta\theta_3 = \Delta\hat{\theta}_3 - \Delta\theta_1$, where $\Delta\hat{\theta}_3$ is calculated using Table 2.

Table 1. Dibit to angle mapping for $\Delta\theta_1$ and $\Delta\theta_2$

00	0
01	$\pi/2$
11	π
10	$3\pi/2$

Table 2. Single bit to angle mapping for $\Delta\hat{\theta}_3$

0	0
1	π

Example: Without loss of generality, suppose that the value of b is set equal to 1 and the previous transmitted symbol $S(i - 1)$ be $3.8284 + 5.2426j$ as follows:

$$S(i - 1) = C(i - 1) + D(i - 1) + E(i - 1) \tag{8}$$

where $C(i - 1) = R_1 e^{j\pi/4}$, $D(i - 1) = R_2 e^{j\pi/4}$ and $E(i - 1) = R_3 e^{j3\pi/4}$. Let a segment of data bits 01011 is to be transmitted in the next symbol $S(i)$. Using the encoding tables, we get the values of angles as $\Delta\theta_1 = \pi/2$, $\Delta\theta_2 = \pi$ and $\Delta\hat{\theta}_3 = 0$; hence $\Delta\theta_3 = 0 - \Delta\theta_1 = -\pi/2$. Using the updating formulas as described above we get $C(i) = -3.1213 + 3.1213j$, $D(i) = -1.4142 - 1.4142j$ and $E(i) = 0.7071 + 0.7071j$. Adding all three components the value of $S(i)$ is calculated to be $-3.8284 + 2.4142j$, refer to Fig. 2.

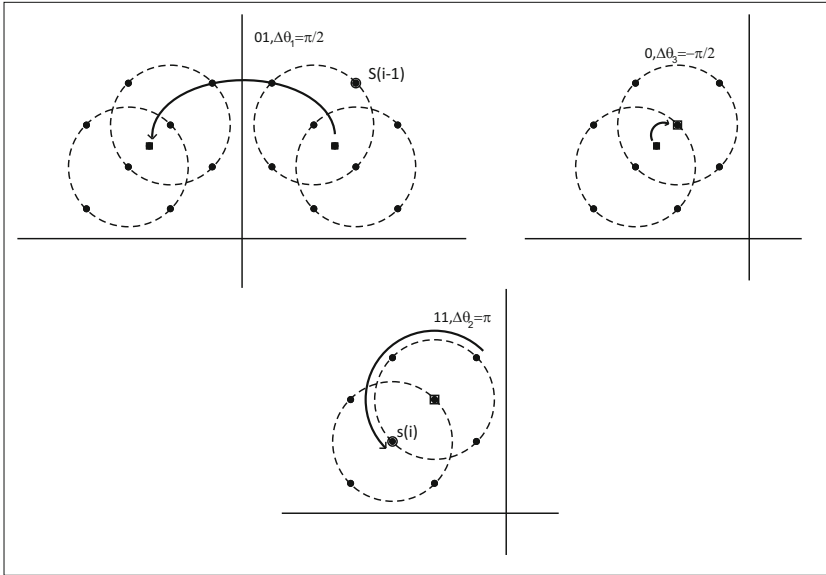


Fig. 2. Illustration of the encoding algorithm

2.2 Decoding

The received signal $X(i)$ is given as $X(i) = S(i)e^{j\phi} + N(i)$, where $S(i)$ is the transmitted signal, $N(i)$ is the additive white Gaussian noise component and ϕ is the phase ambiguity which could take any value from a set of multiples of $\pi/2$. The first step in decoding is to compare the received signal $X(i)$ from each signal point in the constellation diagram and choose the signal with minimum Euclidian distance as the decoded signal $\hat{S}(i)$. Now to determine $\hat{C}(i)$ from $\hat{S}(i)$ we use the equation

$$\hat{C}(i) = R_1 [\text{sgn}(\Re(\hat{S}(i))) + j \text{sgn}(\Im(\hat{S}(i)))] \tag{9}$$

where $\text{sgn}(\cdot)$ is the signum function, $\Re(z)$ and $\Im(z)$ are used to denote real and imaginary components of z , respectively. To decode $\Delta\theta_1$ and hence the first two bits $\hat{C}(i)$ is correlated with $\hat{C}(i-1)$ i.e. multiplied by the complex conjugate of $\hat{C}(i-1)$. As long as both $\hat{C}(i)$ and $\hat{C}(i-1)$ experience the same phase ambiguity ϕ , the signal shall be decoded correctly. The value of $\Delta\theta_1$ is detected as

$$\text{if } \hat{C}(i)\hat{C}(i-1)^* = \begin{cases} R_1^2 & \text{then } \Delta\theta_1 = 0 \\ jR_1^2 & \text{then } \Delta\theta_1 = \pi/2 \\ -R_1^2 & \text{then } \Delta\theta_1 = \pi \\ -jR_1^2 & \text{then } \Delta\theta_1 = 3\pi/2 \end{cases} \tag{10}$$

Now to determine $\hat{D}(i)$ we use the equation

$$\hat{D}(i) = R_2 [\text{sgn}(\Re(\hat{S}(i) - \hat{C}(i))) + j \text{sgn}(\Im(\hat{S}(i) - \hat{C}(i)))] \tag{11}$$

Similar to $\Delta\theta_1$, $\Delta\theta_2$ is calculated from the value of $\widehat{D}(i)$ and $\widehat{D}(i - 1)$ using

$$\text{if } \widehat{D}(i)\widehat{D}(i - 1)^* = \begin{cases} R_2^2 & \text{then } \Delta\theta_2 = 0 \\ jR_2^2 & \text{then } \Delta\theta_2 = \pi/2 \\ -R_2^2 & \text{then } \Delta\theta_2 = \pi \\ -jR_2^2 & \text{then } \Delta\theta_2 = 3\pi/2 \end{cases} \quad (12)$$

Similarly

$$\widehat{E}(i) = R_3[\text{sgn}(\Re(\widehat{S}(i) - \widehat{C}(i) - \widehat{D}(i))) + j \text{sgn}(\Im(\widehat{S}(i) - \widehat{C}(i) - \widehat{D}(i)))] \quad (13)$$

Now $\widehat{E}(i)$ is further rotated by an angle $\Delta\theta_1$ to compensate for the angle subtracted during the encoding phase hence $\widehat{E}(i) \leftarrow \widehat{E}(i)e^{j\Delta\theta_1}$. Finally for $\Delta\theta_3$

$$\text{if } \widehat{E}(i)\widehat{E}(i - 1)^* = \begin{cases} R_3^2 & \text{then } \Delta\theta_3 = 0 \\ -R_3^2 & \text{then } \Delta\theta_3 = \pi \end{cases} \quad (14)$$

As long as the phase ambiguity ϕ is same in the previous and the current detected symbol it will not create any errors in decoding since the decoding is based on the relative change of the angle of the previous and the current detected symbol and not based on their absolute phases. Fig. 3 depicts the architecture of decoding mechanism.

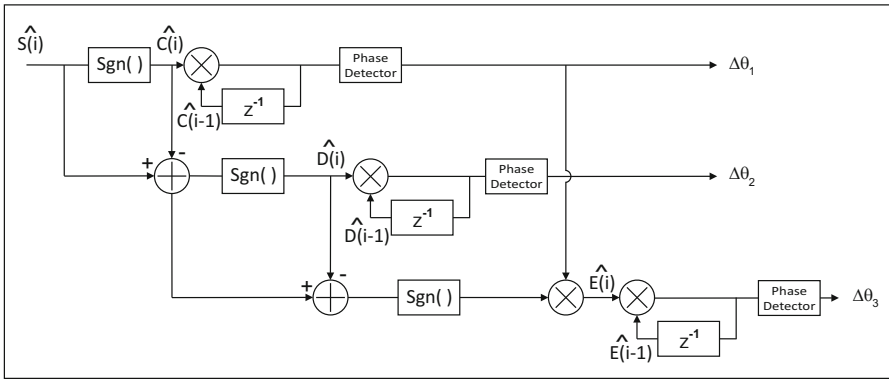


Fig. 3. Three stage decoding scheme for 32-QAM

3 Error Performance Analysis

To determine the probability of bit error for the proposed constellation and encoding scheme we utilize the approach as given in [8] and approximate the probability of bit error as

$$P_b \approx \frac{1}{b_n} \sum_{i=0}^{M-1} \sum_{j=1}^{N_i} P_x(i) P\{\varepsilon_{ij}\} n_b \quad (15)$$

where M is the possible number of signal points transmitted, N_i is the number of nearest neighbors i.e. no. of symbols at d_{\min} from the i th symbol in the constellation diagram. $P_{x(i)}$ is the probability of transmission of symbol. $P\{\varepsilon_{ij}\}$ is the probability of symbol error when symbol ' i ' is erroneously detected as symbol ' j '. n_b is the number of bit errors when symbol ' i ' is erroneously detected as symbol ' j ' and b_n is the number of bits per symbol.

$$\begin{aligned}
 P\{\varepsilon_{ij}\}_{\text{diff}} &= P(S(i) \text{ is incorrect and } S(i-1) \text{ is correct}) + P(S(i) \text{ is correct and } \\
 &\quad S(i-1) \text{ is incorrect}) + P(S(i) \text{ is incorrect and } S(i-1) \text{ is incorrect}) \\
 &= P\{\varepsilon_{ij}\}(1 - P\{\varepsilon_{ij}\}) + (1 - P\{\varepsilon_{ij}\})P\{\varepsilon_{ij}\} + P\{\varepsilon_{ij}\}P\{\varepsilon_{ij}\} \\
 &= 2P\{\varepsilon_{ij}\}(1 - P\{\varepsilon_{ij}\}) + P\{\varepsilon_{ij}\}^2 \\
 &= 2P\{\varepsilon_{ij}\} - P\{\varepsilon_{ij}\}^2
 \end{aligned} \tag{16}$$

Assuming $P\{\varepsilon_{ij}\}$ is small, the higher order term can be neglected from the above expression and we obtain

$$P\{\varepsilon_{ij}\}_{\text{diff}} \approx 2P\{\varepsilon_{ij}\} \tag{17}$$

Hence for differential encoding the probability of bit error is approximated as

$$P_{b,\text{diff}} \approx \frac{2}{b_n} \sum_{i=0}^{M-1} \sum_{j=1}^{N_i} P_x(i) P\{\varepsilon_{ij}\} n_b(i, j) \tag{18}$$

Using the union bound and replacing $P\{\varepsilon_{ij}\}$ with $Q(d_{\min}/(2\alpha))$, we get

$$P_{b,\text{diff}} \approx \frac{2}{b_n} Q\left(\frac{d_{\min}}{2\alpha}\right) \sum_{i=0}^{M-1} \sum_{j=1}^{N_i} P_x(i) n_b(i, j) \tag{19}$$

Let $n_b(i) \triangleq \sum_{j=1}^{N_i} n_b(i, j)$ and $N_b \triangleq \sum_{i=1}^{M-1} P_x(i) n_b(i)$ then (19) can be written as

$$P_{b,\text{diff}} \approx \frac{2N_b}{b_n} Q\left(\frac{d_{\min}}{2\alpha}\right) \tag{20}$$

The value of N_b depends upon the particular bit mapping onto the constellation symbols. For differential encoding, the bit mapping is redefined after each symbol transmission; however, the value of N_b remains unchanged and hence N_b can be calculated without loss of generality using any symbol. Let the previous transmitted symbol $S(i-1)$ be the same as in example of Section 2 i.e. $3.8284 + 5.2426j$. For this particular choice the bit mapping is shown in Fig. 4.

From Fig. 4, the value of N_b may be calculated. For each symbol in the constellation, we compute the number of bit errors that would result if a transmitted symbol is erroneously detected as one of its nearest neighbor, i.e., the symbols lying at d_{\min} from the transmitted symbol. The average of the total bit errors gives the value of N_b , as given by

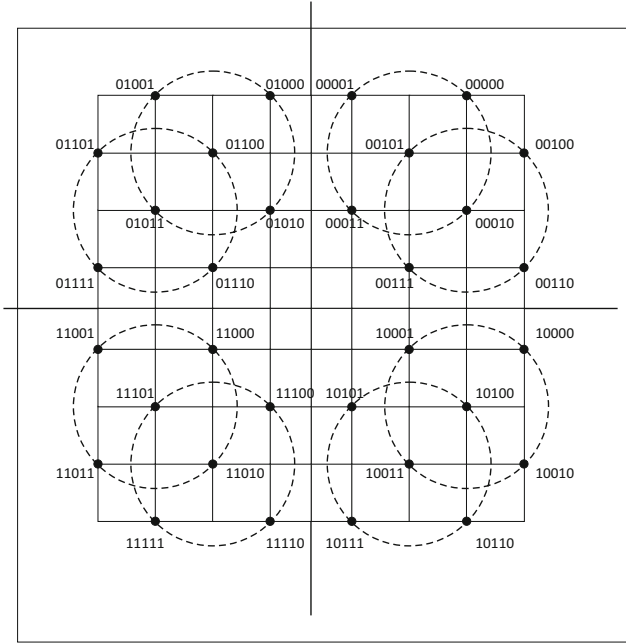


Fig. 4. Bit mapping for the example given in Section 2

$$\begin{aligned}
 N_b &= \frac{4}{32} [(3 + 1 + 1) + (3 + 1) + (2 + 2 + 1) + (1 + 1 + 2 + 3) + \\
 &\quad (2 + 3 + 2 + 1) + (2 + 1) + (1 + 2) + (2 + 1)] \\
 &= 4.75
 \end{aligned}
 \tag{21}$$

The expression for the probability of bit error becomes

$$P_{b,diff} \approx 1.9Q \left(\frac{d_{min}}{2\alpha} \right)
 \tag{22}$$

Now to figure out the probability of bit error in terms of E_b/N_o , we first note that d_{min} is equal to $2b$ and $\alpha = \sqrt{N_0/2}$.

$$P_{b,diff} \approx 1.9Q \left(\frac{2b}{2\alpha} \right) = 1.9Q \left(\frac{b}{\sqrt{N_0/2}} \right)
 \tag{23}$$

Now to determine the relation between b and E_b , we note that the symbol energy is given by $E_{sym} = E[|s_i|^2]$, where $s_i = i^{th}$ vector on constellation diagram

$$E_{sym} = \frac{4}{32} [4b^2 + 4(b + \sqrt{2}b)^2 + 4(b + 2\sqrt{2}b)^2 + 4(b + 3\sqrt{2}b)^2]
 \tag{24}$$

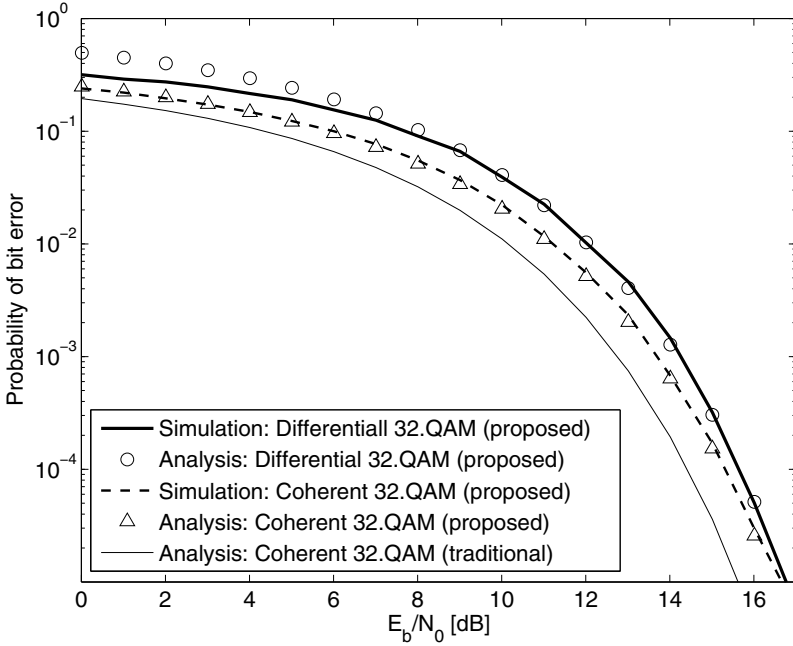


Fig. 5. Analytical and simulated BER curves under AWGN for the proposed differential encoding scheme and its comparison with coherent ones

$$\Rightarrow b = \sqrt{\frac{E_{\text{sym}}}{2(8 + 3\sqrt{2})}} = \sqrt{\frac{5E_b}{2(8 + 3\sqrt{2})}} \quad (25)$$

So the final expression for probability of bit error for differential encoding becomes

$$P_{b,\text{diff}} \approx 1.9Q\left(\sqrt{\frac{E_b}{N_0} \frac{10}{2(8 + 3\sqrt{2})}}\right) \quad (26)$$

To compare our scheme with the traditional cross-shaped 32-QAM coherent modulation scheme, we use the expression for its approximate probability of bit error as given in [9]:

$$P_{b,\text{cross}} \approx \frac{4}{5}Q\left(\sqrt{\frac{15E_b}{31N_o}}\right) \quad (27)$$

4 Results and Conclusion

To verify the performance of the proposed scheme, the simulated as well as the analytical probability of errors are presented in Fig. 5, where, in legend, “proposed” and “traditional” respectively refer to the constellations as depicted

in Fig. 1(a) and 1(b). It can be observed that the simulation results match with the analytical performance very well specifically for higher SNR. The probability of error for coherent demodulation of 32-QAM for the proposed constellation with the bit mapping same as that shown in Fig. 3 is also plotted. The analytical probability of error for the coherent 32-QAM of the proposed scheme can be approximated as half the probability of error of the differential encoding scheme i.e. $P_{b,\text{coherent}} \approx 0.5P_{b,\text{diff}}$. At higher SNR the difference between coherent and non-coherent detection becomes very small. Finally the performance of a classical 32 cross QAM coherent modulation is also plotted for comparison with our scheme. We observe that our scheme does incur a penalty of slightly greater than 1dB when compared with 32 cross QAM coherent detection however our scheme proposes a method for differential encoding that is simple and scalable to higher order odd bit QAM to enable their transmission in such media where coherent detection owing to phase ambiguity is not possible.

References

1. Warrior, D., Madhow, U.: Spectrally efficient non-coherent communication. *IEEE Trans. Information Theory* 48(3) (2002)
2. Hwang, J.K., Chiu, Y.L., Liao, C.S.: Angle differential-QAM scheme for resolving phase ambiguity in continuous transmission system. *Intl. Journal of Communication Systems* 21, 631–641 (2008)
3. Ma, Y., Zhang, Q.T., Schober, R., Pasupathy, S.: Diversity reception of DAPSK over generalized fading channels. *IEEE Trans. Wireless Communications* 4(4), 1834–1846 (2005)
4. Dong, X., Tjhung, T.T., Adachi, F.: Error probability analysis for 16 star-QAM infrequency-selective Rician fading with diversity reception. *IEEE Trans. Vehicle Technology* 47, 924–935 (1998)
5. Weber, W.J.: Differential encoding for multiple amplitude and phase shift keying systems. *IEEE Trans. Communications* 26, 385–391 (1978)
6. Gini, F., Giannakis, G.B.: Generalized differential encoding: a nonlinear signal processing perspective. *IEEE Trans. Signal Processing* 46, 2967–2974 (1998)
7. Wei, R.Y.: Differential encoding by a look-up table for quadrature amplitude modulation. *IEEE Trans. Commun.* 59(1) (2011)
8. Cioffi, J.: Signal processing: Digital communication course reader, p. 39. Stanford University (2007)
9. Xiong, F.: Digital modulation techniques, 2nd edn. Artech House (2006)

Adaptive Wavelets Based Fuzzy NN Control for Active Suspension Model

Laiq Khan, Shahid Qamar*, and Muhammad Umair Khan

COMSATS Institute of Information Technology,
Abbottabad Campus, Pakistan
{laiq,shahidqamar,umairkhan}@ciit.net.pk

Abstract. The objective of this paper is to examine the performance of full car active suspension system by using adaptive wavelet fuzzy-neural network (WFNN) control strategy. The conventional passive suspension system does not provide the passenger comfort and vehicle handling against the road disturbances. In order to improve the passenger's comfort and vehicle's handling an adaptive WFNN is used for full car suspension. WFNN consists of fuzzy linguistic rules. WFNN has more accurate and generalized approximations for non-linear functions. The performance of WFNN is examined as compared to semi-active and passive suspension systems. Simulation is based on the full car mathematical model by using MATLAB/SIMULINK.

Keywords: Morlet Wavelet, Fuzzy logic, Neural Network, Suspension.

1 Introduction

Suspension system is a common component of all the vehicles. Suspension system isolates the vehicle body from the road disturbances to improve ride comfort and good road handling. Ride comfort and road handling performance of a vehicle are generally analyzed by the damping feature of the shock absorbers. Conventional passive suspension system comprises of springs and shock absorbers [3]. Whereas, the semi-active suspension system changes the damping coefficient by the electromagnetic regulator inside the absorber. The important feature of the active suspension system is that peripheral power source is applied to attain the desired suspension objective. The actuator in active suspension system is placed as a secondary suspension system for the vehicle. The controller drives the actuator, which depends on the proposed control law. Initially many researchers assumed that the vehicle models are linear, but these models have some non-linearities, like dry friction on the dampers. These non-linearities can affect the vehicle stability and ride comfort.

As linear controller can provide the ride comfort and better handling performances. Their use is only successful, when the system's states stay close to the region of operating point. Thus, for the better performance of the nonlinear models, nonlinear controllers should be used to give better ride comfort and

* Corresponding author.

handling qualities. [1] presented explicit self tuning adaptive control for active suspension systems. However, this method does not give any information about the robustness issues and ignores the deviation in the shock absorber and the spring. [2] presented a sliding mode controller for active suspension systems. But this sliding mode controller is applied to the model without any reference model. Furthermore, this does not address the problem of robustness and model's uncertainties.

Some optimal control techniques have been proposed for the full car suspension system [4,5]. Also, control approaches have been examined to minimize the vertical motion, roll and the chassis motion of vehicle by [6]. But did not provide any interpretation about the robustness of the system parameter variations. The PID controller is applied on active suspension system by [8].

Fuzzy logic control is perfect for this sort of condition for control of suspension system. Because, fuzzy logic control is a set of linguistic rules, which signifies human thoughts and arranges the estimation to resolve control approaches for the whole process. A variety of simulations showed that the fuzzy logic and observer-based fuzzy sliding-mode control is proficient to give a better ride quality than other common control approaches [7,20]. In [19] the authors used a fuzzy type-2 neural network to increase the ride comfort of the vehicle.

Self-organizing fuzzy controllers have been proposed by [9] to resolve the concern of a fuzzy logic control application. According to the above mentioned studies, [10] proposed a DSP-based self-organizing fuzzy controller for an active suspension system, to reduce the displacement and acceleration in the sprung mass. Also, [11] proposed a fuzzy controller to control the active suspension system.

Since, the aforementioned control techniques applied on active car models did not give enough information about the robustness, sensitivity and rattle space limits. Here, fuzzy wavelet neural network is proposed for the active suspension control. For this, fuzzy logic combines wavelets theory with artificial neural networks and fuzzy logic system. Wavelet transform has the capability to examine nonstationary signals to determine their local details. Fuzzy logic system decreases the complexity and deals with vagueness of the data, where, neural networks have self-learning qualities that raise the precision of the model.

In this study, WFNN control technique is used to enhance the ride comfort and vehicle stability against the road disturbances. The passenger seat is also incorporated in the vehicle model to improve the passenger's comfortability. The paper is divided into 6 sections. Section 2, discusses the full vehicle's model. Section 3 gives the description of the control problem. Section 4, discusses WFNN for full car suspension control. Finally, simulation results and conclusion are given in section 5 and 6.

2 Vehicle's Model

The full-car suspension model is known to be a nonlinear system, which has eight-degrees of freedom. It comprises of only one sprung mass attached to the

four unsprung masses $M_{f,r}, M_{f,l}, M_{r,r}, M_{r,l}$ (front-right, front-left, rear-right and rear-left wheels) at each corner. This model consists of only one seat while, considering other fixed with chassis [13].

The eight degrees of freedom ($x_1, x_2, x_3, x_4, x_5, x_6, x_7 = \theta, x_8 = \phi$) are the four wheels displacement, seat displacement, heave displacement, pitch displacement and roll displacement of the vehicle's suspension system. The model of a full car suspension system is shown in figure 1. The suspension between the

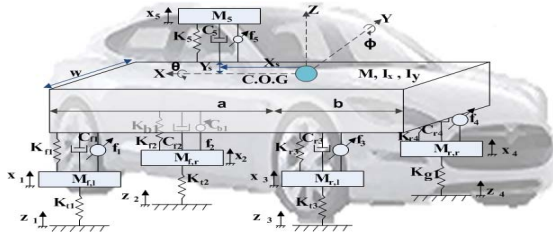


Fig. 1. Full Car Model

sprung mass and unsprung masses is modeled as nonlinear viscous dampers and spring components. The tyres are modeled as simple non-linear springs without damping elements. The actuators provide forces, which are determined by the displacement between the sprung mass and the wheels. The inputs of full car model are four disturbances coming through the tyres and the four outputs are the heave, pitch, seat, and roll displacement [12].

2.1 Mathematical Modeling

The general class of nonlinear MIMO system is described by:

$$y^{(r)} = A(x) + \sum_{i=1}^p \sum_{j=1}^s B_{ij}(x)u_j + \sum_{i=1}^p \sum_{j=1}^s G_{ij}(x)z_j \tag{1}$$

Where

$$x = [y_1, \dot{y}_1, \dots, y_1^{(r_1-1)}, \dots, y_p, \dot{y}_p, \dots, y_p^{(r_p-1)}]^T \in R^r$$

is the overall state vector, which is assumed available and $r_1 + r_2 + \dots + r_p = r$.

$u = [u_1, u_2, \dots, u_s]^T \in R^s$ is the control input vector, $y = [y_1, \dots, y_p]^T \in R^p$ is the output vector and $z = [z_1, \dots, z_s]^T \in R^s$ is the disturbance vector. $A_i(x)$, $i = 1, \dots, p$ are continuous nonlinear functions, $B_{ij}(x)$, $i = 1, \dots, p; j = 1, \dots, s$ are continuous nonlinear control functions and $G_{ij}(x)$, $i = 1, \dots, p; j = 1, \dots, s$ are continuous nonlinear disturbance functions.

Let

$$A = [A_1(x) A_2(x) \dots A_p(x)]^T \tag{2}$$

The control matrix is:

$$B(x) = \begin{bmatrix} b_{11}(x) & \dots & b_{1s}(x) \\ \vdots & \ddots & \vdots \\ b_{p1}(x) & \dots & b_{ps}(x) \end{bmatrix}_{p \times s} \quad (3)$$

The disturbance matrix is:

$$G(x) = \begin{bmatrix} g_{11}(x) & \dots & g_{1s}(x) \\ \vdots & \ddots & \vdots \\ g_{p1}(x) & \dots & g_{ps}(x) \end{bmatrix}_{p \times s} \quad (4)$$

$$y^{(r)} = [y_1^{(r_1)}, y_2^{(r_2)}, \dots, y_p^{(r_p)}]^T$$

$$y^{(r)} = A(x) + B(x).u + G(x).z \quad (5)$$

$$A(\cdot) \in R^{p \times p}; \quad B(\cdot) \in R^{p \times s}; \quad G(\cdot) \in R^{p \times s}$$

The generic non-linear car model is,

$$\dot{y} = f(x) + B(x).u + G(x).z \quad (6)$$

$$y = h(x) \quad (7)$$

$f(x) \in R^{(16 \times 16)}$, $B(x) \in R^{(16 \times 4)}$, $G(x) \in R^{(16 \times 4)}$, state vector $x \in R^{(16 \times 1)}$, $u \in R^{(4 \times 1)}$ and $z \in R^{(4 \times 1)}$.

The above matrices can be shown in state-space form, with state vector x that is also represented in row matrix form.

$$f(x) = [A_1(x) \quad A_2(x) \quad A_3(x) \quad \dots \quad A_{16}(x)]$$

$$x = [x_1 \quad x_2 \quad x_3 \quad \dots \quad x_{16}]^T$$

$A_1(x)$ to $A_8(x)$ are velocity states and $A_9(x)$ to $A_{16}(x)$ are acceleration states of four tires, seat, heave, pitch and roll [13].

The disturbance inputs for each tire individually are represented in the form of z matrix.

$$z = [z_1 \quad z_2 \quad z_3 \quad z_4]^T$$

z_n are n disturbances applied to full car model. u_n are n controllers output to full car model, to regulate the car model disturbances. y_n are n states of car. r_n are n desired outputs for the controller to achieve.

3 Control Problem

The aim of this control strategy is to improve the ride comfort and vehicle stability against the road disturbances. The comfort is examined by the vertical displacement felt by the passenger. The controller goal is to minimize the displacement of the vehicle body with reference to the open-loop, to avoid the suspension travel should not hit the rattle space limits. So, the controller performance is good when it reduces the vehicle vibrations under road disturbances. In this study, a road profile containing pothole and bump has the form, i.e.,

$$z(t) = \begin{cases} -0.15 & 1 \leq t \leq 2 \text{ and } 9 \leq t \leq 10 \\ -0.10 & 4 \leq t \leq 5 \text{ and } 12 \leq t \leq 13 \\ 0 & \text{otherwise} \end{cases}$$

Here -0.15 m and -0.10 m are the amplitudes of two different potholes on the road. Where, -0.15 m pothole is for the front left and rear right tyre, where the -0.10 m pothole is for the front right and rear left tyre. This road profile is very helpful for the calculation of pitch and roll of the vehicle. This type of road profile shows the low frequency high amplitude response.

4 WFNN Structure and Construction

Wavelet transform is a local transformation instead of global transformation of the time and frequency, which can efficiently extract significant data from the signal. It constructs a multi-scale investigation to a signal or a function through dilation and translation. After dilation and translation the wavelet function $\Psi(t)$ can be formulated as

$$\Psi_j(x) = \Psi\left(\frac{x - b_j}{a_j}\right) \tag{8}$$

Where a is dilation factor and b translation factor. Now, the following Morlet wavelet function to act as wavelet radix function [14]:

$$\Psi_j(x) = \cos(5q_j) e^{-\frac{1}{2}(q_j^2)} \tag{9}$$

where

$$q_j = \frac{x - b_j}{a_j} \tag{10}$$

Where $\Psi_j(x)$ is the family of wavelets, $x = x_1, x_2, \dots, x_m$ shows the inputs values, $a_j = a_{1j}, a_{2j}, \dots, a_{mj}$ and $b_j = b_{1j}, b_{2j}, \dots, b_{mj}$ represents the dilation parameters and translation parameters of the mother wavelet $\Psi_j(x)$, respectively. The $\Psi_j(x)$ function is a waveform of limited duration and has a zero mean value.

The output for wavelet neural network is

$$y = \sum_{j=1}^k w_j \Psi_j(x) \tag{11}$$

Where $\Psi_j(x)$ is the wavelet function of the j th part of hidden layer, because, the wavelet networks contain the wavelet functions in the hidden layer's neurons of the network. w_j are the weights connected between the input layer and the hidden layer. Wavelet functions have the capability of time–frequency localization properties [15]. Localization of the i th hidden layer of WNN is found by the dilation parameters and translation parameters of a wavelet function [16].

The proposed WFNN connects TSK fuzzy logic system with wavelet functions. In the WFNN, the THEN part of the fuzzy rules are substituted with wavelet functions instead of constant or linear functions in order to enhance the computational strength of the neuro-fuzzy system. The wavelets can collect the information globally and locally easily by mean of the multiresolution property [17]. The proposed WFNN model has fast convergence and accuracy properties. The fuzzy wavelets rules have the following form:

$$\text{If } x_1 \text{ is } R_{n1} \text{ and } x_m \text{ is } R_{nm} \text{ Then } y_n = \sum_{i=1}^m w_{in} \cos(5q_{il})e^{-\frac{1}{2}q_{il}^2} \quad (12)$$

Where $x_1, x_2, \dots, x_m, y_1, y_2, \dots, y_m$ are the input-output variables and R_{ij} is the membership function of i th rule and j th input, which classified as Gaussian membership function. Wavelet functions are in the consequent part of the rules. Under these fuzzy rules, by using these wavelet functions with different dilation parameters and translation parameters, allows to capture necessary characteristics and behavior of nonlinear system. The structure for WFNN is shown in figure 2.

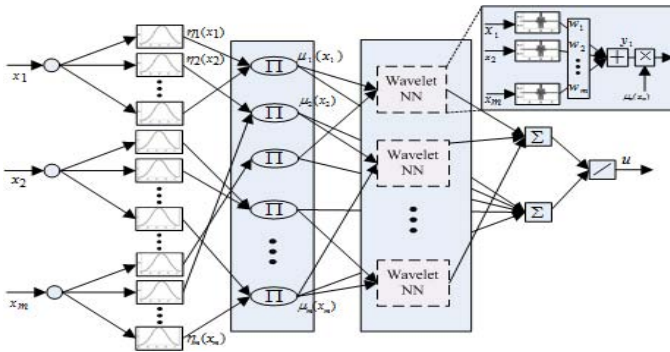


Fig. 2. Structure of WFNN

In the first layer, fuzzy reasoning is performed. In the second layer, every node communicates to individual linguistic term. For each input value, that passes through the system, the membership degree of the fuzzy set is calculated, by which the input value is belongs to. The Gaussian membership function is

$$\eta_j(x_i) = e^{-(x_i - g_{ij})^2 / \sigma_{ij}^2} \quad (13)$$

Where $\eta_j(x_j)$ shows the membership function, g_{ij} and σ_{ij} are the mean and variance of membership function of the j th term of i th input variable. In the third layer, each node shows one fuzzy rule. Here, min operation is used to estimate the output value of the layer. i.e.,

$$\mu_j(x) = \prod_i \eta_j(x_i) \tag{14}$$

where \prod_i is the meet operation and $\mu_j(x)$ are the input values for the next layer. The output value y for the l th wavelet is given by

$$y_l = w_l \sum_{i=1}^m \cos 5 \left(\frac{x_i - b_{il}}{a_{il}} \right) e^{-\frac{1}{2} \left(\frac{x_i - b_{il}}{a_{il}} \right)^2} \tag{15}$$

Therefore, the output for the WFNN can be expressed as:

$$u = \frac{\sum_{l=1}^n \mu_l(x) y_l}{\sum_{l=1}^n \mu_l(x)} \tag{16}$$

Where u is the output for the entire network. The training of the network starts after estimating the output value of the WFNN.

4.1 Parameters Update Rules for Learning

The gradient descent technique is used to speed up convergence and reduce the cost function. However, to speed up the convergence process a momentum is used. To minimize the error between the output value of the system and the desired value, then the gradient descent can expressed as:

$$J = \frac{1}{2} \sum_{i=0}^n (r_i - u_i)^2 \tag{17}$$

Where r_i and u_i are the desired and current output values of the system, n shows the number of the output values of the system, respectively. The update parameters w_l , a_{il} , b_{il} of the consequent part of network, and g_{il} and σ_{il} of the antecedent part of the network can be formulated as:

$$w_l(t + 1) = w_l(t) - \gamma \frac{\partial J}{\partial w_l} + \lambda(w_l(t) - w_l(t - 1)) \tag{18}$$

$$a_{il}(t + 1) = a_{il}(t) - \gamma \frac{\partial J}{\partial a_{il}} + \lambda(a_{il}(t) - a_{il}(t - 1)) \tag{19}$$

$$b_{il}(t + 1) = b_{il}(t) - \gamma \frac{\partial J}{\partial b_{il}} + \lambda(b_{il}(t) - b_{il}(t - 1)) \tag{20}$$

$$g_{ij}(t + 1) = g_{ij}(t) - \gamma \frac{\partial J}{\partial g_{ij}} \tag{21}$$

$$\sigma_{ij}(t + 1) = \sigma_{ij}(t) - \gamma \frac{\partial J}{\partial \sigma_{ij}} \tag{22}$$

Where γ and λ represents the learning rate and momentum, and m and n shows the input values and rules number of the network.

The change in the w_l , a_{il} , b_{il} , g_{ij} and σ_{ij} can be calculated as:

$$\frac{\partial J}{\partial w_l} = (u(t) - r(t))\mu_l(x).\psi(q_l) / \sum_{l=1}^n \mu_l(x) \tag{23}$$

$$\frac{\partial J}{\partial a_{il}} = \delta_l \left(\frac{\cos(5q_{il})e^{-\frac{1}{2}(q_{il}^2)}q_{il}^2 + 5q_{il} \sin(5q_{il})e^{-\frac{1}{2}(q_{il}^2)}}{a_{il}} \right) \tag{24}$$

$$\frac{\partial J}{\partial b_{il}} = \delta_l \left(\frac{\cos(5q_{il})e^{-\frac{1}{2}(q_{il}^2)}q_{il} + 5 \sin(5q_{il})e^{-\frac{1}{2}(q_{il}^2)}}{a_{il}} \right) \tag{25}$$

$$\frac{\partial J}{\partial g_{ij}} = \sum_j \left[\left((u(t) - r(t)) \frac{y_j - u}{\sum_j \mu_j} \mu_j(x_i) \frac{2(x_i - g_{ij})}{\sigma_{ij}^2} \right) \right] \tag{26}$$

$$\frac{\partial J}{\partial \sigma_{ij}} = \sum_j \left[(u(t) - r(t)). \frac{y_j - u}{\sum_j \mu_j(x)} .u_j(x_i) \frac{2(x_i - g_{ij})^2}{\sigma_{ij}^3} \right] \tag{27}$$

where

$$\delta_l = (u(t) - r(t))\mu_l(x).w_l / \sum_{l=1}^n \mu_l(x)$$

In learning process, there is a problem of convergence. Then the gradient descent method shows convergence on the basis of the learning rate and the momentum value [18]. The values of the learning rate and momentum is usually, in interval [0,1]. If the value of the learning rate is high, it make the system unstable and if its value is small, then the convergence process is slow and momentum speed up the learning process. The closed loop control structure for the WFNN is depicted in figure 3.

5 Simulation Results

In this section, the simulation results of seat (with and without controller), heave, pitch and roll displacement are given with respect to three different road profiles. These results are compared with passive suspension and semi-active suspension system.

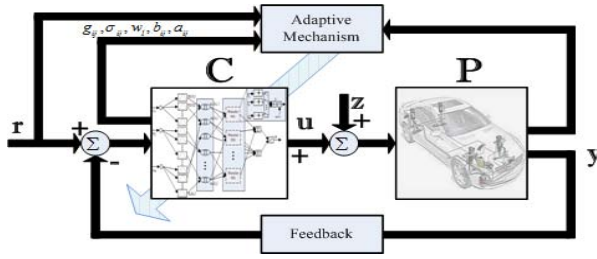


Fig. 3. WFNN based closed-loop control system

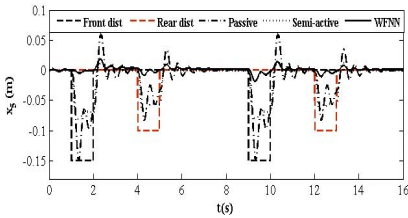


Fig. 4. Seat displacement without controller

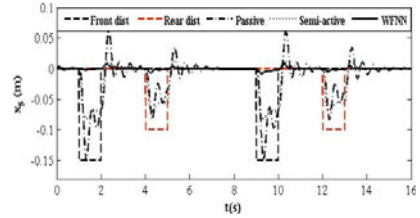


Fig. 5. Seat displacement with controller

The learning rate for the WFNN control is 0.08 for front left tyre, 0.009 for front right tyre, 0.007 for rear left tyre, 0.008 for rear right tyre and 0.003 for the seat controller respectively.

Figures (4) and (5) show that the response of seat is improved as compared to passive suspension and semi-active suspension system. In passive suspension and semi-active suspension, the maximum value for seat displacement is $0.152m$ and 0.080 while, for the WFNN control, the maximum value for seat displacement is $0.025m$. Here, the passenger comfort is increased by 83% as compared to passive suspension and 69% as compared to semi-active suspension system. The response of seat with controller is better than seat without controller. Also, the settling time of WFNN controller is reduced and steady state response is improved as compared to passive suspension. The seat with controller increased the passenger comfortability by 21%.

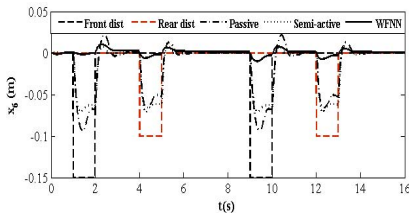


Fig. 6. Heave displacement

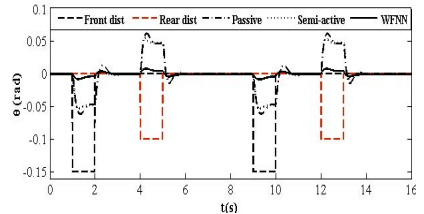


Fig. 7. Pitch displacement

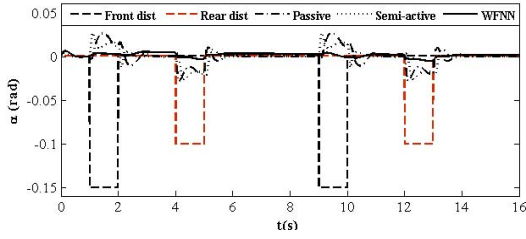


Fig. 8. Roll displacement

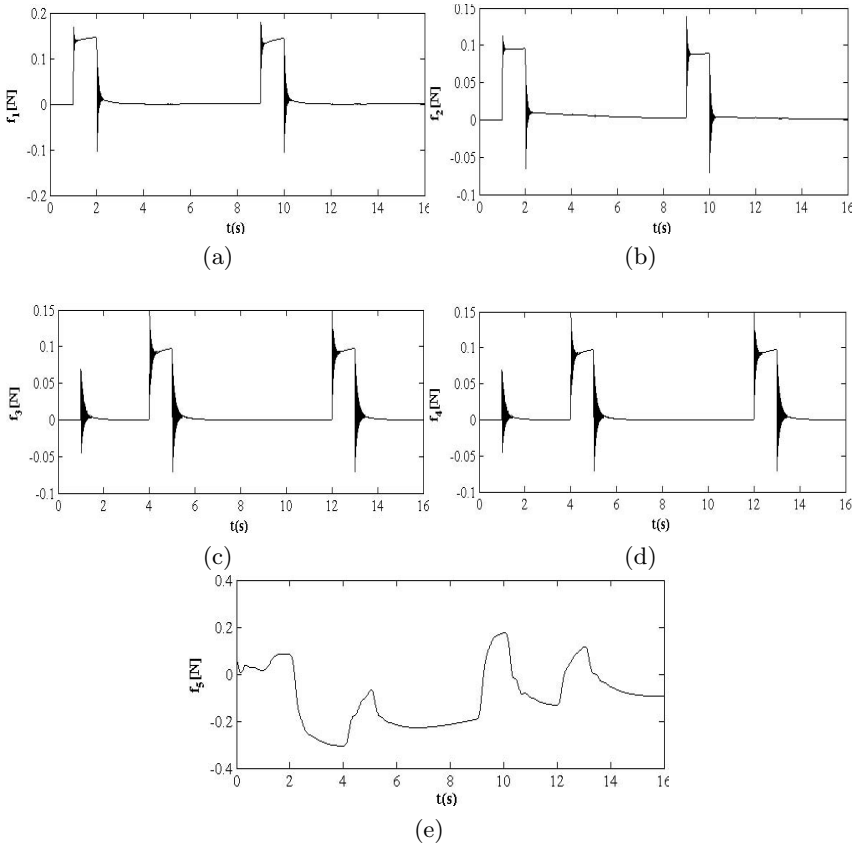


Fig. 9. Control Efforts of WFNN controller: (a) Control effort of front left tyre (b) Control effort of front right tyre (c) Control effort of rear left tyre (d) Control effort of rear right tyre (e) Control effort of passenger seat

Figures (6–8) show that the response of heave, pitch and roll is improved as compared to passive suspension and semi-active suspension system. In passive suspension and semi-active suspension, the maximum value of displacement for

heave is $0.094m$ and 0.070 while, for the WFNN control, the maximum value of displacement for heave is $0.025m$. Here, the value of heave is improved by 83% as compared to passive suspension and 78% as compared to semi-active suspension system. In passive suspension and semi-active suspension, the maximum value of displacement for pitch is $0.061m$ and 0.054 while, for the WFNN control, the maximum value of displacement for pitch is $0.014m$. Here, the value of pitch is improved by 78% as compared to passive suspension and 74% as compared to semi-active suspension system. In passive suspension and semi-active suspension, the maximum value of displacement for roll is $0.028m$ and 0.024 while, for the WFNN control, the maximum value of displacement for roll is $0.013m$. Here, the value of roll is improved by 57% as compared to passive suspension and 46% as compared to semi-active suspension system. Also, the settling time of WFNN controller is reduced and steady state response is improved as compared to passive suspension. This increased the vehicle stability, ride comfort and passenger comfortability.

Here, only the passive suspension hits the rattle space limits but active suspension for the seat, heave, pitch and roll displacement did not reach the rattle space limits.

Figure 9 shows the control efforts of front left, front right, rear left, rear right tyre and seat controllers. From the above results it is observed that the front left and rear right tyre controllers applied more force than other controllers to give passenger comfort and vehicle stability.

6 Conclusion

In this paper, an active suspension system is proposed to ameliorate the passenger safety and vehicle stability by using WFNN control technique. Simulation results of adaptive WFNN are compared with passive and semi-active suspension systems. Performance of the adaptive WFNN reveals that it improves passenger's comfort and vehicle's handling against the road disturbances.

Acknowledgments. Thanks to COMSATS Institute of Information technology for facilitating us in the completion of this research work.

References

1. Sunwoo, M., et al.: An application of explicit self-tuning controller to vehicle active suspension system. In: IEEE Conf. on Decn and Cnt., vol. 4, pp. 2251–2257 (1990)
2. Kim, C., Ro, P.I.: A sliding mode controller for vehicle active suspension systems with nonlinearities. Pr. Instl. Mech. Engn. 212, 79–92 (1998)
3. Giua, A., Seatzu, C., Usai, G.: Semi active Suspension Design With an Optimal Gain Switching Target. Vehicle System Dynamics 31, 213–232 (1999)
4. Chalasani, R.M.: Ride Performance Potential of Active Suspension System Part II: Comprehensive Analysis Based on a Full Car Model. In: Sym. on Siml. and Cntrl of Ground Veh. and Trans. Sys., pp. 205–234 (1996)

5. Elbeheiry, M., Kamopp, D., Abdelraaouf, M.: Suboptimal Control Design of Active and Passive Suspensions Based on a Full Car Model. *Veh. Sys. Dyn.* 26, 197–222 (1996)
6. Crolla, D., Abdel-Hady, M.: Active suspension control: Performance comparisons using control laws applied to a full vehicle model. *Veh. Sys. Dyn.*, 107–120 (1991)
7. Bigarbegian, M., Melek, W., Golnaraghi, F.: A novel neuro-fuzzy controller to enhance the performance of vehicle semi-active suspension systems. *Veh. Sys. Dyn.* 46(8), 691–711 (2008)
8. Kumar, M.S.: Development of Active Suspension System for Automobiles using PID Controller. In: *Proc. of the World Congr. on Engn., London*, vol. 2, pp. 987–993 (2008)
9. Wilson, Sharp, Hassan.: Application of linear optimal control theory to design of active automotive suspensions. *Veh. Sys. Dyn.* 15(2) (1986)
10. Lin, J., Lian, R.J.: DSP-based self-organising fuzzy controller for active suspension systems. *Veh. Sys. Dyn.* 46(12), 1123–1139 (2008)
11. Lian, R., Lin, B., Sie, W.: Self-organizing fuzzy control of active suspension systems. *Intr Jr. of Sys. Sci.* 36(3), 119–135 (2005)
12. Darus, R.: Modeling and control of active suspension for a full car model. Master, dissertation (2008)
13. Rahmi, G.: Active control of seat vibrations of a vehicle model using various suspension alternatives. *Turkish J. Eng. Env. Sci* 27, 361–373 (2003)
14. Peng, J.-Z., Wang, Y.-N.: Fuzzy Wavelet Neural Network Control Based on Hybrid Learning Algorithm. *IEEE Tr. Fuzzy Sy.* 33(2), 51–54 (2006)
15. Zhang, J., Walter, G., Miao, Y., Lee, W.: Wavelet neural networks for function learning. *IEEE Trans. Signal Prs, N-computing* 43(6), 1485–1497 (1995)
16. Chen, Y., Yang, B., Dong, J.: Wavelet networks. *IEEE Trans. NN, Neurocmptng* 69(4-6), 449–465 (2006)
17. Ho, D.C., Zhang, P.A., Xu, J.: Fuzzy wavelet networks for function learning. *IEEE Trans. Fuzzy Syst.* 9(1), 200–211 (2001)
18. Abiyev, R.H.: Fuzzy Wavelet Neural Networks for Identification and Control of Dynamic Plants A Novel Structure and a Comparative Study. *IEEE Trans. on Indl. Elct.* 55(8) (2008)
19. Lin, T.-C., Roopaei, M., Chen, M.-C.: Car Suspension Control By Indirect Adaptive Interval Type-2 Fuzzy Neural Network Control. *Wrld Apl. Sci. Jr.* 8(5), 555–564 (2010)
20. Cheng, C.-P., Chao, C.-H., Li: Design of observer-based fuzzy sliding-mode control for an active suspension system with full-car model. In: *IEEE Intl. Cnf. on Sys. Man and Cybr.*, pp. 1939–1944 (October 2010)

Blind Deconvolution of Blurred Images with Fuzzy Size Detection of Point Spread Function

Salman Hameed Khan¹, Muhammad Sohail¹, Ahmed Rehan¹,
Zeashan Hameed Khan², and Arsalan Hameed Khan³

¹Department of Electrical Engineering, College of E&ME, NUST, Rawalpindi, Pakistan
salman.khan@seecs.edu.pk, sohail_30@ee.ceme.edu.pk,
rehan_eme@yahoo.com

²Center for Emerging Sciences, Engineering & Technology (CESET), Islamabad, Pakistan
zkhan@ceset.pk

³School of Automation, Northwestern Polytechnical University, Xi'an, China
arsalan1@mail.nwpu.edu.cn

Abstract. The objective of present research is to find the correct dimensions of point spread function (PSF), which is a crucial step in blind deconvolution of linearly blurred images. Usually size of PSF is estimated by trial and error, based on user experience. Keeping in view the fuzzy nature of this problem, we have implemented a fuzzy inference system (FIS) in Matlab to efficiently predict the size of PSF. The fuzzy system is based on the common observation that the size of PSF is directly related to the amount of degradation caused to each pixel in the original image. The blurred image is compared with edge extracted image and the PSF size is estimated by accounting for the distortion of edges. The results are encouraging and the method presented in this paper can be used to avoid trial and error based lengthy process of PSF size estimation.

Keywords: fuzzy logic, point spread function, blurred image, deconvolution.

1 Introduction

Blur in an image can be caused by relative motion between the camera and the object being captured, defocused or faulty optical instrument, atmospheric conditions, shallow depth of field or wide angle optical lens. Very short exposure time while capturing image can also induce blur due to less number of photons captured. Confocal optical microscopy, which is used to increase optical resolution of a photo micrograph, also causes distortion in scattered light which causes blurring [1-2].

In case of linear blurring kernel, the process of deblurring or image restoration requires the knowledge of exact PSF so that the blurred image can be deconvolved to obtain true information. PSF accounts for the amount of distortion produced by an optical system. In other words, it determines the spread of a point of light in space caused by optical system. Generally, it is assumed that either the degradation model is known or can be estimated with the partial information provided. In cases, where we

do not have any information about the spatial or frequency components of actual image, PSF and noise, we opt for blind deconvolution method to recover actual image. Blind deconvolution method recovers image and PSF by running the algorithm over and over again in an iterative manner.

Iterative methods perform better in the sense that their result can be evaluated as it progresses. Moreover, iterative methods perform best while restoring the images suffering from a variety of degradations, such as linear, non-linear, signal dependent and spatially invariant blurs because of their flexible way of solving the problem. However it must be noted that in case of linear blurring kernel, it is important in blind deconvolution method to know the correct PSF size. The deconvolution with oversized or undersized PSF results in more blur or ringing in recovered image. Traditionally PSF size is estimated by concerned person based on expert knowledge and previous experience. Our contribution in this work lies in the implementation of fuzzy controller to decide about the appropriate size of PSF.

We have used direct method in fuzzy reasoning due to its simplicity and ease of use. There are two commonly used types of direct FIS, known as Mamdani and Takagi-Sugeno FIS [3]. Mamdani type FIS is used in the current paper due to its widespread acceptance and suitability for human input.

2 Related Work

The incorporation of fuzzy techniques in image deblurring, especially when no prior knowledge of blurring function is at hand, is an important topic with a variety of good results. Blind deconvolution method has been used for removing camera shakes from single photograph to recover the original image [1][4]. A strong image processing background is required for deblurring phenomenon; fuzzy based approach, on the other hand, reduces development time as it requires less tedious work to carry out the realization of problem at hand [3].

Fuzzy logic based techniques have been reported in finding success in image processing applications. For example the problem of finding edges in an image have been addressed with the linguistic rule base offered by fuzzy logic in [2] [5-7] to name a few. In these methods, fuzzy linguistic statements like IF THEN have been used in finding a rule base for threshold and window sizes have been demonstrated. Results have been compared with conventional methods like Sobel and Prewitt demonstrating the success of these simple algorithms. Similarly a method for the estimate of channel degradation termed as 'blur' in image processing has been described in [8] which is based on fuzzy k-nearest neighbor algorithm. The aim in this and other works like [9] is the estimate of the complete blurring kernel. Our work focuses on using fuzzy logic for estimating the size of linear blurring kernel, as variations in it leads to poorer results.

3 Methods

Suppose that we have an image (I), a linear kernel i.e. PSF (H) which is the source of degradation of image (generally irreversible), blurred image (B) and some noise (N)

that has additive effect on our system. The PSF convolves with actual image to give blurred image. This process is given by, [5][10]

$$B=I*H+N \tag{1}$$

We have experimented with three types of PSFs i.e. gaussian, linear motion and circular averaging filters. Gaussian blur is caused due to long exposure time and is given by,

$$H(x,y) = \frac{1}{\sigma\sqrt{2\pi}} e^{-\frac{x^2+y^2}{2\sigma^2}} \tag{2}$$

Circular averaging blur is produced due to out of focus optics. This type of PSF uniformly distorts a disk surrounding a single pixel (center of defocus (c_x,c_y)) and is given by,

$$H(x,y) = c \begin{cases} 1, & \sqrt{(x - c_x)^2 + (y - c_y)^2} \leq \text{radius} \\ 0, & \text{otherwise} \end{cases} \tag{3}$$

where ‘c’ is a constant that acts as a scaling factor [4].

When there is a relative motion between object being captured and the optical instrument, the resulting distortion is modeled by motion PSF. The form of all three blurring kernels is shown in figure 1.

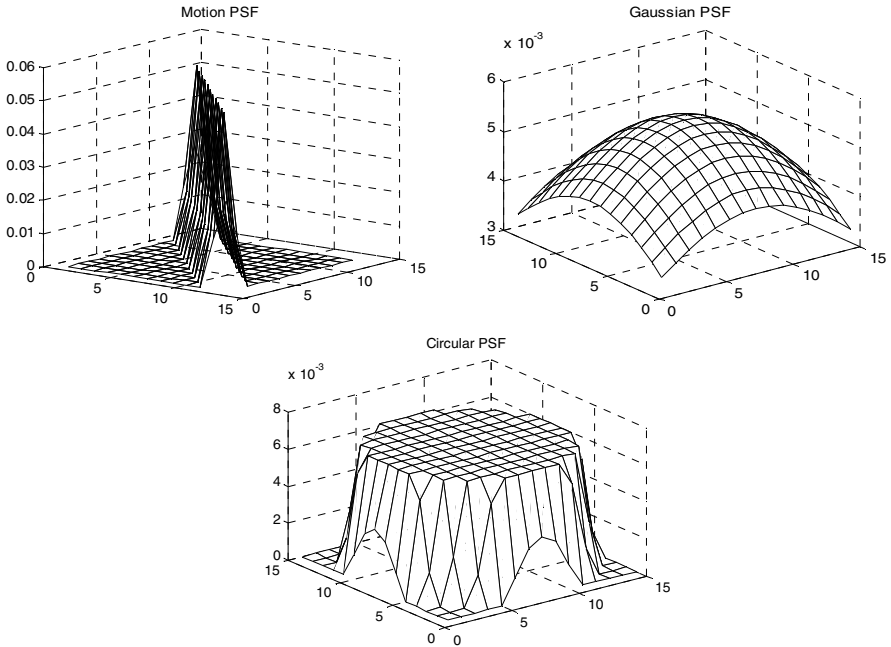


Fig. 1. Motion, Gaussian and Circular Averaging/Out of Focus PSF

3.1 Fuzzy Image Processing

Fuzzy image processing deals with the application of fuzzy sets, rules and techniques to processing of images [11]. The representation and processing in the form of fuzzy sets and membership functions depends largely on problem in hand. First step is the fuzzification of inputs and the last step is defuzzification to get the crisp output. Processing is done in between these two steps and modification of membership values is achieved by mapping inputs to the corresponding outputs as shown in figure 2.

Fuzzy rule based approach is used in our work for calculating outputs. Centroid method was used for defuzzification of fuzzy outputs. Simple min and max operations were used for multiplication and addition.

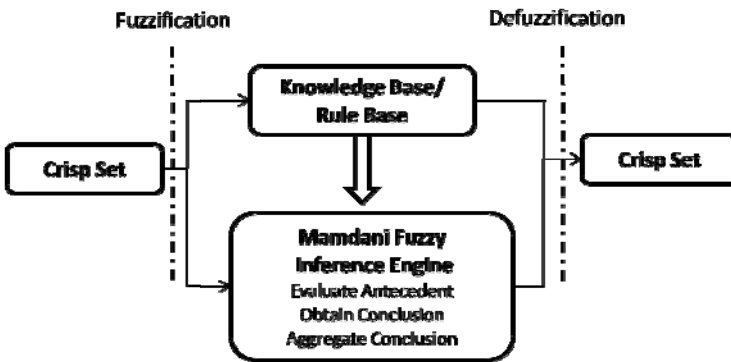


Fig. 2. Fuzzy Inference System

3.2 Fuzzy Membership Functions

Triangular and trapezoidal member functions were used for inputs and output as shown in figure 3. The inputs from the edge image were assigned triangular while inputs from blurred image and output were given triangular and trapezoidal membership functions. The ranges were set to optimize the FIS result.

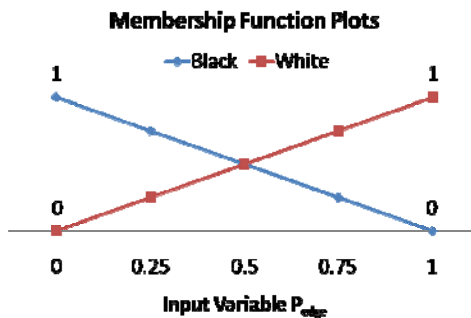


Fig. 3. Fuzzy membership functions for Edge window, Difference window and Output PSF size

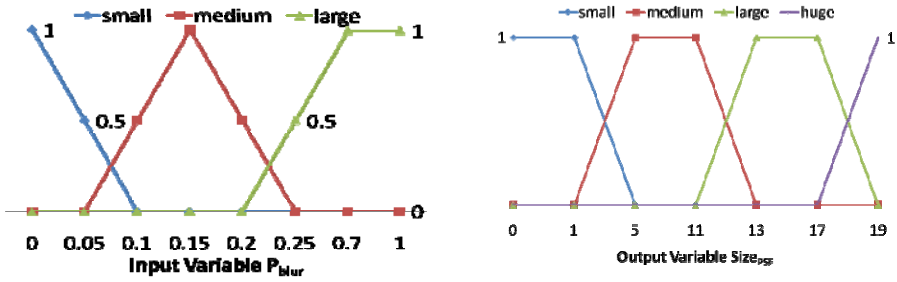


Fig. 3. (continued)

3.3 Fuzzy Rules

Mamdani type FIS controller is used in our application due to its ability to tackle relatively complex problems. Eighteen rules are defined which are shown in table 1.

Table 1. Fuzzy Rule Base for PSF Output

$P1_{edge}$	$P2_{edge}$	$P1_{diff}$	$P2_{diff}$	$P3_{diff}$	$P4_{diff}$	THEN PSF Size
I F Black	White	Small	Large	Large	Small	Medium
		Medium	Large	Large	Medium	Large
		Medium	Medium	Medium	Medium	Medium
		Medium	Small	Small	Medium	Medium
		Large	Large	Large	Large	Huge
		Large	Medium	Medium	Large	Large
		Large	Small	Small	Large	Large
		Small	Small	Small	Small	Small
		Small	Medium	Medium	Small	Small
I F White	Black	Small	Large	Large	Small	Medium
		Medium	Large	Large	Medium	Large
		Medium	Medium	Medium	Medium	Medium
		Medium	Small	Small	Medium	Medium
		Large	Large	Large	Large	Huge
		Large	Medium	Medium	Large	Large
		Large	Small	Small	Large	Large
		Small	Small	Small	Small	Small
		Small	Medium	Medium	Small	Small

3.4 State Diagram of Complete System

The overall working of system is shown in block diagram of figure 4. Edges are detected out of blurred image and fuzzification block makes both blurred and edge images suitable for input to FIS. Proper window size for both images is selected as described in Section 2.5. Difference vector from blurred image frame is augmented with edge window and the resulting vector is fed to FIS. PSF size is predicted and comparison is done to decide whether supposed PSF size was correct or not. Once correct size is found out, blind deconvolution is used to recover the original image.

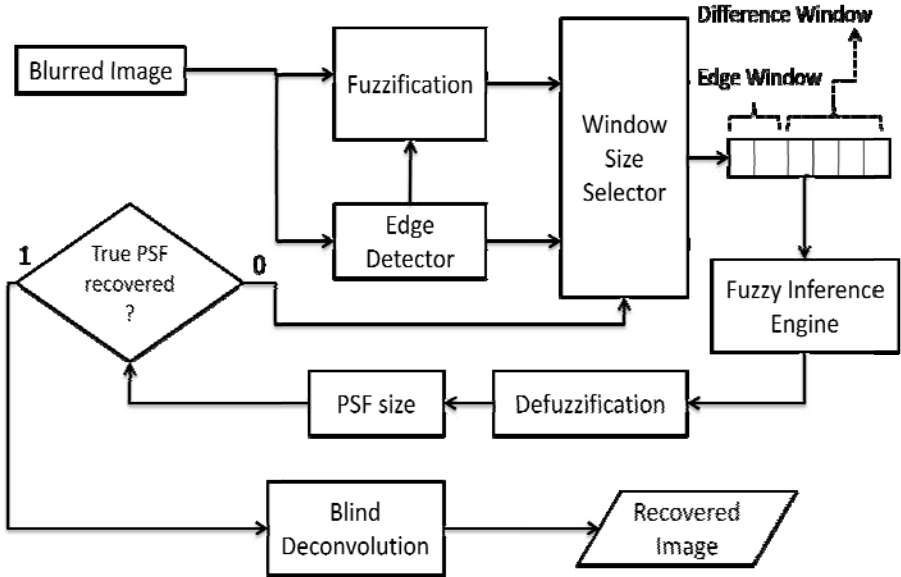


Fig. 4. Algorithm Flow Chart

3.5 Algorithm

Algorithm in the form of high level code is as follows:

Blurring the Image

Step 1: An Image of $M \times N$ dimension is read and is named as A

Step 2: Create a known PSF of a size $p \times q$. Convolve it with original image A to get blurred image B as output.

Determining Size of PSF

Step 3: Calculating edges of blurred image using Sobel edge detection method with threshold (th) . Store this image as C matrix.

Step 4: Fuzzifying the image C by keeping the matrix values in discrete steps between 0 and 1. Fuzzification of blurred image is achieved by first converting it from uint8/uint16 or logical format to double and then normalizing it with 255.

Step 5: Create two windows, one for edge image C and second for blurred image B . Set the size of edge window to be 2. Set initial size of blur window to be 4.

Step 6: Scan through the edge image C of size $N \times M$. The location where edge is detected i.e. sudden transition is detected, in image C , go to image B and get the pixels around this edge. The number of pixels to be stored is determined by size of blur window. Take differences between two immediate values found at both sides of blur window. This will show the strength of effect of PSF. This difference is

calculated in order to keep the input to FIS constant and the origin of this difference is the observation that usually all PSF's have maximum strength at center and it fades away near the corners.

Store the 4 differences in a vector.

Step 7: The edge window and blur window are fed to FIS.

The scaled output PSF size is compared to initially assumed PSF size. Based on this comparison it is decided if the initially assumed PSF size was correct or not. If the PSF size is correct system goes to step 9 other wise step 8.

Step 8: The size of blur window is increased by one pixel on both sides and the control of program is shifted back creating difference vector and Step 5.

Blind Deconvolution

Step 9: Blind deconvolution is performed with blurred image B and obtained PSF size as input. Thirty iterations are performed to get satisfactory restored image.

4 Results

We conducted the experiments on 30 grayscale images obtained from image repositories from Signal and Image Processing Institute, University of Southern California [12] and Visual Information Processing Group, University of Granada [13]. The size of PSF recovered using the FIS showed good results giving correct PSF size in about 86% cases. Even in cases when answer was wrong, PSF size was close to actual size. It is evident that estimating the correct PSF size is important in blind deconvolution for linear blurring kernel case and the results are greatly improved when correct size is calculated.

Two metrics i.e. root mean square error (RMSE) and peak signal to noise ratio (PSNR) are used for analyzing the amount of restoration achieved through the method. Mathematical expressions used for calculating these two parameters over each image are,

$$RMSE = \sqrt{\frac{1}{N^2} \sum_{i=0}^{N-1} \sum_{j=0}^{N-1} [I_{ij} - I'_{ij}]^2} \quad (4)$$

$$PSNR = 20 \log_{10} \left(\frac{2^b - 1}{RMSE} \right) \quad (5)$$

Where, N is the total number of pixels in horizontal and vertical direction, b is bits per sample of linear PCM and I is the original image.

Among the thirty test images, four are shown in figure 5 that were passed through the complete process. The first and the last image shown are 256x256 while the middle two are of size 512x512. Three blurring techniques were used to model blur due to linear motion, high exposure time and out of focus optics (in the same sequence from left to right as shown in figure 6). The restored images are shown in figure 7. Peak signal to noise ratio (PSNR) and root mean square error for all results

are summarized in table 2. Due to limited space, results for only gaussian blur are included. SNR values are increased considerably while RMS errors are reduced in restored image.

Table 2. RMSE and PSNR values for test images





















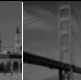










Image	Parameter								
Blurred	RMSE	17.68	11.7	14.63	15.45	12.82	17.07	30.86	11.61
	PSNR	23.2	26.8	24.82	24.35	25.97	23.48	18.34	26.83
Restored	RMSE	9.26	6.39	7.13	7.76	7.30	8.69	16.58	6.393
	PSNR	29.1	32.01	31.06	30.33	30.92	29.35	24.5	32.01
									
Blurred	RMSE	33.3	16.01	16.19	11.70	20.06	23.44	26.29	16.46
	PSNR	17.68	24.0	23.95	26.77	22.08	20.73	19.73	23.8
Restored	RMSE	16.2	8.4	7.63	6.39	9.45	9.81	14.83	8.155
	PSNR	23.9	29.65	30.5	32.0	28.6	28.3	24.7	30.10
									
Blurred	RMSE	23.8	19.1	9.2	11.5	8.3	9.3	10.1	11
	PSNR	20.6	22.49	28.87	26.94	29.7	28.8	28.1	27.3
Restored	RMSE	11.4	10.02	4.30	5.82	4.57	5.14	4.61	5.0
	PSNR	27	28.41	35.46	32.84	34.93	33.9	34.85	34.63
									
Blurred	RMSE	7.2	9.5	18.17	17.53	18.6	18.1		
	PSNR	23.41	28.57	22.94	23.25	22.7	23.1		
Restore d	RMSE	9.62	5.15	8.504	10.18	11.1	8.53		
	PSNR	28.5	34.2	29.5	28.3	27.2	30.0		



Fig. 5. Original grayscale images for test purposes

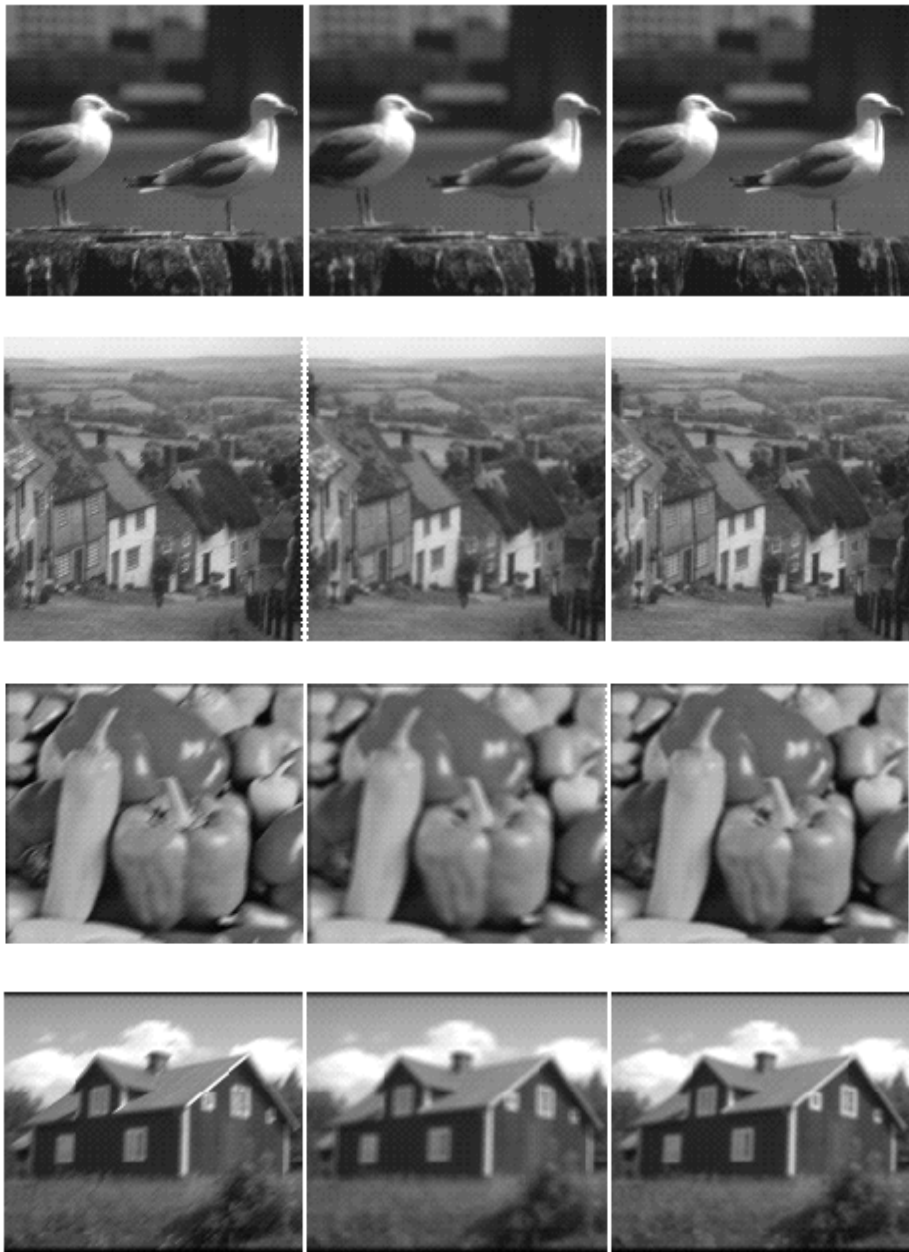


Fig. 6. Blurred images using motion blur (at left), Gaussian (middle) and Circular averaging blur (at right)



Fig. 7. Recovered images that earlier suffered from linear motion blur (at left), Gaussian (middle) and Circular averaging blur (at right)

5 Conclusion and Future Work

The size of PSF in blind deconvolution method is usually estimated by trial and error. This embeds uncertainty or vagueness to the estimation of PSF size. Fuzzy logic is used in this paper to model this vagueness. Based on the amount of distortion produced by PSF on edges, the size of PSF is successfully estimated in this paper. In future, we will explore the possibility of estimating the form of PSF using fuzzy logic in blind deconvolution.

References

1. Fergus, R., Singh, B., et al.: Removing Camera shake from a Single Photograph. ACM Transactions on Graphics, Proc. SIGGRAPH (2006)
2. Liang, L.R., Looney, C.G.: Competitive fuzzy edge detection. Appl. Soft Comput. J. 3, 123–137 (2003)
3. Driankov, D., Hellendorn, H., Reinfrank, M.: An Introduction to Fuzzy Control. Springer, New York (1993)
4. Stefan, W.: Image Restoration by Blind Deconvolution. Diploma Thesis, Technische Universität München (TUM) and Arizona State University (2003)
5. Kaur, K., Mutenja, V., Gill, I.S.: Fuzzy Logic Based Image Edge Detection Algorithm in MATLAB. International Journal of Computer Applications 1 (2010)
6. El-Khamy, S.E., Ghaleb, I., El-Yamany, N.A.: Fuzzy edge detection with minimum fuzzy entropy criterion. In: Proceedings of the Mediterranean Electrotechnical Conference, Cairo, Egypt, vol. 1, pp. 498–503 (2002)
7. Tyan, C., Wang, P.: Image processing-enhancement, filtering and edge detection using the fuzzy logic approach. In: Proceedings of the Second International Conference on Fuzzy Systems, San Francisco, vol. 1, pp. 600–605 (1993)
8. Chen, L., Yap, K.-H.: A Fuzzy K-Nearest-Neighbor Algorithm to Blind Image Deconvolution. In: IEEE International Conference on Systems, Man and Cybernetics, vol. 3, pp. 2049–2054 (2003)
9. Yap, A.K.-H., Guan, L.: A fuzzy blur algorithm to adaptive blind image deconvolution. In: Proceedings of the 7th IEEE International Conference on Control, Automation, Robotics and Vision (ICARCV 2002), Singapore, pp. 34–38 (2002)
10. Sarwal, P., Srinath, M.D.: A Fuzzy Logic System for Channel Equalization. IEEE Transactions on Fuzzy Systems 3, 246–249 (1995)
11. Alshennawy, A.A., Aly, A.A.: Edge Detection in Digital Images Using Edge Detection Technique. World Academy of Science, Engineering and Technology (2009)
12. Signal and Image Processing Institute, University of Southern California, <http://sipi.usc.edu/database/>
13. Visual Information Processing Group, University of Granada, <http://decsai.ugr.es/cvg/CG/base.htm>

Bluetooth Usage Control Policy Enforcement Model

Shahryar Khan and Inayatullah Babar

N.W.F.P University of Engineering and Technology,
Peshawar, Pakistan

engrshahrs@gmail.com, babar@nwfpuet.edu.pk

Abstract. Bluetooth is short range wireless communication mechanism that provides detail specifications for connecting devices. It is used for data transfer over wireless channel however, the functionality is not just limited to this. It provides advanced features that has no alternative in current time that includes low cost, low power, faster data rates and sharing services like Internet, personal area networking etc. Provided with high-end features, Bluetooth requires adequate security implementations for secure and reliable communication. Current security implementations for authentication and encryption are claimed strong enough against security threats. Authorization currently supported by Bluetooth is however, based on simple allowing or denying a resource. Authorization should facilitate user with fine grained control features over resources. This means that authorization mechanism should provide usage control over resources shared using Bluetooth. We propose Bluetooth Usage Control Model (BUCM) that enhances existing security model in usage control features. Using extended model, user can perform fine grain customization of resources. Proposed model is implemented within Android Bluetooth stack. Performance results verify the extended model for minimal overhead in performance.

Keywords: Bluetooth, Android, Usage control, Authorization, Security.

1 Introduction

Nowadays information media trends to converge on wireless technologies such as Wi-Fi, Wi-MAX, Bluetooth and GSM networks. These have replaced traditional wired technologies for data and telephonic communication to a great extent. Among these technologies, Bluetooth, developed by Special Interest Group (SIG) has spread rapidly in recent decade. Bluetooth is found in laptops, printers, wireless keyboard, mice and other peripherals. Majority of cell phones are shipped with a Bluetooth chip that enables variety of functionalities. In mobile systems, Bluetooth communication is used for data transfer, dial-up networking, business card and Internet sharing etc. It supports various Internet Protocol (IP) based services for example mobile IP and cellular IP [1] that are used to access services in public area like airport, shopping mall, museum etc. Bluetooth

connections are made among devices like personal computers, laptops, mobile phones and other peripheral devices. Communication among such devices needs to be secure, reliable and efficient.

Security is major concern in communication done over wireless medium. Unlike wired medium, wireless communication is exposed and therefore more prone to security threats. Bluetooth possess security procedures for authentication, authorization and encryption. These security procedures make use of advanced cryptographic mechanisms to ensure secure authentication and encryption. However, the authorization scheme needs to be refined with some advanced features. These features provide user with fine grained access control procedures over resources shared using Bluetooth. These functionalities come handier to owner who requires resources to be shared and accessed in a fair way.

Example is a wireless Hot-Spot at airport providing Internet to Bluetooth enabled devices. Administration at such places requires to allow usage of Internet or other Bluetooth services on restrictions, for example allowing customers to use Internet at rate of 10 Kbytes per second. This is required to ensure availability and fair usage of services. Unfortunately, Bluetooth does not take care of resource control at such fine level. Framework capable of implementing Bluetooth fine grained authorization policy is required. In this aspect we proceed by proposing a comprehensive model for Bluetooth that is compatible with existing Bluetooth protocol stack and provides a mechanism to define and enforce constraints on services shared over its network. These constraints are defined on Master device which shares resources with Slave devices.

In this paper terms; fine grained access control and usage control are interchangeably used, as both have same context. However, access control and fine grained access control have differentiated meanings. The rest of paper is organized as follows; Section 2 explains motivating example and related work. Section 3 explain Methodology and policy structure with some formal definitions. Section 4 defines target architecture and Section 5 covers implementation details. Section 6 discusses performance evaluation and conclusion.

1.1 Limitations and Contributions

We identify following limitations of Bluetooth protocol in context of fine grained authorization of services.

1. Bluetooth does not provide fine grain control on resources shared with other devices, for example Internet shared on conditional basis.
2. Bluetooth does not allow time based usage of resources, for example allowing access to services during particular time of day.
3. Bluetooth does not allow bandwidth control on Internet sharing in a personal area network.
4. Bluetooth does not provide differentiated allocation of services, for example device allowing access to certain services while denying others.

We address to above limitations by making following contributions:

1. We model our approach by following a standard access control prototype. This enables user to define usage control on shared services.
2. Extended model provides an interface that is used to define policy for usage control.
3. To testify our model we implement the proposed scheme as a framework application on Android OS.
4. Android emulator currently does not emulate Bluetooth [2]. We address to this limitation by connecting Android Software Development Kit (SDK) to x86 based Android Virtual OS. The x86 based Android OS is installed in Virtual box. Thus we enable support of Bluetooth for Android on Virtual machine. This provides complete testing and running of Bluetooth applications on Android.

2 Motivating Example and Related Work

2.1 Bluetooth Usage Control in Tethering

1). Shopping mall is having employees working at shops and daily thousands of customers are served for products and services. In order to update customers with available products, services and other offers, the mall provides Internet facility. Customers having Bluetooth enabled devices connect to access point and are facilitated with various communication services like access to Internet, business card sharing and free messaging. Using these services customers browse through latest items, services available and order them using their device. However in such public places where customers are in hundreds or even more, it's not feasible to provide wired connectivity. Wi-Fi is feasible solution however, few of customers with Wi-Fi embedded devices can utilize this facility. Mobile devices having Wi-Fi chips are expensive and therefore less popular. Conversely, almost all mobile devices comes with Bluetooth chip using which devices connect to Bluetooth access point. The phenomenon is known as tethering as shown in Fig.1. The shopping mall has an administrative section that maintains network services. Administration requires to conditionally allow access these services. They have to make sure that employees and customers uses only allocated set of services. Moreover, no user strives for bandwidth while using Internet service and block suspicious devices using Bluetooth addresses.

2). Consider location where laptop and personal computer (PC) cannot connect to Internet due to absence of wireless and wired connection. However using tethering laptop and PC access Internet without a network card. Bluetooth device possessing Internet access (on cellular network) allows connected devices to access services in a personal area network. In such case, the service providing device becomes Master while other devices connect to it. In this way a personal area network is formed and slave devices utilize services offered by Master device. Internet service is shared using dial-up networking profile. However, Bluetooth does not provide any means to define usages constraints on services. For example, user has Internet data plan of 2 GigaBytes purchased at some cost. Internet

is shared with other devices such as laptop and mobile devices. User utilizes Internet on these devices by tethering to Master device. However, Internet usage exceeds limits and data plan ends without user being informed. This makes situation even worse. User continue to use these services on regular (high) charges which soon drains credit in her account. User in this case requires the cost effective services to be used under constraints and conditions.

Such policies need to be implemented on access point or Master device that provides services to other devices. However, these policies cannot be handled by existing mechanism for Bluetooth. Policy enforcement mechanism is required which handles policies and imposes usage control.

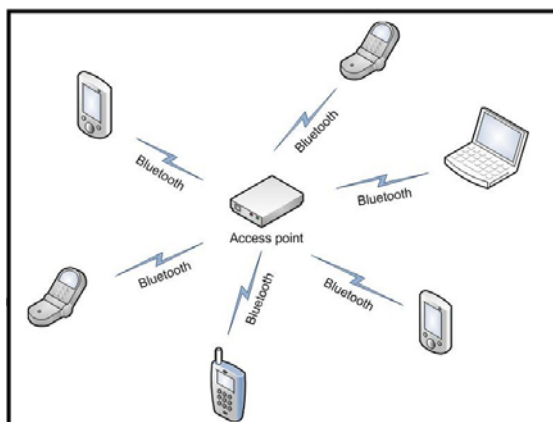


Fig. 1. Common devices connected to Bluetooth access point

2.2 Related Work

Most work done on Bluetooth is regarding authentication and encryption making it more robust against security threats. These involve cryptographic methods that enhances security. Authorization needs to be refined so that user can customize access to these resources according to the situation. Nguyen *et al.* in "Secure authorization, access control and data integrity in Bluetooth" [3] introduces User Authorization and Pairing (UAP) application for Bluetooth. This application has the ability to perform authentication and authorization using RBAC model [3]. Similar to our approach the UAP application authenticates user based on their roles, however usage control on services is absent. It simply allows or denies a resource. UAP does not define any mechanism that allows a resource on conditional basis. In contrast, our approach fine grains access to resources based on defined constraints, for example, time based and transfer rate constraints. Moreover, UAP does not support policy based enforcement. Bandwidth control and load balancing in Bluetooth local area network is discussed by Jesung Kim *et al* [4]. This approach discusses issues in Bluetooth

networks. Similar to our motivating example they discuss LAN infrastructure that is setup using Bluetooth access point. In such scenario number of users exceeds hundreds and therefore Bluetooth access point is unable to handle all requests efficiently. Proposed solution is to have multiple Bluetooth radio in an access point system which divides the load among radios. The scheduling policy uses a kind of round-robin technique to evenly distribute load and handle client devices. However their proposed mechanism does not impose restrictions on accessing resources. Moreover there is no time or usage base constraints that are based on policy. In contrast, our model can adopt their proposed scheme in order to handle hundreds of user requests and share load among the radios. Some related work on usage control on Android platform is done by APEX [5]. APEX facilitates user of mobile device to define constraints using interface known as Poly. These constraints define usage control over resources present on mobile device. The proposed scheme is fine example of imposing restrictions over mobile resources. However, the scheme does not cover any aspect of resources shared over Bluetooth network. Instead of shared resources it only discusses resources that are consumed by user herself. Moreover their scheme is single user approach that defines limitation on self-owned services. In contrast our approach is more generic and defines constraints for resources shared with other devices.

3 Methodology

3.1 Bluetooth Specifications

Our proposed model follows Bluetooth specifications mentioned by Bluetooth specification standard documentation [6]. It operates at Security Mode 2 where authorization and access to services and devices is performed. In Bluetooth protocol, Security Manager performs basic access control functions that simply grants or denies access to services. Usage control is not supported by Security Manager. Our proposed model follows dial-up networking profile [7] according to which device forms connection with other devices. Device having access to Internet is known as Gateway while device connected to Gateway using dial-up services is known as Data terminal [7]. Bluetooth network specifications are mentioned in Personal Area Network (PAN) profile [8]. In PAN profile, Network access point (NAP) refers to device capable of providing Internet. Group of ad-hoc network refers to devices that are connected to one another and transfers data. Finally, PAN user uses the supported services. Bluetooth Internet Gateway [9] defines a Bluetooth model which provides ad-hoc web access for Internet-enabled Bluetooth devices such as PDAs, laptops and WAP mobile phones.

We define three operational modes for authorization of services. These are:

Unrestricted Access: This mode allows unlimited access to a particular resource. This mode includes services that are not cost and security sensitive, moreover the accessing device is trusted.

Fine Grained Access: Our main contribution lies in this mode. Services are subjected to specific conditions before access is granted. Thus services in this

mode are utilized within the specified limitations, for example time period for which access to Internet service is granted.

Always Deny: In this mode services are not allowed for access. This is required if Master device does not trust the Slave device or if a particular resource is restricted based on pre-defined policy.

We identify constraints over Bluetooth services and present them in table1.

Table 1. Constraints over Bluetooth services

Constraint	Description
Time constraint	Defines duration for which a service is accessible
Download constraint	Defines amount of data allowed for download
Bandwidth limit	Defines the rate at which device downloads data
Block list	Defines list of suspicious and non-secure devices
Hybrid constraint	Defines combination of constraints imposed simultaneously

Scope of Constraints: Constraints are imposed at two different levels based on their scope.

Role Level: Constraints for a specific role is implemented at this level. Separate policy file is maintained for each role.

Global Level: This is cumulative level of constraints in which all devices are treated in same fashion. Constraints imposed at this level affects all connected devices using single policy file.

3.2 Policy Structure

Our designed policy is XML based containing set of constraints. Policy created using interface is stored in respective repository. Policy holds information on usage control over shared resources. Policy structure is shown in Fig.2. Note that the role name and Bluetooth address are not mentioned in Policy.xml file. This information is only required to create or edit policy and therefore not stored in policy file itself.

3.3 Formal Definitions

Definition 1. Users are assigned roles based on role hierarchy model. We define a function α that assigns users to the roles they belong.

$$\alpha : U \rightarrow R, \quad (1)$$

$U = \{u1, u2, \dots, un\}$ where U is set of users and $R = \{r1, r2, r3, \dots, rn\}$, R is set of roles, for example,

$$\alpha1 : \{u1\} \rightarrow \{r1\} \quad (2)$$

$$\alpha2 : \{u2\} \rightarrow \{r2\} \quad (3)$$

```

1 <?xml version="1.0" encoding="utf-8"?>
2 <policy>
3 <resource name="status"
4     value="yes"/>
5 <resource name="time_limit"
6     from="08:00" to="16:00"/>
7 <resource name="time_duration"
8     value="01:00"/>
9 <resource name="download_limit"
10    value="5,100"/>
11 <resource name="block_list"
12    value="BC:34:34:FA:VD:02"/>
13 </policy>

```

Fig. 2. XML Policy Structure

Definition 2. User requests Master device to grant access to service. In response, Master device authorizes requester for specified set of services. Requested services denoted by set S while services for which requester is authorized is denoted by set S' . The set of granted services is always equal subset of requested services.

$$S' \subseteq S \quad (4)$$

Definition 3. Resources are granted to users based on their role. We define function β that assigns set of service S to respective roles R .

$$\beta : S \rightarrow R \quad (5)$$

$S = \{s1, s2, s3, \dots, sn\}$ where S is set of services, for example, employees $r1$ are assigned different set of services as compared to customers $r2$.

$$\beta1 : \{s1, s2\} \rightarrow \{r1\} \quad (6)$$

$$\beta2 : \{s1\} \rightarrow \{r2\} \quad (7)$$

Definition 4. We have two kinds of policies stored on device Pol ; Global policy defined by G_Pol and role specific policy defined by R_Pol .

$$Pol1 \rightarrow G_Pol \quad (8)$$

$$Pol2 \rightarrow r1_Pol \quad (9)$$

$$Pol3 \rightarrow r2_Pol \quad (10)$$

where, $r1_Pol$ and $r2_Pol$ defines policies for $role1$ and $role2$ while G_Pol defines global policy on device, respectively.

4 Bluetooth Usage Control Model (BUCM)

Existing Bluetooth protocol contains Security Manager that is used for setting appropriate security requirements that includes authentication, authorization and encryption specifications that should meet for incoming connection. Security Manager specifies whether these requirements are applied or not for a particular service. Tasks of Security Manager includes storing security information on services and devices, enforcing authentication and encryption. Moreover, it asks user to enter PIN so that a trusted relationship is established between devices. Note that Security Manager does not fine tune the authorization mechanism. We augment our proposed Bluetooth Usage Control Model (BUCM) within Bluetooth protocol to achieve fine grain authorization mechanism as shown in Fig.3a. BUCM comes in action after Security Manager processes and grants access to resource. BUCM implements usage control and consists of several modules including couple of repositories and a GUI as shown in Fig.3b.

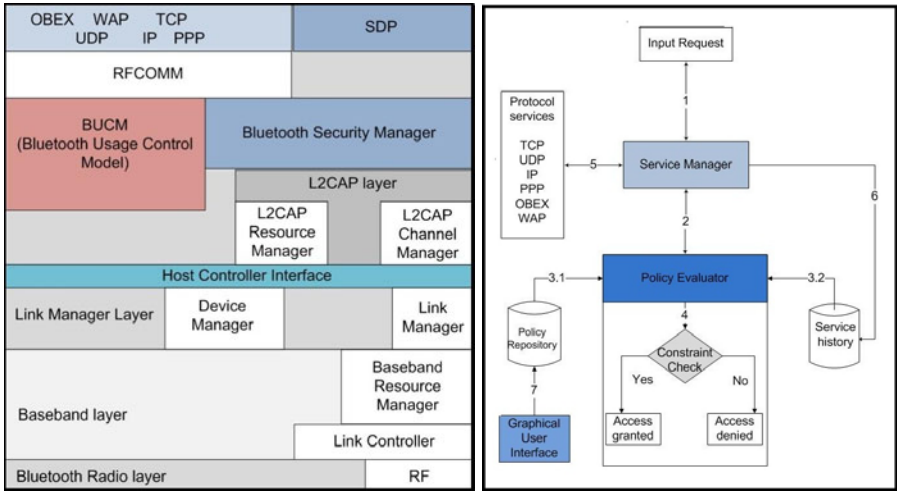


Fig. 3. a). Extended Bluetooth architecture, b). Bluetooth Usage Control Model

GUI: Proposed framework has a GUI which is password protected. The interface is used to create or modify policy. The policy is then stored as XML file in policy repository.

Service Manager: Incoming request to access a service is received by Service Manager. It is at this point whether the request is granted or denied. The request is passed to Policy Evaluator. Service Manager also updates Service History upon access to service.

Policy Evaluator: It is core module that evaluates decision to grant or deny access to services. Evaluation is based on comparison of constraints extracted

from Service History and Policy file. If Service History exceeds limits, further access is denied.

Service History: This module maintains record for each service usage using its respective attributes. As long as a service is accessed the attributes are updated and sent to Policy Evaluator for evaluation.

Policy Repository: This repository stores and maintains both Role specific and Global system policies. Policy contents (in form of attributes) are sent to Policy Evaluator for comparison.

5 Implementation

We implement our proposed scheme on Android due to number of reasons. Android is Open Source mobile platform. Its source code is freely available which makes it favorable for research and development. Manufacturers and application developers choose Android because of its open libraries and high-end features. Android provides SDK for application development that aids developer to develop applications.

5.1 Limitations of Android Emulator

Android emulator is a convenient tool for developing and testing applications without a real handset, but it is not as a real device. Bluetooth support is not available on Android emulator, even in latest version of its provided Application Program Interface (API) [2]. Emulating Bluetooth functionality is core requirement for researchers and developers. We counter this by emulating Bluetooth using x86 based Virtual OS of Android. We installed Android latest available x86 firmware that is Froyo version 2.3 on Sun Oracle Virtual box Manager. We connect Android Virtual OS to SDK using Eclipse tool and adb command shell. This is done using IP address and adb commands. Testing applications on eclipse results in launching Android Virtual OS with Bluetooth support.

5.2 Existing Bluetooth Implementation

BluetoothAdapter: This class provides; discovery of Bluetooth devices, query of paired devices, instantiate Bluetooth device using MAC address and enable listening from other devices. `getBondedDevices()` returns set of paired devices. **BluetoothSocket:** This classes implement sockets for input and output data streams. It is same as TCP socket in functionality and is used for establishing connections and exchange of data. Data is transferred by creating `InputStream` and `OutputStream`. `BluetoothServerSocket` class implements server socket for connection. `BluetoothClass` provides general information on capabilities of a Bluetooth device. Bluetooth socket provided by Android API's is implementation of RFCOMM. This provides connection-oriented and streaming transport over Bluetooth. BUCM comes in action after `connect()` method (of RFCOMM

socket) and attempts to make connection to remote device. BUCM checks for policy and usage constraints. If a resource is allowed according to policy, RFCOMM socket is allowed to retrieve Input stream and Output stream objects by calling `getInputStream()` and `getOutputStream()` methods, respectively.

5.3 Bluetooth Classes and Methods Used in Implementation

We coded the following methods for implementing our proposed scheme.

`checkBTPolicy()`: It reads contents of Policy.xml file and extracts information in the form of attributes. `updateBTPolicy()`: This method updates Policy.xml file after changes are made and saved using GUI.

`checkTimeLimit()`: This method checks time attributes extracted from policy by comparing it with system time. `checkTimeDuration()`: This method checks time duration for which the resource is accessed. The time duration is compared with the Android system timer.

`device.getName()`: This method gives the name while the `BluetoothAdapter.getDefaultAdapter(). getAddress()` gives address of the device.

`BluetoothDevice` class represents remote Bluetooth device with which connection is established. It gives information of the device name, address, class and bonding state. `checkBlockList()`: It checks if address of connecting device is in Block list. These methods are defined in `PolicyEvaluator` class.

`SettingActivity`: This class implements GUI, using which user enters details for policy which is then saved to the policy repository. `BrowserActivity`: This class is present in android.webkit package that manages downloaded data while browsing Internet. `checkTimeLimit()` and `checkTimeDuration()` methods checks time constraints for Internet.

`IsInternetLimit Exceed()` method checks amount of data downloaded while browsing Internet. This information is sent to `PolicyEvaluator` class. `updateInternetCounter()` method implements a counter that sums browser activity and sent it to `PolicyEvaluator` class. `CoreTask`: It is pre-defined class having `getDataTraffic()` method which returns traffic usage information on interface level. `BandwidthRateLimit()` gets traffic usage information from `getDataTraffic()` method to limit Internet rate. There are few other methods involved which are skipped from discussion. Flow of implemented classes and methods is shown in Fig.4.

6 Performance Evaluation and Conclusion

We performed evaluation tests in order to testify performance of our implemented model. We developed our model as a framework application and port it to developer's version of Android known as Android Developer Phone (ADP). The ADP we used is Android Dev Phone 1 (first version) of HTC Dream (known as the T-Mobile G1). ADP is used to run and test custom developed OS and framework applications. We calculate mean of execution time of our implemented methods in milliseconds as shown in Performance evaluation chart

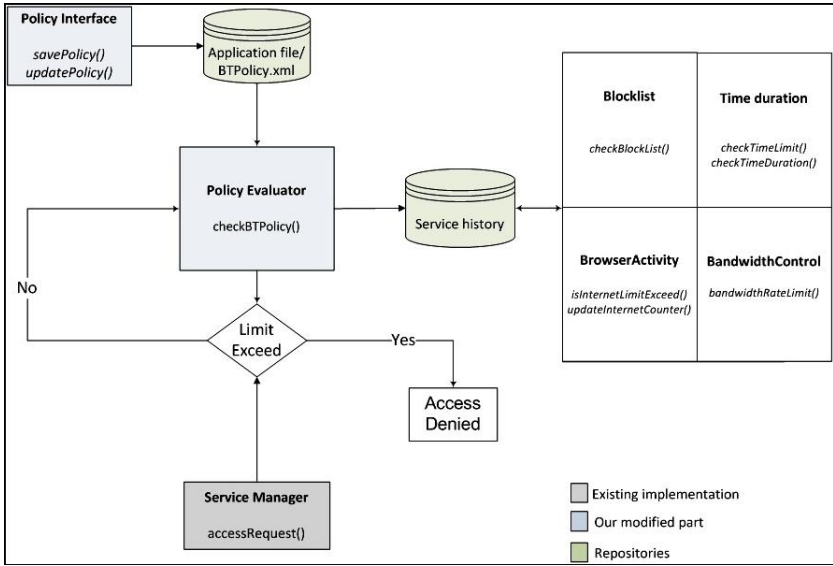


Fig. 4. Classes and methods involved in implementing proposed model

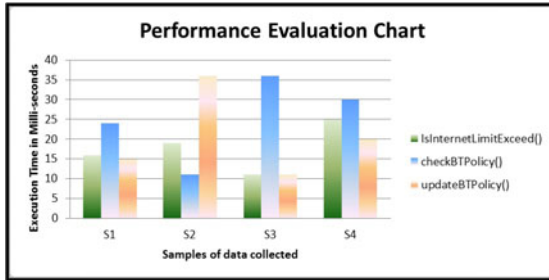


Fig. 5. Performance Time execution chart

(Fig.5). Execution time is calculated using `system.nanoTime()` method. Methods like `getBondedDevices()`, `device.getname()` and `getAddress()` are executed when the device requests for information of pairing process or checks block list and not recalled during policy enforcement, so we can exclude its execution time. Methods like `checkTimeLimit()`, `checkTimeDuration()`, `checkBlockList()` compares resource attributes with policy attributes. Execution time of these methods are short and varies in milliseconds. We include execution time for methods like `checkBTPolicy()` and `updateBTPolicy()` as it requires reading and writing to Policy.xml file. Overhead for these methods reach to maximum of 35 milliseconds which is less. We calculate memory consumption of Policy Evaluator. Current memory of RAM consumed by Policy Evaluator is 12 Mbytes while peak value reaches to 15 Mbytes. Memory consumption of Policy

Evaluator shows that it consumes less memory compared to other applications running in Android. Normally applications consumes average of 20 to 40 Mbytes in memory. Bluetooth Internet access points are nowadays more powerful, providing faster dial-up services to clients. Simulation result shows that Bluetooth access point is faster and efficient compared to dial-up modem. [10].

Conclusion

Authorization is one of essential security requirements in wireless networks. Authorization scheme currently provided by Bluetooth is binary. Access to service is either is allowed or denied. This needs to be fine grained providing user with more refined control over the shared resources. For this purpose we develop a comprehensive model that enables user to share resources conformed to policy. Proposed model widens concept of authorization. Policies are created using GUI. Resources shared with devices are thus subjected to constraints defined in policy file. We implement proposed model as framework application for Android. Proposed scheme can be incorporated in devices that uses Bluetooth.

References

1. Albrecht, M., Frank, M., Martini, P., Schetelig, M., Vilavaara, A., Wenzel, A.: Inst. of Comput. Sci. IV, Bonn Univ.: IP services over Bluetooth: leading the way to a new mobility. In: Local Computer Networks, LCN 1999 Conference (1999)
2. Limitations of Android emulator.: Using the Android Emulator, <http://developer.android.com/guide/developing/devices/emulator.html>
3. Nguyen, L., Safavi-Naini, R., Susilo, W., Wysocki, T.: Centre for Comput. Security Res. In: 10th IEEE International Conference on Secure Authorization, Access Control and Data Integrity in Bluetooth, ICON 2002, pp. 428–433. Wollongong Univ., Australia (2002) ISSN: Print ISBN: 0-7803-7533-5
4. Kim, J., Kim, J., Lim, Y., Yoon, J., Min, S.L., Ma, J.S.: A Bluetooth-based high-performance LAN access point incorporating multiple radio units. In: Proc. Int. Conf. on Comm. in Computing CIC, Las Vegas (2001)
5. Nauman, M., Khan, S.: Design and Implementation of a Fine-grained Resource Usage Model for the Android Platform. The International Arab Journal of Information Technology 8(4) (October 2011)
6. Scarfone, K., Padgett, J.: Guide to Bluetooth security Special publication 800-121. National Institute of Science & Technology US Department of Commerce
7. Bluetooth Tutorial - Profiles Table of Contents, <http://www.palwireless.com/infotooth/tutorial/profiles.asp>
8. Bluetooth PAN profile.: Personal Area Networking Profile, grouper.ieee.org/groups/802/15/Bluetooth/PAN-Profile.pdf
9. Nicolas Rouhana University, Nicolas Rouhana.: Bluetooth Web Internet Gateway (2002), <http://citeseerx.ist.psu.edu/viewdoc/summary?doi=10.1.1.19.4024>
10. Lim, Y., Kim, J., Min, S.L., Ma, J.S.: Dept. of Mech. Eng., Seoul Univ. Performance evaluation of the Bluetooth-based public Internet access point. In: Proceedings of 15th International Conference on Information Networking (2001)

A Comparative Study on Particle Swarm Optimization and Genetic Algorithms for Fixed Order Controller Design

Faizullah Mahar¹, Syed Saad Azhar Ali¹, and Zuhaibuddin Bhutto²

¹Department of Electronics Engineering Iqra University, Karachi, Pakistan

²Department of Computer System Engineering Balochistan University of Engineering and Technology, Khuzdar

lakhvi@yahoo.com, saadazhar@iqra.edu.pk,

zuhaib_bhutto@hotmail.com

Abstract. This article deals with a performance evaluation of particle swarm optimization (**PSO**) and genetic algorithms (**GA**) for fixed order controller design. The major objective of the work is to compare the ability, computational effectiveness and efficiency to solve the optimization problem for both algorithms (**PSO** and **GA**). All simulation has been performed using a software program developed in the Matlab environment. As yet, overall results show that genetic algorithms generally can find better solutions compared to the **PSO** algorithm. The primary contribution of this paper is to evaluate the two algorithms in the tuning of proportional integral and derivative (**PID**)-controllers and minimization of cost function and maximization of robust stability in the servo system which represents a complex system. Such comparative analysis is very important for identifying both the advantages and their possible disadvantages.

Keywords: Evolutionary algorithm, optimization, robustness performance and **PID** controller.

1 Introduction

Particle Swarm Optimization (**PSO**) is a relatively new heuristic search technique, whose functioning is inspired by the swarming [1]. **PSO** is similar to genetic algorithm (**GA**), in terms of both evolutionary heuristic search techniques are population-based [2]. The **GA** has been popular in academic world and the industry mostly for the reason that of its easiness in implementation, and the aptitude to efficiently solve extremely nonlinear, mixed integer optimization problems of complex engineering systems [3]. This paper an attempt is made to inspect the claim that **PSO** has the same effectiveness as the **GA** in finding the global optimal solution. By implementing analysis the performance comparison of the **GA** and **PSO** has been implemented in design optimization problems.

The **PSO** was invented by Kennedy in **PSO**, a set of randomly initial swarm propagates in the design space towards the optimal solution over a number of moves based on large amount of information about the design space that is assimilated and

shared by all members of the swarm [4]. **PSO** is inspired by the ability of flocks of birds, schools of fish to adapt to their environment, find rich sources of food [5].

The **GA** was introduced in the mid 1970s by John Holland. The **GA** is inspired by the principles of genetics and evolution, and mimics the reproduction behavior observed in biological populations. The **GA** employs the principal of —survival of the fittest|| in its search process to select and generate individuals that are adapted to their design objectives. Therefore, over a number of generations, desirable traits will evolve and remain in the composition of the population. The **GA** is well suited to and has been extensively applied to solve complex design optimization problems because it can handle both discrete and continuous variables and nonlinear objective and constrain functions without requiring gradient information.

Currently, the most of industrial processes are controlled by the well-established **PID** control. The parameters K_p , K_i , K_d are selected to meet prescribed performance criteria, classically specified in terms of rise and settling times, overshoot, and steady state error [6]. The reputation of **PID** control can be credited to its simplicity and to its good performance in a wide range of operating conditions. Moreover, the controllers designed with the aid of modern control techniques are usually of high order, difficult to implement [7].

Also, the design procedures of **PID** controllers are simple, although, the tuning parameters are the trickiest ones in a **PID** controller, as optimal tuning parameters are difficult to find [8]. Therefore, researchers introduced advanced controllers such as **PID** self-tuning, model-based adaptive control, model predictive control, fuzzy control, optimal control, expert control, robust control, etc.

The other methods including optimal control, expert control, neural networks, etc., have been developed to address the issues of complexity. However, most require some kind of process model and high-level expertise. It is difficult to develop a general-propose, user-friendly, smart control system based on these control methods.

Recently, the evolutionary computations have purposed **GA** [9, 10] and **PSO** [11, 12] as open paths to a new generation of advanced process control. These advanced techniques to design industrial control systems are, in general, dependent on getting *optimum performance*, since the real world processes are very *complex*. The controller when facing with various types of disturbance those are unknown in most practical applications. Usually such an optimum system performance is defined by a continuous function which is obtained by minimizing the cost function (**CF**) and maximizing the robust stability.

The **GA** and **PSO** is non-gradient based optimization algorithm and belong to probabilistic search algorithms, which have attracted much interest from the research community [13-14]. These algorithms normally mimic some natural phenomenon. **GAs** have been widely applied to the design of controllers, used a standard **GA** to determine initial estimates for the values of **PID** parameters. **GAs** is tested for **PID** controller for nonlinear process and showed robustness and efficiency [10, 15 and 16] other several applications of **GA** appeared in [4, 7, and 17]. The **PSO** have also been used for tuning **PID** controller [18- 20] and have proved successful results.

The major objective of this paper is to compare the computational effectiveness and efficiency of two algorithms **GA** and **PSO**. The primary motivation of this work is to present a complete treatment on the design and application of **PSO** and **GA** for **CF** minimization and robust stability maximization in the presence of uncertainties.

2 Problem Formulation

To formulate the problem as an optimization and search problem, the original plant will be shaped by choosing the weighting functions and minimizing the **CF** of shaped plant. A set of controller parameters in pre-specified low fixed order controller is optimized by using **PSO** and **GA**. The lowest achievable value of gamma and corresponding maximum stability margin is calculated by the following equation [23]

$$\gamma = \varepsilon_{\max}^{-1} = \sqrt{1 + \lambda_{\max}(XZ)} \tag{1}$$

A controller K_{∞} stabilizes the original closed loop system and minimizes gamma.

$$\gamma = \underset{k}{\text{stab}} \left\| \begin{bmatrix} I \\ K_{\infty} \end{bmatrix} (I + G_s K_{\infty})^{-1} M^{-1} \right\|_{\infty} \tag{2}$$

The singular values of original plant are shaped $G_s = W_1 G_0 W_2$ by choosing W_1 and W_2 . The original plant G_0 and weighting functions are combined to form a shaped plant G_s . The weighting functions are chosen as:

$$W_1 = K_w \frac{s + \alpha}{s + \beta} \tag{3}$$

Where k_p, k_i, k_d are positive numbers, β is selected as small number ($\ll 1$) for integral action. The final controller is constructed by multiplying K_{∞} with weighting functions W_1 and W_2 as shown in Eq. (4)

$$K(s)_{\text{final}} = W_1 K_{\infty} W_2 \tag{4}$$

Assume that $K(p)$ is structure specified controller. The structure of controller is specified before starting the optimization process [27]. The p controller structure is taken as vector p of the controller parameters is given by $p = [k_p, k_i \text{ and } k_d]$. A set of controller parameters p is evaluated to minimize **CF**. By using eq. (4) controller $K(p)$ can be written as:

$$K(p) = W_1 K_{\infty} W_2 \tag{5}$$

It is assumed that W_1 and W_2 are invertible, therefore,

$$K_{\infty} = W_1^{-1} K(p) W_2^{-1} \tag{6}$$

By substituting eq. (6) in eq. (2), the H_{∞} -norms of the transfer matrix from disturbances to states, which has to be, minimized i.e. **CF** is written as:

$$\|T_{zw}\|_{\infty} = \left\| \begin{bmatrix} I \\ W_1^{-1} K(p) \end{bmatrix} (I + G_s W_1^{-1} K(p) (I \ G_s)) \right\|_{\infty} \tag{7}$$

The **PID** control is a linear control methodology [13]. The structure of **PID** controllers is very simple. They operate on the error signal; this is the difference between the desired output and the actual output and generates the actuating signal that drives the plant [14]. The **PID** controller has three terms: The basic three term structure of a

SISO PID controller is shown in Fig.1

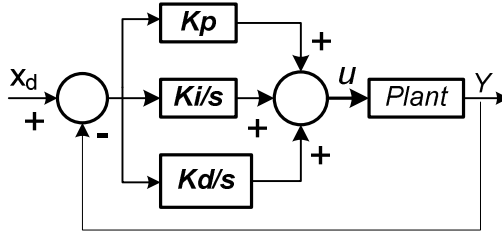


Fig. 1. PID Controller

Here X_d is the reference signal to track, X is the state of the system to control and u is the control action generated by the **PID** controller. K_p , K_i and K_d are the gains of the proportional, integral and derivative terms. These **PID** controllers have been found to be reasonably effective and easy to implement. Consequently, the **PID** controller is the standard controller design in the process industries. The **PID** standard form is given by the equation

$$u = K_p \cdot e + k_i \int e \cdot dt + k_D \cdot \frac{de}{dt} \tag{8}$$

The variety of **PID** controllers tuning techniques has been developed such as Ziegler-Nichols (**ZN**) [21-22]. However, since they rely on a minimum amount of dynamic information by making a certain assumption about nature of the controlled process, such as linearity, weak interactions within the process, absence of noise.

3 Particle Swarm Optimization

In recent years, **PSO** procedure appeared as promising technique for managing the optimization problems. **PSO** is population based technique that has many key advantages over other techniques. The **PSO** is general purpose optimizer that solves the wide range of optimization problems. In this work, the basic **PSO** algorithm that is explained in [24] has been implemented.

$$V_{id} = w \times V_{id} + c_1 \times Rand() \times (P_{id} - x_{id}) + c_2 \times Rand() \times (g_d - x_{id}) \tag{9}$$

$$x_{id} = x_{id} + V_{id} \tag{10}$$

$V_{id} \rightarrow$	Velocity of each particle in each dimension
$I \rightarrow$	Particle
$D \rightarrow$	Dimension
$W \rightarrow$	Inertia Weight
$c_1, c_2 \rightarrow$	Constants
$\text{Rand} () \rightarrow$	Random
$P_{id} \rightarrow$	Best position of each particle
$g_d \rightarrow$	Best position of swarm
$x_{id} \rightarrow$	Current position of each particle in each dimension

4 Genetic Algorithm GA

The literatures contain many versions of the **GA**. In this study, a basic **GA** with tournament selection, uniform crossover and one bit mutation is employed to solve the optimization problem. The **GA** represents the design variables of each individual design with that are referred to as chromosomes. It is important to note that the **GA** works with design parameters that allows for a combination of discrete and continuous parameters in one problem statement.

GA is a search method, starts the process with randomly initialization of population of 10 individuals. Then the fitness of each individual is calculated. The transmission of one population to next takes place by means of the genetic operators such as selection, crossover and mutation. The process chooses the fittest individual from the population to continue in the next generation [20]. Cross over randomly chooses a locus.

5 Simulation Results

The transfer function of original plant is shown in eq. (11)

$$G(s) = \frac{551.1e^{-0.12s}}{(s^2 + 43.26s + 536.9)} \tag{11}$$

To design the stabilizing controller by using H_∞ LSDP, the weighting functions are chosen as:

$$W_1 = \frac{0.80s + 4}{s + 0.001} \quad \text{and} \quad W_2 = I \tag{12}$$

Where I is the identity matrix, with these weighting functions the shaped plant is computed as:

$$G_S(s) = \frac{413.5s + 2205e^{-0.12s}}{s^3 + 43.26s^2 + 536.9s + 0.5369} \tag{13}$$

The stabilizing controller K_∞ is obtained by using H_∞ loop shaping design procedure is,

$$K_{\infty}(s) = \frac{413.5s + 2205}{s^3 + 43.36s^2 + 5369s + 0.5369} \quad (14)$$

By using the H_{∞} LSDP the final controller is obtained as:

$$K(s) = \frac{310.1s^2 + 3308s + 8221}{s^4 + 43.26s^3 + 537s^2 + 1.07s + 5.36 \times 10^{-2}} \quad (15)$$

The controller obtained by H_{∞} LSDP Eq. (15) is of 4th order which is double than that of the plant and its structure is complex as well. The investigation has been performed for **PID** controller as a fixed structure controller k_p , k_i and k_d are the controller parameters which are evaluated by using **PSO** and **GA**. The specific controller structure is expressed in equation

$$K(p) = k_p + \frac{k_i}{s} + k_d s \quad (16)$$

For **PSO**, The swarm size was limited to 10 particles. The velocity of each particle is randomized to a small value to provide initial random motion to the swarm. The most important factor is maximum velocity parameters which affect the convergence speed of the algorithm. The C1 and C are 3.0 and 2.5 correspondingly. The optimal solution of controller parameters was obtained which has satisfied stability margin of 0.716. The computed optimal values of controller parameters are shown in Eq. (17). The step response presents rise time 1.25 sec., about 2.5% overshoot and the settling time is about 1.23 sec.

$$K(p)^* = 0.939 + \frac{0.890}{s} + 0.212 s \quad (17)$$

For **GA**, the simulation started with population size of 10, tournament selection and single bit wise mutation was used. GA converged on 4th generation and gave optimal **CF** of 1.396. This has satisfied stability margin of 0.716. Obtained optimal values of controller parameters are shown in eq. (18).

$$K(p)^* = 0.833 + \frac{0.670}{s} + 0.322 s \quad (18)$$

The step response present 0.66 seconds rise time, 14% overshoot and the settling time 2.73 seconds, the results obtained clearly shows the effectiveness of proposed scheme.

To investigate PID controller parameters **ZN** technique was employed to find the values of specified controller parameters. Controller parameters were obtained experimentally by using **ZN** techniques based on the unit step response of the nominal plant. The controller parameters obtained using **ZN** technique is shown in eq. (19).

$$K(p)^* = 4.495 + \frac{12}{s} + 3.90s \quad (19)$$

The closed loop step response of the system present an over shoot of about 58 %, rise time 0.25 sec. and settling time 3.7 sec.

6 Comparison and Performance Analysis

The aim of control system design is to achieve desired time domain performance of the controlled system; usually this action is represented in terms of percentage overshoot, rise time and settling time etc.

Comparisons on performances between different controllers are represented in table 1 & 2. The settling time, oscillations and overshoot are compared. It is observed from the table 1 that the designed **GA-PID** controller exhibits comparatively good performance with very less settling time, overshoot and transient oscillations. The simulation results verify that **GA** method has better efficiency in solving optimization problem.

Table 1. Comparisons of Steady State Responses

	PSO	GA	ZN
Rise Time	2.87	2.73	3.7
%Overshoot	2.5%	14%	58%
Settling Time	1.26	0.66	0.25

The **GA**-based controller outperforms the **PSO**- based and Ziegler-Nichols (**ZN**) tuned controller in terms of settling time, rise time and percentage overshoot. However the optimized Cost function of both PSO and GA are almost equal Fig. 2 compares the performance of the **ZN** tuned designed controller with the **PID** tuned controller by the PSO and GA.

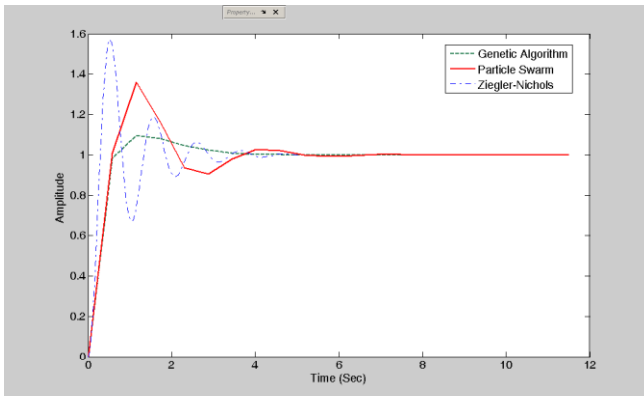


Fig. 2. Shows the step response PSO, GA and ZN

The **CF** value and the parameters of the controller optimized using **GA** and **PSO** were compared to that obtained by using **ZN** method. Results shown in table 2, indicates that **GA** and **PSO** gave much better solutions than conventional **ZN** technique.

Table 2. Comparison of PID Parameters Cost Function

Parameters	ZN	GA	PSO
k_p	4.495	0.833	0.939
k_i	12	0.760	0.890
k_d	3.90	0.322	2.12
Cost Function	2.38	1.395	1.396

The **PID** gains obtained by using **Z-N** method are quite high values as compared to **GA** and **PSO** methods. High controller gains may cause high frequency oscillations and saturation in the controller circuit. Moreover, the **CF** values of **GA** and **PSO** are also much better than **Z-N** method.

6.1 Controller Structure

The controller obtained from H_∞ **LSDP** in Eq. (16) is of 4th order, double as compared to the original plant under consideration and has complex structure as well. The controllers designed by using **PSO** and **GA** showing approximately equivalent performances have much lower order, i.e. fixed as first order.

6.2 Overall Performance

The overall performances of control system were tested for closed loop response with three controllers **PSO**, **GA** and **Z- N**, results are shown in Fig. 2, the results of overall performance comparison clearly show the advantage of using the **GA** -controller due to its best performance with respect to time domain specifications, and **CF** value.

6.3 Convergence Behavior

The comparisons were made in terms of convergence behavior; good cost function convergence values are reflected as shown in cost function versus iteration plots Fig.3 and Fig. 4, when evaluate the optimal values of **CF** obtained using **GA** and **PSO**. It seems quite clear the benefit of using **PSO** for this type of optimization problem, since it provides optimal **CF** in fewer generations. Moreover the two algorithms almost converge to the same value of **CF**.

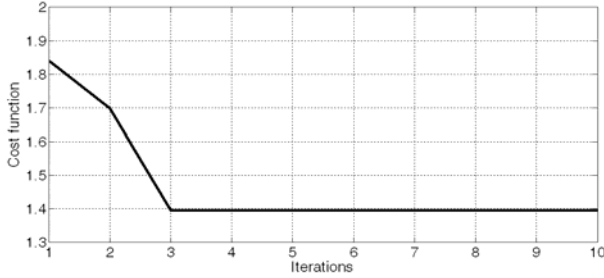


Fig. 3. Conversion of cost function versus the generation of PSO

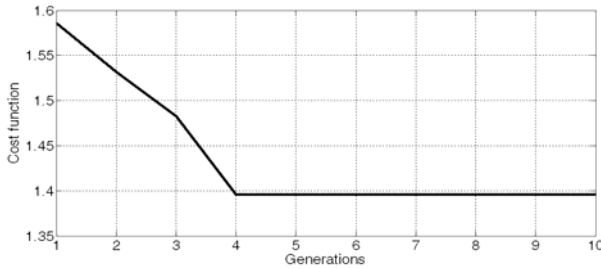


Fig. 4. Conversion of cost function versus the generation of GA

6.4 Robustness Check

In order to validate the suitability and robustness of designed controllers, some parameters of the nominal plant in Eq. (11) were varied as follows:

$$G_{\Delta}(s) = \frac{551.1e^{-0.12s}}{(8s^2 + 43.26s + 536.9)} \tag{20}$$

The designed optimal controller Eq. (20), obtained by running **GA** was implemented to control the perturbed plant Eq. (20).

The step response of perturbed plant is almost same as step response of original plant with some difference in settling time. The result shown in Fig. 5 demonstrates that the designed controller from the proposed scheme have reasonably good performance and robustness.

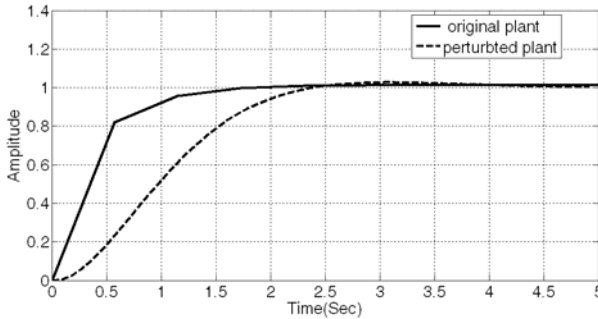


Fig. 5. Conversion of cost function versus the generation of PSO

7 Conclusion

In this work, we have presented a comparison study of using **PSO** and **GA** algorithms for the tuning of **PID** controllers. For processes which represent a subsystem of complex industrial processes. Simulation results showed that the **PID** control tuned by **GA** provides an adequate closed loop response. The proposed **GA** based **PID** controller provides an acceptable stability between frequency overshoot and transient oscillations with zero steady state error. The simulation results express the success of the proposed approach of controller design. This work can be extended by including non-linear parameters to the system modeled and there by comparison can be made with respect to linear system.

References

1. Kennedy, J., Eberhart, R.: Particle Swarm Optimization. In: Proceedings of the IEEE International Conference on Neural Networks, Perth, Australia, pp. 1942–1945 (1995)
2. Kennedy, J., Eberhart, R.: Swarm Intelligence, 1st edn. Academic Press, San Diego (2001)
3. Goldberg, D.: Genetic Algorithms in Search, Optimization and Machine Learning, pp. 1–25. Addison-Wesley, Reading (1989)
4. Venter, G., Sobieski, J.: Particle Swarm Optimization. In: 43rd AIAA/ASME/ASCE/AHS/ASC Structures, Structural Dynamics, and Materials Conference AIAA 2002-1235, Denver, CO (April 2002)
5. Ahmad, S., Pedrycz, W.: A Comparative Study of Genetic Algorithms, Particle Swarm Optimization, and Differential Evolution in Problem of Feature Selection through Structure Retention. In: Proc. GEM, pp. 49–54 (2010)
6. Astrom, K., Haggglund, T.: The future of PID control. Control Engineering Practice 9, 1163–1175 (2001)
7. Astrom, K., Haggglund, T.: PID controllers: Theory, design, and tuning, 2nd edn. Instrument Society of America (1995)
8. Cipperfield, A., Flemming, P., Fonscea, C.: Genetic Algorithms for Control System Engineering. In: Proceedings Adaptive Computing in Engineering Design Control, pp. 128–133 (1994)

9. Houck, C., Joines, J., Kay, M.: A Genetic Algorithm for Function Optimization: A MATLAB Implementation. *ACM Transactions on Mathematical Software* (1996)
10. Kennedy, J., Spears, M.: Matching Algorithms to Problems: An Experimental Test of the Particle Swarm and Some Genetic Algorithms on the Multimodal Problem generator. In: *Proceedings IEEE International Conference of Evolutionary Computation* (1998)
11. Kennedy, J., Eberhart, C.: Particle Swarm Optimization. In: *Proceedings of the IEEE International Conference on Neural Networks, Australia*, pp. 1942–1948 (1995)
12. Easter, S., Subramanian, S., Solomon, S.: Novel technique for PID tuning by particle swarm optimization. In: *Proceedings 7th Annu. Swarm Users/Researchers Conf.* (2003)
13. Flemming, P., Purshouse, R.: Evolutionary Algorithms in Control System Engineering: A Survey. *Control Engineering Practice* 10, 1223–1241 (2002)
14. Gaing, Z.L.: A particle swarm optimization approach for optimum design of PID controller in AVR system. *IEEE Transactions on Energy Conversion* 19(2), 384–391 (2004)
15. Goldberg, D.: *Genetic Algorithms in Search, optimization, and Machine Learning*. Addison-Wesley (1989)
16. Herrero, J., Blasco, X., Martinez, M., Salcedo, J.V.: Optimal PID Tuning with Genetic Algorithms For Non Linear Process Models 15th Ifac, Span (2002)
17. Kennedy, J., Eberhart, C.: *Swarm Intelligence*. Morgan Kaufman (2001)
18. Michalewicz, Z., Dasgupta, D.: *Evolutionary Algorithms in Engineering Applications*. Springer, Heidelberg (1997)
19. Wang, Q., Spronck, P., Tracht, R.: An Overview of Genetic Algorithms Applied To Control Engineering Problems. In: *Proceedings of the 2nd International Conference on Machine Learning and Cybernetics* (2003)
20. Wang, P., Kwok, D.P.: Optimal Design of PID process controllers based on genetic algorithms. *Control Engineering Practice*, 641–648 (1994)
21. Zheng, Y., Ma, L., Zhang, L., Qian, J.: Robust PID Controller Design using Particle Swarm Optimizer. In: *Proceedings of IEEE International Symposium on Intelligence Control*, pp. 974–979 (2003)
22. Ziegler, J., Nichols, N.: Optimum settings for automatic controllers. *Transactions of ASME* 64, 759–768 (1942)
23. Mahar, F., Saad Azhar, S.: PSO Based Fixed Order Controller Design and System Simulation. In: *International Conference on Soft Computing and Pattern Recognition (SoCPaR 2010)*, France, vol. 1, pp. 152–155 (2010)
24. Mahar, F., Saad Azhar, S.: Immune Algorithm Based Fixed Order Controller Design and System Simulation. In: *IEEE International Symposium on Signals, Systems and Electronics, Nanjing, China*, vol. 1, pp. 18–25 (2010)

Design of WLAN Patch and UWB Monopole Antenna

Faraz Mahmood¹, Syed Muhammad Usman Ali^{2,3}, Mahmood Alam⁴,
and Magnus Willander³

¹ Research and Development, Downlink Radio Design, PDU Hardware Design Department,
Ericsson AB, Sweden

faraz.mahmood@ericsson.com

² Department of Electronic Engineering, NED University of Engineering and Technology,
Karachi, Pakistan

uashah68@neduet.edu.pk

³ Physical Electronics and Nanotechnology Division, Campus Norrköping,
Linköping University, SE-60174 Norrköping, Sweden

syéal@itn.liu.se

⁴ Geo Physics/Earth and Environmental Sciences Bahria University, Karachi, Pakistan

Abstract. This paper demonstrates the comparative analysis of the performances of two antenna designs, half wavelength Wireless Local Area Network (WLAN) patch antenna and a broadband Ultra wideband (UWB) monopole antenna. Both the antenna designs have been simulated utilizing the Advanced Design System (ADS) tools. During the investigations, it has been observed that the low profile antenna with its wide impedance bandwidth, quasi-Omni directional radiation pattern and high efficiency is quite promising for the existing communication and surgical instruments. In this work, we have simulated and measured the different essential parameters such as input reflection; voltage standing wave ratio (VSWR), radiation pattern, simulated current distributions and the efficiency of the proposed designs are also presented and analyzed. Measured results were taken using a Vector Network Analyzer (VNA).

Keywords: Voltage standing wave ratio, broadband antenna, Input reflection, low profile, Efficiency, Impedance bandwidth.

1 Introduction

An antenna is a transducer that converts electrical energy into electromagnetic waves (EM) in a transmitter and vice versa in a receiver. The alternating current fed into a transmitting antenna generates a corresponding alternating EM field which propagates in space and induces a voltage in the receiver. The antennas are categorized on the basis of physical structure like wire antenna, reflector antenna, aperture antenna, micro-strip antenna etc. Patch antenna is a micro-strip type having a conductor of specific length of half the wavelength separated from a ground plane by a dielectric. Current is fed into the conductor at the edge of the patch. Patch antenna relatively has a narrow bandwidth of operation and radiation field is mainly attributed to the fringing fields around the edges. The compact size of a patch antenna makes it suitable for fabrication on a printed circuit board. Patch antennas find widespread applications in radio frequency identification (RFID) tags, Bluetooth, wireless local

area networks. Monopole is a wire type antenna with a conductor placed perpendicular to larger ground plane. The feeding point is the lower end of the conductor. Radiations emitting from the conductor get reflected by the ground plane and reflected radiation field can be attributed to an equivalent image conductor. The radiation pattern from a monopole antenna is isotropic and directivity twice as that of dipole antenna owing to the fact that no radiation occurs below the ground plane. Walkie talkie, older cell phones, car mounted antennas are some of the generic applications of monopole.

2 Antenna Parameters

There are various parameters for an antenna which decide the operation, characteristics of propagation and efficiency. Resonant frequency, bandwidth, input reflection coefficient (S_{11}), voltage standing wave ratio (VSWR), antenna efficiency, radiation pattern, directivity are major arguments for design of an antenna. Resonant frequency determines the physical structure of the radiating elements and dimensions are inversely related to the frequencies. The range of frequencies in which antenna radiates is the bandwidth. In a patch antenna the spacing between the conductor and the ground plane and width of the conductor affects the bandwidth. The designed monopole antenna has a bandwidth of 4.5 to 10 GHz. VSWR and S_{11} are the parameters indicating the extent to which the driving circuitry is matched to the antenna. VSWR ranges from one to infinity corresponding to the mismatch and higher value degrades the antenna performance [1]. The radiation patterns are plotted on both elevation and azimuthal angles. It is desirable to have the larger radiation in the direction of the receiver which is represented by term directivity [2]. Beam width represents the angular width in which maximum radiation occurs. Patch antennas are directional compared to monopole antenna. Antenna efficiency can be described in terms of matching, resistive losses and radiation losses. Distance metrics such as far field region and near field are also the criteria for antenna design to particular application.

3 Antenna Design Specifications

The different parameters that need to be considered for designing and fabricating the antenna are discussed in this paper. Matlab scripts written to simulate the operation of antenna provide a better visualization. The specifications which decide these parameters are listed in Table 1.

Table 1. Specifications For Patch And Wideband Monopole Antenna

Roger's substrate	R04350B
Height	0.254 mm
Permittivity	3.48
Loss tangent	0.004
Metal thickness	18 μm
Conductivity	5.8e7 S/m
Patch antenna Centre frequency	2.4 GHz
Monopole bandwidth	4.5-10 GHz

The specifications mentioned in table 1 are for Rogers R04350B used for the simulations in ADS also the same substrate has been used to Fabricate the Prototype of Monopole antenna as shown in Fig.7 below. ADS is a 2.5D electromagnetic simulator that uses Method of Moments (MoM) to solve Maxwell equations. The MoM is a numerical technique used to solve differential and integral equations [3].

4 Patch Antenna Design

The patch antenna is designed to operate at a resonant frequency 2.4 GHz. Considering the fringing effect the antenna length was calculated utilizing matlab scripts. The width of 41.8 mm and length of 33.5 mm resulted from the design. The input impedance of the antenna is controlled by the width because the increase in surface area of the conductor lowers input impedance [4]. Edge resistance can also be matched by probe feed or inset feed line. Inset feed line was chosen for our design. Inset feed line extends the transmission line of characteristic impedance 50Ω into the conductor plate until the input impedance of the antenna becomes equal to 50Ω . We used an inset width of 2 mm and inset feed length was experimentally determined by momentum tool in Advanced Design System (ADS) which results in best matching. VSWR measurements revealed a value of 2 which is a standard for antennas for handheld devices. Skin effect was also observed which makes the current flow on the sides of the antenna at larger frequencies.

Fig. 1, shows the layout of Patch antenna having a dimension of 42mm x 33.5 mm with inset feeding used to produce a Perfect match at the resonant frequency.

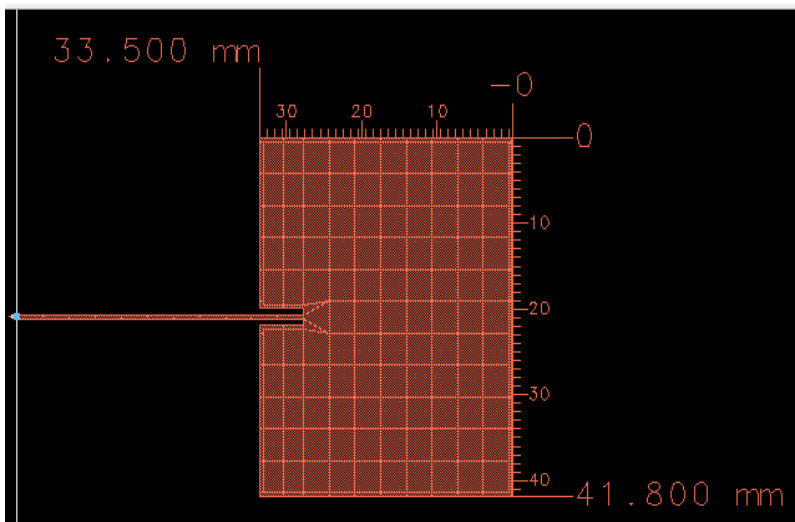


Fig. 1. Layout of Patch Antenna

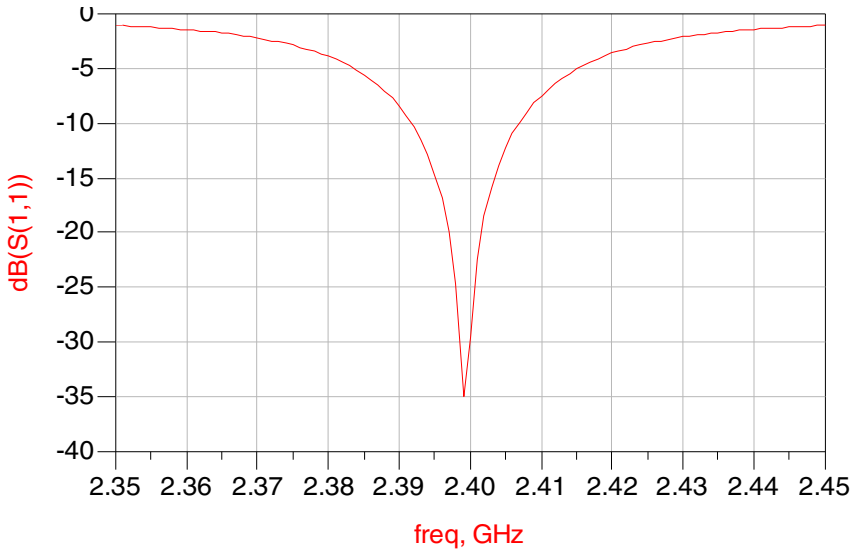


Fig. 2. S11 response of patch antenna

Fig. 2, shows the input reflection S_{11} below -10 dB at 2.4 GHz which is considered as a primary requirement for any antenna design.

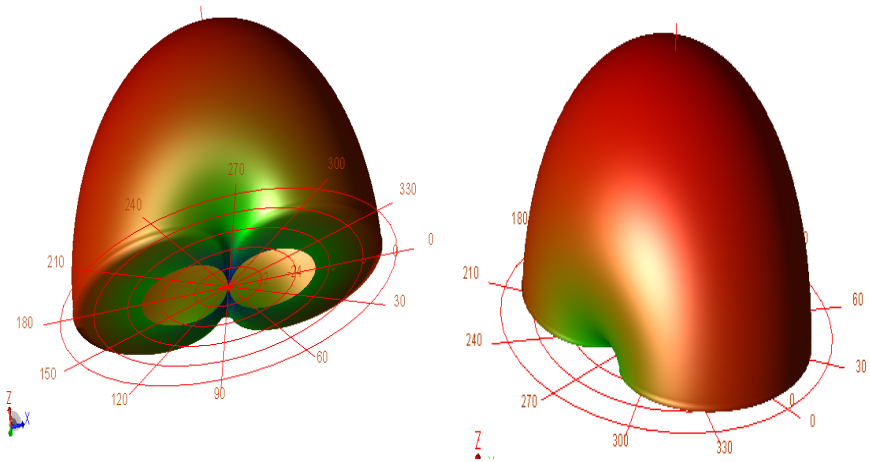


Fig. 3. Radiation Pattern of Patch antenna

Fig. 3 shows a highly directional radiation pattern at the resonant frequency for a Patch antenna, fig 3 shows different 3 directional views of the radiation pattern.

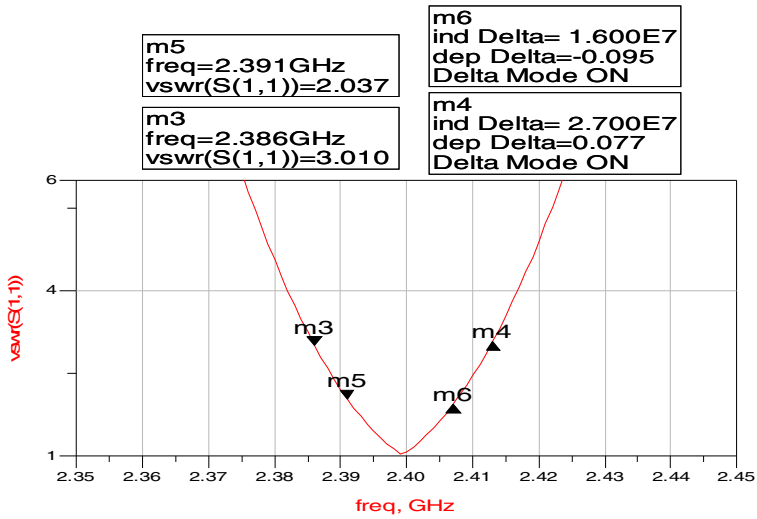


Fig. 4. Voltage standing wave ratio of Patch antenna

Fig. 4 shows the voltage standing wave ratio for Patch antenna at 2.4 GHz equal to 2 which corresponds to input reflection of 10 dB.

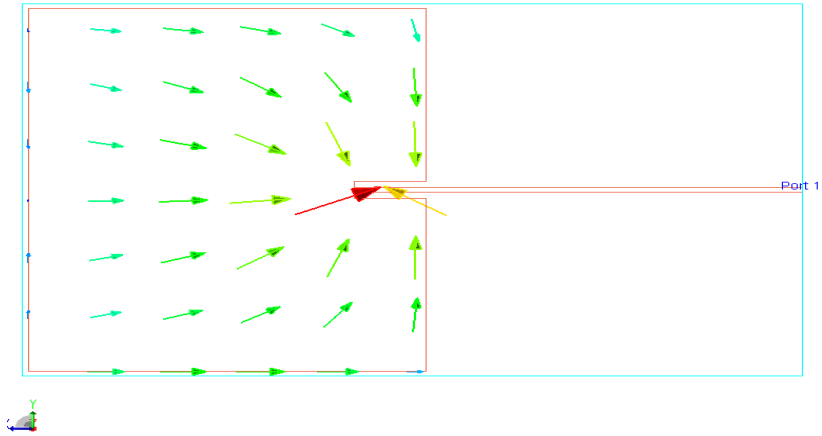


Fig. 5. Simulated Current distribution at 2.4 GHz

Fig. 5 shows a simulated distribution of the imaginary parts of electric currents for antenna operating at resonant frequency.

5 Monopole Antenna Design

Monopole antenna operation is much dependent on the large ground plane which is used as reference for input feed current [5]. The shape of the monopole antenna varies the impedance bandwidth of operation and circular or rectangular shapes provide a larger impedance bandwidth [6]. References [7-8] investigate the ground planes especially, square and circular planes for monopole antennas.

Parallel ground plane are employed to miniaturize antenna and with a slight impact in radiation pattern. Experimental investigation was done based on a square and a rectangular ground plane structures. Values of S_{11} over impedance bandwidth were measurement criteria for the analysis by maintaining either width or length constant for two ground planes. It has been observed that the width change has a greater effect than length when having a large ground plane as shown in figure 6 below [7].

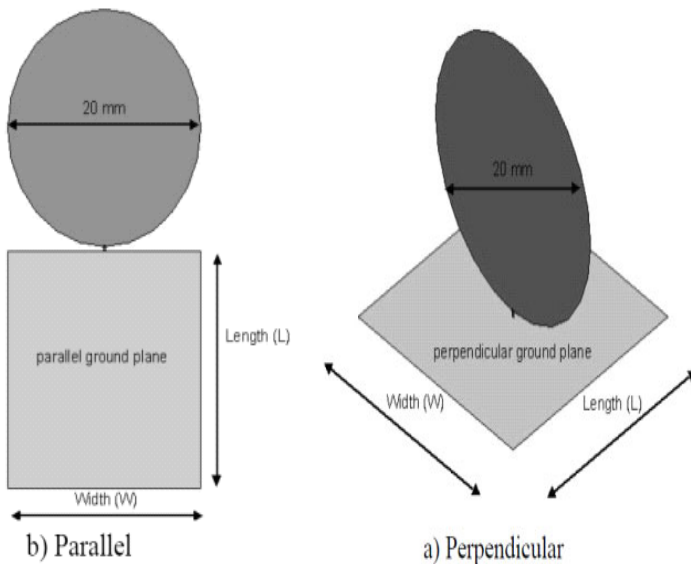


Fig. 6. Showing perpendicular and parallel ground planes

The monopole antenna is always regarded as equivalent to one half of a dipole and correspondingly the length of the antenna is one quarter of wavelength ($\lambda/4$) [9]. The design we prepared was a square monopole antenna with conductor and ground plane on opposite sides of the dielectric. The antenna is composed of alternate free space and metallic layers on the Roger's substrate R04350B. The dimension of the antenna is calculated from its lowest frequency considering nearing value of 5.5 GHz. The calculated antenna linear dimension is a square of side 13.6 mm [10].

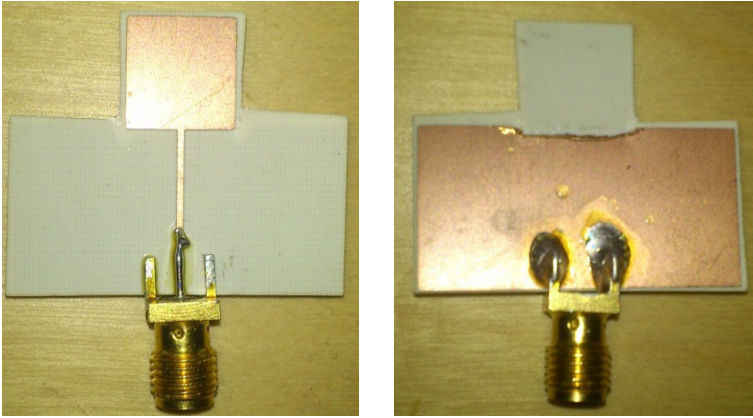


Fig. 7. Prototype of Monopole antenna showing the top and bottom view

Figure 7 shows the Prototype of broadband Monopole antenna fabricated using Rogers 4350B having a permittivity of 3.48.

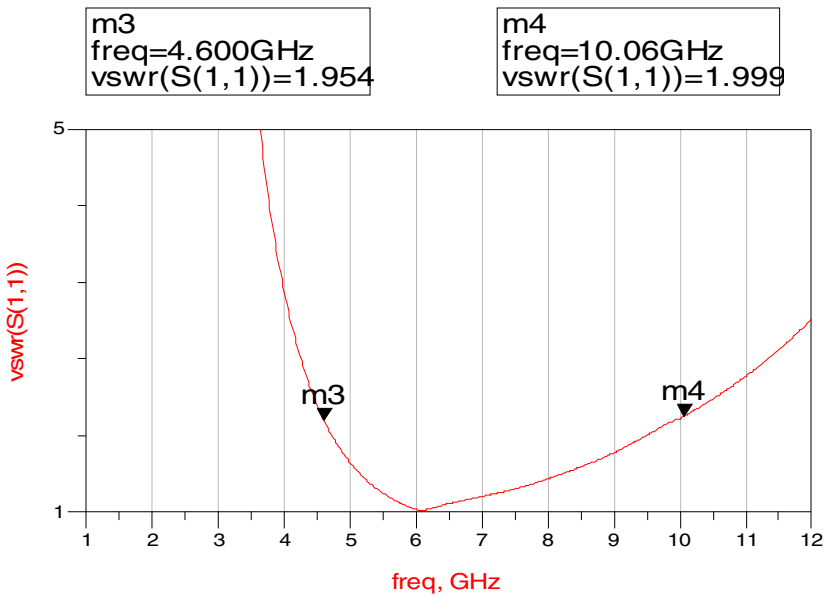


Fig. 8. Simulated Voltage standing wave ratio of Monopole Antenna

Fig. 8 shows the simulated Voltage standing wave ratio less than 2 in the frequency band from 4.5 to 10 GHz. The markers m3 and m4 show the region where VSWR is less than 2 which is an important criterion for antennas for wireless applications.

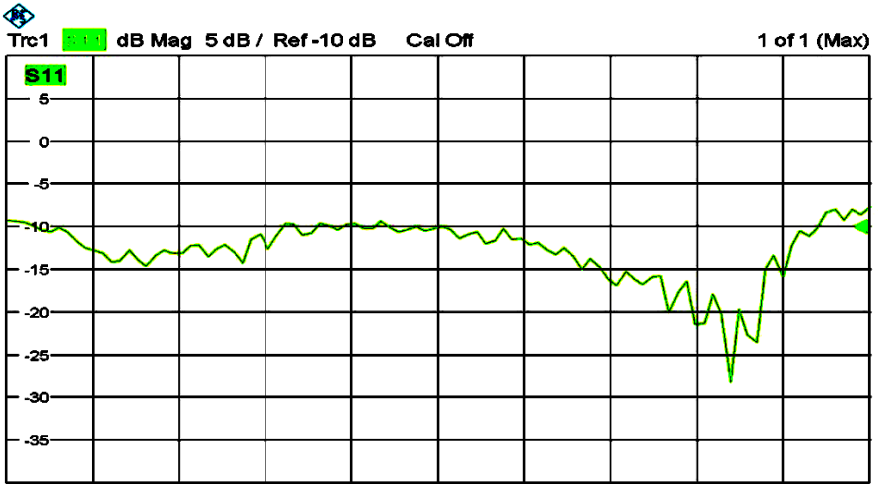


Fig. 9. Measured Return Loss of wideband Monopole antenna

Fig. 9 shows the measured results obtained from Rohde and Schwarz Vector Network analyzer the results show a very broadband Input reflection response in the frequencies of interest.

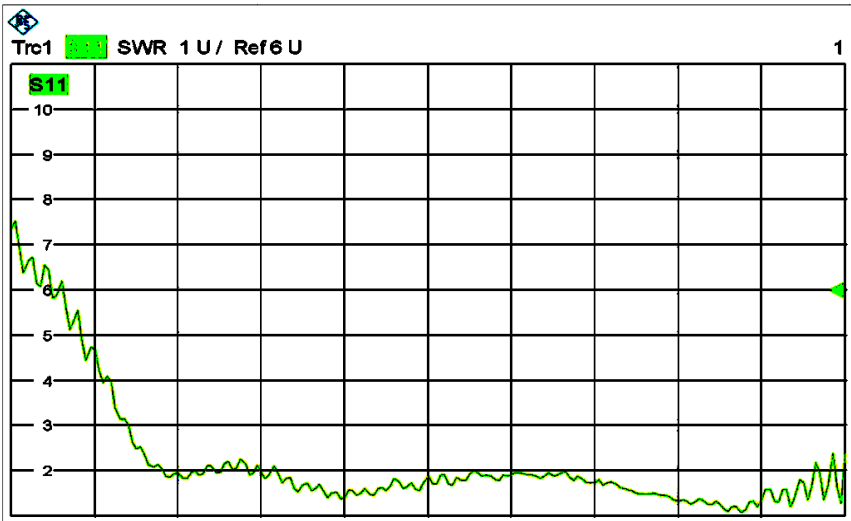


Fig. 10. Measured Voltage standing wave ratio of Monopole antenna

Fig. 10 shows the measured VSWR < 2 in a broadband range of frequencies which is suitable for any wireless application based antenna.

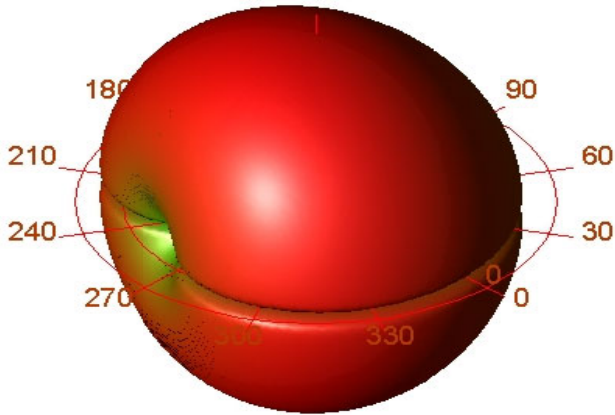


Fig. 11. Omni Directional Radiation pattern of Monopole antenna

Fig. 11 shows the radiation pattern of a 2 Dimensional radiator at 900 MHz having a very uniform Omni-directional and nearly linearly polarized pattern at both the lowest and highest frequencies of design.

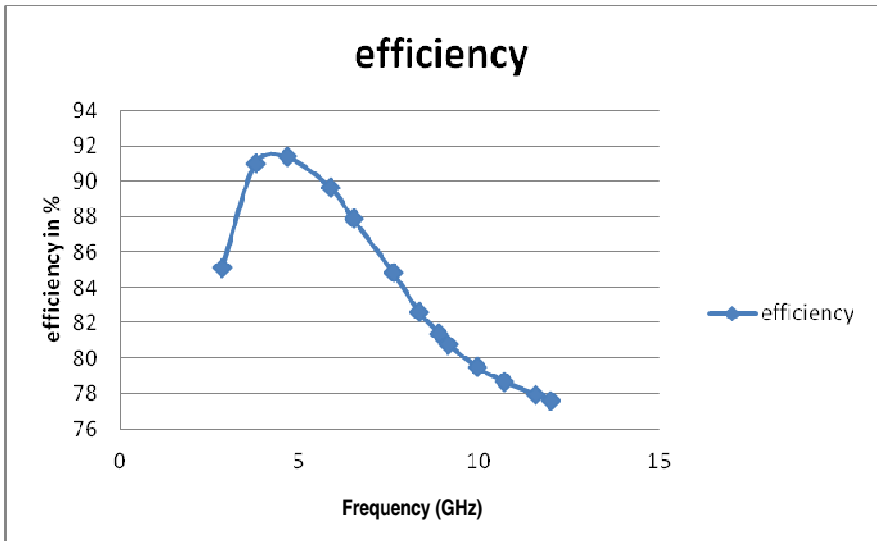


Fig. 12. Measured Efficiency of Broadband Monopole antenna

Fig. 12 shows high efficiency in the frequencies from 4 to 10 GHz although the efficiency is not high at the higher frequencies as compared to that at the lower frequencies but still it is quite high for a UWB antenna.

Table 2. Dimensions of Fabricated Monopole Antenna

P	0.2 mm
Ground width	30 mm
Antenna Length	10 mm
Ground Height	15 mm

Table 2 shows the dimensions of the fabricated monopole antenna shown in fig.7 as table 2 shows clearly a minaturized design.

6 Conclusion

This paper discusses the design and analyses of the patch and UWB monopole antenna. It has been observed that the patch antenna operates at a lower bandwidth and this can be improved by increasing the thickness of the substrate between the conductor patch and the ground plane. The directivity is higher compared to monopole antenna because of the larger ground plane which causes energy in the back side lobe to be added front side lobe. Similarly, the monopole antenna approximates to an omnidirectional antenna and directivity improves at higher frequencies because electrical length gets smaller at higher frequencies. It was desired that the antenna has a larger bandwidth to avoid shift in the frequency and better performance in presence of other disturbing sources. Due to slight variation in precision the operating frequency may shift to a large extent. The bandwidth improves with substrate thickness and skin effect causes current to be concentrated at the edges at high frequencies. These antennas can find much application including Wireless Orthopedic Pin for Bone Healing and Growth, Real-Time Non coherent UWB Positioning Radar, Real-time UWB indoor positioning system with millimeter 3-D dynamic accuracy.

References

1. Clarke, R., Karunaratne, R., Schrader, C.: Ultra-Wideband Antenna, EE198B (fall 2004)
2. Balanis, C.A.: Antenna Theory, Analysis and Design, 2nd edn. John Wiley & Sons, Inc. (1982) ISBN: 0-471-59268-4
3. Agilent Technologies Inc. Advanced Design System (ADS), <http://www.agilent.com/find/eesof-ads> (viewed (September 9, 2011))
4. Ray, K.P.: "Research Article" Design Aspects of Printed Monopole Antennas for Ultra-Wide Band Applications. Hindawi Publishing Corporation (2008)
5. Sharkawy, M.H.A., Eldek, A.A., Elsherbeni, A.Z., Smith, C.E.: Design of Wideband Printed Monopole Antenna Using WIPL-D: ACES (April 2004)
6. Hamed, M.: Study of multi-band and ultra-wideband antennas 6-8.5 GHz. Master Thesis at Linköping university, LiTH-ITN-PR-07/018—SE
7. Liang, J.L., Chiau, C.C., Parini, C.G.: Analysis and design of UWB disc monopole antennas. IEEE Transactions on Antennas and Propagation 46(2), 294–295 (1998)
8. Gandhi, O.P., Lazzi, G., Furse, C.M.: MONOPOLE ANTENNAS Electrical & Computer Engineering Department University of Utah Salt Lake City, UT 84112-9206
9. Fundamentals of antenna theory Monopole, Antenna-Theory, <http://www.Antenna-Theory.com> (visited January 7, 2012)
10. Pozar, D.M.: Microwave Engineering, 3rd edn. John Wiley & Sons (2005)

Single-Bit Ternary FIR Filter in FPGA Using Canonical Signed Digit Encoding

Tayab D. Memon, Abdullah Alhassani, and Paul Beckett

School of Electrical and Computer Engineering,
Royal Melbourne Institute of Technology (RMIT),
Melbourne, Victoria, 3001
{tayab.memon, pbeckett}@rmit.edu.au,
eng_alhassani@hotmail.com

Abstract. Sigma-delta modulation based single-bit ternary DSP algorithms have been extensively studied in the literature. More recently, FPGA based design and analysis of ternary FIR filter with distributed arithmetic (DA) algorithm have been reported in comparison equivalent multi-bit systems. In this paper, we present the design and synthesis of single-bit ternary and multi-bit (i.e., conventional) FIR filters using a more complex but efficient encoding technique called canonical signed digit (CSD) in both pipelined and non-pipelined modes. Both filter types are coded into VHDL and synthesized using small commercial FPGA devices in Quartus-II. Synthesis results show that in pipelined mode single-bit ternary FIR filter offers approximately 90% better clock performance than multi-bit FIR filter. Single-bit ternary FIR filter achieved clock frequency of 370 MHz using Stratix-III device that can easily process a 6-MHz video signal transmission. The single-bit DSP systems are highly beneficial for mobile communication purpose.

Keywords: Sigma-delta Modulation, CSD Encoding, FPGA Implementation, Ternary FIR-like Filter, VHDL.

1 Introduction

Short Word Length (SWL, often single-bit) sigma delta modulated general purpose DSP applications have been shown to be hardware efficient and easy to implement [1-2]. Sigma-delta modulation, which is already widely accepted for data conversion purpose (i.e., ADC/DAC), can be utilized to generate the filter coefficients in a ternary format $\{+1, 0, -1\}$ [1]. In this way, DSP algorithms developed using SWL techniques result in simple multiplication, which can be performed via simple AND-OR logic gates or a very small look up table (LUT) [3]. As multiplication is the most complex part of multi-bit signal processing, the SWL approach can lead to significantly reduced silicon space and power consumption. A single-bit ternary FIR filter, which assumes that the coefficients are from the ternary set of $\{+1, 0, -1\}$ [4], is reported in [5] using a 2's complement technique. In [5], the authors has shown that

the single-bit ternary FIR filter has a better area-performance results than its equivalent multi-bit filter (i.e., using a conventional approach).

In multi-bit systems, canonical signed digit (CSD) encoding technique has proved to be an efficient way of hardware implementation that reduces chip area and improves the performance of system [6-7]. In this paper, we extend the work reported in [8,5] and compare the single-bit ternary FIR filter with multi-bit systems using a more complex but efficient CSD encoding technique.

The remainder of this paper proceeds as follows. In section 2, we discuss about ternary FIR filter that is followed by introduction to CSD encoding technique. Section 3, discusses the VHDL design and synthesis of the two filters. Simulation and results are discussed in section 4 that if followed by conclusion and point to future in section 5.

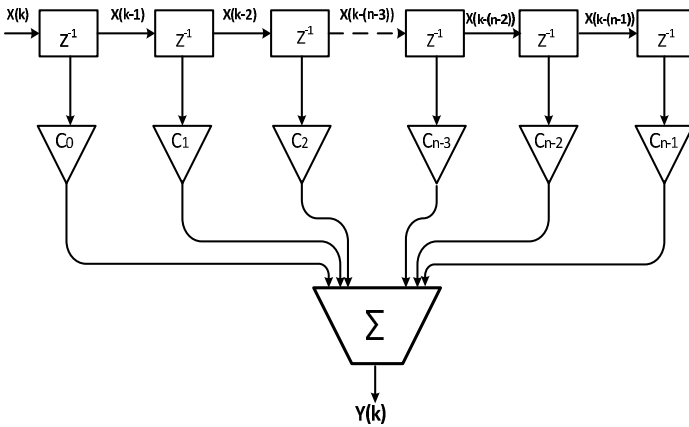


Fig. 1. Architecture of single-bit ternary FIR filter

2 Ternary FIR Filter

As shown in Fig 1 , the single-bit ternary FIR filter architecture is essentially the same as a conventional filter except that it draws its coefficients from a ternary set i.e., $\{+1,0,-1\}$. The overall filter operation can be defined as the convolution of ternary taps (h_i) with an input bit-stream (x_i) given below:

$$y(k) = \sum_{i=0}^M h_i x_{i-k} \tag{1}$$

where M is the order of the single-bit ternary FIR filter (\equiv Number of ternary taps), which depends upon the OSR of sigma-delta modulator. These ternary taps are generated after passing target impulse response (TIR) through a second order sigma-delta modulator as shown in Fig 2. Target Impulse Response (TIR) can easily be generated using commonly available filter design techniques. We have used the Remez exchange algorithm to generate the TIR taps in MATLAB. In this work, we have considered the TIR of a speech filter that is reported in [8].

Two filters are compared in hardware on the basis of approximate equivalent spectral characteristics. The spectral characteristics are determined by signal-to-noise ratio parameter. The single-bit ternary system proposed here is originated from sigma-delta modulation therefore SNR is denoted as signal-to-quantization noise ratio (SQNR). In a typical environment each bit adds 6-dB SNR. For example 60-dB SNR can be expected from a 12-bits multi-bit system theoretically. Similarly single-bit systems SQNR depends upon the OSR. The SQNR for second order sigma-delta modulator (see Fig 2 can be defined as:

$$SQNR = 10\log(\sigma_x^2) - 10\log(\sigma_e^2) - 10\log\left(\frac{\pi^4}{5}\right) + 15.05 r(dB) \tag{2}$$

where σ_x^2 is signal power and σ_e^2 is noise power that is called in-band noise power defined as below:

$$\sigma_{ey}^2 = \sigma_e^2 \frac{\pi^4}{5} \left(\frac{2f_B}{f_s}\right)^5 \tag{3}$$

where $2f_B / f_s = 1/OSR$.

Increasing the OSR decreases the in-band noise power and increases the SQNR. For example OSR of 32 can achieve a SQNR 64 and 73 with binary and ternary encoding correspondingly [9]. In this paper we have considered a speech filter with Nyquist rate having 32 multi-bit taps [8]. For the example chosen, to achieve a SNR of 60-dB and 80-dB we have used 12-bit and 16-bit wide taps with same number of data widths (discussed in section 4). For the equivalent level of spectral characteristics we have used OSR of 32 and 64 [5].

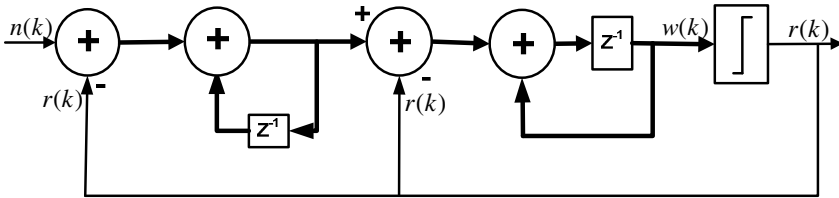


Fig. 2. Second order sigma-delta modulator

3 Canonical Signed Digit (CSD)

Canonical Signed Digit (CSD) is an important classical techniques that has been widely adopted due to its reduced complexity and better area-performance tradeoffs as reported in [6,10]. The technique was first reported in 1960 by Reitwiesner [11] and further improved by many researchers (see [12], for example). Using the CSD encoding technique, the number of nonzero digits can be reduced thereby minimizing the partial products, leading to a more efficient hardware implementation. The two

important properties of CSD are that no two adjacent digits are nonzero and each representation of a number is unique [13]. This implies that there are at most $N/2$ non-zero digits for an N -bit number while, for a 2's complement number there can be N non-zero digits for N -bit number. A 2's complement number, a , can be represented in CSD encoding by the following relationship:

$$a = -a^n 2^n - 1 + \sum_{i=0}^{n-2} a_i 2^i = \sum_{i=0}^{n-1} c_i 2^i \tag{4}$$

where $a_i \in (0, 1)$ and $c_i \in (-1, 0, +1)$. The ternary nature of the canonical system is of great importance as it represents a given number with fewer non-zero digits than is the case in 2's complement. For example, in the four-bit two's complement representation of 15 (1111), all four bits are non-zero while the equivalent CSD encoding ($\bar{1}0001$) has only two. Similarly, the 8-bit CSD encoding of $-25 = 00\bar{1}0100\bar{1}$ compares favorably with its 2's complement representation: 1110111. Additionally, in contrast to the 50% probability that a digit is zero in 2s complement, an n -bit CSD number exhibits a probability of $2/3$ that an individual bit will be zero. This tends to $1/3$ as n becomes larger, as given by the relationship [13]:

$$P(|c_i| = 1) = 1/3 + (1/9n) [1 - (-1/2)^n] \tag{5}$$

These characteristics make CSD highly useful for general purpose DSP applications, especially filters as the smaller number of non-zero digits in the CSD scheme simplifies the multiplication process, which can most easily be realized using shifters, adders and subtractors.

The operation of a CSD multiplier is quite simple. The multiplicand is either added to or subtracted from the accumulator depending on the least significant bit (LSB) of the multiplier e.g. (+1, -1), with no operation being required in the case of a zero. The accumulator is then right shifted by one-bit with sign extension (see Fig 3). These operations are repeated from the LSB of the multiplier until the most significant bit (MSB). The accumulator is reset before a new multiplication is started.

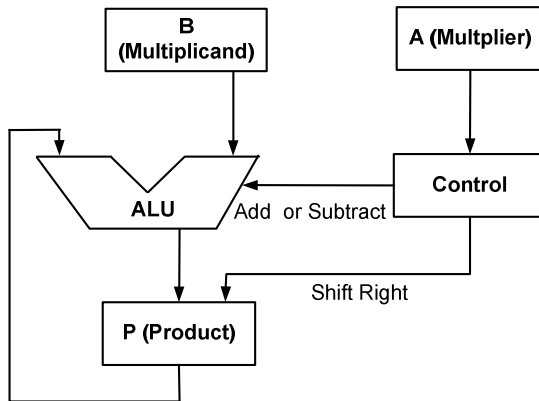
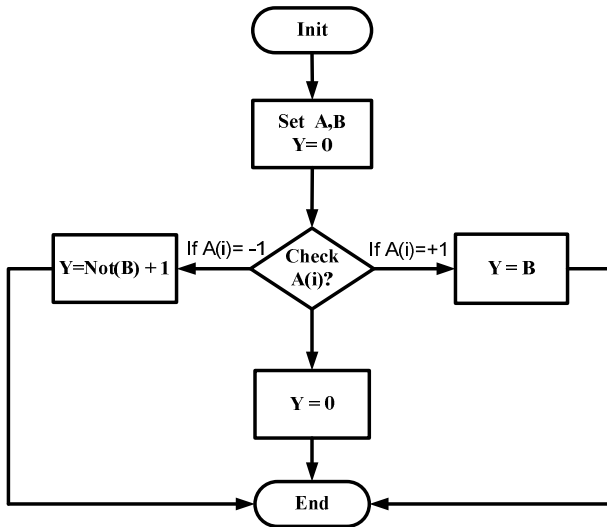


Fig. 3. Typical CSD Multiplier Data Path

3.1 Single-Bit CSD Multiplier

In the particular case of single-bit ternary encoding, the CSD multiplier becomes trivial. The proposed CSD multiplier shown in Fig 4 only requires add or subtract operation. The shift operation is unnecessary because we are dealing with only a single-bit. Moreover, as the multiplicand and the multiplier are in single-bit format, the product is a single-bit as well. This can be mapped efficiently to a small LUT in FPGA. This hardware simplicity offers a distinct advantage to single-bit CSD FIR filter implementation.



A: Multiplier; B: Multiplicand

Fig. 4. Flow chart of the single-bit ternary CSD Multiplier

3.2 Multi-bit CSD Multiplier

The basic structure of multi-bit CSD multipliers is similar to the single-bit case, except that a shift operation is required. As shown in Fig 5, the multiplication starts from the LSB and depending on the value of the multiplier (e.g. +1, 0 and -1), the multiplicand is either added to or subtracted from the result. The result is then shifted right by one bit with sign extension, resulting in a $2N$ -bit result for N -operands.

4 FPGA Design of FIR-Like Filter

As can be seen from (1.1) and Fig 1, the overall architecture of the transversal FIR filter consists of a tapped delay line followed by the multiplication and, finally, the addition of the partial products. The hardware architecture of the filter with CSD encoding is identical to the 2's complement structure except that the coefficients are

encoded using CSD. Designs for both filters are coded in VHDL and synthesized using small commercial Cyclone-III and Stratix-III that are suited for general purpose DSP applications without necessarily containing specialized DSP components.

The order of single-bit filters that is defined by the multiplication of OSR with Nyquist rate filter order i.e., $M = N \times OSR$. Where M is the order of single-bit filter and N is the Nyquist rate filter order. Therefore, large number of ternary taps is required to achieve equivalent spectral performance of two systems. The large filter order already arising from the high OSR required by sigma-delta modulation was further increased by the CSD encoding. To map CSD encoding in VHDL, one extra bit was added to each single-bit to represent its sign, significantly increasing the required extra hardware resources.

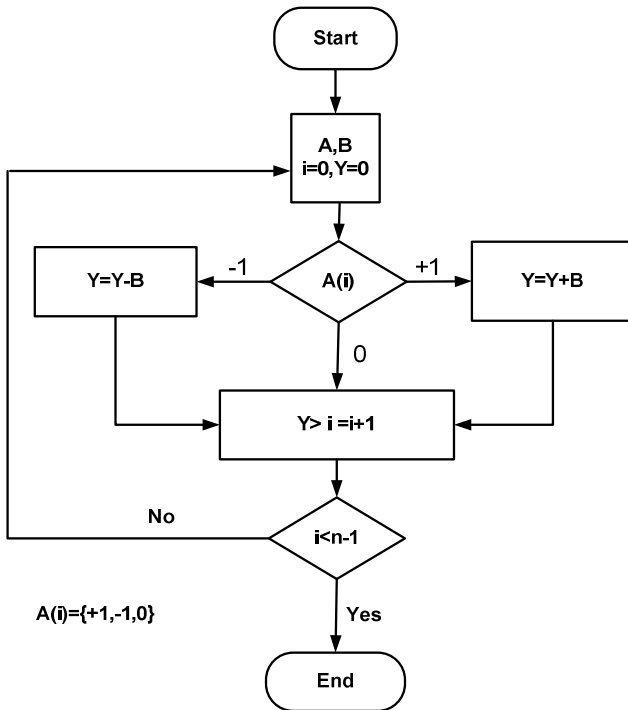


Fig. 5. The Flowchart of a Multi-bit CSD Multiplier

In this paper, Nyquist (i.e., multi-bit) filters of orders 32 and 64 are used as baseline examples to demonstrate the area-performance characteristics of the two approaches (as discussed in section-2). Equivalent spectral performance can be achieved by the single-bit filter at OSRs of 32 and 64. The equivalent multi-bit filter with coefficients and data bit widths of 12 and 16 are synthesized in Quartus-II. In conventional multi-bit filters, the coefficient bit-width is a critical determinant of performance, especially signal-to-noise (SNR) ratio. Both of the designs are synthesized using pipelined and non-pipelined modes. In pipelined mode, extra

registers are used in between each adder stage. The trade-offs involve a small increase in hardware area and greater latency in exchange for increased throughput.

5 Results and Discussion

The two filters are synthesized using VHDL and simulated in pipelined and non-pipelined modes using small commercial FPGA devices Cyclone-III and Stratix-III available from Altera[®]. In both modes of operation, the single-bit ternary FIR filter outperforms in corresponding to its multi-bit system.

The synthesized results are shown in Table 1 and Table 2. The number of LUTs represents the total LUTs occupied by the design out of the available resources of a device. The maximum clock frequency (i.e., F_{MAX}) is determined by synthesizing the results in timing mode and represents the maximum clock achieved by the device at zero slack. Similar to the LUTs, total number of registers is percentage of registers used by the design from available number on the device.

In general, it can be seen that the multi-bit filter occupies a higher chip area (i.e., LUTs) than single-bit filter. On the contrary, the number of registers required by single-bit filter is always higher due to higher number of taps that ends with a bigger adder tree in comparison to multi-bit system. Due to FPGA cell architecture that embodies registers it cannot be counted as disadvantage of the design.

In non-pipelined mode, the single-bit filter is capable of achieving the maximum operating frequency (F_{MAX}) of 118.44 MHz using the Stratix-III device. This represents an average approximately 58% and 70% better performance than the multi-bit filters with bit-widths of 12 and 16, respectively.

As expected, in the pipelined mode the number of registers is almost double in both filters and its performance is superior. From Table 1 and Table 2 it is evident that the single-bit filter has better performance compared to multi-bit filter in pipelined mode. However, when using the Cyclone III device, the performance of the multi-bit filter is decreased by a small amount. The limited effect of pipelining on the multi-bit filter can be understood by the fact of complex multiplier stages that are primarily critical path and restricts the design from achieved higher throughput. Using pipelining in every stage within the multiplier block may be the appropriate solutions to achieve fast and better results. In this work, we have taken more general approach

Table 1. Pipelined and Non-pipelined area-performance results for Single-bit and Multi-bit FIR filter with Cyclone-III device

Taps #	BW	Non-Pipelined			Pipelined		
		LUTs	Registers	F_{MAX}	LUTs	Registers	F_{MAX}
1024	1	10,196 (9%)	6,156 (5%)	63.87	13,410 (11%)	12,274 (10%)	213
32	12	18,554 (16)	1,917 (2%)	53.67	19,132 (16)	3,409 (3%)	26.75
2048	1	20,351 (17)	12,301 (7%)	53.67	26,810 (23)	24,561 (21%)	185
32	16	33,025 (28)	2,565 (2%)	18.57	33,774 (28)	4,553 (4%)	17.92

Table 2. Pipelined and Non-pipelined area-performance results for Single-bit and Multi-bit FIR filter with Stratix-III device

Taps #	BW	Non-Pipelined			Pipelined		
		LUTs	Registers	F _{MAX}	LUTs	Registers	F _{MAX}
1024	1	6,876 (3%)	6,158 (2%)	118.44	6,957(3%)	12,274(5%)	370
32	12	17,989 (7%)	1,918 (<1%)	50.40	17,885 (7%)	3,409 (1%)	51.38
2048	1	13,740 (5%)	12,301(5%)	99.70	13,767 (5%)	24,561 (9%)	322
32	16	32,846 (12%)	2,565 (<1%)	35.27	32,642 (12%)	4,553 (2%)	35.83

BW: Bit Width.

that can be considered in worse case so we are not considering these options at this stage. Here, again the single-bit filter results an average 87 % and 91 % better performance than the multi-bit filter with bit-widths of 12 and 16, respectively.

It is clear that the single-bit filter implementation significantly outperforms than the multi-bit filter in terms of area-performance. The superior performance of the single-bit filter is due to trivial multiplication stages.

6 Conclusion

In this paper, CSD techniques have been considered in the design of FIR filter. Two architectures, the single-bit ternary and multi-bit FIR filters, have been considered and their area-performance tradeoff is shown by synthesize two designs using small commercial FPGA devices.

In contrast with the multi-bit CSD FIR filter, the single-bit filter offers better area-performance tradeoff in non-pipelined as well as pipeline modes, it has a compact operation (i.e. single-bit operation), less power utilization and a lower cost than the multi-bit filter.

In future, we expect to find the comparison of single-bit designs using different available encoding techniques and find the optimized encoding technique for single-bit DSP systems hardware implementation.

References

1. Thompson, A.C., O'Shea, P., Hussain, Z.M., Steele, B.R.: Efficient Single-Bit Ternary Digital Filtering Using Sigma-Delta Modulator. *IEEE Letters on Signal Processing* 11(2), 164–166 (2004)
2. Thompson, A.C., Hussain, Z.M., O'Shea, P.: Efficient Digital Single-Bit Resonator. *IEEE Electronic Letters* 40(22), 1396–1397 (2004)
3. Sadik, A.Z., Hussian, Z.M., O'Shea, P.: Structure for single-bit digital comb filtering. In: *Proc. APCC 2005*, pp. 545–548 (October 2005)
4. Benvenuto, N., Franks, L.E., Hill Jr., F.S.: Realization of finite impulse response filters using coefficients +1, 0, and -1. *IEEE Transactions on Communications COMM-33(10)* (October 1985)

5. Memon, T.D., Beckett, P., Sadik, A.Z.: Power-Area-Performance Characteristics of FPGA based sigma-delta modulated FIR Filters. *Journal of Signal Processing Systems, JSPS* (accepted November 2011)
6. Lee, H., Sobelman, G.E.: FPGA-based digit-serial CSD FIR filter for image signal format conversion. *Microelectronics Journal* 33(5-6), 501–508 (2002)
7. Hewlitt, R.M., Swartzlantler Jr., E.: Canonical signed digit representation for FIR digital filters. In: *IEEE Workshop on Signal Processing Systems*, pp. 416–426. IEEE (2000)
8. Memon, T.D., Beckett, P., Sadik, A.Z.: Single-bit and Conventional FIR Filter Comparison in State-of-Art FPGA. In: *5th IEEE ICMENS 2009*, December 28-30, pp. 72–76 (2009)
9. Schreier, R., Temes, G.C.: *Understanding delta-sigma data converters*. IEEE Press, New Jersey (2005)
10. Hewlitt, R.M., Swartzlantler Jr., E.: Canonical signed digit representation for FIR digital filters. In: *IEEE Workshop on Signal Processing Systems*, pp. 416–426 (2000)
11. Reitwiesner, G.W.: Binary arithmetic. *Advances in Computers* 1, 231–308 (1960)
12. Lim, Y.C., Evans, J.B., Liu, B.: Decomposition of binary integers into signed power-of-two terms. *IEEE Transactions on Circuits and Systems* 38(6), 667–672 (1991)
13. Ma, G.K., Taylor, F.J.: Multiplier policies for digital signal processing. *IEEE ASSP Magazine* 7(1), 6–20 (1990)

A Parametric Analysis of Stream Based Joins

Muhammad Asif Naeem¹, Gillian Dobbie¹, Gerald Weber¹,
and Imran Sarwar Bajwa²

¹ Department of Computer Science, The University of Auckland,
Private Bag 92019, Auckland, New Zealand

² School of Computer Science, The University of Birmingham,
Edgbaston, Birmingham, UK
mnae006@aucklanduni.ac.nz, {gill,gerald}@cs.auckland.ac.nz,
i.s.bajwa@cs.bham.ac.uk

Abstract. Online stream processing is an emerging research area in the field of computer science. Common examples where online stream processing is important are network traffic monitoring, web log analysis and real-time data integration. One kind of stream processing is used to relate the information from one data stream to other data stream or disk-based data. A stream-based join is required to perform such operations. A survey of the literature shows a number of join operators which can process the stream in an online fashion, but each approach has advantages and disadvantages. In this paper we address a number of well known join operators by grouping them into two categories. In first category we discuss those operators which take all their inputs in the form of stream while in the second category we consider operators in which one input resides on the disk. At the end of the paper we summarise our comparisons for each category on the basis of some key parameters. We believe that this exercise will contribute in further exploring this area.

Keywords: Stream-based joins, Data transformation, Performance analysis.

1 Introduction

A stream-based join is an operation to combine the information coming from two different data sources in the form of streams. They are important in the computer science field, but also in many other areas. An example where such a join plays an important role is in the field of networking, where two streams of data packets can be joined using their packets *id's* to synchronize the flow of packets through routers. Another example is an online auction system which generates two streams: one stream for opening an auction while the other stream consists of bids on that auction. A stream-based join is required to relate the bids with the corresponding opened auction.

Stream-based joins are also important in scenarios where one input is in the form of stream while the other input comes from disk. For example, in the context of near-real-time data warehousing during the transformation phase, the source

updates occurring at data source level are propagated in the form of stream while the master data is stored on the disk. A stream-based join is required to combine that stream of updates with the disk-based master data.

The stream-based joins are different from conventional static join operators [1][2][3]. In the case of stream the input tuples are propagated to the join operator continuously and the output tuples are required in an online fashion.

The graphical representations of stream-based join are shown in Figure 1. In Figure 1(a) both inputs of the join are in the form of stream and each tuple $s_1 \in S_1$ and $s_2 \in S_2$ are joined together while θ is join condition. Later in this paper we use term Stream-Stream for this category of join. In Figure 1(b) one input is provided in the form of stream while the other input comes from disk at run time. Each tuple of stream $s \in S$ is joined with the disk tuple $r \in R$ under the specified join condition θ . The tuple is generated as an output if it matches with any of the disk tuple. We use term Stream-Disk for this category of join.

This paper provides an overview of stream-based join operators. As stated above, we divide the stream-based joins into two categories. In first category, we review those join operators whose both inputs are in the form of stream. In second category, we consider those join algorithms in which one input comes in the form of stream while the other input comes from the disk. At the end of the paper, we perform a summarized comparison of all the approaches discussed with respect to different parameters.

The remainder of the paper is organized as follows. Section 2 describes the basics semantics of stream-based joins. In Section 3 we present the review of well know join approaches under Stream-Stream category. Section 4 describes a number of popular join approaches that come under Stream-Disk category. In Section 5 we present an analysis of all approaches, basing our evaluation on a number of important parameters. Finally Section 6 concludes the paper.

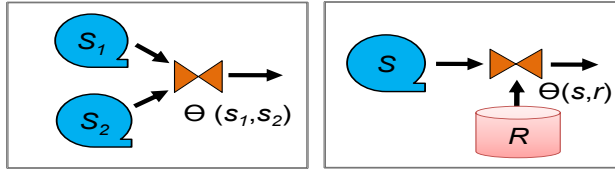
2 Basic Semantics

2.1 Semantics of Join between Streams

A stream is a combination of an unlimited number of tuples of the form $\langle s, t \rangle$ where s is a tuple and t is timestamp for that tuple. The two streams S_1 and S_2 are joined together by maintaining their join state separately. A join state of S_1 keeps the record of all tuples of stream S_1 that it has received to that point. Similarly the join state of S_2 keeps the record of all tuples received from stream S_2 . When the tuple $s_1 \in S_1$ arrives, it is stored in the join state table for S_1 , probed into the join state table of S_2 and join output is generated. Similar operations are performed for stream S_2 .

2.2 Semantics of Joins between Streams and Database Relations

In this type of join each stream tuple is joined with the database relation. Normally the database is stored on the disk. The main issue with these semantics of



(a) Both inputs are in the form of stream (b) One input is stream while the other is disk-based

Fig. 1. Graphical representation of stream-based joins

joins is that the disk I/O cost to access the database is a significant and dominant factor. On the other hand the stream arrival rate is fast and therefore it is necessary to amortize the dominant I/O cost on the fast stream. A number of approaches are available in the literature which address this issue. We will discuss them in our later sections.

3 Stream-Stream

3.1 Symmetric Hash Join (SHJ)

Symmetric Hash Join (SHJ) [4] has exploited the concepts of the traditional hash join algorithm by eliminating the delay for the input stream. SHJ maintains the hash tables for both input streams in memory, as shown in Figure 2. Each newly arrived tuple from one stream is joined with the other stream already stored in hash table and the output for joined tuple is generated. After generating the output, the tuple is stored into its own hash table. The algorithm can generate the output as early as the new tuple arrives. However, it needs to store both inputs in memory. Moreover, the algorithm has the capability to implement the sliding-window features.

3.2 Double Pipelined Hash Join (DPHJ)

The double Pipelined Hash Join (DPHJ) [5] is another extension of symmetric hash join and is based on two stages. In the first stage, which is similar to the SHJ, the algorithm joins the tuples which are in memory. In second stage the algorithm marks the tuples which are not joined in memory and joins them on the disk. In DPHJ duplication of tuples is possible in the second phase when all tuples from both inputs have been read and the final clean-up stage is executed. This algorithm is suitable for medium sized data and does not perform well for large sized data.

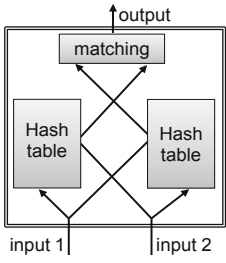


Fig. 2. Symmetric Hash Join [4]

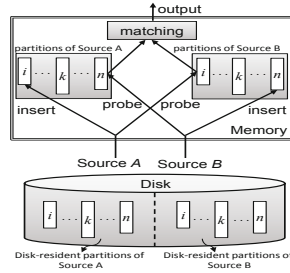


Fig. 3. Graphical interpretation of XJoin [6]

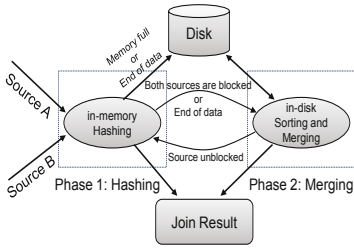


Fig. 4. An overview of Hash-Merge Join [8]

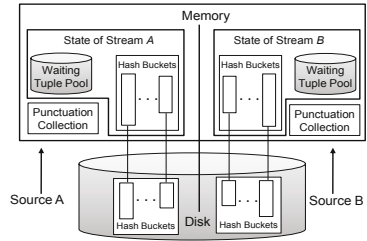


Fig. 5. Framework of MJoin [9]

3.3 XJoin

XJoin [6] is also an extended form of SHJ developed to handle memory overflow by flushing the largest single partition on disk. XJoin presents a three stage strategy for switching its execution state between disk and memory.

First Stage: The first stage of XJoin is quite similar to the standard Symmetric Hash Join, containing only one difference: the tuples are organized in partitions both in memory and on disk. Each partition has two parts. One part exists in memory while the other part exists on disk, as shown in Figure 3. On the arrival of an input tuple from Source A the algorithm stores the tuple into the relative memory partition and probes it into the corresponding partition of Source B. If sufficient space is not available in memory then the algorithm chooses one partition, flushes all its tuples on disk and resumes the usual process. The first stage continues until the tuples are received from at least one input. In the case when the algorithm does not receive any tuple from either input up to a particular time period, it blocks the first stage and starts the execution of second stage. The first stage is terminated permanently when both inputs are finished.

Second Stage: The second stage starts its execution when the first stage is blocked. In the second stage the algorithm selects a partition, reads the tuples

from disk-resident part of that partition and one by one probes them into the corresponding memory partition of the other source. If the tuples match the algorithm generates that tuple as an output. When all the tuples of selected disk-resident partition are processed the algorithm checks the inputs status. If any input resumes producing tuples the algorithm switches back to the first stage. Otherwise it continues the second stage by selecting a different disk-resident part.

Third Stage: The third stage is also called the clean-up stage and it starts when both inputs are finished. The main objective of this stage is to make sure that all the tuples of both inputs are produced as an output.

XJoin uses a timestamps approach to detect the duplicates tuples. Each tuple is assigned an arrival time when it loads into memory and a departure time when it flushes to the disk. The overlapping of timestamps for any two tuples indicates the duplication of tuple. However, in XJoin the strategy of detecting the duplicate tuples is not effective and a flushing policy is also required in order to transfer the extra tuples to the disk.

3.4 Progressive-Merge Join (PMJ)

Progressive-merge join (PMJ) [7] is an enhanced version of the traditional sort-merge join. The PMJ algorithm reads both input data sets simultaneously equal to the available memory size. Once the data is read the algorithm sorts both data sets, joins them together and then flushes both data sets on the disk. After finishing the input data, the algorithm joins the disk-resident data using a sort-merge join technique, while the join results are produced during the merging phase. However, the PMJ algorithm cannot generate the output as fast as the input tuples arrive. Moreover there is a high probability of generating duplicate tuples.

3.5 Hash-Merge Join (HMJ)

Hash-Merge Join (HMJ) [8], also one from the series of symmetric joins, is based on push technology and consists of two phases, hashing and merging. A graphical overview of HMJ is shown in Figure 4. The algorithm begins with the hashing phase. During this phase the algorithm reads the input tuples from two remote data sources and loads them into the hash-buckets exists in memory. The algorithm then joins these hash-based tuples and generates the output accordingly. If the memory is fully occupied, the algorithm flushes a particular part of memory on the disk. The second merging phase of the algorithm starts when both the input sources are blocked. During this phase the disk-resident tuples are joined together. Once any source is unblocked the algorithm switches to the first phase again. This switching between two phases continues until all the data is processed. HMJ uses an effective flushing strategy that helps to keep memory distribution balanced between the two inputs. Moreover, as the algorithm flushes a pair of partition (one from each source) on disk, no timestamp is required to

avoid the duplicate tuples. However, the sorting of both partitions is required in each flushing.

3.6 MJoin

None of the above three approaches consider the metadata about the stream. Therefore, they are unable to recognize data which is no-longer required and by drooping it the overhead can be reduced. In addition, all the join approaches discussed above focus on throughput optimization while ignoring the other optimization goals related to stream metadata, which are equally important.

MJoin [9], a generalized form of XJoin, extends the symmetric binary join operators to handle multiple inputs. MJoin is the first algorithm that considers both static and dynamic metadata to optimize the join execution. The algorithm uses a separate hash table for each input. Figure 5.9 presents a working framework for the MJoin algorithm. On the arrival of a tuple from an input, it is stored in the corresponding hash table and is probed into rest of the hash tables. It is not necessary to probe all hash tables for each arrival, as the sequence of probing stops when a probed tuple does not match in a hash table. The methodology for choosing the correct sequence of probing is determined by performing the most selective probes first. The algorithm uses a coordinated flushing technique that involves flushing the same partition on disk for all inputs. To identify the duplicate tuples MJoin uses two timestamps for each tuple, arrival time and departure time from memory.

3.7 Early Hash Join (EHJ)

Early Hash Join (EHJ) [10] is an improved version of XJoin. In EHJ each input is stored in a separate hash table. When the tuple from one input arrives, it is probed into the hash table of the other input and if the tuple matches then that tuple is generated as an output. After generating the output the tuple is added into its own hash table. The default reading strategy for the in-memory phase is alternative, i.e. the tuples from both inputs are read alternatively. However at any time the user can change the reading strategy to optimize the output rate. In cases when the memory gets filled the algorithm switches to the second phase, which is called the flushing phase. The algorithm implements a biased flushing policy, which is based on two rules: (a) the algorithm first selects the largest and non-frozen partition of larger relation for flushing; (b) when no such partition is found the algorithm then selects the smallest and non-frozen partition of the smaller relation. When both inputs are finished the algorithm starts its last phase, called the clean-up phase, and processes the tuples which have been missed in first two phases.

For all the approaches discussed above, as the algorithms take all inputs in the form of streams, they are not adaptive in the context of real-time data warehousing where one input comes from disk.

4 Stream-Disk

4.1 Index Nested Loop Join (INLJ)

Index-Nested-Loop Join (INLJ) [11] is a traditional join algorithm that can be used to join the stream data with the disk-based data. In INLJ, a stream S is scanned tuple by tuple and the look-up relation R is accessed using a cluster-based index on the join attribute. Although this join algorithm can deal with a bursty stream, it requires extra time to maintain an index on the join attribute. It also processes one tuple at a time, reducing the throughput. A graphical overview of an INLJ is shown in Figure 6.

4.2 Mesh Join (MESHJOIN)

Mesh Join (MESHJOIN) algorithm [12,13] has been introduced particularly for the scenarios like real-time data warehouses. One input of the join is end user updates that come in the form of stream, while the other input is master data that resides on the disk and is accessed during the join execution. The key objective of this join is to amortize the fast stream of updates with the slow disk access rate. To achieve this objective the algorithm keeps a number of chunks of stream in memory at the same time. In MESHJOIN, the disk-based master data (also called disk-based relation R) is traversed cyclically in an endless loop and every stream tuple is compared with every tuple in R . Therefore every stream tuple stays in memory for the time that is needed to run once through R .

The crux of MESHJOIN is that with every iteration a new chunk of stream tuples is also read into the main memory. Each of these chunks will remain in the main memory for one full circle in the continuous traversal of R . The sets therefore leave the main memory in the order that they enter it and their time of residence there is shifted from chunk to chunk. This leads to the staggered processing pattern of MESHJOIN. In the main memory they are organized with a queue, each chunk defining one partition of the queue. At each point in time, going through the partitions from the back of the queue to the front, each partition will have seen a larger number of iterations than the previous, and started on a later position in R (save when the traversal of R resets to the start of R). Figure 7 provides a pictorial representation of the MESHJOIN operation in the moment that a part R_2 of R is read into the disk buffer but not yet processed.

This is an adaptive approach with respect to the stream amortizing. However, there are some research issues that need to be discussed further, such as inefficient memory distribution among the join components, ineffective strategy for accessing the disk based relation, and inability to deal with intermittences.

4.3 Partitioned-Based Approach

A partition-based approach [14] has been introduced to deal with intermittency in the stream. Similar to MESHJOIN, the partitioned-based algorithm also divides the disk-based-relation R into segments using a space partitioning technique. A subset of these segments resides in memory. A wait-buffer, another

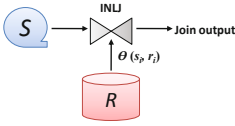


Fig. 6. An example of Index Nested Loop Join (INLJ)

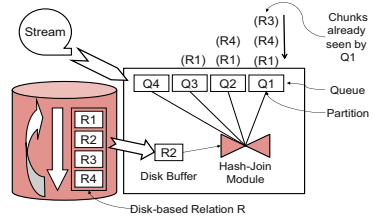


Fig. 7. MESHJOIN right before processing of R_2 [15]

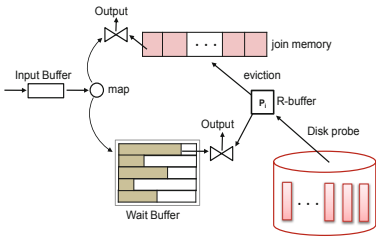


Fig. 8. A graphical framework for partitioned-based algorithm [14]

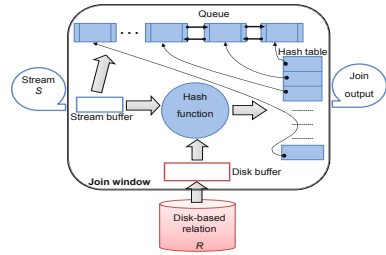


Fig. 9. Architecture of HYBRID-JOIN [16]

memory-based component, contains parallel slots which are equal in number to the disk segments. For each stream update tuple, provided the required disk tuple is available in the memory, the join is performed. If the tuple is not available in the memory the stream tuple is mapped into the corresponding slot of the wait-buffer. The disk invokes operation is based on following conditions: (i) the number of stream tuples in any slot of the wait-buffer crosses the threshold value or (ii) the memory space allocated for the wait-buffer is full. The graphical representation of the partitioned-based join is shown in Figure 8.

As a general observation the join attribute values waiting in the slots of the wait buffer, which are not frequent in the input stream, need to wait longer than in the original MESHJOIN algorithm, because of not reaching the threshold limit. In addition the author focuses on the analysis of the stream buffer in terms of back log tuples and the delay time rather than analysing the algorithm in terms of service rate. The authors do not provide a cost model for their approach. In addition, the algorithm requires a clustered-based-index or an equivalent sorting on the join attribute and it does not prevent starvation of stream tuples.

4.4 Reduced Mesh Join (R-MESHJOIN)

R-MESHJOIN (reduced Mesh Join) [15] is an enhanced form of MESHJOIN which resolves one issue related to an inefficient distribution of memory among

the join components. In MESHJOIN, due to unnecessary constraints, the memory distribution among the join components was not optimal. One drawback of this is that varying the size of the relation on disk also varies the memory sizes for each join component; this is counter-intuitive. In R-MESHJOIN this problem is removed by eliminating the unnecessary constraints in the join components. Moreover, R-MESHJOIN operates at one degree more freedom than MESHJOIN. However, R-MESHJOIN implements the same strategy as the MESHJOIN algorithm for accessing the disk-based relation.

4.5 Hybrid Join (HYBRIDJOIN)

One recent attempt in the form of HYBRIDJOIN (Hybrid Join) algorithm [16] has been made to address the issue of accessing the disk-based relation. An effective strategy for this is introduced in HYBRIDJOIN. The HYBRIDJOIN does not read the entire disk relation sequentially but instead accesses it using an index. This not only reduces the stay of every stream tuple in the join window, but also minimizes the disk I/O cost by guaranteeing that every page read on R is at least used for one stream tuple, while in MESHJOIN and R-MESHJOIN there is no guarantee. To amortize the disk read over many stream tuples, the algorithm performs the join of disk pages with all stream tuples currently in memory. This approach will guarantee that HYBRIDJOIN is never asymptotically slower than MESHJOIN and R-MESHJOIN.

Another advantage of HYBRIDJOIN is that it can deal with bursty stream; inability to do this was one limitation in both MESHJOIN and R-MESHJOIN. To deal with the intermittencies in the stream, for each iteration the algorithm loads a disk page into memory and checks the status of the stream buffer. If no stream tuples are available in the stream buffer, the algorithm does not stop but continues its disk invoking and probing of disk tuples in the hash table. However, the queue keeps on shrinking continuously and will become empty when all tuples in the hash table are joined. When tuples arrive from the stream, the queue starts growing again. The execution architecture for HYBRIDJOIN is shown in Figure 9.

4.6 Extended Hybrid Join (X-HYBRIDJOIN)

The X-HYBRIDJOIN [17] algorithm is an extension of HYBRIDJOIN. Although the HYBRIDJOIN algorithm efficiently amortizes the fast input stream, using an index-based approach to access the disk-based relation and can deal with bursty streams, its performance could still be improved if current market characteristics are taken into consideration. Current market analysis models show that a few products are bought with higher frequency than other products [18]. Therefore, in the input data stream, the sales transactions related to that limited number of products are most frequent and during the join operation they need to join with a particular portion of the disk-based relation. The HYBRIDJOIN algorithm does not consider this aspect and reads the required page from the disk each time. That increases the disk I/O cost significantly.

Table 1. Comparison of Stream-Stream join approaches

Algo. Name	Storage of inputs in Memory	Inputs	Multiple joins capability	Sliding window Feature	Chances of Duplicate tuples	I/O Complexity	Initial delay	Consider stream metadata
SHJ	completely	two	limited	yes	medium	n/a	no	no
DPHJ	partially	two	limited	yes	medium	low	no	no
XJoin	partially	two	limited	yes	medium	high	no	no
PMJ	partially	two	limited	yes	high	medium	yes	no
HMJ	partially	two	limited	yes	low	low	no	no
MJoin	partially	\geq two	high	yes	low	low	no	yes
EHJ	partially	two	limited	yes	low	low	no	no

Table 2. Comparison of Stream-Disk join approaches

Algorithm Name	Input stream	Disk data	Index on disk data	Join type	Stream back-log	Stream amortizing	Initial delay	Un-process tuples
INLJ	bursty	sort, unsort	clustered	1:M	high	very low	no	no
MESHJOIN	cont.	sort, unsort	clustered, non-clus.	1:M, M:N	low	medium	yes	yes
Partitioned-based Join	bursty	sort	non-clus.	1:M	low	medium	no	yes
R-MESHJOIN	cont.	sort, unsort	clustered, non-clus.	1:M, M:N	low	medium	yes	yes
HYBRIDJOIN	bursty	sort	clustered	1:M	low	high	no	no
X-HYBRIDJOIN	bursty	sort	clustered	1:M	low	highest	no	no

In X-HYBRIDJOIN one key component, the disk buffer (used to store disk-based data), is divided into two equal parts. One part is swappable while the other part is non-swappable. The algorithm stores a particular part of disk-based relation in the non-swappable part, which is quite frequent in stream. The key benefit of this is as follows. For each iteration, when the disk page is loaded into the swappable part of the disk-buffer, apart from matching only with that page as in HYBRIDJOIN, the algorithm matches both parts of the disk-buffer with all the stream tuples available in the memory without any extra disk I/O cost. As a result, this reduces the I/O cost substantially and consequently improves the performance.

5 Analysis

Having provided a detailed description of each well known join operator in Sections 3 and Section 4 we turn now to comparing the different approaches on the basis of some key parameters. A separate comparison is made for each

category. Table 11 presents the comparisons of Stream-Stream approaches. From the table it is clear that all approaches except SHJ store the inputs partially in memory. When the available memory becomes filled, algorithms generally select one partition as a victim each time and flush it on the disk. Therefore, at one time they can store a portion of stream in memory. The table shows MJoin is the only algorithm that can accept more than two inputs and that has the capability of multiple joins. One other feature of MJoin is that it is the only join operator that considers both static and dynamic metadata data of stream in order to optimize the performance.

All the algorithms except PMJ have the capability to generate the output as soon as the tuple is received. In PMJ the algorithm first reads the data according to the available memory and then sorts it. Due to the sorting feature, the algorithm cannot generate the output as soon as the tuple is received. Some techniques, such as SHJ, DPHJ, XJoin and PMJ, are also likely to generate duplicate tuples.

A summarized comparison of Stream-Disk approaches is presented in Table 12. In a realistic scenario, the stream would be of bursty nature. The parameters for comparison we considered for Table 12 are slightly different from the parameters in Table 11. The reason for considering different parameters is the different nature of inputs. From the table it can be observed that HYBRIDJOIN and X-HYBRIDJOIN are the only two approaches that cover all the features. Comparing these two, X-HYBRIDJOIN is the one that amortizes the maximum disk I/O cost over fast input stream.

6 Conclusions

Stream processing is an emerging area in different fields (networking, databases, data warehousing, etc) of computer science. Stream-based join operators are required to process the stream data. A considerable amount of literature has been published on these stream-based join operators. In this paper we divide these join operators into two main categories with respect to the nature of their inputs. Category Stream-Stream consists of those join operators whose all inputs are in the form of stream while Category Stream-Disk contains those join operators in which one input is in the form of stream and the other is disk-based. We have discussed a number of well known approaches in both categories and finally presented our analysis of these approaches based on different features. For further clarity we have performed our analysis for each category separately. These kinds of comparisons will certainly be helpful in exploring such areas further.

References

1. Liu, L., Pu, C., Tang, W.: Continual Queries for Internet Scale Event-Driven Information Delivery. *IEEE Trans. on Knowl. and Data Eng.* 11(4), 610–628 (1999)
2. Arasu, A., Babcock, B., Babu, S., McAlister, J., Widom, J.: Characterizing memory requirements for queries over continuous data streams. *ACM Trans. Database Syst.* 29(1), 162–194 (2004)

3. Avnur, R., Hellerstein, J.M.: Eddies: continuously adaptive query processing. *SIGMOD Rec.* 29(2), 261–272 (2000)
4. Wilschut, A.N., Apers, P.M.G.: Dataflow query execution in a parallel main-memory environment. *Distrib. Parallel Databases* 1(1), 103–128 (1993)
5. Ives, Z.G., Florescu, D., Friedman, M., Levy, A., Weld, D.S.: An adaptive query execution system for data integration. *SIGMOD Rec.* 28(2), 299–310 (1999)
6. Tolga, U., Michael, J.F.: Xjoin: A reactively-scheduled pipelined join operator. *IEEE Data Engineering Bulletin* 23(2), 27–33 (2000)
7. Dittrich, J., Seeger, B., Taylor, D.S., Widmayer, P.: Progressive merge join: a generic and non-blocking sort-based join algorithm. In: *VLDB 2002: Proceedings of the 28th International Conference on Very Large Data Bases*, Hong Kong, China, pp. 299–310 (2002)
8. Mohamed, F.M., Ming, L., Walid, G.A.: Hash-merge Join: A Non-blocking Join algorithm for Producing Fast and Early Join Results. In: *ICDE 2004, Proceedings of IEEE 20st International Conference on Data Engineering*, Boston, MA, USA, pp. 251–263 (2004)
9. Ding, L., Rundensteiner, E.A., Heineman, G.T.: MJoin: a metadata-aware stream join operator. In: *Proceedings of the 2nd International Workshop on Distributed Event-Based Systems*, pp. 1–8. ACM, New York (2003)
10. Lawrence, R.: Early hash join: a configurable algorithm for the efficient and early production of join results. In: *VLDB 2005: Proceedings of the 31st International Conference on Very Large Data Bases*, pp. 841–852. VLDB Endowment, Trondheim (2005)
11. Ramakrishnan, R., Gehrke, J.: *Database Management Systems*. McGraw-Hill, Inc., New York (1999)
12. Polyzotis, N., Skiadopoulos, S., Vassiliadis, P., Simitsis, A., Frantzell, N.: Meshing Streaming Updates with Persistent Data in an Active Data Warehouse. *IEEE Trans. on Knowl. and Data Eng.* 20(7), 976–991 (2008)
13. Polyzotis, N., Skiadopoulos, S., Vassiliadis, P., Simitsis, A., Frantzell, N.E.: Supporting Streaming Updates in an Active Data Warehouse. In: *ICDE 2007, Proceedings of IEEE 23rd International Conference on Data Engineering*, Istanbul, Turkey, pp. 476–485 (2007)
14. Chakraborty, A., Singh, A.: A partition-based approach to support streaming updates over persistent data in an active datawarehouse. In: *IPDPS 2009: Proceedings of the 2009 IEEE International Symposium on Parallel & Distributed Processing*, pp. 1–11. IEEE Computer Society, Washington, DC, USA (2009)
15. Naem, M.A., Dobbie, G., Weber, G.: R-MESHJOIN for Near-real-time Data Warehousing. In: *DOLAP 2010: Proceedings of the ACM 13th International Workshop on Data Warehousing and OLAP*. ACM, Toronto (2010)
16. Naem, M.A., Dobbie, G., Weber, G.: HYBRIDJOIN for Near-real-time Data Warehousing. *IJDWM: International Journal of Data Warehousing and Mining* 7(4), 21–42 (2011)
17. Naem, M.A., Dobbie, G., Weber, G.: X-HYBRIDJOIN for Near-real-time Data Warehousing. In: *Fernandes, A.A.A., Gray, A.J.G., Belhajjame, K. (eds.) BNCOD 2011. LNCS, vol. 7051*, pp. 33–47. Springer, Heidelberg (2011)
18. Anderson, C.: *The Long Tail: Why the Future of Business is Selling Less of More*. Hyperion (2006)

Efficient Usage of Memory Resources in Near-Real-Time Data Warehousing

Muhammad Asif Naeem¹, Gillian Dobbie¹, Gerald Weber¹,
and Imran Sarwar Bajwa²

¹ Department of Computer Science, The University of Auckland,
Private Bag 92019, Auckland, New Zealand

² School of Computer Science, The University of Birmingham,
Edgbaston, Birmingham, UK
mnae006@aucklanduni.ac.nz, {gill,gerald}@cs.auckland.ac.nz,
i.s.bajwa@cs.bham.ac.uk

Abstract. In the context of near-real-time data warehousing the user's updates generated at data source level need to be stored into warehouse as soon as they occur. Before loading these updates into the warehouse they need to be transformed, often using a join operator between the stream of updates and disk-based master data. In this context a stream-based algorithm called X-HYBRIDJOIN (Extended Hybrid Join) has been proposed earlier, with a favourable asymptotic runtime behavior. However, the absolute performance was not as good as hoped for. In this paper we present results showing that through properly tuning the algorithm, the resulting "Tuned X-HYBRIDJOIN" performs significantly better than that of the previous X-HYBRIDJOIN, and better as other applicable join operators found in literature. We present the tuning approach, based on measurement techniques and a revised cost model. To evaluate the algorithm's performance we conduct an experimental study that shows that the Tuned X-HYBRIDJOIN exhibits the desired performance characteristics.

Keywords: Near-real-time data warehousing, Data transformation, Stream-based joins, Tuning and performance optimization.

1 Introduction

To fulfill the businesses need for the latest information, proprietary data warehouses are upgraded towards a near-real-time mode of operation. This requires that the end user's updates generated at data source level are propagated to the data warehouse in an online fashion. These data source level updates are not in the data warehouse format, and therefore it is necessary to transform them into the required format. A common example for this is the replacement of a data source key with a unique warehouse key or surrogate key. Another scenario is when more information is required to enrich to the source data. Normally this task is performed in the transformation phase of ETL (Extraction, Transformation, and Loading). For that purpose, a join operator is required between the stream of updates and the disk-based master data.

There are some known issues concerning the stream-based join operator which are subject of ongoing research. Firstly there is a bottleneck during join execution, since both inputs of the join come from different sources with different arrival rates. The stream input is fast and bursty while the disk input is comparatively slow. Secondly, because this kind of join algorithm normally executes with limited available resources, the optimal utilization of these available resources is very important.

To overcome these challenges a novel stream-based join algorithm called X-HYBRIDJOIN (Extended Hybrid Join) [1] was proposed recently by the authors. This algorithm not only addressed the issues described above but also was designed to take into account the typical characteristics of market data, commonly known as the 80/20 sale Rule [2]. According to this rule 80 percent of sale focus on only 20 percent of the products, i.e., one observes a Zipfian distribution. Although the authors presented an adaptive algorithm to adopt the typical characteristics of market data, the components of the algorithm are not tuned to make efficient use of available memory resources. Further details about this issue are provided in Section 2.

On the basis of these observations, we propose a revised X-HYBRIDJOIN with name Tuned X-HYBRIDJOIN. We revise the existing cost model of X-HYBRIDJOIN and also tune the join component based on that cost model. As a result the available memory is distributed among all components optimally and consequently it improves the performance of algorithm significantly.

The rest of the paper is structured as follows. The related work to our approach is presented in Section 6. Section 2 describes our observations about the current approach. In Section 3 we present our proposed solution along with the revised cost model. Section 4 presents the tuning of X-HYBRIDJOIN based on the revised cost model. The experimental study is discussed in Section 5 and finally Section 7 concludes the paper.

2 Preliminaries and Problem Definition

This section presents a working overview of X-HYBRIDJOIN along with the research issue we explore in this paper. In the field of real-time data warehousing X-HYBRIDJOIN is an adaptive algorithm for joining the bursty data stream with disk-based master data. Although the typical characteristics of market data are considered, optimal settings for the available limited memory resources are not considered. We first explain the major components of X-HYBRIDJOIN and the role of each component. Figure 1 presents an abstract level working overview of X-HYBRIDJOIN where m is the number of partitions in the queue to store stream tuples and n is the number of pages in disk-based relation R . The relation R is assumed to be sorted with respect to the access frequency. The stream tuples are stored in the hash table while the join attribute values are stored in the queue. The queue is implemented using a doubly linked-list data structure to allow the random deletion of matching tuples. The disk buffer is used to load the disk pages into memory. To make efficient use of the disk-based relation R by

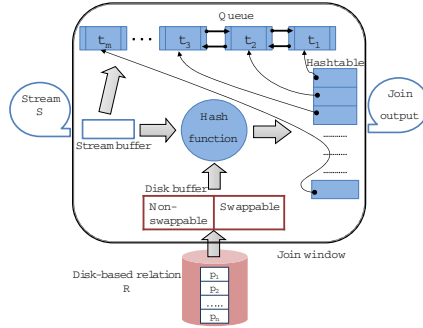


Fig. 1. X-HYBRIDJOIN working overview

minimizing the disk access cost, the disk buffer is divided into two equal parts. One is called the non-swappable part which stores a small but most frequently used portion of disk-based relation R into memory on a permanent basis. The other part of the disk buffer is swappable and for each iteration it loads the disk page p_i from relation R into memory.

Before the join process starts X-HYBRIDJOIN loads the most frequently used page of disk-based relation R into the non-swappable part of the disk buffer. During the join process, for each iteration the algorithm dequeues the oldest join attribute value from the queue and using this value as an index it loads the relevant disk page into the swappable part of the disk buffer. After loading the disk page into memory the algorithm matches each of the disk tuples available in both the swappable and non-swappable parts of the disk buffer with the stream tuples in the hash table. If the tuple match, the algorithm generates the resulting tuple as output and deletes the stream tuple from the hash table along with its join attribute value from the queue. In the next iteration the algorithm again dequeues the oldest element from the queue, loads the relevant disk page into the swappable part of the disk buffer and repeats the procedure.

X-HYBRIDJOIN minimizes the disk access cost and improves performance significantly by introducing the non-swappable part of the disk buffer. But in X-HYBRIDJOIN the memory assigned to the swappable part of the disk buffer is equal to the size of disk buffer in HYBRIDJOIN [3] and the same amount of memory is allocated to the non-swappable part of the disk buffer. In the following we will show that this is not optimal. The problem that we consider in this paper is to tune the size of both parts of the disk buffer so that the memory distribution among these two components is optimal for the performance of the algorithm.

3 Proposed Solution

As a solution for the stated problem we propose a tuning module for the existing X-HYBRIDJOIN. The tuning procedure is based on both a measurement

strategy and the cost model. In this section we first revise the cost model, calculated in X-HYBRIDJOIN. We then describe the four components on which the average input size w of the algorithm is based. Once the cost and the value for w are determined, tuning is performed on the basis of these parameters.

3.1 Cost Calculation

In this section we revise the cost formulas derived in X-HYBRIDJOIN. The reason for this revision is that X-HYBRIDJOIN uses equal memory for both the swappable and non-swappable parts of the disk buffer, and therefore the formulas do not apply for other relative sizes. Following the style of cost modeling used for MESHJOIN, the cost for any algorithm is expressed in terms of memory and processing time. Equation 1 describes the total memory used to implement the algorithm while Equation 2 calculates the processing cost for w tuples.

Memory Cost. Since the optimal values for the sizes of both the swappable part and non-swappable part can be different, we assume k pages for the swappable part and l pages for the non-swappable part. Overall the largest portion of the total memory is used for the hash table while a much smaller amount is used for each of the disk buffer and the queue. The memory for each component can be calculated as given below:

Memory for the swappable part of disk buffer (bytes) = $k \cdot v_P$ (where v_P is the size of each disk page in bytes).

Memory for the non-swappable part of disk buffer (bytes) = $l \cdot v_P$.

Memory for the hash table (bytes) = $\alpha[M - (k + l)v_P]$ (where M is the total allocated memory and α is memory weight for the hash table).

Memory for the queue (bytes) = $(1 - \alpha)[M - (k + l)v_P]$ (where $(1 - \alpha)$ is memory weight for the queue).

The total memory used by the algorithm can be determined by aggregating the above.

$$M = (k + l)v_P + \alpha[M - (k + l)v_P] + (1 - \alpha)[M - (k + l)v_P] \quad (1)$$

Currently we are not including the memory reserved for the stream buffer because it is small (0.05 MB was sufficient in all our experiments).

Processing Cost. In this section we revise the processing cost for X-HYBRIDJOIN. We denote the cost for one iteration of the algorithm by c_{loop} and express it as the sum of the costs for the individual operations. We first calculate the processing cost for each component separately.

Cost to read the non-swappable part of disk buffer (nanoseconds) = $c_{I/O}(l \cdot v_P)$.

Cost to read the swappable part of disk buffer (nanoseconds) = $c_{I/O}(k \cdot v_P)$.

Cost to look-up the non-swappable part of disk buffer in the hash table (nanoseconds) = $d_N c_H$ (where $d_N = l \frac{v_P}{v_R}$ is the size of the non-swappable part of disk buffer in terms of tuples, v_P is size of disk page in bytes, v_R is size of disk tuple in bytes, and c_H is look-up cost for one disk tuple in the hash table).

Cost to look-up the swappable part of disk buffer in the hash table (nanoseconds) = $d_S c_H$ (where $d_S = k \frac{v_P}{v_R}$ is the size of the swappable part of disk buffer in terms of tuples).

Cost to generate the output for w matching tuples (nanoseconds) = $w \cdot c_O$ (where c_O is cost to generate one tuple as an output).

Cost to delete w tuples from the hash table and the queue (nanoseconds) = $w \cdot c_E$ (where c_E is cost to remove one tuple from the hash table and the queue).

Cost to read w tuples from stream S into the stream buffer (nanoseconds) = $w \cdot c_S$ (where c_S is cost to read one stream tuple into the stream buffer).

Cost to append w tuples into the hash table and the queue (nanoseconds) = $w \cdot c_A$ (where c_A is cost to append one stream tuple in the hash table and the queue).

As the non-swappable part of the disk buffer is read only once before execution starts, we exclude it. The total cost for one loop iteration is:

$$c_{loop}(\text{secs}) = 10^{-9} [c_{I/O}(k \cdot v_P) + (d_N + d_S)c_H + w(c_O + c_E + c_S + c_A)] \quad (2)$$

Since in every c_{loop} seconds the algorithm processes w tuples of stream S , the performance or service rate μ can be calculated by dividing w by the cost for one loop iteration.

$$\mu = \frac{w}{c_{loop}} \quad (3)$$

4 Tuning

The stream-based join operators normally execute within limited memory and therefore tuning of join components is important to make efficient use of the available memory. For each component in isolation, more memory would be better but assuming a fixed memory allocation there is a trade-off in the distribution of memory. Assigning more memory to one component means less memory for other components. Therefore we need to find the optimal distribution of memory among all components in order to attain maximum performance. A very important component is the disk buffer because reading data from disk to memory is very expensive.

In our approach we first perform the tuning through performance measurements by considering a series of values for the sizes of the swappable and non-swappable parts of the disk buffer. We also derive a mathematical model for tuning from the cost model. Finally, we compare the tuning results of both approaches to validate our cost model. The details about the experimental setup is presented in Table II.

4.1 Tuning through Measurements

In this section we present the tuning of the key components of X-HYBRIDJOIN through measurements. In our measurement approach we test the performance on particular memory settings for swappable and non-swappable parts rather than on every contiguous value.

Our measurement approach assumes the size of total memory and the size of the disk-based relation are fixed. The sizes for the swappable and non-swappable

Table 1. Data specification

Parameter	value
Disk-based data	
Size of disk-based relation R	0.5 million to 8 million tuples
Size of each tuple v_R	120 bytes
Stream data	
Size of each tuple v_S	20 bytes
Size of each node in queue	12 bytes
Benchmark	
Based on	Zipf's law
Characteristics	Bursty and self-similar

parts vary in such a way that for each size of the swappable part the performance is measured against a range of sizes for the non-swappable part. By changing the sizes for both parts of the disk buffer the memory sizes for the hash table and the queue are also affected.

The performance measurements for varying the sizes of both swappable and non-swappable parts are shown in Figure 2. The figure shows that the performance increases rapidly by increasing the size for the non-swappable part. After reaching a particular value for the size of non-swappable part the performance starts decreasing. The plausible reason behind this behavior is that in the beginning when the size for the non-swappable part increases, the probability of matching stream tuples with disk tuples also increases and that improves the performance. But when the size for the non-swappable part is increased further it does not make a significant difference in stream matching probability. On the other hand, due to higher look-up cost and the fact that less memory is available for the hash table the performance decreases gradually. We see a similar behavior when we test the performance for the swappable part. In this case, after attaining the maximum performance it decreases rapidly because of an increase in the I/O cost for loading the growing swappable part. From the measurements shown in the figure it is possible to approximate the optimal settings for both the swappable and non-swappable parts by finding the maximum on the two-dimensional surface.

4.2 Tuning Based on Cost Model

We now derive a mathematical mode for tuning from the cost model presented in Section 3.1. From Equation 3 it is clear that the service rate depends on the size of w and the cost c_{loop} . To determine the optimal settings it is first necessary to calculate the size of w . The value of w in X-HYBRIDJOIN is the sum of w_S and w_N as in Equation 4.

$$w = w_S + w_N \quad (4)$$

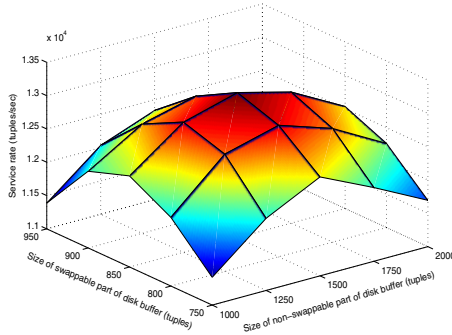


Fig. 2. Tuning of X-HYBRIDJOIN using measurement approach

where w_S represents the number of stream tuples processed through the swappable part of the disk buffer and w_N represents those which processed through the non-swappable part of the disk buffer. In X-HYBRIDJOIN the values for w_S and w_N depend upon the following four components.

- a. Size of swappable part of the disk buffer in tuples (d_S).
- b. Size of non-swappable part of the disk buffer in tuples (d_N).
- c. Size of the disk based relation in tuples (R_t).
- d. Size of the hash table in tuples (h_t).

In the following we present the effect of each component on both w_S and w_N by conducting different experiments.

a. Effect of the Swappable Part of the Disk Buffer on w_S and w_N : In our first experiment, in order to show the effect of the swappable part of the disk buffer on both w_S and w_N , we consider the values for other parameters (d_N , R_t , h_t) to be fixed. We increase the size of the swappable part exponentially and measure the value for both w_S and w_N against every setting. Figure 3(a) presents the results of our experiment. It can be observed from the figure that by increasing the size for the swappable part of the disk buffer, both w_S and w_N also increase equally. The reason for this behavior is that when the size of the swappable part increases, more stream tuples are matched with this part of the disk buffer and that increases the stream input size for the next iteration. In the next iteration when more stream tuples come in, due to the Zipfian distribution, the matching probability with the non-swappable part of the disk buffer increases equally. Therefore, both w_S and w_N are directly proportional to the size of the swappable part of the disk buffer.

$$w_S \propto d_S \qquad (5) \qquad w_N \propto d_S \qquad (6)$$

b. Effect of the Non-swappable Part of the Disk Buffer on w_S and w_N : In this experiment we observe the effect of the non-swappable part on both w_S and w_N by fixing the values of the other parameters (d_S , R_t , h_t). Figure 3(b)

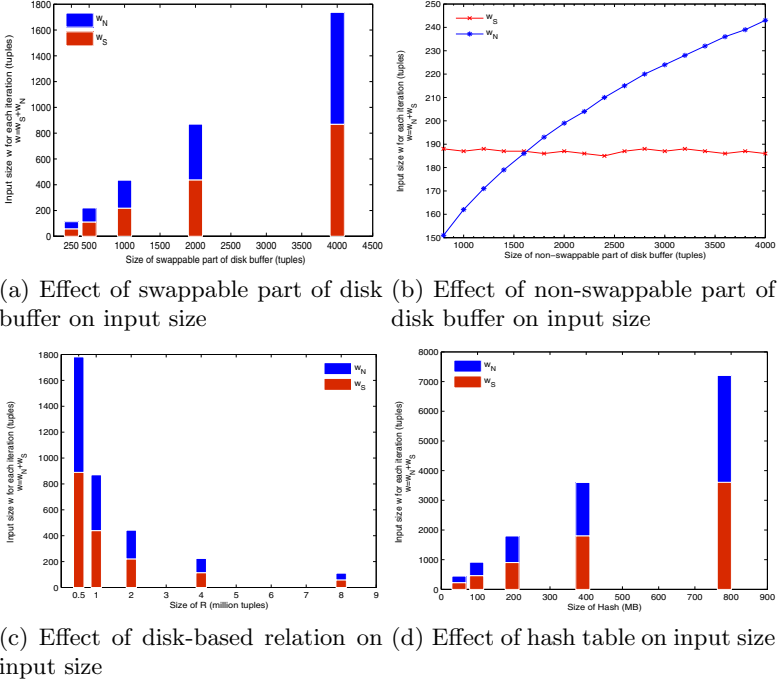


Fig. 3. Effect of join components on input size w

shows the results of our experiment where the size of the non-swappable part of the disk buffer increases sequentially and we measure the values for both w_S and w_N against every setting of d_N . From the figure it is clear that the increment in the size of the non-swappable part only increases w_N , without effecting w_S . Moreover, the rate of increasing w_N is by some power factor. This behavior can be explained as; initially by increasing the size of the non-swappable part it increases the probability of matching more stream tuples w_N rapidly, because the non-swappable part contains highly used pages of disk-based relation R . By increasing the size for the non-swappable part further, the probability of matching stream tuples w_N does not increase with the same rate because the frequency of matching the stream tuples with disk-pages (which are stored at later positions of non-swappable part) decreases. Therefore the relationship between the w_N and the size of non-swappable part of disk buffer d_N can be interpreted by the given equation,

$$w_N \propto d_N^P \quad (7)$$

where P is the power factor whose value in our settings is equal to 0.2955.

c. Effect of Size of Disk-Based Relation R on w_S and w_N : To observe the effect of R on both w_S and w_N we conducted one experiment in which we

increase the size of the disk-based relation R exponentially while keeping the values for all other parameters (d_N, d_S, h_t) fixed. The results of this experiment are shown in Figure 3(c). From the figure it is clear that the change in the size of R affects both w_S and w_N inversely. We explain this as follows: by incrementing the size of R it equally decreases the probability of matching the stream tuples for both swappable and non-swappable parts of the disk buffer. Therefore, the relationship of R with both w_S and w_N can be represented by Equations 8 and 9 respectively.

$$w_S \propto \frac{1}{R_t} \tag{8} \qquad w_N \propto \frac{1}{R_t} \tag{9}$$

d. Effect of Hash Table Size on w_S and w_N : In this experiment we examine the effect of hash table size on both w_S and w_N . We increase the size of the hash table sequentially while the values for other parameters (d_N, d_S, R_t) are fixed. The measured values for both w_S and w_N against every setting for the hash table size are shown in Figure 3(d). The values for both w_S and w_N increase at an equal rate by increasing the size of the hash table. The reason is that by increasing the size of the hash table more stream tuples can be accommodated in memory and therefore, the probability of matching both swappable and non-swappable parts also increases. Hence, both w_S and w_N are directly proportional to the size of the hash table and this relationship is represented by Equations 10 and 11.

$$w_S \propto h_t \tag{10} \qquad w_N \propto h_t \tag{11}$$

After observing the effect of individual components on w_S and w_N , we can derive a formula to calculate the values for w_S and w_N .

Using Equations 5, 8 and 10, w_S can be calculated as below

$$w_S = k_1 \frac{d_S h_t}{R_t} = k_1 \frac{d_S h_t}{R_t} \tag{12}$$

where k_1 is constant and its value in our settings is 1.7147.

Similarly using Equations 6, 7, 9, and 11, w_N can be calculated as below.

$$w_N = k_1 k_2 \frac{d_S d_N^P h_t}{R_t} = k_1 k_2 \frac{d_S d_N^P h_t}{R_t} \tag{13}$$

where k_1, k_2 , and P are constants. The values for k_1 and P are already mentioned while the value for k_2 in our settings is 0.11305.

Once the formulas for w_S and w_N are determined, the formula to calculate w can be derived by putting the values of w_S and w_N from Equations 12 and 13 into Equation 4, as shown in Equation 14.

$$w = \frac{k_1 d_S h_t}{R_t} (1 + k_2 d_N^P) \tag{14}$$

Now we have formulas to calculate w and the cost c_{loop} required to process these w tuples therefore, by putting the values of w and c_{loop} from Equations 14 and 2 in Equation 3 and simplifying it we get:

$$\mu = \frac{k_1 d_S h_t (1 + k_2 d_N^P) 10^9}{k_1 d_S h_t (1 + k_2 d_N^P) (c_O + c_E + c_S + c_A) + R_t [c_{I/O}(d_S) + (d_N + d_S) c_H]} \quad (15)$$

In the above equation, the service rate μ depends on four parameters: the size of the swappable part of the disk buffer d_S , the size of the non-swappable part of the disk buffer d_N , hash table size h_t and the size of disk-based relation R_t . We know that for the tuning of a particular settings R_t can be assumed fixed. From Section 3.1 it is clear that the size of the hash table h_t depends upon the sizes of both swappable d_S and non-swappable d_N parts of the disk buffer. Therefore, using Equation 15 we can find the values of d_S and d_N at which the algorithm performs optimally.

4.3 Comparisons of Both Approaches

To validate our cost model we compare the tuning results based on the measurement approach with those that we achieved through cost model.

Swappable Part: In this experiment we compare our tuning results for the swappable part of the disk buffer using both the measurement and cost model approaches. The tuning results of each approach (with 95% confidence interval in case of measurement approach) are shown in Figure 4 (a). From the figure it is evident that at every position the results in both cases are similar, with only 0.5% deviation.

Non-swappable Part: Similar to before, we also compare the tuning results of both approaches for the non-swappable part of the disk buffer. The results are shown in Figure 4 (b). Again, we can see from the figure, the results in both cases are nearly equal with a deviation of only 0.6%.

5 Experimental Study

To strengthen our arguments we performed an experimental evaluation of X-HYBRIDJOIN with and without the tuning module using the synthetic datasets.

In X-HYBRIDJOIN kinds of algorithms, the total memory and the size of the disk-based relation are the common parameters that vary frequently. Therefore, in our experiments we compare the performance by varying both parameters individually.

Performance Comparisons for Different Sizes of R : In this experiment we compare the performance of X-HYBRIDJOIN with and without tuning by varying the size of R . We assume that the size of R varies exponentially while the total memory budget remains fixed (50MB) for all values of R . For each value of R we run X-HYBRIDJOIN algorithm both with and without optimal settings, and measure the performance in both cases. The performance results we measured are shown in Figure 5 (a). From the figure it is clear that for

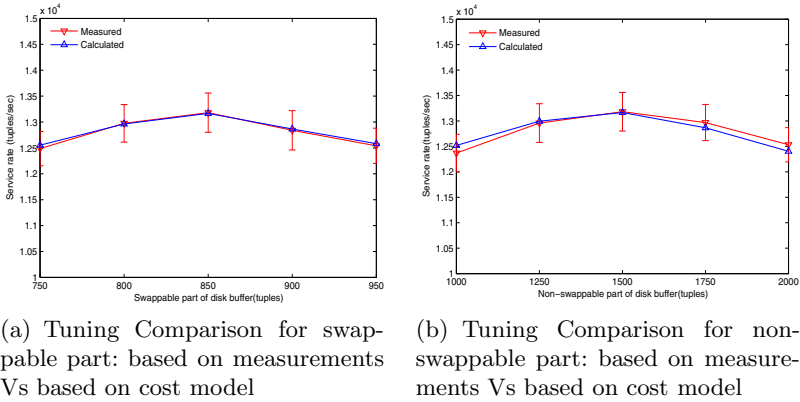


Fig. 4. Comparisons of tuning results

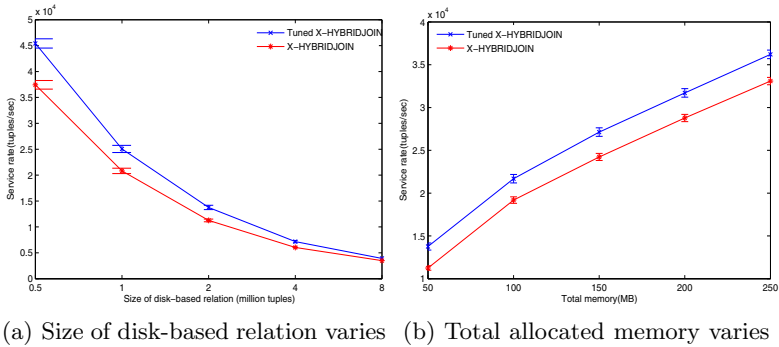


Fig. 5. Performance comparisons: Tuned X-HYBRIDJOIN Vs X-HYBRIDJOIN without tuning

all settings of R the Tuned X-HYBRIDJOIN performs significantly better than X-HYBRIDJOIN without tuning.

Performance Comparisons for Different Memory Budgets: In our second experiment we analyse the performance of X-HYBRIDJOIN and Tuned X-HYBRIDJOIN using different memory budgets while the size of R is fixed (2 million tuples). Figure 5(b) depicts the comparisons of both approaches. From the figure it can be observed that for all memory budgets the Tuned X-HYBRIDJOIN performs significantly better than X-HYBRIDJOIN without tuning. This improvement increases gradually as the total memory budget increases.

6 Related Work

Some techniques have already been introduced to process the join queries over continuous streaming data [45]. In this section we will elaborate only those which are directly related to our problem domain.

A stream-based algorithm called Mesh Join (MESHJOIN) [6,7] was designed specifically for joining a continuous stream with disk-based data in an active data warehouse. R-MESHJOIN (reduced Mesh Join) [8] is a revised version of MESHJOIN that focuses on the optimal distribution of memory among the join components. A recent piece of work introduces a novel stream-based join called HYBRIDJOIN (Hybrid Join). Although this is an adaptive approach but it is suboptimal with respect to stream data with Zipfian distribution.

7 Conclusions

In this paper we investigated a stream-based join algorithm called X-HYBRID JOIN. Our main observation about X-HYBRIDJOIN is that the tuning factor is not considered but it is necessary, particularly when limited memory resources are available to execute the join operation. By omitting the tuning factor, the available memory cannot be distributed optimally among the join components and consequently the algorithm cannot perform optimally. In this paper, we revise the cost model for X-HYBRIDJOIN and propose its tuning based on this cost model. To strengthen our arguments we implemented a prototype of Tuned X-HYBRIDJOIN and compared the performance with the existing approach.

References

1. Naeem, M.A., Dobbie, G., Weber, G.: X-HYBRIDJOIN for Near-real-time Data Warehousing. In: Fernandes, A.A.A., Gray, A.J.G., Belhajjame, K. (eds.) BNCOD 2011. LNCS, vol. 7051, pp. 33–47. Springer, Heidelberg (2011)
2. Anderson, C.: *The Long Tail: Why the Future of Business is Selling Less of More*. Hyperion (2006)
3. Naeem, M.A., Dobbie, G., Weber, G.: HYBRIDJOIN for Near-real-time Data Warehousing. *IJDWM: International Journal of Data Warehousing and Mining* 7(4), 21–42 (2011)
4. Golab, L., Tamer Özsu, M.: Processing Sliding Window Multi-Joins in Continuous Queries over Data Streams. In: *VLDB 2003*, Berlin, Germany, pp. 500–511 (2003)
5. Babu, S., Widom, J.: Continuous queries over data streams. *SIGMOD Rec.* 30(3), 109–120 (2001)
6. Polyzotis, N., Skiadopoulos, S., Vassiliadis, P., Simitsis, A., Frantzell, N.E.: Supporting Streaming Updates in an Active Data Warehouse. In: *ICDE 2007: IEEE 23rd International Conference on Data Engineering*, Los Alamitos, CA, USA, pp. 476–485 (2007)
7. Polyzotis, N., Skiadopoulos, S., Vassiliadis, P., Simitsis, A., Frantzell, N.: Meshing Streaming Updates with Persistent Data in an Active Data Warehouse. *IEEE Trans. on Knowl. and Data Eng.* 20(7), 976–991 (2008)
8. Naeem, M.A., Dobbie, G., Weber, G.: R-MESHJOIN for Near-real-time Data Warehousing. In: *DOLAP 2010: Proceedings of the ACM 13th International Workshop on Data Warehousing and OLAP*. ACM, Toronto (2010)

Classifier Ensemble Framework Based on Clustering Method

Hamid Parvin, Sajad Parvin, Zahra Rezaei, and Moslem Mohamadi

Nourabad Mamasani Branch, Islamic Azad University, Nourabad Mamasani, Iran
hamidparvin@mamasaniiu.ac.ir,
{s.parvin, rezaei, mos.mohamadi}@iust.ac.ir

Abstract. This paper proposes an innovative combinational method how to select the number of clusters in the Classifier Selection by Clustering (CSC) to improve the performance of classifier ensembles both in stabilities of their results and in their accuracies as much as possible. The CSC uses bagging as the generator of base classifiers. Base classifiers are kept fixed as either decision trees or multilayer perceptron during the creation of the ensemble. Then it partitions the classifiers using a clustering algorithm. After that by selecting one classifier per each cluster, it produces the final ensemble. The weighted majority vote is taken as consensus function of the ensemble. Here it is probed how the cluster number affects the performance of the CSC method and how we can switch to a well approximation option for a dataset adaptively. We expand our studies on a large number of real datasets of UCI repository to reach a well conclusion.

Keywords: Decision Tree, Classifier Ensembles, Bagging, AdaBoosting.

1 Introduction

Although the more accurate classifier leads to a better performance, there is another approach to use many inaccurate classifiers specialized for a few data in the different problem spaces and using their consensus vote as the classifier. This can lead to a better performance due to the reinforcement of the consensus classifier in the error-prone feature spaces. In General, it is ever-true sentence that combining diverse classifiers usually results in a better classification [1]-[2].

Giacinto and Roli propose a clustering and selection method to deal with the diversity generation problem [3]. They first produce a large number of classifiers with different initializations, after that they select a subset of them according to their distances in their output space. They don't take into consideration how the base classifiers are created. In this paper it is explored that usage of Bagging and Boosting as the sources of diversity how can affect on their methods. Besides it is explored that selection of a classifier from each of clusters how can be done better.

Generally, there are two important challenging approaches to combine a number of classifiers that use different train sets. They are Bagging and Boosting. Both of them are considered as two methods that are sources of diversity generation.

The term Bagging is first used by [4] abbreviating for Bootstrap AGGREGatING. The idea of Bagging is simple and interesting: the ensemble is made of classifiers built on bootstrap copies of the train set. Using different train sets, the needed diversity for ensemble is obtained. Breiman [5] proposes a variant of Bagging which it is called Random Forest [6]. Random Forest is a general class of ensemble building methods using a decision tree as the base classifier. Random Forest algorithm which is one of the well known versions of Bagging classifier [2] is implemented and compared with the proposed method. Boosting is inspired by an online learning algorithm called Hedge(β) [7]. Another version of these algorithms is arc-x4 which performs as another version of recently ADAboost [2].

Giacinto and Roli propose a clustering and selection method [3]. They first produce a large number of MLP classifiers with different initializations. After that they partition them. They select one classifier from each cluster of the partition. Finally they consider them as an ensemble and aggregate them to produce final decisions.

Parvin et al. propose a framework for development of combinational classifiers. In their framework, a number of train data-bags are first bootstrapped from train dataset. Then a pool of weak base classifiers is created; each classifier is trained on one distinct data-bag. After that to get rid of similar base classifiers of the ensemble, the classifiers are partitioned using a clustering algorithm. The partitioning is done considering the outputs of classifiers on train dataset as feature space. In each partition, one random classifier is selected to participate in final ensemble. Then, to produce consensus vote, different votes (or outputs) are gathered out of ensemble. After that the weighted majority voting algorithm is applied over them. The weights are determined using the accuracies of the base classifiers on train dataset [8].

2 Classifier Selection by Clustering

The main idea behind the classifier selection by clustering method is to use the most diverse set of classifiers obtained by Bagging or Boosting mechanism. Indeed a number of classifiers are first trained by the two well-known mechanisms: Bagging or Boosting. After that the produced classifiers partitioned according their outputs. Then the nearest classifier to the head of each produced cluster is selected. Since each cluster is produced according to classifiers' outputs, it is highly likely that selecting one classifier from each cluster, and using them as an ensemble can produce a diverse ensemble that outperforms the traditional Bagging and Boosting, i.e. usage of all classifiers as an ensemble.

In training phase of the classifier selection by clustering method by Bagging, n subsets of dataset are bootstrapped with b percent of the train dataset. Then a classifier is trained on each of those subsets. Each classifier is also then tested over the whole of train dataset and its accuracy is calculated after that. The output of i th classifier over train dataset is denoted by O_i and its accuracy is denoted by P_i .

In training phase of the classifier selection by clustering method by Boosting, a subset of dataset containing b percent of train dataset is again selected. Then the first classifier is trained on this subset. After that the first classifier is tested on the whole train dataset which this results in producing the O_1 and P_1 . Using O_1 , the next subset of b percent of train dataset is obtained. This mechanism is continued in such a way

that obtaining i th subset of b percent of train dataset is produced considering the O_1, O_2, \dots, O_{i-1} . For more information about the mechanism of Boosting, the reader can refer to Kuncheva [2].

In final part of the method a dataset whose i th dataitem is O_i is first produced. Features of this dataset are real dataitems of under-leaning dataset. A new dataset having n classifiers and N features is available, where n is a predefined value showing the number of classifiers produced by Bagging or Boosting and N is the cardinality of under-leaning datasets. After producing the mentioned dataset, the dataset is partitioned by use of a clustering algorithm that this results in some clusters of classifiers. Each of the classifiers of a cluster has similar outputs on the train dataset; it means these classifiers have low diversities, so it is better to use one of them in the final ensemble rather than all of them. For escaping from outlier classifiers, the clusters which contain number of classifiers smaller than a threshold are ignored.

3 Experimental Study and Discussion

Evaluation metric based on which an output of a classifier is computed is discussed in the first subsection of this section. The details of the used datasets are given in the subsequent section. Then the settings of experimentations are given. Finally the experimental results are presented.

The accuracy is taken as the evaluation metric throughout all the paper. All the experiments are done using 4-fold cross validation. The results obtained by 4-fold cross validation are repeated as many as 10 independent runs. The averaged accuracies over the 10 independent runs are reported.

The proposed method is examined over 13 different standard datasets and one artificial dataset. It is tried for datasets to be diverse in their number of true classes,

Table 1. Details of used dataset

Dataset Name	# of dataitems	# of features	# of classes	Data distribution per classes
Breast Cancer*	404	9	2	444-239
Balance Scale*	625	4	3	288-49-288
Bupa*	345	6	2	145-200
Glass*	214	9	6	70-76-17-13-9-29
Galaxy*	323	4	7	51-28-46-38-80-45-35
Half-Ring*	400	2	2	300-100
SAHeart*	462	9	2	160-302
Ionosphere*	351	34	2	126-225
Iris*	150	4	3	50-50-50
test Monk1	412	6	2	216-216
test Monk2	412	6	2	216-216
test Monk3	412	6	2	216-216
train Monk1	124	6	2	62-62
train Monk2	169	6	2	105-64
train Monk3	122	6	2	62-60
Wine*	178	13	3	59-71-48
Yeast*	1484	8	10	463-5-35-44-51-163-244-429-20-30

features and samples. A large variety in used datasets can more validate the obtained results. Brief information about the used datasets is available in Table 1. These real datasets are available at UCI repository [9]. The details of half-ring dataset can be available in [10].

Note that some of datasets which are marked with star (*) in Table 1 are normalized. All experiments are done over the normalized features in the stared dataset. It means each feature is normalized with mean of 0 and variance of 1, $N(0, 1)$.

The measure of decision for each employed decision tree is taken as Gini measure. The threshold of pruning is set to 2. Also the classifiers' parameters are fixed in all of their usages.

All multilayer perceptrons which are used in the experiments have two hidden layers including 10 and 5 neurons respectively in the first and second hidden layers, as well as they are iterated 100 epochs.

In all experiments n , b and threshold of accepting a cluster are set to 151, 30 and 2 (i.e. only the clusters with one classifier is dropped down) respectively. All the experiments are done using 4-fold cross validation. Clustering is done by k-means clustering algorithm with different k parameters.

Table 2 shows the accuracies of different methods by considering a DT as each of the base classifiers. Table 3 shows the accuracies of different methods by considering a MLP as each of the base classifiers. The parameter r is set to 33 to reach the results of the Table 2 and Table 3.

While we choose only at most 22 percent of the base classifiers of Bagging, the accuracy of their ensemble outperforms the full ensemble of them, i.e. Bagging Method. Also it outperforms Boosting method and proposed method based on Boosting method.

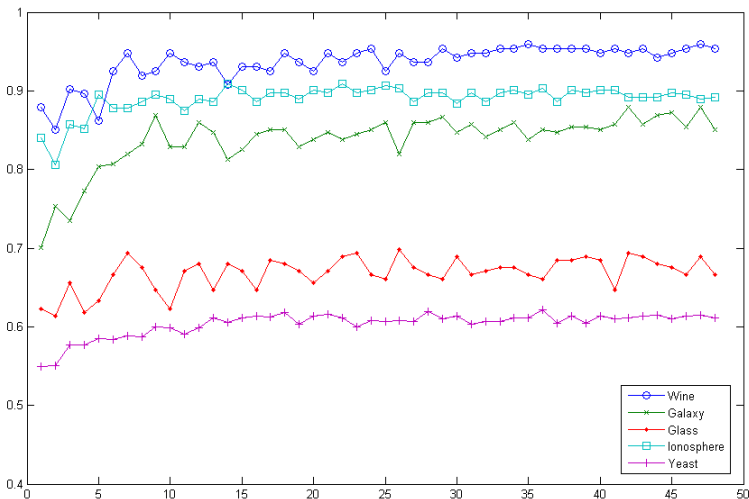


Fig. 1. The performance of CSC by boosting over some dataset with $n=151$ and different r and MLP as base classifier

Table 2. Comparison of the results by considering Decision Tree as base classifier. * shows the dataset is normalized, and 4 fold cross validation is taken for performance evaluation. ** shows that the train and test sets are predefined and averaged over 10 independent runs.

	Arc-X4	Random Forest	Classifier Selection By RF	Classifier Selection By Arc-X4	Cluster and Selection
Breast Cancer*	95.74	96.32	96.47	95.05	93.68
Balance Scale*	94.44	93.60	94.72	94.24	94.44
Bupa*	70.64	72.09	72.97	66.28	64.53
Glass*	65.04	70.28	70.28	62.26	60.85
Galaxy*	70.59	73.07	72.45	70.28	70.94
Half-Ring*	97.25	95.75	97.25	95.75	95.75
SAHeart*	70.00	71.30	72.61	69.70	68.04
Ionosphere*	90.31	92.31	91.45	89.74	87.64
Iris*	96.62	95.27	96.62	95.95	94.59
Monk problem1**	98.11	97.49	98.76	97.37	98.34
Monk problem2**	97.01	86.64	97.62	86.73	97.14
Monk problem3**	87.29	96.92	96.97	96.34	87.31
Wine*	96.07	97.19	97.19	95.51	92.61
Yeast*	53.17	53.98	53.98	52.09	54.51
Average	84.45	85.16	86.38	83.38	82.88

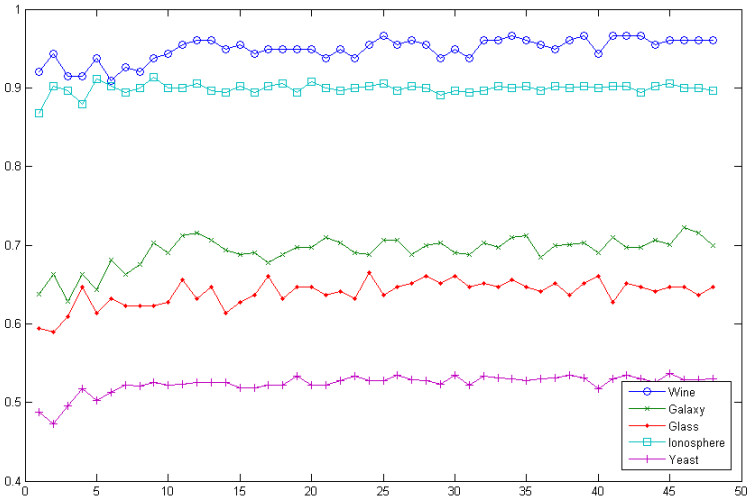


Fig. 2. The performance of CSC by boosting over some dataset with $n=151$ and different r and DT as base classifier

Because the classifiers selected in this manner (by Bagging along with clustering), have different outputs, i.e. they are as diverse as possible, they are more suitable than ensemble of all them. It is worthy to mention that the Boosting is inherently diverse enough to be an ensemble totally; and the reduction of ensemble size by clustering destructs their Boosting effect. Take it in the consideration that in Boosting ensemble, each member covers the drawbacks of the previous ones.

To see how the parameter r affects over the performance of classification over CSC methods (by bagging, boosting and Gianito [3]) with two base classifiers (MLP, DT), take a look at Fig. 1 and Fig. 6.

These figures depict the accuracies of different method by 4-fold cross validation on some benchmarks. As it is inferred from these figures, increasing the cluster number parameter r is not always resulted in the improvement in the performance.

The performances of CSC by boosting over some dataset with $n=151$ and different r are depicted in Fig 1 and Fig 2 respectively while MLP and DT are used as base classifier. The same results are depicted in Fig 3 and Fig 4 for CSC by Gianito's method. Fig 5 and Fig 6 finally represent the performances of CSC by bagging method.

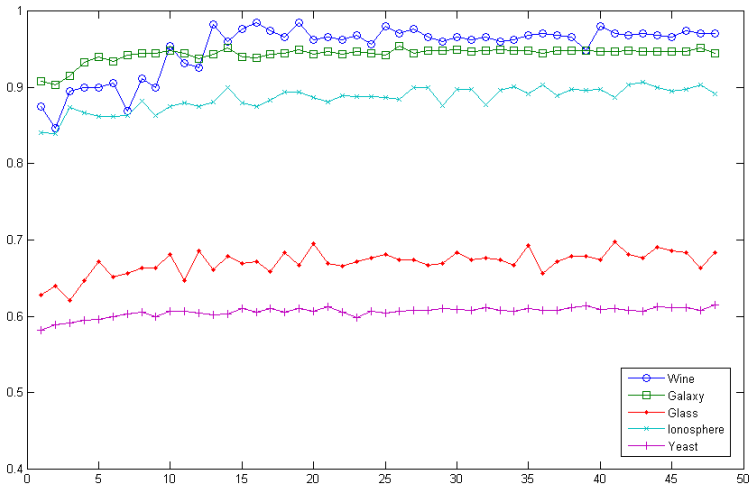


Fig. 3. The performance of Gianito's method over some dataset with $n=151$ and different r and MLP as base classifier

Indeed an $r=15$ is a well choice for all of the datasets. It means that if the classifier number parameter, n , is 151 then $r=15$ is a well value for the cluster number parameter. In other words, using 10 percent of the base classifiers in the final ensemble can be a good option.

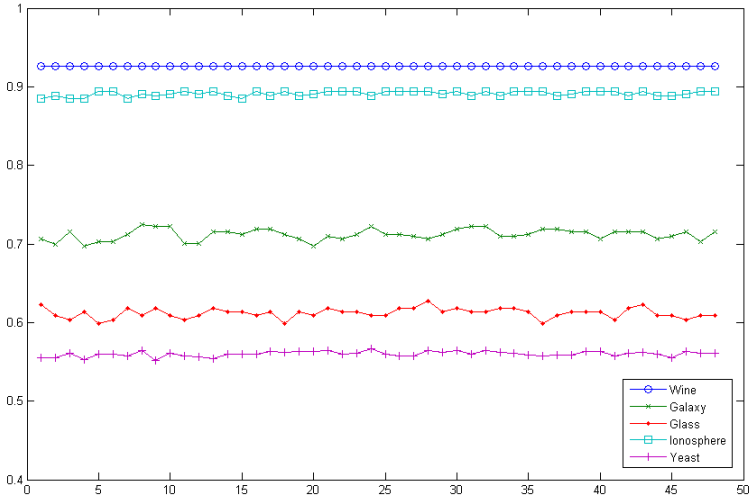


Fig. 4. The performance of Gianito's method over some dataset with $n=151$ and different r and DT as base classifier

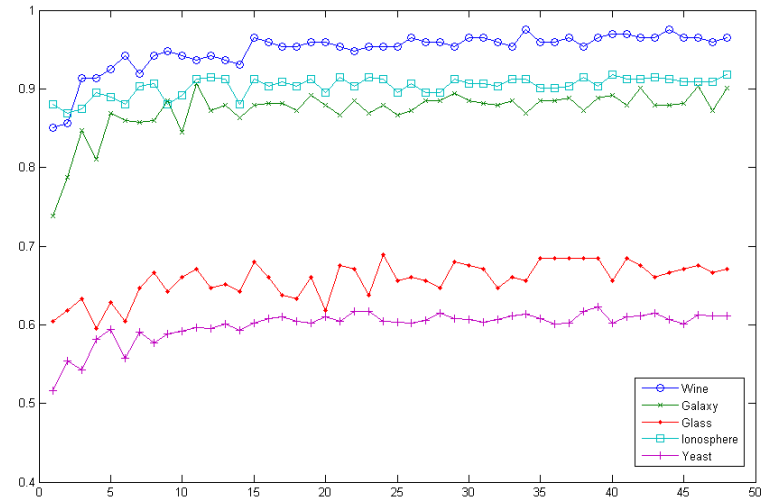


Fig. 5. The performance of CSC by bagging over some dataset with $n=151$ and different r and MLP as base classifier

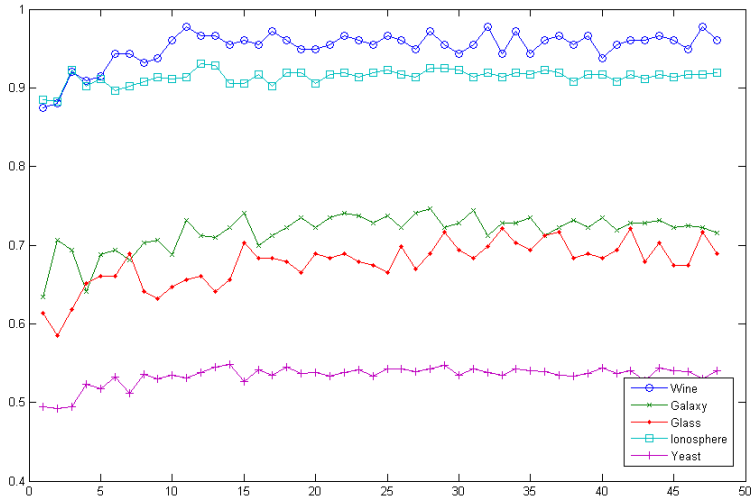


Fig. 6. The performance of CSC by bagging over some dataset with $n=151$ and different r and DT as base classifier

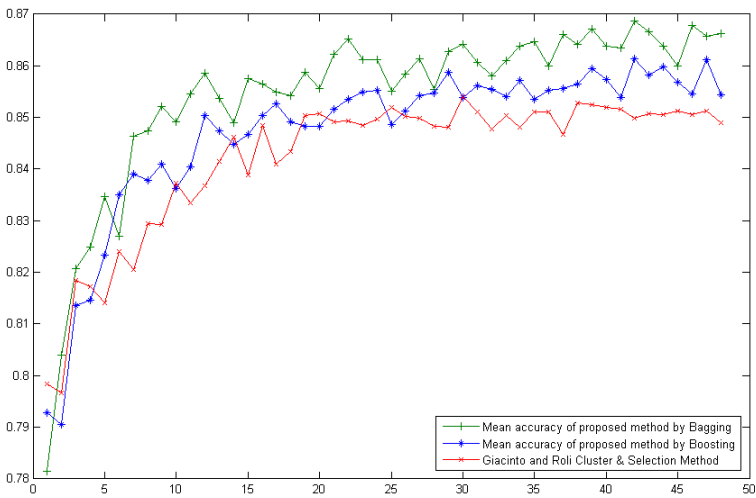


Fig. 7. The performance of CSC methods averaged over 14 datasets of Table 1 with $n=151$ and different r and MLP as base classifier

Indeed in this option, a classifier is selected from a cluster of classifiers that contains about 10 classifiers, so it gives the method the ability to select each classifier from a good coverage of classifiers.

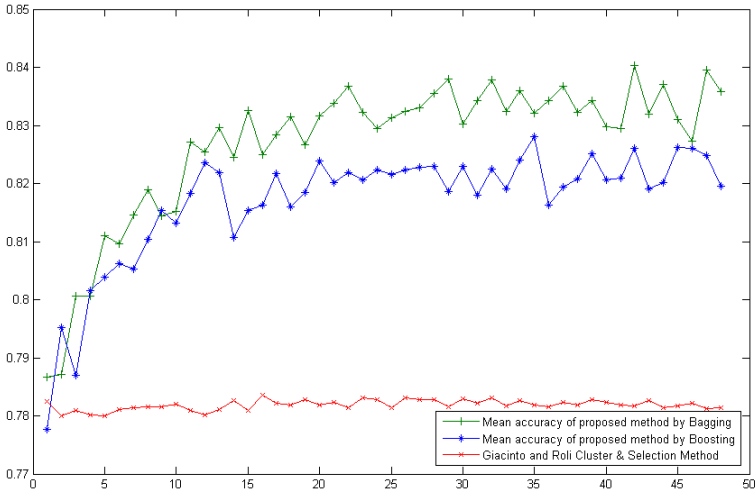


Fig. 8. The performance of CSC methods averaged over 14 datasets of Table 1 with $n=151$ and different r and DT as base classifier

Table 3. Comparison of the results by considering MLP as base classifier. * shows the dataset is normalized, and 4 fold cross validation is taken for performance evaluation. ** shows that the train and test sets are predefined and averaged over 10 independent runs.

	Arc-X4	Bagging	Classifier Selection By Bagging	Classifier Selection By Arc-X4	Cluster and Selection
Breast Cancer*	97.06	96.91	96.91	96.47	96.19
Balance Scale*	93.27	91.99	91.35	92.95	95.75
Bupa*	70.06	71.22	72.09	68.02	71.98
Glass*	66.04	66.98	67.45	66.04	67.05
Galaxy*	87.00	85.62	85.62	84.52	87.00
Half-Ring*	97.25	95.75	97.25	97.25	97.25
SAHeart*	73.04	72.39	71.52	71.09	70.18
Ionosphere*	90.03	88.51	90.31	87.64	88.51
Iris*	96.62	96.62	97.97	97.33	93.33
Monk problem1**	98.06	92.23	98.43	97.87	98.34
Monk problem2**	87.35	85.68	87.41	87.23	87.21
Monk problem3**	97.09	95.87	97.33	96.99	96.77
Wine*	96.59	96.06	97.19	95.51	95.23
Yeast*	60.85	61.19	61.19	60.85	60.56
Average	86.45	85.50	86.57	85.70	86.10

The Fig. 7 and Fig. 8 depict the averaged accuracies over all 14 different datasets. Fig. 7 reports the performances of the framework by using the MLP as base classifier.

Fig. 8 reports the performances of the framework by using the DT as base classifier.

As it is illustrated in the Fig. 7 and Fig. 8, usage of bagging as generator of classifiers for CSC method is better than Boosting and Giacinto and Roli's methods. Also it is concluded that using $r=33$ instead of $r=15$ is a better choice for all of the 14 datasets. In other words, using 22 percent of the base classifiers in the final ensemble can be a better option.

Comparing the Fig. 7 and Fig. 8 one can find out that the using the decision tree as base classifier increases the gap between the three approaches to generate the base classifiers. It is due to special feature of the decision tree. Because it is very sensitive to its train set, the use of decision tree as base classifier is very consistent with the Bagging mechanism.

4 Conclusion and Future Works

In this paper, we have proposed a new method to improve the performance of classification. The proposed method uses Bagging as generator of the base classifiers. Then using k-means we partition the classifiers. After that we select one classifier per a validated cluster.

Also it is concluded that using 22 percent of the base classifiers in the final ensemble can be a well option generally.

Using the decision tree as base classifier increases the gap between the three approaches to generate the base classifiers. It is due to special feature of the decision tree. Because it is very sensitive to its train set, the use of decision tree as base classifier is very consistent with the Bagging mechanism.

While we choose only at most 22 percent of the base classifiers of Bagging, the accuracy of their ensemble outperforms the full ensemble of them. Also it outperforms Boosting.

As a future work, one can turn to research on the variance of the method. Since it is said about Bagging can reduce variance and Boosting can simultaneously reduce variance and error rate.

References

1. Günter, S., Bunke, H.: Creation of Classifier Ensembles for Handwritten Word Recognition Using Feature Selection Algorithms. In: Proceedings of the Eighth International Workshop on Frontiers in Handwriting Recognition (IWFHR 2002), August 06-08, p. 183 (2002)
2. Kuncheva, L.I.: Combining Pattern Classifiers, Methods and Algorithms. Wiley, New York (2005)
3. Giacinto, G., Roli, F.: An approach to the automatic design of multiple classifier systems. Pattern Recognition Letters 22, 25–33 (2001)
4. Breiman, L.: Bagging Predictors. Journal of Machine Learning 24(2), 123–140 (1996)
5. Breiman, L.: Random Forests. Machine Learning 45(1), 5–32 (2001)

6. Yang, T.: Computational Verb Decision Trees. *International Journal of Computational Cognition* 4(4), 34–46 (2006)
7. Freund, Y., Schapire, R.E.: A Decision-Theoretic Generalization of On-Line Learning and an Application to Boosting. *J. Comput. Syst. Sci.* 55(1), 119–139 (1997)
8. Parvin, H., Minaei-Bidgoli, B., Beigi, A.: A New Classifier Ensembles Framework. *Knowledge-Based and Intelligent Information and Engineering Systems*, 110–119 (2011)
9. Blake, C.L., Merz, C.J.: UCI Repository of machine learning databases (1998), <http://www.ics.uci.edu/~mllearn/MLRepository.html>
10. Minaei-Bidgoli, B., Topchy, A.P., Punch, W.F.: Ensembles of Partitions via Data Resampling. In: *ITCC*, pp. 188–192

Usability Cost Benefit Analysis Using a Mathematical Equation

Samina Rajper¹, Abdul Wahid Shaikh², Zubair A. Shaikh³, and Imran Amin¹

¹ Department of Computing, SZABIST, Karachi
Samina.rajper@gmail.com

² Department of Computer Science, SALU, Khairpur

³ Department of Computer Science, FAST-NU, Karachi

Abstract. The software development is a key area in Software Engineering. Several mathematical models have been emerged and implemented for the cost benefit analysis of the software development effort. The most dominant model is Bohem's COCOMO. On the other hand, Usability is also an important characteristic of the software or system. But, there is no defined mathematical model to calculate the effort spent for the process of usability. However, several theoretical cost benefit analysis models are defined by various authors. The present study is conducted to analyze different usability cost benefit justification models. Further, on the basis of general cost benefit analysis framework by Mayhew, a mathematical model is defined. The purpose of present study is to provide a mathematical equation to usability cost benefit analysis process.

Keywords: Usability, Cost Benefit Justification, Mathematical Model, Equation, COCOMO.

1 Introduction

There are many quality attributes defined by International Standard Organization to verify the quality standard of the product. Usability is also one of the major ISO 9126 defined quality characteristics. According to ISO 9126; usability can be defined by three attributes, i.e., efficiency, effectiveness and satisfaction. However, the usability is also defined by ISO 9241-11 that the extent to which a particular group of users can use the product and acquire the specified goals with efficiency, effectiveness and satisfaction in context of specified use. Summing up that usability can be defined as the qualification of the product that makes it understandable, learnable, and easy to use under specified conditions for particular goals [1].

There are several potential benefits of usability and on the same time many people (e.g., staff, users, management etc.) are the main beneficiaries of the usability. But it is questionable that usability cannot be incorporated into the organizations as a main activity in product development process [2] and organizations are unable to exercise usability as the main phase of the product development life cycle. In fact, the usability and product life are directly proportional to each other, i.e., the more usable product the long lasting product it is and again a user centered product will has a long line of users.

The current study is conducted to represent mathematically the general framework given by Mayhew and Tremaine with different identified attributes to analyze the cost and benefit of usability of the product. The purpose of formulating the already defined general framework by mathematical equations is to provide a refined mathematical model to the general theoretical framework of usability cost benefit justifying model.

Many research works has been done to direct the organizations or usability engineering teams towards simple cost and benefit calculation models of usability as to gain the long lasting benefits of user centered designs. In section 2, cost benefit analyses will be discussed.

2 Cost Benefit Analyses and Models

All the products, softwares or systems can be thought beneficial in terms of how much return on investment is achieved. In Software Engineering life cycle or Software Development life cycle of product, COCOMO (Constructive cost model by Boehm) [3-7] is used as a reliable approach for calculating the cost incurred and estimated benefits for return on investment on the project. But, there is no such formulated model is defined for usability cost benefit calculation. However, there is some published work on cost benefit analyses for usability also. That work can lead towards some organized and defined formulation.

3 Cost Benefit Analysis Models

The cost benefit justification can be understood as a method of examining the project for the purpose of investment. The cost benefit analysis method needs to identify and simulate the data on which the decision can be made [8]. The usability cost benefit justification has the main goal to estimate the costs and benefits for specific usability activities. These activities may be prototyping, usability testing, heuristic evaluation etc. [9]. The analysis can be done in four steps [9].

1. Selection of usability techniques
2. Determination of the appropriate unit of measurement
3. Estimate the benefit's magnitude
4. Finally, translating the assumed benefits into financial figure

The general three steps to proceed for the cost-benefit method are identified as follows [10].

1. Identification of the financial value of cost benefits variables for the expected project.
2. Using the simple techniques to analyze the relationship between expected costs and benefits for the expected projects.
3. Decide for investment.

In the current study, the purpose of discussing different models is just to know that how different authors identified different attributes to calculate the usability cost and benefits for different types of application, i.e., Internal users, vendor company, web applications etc. also, to describe that why the Model given by Mayhew is selected as the base for the Mathematical Equation during the present study. There are some models published in [11]. It is observed that different models have identified various attributes to calculate cost of usability and also predicted potential benefits for various applications are different. As in [12], cost benefit justification is discussed from the perspective of Vendor Company. This model identifies that following three areas can be used for benefit justification for a vendor company [13].

1. Increased sales
2. Decrease support costs
3. Decrease development costs.

But, there is no mathematical formula given to represent their overall method. However, the usability benefits are calculated via the cost benefit analysis of human factors at work. Following are the some identified benefits for representing the cost benefit analysis model by Karat [13-15].

1. Increased sales
2. Increased productivity
3. Reduce personnel costs via smaller staff turnover.

Bevan [16] proposed the potential benefits for an organization in the areas of development, sales, use and support. According to the author [16] the benefits can be achieved in terms of development, sales and support by a vendor company. However, the use and support are the identified areas to gain benefit by customers [16].

However, Mayhew and Tremaine [17] represented a general framework for cost-benefit analysis of usability by focusing attention on the benefits which can be important for the audience for analysis. Their general framework created room for all type of applications to justify cost and benefit for usability perspective according to their interest. In section 4, the theoretical overview of the general approach presented by [17] is discussed also it is attempting to answer that why the mentioned model [17] is selected for the basis of Mathematical Model presented in this study?

4 Why an Equation on the Basis of Cost Benefit Justification Model by Mayhew and Tremaine?

After a detailed literature review of different cost benefit analysis models and approaches for the purpose of current study, i.e., to propose a mathematical model or representation of usability cost benefit justification, it is come to know that different authors identified different attributes for calculating the potential benefits of the projects. While the general frame work [17] provides an overall framework for calculating the usability cost benefit for the application of any type also with any attributes. Software process development needs the usability cost benefit analysis for the following two reasons [17].

1. This justification represents usability as an important cost saving method.
2. To be helpful in planning usability engineering program for any development project.

In software development industry, there are several types of application which need to be analyzed for the investment purpose. Therefore, the author suggested in [17] to follow the following steps to conduct a usability cost benefit justification.

1. Devise the usability engineering plan for the project. It means that the project should be analyzed systematically via usability engineering life cycle.
2. Usability engineering life cycle can be followed by incorporating the project in its each phase; which are:

- Requirements Analysis,
- Design/Testing/Development
- Installation.

However, each phase is comprised of different tasks. A usability engineering task is an activity that produces a work product that is must for the later usability engineering steps [17]. However, a technique is a particular methodology for carrying out a task to fulfill a goal. For following the general approach to justify usability cost benefits as already mentioned in the first step, a usability engineering plan is laid out. This plan will specify certain techniques to be used for each usability engineering life cycle task. The techniques will be broken down into the steps and the personnel cost and equipment cost will be specified at each step. The cost of each task can be calculated by multiplying the total number of hours for each type of personnel by their current hourly wage, i.e., fully loaded. The term “Fully loaded” includes salary, benefits, office space, equipment, utilities, and other facilities. Finally, adding up personnel costs for all type of personnel [17].

In the next step, the overall estimated or predicted benefit is to be calculated. The list of potential benefits varies from application type to application type. The selection of the list of potential benefits depends upon the organization. However, the identified attributes for different types of organization to calculate the benefits are given in Table 1.

Table 1. Identified benefit attributes for Internal users and Vendor Companies [17]

Development organization for Internal users	Vendor Company
Increased user productivity	Increased sales
Decreased user errors	Decreased Customer Calls for Service

Table 2. Depicts the identified areas of benefits for different types of web sites [17]

E-Com	Funded by Advertisements	Product Information	Customer Service	Intranet
Increased buy-to-look ratios of Visits	Increased number	Savings from changes in earlier Lifecycle	Savings from changes in earlier Lifecycle	Savings from changes in earlier Lifecycle
Decreased Abandoned shopping carts	Increased Return Visits	Increased Sales leads	Decreased costs of traditional customer Service Channels	Decreased use of live customer service
Increased Return Visits	Increased length of visits	-----	-----	Decreased Training costs
Decreased Failed Searches	Decreased failed searches	-----	-----	Increased user productivity
Decreased Costs of Other Sales Channels	Savings from changes in earlier lifecycle	-----	-----	Decreased user errors

The area of web sites also consists of different types of the web sites. Table 2 represents the identified expected potential benefits for different types of websites. It is observed from the framework [17] that total calculation of usability estimation for a project depends upon two factors, i.e., total cost invested (Cost estimation) and total benefit gained (Gain estimation). If the correct or a near to correct analysis is made then the decisive factor for the project can be achieved, i.e., “Estimate or Analysis”. Summing up the discussion here, it is analyzed that usability cost benefit justification is equally important for all type of organizations. Different types of organizations may involve in varying type of products development; hence the usability will vary from one to another product. Variant types of products usability cost analyzing procedure will be different but the general framework suggests to follow the usability engineering Plan by involving the usability engineering life cycle into the project under consideration. The usability engineering plan can be different from one to another [17]. The procedure is as follows:

1. Breaking up phases into tasks
2. The task will be accomplished by some techniques
3. Each task accomplishing technique will be carried out by some personnel.

Therefore, the total cost estimation for each phase will depend upon the cost of number of hours of user and wages and finally the number of users involved to complete one step. This procedure will be repeatedly followed until the total cost for all the phases will be calculated. This cost will be compared to the potential benefits gained from the product. The decision for the investment on the project will depend upon the difference of the usability benefits and cost. From the overview of Cost benefit justification model by [17], it is found that this is the most general framework for usability cost benefit inspection and almost all types of attributes involved in various types of applications are discussed. Therefore, this model is chosen for the Mathematical model during this study.

In the next section, it will be discussed that how the identified techniques for calculating the total usability cost for the project and the identified potential benefits for the organization can be represented by a mathematical model.

5 Formulation of Mathematical Model for Usability Cost Benefit Justification

In this section, the basic steps towards the final equation for calculating the usability cost benefit for a product on the basis of discussed model [17] will be discussed.

The usability cost benefit justification mathematical model on the basis of general framework by Mayhew [17] can be achieved by first demonstrating the cost calculation methodology step by step using the proposed mathematical model and then calculation of potential benefits. Finally, the theoretical general framework will be re-pictured by a general equation to justify the usability cost for any project.

5.1 Usability Cost Calculation

According to the Mayhew framework [17], it is necessary first to start with Usability engineering plan.

— Step 1: Usability Engineering Plan

Following up a usability engineering plan will be helpful to identify the usability engineering tasks and techniques, will be employed and broken down into required staff and hours. Devising the usability plan for any project is a very important step while analyzing its cost invested and benefits gained (predicted) because the plan varies from project to project; hence the tasks and techniques and involved users and their working hours and wages will also be different from one plan to another [17]. Therefore, it can be said that the usability engineering plan can be unique for any project. To reach the required mathematical format of this theory, it is needed to analyze any example. Table 3 is used to depict any hypothetical example to understand:

- How the phases of usability engineering life cycle will be involved in usability plan?
- How the phases are broken up into steps/tasks/techniques?
- How each step/task/technique is carried out by involving different type of staff?
- How to start calculating the wages for each and every staff participating in usability plan?

Table 3. Depicts the Usability engineering Plan for any project [17]

Phase	Task	User-1@ \$200 for 2 Hrs	User-n @ \$a for anyHrs	Total
1. Requirement Analysis	user profile	60	100	Total\$
---	Usability Goals			
--	-----			
All Phases	all task	wages	wages	Total\$

Table 3 shows the procedure that first break up phases into tasks and employing different types of users at different wages working for different hours per year to accomplish the tasks to complete one phase and the same procedure will be followed for other phases

Note that the values represented in Table 3 are assumed. The calculation will be done by taking the wages according to the rules of any organization. The users may be any staff, e.g., usability engineers, manager, Quality assurance staff etc. Users in this case can be defined as who are expected to participate according to the usability engineering plan.

– Step 2: Deciding the Analysis Parameters

After laying down the usability engineering plan, the next step is to select the analysis parameters for the application. Analyze and decide the parameters for cost calculation and potential benefit calculation. For example the cost calculation may involve the any parameters for an application for internal users [17]. Table 4 is the representation of an example of some identified analysis parameters for an application for internal users. The application may be used for a limited staff, i.e., 200-250 in a bank or insurance company etc.

Table 4. Depicts the Analysis Parameters for an application for internal users [17]

Analysis Parameters	Values
Number of Users	250
Users work days per year	230
Users fully loaded hourly wage	\$25
Developer fully loaded hourly wage	\$175
Usability Engineer fully loaded hourly wage	\$175
Manager fully loaded hourly wage	\$200

It is analyzed from Table 3 and 4 that the number of users, types of users, number of working hours and value for wages vary from application to application. Therefore, the above scenario can be generalized as represented using Table 5.

Table 5. Depicts the Generalized form for Analysis Parameters for any application

Analysis Parameters	Values
Number of Users	n
Users work days per year	n
Users fully loaded hourly wage	n
Developer fully loaded hourly wage	n
Usability Engineer fully loaded hourly wage	n
Manager fully loaded hourly wage	n
n	n

Note that ‘n’ shows that values for the variables or analysis parameters may be any and the number of analysis parameters may vary from application type to application type.

It is added here that the analysis parameters for one application will be different from another application. For example; in comparison of analysis parameters for an internal application (as stated above), the analysis parameters for calculating the cost for a commercial application by a vendor company will be different and might be current typical sales (in units), User fully loaded hourly wage, Developer fully loaded hourly wage, Usability engineer fully loaded hourly wage, Manager fully loaded hourly wage, Customer support fully loaded hourly wage etc. [17]

Hence, it is observed from the analysis parameters for calculating the usability cost and benefit, the number of parameters and type of parameters will be different from one application to another. Therefore, the parameters will be supposed as “n” for any application.

Following the calculation in Table 3.the equation can be formed as follows:

1. Calculating the cost of each user by multiplying the number of working hours by fully loaded wages and number of users involved.

For example; two usability engineers are involved for 30 hours at \$175 = 2x30x175 = \$10500. This implies that “n” users of any type, e.g., manager are engaged on some hrs and wages:

$$User = n \times hrs \times wages \tag{1}$$

2. For the accomplishment of one task several users of various types can be involved, therefore, the number of users is assumed as “u”. Total cost for one task or technique will be acquired by summation of cost of all users involved in the task. Hence, the equation will be:

$$Task = \sum_{u=1}^m (Users_u) \therefore users = user1 + user2 + \dots + user_m \tag{2}$$

3. Accomplishment of one phase depends upon the accomplishment of many tasks or techniques. Hence, the summation of cost for all; suppose “o” tasks will be the cost of one phase. Therefore, the required equation will be:

$$Phase = \sum_{s=1}^o Task_s \therefore Task_s = Task1 + Task2 + \dots + Task_o \tag{3}$$

4. The whole usability engineering plan will be dependent of many phases. Let the number of phases are “k”, depend upon the devised plan for the project. The total cost for the plan will be a sum of all cost invested for each phase. Hence, the required equation will be:

$$TotalUsabilityCost = \sum_{i=1}^k Cost_i \therefore i = phase1 + phase2 + \dots + phase_k \tag{4}$$

The analysis of usability cost benefit justification involves calculation of cost estimated for all phases of usability engineering plan but also to calculate the predicted potential benefits for the project is required. Therefore, in the next step the identified potential benefits for the projects will be calculated and modeled into the equations required.

5.2 Usability Potential Benefit Calculation

In section 4, Table 1 and Table 2 are used to depict the predicted usability benefits for different types of the applications. Hence, the number of potential benefits and the nature of the potential benefits will be assumed as “z”, depending on the project type.

Suppose that the predicted potential benefits for an application for internal users are depicted here in Table 6, also the calculation procedure is shown as well [17]:

The number of relevant potential benefits for any application/project varies from one to another. From the Table 6, it is observed that each potential benefit can be calculated by multiplying all the variables involved. The product of all variables involved will result the total potential benefit gain for any application. It is analyzed here:

Table 6. Calculation of predicted potential benefits for internal user’s application[17]

Identified Potential Benefit Areas	Calculation	Total
Increased Productivity =	No: of days x No: of users x No: of transactions x Hrs saved or transaction x hourly rate	
	250x230x100x 0.001389x\$25	\$199,652.78
Decreased errors =	No: of users x No: of days x no: of eliminated errors x hrs saved per error x hourly rate	
	250x230x1.0x0.03333x\$25	\$47,916.67
<i>z</i>	$v_1 \times v_2 \times \dots \times v_p$	Total \$xyz

– Total Product of all variables involved in any one identified potential benefit will be the value for that potential benefit (i.e., as stated in Table 6). Therefore the required equation for this procedure will be:

$$PB = \prod_{a=1}^p V_a \because a = v_1 \times v_2 \times \dots \times v_p \tag{5}$$

– Any application can involve more than one predicted potential benefits. Therefore, the sum of all potential benefits involved in any application is required to predict the value of total benefit. Hence, the number of potential benefits can be from one to any. Therefore, the required equation will be equation (6):

$$TotalPotentialBenefit = \sum_{jk=1}^z PB_{jk} \because jk = PB_1 + PB_2 + \dots + PB_z \tag{6}$$

It is important to note here that the net benefit calculation for any application needs to calculate the predicted benefits for first year and for five year or life time too. The equation 6 is proposed to calculate the net benefit calculation for first year. It is supposed here that if the net benefit expected for the first year is less than the total calculated cost on the project then the project should be rejected to proceed.

5.3 Total Usability Cost Benefit Justification

From the theoretical model [17], it is analyzed that the decisive factor to proceed the project should be the difference between the total cost calculated and the net benefits

expected for the application. Therefore, from equation (4) and (6), the Justification can be done using the equation (7):

$$UCJ = TPB - TUC \quad (7)$$

Here:

UCJ = UsabilityCostJustification

TPB = TotalPotentialBenefit

TUC = TotalUsabilityCost

6 Conclusion

The objective of the conducted study is to represent a Mathematical Model for Usability Cost Benefit Justification as the software or product development process already has. The presented Mathematical Model is based on the theoretical framework by Mayhew [17]. It is necessary to have refined form of any theoretical model because the refined forms convince for further improvements in the models or frameworks. The represented mathematical model convinces for further improvements for example to have some coefficients and drivers according to the complexity of the application type. However, the undertaken study successfully provides a simple equation for Usability Cost Benefit Justification.

References

1. ISO/IEC 9126-1.:Software Engineering, Product quality, Part 1: Quality model. International Standard (2001)
2. Ohnemus, K.: Incorporating Human Factors in the System Development Life Cycle: Marketing and Management Approaches. In: IPCC 1996, pp. 46–53. IEEE, Los Alamitos (1996)
3. Boehm, B.W.: Software Engineering Economics. Prentice-Hall (1981)
4. Boehm, B.W.: Anchoring the Software Process. IEEE Software 13(4), 73–82 (1996)
5. Boehm, B.W.: Making RAD Work for your Project. Extended version of, IEEE Computer Column; USC Technical Report USC-SCE-99-512 (March 1999)
6. Boehm, B.W., et al.: Software Cost Estimation with COCOMO II, 1st edn. Prentice Hall PTR (2000)
7. Boehm, B.W., et al.: COCOMO II Model Definition Manual. Version 2.1. The University of Southern California (2000)
8. Rajanen, M.: Different Approaches to Usability Cost-Benefit Analysis. In: Remenyi, D., Brown, A. (eds.) Proc. ECITE 2006, pp. 391–397. Academic Press, Reading (2006)
9. Donahue, G.: Usability and the Bottom Line. IEEE Software 18(1), 31–37 (2001)
10. Burrill, C.W., Ellsworth, L.W.: Modern Project Management: Foundations for Quality and Productivity, pp. 209–223. Burrill-Ellsworth Assoc., New Jersey (1980) ISBN: 0-935-31000-2
11. Bias, R., Mayhew, D.: Cost-Justifying Usability. An Update for an Internet Age, 2nd edn. Academic Press, London (2005)

12. Ehrlich, R.: Cost Justification of Usability Engineering in Vendor's company. In: Bias, R., Mayhew, D. (eds.) *Cost-Justifying Usability An Update for Internet Age*, 2nd edn., pp. 185–213. Academic Press (2005)
13. Rajanen, M., Jokela.: Analysis of Usability Cost benefit Justification Models. Department of Information Processing Science. University of Oulu, Finland, mikko.rajanen@oulu.fi
14. Karat, C.M.: A Business Case Approach to Usability Cost Justification. In: Bias, R., Mayhew, D. (eds.) *Cost-Justifying Usability*, pp. 45–70. Academic Press, London (1994)
15. Karat, C.M.: A Business Case Approach to Usability Cost Justification for the web. In: Bias, R., Mayhew, D. (eds.) *Cost-Justifying Usability an Update for Internet Age*, 2nd edn., pp. 130–169. Academic Press, London (2005)
16. Bevan, N.: Cost Benefit Analysis. TRUMP report (September 2000)
17. Mayhew, D., Tremaine, M.: A Basic Framework for Cost-Justifying Usability Engineering. In: Bias, R., Mayhew, D. (eds.) *Cost-Justifying Usability*, 2nd edn., pp. 41–101. Academic Press, London (2005)

Efficient FPGA Implementation of Secure Hash Algorithm Grøstl – SHA-3 Finalist

M. Muzaffar Rao, Kashif Latif, Arshad Aziz, and Athar Mahboob

National University of Sciences and Technology (NUST), H-12 Islamabad, Pakistan
{Mrao,kashif,athar}@pnec.edu.pk, arshad@nust.edu.pk

Abstract. Cryptographic hash functions are used for digital signatures; message authentication codes (MACs) and other forms of authentication. National Institute of Standards and Technology (NIST) announced a publicly open competition for selection of new standard Secure Hash Algorithm called SHA-3. Hardware performance evaluation of the candidates of this competition is a vital part of this contest. In this work we present an efficient FPGA implementation of Grøstl, one of the final round candidates of SHA-3. We show our results in the form of chip area consumption, throughput and throughput per area. We compare and contrast these results with other reported implementations of Grøstl. Our design ranks highest in terms of throughput per area, achieving figures of 5.47 Mbps/slice on Virtex 7 and 5.12 Mbps/slice for Grøstl-256 on Virtex 6.

Keywords: SHA-3, Grøstl, Hash Functions, High Speed Hardware, FPGA.

1 Introduction

A hash function is a process whose input is random block of data and output is a fixed-size bit string, which is known as the hash value. It is in this way that an accidental or intentional change in the message will change the hash value drastically. There are various cryptographic hash functions but many of them have been found in a weak position with respect to security.

In 2004, Xiaoyun Wang et al presented the collisions for MD4, MD5, HAVAL-128 and RIPEMD [1]. In 2005, Professor M. Szydło found that it is possible to find a collision in SHA-1 in 2^{63} operations [2]. Before, it was thought that 2^{80} operations are required to find a collision in SHA-1 for a 160-bit block length. M. Stevens reported a collision attack on MD5 in 2006 [3]. The algorithmic similarity of SHA-2 with SHA-1, make this algorithm's security susceptible. Although, no attack on SHA-2 has been reported yet.

In view of the security dilemma of hash functions, National Institute of Standards and Technology (NIST) USA has announced a public competition in the Federal Register Notice published on November 2, 2007 [4] to develop a new cryptographic hash algorithm called SHA-3. In response to NIST's announcement 64 submissions were reported, out of which 51 entries fulfilled the minimum submission requirements

and were selected as the first round candidates. These candidates were reduced to 14 in round 2 and further reduced to 5 in round 3 of the competition. Five short listed candidates selected for final round are BLAKE, Grøstl, JH, Keccak and Skein. The tentative time-frame for the end of this competition and selection of finalist for SHA-3 is in 4th quarter of 2012 [5].

This paper describes efficient FPGA implementation of Grøstl. Implementation results are shown for latest Xilinx FPGAs; Virtex-5, Virtex-6 and Virtex-7. The remainder of this paper is organized as follows. We briefly give an overview about cryptographic hash functions in section 2. Section 3 gives brief description of Grøstl. In Section 4 we present the efficient FPGA implementations of Grøstl. In section 5 we give the results of our work and in section 6 compare it with previous implementations of Grøstl. Finally, we provide some conclusions in Section 7.

2 Cryptographic Hash Functions

A cryptographic hash function is a process whose input is random block of data and output is a fixed-size bit string, which is known as the (Cryptographic) hash value. The input data is often called the “message”, and the hash value is known as the “message digest”. It is in this way that a fortuitous or intentional change to the message will change the hash value. The ideal cryptographic hash function has following major or significant properties:

- It is very difficult to find out two inputs that produce the same message digest.
- It is easy to compute the hash value for any given message.
- It is very hard to find a message that has a given hash.
- It is infeasible to modify a message without changing its hash.

Hashes are not encryptions. Encryption converts plain text into cipher text and by using the right key it converts it back. The two texts roughly correspond to each other with respect to size. “Encryption” is a two-way operation. On the other hand, hash functions convert a stream of data into a fixed size hash value. No matter, how long the message is but its hash value will be of fixed size bit string and it’s strictly a one way operation. Cryptographic hash functions have many information security applications, particularly in digital signatures and message authentication codes (MACs). Moreover, these can be used for fingerprinting, for data indexing in hash tables and to detect duplicate data or uniquely identify files, and as checksums to detect accidental data corruption during communication.

3 Brief Description of Grøstl

P. Gauravaram et al. designed and proposed the Grøstl hash function for SHA-3 [6]. Grøstl is an iterated hash function built from two fixed, large, distinct but similar permutations P and Q . Grøstl is a byte-oriented SP-network which is based on

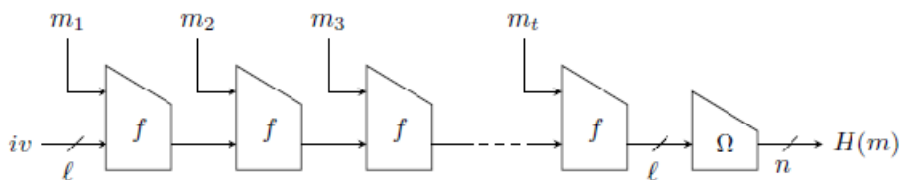


Fig. 1. The Grøstl Hash function

components of AES [7]. These components are named as AddRoundConstant, SubByte, ShiftBytes and MixBytes. The Grøstl has two variants Grøstl-512 and Grøstl-1024. The construction of Grøstl hash function is shown in Fig. 1. The Grøstl hash functions iterate the compression function f as follows. The message M is padded and split into l -bit message blocks $m_1, m_2, m_3, \dots, m_t$ and each message block is processed sequentially. An initial l -bit value $h_0 = iv$ is defined, and subsequently the message blocks m_i are processed as:

$$h_i \leftarrow f(h_{i-1}, m_i) \quad \text{for } i = 1, \dots, t$$

Hence, f maps two inputs of l -bits each to an output of l -bits. The first input is called the chaining input, and the second input is called the message block. For Grøstl variants returning up to 256 bits, l is defined to be 512. For larger variants, l is 1024 bits. After the last message block has been processed, the output $H(M)$ of the hash function is computed as:

$$H(M) = \Omega(h_t)$$

Compression Function of Grøstl: The compression function f is based on two underlying l -bit permutations P and Q . It is defined as follows:

$$f(h, m) = P(h \oplus m) \oplus Q(m) \oplus h$$

The construction of f is described in Fig. 2. The internal state consists of two 8x8-byte matrices for Grøstl-512 and two 8x16-byte matrices for Grøstl-1024. The permutation Q operates on a message block and permutation P operates on XOR of message and chaining hash value or initial value. Each permutation P and Q is iterated 10 times for Grøstl-512 and 14 times for Grøstl-1024. The next chaining value of hash is calculated by XORing the outputs of P , Q and previous chaining hash value. After processing of all message blocks final hash is transformed applying permutation P on chaining hash and XORing it with permuted value, as shown in Fig. 3. The resulting hash digest may be truncated to any desired length.

The P and Q Permutations: P and Q permutations are consists of components from AES. Both permutations are similar and follow same steps except used different round constants and different arrangements in ShiftBytes step. We briefly define here the four steps involved in these permutations. For details, we refer to original submission document of Grøstl [6].

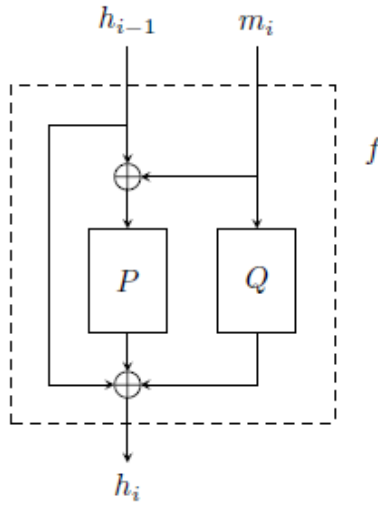


Fig. 2. The Grøstl compression function f

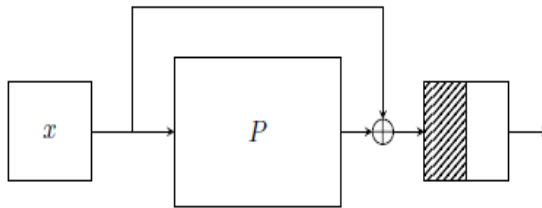


Fig. 3. The Grøstl output transformation

AddRoundConstants: The AddRoundConstant transformation adds a round-dependent constant to the state matrix A . The AddRoundConstant transformation in round i (starting from zero) updates the state A as:

$$A \leftarrow A \oplus C[i]$$

Where $C[i]$ is the round constant used in round i . P and Q have different round constants, which are defined in [6].

SubBytes: The SubBytes transformation substitutes each byte in the state matrix by another value, taken from the s-box S . This s-box is the same as the one used in AES and its specification can be found in [7].

ShiftBytes and ShiftByteWide: ShiftBytes and ShiftByteWide cyclically shift the bytes within a row to the left by a number of positions. Let $\sigma = [\sigma_1, \sigma_2, \dots, \sigma_7]$ be a list of distinct integers in the range from 0 to $v - 1$. Then, ShiftBytes moves all bytes in row i of the state matrix σ_i positions to the left, wrapping around as

necessary. The vector σ in ShiftBytes respectively ShiftBytesWide is different for P and Q . For ShiftBytes in P , use $\sigma = [0,1,2,3,4,5,6,7]$ and for ShiftBytes in Q , use $\sigma = [1,3,5,7,0,2,4,6]$. Similarly, for ShiftBytesWide in P and Q , use $\sigma = [0,1,2,3,4,5,6,11]$ and $\sigma = [1,3,5,11,0,2,4,6]$ respectively. The transformations ShiftBytes for P and Q in Grøstl-512 are illustrated in Fig. 4.

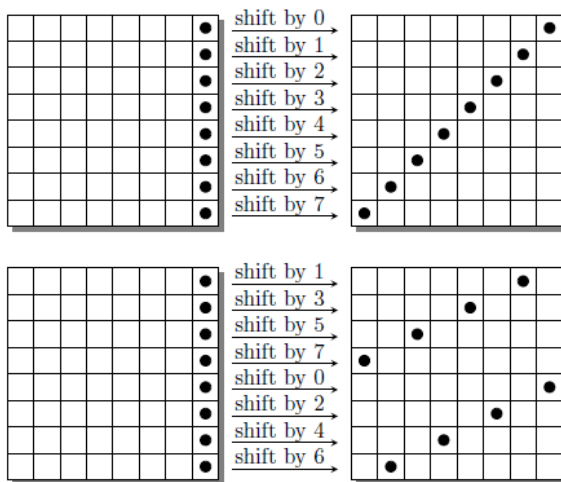


Fig. 4. The ShiftBytes transformation of permutation P_{512} (top) and Q_{512} (bottom)

MixBytes: In the MixBytes transformation, each column in the matrix is transformed independently. MixBytes multiplies each column of A by a constant 8×8 matrix B in F_{256} . Hence, the transformation on the whole matrix A can be written as the matrix multiplication:

$$A \leftarrow B \times A$$

The matrix B is specified as:

$$B = \begin{bmatrix} 02 & 02 & 03 & 04 & 05 & 03 & 05 & 07 \\ 07 & 02 & 02 & 03 & 04 & 05 & 03 & 05 \\ 05 & 07 & 02 & 02 & 03 & 04 & 05 & 03 \\ 03 & 05 & 07 & 02 & 02 & 03 & 04 & 05 \\ 05 & 03 & 05 & 07 & 02 & 02 & 03 & 04 \\ 04 & 05 & 03 & 05 & 07 & 02 & 02 & 03 \\ 03 & 04 & 05 & 03 & 05 & 07 & 02 & 02 \\ 02 & 03 & 04 & 05 & 03 & 05 & 07 & 02 \end{bmatrix}$$

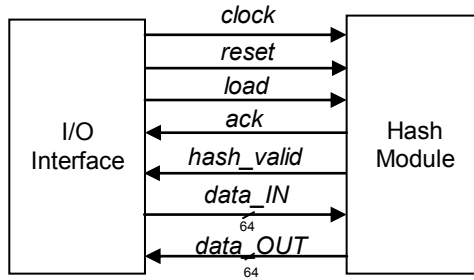


Fig. 5. Input/Output Interface

4 Implementation

Our design is fully autonomus with complete I/O interface. We targeted for efficient implementation but keeping in mind the hardware performance comparison with previously reported implementations. We assure this approach by catering common development environment and use of same set of chip resources. We assured it by forcing our designs to map on LUT based logic and not to use dedicated hardware resources like BRAMs, Multipliers and DSPSlices. Memory is also implemented using distributed ROM because it utilizes the LUT resources and memory requiremet of the algorithm is reflected in terms of utilized area.

4.1 I/O Interface

The developed input/output interface is shown in Fig. 5. All I/O transactions are synchronized. Each I/O is sampled at the rising edge of clock pulse. The input cycle is initiated by I/O interface by setting *load* signal to high. Hash Module acknowledges the request if it is able to receive data by setting *ack* signal to high. After receiving acknowledgment, I/O interface make available 64-bit word of data at each rising edge of clock pulse. During the transaction of data, *ack* signal remains at logic high. After receiving desired amount of input words Hash Module sets the *ack* signal to low. Accordingly, I/O interface pulls the *load* signal to low if no more transactions are required. If message blocks are still present, *load* signal will remain high but Hash Module acknowledges it after one clock cycle from the previous transaction. In the same way when Hash Module is ready with a valid hash value it signals the I/O interface by putting *hash_valid* signal to high. After putting *hash_valid* signal hash module outputs 64-bit words on each rising edge of clock cycle until the desired hash length is achieved. I/O interface is designed in a way that it does not affect the ongoing processing within hash module. That is, we can make I/O transactions at the same time while hash of a message block is in progress.

4.2 Control and Data Paths

Hash module consists of two major parts, the control path and the data path. Block diagram of hash module separated in control path and data path is depicted in Fig. 6. Control path consists of Finite State Machine, State register, clock and counter. Data path consists of Input registers, Hash Core, Intermediate registers and Output registers. Input registers of data path consist of a Serial In Parallel Out (SIPO) register and other registers to store message and other input parameters like constant values.

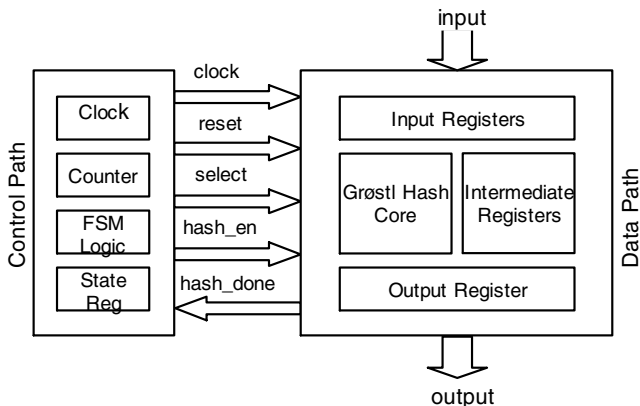


Fig. 6. Hash Module separated in Control and Data paths

Hash Core is the main arithmetic logic unit of the Grøstl hash algorithm. Intermediate registers are utilized to store intermediate results of the hash algorithm. Output register contains the resulting hash and it is a Parallel In Serial Out (PISO) register to serially output the result.

4.3 Datapath of Grøstl

The data path implemented for Grøstl is shown in Fig. 7. The compression function of Grøstl consists of two separate permutations P and Q . These permutations are almost identical and can be implemented in parallel. Two differences between P and Q are in the step of AddRoundConstant, where different round constants are used, and in ShiftByte step, where different scheme is used to circular shift the bytes left. AddRoundConstant step is a simple eight byte XOR operation of input matrix with round constant. SubByte is AES S-box substitution; it is implemented using combinational logic which utilize the internal logic structure of inversion in Galois Field $GF(2^8)$ and affine transformation, as described in [8]. ShiftByte is circular shift of bytes in matrix; it is implemented through simple re-labeling of the bytes in matrix. MixByte step multiplies each column of the matrix to a constant 8×8 matrix in Galois Field $GF(2^8)$. This step is implemented as combinational logic described in [8]. In the beginning of every hash process message block (msg) is directly pass on to Q

permutation. The P permutation operates on XOR of msg and initial value (IV) or chaining hash value. Both permutations P and Q iterated 10 times for Grøstl-512 and 14 times for Grøstl-1024. After completion of desired number of rounds next chaining hash value is obtained by XORing outputs of P , Q and previous chaining value. This process continues till the end of all message blocks. At the end, resulting chaining hash is again permuted through permutation P and XORed with permuted value to obtain final hash digest.

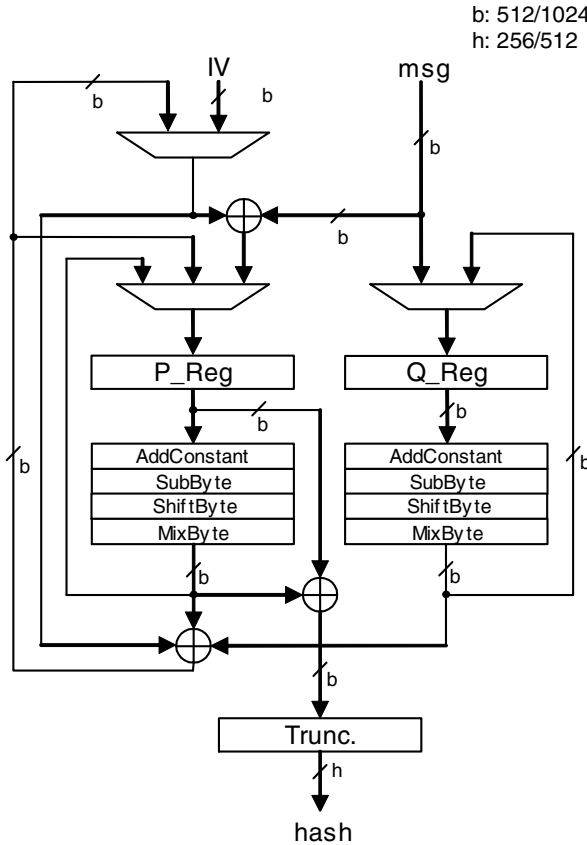


Fig. 7. Data path of Grøstl

5 Implementation Results

The design has been implemented on Xilinx Virtex 5, Virtex 6 and Virtex 7. Detailed device specifications are: Virtex 5 LX30T, speed grade 3, package FF323 (5vlx30tff323-3), Virtex 6 LX75T, speed grade 3, package FF784 (6vlx75tff784-3) and Virtex 7 285T, speed grade 3, package FG1157 (7v285tffg1157-3). The resulting

clock frequencies and area utilization after place and route are reported. Table 1 shows achieved area consumption (*Area*), clock frequency (F_{max}) and time delay (T) for implemented design.

Table 1. Results for Grøstl Implementation

Device	Grøstl-256			Grøstl-512		
	<i>Area</i> [Slices]	F_{max} [MHz]	T [ns]	<i>Area</i> [Slices]	F_{max} [MHz]	T [ns]
Xilinx Virtex 7	1494	159.69	6.26	2665	151.72	6.59
Xilinx Virtex 6	1467	146.87	6.81	2359	125.44	7.97
Xilinx Virtex 5	1419	121.03	8.26	2523	101.22	9.88

5.1 Throughput

From these results we can calculate throughput of our design. The throughput TP of a given design can be calculated by:

$$TP = \frac{Block\ Size}{T_{hash}} \tag{2}$$

Where *Block Size* is the block size of message in bits. T_{hash} is the total time required to calculate hash value which is given by:

$$T_{hash} = T \cdot N_{clk} \tag{3}$$

Where T is the time period of the system clock and N_{clk} is the number of clock cycles required for a valid hash output. Table 2 shows these parameters and throughput results for Grøstl-256 and Grøstl -512.

Table 2. Throughput Results

Device	Grøstl-256					Grøstl-512				
	N_{clk} [cycles]	<i>Block Size</i> [bits]	T [ns]	T_{hash} [ns]	TP [Gb/s]	N_{clk} [cycles]	<i>Block Size</i> [bits]	T [ns]	T_{hash} [ns]	TP [Gb/s]
Xilinx Virtex 7	10	512	6.26	62.6	7.59	14	1024	6.59	92.26	11.10
Xilinx Virtex 6	10	512	6.81	68.1	9.62	14	1024	7.97	111.58	9.17
Xilinx Virtex 5	10	512	8.26	82.6	6.20	14	1024	9.88	138.32	7.40

5.2 Throughput Per Area

Throughput per area is a significant performance measure, such that it combines the performance effect of both area and speed in a single value. It measures the contribution of each unit area to throughput and hence the efficiency of the implementation.

From the results given above, we can calculate throughput per area of our designs. The throughput per area TPA of a given design can be calculated by:

$$TPA = \frac{TP}{Area} \quad (4)$$

Where TP is the throughput of the design. $Area$ is the occupied area of the design on the chip. In our case we have chosen the number of slices as a unit of area consumption, as it is a worldwide standard practice. Table 3 shows throughput per area results.

Table 3. Throughput per Area Results

Device	Grøstl-256			Grøstl-512		
	TP [Gb/s]	$Area$ [Slices]	TPA [Mb/slice]	TP [Gb/s]	$Area$ [Slices]	TPA [Mb/slice]
Xilinx Virtex 7	7.59	1494	5.47	11.10	2665	4.16
Xilinx Virtex 6	9.62	1467	5.12	9.17	2359	3.89
Xilinx Virtex 5	6.20	1419	4.37	7.40	2523	2.94

6 Comparison with Previous Work

Table 4 shows the comparison of results with previously reported implementations in terms of throughput, area and throughput per area.

Table 4. Comparison of Grøstl Implementations. F_{max} in MHz, $Area$ in Slices, TP in Gbps and TPA in Mbps/Slice

Author(s)	Device	Grøstl-256				Grøstl-512			
		F_{max}	$Area$	TP	TPA	F_{max}	$Area$	TP	TPA
This work	Virtex 7	159.69	1494	7.59	5.47	151.72	2665	11.10	4.16
This work	Virtex 6	146.87	1467	9.62	5.12	125.44	2359	9.17	3.89
This work	Virtex 5	121.03	1419	6.20	4.37	101.22	2523	7.40	2.94
Baldwin et al.[9]	Virtex 5	78.06	2579	3.24	1.26	113.12	4525	3.62	0.80
Matsuo et al. [10]	Virtex 5	154	2616	1.97	0.75	-	-	-	-
Kris Gaj et al. [11]	Virtex 5	355.87	1884	8.676	4.61	180.15	3466	6.36	1.84
E. Hom. et al. [12]	Virtex 6	-	2630	9.34	3.55	-	5106	11.57	2.27
E. Hom. et al. [12]	Virtex 5	-	2591	8.081	3.12	-	5254	10.12	1.93

Most of previously reported results are for second round specifications of the algorithm [9-11]. However, in final round specifications, Grøstl algorithm has been tweaked. E. Homsirikamol et al. [12] discussed and reported their results for various architectures of Grøstl. For performance comparison, we considered the results of architecture most similar to our work. We are not using BRAM as used in architecture of B.Jungk ,S. Reith[13] that's why did not included it in table 4. Although our results are better in terms of slices and TPA for Grøstl-512 and in terms of slices for Grøstl-256 as compare to [13]. Our results for Virtex 5, Virtex 6 and Virtex 7 are far ahead from all previously reported work in terms of area, throughput and throughput per area.

7 Conclusion

In this work we have presented efficient FPGA implementation of SHA-3 finalist: Grøstl. We reported the implementation results on Xilinx Virtex 7, Virtex 6 and Virtex 5. We reported the performance figures of our implementation in terms of area, throughput and throughput per area and compared it with previously reported implementation results. Results achieved in this work are exceeding the implementations reported so far. We compared and contrasted the performance figures of Grøstl-256 and Grøstl-512 on Virtex 5, Virtex 6 and Virtex 7. To the best of our knowledge, our design ranks highest in terms of throughput per area with respect to all reported high speed architectures for Grøstl to date, on all devices.

References

1. Wang, X., Lai, X., Feng, D., Yu, H.: Collisions for hash functions MD4, MD5, HAVAL-128 and RIPEMD. Cryptology ePrint Archive, Report 2004/199, pp. 1–4 (2004), <http://eprint.iacr.org/2004/199>
2. Szydło, M.: SHA-1 collisions can be found in 2^{63} operations. CryptoBytes Technical Newsletter (2005)
3. Stevens, M.: Fast collision attack on MD5. ePrint-2006-104, pp. 1–13 (2006), <http://eprint.iacr.org/2006/104.pdf>
4. Federal Register. Notices 72(212) (November 2, 2007), http://csrc.nist.gov/groups/ST/hash/documents/FR_Notice_Nov07.pdf
5. National Institute of Standards and Technology (NIST): Cryptographic Hash Algorithm Competition, <http://www.nist.gov/itl/csd/ct/>
6. Gauravaram, P., Knudsen, L.R., Matusiewicz, K., Mendel, F., Rechberger, C., Schlffer, M., Thomsen, S.S.: SHA-3 Proposal Grøstl Version 2.0.1 (2011), <http://www.groestl.info/>
7. Daemen, J., Rijmen, V.: The Design of Rijndael – AES Advanced Encryption Standard. Springer, New York (2002)
8. Gaj, K., Chodowicz, P.: Chapter 10: FPGA and ASIC Implementations of AES – Cryptographic Engineering. Springer, Heidelberg (2009)

9. Baldwin, B., Hanley, N., Hamilton, M., Lu, L., Byrne, A., Neill, M., Marnane, W.P.: FPGA Implementations of the Round Two SHA-3 Candidates. In: 2nd SHA-3 Candidate Conference, Santa Barbara, August 23-24, pp. 1–18 (2010)
10. Matsuo, S., Knezevic, M., Schaumont, P., Verbauwhede, I., Satoh, A., Sakiyama, K., Ota, K.: How Can We Conduct Fair and Consistent Hardware Evaluation for SHA-3 Candidate? In: 2nd SHA-3 Candidate Conference, Santa Barbara, August 23-24, pp. 1–15 (2010)
11. Gaj, K., Homsirikamol, E., Rogawski, M.: Comprehensive Comparison of Hardware Performance of Fourteen Round 2 SHA-3 Candidates with 512-bit Outputs Using Field Programmable Gate Arrays. In: 2nd SHA-3 Candidate Conference, Santa Barbara, August 23-24, pp. 1–14 (2010)
12. Homsirikamol, E., Rogawski, M., Gaj, K.: Comparing Hardware Performance of Round 3 SHA-3 Candidates using Multiple Hardware Architectures in Xilinx and Altera FPGAs. In: ECRYPT II Hash Workshop 2011, Tallinn, Estonia, May 19-20, pp. 1–15 (2011)
13. Jungk, B., Reith, S.: On FPGA-Based Implementations of the SHA-3 Candidate Grøstl. In: 2010 International Conference on Reconfigurable Computing and FPGAs (ReConFig), December 13-15, pp. 316–321 (2010)

Capture Largest Included Circles: An Approach for Counting Red Blood Cells

Saima Rathore, Aksam Iftikhar, Ahmad Ali, Mutawarra Hussain, and Abdul Jalil

Department of Computer and Information Sciences, PIEAS, Islamabad, Pakistan
saimarathore_2k6@yahoo.com, aksam_444@hotmail.com,
{ahmadali,mutawarra,jalil}@pieas.edu.pk

Abstract. Complete Blood Count (CBC) is a standard medical test that can help diagnose various conditions and diseases. Manual counting of blood cells is highly tedious and time consuming. However, new methods for counting blood cells are customary employing both electronic and computer-assisted techniques. Image segmentation is a classical task in most image processing applications which can be used to count blood cells in a microscopic image. In this research work, we have employed a few existing segmentation techniques, and also proposed a new scheme to count total blood cells in a smear microscopic image. The proposed technique, called Capture Largest Included Circles (CLIC), is a parameterized segmentation algorithm that captures largest possible circles in an object boundary. The algorithm is perfectly suited for appliance in counting blood cells because of high circularity ratio of cells. Comparative study of segmentation by CLIC and a few other state-of-the-art segmentation algorithms such as Distance Regularized Level Set Evolution (DRLSE), Watershed segmentation and Pixcavator (a topology-based segmentation) is also part of this research work. Results have proven the superiority of CLIC over other schemes, especially in case of diseased red blood cells.

Keywords: Red blood cells, Level set, Watershed, Pixcavator, CLIC.

1 Introduction

Red Blood Cell (RBC) counting is one of the most commonly performed medical tests as it plays vital role in the diagnosis of various diseases like Alport syndrome and Anemia[1]. Blood smear is examined under microscope and count of each type of cells is obtained. Counting process, when performed manually, proves to be tedious, time consuming and subjective. Results vary from person to person and even for one person at different turns. Precision of the process is also very low because of subjective evaluation by histopathologists. Moreover, factor of human error adds to the delicacy of the process. Therefore, some automatic and accurate mechanism is required to cope with the aforementioned problems. Automatic blood cells inspection may be performed with the help of automatic flow cytometry, but algorithms based on image processing and computer vision techniques reduce analysis cost. Therefore,

researchers have been putting their efforts in this direction since last decade and have proposed various automatic, computer-aided blood cell counting techniques.

Counting of RBC is the overall task at hand. It comprises of several steps; out of which segmentation and counting of cells are the two most important phases. Our work is primarily focused on these two steps of automatic computer-aided RBC counting. We have applied traditional image segmentation approaches to blood cells microscopic images to count the number of cells but our main contribution is to present a new scheme for RBC counting, called CLIC. CLIC is a parameterized segmentation algorithm that captures largest possible circles in an object boundary in an efficient way. Results reveal that the proposed scheme outperforms classical image segmentation algorithms.

Rest of paper is organized as follows. Section2 investigates literature on automatic computer-aided segmentation and counting of RBC. Section3 reviews watershed, DRLSE and Pixcavator algorithms. Section4 presents in detail the CLIC approach. Section 5 elaborates the results of applying the said techniques on sample blood cells microscopic images. Section 6 supplies a performance overview whereas section7 concludes the paper.

2 Previous Work

Segmentation and counting of the RBC in a microscopic blood smear image is a potential research problem due to its medical significance. Researchers have been putting serious efforts for this purpose, and much encouraging and accurate results have been produced as a result of these endeavors. Following text states a brief survey of literature related to the computer vision based blood cells segmentation and counting.

Boray et al. [2] employed watershed transform in combination with Radon transform to obtain effective segmentation of peripheral microscopic blood images. Initially, they applied a special form of watershed transform, called minimum area watershed transform, to obtain initial segmentation. This initial segmentation served to locate markers in the image using circle Radon transform. The result of applying circle Radon transform is utilized subsequently in a marker controlled watershed transform to obtain final segmentation result. The results were evaluated on a benchmark set and a segmentation rate of 95% was achieved. Similarly, Ruberto et al. [3] claimed to propose a more accurate approach to segment blood images than the classical watershed algorithm. They used gray scale granulometries on blood images for this purpose. Gray scale granulometries were based on opening with non-flat disk-shaped structuring elements. The non-flat nature of structuring element helped to enhance the circular shape of blood cells as well as their compactness. Then, they have employed a flat disk-shaped structuring element to separate occluded cells. A similar approach to [3] was adopted by Dorini et. al. [4]. They also used morphological operators for segmentation of white blood cells in blood smear image. But, they improved the segmentation accuracy by incorporating the scale-space properties of a toggle operator. Similarly, an excellent work in the field of granulometry for blood

cell counting was performed by Theera et al [5]. Authors estimated blood cell counts against each category according to cell-age. They utilized non-homothetic theory for their purpose because each cell class is attributed to a random grain and non-homothetic theory is ideal for such a problem. After applying the approach, authors demonstrated low counting error for different cell categories.

Theerapattanakul et al. [6] utilized the benefits of snake/active contour to segment white blood cells in microscopic blood smear images. They started by thresholding the image to obtain a binary image that was used to compute the locations of nuclei of white blood cells. Then they cropped the smear image in the vicinity of found nuclei and applied the active contour method on each cell. They placed the round shaped snake at the center of the nuclei and the snake was allowed to expand. After sufficient iterations, the snake evolved to the shape of white blood cell hence segmenting the cell from the image. This process of cropping each cell with its neighborhood and evolving round shaped snake inside that cell was carried out for the whole image to segment all possible white blood cells in the image. In the end, authors demonstrated visual results of their approach and proved effectiveness of their approach.

Seongeun et al. [7] extracted Leukocytes (white blood cells) from blood smear images using region-based active contour approach. Regional statistics were used to avoid the problem associated with initialization of the contour. They were also utilized to attract the evolving contour towards the boundaries of white blood cells. To control the contour deformation near edges of Leukocytes, they used an additional regularizer. Specifically, the active contour model used in this approach was the level set method. The results of applying this method on an image database were compared with those of already categorized by expert hematologists. To be precise, nucleus of different types of cell images (Neutrophil, Lymphocyte, Monocyte and Eosinophil respectively) were segmented with an accuracy of 91.40, 95.45, 90.83, 88.43 percent and cytoplasm were segmented with an accuracy of 93.60, 95.10, 91.82, 91.41 and 93.02 percent respectively.

Acton proposed a new external force [8] in the active contour model for tracking Leukocytes from intra vital microscopic video imagery. The proposed force field, referred to as Motion Gradient Vector Flow (MGVF), takes hemodynamic direction of flow into consideration. This force adds to the classical Gradient Vector Flow (GVF) proposed by Xu and Prince [9] and it is realized in the active contour model by minimizing an energy functional which considers motion direction and image gradient magnitude into its formulation. The proposed active contour model employing the MGVF was evaluated against the classical GVF on intra vital microscopic video imagery. It was shown that root mean square error of tracking Leukocytes at different frame rates for MGVF was much less than GVF.

3 RBC Counting Techniques

Several methods have been proposed by researchers for RBC segmentation and counting with each having its own merits and demerits. In this study, we have used three traditional segmentation techniques for RBC counting.

3.1 Watershed Segmentation

Watershed scheme [10] is inspired by the watershed in hilly areas. It finds watershed lines that represent low intensity areas around high intensity objects. Core of watershed segmentation is internal and external markers. Internal markers are exploited to limit the number of regions by specifying the objects of interest; mainly they are used as seed points for region growing. However, external markers are best candidates for representing image background. Watershed, in a standalone position, can perform reasonably well however in order to make the segmentation process more effective, we used a sequence of morphological operations in pre-processing and post-processing phases.

3.2 Distance Regularized Level Set (DRLS) Evolution

Level set is a viable method for capturing dynamic interfaces using contour evolution. The key ideas of level set method were established by Dervieux and Thomasset [11], [12] but level sets did not attain significant attention before Osher and Sethian [13]. After its theoretical birth in 1988, level set method has found various applications in the fields of computational physics, fluid mechanics, computer graphics, image processing and computer vision. The evolution of level set has witnessed many flavors and variants. DRLSE [14] is one such variation that not only does away with the burden for re-initialization but also permits greater flexibility in the selection of initial Level Set Function (LSF). In our implementation, we have used a binary step function which is extremely efficient to generate. Also, a finite difference scheme is employed as proposed in [14].

3.3 Pixcavator

Pixcavator is one of latest segmentation techniques that have been developed for counting RBC. In pixcavator [15], Saveliev et al. extended the idea of [16] and exploited the topological relationship between different objects in the image to identify and count number of cells in the image. Though, scheme is developed only for RBC counting, yet it has proven to be simple and effective. It can be used in other scenarios with minor modifications.

Counting the number of blood cells after segmenting them in a microscopic blood smear image is simply a task of listing the number of connected components in the image. If the segmentation is performed accurately and the cells are separated after processing, then cells constitute different connected components in the image. In our work, we have applied three classical and one newly proposed technique. The output from these segmentation techniques is an image containing connected components in place of blood cells which can then be counted easily using a simple connected component counter algorithm.

4 Proposed RBC Counting Solution

Counting of red blood cells, though seems simple, is actually a challenging task. Several algorithms proposed in the past exhibit good performance for healthy cells but performance degrades gradually as the cells become diseased. We have proposed a very simple, straight forward yet effective algorithm, **CLIC** for counting red blood cells. We have followed the idea of [17, 18] and modified their algorithm to meet the specific needs of the problem at hand. In [17], initially they found 4-connectivity based connected components from the image. Then, they fitted all possible circles in the connected components by iteratively processing individual components. However, they slightly varied the algorithm in [18]. In the first step, they made connected components and found only one largest possible circle from each component. In successive iterations, they found remaining pixels that are not part of any circles, made connected components of those pixels and fitted only one largest possible circle in each component. Process continued until all the remaining components have size smaller than an area threshold. Both the schemes perform equally well in terms of segmentation accuracy but second scheme works very efficiently as far as memory utilization and CPU processing is concerned.

In our work, we have combined both the algorithms and simplified them. Our algorithm has proven to be computationally faster because instead of working on connected components, we have processed whole image at once. Several other variations that we have introduced in our algorithm are pre-processing, and customized circle growing in post-processing phase.

4.1 Capture Largest Included Circle Algorithm

Sequential steps of CLIC are:

Step1. Read the input image.

Pre-Processing

Step2. Convert the image to binary if it is colored or grayscale.

Step3. Perform morphological operation of dilation and hole filling.

Step4. Remove areas of image smaller than an area threshold.

Step5. Perform rigorous erosioning.

Algorithm

Step6. Specify maximum and minimum possible radius threshold.

Step7. Generate simulated circle of given radius (largest).

Step8. Iterate the circle on the entire image and match where, in the image, such pattern exists.

Step9. In case pattern found and the underlying image pixels are not already part of some other circle, a circle exists at that place.

Step10. Mark the remaining pixels that are not part of any circle.

Step11. Decrement the radius value and continue from step7 (use unprocessed pixels in each next iteration).

Post-Processing

Step12. Approximate exact appearance of cells.

It is worth to be noted that in step 08 of the algorithm, a simulated circle of given radius is treated as a pattern, comprising of pixels. Pattern is overlapped at each image pixel and it is checked whether the underlying pattern is similar to circle or not.

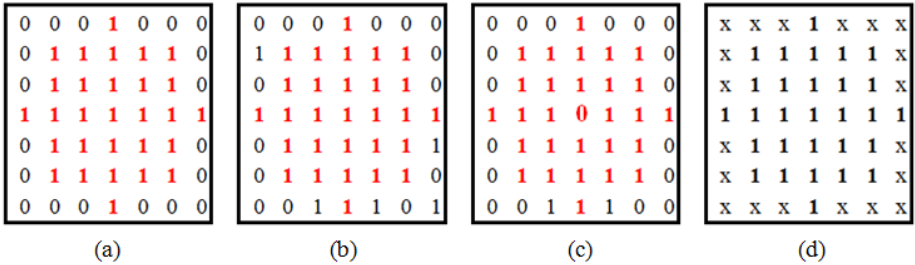


Fig. 1. (a) Simulated circle, (b) & (c) sample image portions, (d) points of matching

In circle matching, only those pixels of circle and underlying image are matched where ‘1’ lies in circle pattern. Matching does not care rest of the pixels of the image and circle. This phenomenon is depicted in Fig. 1(d). In Fig1, point of contact of image and circle is row number 4 and column number 4 of the given samples. Algorithm will detect circle (red pixels) in Fig. 1(b) by ignoring the ‘1’s outside circle boundary whereas it will not detect circle in Fig. 1(c) because of middle zero.

In step 12 of the algorithm, once circles are located at different places in the image, then in order to approximate the exact appearance of underlying red blood cells, a customized connected component analysis is performed. Here, we start from the detected circle boundary and move outside. In each outer layer, we add a pixel to the circular object if three pixels in the inner layer bear 8-connectivity to the pixel and no other 3 pixels that are not part of current circular object, share 8-connectivity to this pixel. Although, a circle may penetrate in another circle but that happens very rare because erosioning have already defined boundaries between objects.

4.2 Circle Generation and Connected Components Removal

Component removal and circle generation algorithms are further elaborated in Fig. 2. In connected components removal, components with size smaller than an area threshold are removed because of obvious reason that they are smaller enough to contain circles. Removal of connected components is based on a pre-defined area threshold; area is actually number of pixels of connected component. This step greatly simplifies the algorithm as number of connected components, generated because of noise, reduces to a great extent.

In circle generation step, circles of different radii are generated in successive iterations. A rectangular array having rows and columns, equal to two times the given radius, is spawned. Center of rectangle is treated as center of circle and for each pixel, it is checked whether it lies inside or outside circle boundary. Array indices are marked accordingly; 1 for pixels inside and on boundary and 0 for pixels outside boundary. In circle generation, maximum and minimum radii were chosen to be 15 and 8 respectively. These radii were selected after a rigorous analysis of several images of red blood cells.

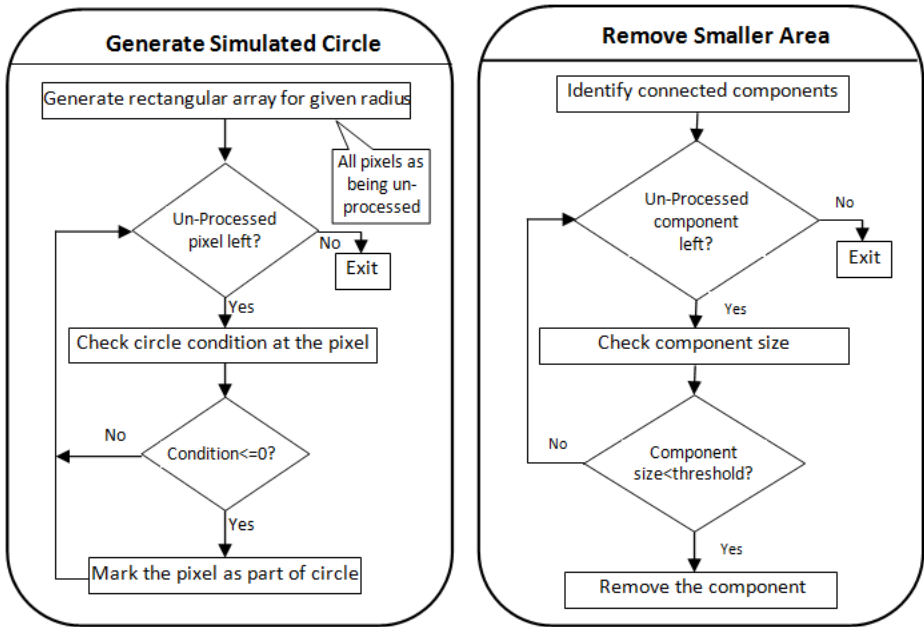


Fig. 2. Circle Generation and Connected Component Removal Algorithm

5 Experimental Results

We carried out experiments on a set 15 images out of which 8 images were healthy and 7 were diseased. Segmentation was performed by using watershed, level set, Pixcavator and our scheme. Several configurable parameters of the algorithms are dumped in Table. 1 whereas Fig. 3 provides a pictorial view of segmentation results.

Table 1. Configurable Parameters of Segmentation Algorithms

Parameter Name = Value (Range of Values)

Watershed	Pixcavator
Type of structuring element = disk	shrink factor = 1
Radius of disk = 8	
(preprocessing for extracting markers)	
Level Set	CLIC
time step = 4, lambda = 5	component size threshold = 50
mu = 0.2/time step, epsilon = sigma = 1.5	min radius = 08
alpha = -5(healthy), -2(diseased)	max radius = 15

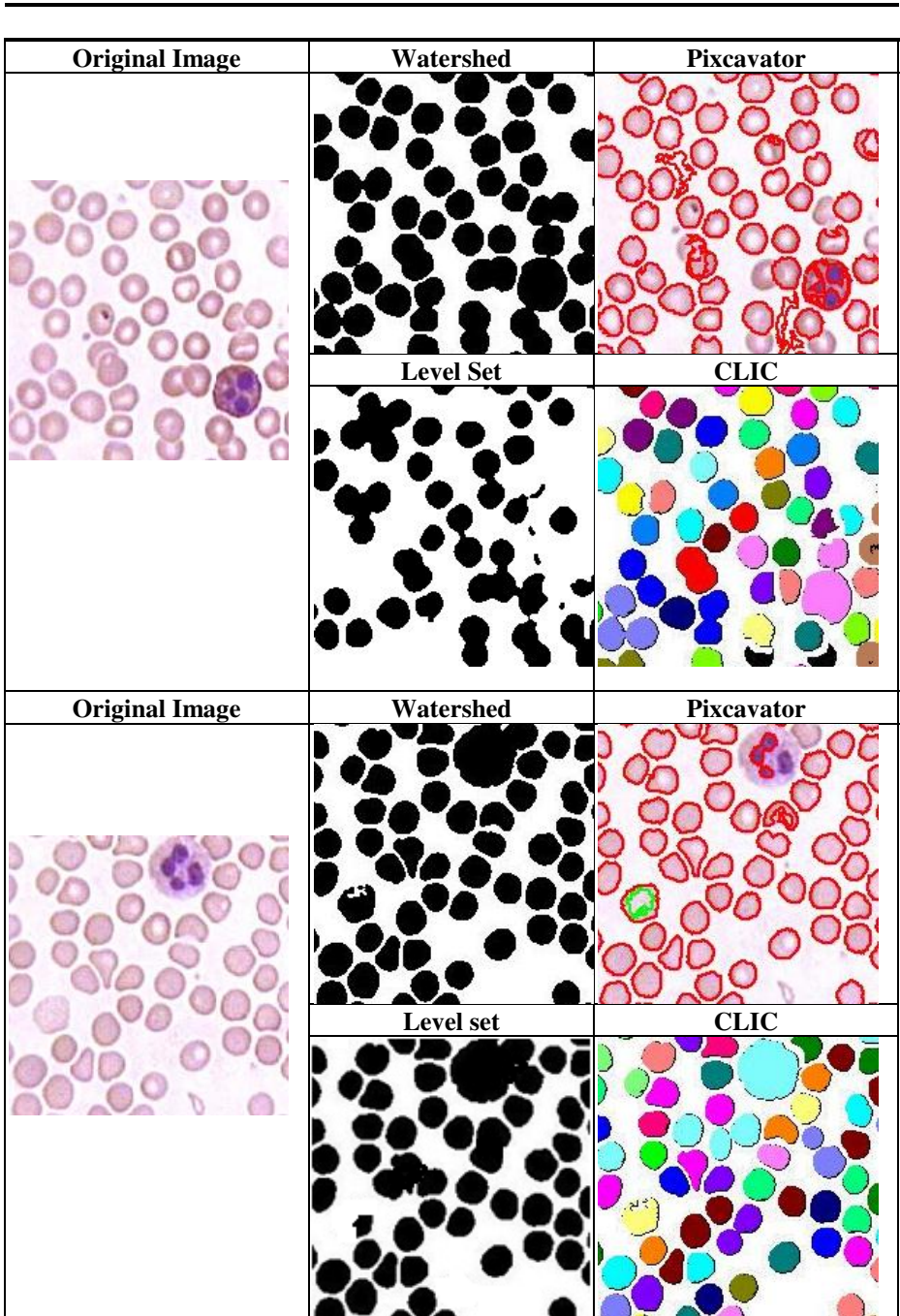


Fig. 3. Results of Segmentation Algorithms

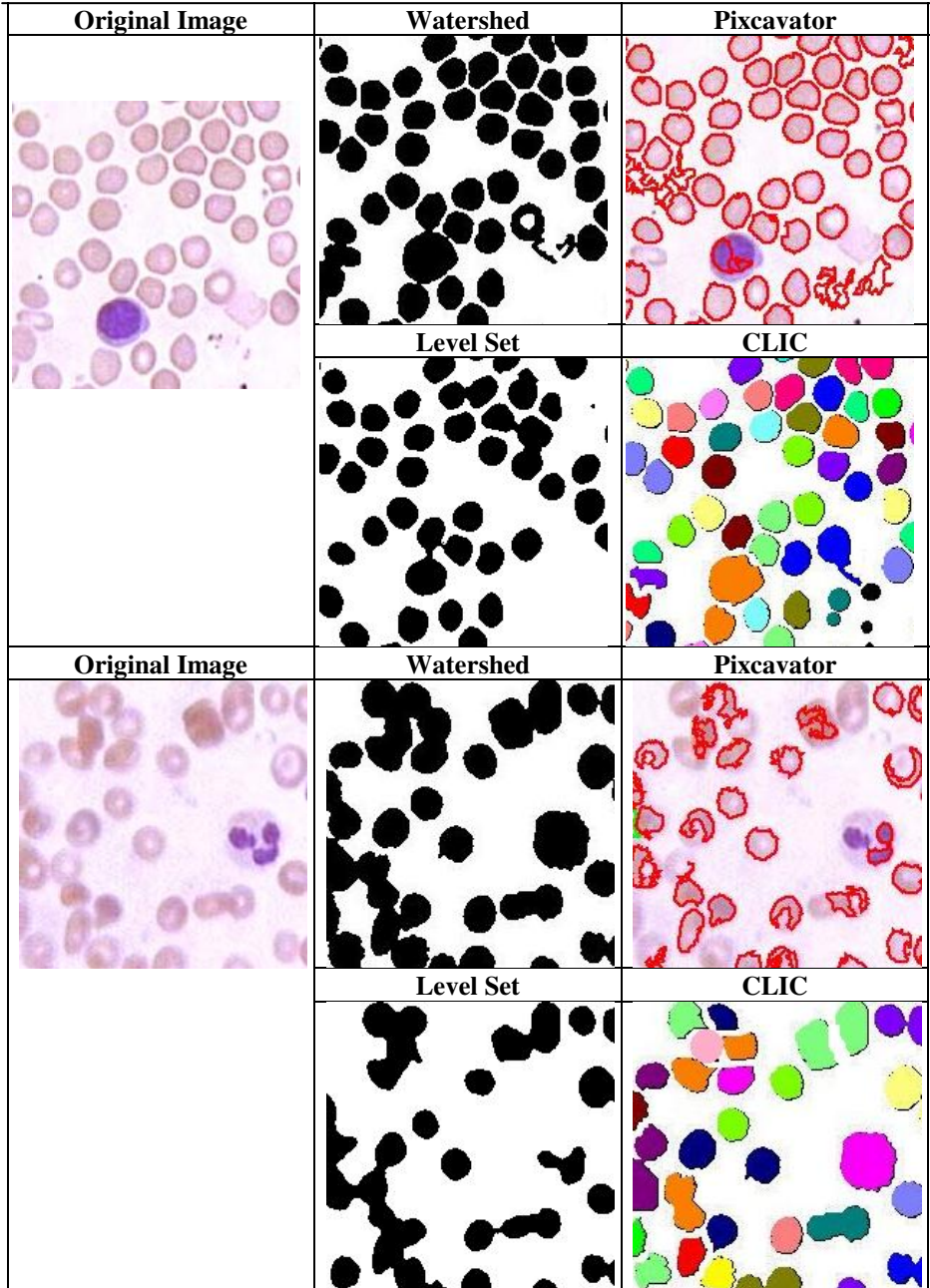


Fig. 3. (continued)

Segmentation results, shown here, are not the entire RBC images. In order to provide a clearer and enlarged view of segmentation, same portion has been cropped from the respective images. Original resolution was 400x670 but we have cropped 100x100 sections from the images starting from 100th row and 100th column. However, Table2. lists total number of cells detected in images. Second column depicts image category whereas third column lists total cells counted using manual segmentation. Remaining columns show segmentation results for individual algorithms.

6 Discussion

Segmentation results lead to a set of very important conclusions. Counting of RBC from diseased image is more error-prone as compared to counting from a healthy image. This effect is painted in Table2. where we see that segmentation results for healthy images are much superior to that of diseased images regardless of the choice of segmentation algorithms. As far as individual algorithms are concerned, level set faces major challenges in segmentation of both the healthy and diseased images; weak edges of cells prevent contour from penetrating through the middle regions of the image. Hence level set becomes unable to capture smaller details in the image. Watershed and Pixcavator both share a comparable level of performance in case of healthy images but the performance of watershed degrades drastically in case of diseased images, where it detects only half of the circles as detected by Pixcavator. Watershed, though segments the image to reasonable level, does not respects natural boundaries between different cells hence it treats multiple individual cells as one merged component.

Table 2. Total cells segmented using individual algorithms

Image	Category	Total	Watershed	Pixcavator	DRLSE	CLIC
1	Healthy	415	269	322	167	326
2	Healthy	398	346	341	124	371
3	Healthy	370	318	334	197	352
4	Healthy	406	352	346	150	368
5	Healthy	457	401	378	167	393
6	Healthy	356	297	308	106	310
7	Healthy	395	321	345	147	361
8	Healthy	342	258	286	158	311
9	Diseased	243	80	148	71	160
10	Diseased	292	100	180	89	210
11	Diseased	252	110	154	78	198
12	Diseased	281	90	165	102	238
13	Diseased	192	84	134	67	169
14	Diseased	234	108	157	98	158
15	Diseased	247	123	198	105	201

Our algorithm performs much better in both the cases. Though, there is only a slight improvement in case of healthy images but our algorithm outclasses other segmentation algorithms for diseased cells. From Fig. 3, it is evident that cells that have either not been detected or have not been separated by other segmentation schemes, have been correctly detected and separated in CLIC. Fig. 4 clearly depicts the best percentage accuracy of CLIC both for healthy and diseased cells.

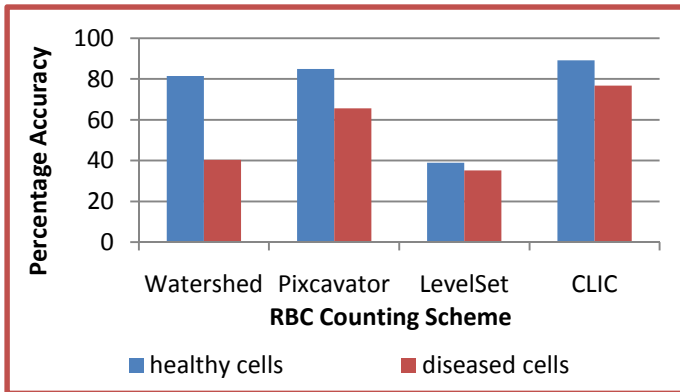


Fig. 4. Percentage Accuracy of segmentation techniques for healthy and diseases cells

7 Conclusion and Future Work

Counting the number of blood cells in a blood smear image is a standard medical test that plays vital role in diagnosis of various diseases. Several computer vision techniques exist for fast, accurate and cost effective counting of these blood cells. Segmentation is the major task in computer vision domain through which a total count of blood cells is obtained. In this work, we have applied several segmentation techniques to segment and subsequently count the number of blood cells. Our main contribution is to present a new technique for RBC counting and compare its results with other classical segmentation approaches like watershed and level set. Results have proven the superiority of our proposed scheme especially in case of diseased images.

Though segmentation results are quite promising, CLIC is still a naive idea in the field of RBC counting. It can further be fine-tuned to produce more robust results. The circle size is currently fixed and is specified as parameter to the CLIC algorithm. In future, an adaptive circle size may be introduced that may increase the accuracy and effectiveness of CLIC. Also, several other performance parameters and state-of-the-art segmentation algorithms may be added to provide better comparative study.

References

1. <http://www.nlm.nih.gov/medlineplus/ency/article/003644.htm> (site last visited on November 28, 2011)
2. Tek, F.B., Dempster, A.G., Kale, I.: Blood cell segmentation using minimum area watershed and circle radon transformations. In: Ronse, C., et al. (eds.) *Mathematical Morphology: 40 Years*, pp. 441–454 (2005)

3. Ruberto, C., Dempster, A., Khan, S., Jarra, B.: Segmentation of blood images using morphological operators. In: International Conference on Pattern Recognition, pp. 3401–3405 (2000)
4. Dorini, L.B., Minetto, R., Leite, N.J.: White blood cell segmentation using morphological operators and scale-space analysis. In: Computer Graphics and Image Processing, SIBGRAPI (2007)
5. Umpon, N.T., Dougherty, E.R., Gader, P.D.: Non-homothetic granulometric mixing theory with application to blood cell counting. *Pattern Recognition* 34, 2547–2560 (2001)
6. Theerapattanakul, J., Plodpai, J., Pintavirooj, C.: An efficient method for segmentation step of automated white blood cell classifications. In: Proc. IEEE Region 10 Conf. TENCON, vol. 01 (2004)
7. Eom, S., Kim, S., Shin, V., Ahn, B.-H.: Leukocyte Segmentation in Blood Smear Images using Region-Based Active Contours. In: Blanc-Talon, J., Philips, W., Popescu, D., Scheunders, P. (eds.) ACIVS 2006. LNCS, vol. 4179, pp. 867–876. Springer, Heidelberg (2006)
8. Ray, N., Acton, S.T.: Motion gradient vector flow: An external force for tracking rolling leukocytes with shape and size constrained active contours. *IEEE Trans. on Medical Imaging* 23(12) (2004)
9. Xu, C., Prince, J.L.: Snakes, shapes, and gradient vector flow. *IEEE Trans. Image Processing* 07, 359–369 (1998)
10. Gao, H., Xue, P., Lin, W.: A new marker based watershed algorithm. In: Proceedings of International Symposium on Circuits and Systems (2004)
11. Dervieux, A., Thomasset, F.: A finite element method for the simulation of Rayleigh-Taylor instability. *Lecture Notes Math.*, vol. 771, pp. 145–158 (1980)
12. Dervieux, A., Thomasset, F.: Multi-fluid incompressible flows by a finite element method. *Lecture Notes Phys.*, vol. 141, pp. 158–163 (1980)
13. Osher, S., Sethian, J.: Fronts propagating with curvature-dependent speed: Algorithms based on Hamilton-Jacobi for mulations. *J. Comput. Phys.* 79(01), 12–49 (1988)
14. Li, C., Xu, C., Gui, C., Fox, M.D.: Distance regularized level set evolution and its application to image segmentation. *IEEE Trans. Image Process.* 19(12), 3243–3254 (2010)
15. Saveliev, P., Pahwa, A.: A topological approach to cell counting. In: Proceedings of Workshop on Bio-Image Informatics: Biological Imaging, Computer Vision and Data Mining (2008)
16. Saveliev, P.: A graph, non-tree representation of the topology of a gray scale image. In: Astola, J.T., Egiazarian, K.O. (eds.) Proceedings of SPIE — The International Society for Optical Engineering, Bellingham, WA 2011 Image Processing: Algorithms and Systems IX, vol. 7870, pp. 1–19 (2011)
17. Tosun, A.B., Kandemir, M., Sokmensuer, C., Demir, C.G.: Object oriented texture analysis for the unsupervised segmentation of biopsy images for cancer detection. *Journal of Pattern Recognition* 42, 1104–1112 (2009)
18. Tosun, A.B., Sokmensuer, C., Demir, C.G.: Unsupervised tissue image segmentation through object oriented texture. In: IEEE International Conference on pattern Recognition (2010)

Enhanced Image Encryption Techniques Using Modified Advanced Encryption Standard

Faisal Riaz¹, Sumira Hameed², Imran Shafi¹,
Rakshanada Kausar², and Anil Ahmed²

¹ Department of Computing and Technology, Iqra University
Islamabad Campus, Islamabad, PK

fazi_ajku@yahoo.com, imranshafi@iqraisb.edu.pk

² Department of Computer Sciences, Mirpur University
of Science and Technology, AJK

{sa_scud,kausar_sadia}@yahoo.com, anilahmed08@gmail.com

Abstract. Protecting multimedia data has become an important and sensitive issue since vast exchange of multimedia data on the internet. For this purpose usually naïve approach is used which provides high level of security but it also need special, costly hardware for real time encryption. Such approach is not practical in situations where we have limited processing power, low bandwidth, and small storage of data. So there is an apparent tradeoff between security and the speed of encryption algorithms. In such situations selective encryption is suggested. We have proposed three new selective encryption techniques for image encryption. We modify AES and make it light and faster. We test our proposed techniques with Modified Advance Encryption Standard on text and images using c# .NET .Achieved results help us to conclude that selective image encryption techniques with MAES can be a better approach to decrease image encryption time.

Keywords: Target area identification function (TAIF), cryptography, Selective encryption (SE), Data Encryption Standard (DES), Modified Advanced Encryption Standard (M-AES).

1 Introduction

Network security (NS) has proven its worth in last few years by protecting user's data over vulnerable computer networks. Security of data storage and transformation is a very sensitive issue because of fast exchange of digital data. The common technique which is used to secure data traffic on the network is cryptography which deals with the encryption of data. Data can be audio files, video files, or text images. Image encryption has its applications in various fields like military communication, internet communication, machine vision etc. Security in transmission and storage of digital images has its importance in today's image communications and confidential video conferencing [1]. As an example only on face book users uploads 14 millions photos per day [2].The arising problem is to protect intellectual properties of valuable digital

masterpieces while making it accessible for public use [3]. Images are less sensitive and also need much computation for encryption as compare to text. In case of still images security is often achieved by using naïve approach (completely encrypting the image) [4].

But large size of images causes certain challenges for encryption [5]. So our research is concerned with new approaches towards image encryption that can overcome the problems of naïve approach. Such techniques are based on encrypting only certain parts of the images using selective image encryption approach (SE).

There are number of fields where selective encryption is needed. One of example of such application is multimedia processing and encrypting images acquired by a surveillance camera [6].

These new selective encryption techniques for images will reduce computational load from cipher end. For further improvement in cipher we have modified Advance Encryption Standard called M-AES. As M-AES is the modification of AES. The paper is organized as follows. Section 2 elaborates about the existing system and its problems. Proposed techniques and structure of modified AES is discussed in Section 3. Experimental results are conversed in section 4. The paper is concluded in section 5. Section 6 illustrate about future work.

2 Existing System and Their Problems

Security of data storage and transformation is a very sensitive issue. In some cases we have limited processing power, low bandwidth, and small storage for data. In such cases there is a tradeoff between amount of encrypted data and computational resources [6]. Some of the existing image encryption algorithms and their problems are discussed in next section.

Van Droogenbroeck and Benedett work focused on image degradation rather than providing high level security by encrypting only 4-5 LSB of an image. Whereas LSB do not have similarity with original image since most significant bits are usually similar with original image as compared to least significant bits [7]. It will result in image quality degradation but image will be still recognizable. Podesser-Schmidt-Uhl Algorithm provides high level security rather than quality degradation. They suggest that user describe its security level and according to its requirement bitplanes will be encrypted which will increase encrypted bit planes and as a result it will lead us to naïve approach.

Cheng and le suggested a compression scheme in 2002 on compressed data to reduce encryption time without having any impact on compression algorithm. The scheme divided compressed data into two parts; an important information and unimportant information. Encryption is carried out only on important information. This scheme is not tunable as static parameters are encrypted. The size of important information can vary from 14% to 50%. Chances of brute force attack can increase in the presence of low information image. So the security level of this scheme can consider low. In 2002 Podesser et.al, proposed a methodology to encrypt only selective bitplanes. Their experiment show that encrypting only MSB's is not secure and

encrypting only 2 or 3 bitplane can only degrade the visual quality of image. It results in increased size of data so it is not suitable for compressed data. AES algorithm is used in this method to encrypt at least 3 bitplanes out of 8 to achieve good security level. But the chance of replacement attack can't be ignore. This attack does not break AES but can replace the encrypted data. The security level of this scheme can consider medium. In 2006 a scheme was proposed by Y.V.Subba Rao et.al in which image is divided into two parts; correlated data and uncorrelated data. First part is encrypted with the data of second part. On the other hand second part is not encrypted. In the end encrypted first part and unencrypted second parts are combined. The degradation of visual quality can be achieved by encrypting four MSB plane. In 2008 an encryption method was suggested by Nidi s. Kulkarni et. al, to scramble the image with the help of random vector and then change its pixel values by using substitution method. It is efficient and suitable for any size of grayscale image. Security level can consider moderate as chances of brute force attack can't be ignored.

3 Proposed Technique

Encrypting images need much more computation than text that's why image encryption is slower than text encryption. So aim of this research is to increase the encryption speed.

3.1 Selective Image Encryption Techniques

We have suggested following image encryption techniques given below:

- Encrypting specific area of images
- Encrypting 3-D components of images
- Encrypting symmetric objects images

Encrypting specific area of images. During data transfer on network we can't compromise on security but on the other hand we also need fast communication. There are some cases where fast communication is preferred on high security. In such cases we have suggested to identify target area of objects and encrypt it. The result will be fast encryption and transmission of data.



Fig. 1. Original Image and Target Area

Figure 1 is target image need to encrypt. After analysis of this image we conclude that if we don't encrypt blue background and area below neck no one can recognize the person in image. The target area of image is shown in fig 1. This is the area from where we can recognize our object.

If we encrypt only this target area the encryption algorithm will need less computation and the result will be decrement of burden from encryption algorithm. So less computation will need less processing power, storage and will save our valuable resources.

Face Recognition

In this proposed technique our aim is to identify target area. Target area is to extract face including hair. We will ignore or subtract background and remaining part of body from image.

Face recognition have certain challenges that hampers its widespread adoption [8]. The first step in automatic face recognition system is to localize face region in a cluttered background [9].

Face detection is used as a precursor for face recognition [10]. There are number of methods that can be used for face detection and recognition. We use skin color. As color processing is much faster than processing other facial features [11]. We have developed our own face extraction algorithm for the identification of target area. The pseudo code of face extraction algorithm is as follow:

Pseudo code of face extraction algorithm.

```

oriFace =: imread('E\user\guest\face\sub6.12.jpg')
copy =: oriFace
rgb =: size(copy)
[MN] =: size(copy)
r =: single(M * N)
g =: single(M * N)
b =: single(M * N)
Chrome =: rgb2ycbcr(copy)
fori =: 1 tosize(Chrome, 1)
forj := 1 tosize(Chrome, 2)
if 105 min Chrome(i, j, 1) min 117 && Chrome(i, j, 3) max 128
r(i, j) =: copy(i, j, 1)
g(i, j) =: copy(i, j, 2)
b(i, j) =: copy(i, j, 3)
else
copy(i, j, 1) =: 255
copy(i, j, 2) =: 255
copy(i, j, 3) =: 255
endif
endfor
endfor

```

```

rgb =: cat(3,r,g,b)
figure,imshow(rgb)
imshow(uint8(rgb),'InitialMagnification','fit')

```

Encrypting 3-Dimensional Components of Images

An object can have two or three dimensions. Most of the things around us are usually 3 dimensions which are height, width, and depth. Digital image are two dimensional and have capability to represent 3 dimensions.

When video camera takes still images or video of any object then they are clearly view able and recognizable due to the different intensity of lights which make 3-D effects of the object clear and viewable and these 3-D components help us to recognize the object. Suppose if the object we want to encrypt is human being than the 3-D components or faces features need to be encrypted are:

- Eyes with eyes brows
- Front part of nose up to upper lip
- Chin
- Lips
- Upper 40 % area of cheeks
- If we hide or encrypt only those parts of object within image the image will not be recognizable as shown in fig 3.2(a)

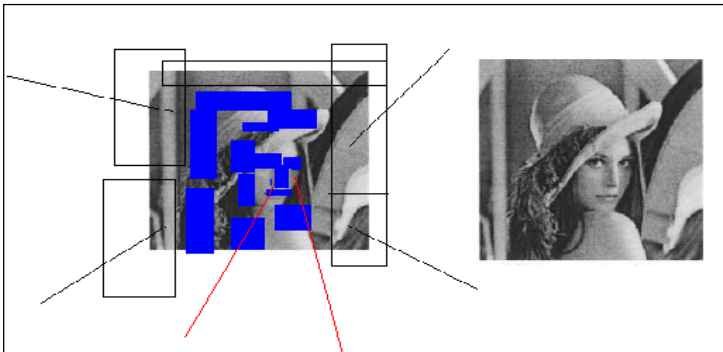


Fig. 2. (a) Encrypted 3-d components of Lena (b) Original image of Lena

In the figure 2 (a) it can be seen that some area has been marked with rectangles are not important to encrypt. The 3-D components are marked with blue color. By encrypting only these components the target area of image will reduce more than first proposed approach.

In this technique we need to encrypt certain facial features. Facial feature extraction consists in localizing the most characteristic face components (eyes, nose, mouth, etc.) within images that depict human faces [12]. Face features are detected usually using skin color and their relative position [13].

Edge based method can also be used for face feature localization and extraction. But the problem with it is that it can easily be affected by noise [14].

Face feature extraction is a very difficult task due to complication of human face structure and the diversity of face features and shooting angle [15]. Morphology based scheme is used to enhance corner features.

Encrypting Symmetric Objects Images

In our third technique we suggest to encrypt symmetric object. The important area in a human image is face. It is well-known that the “face is roughly symmetrical” [16]. This technique is suggested specifically for passport size and National ID card size images.

If we divide the image into two equal halves and encrypt only one half and paste it on the other side the encryption time and computation will be reduced. As a result burden from encryption algorithm will be decrease and speed of image encryption will be increase.

3.2 Modified Advanced Encryption Standard (M-AES)

To overcome the problem of high calculation and computational overhead, we analyze the Advanced Encryption Standard (AES) and modify it, to reduce the calculation of algorithm and for improving the encryption speed. In comparison to the modified AES algorithm proposed by M. Zeghid et. al, we have practice changes in the structure of AES, where as their proposed modification consist of original structure of AES, A5/1 and W7 key stream generators[17].

In our proposed M-AES the block length and the key length are specified according to AES specification: three key length alternatives 128, 192, or 256 bits and block length of 128 bits. While the number of rounds in AES depends upon the size of input data and key [18]. We assume a key length of 128 bits, which is most commonly implemented.

In Modified-AES encryption and decryption process resembles to that of AES, in account of number of rounds, data and key size. The round function consists of four stages. To overcome the problem of high calculation we skip the Mixcolumn step and add the permutation. Mixcolumn gives better security but it takes large calculation that makes the encryption algorithm slow [19]. The other three junctures remain unbothered as it is in the AES. A single 128-bit block is the input to the encryption and decryption algorithms. This block is a 4×4 square matrix consisting of bytes. This block is copied into the state array. The state array is modified at each stage of encryption or decryption. Similarly the 128-bit key is also depicted into a square matrix.

The 128-bit key is expressed into an array of key schedule words: each word is of four bytes. The totals key schedule words for ten rounds are 44 words; each round key is similar to one state. The block diagram of the M-AES algorithm with 128 bits data is shown in figure 3.

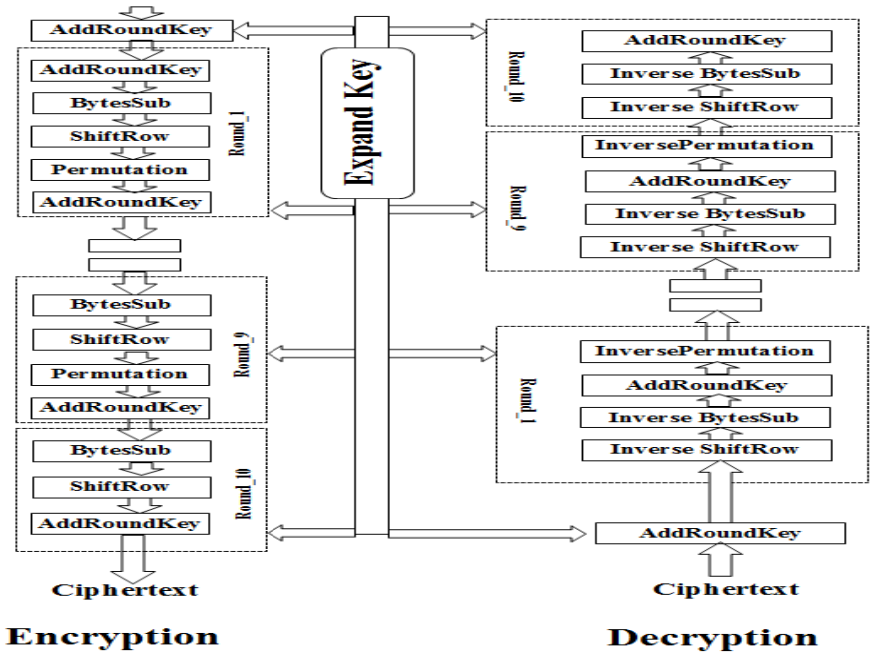


Fig. 3. Structure of M-AES

The algorithm is divided into four operational blocks where we observe the data at either bytes or bit levels and the algorithm is designed to treat any combination of data and is flexible for key size of 128 bits. These four operational blocks represent one round of Modified-AES. [19,20]

Rounds of Modified-AES Algorithm

There are 10 rounds for full encryption. The four different stages that we use for M-AES Algorithm are:

- Substitution bytes
- ShiftRows
- Permutation
- AddRoundKey

Substitution Bytes, ShiftRows and AddRoundKey remain unaffected as it is in the AES. Here the important function is Permutation which is used instead of Mixcolumn. Permutation is widely used in cryptographic algorithms. Permutation operations are interesting and important from both cryptographic and architectural points of view. Tables characterize the permutation and its contrary; the Data Encryption Standard (DES) algorithm will provide us permutation tables. The inputs to the IP (Initial Permutation) table consist of 64 bits. Modified-AES algorithm takes 128 bits as input. The functions Substitution Bytes and ShiftRows are also interpreted as 128 bits

whereas the Permutation function takes 64 bits. We divide the consequential bits of ShiftRows function into two parts of 64 bits and then take each part of 64 bits as input of permutation tables and shift bits one by one according to that table. We fetch one bit from the source, and put it into the correct position in the destination. Each bit of a block is subject to initial permutation, which can be represented by the IP table, showed in Figure 4. In the permutation table each entry indicates a specific position of a numbered input bit consisting of 64 bits in the output. While reading the table from left to right and then from top to bottom, we observe that the 58th bit of the 64-bit block is in first position, the 50th is in second position and so forth.

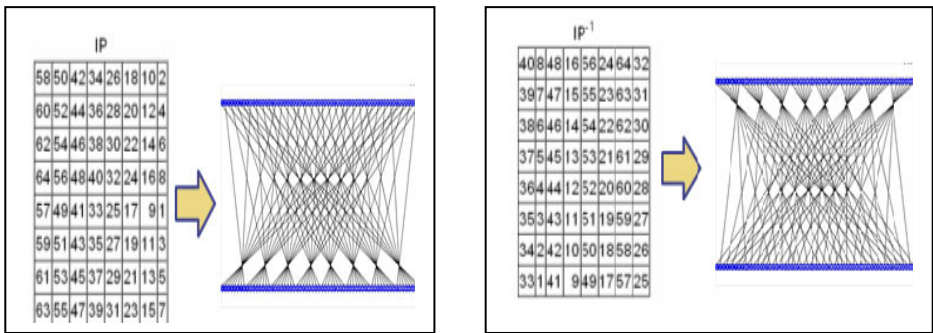


Fig. 4. IP Table and Inverse IP Table

After applying permutation on both sections of 128 bits we again combine both sets of 64 parts into a complete set of 128 bits and then perform next remaining functions of algorithm. If we take the inverse permutation it gives again the original bits, the output result is a 64-bit cipher text. The inverse permutation is performed according to table shown in Figure 4.

For the full decryption of Modified-AES algorithm the transformation processes are, Inv-Bytesub, Inv-Shiftrows, Inv-Permutation, and the Addroundkey, which are performed in 10 rounds as it is in the encryption process.

4 Testing of Proposed Technique

In this research paper we have only tested specific area encryption technique. For this purpose Image is first feed to face extraction algorithm and the resulting processed image is feed to M-AES. Then the original full image is also feed to M-AES to make a comparison in terms of image encryption efficiency. We perform 50 such tests. Some of them are shown in table 5.1. Different images with different dimensions along with original encryption time are shown in first two columns. After passing through our face extraction algorithm the same images have got less dimensions and less encryption time using M-AES as shown in last two columns of table 1.

Table 1. Encryption results for original and processed images using M- AES

Dimensions of image	Original image encryption time	Target image dimensions	Target image encryption time
96*96	00:00: 02.5428000	60*73	00:00: 01.5444000
144*178	00:00: 15.3972000	76*112	00:00: 02.2308000
170*164	00:00:18.5328000	126*138	00:00: 07.6596000
192*192	00:00: 31.4808000	64*88	00:00: 02.3556000
184*209	00:00: 34.2732000	135*166	00:00:12.1992000

A comparison bar chart shown in figure 5 has been generated on data achieved in result of tests performed in table 5.1. From the bar chart it is obvious that using MAES and face extraction algorithm for specific image encryption can enhance the image encryption performance as compare to the full image encryption using MAES.

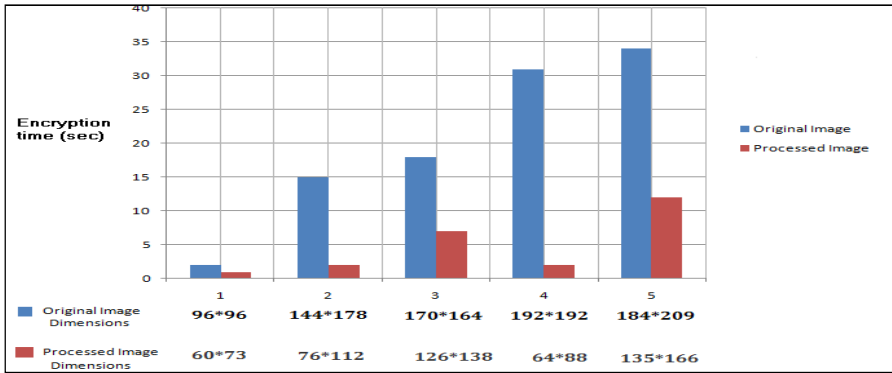


Fig. 5. Encryption results for processed & original image using M-AES

We also feed the processed image using face extraction algorithm and original image to AES in order to compare the efficiency of our M-AES. In table 5.2 results achieved on different images using AES with full image and specific area encryption technique are given. For example Clearly in case of 160*157 dimension image encryption time with specific area encryption technique is approximately 36 seconds faster as compare to the full image encryption using AES. Other obvious differences can be seen clearly in table 2.

Table 2. Encryption results for original and processed images using AES

Dimensions of image	Original image encryption time	Target image dimensions	Target image encryption time
80*103	00:00:05.4843750	77*110	00:00:05.8125000
160*157	00:00:47.0937500	84*142	00:00:11.1718750
144*178	00:00:50.2031250	71*110	00:00:05.0312500
150*180	00:00:54.6250000	91*177	00:00:20.0312500
191*194	00:01:41.3125000	105*174	00:00:25.2812500

The above table shows required encryption time between original image and processed image using AES.

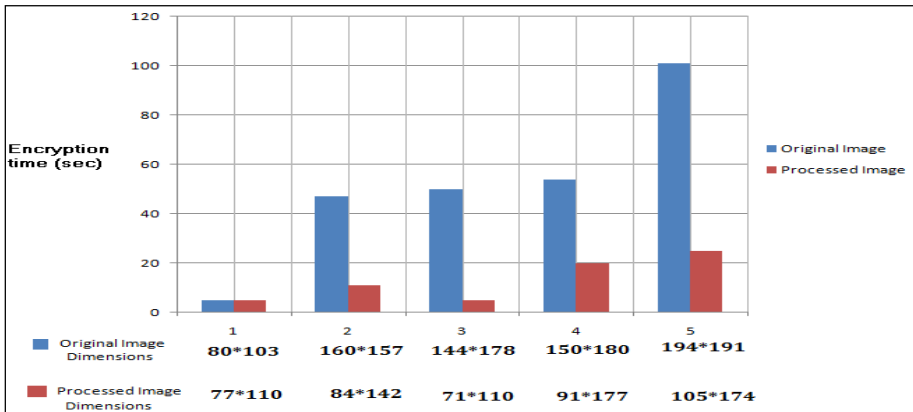


Fig. 6. Encryption results for processed & original image using AES

The above bar chart drawn on results obtained in table 2 is shown in figure 6. It clearly shows required encryption time for original image and processed image using AES. Here again encryption using our proposed specific area technique has been dominated full image encryption.

5 Conclusion

Fast and light encryption algorithms are usually very attractive for multimedia applications especially for image and video transmission. Our proposed modification in AES and proposed selective image encryption techniques prove that selective image encryption is faster than naïve approach.

6 Future Work

Future directions of our work include implementation of remaining two image encryption techniques. We are focusing our future work on different scenarios relating to security analysis of M-AES.

References

1. Shtewi, A.A., et al.: An efficient modified advanced encryption standard (MAES) adapted for image cryptosystems. *International Journal of Computer Science and Network Security* 10(2) (February 2010), http://paper.ijcsns.org/07_book/201002/20100234.pdf (accessed August 8, 2010)
2. Becker, B.C., Ortiz, E.G.: Evaluation of face recognition techniques for application to facebook, <http://www.enriquegortiz.com/publications/FacebookPaper.pdf> (accessed August 11, (2010)
3. Triet, T., Duc, D.A.: Applying the AES and its extended versions in a general framework for hiding information in digital images, <http://www.springerlink.com/index/r31323122763062p.pdf> (accessed August 8, 2010)
4. Ismail, I.A., et al.: A digital image encryption algorithm based a composition of two chaotic logistic maps. *International Journal of Network Security* 11(1), 1–10 (2010), <http://ijns.femto.com.tw/contents/ijns-v11../ijns-2010-v11-n1-p1-10.pdf> (accessed August 18, 2010)
5. Riaz, F., et al.: Modified advanced encryption standard for text and Images. In: Zebist Conference (January 2010)
6. Rodriguesa, J.M., et.al.: Selective encryption of human skin in JPEGImaes, http://hal.archivesouvertes.fr/docs/00/12/95/20/PDF/06_ICIP.pdf (accessed August 09, 2010)
7. Image Encryption Algorithm, *Multimedia Systems and Applications, I*, Vol. 28, *Multimedia Encryption and Watermarking, Part II*, pp. 79-120, <http://www.springerlink.com/content/pm50106971353471/fulltext.pdf>
8. Kakadiaris, I., et.al.: 3D face recognition, <http://citeseerx.ist.psu.edu/viewdoc/download?doi=10.1.1.80> (accessed August 10, 2010)
9. Srikantaswamy, R., Sudhaker Samuel, R.D.: A novel face segmentation algorithm from a video sequence for real-time face recognition, <http://downloads.hindawi.com/journals/asp/2007/051648.pdf> (accessed August 10, 2010)
10. Aarabi, P., et al.: Face detection using information fusion, http://www.isif.org/fusion/.../fusion07CD/Fusion07/pdfs/Fusion2007_1306.pdfon2007_1306.pdf (accessed August 11, 2010)
11. Singh, S.K., et al.: A robust skin color based face detection algorithm. *Tamkang Journal of Science and Engineering* 6(4), 227–234 (2003)

12. Wu, J.C., et al.: An automatic approach to facial feature extraction for 3-D face modeling. *IAENG International Journal of Computer Science* 33, http://www.iaeng.org/IJCS/issues_v33/issue_2/IJCS_33_2_1.pdf (accessed August 12, 2010)
13. Zhu, Y., Cutu, F.: Face detection using half-face templates, <ftp://ftp.cs.indiana.edu/pub/techreports/TR572.pdf> (accessed August 11, 2010)
14. Gu, H., Su, G., Du, C.: Feature Points Extraction from Faces, <http://citeseerx.ist.psu.edu/viewdoc/download?doi=10.1.1.110...pdf> (accessed August 12, 2010)
15. <http://citeseerx.ist.psu.edu/viewdoc/download?doi=10.1.1.63.2881...pdf> (accessed August 12, 2010)
16. Harguess, J., Aggarwal, J.K.: A case for the average-half-face in 2D and 3D for face recognition, http://cvrc.ece.utexas.edu/Publications/harguess_cvp (accessd August 10, 2010)
17. Zeghid, M., et al.: A Modified AES Based Algorithm for Image Encryption. *International Journal of Computer Sciences & Engineering* 1(1), 70–75 (2007)
18. Wright, M.A.: The advanced encryption standard, <http://linkinghub.elsevier.com/retrieve/pii/S1353485801010182> (accessed August 8, 2010)
19. Noo-intara, P., et al.: Architectures for MixColumn Transform for the AES, http://ww.kmitl.ac.th/~kchsomsa/somsak/papers/icep04_163.pdf
20. Krishnamurthy, G.N., Ramaswamy, V.: Making AES Stronger: AES with Key Dependent S-Box. *IJCSNS International Journal of Computer Science and Network Security* 8(9), 388–398 (2008)

Virtual Instrumentation for Control Applications

Syed Ali Asad Rizvi, Sham Sunder, Farah Haroon, and Ashab Mirza

Institute of Industrial Electronics Engineering (IIEE)-PCSIR, Karachi, Pakistan
{s.ali.asad,ss.lohana, farah, ashab}@iiee.edu.pk

Abstract. The virtual instrumentation (VI) is rapidly replacing classical analog as well as digital instrumentation systems owing to the availability of high performance microprocessors based PCs, fast Analog-to-Digital Converters (ADCs) and sophisticated data communication technology. Therefore, investigation of more and more efficient and effective VI based solutions to modern instrumentation problems is one of the main research areas for design engineers. The work presented in this paper is application oriented and thus the contribution of the paper is how to instigate the already known control algorithms in NI LabVIEW. Instead of relying on commercially available expensive hardware, a low-cost self-developed DAQ card is employed. The elaboration of the idea is carried out by designing a VI based DC drive and a thermal system. Modeling, PID controller and user-interface development is presented for both examples. The positive results of this study establish the utility of virtual instrumentation especially for control applications.

Keywords: Virtual instrumentation, DAQ, LabVIEW, digital control, thermal system, DC drive.

1 Introduction

The idea of using software practices in engineering education has been widely explored [1]. From design simulation to implementation phases, the role of software has been proven outstanding. Another trend that we have been experiencing is the replacement of existing bulky electronics hardware with computer programs by bearing the functionality of the real one. This is what virtual instrumentation is all about. The key idea is that an engineer can use routines running on a computer combined with data acquisition hardware to define a custom built-to-order test and measurement system.

An important contribution of our work is the realization of graphical programming language not only for data acquisition and measurement as in [2] but also for designing intelligent controllers for real time control purpose. The DC drive application in this paper extends the work in [3] where only the monitoring system of drives for performance analysis is provided. The thermal system application also enhances the work in [4] in which a VI based ON-OFF controller is developed whereas; a PID controller is exercised for both control applications presented in this paper.

The paper is organized in five sections. The inclination of software oriented practices in engineering systems is presented in Section 1. An overview of virtual instrumentation is provided in Section 2. The design of a low-cost DAQ card solution to practice instrumentation and control experiments is carried out in Section 3. However, a major portion of the work presented in this paper is explored in Section 4 in which the VI focused design of an Insulated Gate Bipolar Transistor (IGBT) based DC drive and a thermal feedback control system is explained. Finally, Section 5 concludes the work in the light of the results of the applications presented.

2 Virtual Instrumentation

An instrument is a device designed to collect data from an environment or a system under test and to display information based on the acquired data. Common examples of traditional instruments that we encounter in our labs are oscilloscope, function generator, multi-meter, spectrum analyzer etc. In contrast, the more exigent is VI which is the use of customizable software and modular measurement hardware for the creation of user-defined measurement systems.

Traditional instrumentation systems involve a general workflow in which a physical phenomenon such as temperature, pressure etc. is converted into electrical signals using sensors; followed by a signal conditioning unit and a measurement equipment. Whereas in a virtual instrumentation system, the measurement equipment is replaced by a DAQ which is followed by a personal computer (PC) equipped with measurement software. The flow of signals in these two practices is shown in the Fig. 1 which shows that there exists a major difference due to the presence of DAQ and computing platform instead of an actual instrument.

The first two stages including the sensors/transducers and the signal conditioning are essentially found in both techniques. This is so because they are directly

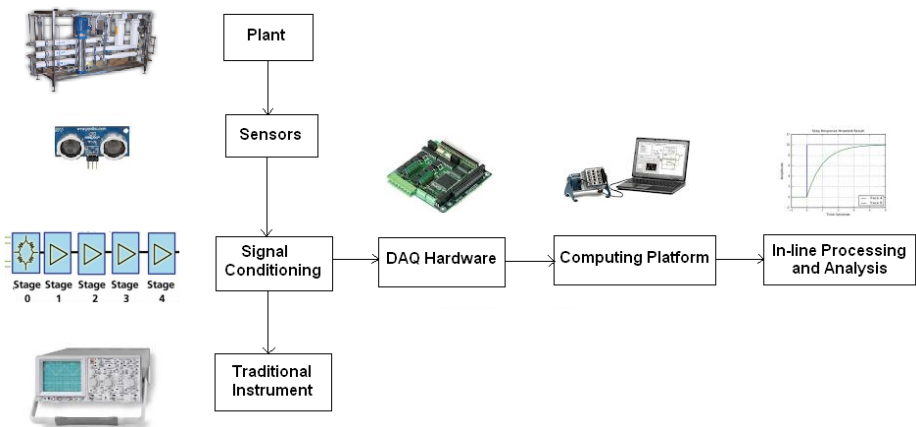


Fig. 1. Signal flow in Traditional and Virtual Instrumentation systems

associated with the characteristics of the physical quantity being measured and are not concerned with how the measurement obtained will be viewed and/or processed by subsequent stages. The presence of software programs in VI contrasts it from the conventional instrumentation. Consequently, this new paradigm has its own set of characteristics. Table 1 summarizes the differences between the two approaches.

Table 1. Differences between traditional and virtual instrument

Conventional Instrumentation	Virtual Instrumentation
Pre-defined hardware components	User-defined measurement system
Limited functionality due to hardcoded functions	Versatile functionality using customizable software
Complex and expensive hardware	Complex hardware functionality implemented on software
Re-calibration is required	Re-calibration is not required
Bulky and stimulus specific	Compact and portable

A virtual instrument system comprises of three main components that are:

- Flexible software
- Modular data acquisition hardware (DAQ)
- Computing platform (e.g. PC)

The flexible software is the computer program on which the virtual instrument is made; modular hardware is a plug-in input/output data acquisition hardware that transforms the real world signals into digital form. The third important component is the computing platform for e.g. a PC that provides the interface between flexible software and data acquisition hardware along with the necessary synchronization between the first two components.

3 Development of IIEE USB DAQ Hardware

The aim of this activity is to develop a low-cost DAQ hardware instead of relying on commercially available expensive cards for low speed applications [5]. This DAQ card is now a patented [6] property of authors' engineering institute, IIEE.

USB interface has been utilized instead of PCI card owing to its portability feature [7]. For this reason this DAQ features USB connectivity and is a USB powered device. The heart of this device is an USB microcontroller.

This card is designed to work with popular programs used for virtual instrumentation and control applications such as Mathworks MATLAB and National Instruments LabVIEW. The usage, however, is not restricted to only the commercial softwares because a number of applications have also been developed in Microsoft Visual Studio programming environment. A block diagram of IIEE DAQ card is presented in the Fig. 2 which reveals its quick specifications. In the control applications discussed in this paper, we will be concerned with analog input channels that are of 5V range and two raw PWM generators. They can be used in either filtered or unfiltered mode.

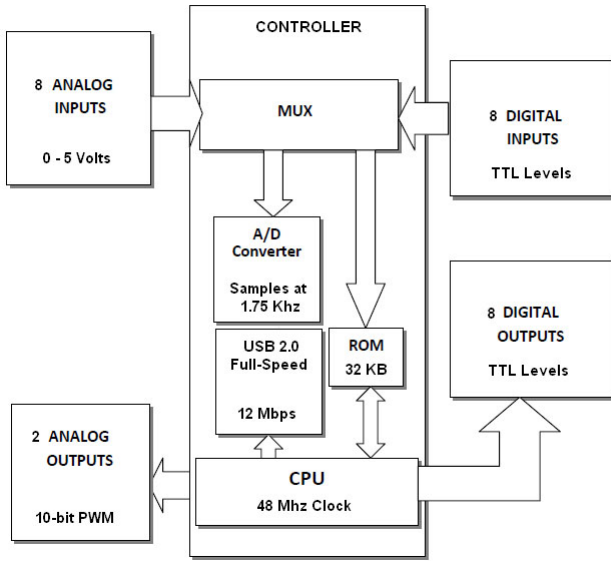


Fig. 2. Block diagram of IEEE DAQ Card

4 Virtual Instrumentation in Control Applications

Virtual instrumentation covers a broad spectrum of industrial and laboratory control applications. These systems are even found in industrial processes. Two examples are presented with VI as the main focus of their design.

4.1 IGBT Based DC Drive

A DC Drive is designed which is based on IGBT power electronic converter (PEC). A DC Motor rated at 75 V and 2.1 A with 3000 RPM speed is used for demonstration. The specifications of IGBTs are 600V and 40A. An external load in the form of another motor is used to evaluate the constant speed capability of the drive using shaft coupling. Our objective is to develop a virtual instrument to monitor and control the speed. For this purpose we use IEEE DAQ as discussed in Section 3.

A block diagram of the proposed design is shown in the Fig. 3. The measurement of motor speed is carried out using the analog channels and control signals are generated through the PWM channels of the DAQ. The PEC incorporates a half-bridge IGBT driver circuit which accepts the DAQ originated PWM signals and transforms them into high voltage level PWM signals of 75V. A PID controller is employed as shown in the block diagram. This controller along with visual user-interface for monitoring and control of the motor speed is developed in LabVIEW which comes under the umbrella of virtual instrumentation.

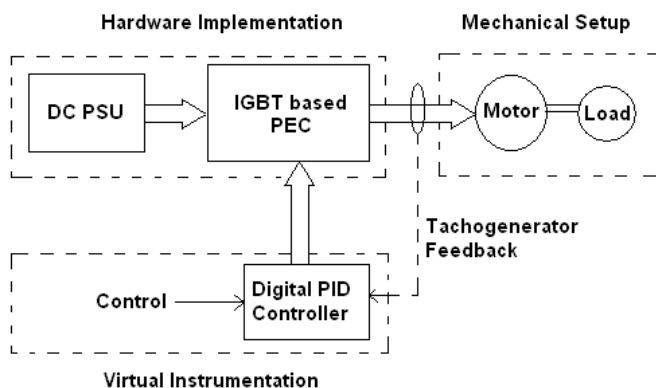


Fig. 3. Block diagram of IGBT based DC Drive

Modeling of DC Motor. In this section we develop a mathematical model of the DC motor and deduce a transfer function for voltage and speed. The motor torque ‘T’ is related to the armature current ‘i’ by a constant factor K:

$$T = Ki \quad (1)$$

The back emf, V_b , is related to the angular velocity by:

$$V_b = K\omega = K \frac{d\theta}{dt} \quad (2)$$

We can write the following equations based on the Newton’s law combined with the Kirchhoff’s law:

$$J \frac{d^2\theta}{dt^2} + b \frac{d\theta}{dt} = Ki \quad (3)$$

$$L \frac{di}{dt} + Ri = V - K \frac{d\theta}{dt} \quad (4)$$

The Laplace transform of (3) and (4) can be written as:

$$Js^2\theta(s) + bs\theta(s) = KI(s) \quad (5)$$

$$LsI(s) + RI(s) = V - Ks\theta(s) \quad (6)$$

$$I(s) = \frac{V - Ks\theta(s)}{R + Ls} \quad (7)$$

$$Js^2\theta(s) + bs\theta(s) = K \frac{V - Ks\theta(s)}{R + Ls} \quad (8)$$

Hence, the transfer function from the input voltage ‘V’ to the angular velocity $\omega(s)$ is:

$$G(s) = \frac{\omega(s)}{V(s)} = \frac{K}{(R + Ls)(Js + b) + K^2} \quad (9)$$

The model assumes that rotor and shaft are rigid. Also, the effect of change of coupling factor when a load motor is driven through shaft couplers is ignored.

Digital PID Controller Design. The PID controller is the most common form of controllers and there are several algorithms [8] for implementation of a digital PID. Depending upon the design requirements, one algorithm may be better suited than the other. The PID equation that serves as the basis for implementing digital PID is given by equation (10).

$$m(n) = Kp e(n) + KiTs(n) + \frac{Kd}{T}[e(n) - e(n-1)] \quad (10)$$

Where, Kp , Ki and Kd are the gain parameters, T is the sampling time, $e(n)$ is the error at n^{th} sample and $s(n)$ is the sum term of the integral.

The pseudo code for the control law given in equation (10) is as follows:

```

1: Start
2: Initialize  $Kp$ ,  $Ki$ ,  $Kd$ ,  $T$ ,  $s[n]$ 
3: Initialize PID equation
4: forevery  $e[n]$  {
5:      $P := Kp * e[n]$ 
6:      $s[n] := s[n-1] + e[n]$ 
7:      $I = Ki * T * s[n]$ 
8:      $D := Kd * (e[n] - e[n-1]) / T$ 
9:      $m[n] := P + I + D$ 
10:    if ( $m[n] > m_{\max}$ )
11:         $m[n] := m_{\max}$ 
12:    }
13: End

```

Pseudo code 1: Algorithm for PID Controller

A simple conditional limit of exceeding the sum term may be added to prevent integral windup. This added flexibility of controller modification is a clear advantage of using a software solution provided by virtual instrumentation. Finally, a LabVIEW block diagram-m code for the PID controller is developed as shown in Fig. 4.

The PID controller output is meaningless for DAQ PWM channels until it is converted to its equivalent PWM form. As we know that valid PWM duty-cycle ranges lie between 0 – 100% which means that there is a need to devise a method of PID to PWM conversion. This can be achieved using equation (11) as,

$$PWM = \frac{PID_{out}}{PID_{max}} \times 100 \quad (11)$$

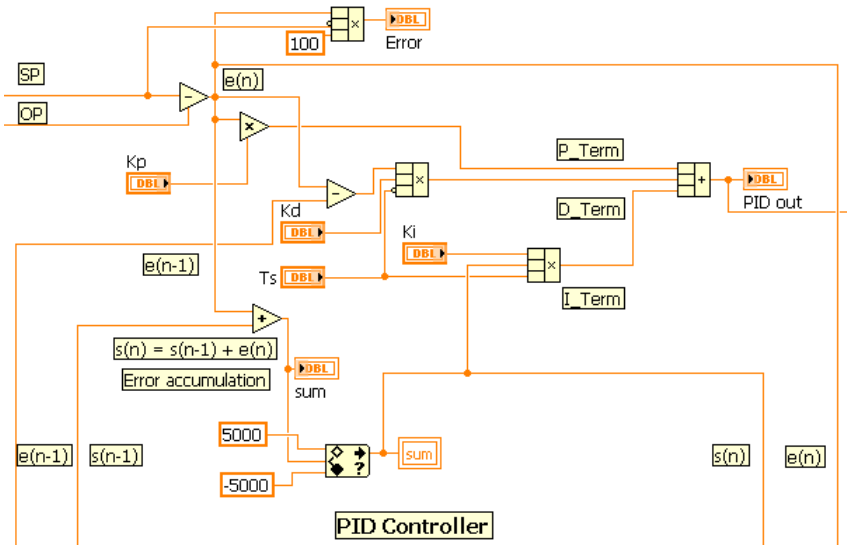


Fig. 4. LabVIEW Implementation of PID Controller

where, PID_{out} is the controller output and PID_{max} is its maximum value. The next question that immediately arises here is the value of PID_{max} that must be kept. Using computer simulation the output of PID controller is determined for safe gain ranges. The PID output values remained within 5000. Thus, PID_{max} can be assigned this value. In this way PWM actuation signals are generated.

Results of VI in DC Drive. The user-interface for DC Drive system is shown in the Fig. 5. There are controls for PID tuning, set-point control, output speed, PEC status

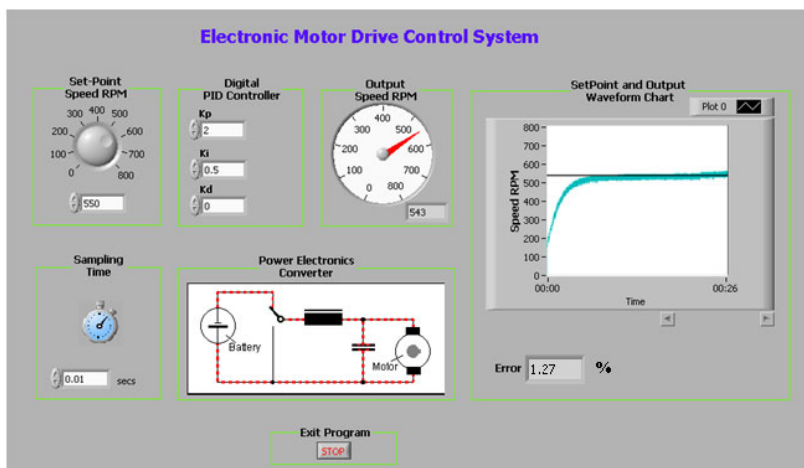


Fig. 5. Front Panel VI for DC Drive System

and I/O response plots for measuring transient and steady-state response of the drive. To improve the user interaction, the status of PWM switching circuit (not actual PWM circuit but a simplified motor switching animation) is updated by the use of animated indicators at the front panel. The effect of PID tuning and sampling rate can be observed in the wave-form chart that are also updated in real-time; thereby increasing our sense of transient specifications being changed with respect to the gains and the sampling interval.

The results displayed in the response show that the motor approaches the set-point in 5 seconds with time constant of 2.3 seconds and an error of 1.3 %. A low-pass filter is employed to reduce spikes arising from vibrations due to imperfect coupling between the drive and load motors. However, the use of filter slows down the transient response as well.

4.2 Thermal Feedback Control System

The objective in this task is to design a digital measurement and control system with temperature as the physical quantity of interest. The body of this system comprises a wooden box which provides a closed environment. However, an external disturbance in the form of heat-loss is present and therefore a digital PID controller is designed. A sketch of this system is shown in the Fig. 6. An electric bulb and a cooling fan are the means of actuation.

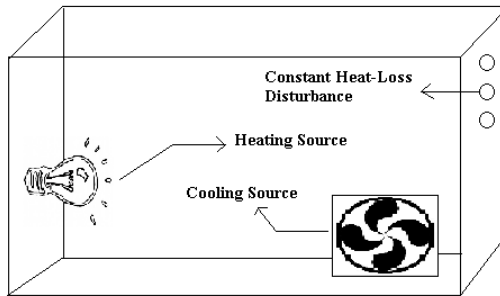


Fig. 6. Physical description of the thermal system

The essential parts of the overall system are shown in block diagram of Fig. 7. The plant in this case is the wooden chamber whose temperature is being controlled using continuous control technique of PWM actuation. The bulb is triggered with these PID proportional PWM command signals.

The actual response of the physical system is practically determined and the data is plotted in Fig. 8. The system can be approximated by first order differential equation like that of simple RC network [9]. The temperature response may be given by

$$T(t) = (T_{ss} - T_a)(1 - e^{-\frac{t}{\tau}}) + T_a \tag{12}$$

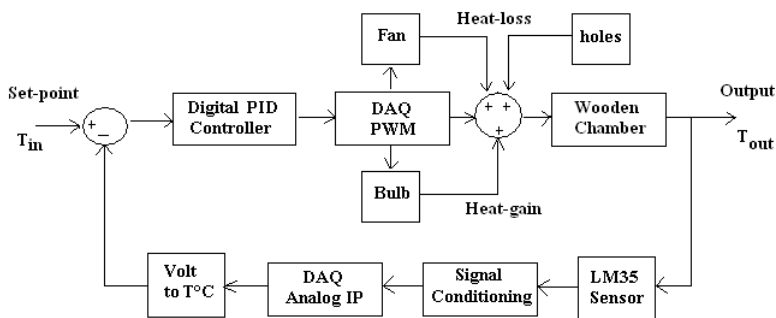


Fig. 7. Block diagram of thermal feedback control system

where, $T(t)$ is the temperature at time t , T_{ss} is the steady-state temperature, T_a is the ambient temperature, and τ is the time constant.

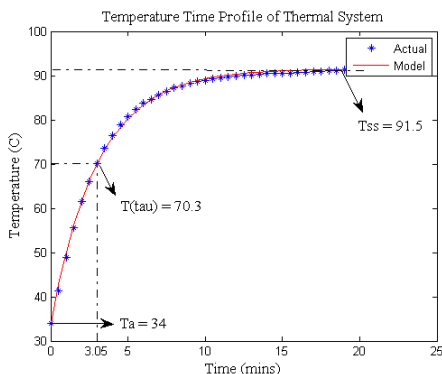


Fig. 8. Plot of temperature function of the system with respect to time

Cooling Source. The fan is used to achieve rapid heat-loss by cooling at a higher rate than achieved by natural convection. It obeys the Newton's Law of Cooling given by:

$$\frac{dT}{dt} = -k\omega_{fan}(T - T_a) \tag{13}$$

The minus sign in equation (13) shows falling temperature. The solution is given by:

$$T(t) = T_a + (T_i - T_a)e^{-k\omega_{fan}t} \tag{14}$$

where, k is the constant factor related to wooden box, ω_{fan} is the fan angular speed (assumed constant), T_i is the initial temperature before cooling, T_a is the ambient temperature and T is the temperature at time t .

Steady-State and DC gain. The response shown in the Fig. 8 is a general open-loop response of the system. Instead of reaching the maximum value of 100 °C a lower set-point of about 91 °C is provided. The system is able to achieve this temperature and has no steady-state error. However, the transient response speed can be improved.

The first order transfer function of the system is obtained from its mathematical model equation and is given by:

$$H(s) = \frac{1}{s\tau + 1} \quad (15)$$

Controller Design and Implementation. In this section we design a controller for thermal system given by transfer function given in equation (13). We use Matlab for determining the proper gains to achieve better transient response as in [10]. Once a controller is designed, it can be implemented in LabVIEW as has been done for the drive application.

The system is subjected to step-input and the responses are shown in the Fig. 9. The PI controller ($K_p = 2.5$, $K_i = 1$) has significantly improved the overall transient response of this thermal system. Particularly, there is a reduction in rise-time and settling-time as compared to the open-loop response. However, the integral gain should be kept only a fraction of the proportional gain to prevent overshoots.

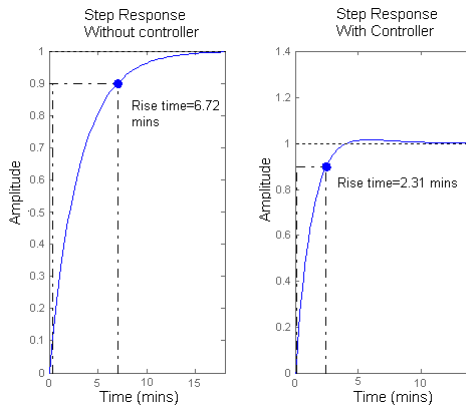


Fig. 9. Step Response with and without controller

Results of VI in Thermal Feedback System. The visual interface shown in Fig. 10 is very similar to the one used in previous application. The controller can be implemented using the earlier code of our DC drive application with a change of gain parameters and PID_{max} value. The optimum measurement and control range is above room temperature and below 100 °C.

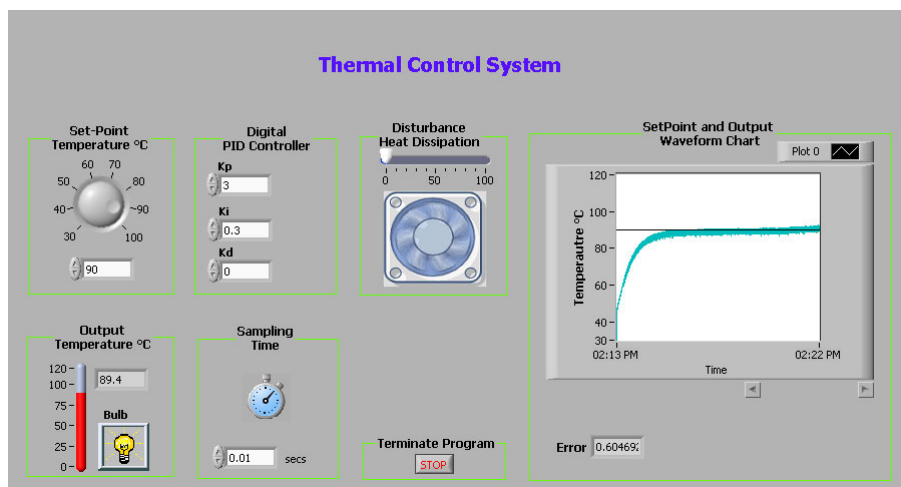


Fig. 10. Front Panel VI for thermal feedback control system

When the fan is used to introduce disturbance intentionally, the error initially increases but the bulb PWM actuation is also increased further to counteract it. The practical gains were found to be close to the ones determined using simulation. The final response obtained after some slight tuning is shown in the Fig 11.

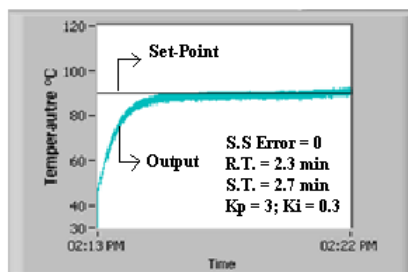


Fig. 11. Final PI tuned system response

5 Conclusion

The applications presented in this paper are based on a hardware software co-design technique. This strategy minimizes the hardware involvement and consequently reduces the overall system cost. The virtual instrumentation techniques allow rapid application development. The portability and large storage capability offered by new PCs enables to carry large number of virtual instruments anywhere. Since, commercially available DAQ cards are expensive, therefore it is imperative to design and develop such systems locally. In the light of the results of both VI based designs,

it is found that is possible to perform laboratory control experiments without relying on dedicated hardware. However, better results were obtained for slow systems (thermal) than for fast mechanical systems (drive). These limitations are not associated with the VI approach itself and therefore can be overcome by employing a fast DAQ along with careful modeling and better implementation of the system under consideration.

Acknowledgements. This work was supported by the authors' institution, IIEE.

References

1. Ugurlu, Y.: Measuring the Impact of Virtual Instrumentation for Teaching and Research. In: IEEE Global Engineering Education Conference (EDUCON), pp. 152–158 (2011)
2. Portillo, E., Cabanes, I., Marcos, M., Orive, D., Sanchez, J.A.: Design of a Virtual-Instrumentation System for a Machining Process. *IEEE Transactions on Instrumentation and Measurement* 56(6), 2616–2622 (2007)
3. Eren, H., Fung, C.C.: A Virtual Instrumentation of Electric Drive Systems for Automation and Testing. In: Proceedings of the 17th IEEE Instrumentation and Measurement Technology Conference, IMTC, vol. 3, pp. 1500–1505 (2000)
4. Prema, K., Kumar, N.S., Sunitha, K.A.: Online Temperature Control Based on Virtual Instrumentation. In: International Conference on Control, Automation, Communication and Energy Conservation, pp. 1–4 (2009)
5. Tang, Z., Xian, F., Fen, L.: Design and Implementation of a Temperature Control System Base on Convenient DAQ. In: 27th Chinese Control Conference, CCC, pp. 374–376 (2008)
6. Mirza, A., et al.: IPO Pakistan patent 14063: USB Data Acquisition Card. Issued (June 29, 2011)
7. Chen, J., Zeng, X., Zhang, C.: The Portable Data Acquisition System of Cutting Tool Condition Monitoring Based on Labview & Wavelet Analysis. In: International Conference on Computer Application and System Modeling (ICCASM), vol. 7, pp. 375–378 (2010)
8. Seborg, D.E., Edgar, T.F., Mellichamp, D.A., Doyle, F.J.: *Process Dynamics and Control*, 3rd edn., pp. 145–146. John Wiley and Sons (2010)
9. Bolton, W.: *Control Systems*, 1st edn., Newnes, pp. 49–50 (2002)
10. Hellerstein, J., Diao, Y., Parekh, S., Tilbury, D.M.: *Feedback Control of Computing Systems*, pp. 332–333. Wiley-IEEE (2004)

Data Management in Mobile Wireless Sensor Networks

Syeda Nida Sahar and Faisal Karim Shaikh

IICT, Mehran University of Engineering and Technology, Jamshoro
enr_nida_sahar@hotmail.com, faisal.shaikh@faculty.muett.edu.pk

Abstract. Currently, data management schemes in Wireless Sensor Networks (WSNs) are finding their way in evolving network technologies such as Peer-to-Peer (P2P) networks. Many P2P protocols have been applied in WSN to accomplish the same due to similarities between P2P and WSNs. Alongside, there are differences between them too making the P2P protocols inefficient in WSNs. Furthermore, to increase the efficiency and to exploit the delay tolerant nature of WSNs, where ever possible, the mobile WSNs are gaining importance. Thus, creating a three dimensional problem space to consider, i.e., mobility, WSNs and P2P. In this paper we propose an efficient algorithm for data management in mobile WSNs. The implementation and deployment of proposed algorithm in real scenario is also presented.

Keywords: Mobile Wireless Sensor Networks, Peer-to-Peer, Data Transport and Management.

1 Introduction

Data management is a process of developing data architecture and procedures that deal with data and are executed on a regular basis. If the data is properly managed it will be easily accessed by others in a reliable manner. The data management is important for every type of network either it is wired or wireless. The data management in wired networks has been reached their maturity during past decades [1]. In contrast, data management in evolving networks, i.e., Peer-to-Peer (P2P), Mobile Ad Hoc Networks (MANETs) and Wireless Sensor networks (WSNs), are still uncharted terrain [1]. Recent works have witnessed an increasing interest in the field of WSN for collecting and processing data (data management) in a distributed manner from either static or mobile scenarios [2].

Data management in WSNs is different from traditional database systems because of its low capabilities or limited resources [3]. But traditional approaches are still being used in WSN especially P2P approaches because of certain similarities between WSN and P2P systems, e.g., each node in the network shares other node's resources, does not have permanent connectivity, has equal responsibilities and is fully independent regarding its own resources, has separate ID and behaves as a router when forwarding the data [4]. Along with similarities there are also differences with P2P systems such as scarce resources, which cause P2P data management protocols to inefficiently utilize the resources of WSNs. The advantage of applying P2P

technology in WSN is to exploit the decentralized approaches, which reduces the number of transmissions for data retrieval and replication process. The replication process assures reliability in case of node failures which is frequent in WSNs. To make use of these advantages and to overcome the problem of inefficient use of resources many protocols are developed and tested [5, 6, 7]. Unfortunately, these protocols are developed only for static networks and provide no support for the mobility.

The data management in mobile networks is a more challenging than static networks. In Mobile WSNs (MWSN), a subset of nodes changes their location in order to collect and disseminate the data instead of routing the data in order to efficiently utilize the network resources [8]. This paper explores how to support mobile nodes in an established static network of Virtual Cord Protocol (VCP) which is using P2P approaches for data management. Furthermore, we present the implementation and deployment of the proposed algorithms in real world scenario for the proof of concept.

Let us consider a scenario of smart hospital where the environment is monitored and controlled by the WSN. The hospital rooms and corridors are equipped with static wireless sensor nodes and the data inside the network is managed by P2P system similar to [4, 7]. The patients and their data plays major role in clinical support system. The patients are generally mobile and their movement cannot be restricted in order to send data towards the base station. The major issue here is how to integrate mobile patients with the existing WSN such that the data gather by the patients (e.g., heart rate, blood pressure, etc.) can be transported to the base station. This paper presents algorithms to detect the presence of WSN and transferring the data to the network. After receiving the data, the WSN transport it to the base station [4, 9].

The rest of paper is organized as follows. Section 2 briefly describes system models and mobility model. Section 3 explores the related work. Section 4 presents different processes of proposed scheme. Implementation and deployment of proposed scheme is discussed in Section 5. Section 6 comprises of result analysis and the Section 7 concludes our work.

2 Models

In this section we first describe the considered system model then briefly elaborate the mobility model.

2.1 System Model

In a finite network, consider a WSN has N nodes numbered [0 to $N-1$] where node numbered 0 is a sink. Each node has sensors and except sink each node has small memory, less computational resources, limited radio communication and less power. Whereas, sink node has more capabilities than other nodes in the network, e.g., continuous power supplies, more memory and high computational resources. The static network senses data, hash it and store it at a node having virtual position closest

to hashed value. These nodes also respond to a request that is generated by the base station. While the mobile nodes sense the data and send data towards the base station through a static node that is nearest to the base station. In this work, we consider only a single mobile node in the network.

2.2 Mobility Model

The mobile nodes inside WSN can move either in a random, predictable or fixed fashion. In random mobility node can move anywhere in the network and its movement is unpredictable. For predictable mobility pattern the movement of the node can be predicted. Whereas, for fixed mobility pattern the movement of a node is known in advance. Irrespective of mobility pattern our proposed system can be deployed in all scenarios but for proof of concept we consider fixed mobility pattern.

3 Related Work

In P2P, no single node controls the network and each node is a peer to all other computers in the network. There is no centralized management in this approach. P2P has provided much flexibility to applications and solved most of the problems of WSN [10].

In the same way, VCP-inspired by structured P2P technology-provides efficient data management using the routing techniques with DHT services [5, 6, 7]. It uses virtual positions for data transport, where each node maintains a successor, a predecessor and a routing table to store information of its neighbors. Each node in the network can have a maximum of two virtual neighbors and can broadcast a message to update the other nodes about its current status and to assign virtual positions to the new nodes. All the nodes are responsible to hold information of their single hop neighbors only, so the functionality of each node would not be affected by the size of the network. In [4, 9] VCP has been implemented on mica2 sensor nodes and its applicability in real world scenario has been shown. The major drawback with VCP and related approaches [5] is that they do not support mobility.

Mobile Wireless Sensor Network, as its name suggests, has the presence of mobile nodes in the network [11]. MWSN has advantages over static WSN as it causes improved coverage, superior channel capacity and enhanced target tracking [11]. This evolving technology can be applied for land [12], ocean [13] and air [14] exploration and monitoring, Habitant Monitoring [15], automobile applications [16] and also on other scenarios. MWSN can derive their coordination with other nodes either through the dedicated coordinates or through the communication with other nodes in the network [2]. Recently, data management techniques have been proposed for MWSN [2]. In these techniques data are sent either periodically or on demand. But still research is going on for efficient data management in MWSN. The main drawback of these techniques is that they do not exploit P2P advantages and their major focus is on exploiting mobility only.

4 Aiding Mobility for P2P Data Management in WSNs

In this section, a brief overview of our approach is presented. Next, the process of network discovery and table update is explained in order to transport and manage the data using P2P techniques for mobile WSNs.

4.1 Overview

Since, VCP is designed to work for static WSNs only [4, 9], we have extended it to support mobile nodes in the network. As static nodes are programmed with VCP, hence each static node in the network is assigned virtual position by a node that is already part of the network. Each node is responsible to sense data from environment, hash it and store at a node having closest virtual position to the hashed value. In addition to this, we allow these nodes to behave as a router for the data from mobile nodes towards the base station. When the mobile node wants to send the data it first discovers the network around it. After discovery the mobile node selects a static node which is nearer to the base station by exploring the distributed hash table of the nodes inside the network. Once, the data is handed over to the static sensor node the data will be transported to the base station using P2P approach, i.e., VCP.

4.2 Network Construction

The network starts with a static preprogrammed initial node having virtual position either S (Start point) or E (End point). If a new static sensor node is added in the network then it will be assigned a virtual position by a node that is already part of the network (called old node) as all communication in the static network will be done using node virtual positions[4, 9]. After having a virtual position each node start broadcasting a *HELLO* message to update other nodes about its current virtual position and start sensing data. This data will be hashed and stored at a node having virtual position closest to the hashed value. If a mobile node wants to send data in the network it will update its routing table and send data towards the base station through its nearest single hop neighbor (static node).

4.3 Network Discovery and Mobile Node Data Management

The mobile node data transport is carried out using the single hop neighbors. If the source and the destination nodes cannot directly communicate with each other, then the data will be sent to a node having the closest virtual position towards the destination as shown in Fig. 1 and its Pseudo code is explained in algorithms 1 and algorithm 2. It is expected that a mobile node is continuously moving. Considering the Fig. 1 the data transport process for the mobile node is as follows:

At point 1, mobile node is in communication range of only node 0.75. The Mobile node will send data to node 0.75. Node 0.75 will search in its routing table and finds node 0.5 that is nearest to node 0.5. Node 0.75 will send data to node 0.5 for further process. Node 0.5 finds a base station (node 0.0) in its routing table and sends data to base station.

At point 2, mobile node is in communication range of two nodes, node 0.75 and 0.875, but since node 0.75 is nearest to base station it will send data to node 0.75.
 At point 3, mobile node is in communication range of only 0.875. Now mobile node will communicate with node 0.875 to transport data.

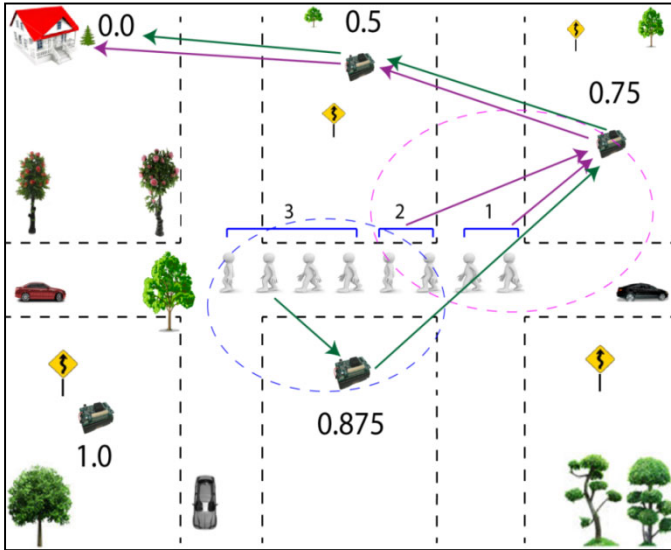


Fig. 1. Data Transport and Management of Mobile Node

Before stating algorithms of data management following are certain terms used in all the algorithms, i.e., NT = Neighbor Table of a node or an array of neighbor table, NT[MIN] = minimum number in the sorted table (NT[1]), NT[MAX] = maximum number in the sorted table(NT[LAST]), BS = Base Station

<pre> 1. if NT != null then 2. Sense Data 3. call Send(Data) 4. end if </pre>	<pre> 1. if BS<NT[min] then 2. SendData(NT[MIN]) 3. end if 4. if (BS>NT[MAX]) then 5. SendData(NT[MAX]) 6. end if 7. if BS>=NT[MIN]&&BS<=NT[MAX] 8. for(int i=1;i<= MAX;i++) 9. if(BS <= NT[i]) 10. SendData(NT[i]) 11. exit for 12. end if 13. end for 14.end if </pre>
Alg. 1: Sense data from environment	Alg. 2: Sending of data

4.4 Routing Table Update for Mobile Node

To route a message from source to destination accurately each node must update its routing table. The routing table update process of static nodes is explained in [4, 9]. In this paper we will discuss routing table update process of mobile node only that is required because of two reasons: first, to update the current virtual position of its neighbors and their existence in the network. Second, as it is a mobile node its neighbors will be changed continuously. The routing table update process of mobile node is shown in Fig. 2 whereas its pseudo code is depicted in Algorithm 3 and Algorithm 4. Each static node broadcasts a *HELLO* message to update its current status to other nodes in the network.

At point 1, mobile node is receiving a *HELLO* message of node 0.75 and updates its routing table with node 0.75.

At point 2, mobile node is receiving a *HELLO* message of another node 0.875 and adds this node in its routing table.

At point 3, mobile node is out of communication range of node 0.75 and a *HELLO* message of node 0.75 is not received by the mobile node. The Mobile node will remove node 0.75 from its routing table as shown in Fig. 2.

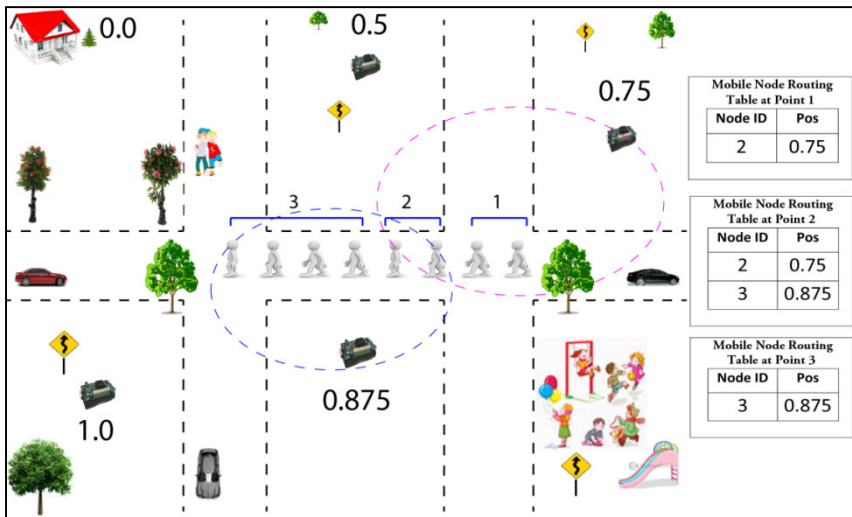


Fig. 2. Routing Table Update Process of Mobile Node

5 Real World Deployment Setup

In this section, real world deployment setup is discussed. First, hardware and software tools are discussed then deployment scenario is explained. In last implementation and execution details are presented.

5.1 Hardware and Software Tools

Six mica2 sensor nodes have been used for the implementation of VCP with the mobile node scenario. Five sensor nodes have MTS301 sensor boards and one sensor node is attached to MIB510 programming board to make the base station. TinyOS-1.1.15 has been used for programming the mica2 sensor nodes.

<pre> 1. if SN ∈ NT 2. Update SN presence 3. else 4. call ADD(SN) 5. end if </pre>	<pre> 1. if(NT == Null) then 2. Add SN in NT[MIN] 3. MAX = MIN 4. end if 5. if SN> NT[MAX] 6. Add SN in NT[MAX+1] 7. MAX = MAX + 1 8. end if 9. if SN<NT[MIN] 10. for (int i=MAX;i>= MIN;i--) 11. NT[i+1] = NT[i] 12. end for 13. NT[MIN] = SN 14. end if 15. if (SN>NT[MIN] && SN<NT[MAX]) then 16. for (int i=MIN;i<=MAX;i++) 17. if(SN< NT[i]) then 18. for(int j=MAX+1;j>=i;j--) 19. NT[j] = NT[j-1] 20. end for 21. NT[i] = SN 22. exit for 23. end if 24. end for 25. end if </pre>
<p>Alg. 3: Received a <i>HELLO</i> message from a node</p>	<p>Alg. 4: Adding a sensor node to the network</p>

5.2 Deployment Scenario

Six mica2 sensor nodes have been deployed in a hospital scenario. Five sensor nodes are static and one node is mobile. Among five static nodes, one node is the base station and four are randomly distributed in lobbies. One node is attached to a patient that behaves as a mobile node. Each static node has VCP functionality and sense light and sound reading from environment. For light data, when there is darkness then

the lights will automatically on and in brightness lights will automatically off in lobbies. For sound data, when there is a noise, node will send report to the base station to take an action. For mobile nodes these static nodes will behave as a router towards base station. The mobile node will send continuous information about patient health to the base station to take an immediate action.

As shown in Fig. 3 two nodes (ID 1 and ID 2) have been placed in lobby of the female ward and two nodes (ID 3 and node 4) have been placed in lobby of the male ward. One node has been placed in information desk that behaves as a base station having ID 0. Nodes having IDs 1 and 4 are in direct communication with the base station and are at single hop. Whereas node having ID 2 is in communication range of node having ID 1 and node having ID 3 is in communication range of node with ID 4. These nodes are at hop 2. A node attached to a patient is present at the private room of the male ward and he is walking in the lobby.

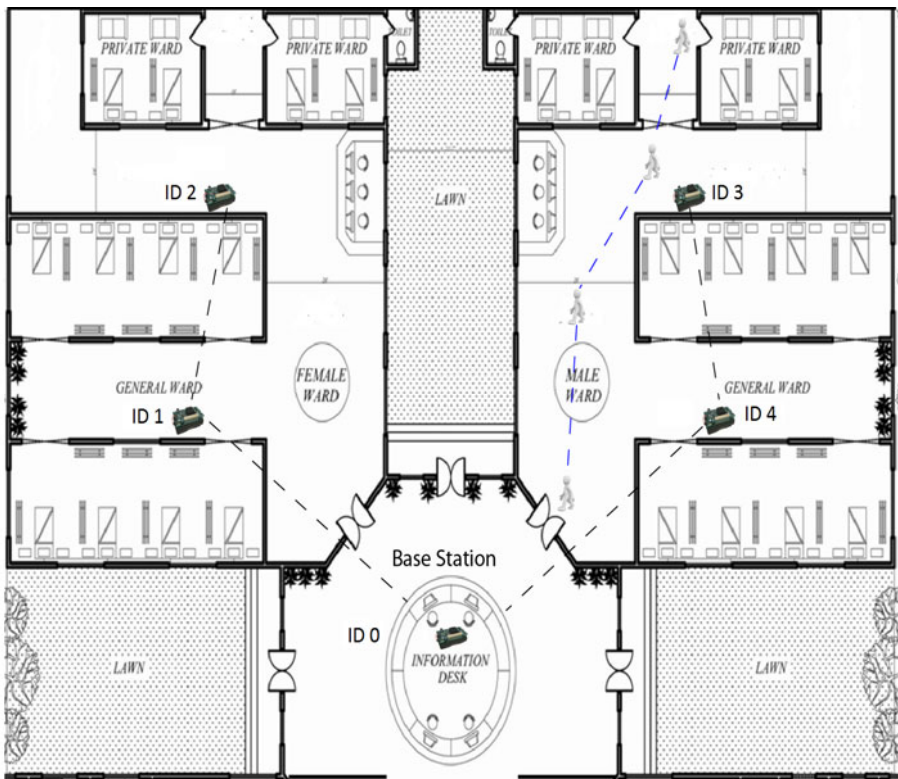


Fig. 3. Mobility in VCP Deployment Scenario

5.3 Hardware Implementation

Static Network: The unique source address to each node is assigned and the nodes that are not part of the network are assigned a virtual position *-1.0*. Each node that

becomes part of the network starts broadcasting a *HELLO* message after every second along with the other network functions including sensing light and sound from the environment and maintaining the routing table. A variable *SET_POS* is used to check the status of the node to determine if the node is busy in setting the virtual position or not. This variable prevents the assignment of same virtual positions to multiple nodes and it also prevents assignment of two different virtual positions to a single node. The virtual positions are allocated between value *S* and *E*(0 and 1). Once the virtual positions are assigned, the data transmission is carried out using the single hop neighbors.

Mobile Network: The mobile node starts sensing data after receiving at least a *HELLO* message from a node in the network. It senses data after every second and send report to the base station using static network.

6 Results

The performance of the proposed scheme is evaluated with respect to the reliability of the scheme. The reliability is measured by number of packets generated by the mobile node to the number of packets received at the base station. The mobile node sends a packet to the base station after every second. The results are obtained by repeating experiments many times.

The graph (Fig. 4) shows the number of packets received at the base station at the interval of one second. From graph (Fig. 4) it is clear that the PRR at hop 1, means when the mobile node is directly communicating with the base station, is approximately 100%. At hop 2 it is 98% and hop 3 PRR is 92%.

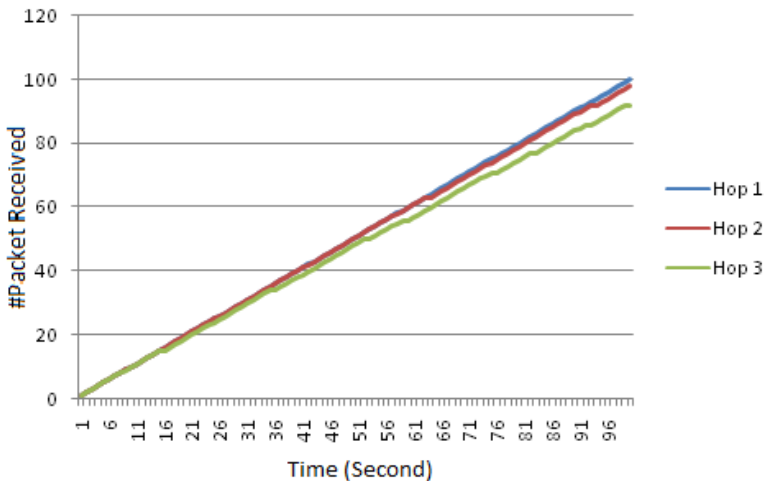


Fig. 4. Packet Receive Rate Vs Time

The mobile node when communicates with its router its PRR at its router is approximately 99% and when it directly communicate with base station its PRR is 100%. For example, if the mobile node is sending a packet/message to node 4 as shown in Fig. 3, the PRR at node 4 will be 99% approximately. The remaining packet loss as shown in the graph (Fig. 4) is due to MAC layer collisions as mentioned in our previous work [4].

The above graph (Fig. 4) shows PRR at different hops when a mobile node is moving within communication range of 1st hop, 2nd hop and directly with base station. But there will be a certain amount of packet loss when mobile node switches from one router to another for example in Fig. 3, when the mobile node is near private room it is in communication range of node 4. When this node reaches near kitchen it is out of communication range of node 4 and now it has to communicate with the base station through node 5 but this information about node 4 is not immediately acquired by the mobile node. Because if a *HELLO* message of a node is not received by the mobile node then it waits for three seconds. If within this period, a *HELLO* message of that node is not received then mobile node will eliminate this node record from its routing table. But within this period the mobile node tries to communicate with that node and due to this reason packets will be lost. The following graph (Fig. 5) shows total number of PRR at the base station by the mobile node. As shown in the graph (Fig. 5) overall PRR at the base station is 95% and there is a loss between 4 to 6 packets when mobile node switches from one router to another.

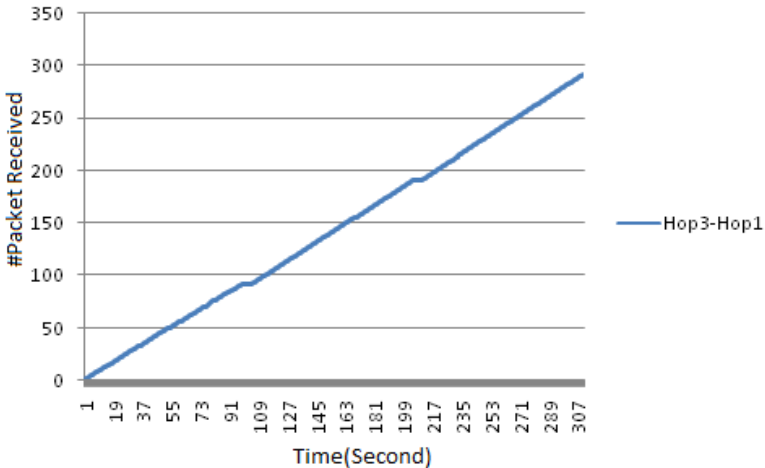


Fig. 5. Packet Receive Rate Vs Time (Total PRR during movement)

7 Conclusion

The objective of this paper is to add mobility in structured P2P based data management protocol called Virtual Cord Protocol. Different processes of this

proposed scheme have been discussed including network construction, data transport and management and routing table update. The implementation and deployment of static network with a mobile node is shown in a hospital scenario. The future work involves adding more mobile nodes in the network to interact with the static nodes as well as among each other in the network. This research is limited to one way communication for mobile nodes (i.e., sending data from mobile node towards base station). We will extend this research by sending queries from the base station to mobile nodes in the network.

Acknowledgment. This research is supported by TL Department, Mehran University of Engg. & Technology, Jamshoro. We are thankful to Dr. Mukhtiar Unar for providing access to the hardware and for necessary arrangements for the execution of the scenario.

References

1. Boncz, P.A., et al.: P2P, Ad Hoc and Sensor Networks –All the Different or All the Same? In: Proc. of Scalable Data Management in Evolving Networks (2007)
2. Chen, M., et al.: Mobile Agent Based Wireless Sensor Networks. *J. Comp.* 1(1), 14–21 (2006)
3. Akyildiz, I.F., Vuran, M.C.: *Wireless Sensor Networks*. John Wiley and Sons (2010)
4. Sahar, S.N., Shaikh, F.K., Jokhio, S.H.: P2P based Data Management WSNs: Experiences and Lessons Learnt from a Real-world Deployment. *MURJET* 30(4) (October 2011)
5. Awad, A., Sommer, C., German, R., Dressler, F.: Virtual Cord Protocol (VCP): A Flexible DHT-like Routing Service for Sensor Networks. In: Proceedings of 5th IEEE International Conference on Mobile Ad-hoc and Sensor Systems (MASS 2008), Atlanta, GA, pp. 133–142 (September 2008)
6. Awad, A., German, R., Dressler, F.: Efficient Service Discovery in Sensor Networks using VCP. In: Proceedings of 15th ACM International Conference on Mobile Computing and Networking (MobiCom 2009), Demo Session, Beijing, China (September 2009)
7. Awad, A., German, R., Dressler, F.: P2P-based Routing and Data Management using the Virtual Cord Protocol (VCP). In: Proceedings of 9th ACM International Symposium on Mobile Ad Hoc Networking and Computing (MobiHoc 2008), Poster Session, Hong Kong, China, pp. 443–444 (May 2008)
8. Khelil, A., Shaikh, F.K., Ali, A., Suri, N.: gMAP: Efficient Construction of Global Maps for Mobility assisted WSNs. In: Proc. of WICON (2009)
9. Sahar, S.N., Shaikh, F.K., Jokhio, S.H.: Peer-to-Peer Wireless Sensor Networks for Efficient Data Transport and management. In: Proc. of SCONEST (2011)
10. Gutierrez, G., Mejias, B., Van Roy, P., Velasco, D., Torres, J.: WSN and P2P: a self-managing marriage. In: Proceedings of 2008 Second IEEE International Conference on Self-Adaptive and Self-Organizing System Workshops, Venice, Italy, pp. 198–201 (2008)
11. Zeinalipour-Yazti, D., Chrysanthis, P.K.: Mobile Sensor Network Data Management. In: Ozsu, M., Tamer; Liu, L. (eds.) *The Encyclopedia of Database Systems, EDDBS* (2009) ISBN: 978-0-387-49616-0
12. Dantu, K., et al.: Robomote: Enabling mobility in sensor networks. In: ACM Int. Conf. on Information Processing in Sensor Networks-SPOTS (2005)

13. Nittel, S., Trigoni, N., Ferentinos, K., Neville, F., Nural, A., Pettigrew, N.: A drift-tolerant model for data management in ocean sensor networks. In: ACM Workshop on Data Engineering for Wireless and Mobile Access (2007)
14. Allred, J., Hasan, A.B., Panichsakul, S., Pisano, B., Gray, P., Huang, J.-H., Han, R., Lawrence, D., Mohseni, K.: SensorFlock: An Airborne Wireless Sensor Network of Micro-Air Vehicles. In: ACM Int. Conf. on Embedded Networked Sensor Systems (2007)
15. Sadler, C., Zhang, P., Martonosi, M., Lyon, S.: Hardware Design Experiences in ZebraNet. In: ACM Int. Conf. on Embedded Networked Sensor Systems (2004)
16. Eriksson, J., Girod, L., Hull, B., Newton, R., Madden, S., Balakrishnan, H.: The Pothole Patrol: Using a Mobile Sensor Network for Road Surface Monitoring. In: ACM Int. Conf. on Mobile Systems, Applications and Services (2008)

Implementation of Load Shedding Apparatus for Energy Management in Pakistan

Hira Sakrani¹, Tooba Tariq Butt², Moezul Hassan^{3,*},
Sarmad Hameed³, and Imran Amin³

¹ National University of Science and Technology, IME Department, Pakistan
hira_sakrani@hotmail.com

² NED University of Engineering and Technology, Electronics Department, Pakistan
toobatarigbutt@gmail.com

³ SZABIST, Centre of Renewable Energy, Pakistan
{moez.hassan, imran.amin, sarmad.hameed}@szabist.edu.pk

Abstract. Uninterrupted power supply is one of the key problems faced by the citizens of Pakistan. The growing residential and commercial sector has further taken a serious toll on the economy and progress of the country.

The power generation & distribution utilities currently heading the charge of supplying electricity to Pakistan have had many struggles with the crippling infrastructure of this sector. Until such time that line losses are substantially reduced and new power units come online to cater for the increasing demand there needs to be devised a method for planning and maintaining a scheduled Load Shedding policy across the country to provide some relief to the citizens and facilitate industrial and commercial growth. For this purpose Pakistan's power companies are implementing a state of the art Supervisory Control & Data Acquisition (SCADA) system for carrying out the activities of the Load Dispatch Centre.

The scope of this design is to incorporate the "Load Shedding Apparatus" in conjunction with the existing Load Shedding policy of the country and develop a miniature system that provides a holistic observation of an entire power company's grid system and real time values of load generation and utilization.

Keywords: Load shedding, Simatic Manager, Windows Control Center (WinCC), feeders.

1 Introduction

Electricity is the most widely utilized commodity in today's era. According to Shah, S. *et al*, the economic and commercial growth of a country is reflected through its surging power demand[1].

The generation, transmission, distribution & retail supply of electricity in Pakistan is currently undertaken by several public and private sector utilities. Despite rising

* Corresponding author.

electricity demand over the past several years no worthwhile measures were taken, as depicted by Dr. Noor ul Haq in IPRI Fact file, to make this necessity feasible and accessible to all [2]. In the Report and Recommendations of the President to the Board of Directors issued by Asian Development Bank, Pakistan is now at a stage where it faces an unprecedented dearth of energy with unplanned load shedding reaching up a huge 8-10hrs for urban dwellers and up to 20hrs for rural consumers[3]. Until such time that substantial investments are made in the power sector to offset this dilemma power utilities need to devise a scheduled load shedding policy to facilitate some form of economic stability and growth in the country. The designed system's load shedding policy is based on selectively shedding blocks of load (on the 11Kilovolt lines) in the interconnected power system in accordance with pre-determined area priorities[4, 5] so that the transmission system continues in operation when the generating and the tie-line capabilities are inadequate to meet normal total load demands. The system is divided into three types of feeders namely

1. Residential feeders: connected to houses, apartments, colonies etc.
2. Industrial feeders: connected to large scale and medium scale industries
3. Exempted feeders: connected to hospitals, airports, high courts etc. These feeders are exempt from shedding unless a major blackout occurs which leads to shedding from several of these areas or a devastating blackout occurs which causes the power in the entire city to drop[6].

To prepare for selective load shedding the entire system distribution feeders (residential, commercial & industrial) are reviewed on an annual basis. The feeders are assigned a priority based on their overall customer mix. The feeders with similar priorities are then amalgamated into groups. The groups have been assigned priority in terms of both planned and emergency load shedding programs. The groups with the lowest priority are subjected to load shedding first whereas the groups with higher priority suffer the least amount of load shedding and are typically the first to be restored.

2 System Description

The simulation has been carried out using the Simatic Manager S7 and Windows Control Center (WinCC)[7]. The preliminary idea behind designing the program is to maintain the system stability in response to the varying generating power and the prevailing loads in an area[8].

The key feature of this project is the design of the Basic Signaling Display as shown in Fig. 1. The interactive toolbar allows navigation to the various display elements in the software and provides easy access to the recognition and detection of the generated alarms[9]. The voltages level designs have been chosen so that other simulations can be incorporated without any major changes required (e.g. interlocking, import target violation etc.)

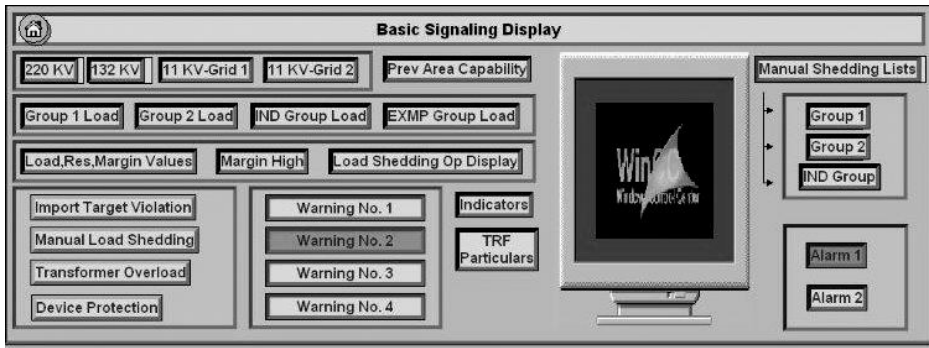


Fig. 1. Basic Signaling Display

220KV lines are designed using double bus bar scheme[10] shown in Fig. 2. Three generating units have been considered. G1, G2 and G3 with max generating capacity of 25, 40 and 15MW bringing the system's maximum generating capacity equals to 80MW.

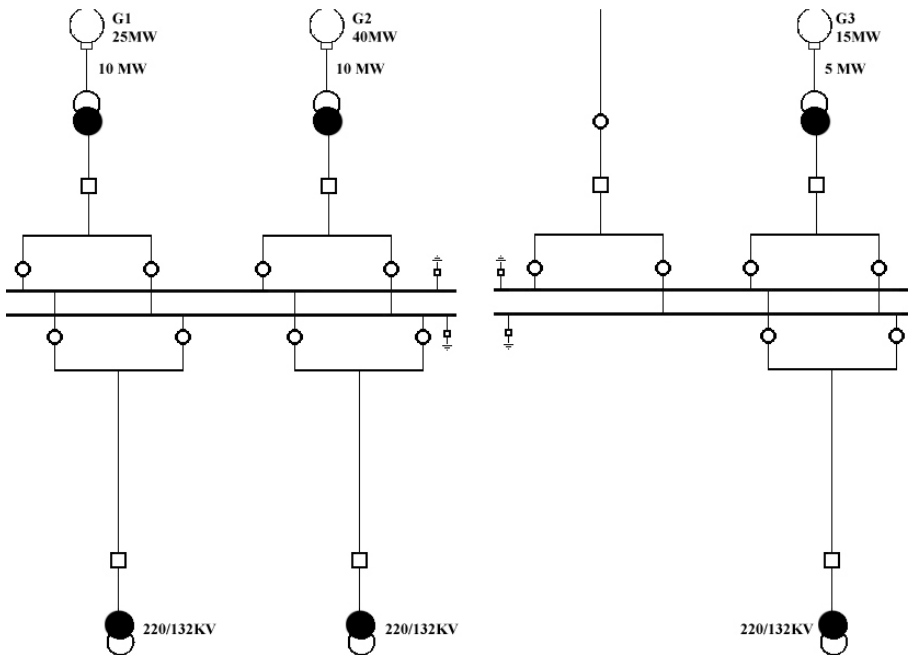


Fig. 2. 220KV Double Bus bar Scheme

The ring bus arrangement has been used in the design of the 132KV lines shown in Fig. 3.

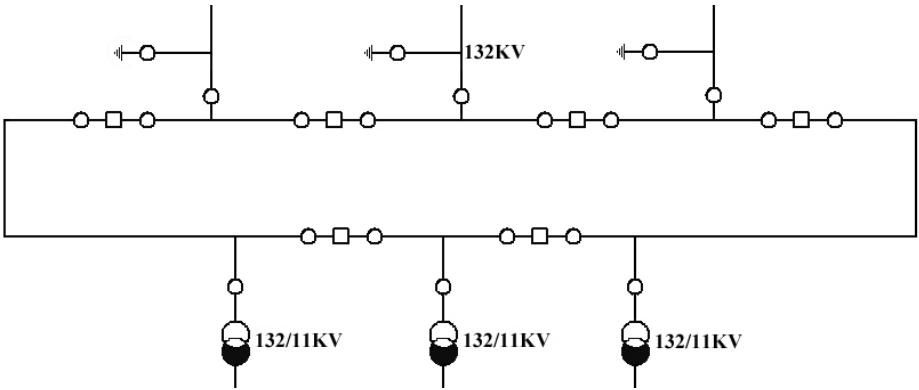


Fig. 3. 132KV Ring Bus Arrangement

We have designed a two-grid 11KV system, with each grid station supplying to 16 single bus bar 11KV feeders. Screenshot of Grid-2 is shown in Fig. 4.

- The residential group G1 comprises of feeders 1, 5, 9, 11 (Higher priority)
- The residential group G2 comprises of feeders 2, 6, 7, 10 (Lower priority)
- The industrial group comprises of feeders 4, 8, 3, 12
- And the exempted feeder group comprises of feeders 13, 14, 15, 16

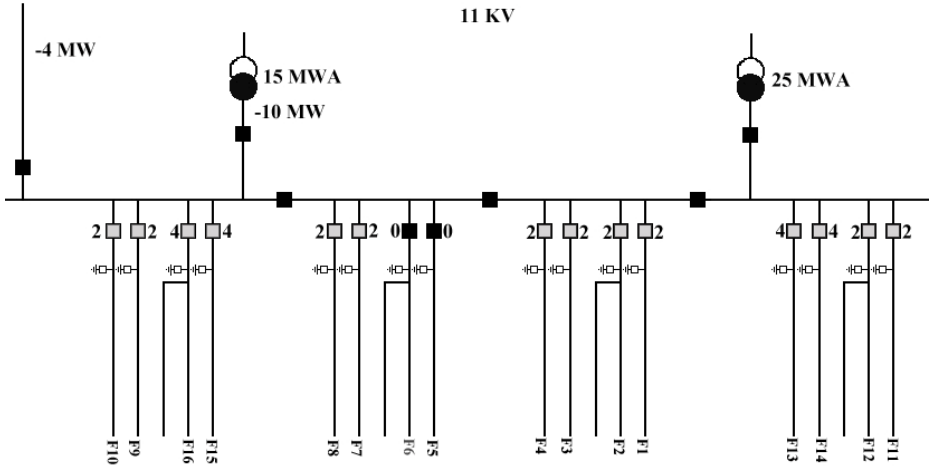


Fig. 4. 11KV Grid-2

3 Load Shedding Program Overview

The prevailing Area Capability of the system is compared with the prevailing Area Load to produce a value indicative of the Prevailing Area Reserve Power. The value

is then compared with the Preferred System Reserve and the difference is defined as the Prevailing Area Margin. Nathan Cohn proposed in his patent, Load Shedding Apparatus, that the load is shed on the basis of the margin value being greater than or less than zero[11].

3.1 Prevailing Area Capability (C)

$$C = \sum Gn \quad (1)$$

Where $\sum Gn$ is the sum of the MW inputs of each generator.

3.2 Prevailing Area Load (L)

$$L = \sum Fn \quad (2)$$

Where $\sum Fn$ is the MW utilization of power in the system, determined by summing up the respective feeder inputs.

3.3 Prevailing Area Reserve Power (R)

$$R = C - L \quad (3)$$

3.4 Preferred Area Reserve Power (P)

It is an arbitrary load value above which the system would prefer that the Current System Reserve be[12, 13].

3.5 Prevailing Area Margin (M)

$$M = R - P \quad (4)$$

4 Load Shedding Program Simulation

4.1 Prevailing Area Margin Greater than Zero

The margin being greater than zero signifies that the generation is in excess to load being used. In this case the Prevailing Area Margin value is compared simultaneously to each generator input. The generator inputs being less than the margin value are then available to be turned OFF. This is done so as to save the amount of fuel cost utilized in running the generating stations. The case is shown in Fig. 5.

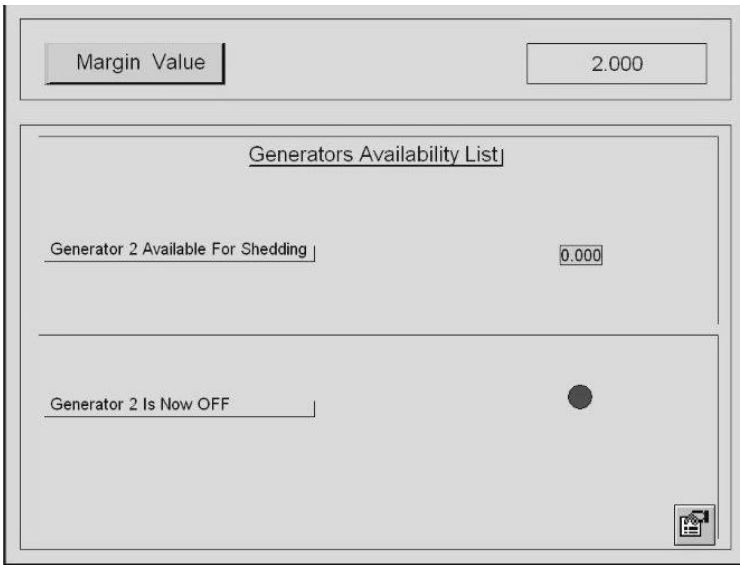


Fig. 5. Prevailing Area Margin > Zero

4.2 Prevailing Area Margin Less Than Zero

This is the case where the demand of electricity is greater than the generation of electricity. The optimum value of prevailing area margin should be equal to zero. In order to achieve this value two effective ways have been considered, including the increase of system generation and the decrease of load demand. The former solution is not achievable in present scenario as the generation capacity is already stretched to its limits in supplying power to an already overloaded system[2] therefore it is in this case that shedding of excess load is required and thus comes into picture the prioritization of loads[14, 15]. In order to achieve the feasibility of turning OFF a single feeder while the group is kept ON or keeping a single feeder ON while the group is OFF (being subjected to load shedding), a Functional Block diagram was created in Simatic Manager, shown in Fig. 6.

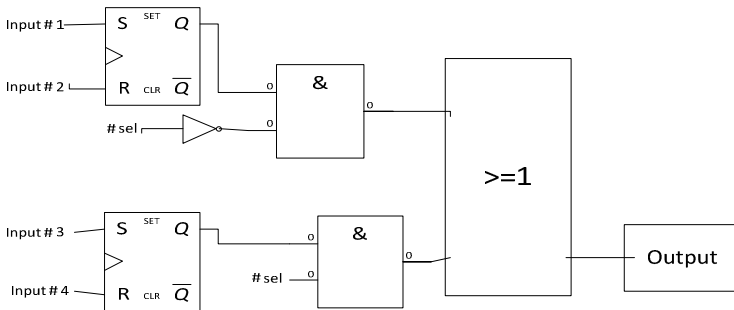


Fig. 6. Functional Block Diagram

Where,

- Input 1 is to switch Group ON
- Input 2 is to switch Group OFF
- Input 3 is to switch a particular feeder ON
- Input 4 is to switch a particular feeder OFF
- Sel is the selection switch used to select any particular feeder and thus make it available for shedding.
- Output displays feeder ON/OFF status.

We check the WinCC screen Load shedding Operating Display shown in Fig. 7. If the red button is being displayed it means that case 2 is valid and load shedding is required.

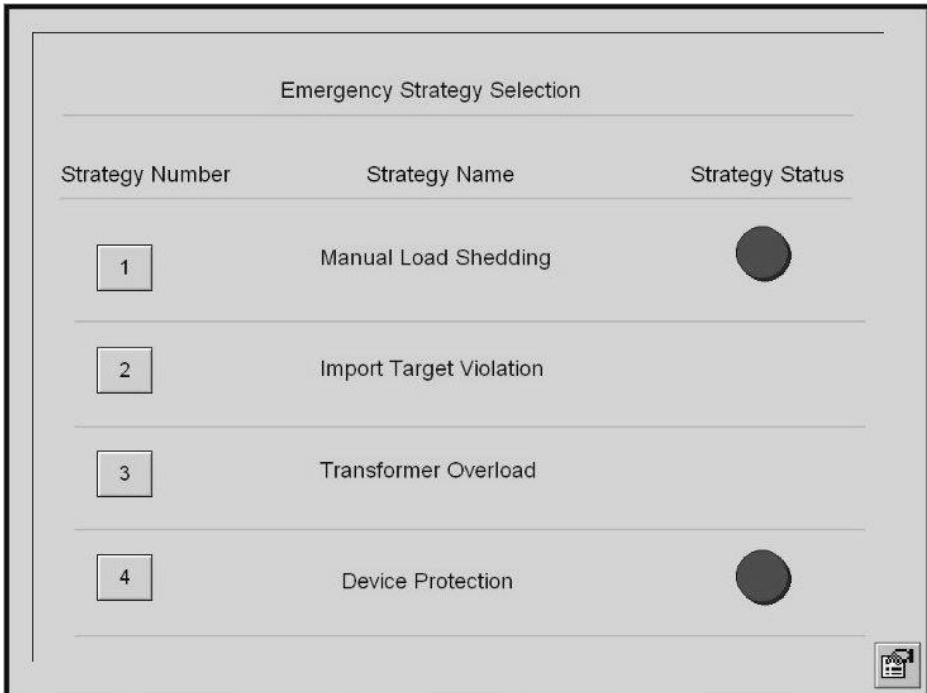


Fig. 7. Load Shedding Operating Display

Clicking on Strategy number “1”, we come to the Manual load shedding screen shown in Fig. 8. From here we can see our Prevailing Area Margin, we are also provided with the option of shedding load from any or all of the three available set of feeders.

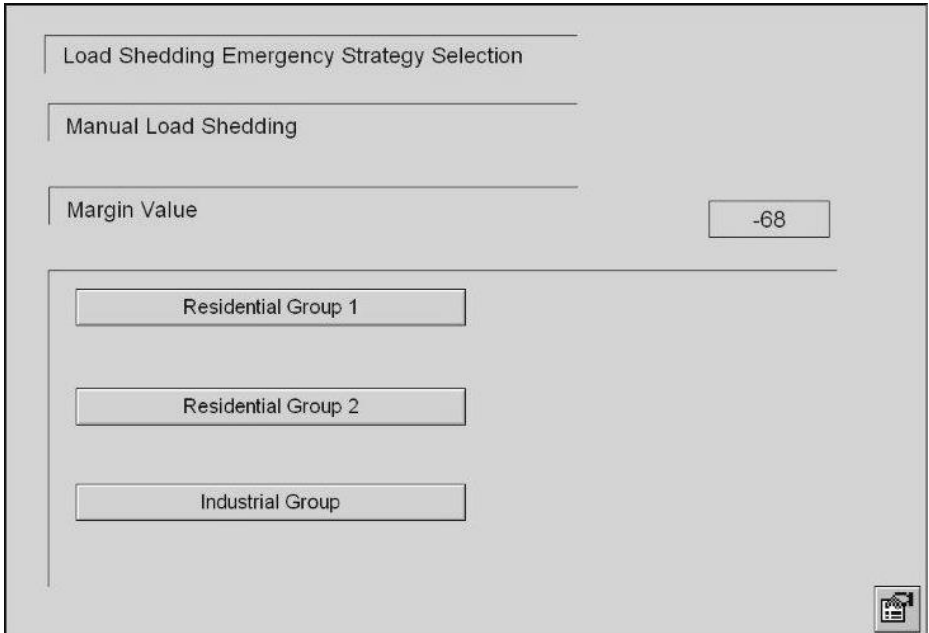


Fig. 8. Manual Load Shedding Screen

Deciding to shed feeders of Group 2 as it is of lower priority we select the “Residential Group 2” button and are brought to the screen “Manual Load shedding List of Group 2” shown in Fig. 9.

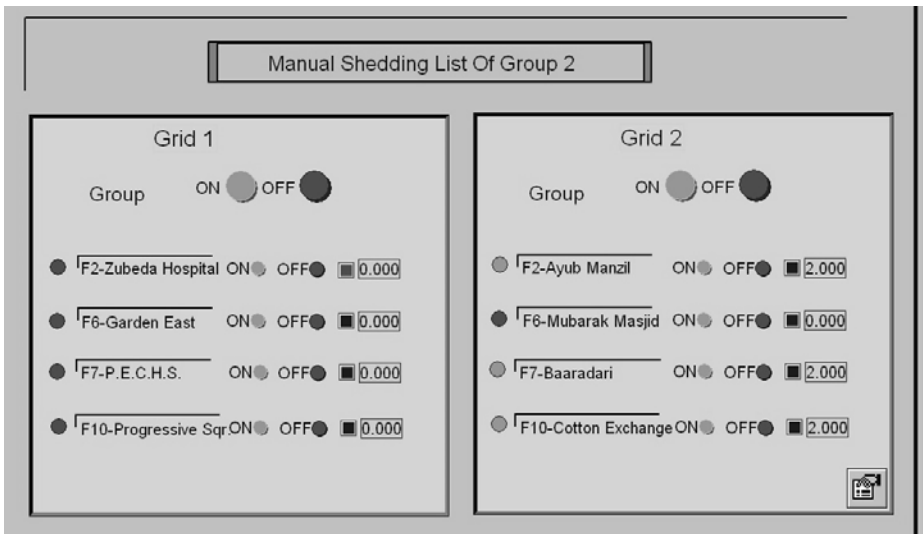


Fig. 9. Manual Load Shedding List of Group -2

- 1: input 1
- 2: input 2
- 3: input 3
- 4: input 4
- 5: Sel
- 6: feeder load input value (0.00 indicates feeder in being subjected to load shed)
- 7: feeder ON/OFF status (green indicates ON and red indicates OFF status)
To turn OFF F2-Zubeda Hospital feeder of Residential Group 2, grid 1
- Input 1: 1
- Input 2: 0
- Input 3: 0
- Input 4: 1
- Sel: 1
- Output: 0 (this value is fed to the status indicator 7, which turns red upon receiving 0)

5 Results and Discussions

The overview of Load shedding policy and its implementation through the application of load shedding apparatus[11] has been described in this paper. The features of the system have been designed similar to the state of the art SCADA [16] being implemented in Pakistan so that it serves not only as a guideline towards understanding the existing system but also provides the flexibility of incorporating our design into it.

The primary achievement of the design is centralized monitoring and control of the entire generation, transmission and distribution system at all times. Such a system would significantly reduce the cost of labor, supply-chain, maintenance etc. it would also provide better decision making and immediate action, on part of the supervisors and operators, in stress situations.

Further, the option of shedding any or all feeders from the system will provide ease of operation in cases of scheduled, preventive maintenance, breakdowns etc.

At every stage the design provides real-time values of generation and load utilization. Also the design provides maximum ease of navigation. The indicators used in the design have been defined onto separate screens to eradicate any complexity in understanding.

A database of the details related to each transformer is maintained in the system shown in Fig. 10 and is of viable use in cases of overloading conditions, maintenance activities, breakdowns etc.

Transformer Particulars	
Name Of Substation	GRID 1
Make	ELTA
Rating	10MVA
Sr. Number	6005262
Type	Three Winding Transformer
Year Of Commissioning	2000 (Year Of Manufacture 1999)
Last Routine Maintenance Work Carried Out	01-11-2007 (planned)

Fig. 10. Transformer Particulars

6 Conclusion

The purpose of this research was to miniaturize the existing national grid system of Pakistan and implement Nathan Cohn's patented "Load Shedding Apparatus" [11] to carry out scheduled load shedding in view of the prevailing system priorities. The design facilitates understanding of the load shedding mechanism, a boon which has become an integral part of our everyday lives and aids the system operators in better functioning.

The authors encourage expansion and future research in this design, some of which are

- Expansion of the design to include PMT (pole mounted transformer) load values or even individual customer loads. Control can then be carried not only on feeder level but rather individual customers can be catered accordingly. This will substantially reduce circular debt due to theft of electricity and non-payment of bills.
- Daily demand supply position summary which will have details of the generation and supply of the system, temperature and weather variables, the public or unplanned holiday details and also the calculations of the peak morning and evening loads. This will help maintain a database which would further assist in load forecasting.

Acknowledgments. We are immensely grateful to Karachi Electric supply Company (KESC) officials for giving us an insight into their world and for educating us with their valuable operating experience and system data. Also, we are very thankful to the Electronics Dept, NED University of Engineering and technology for supporting us in our venture and for guiding us throughout the process.

References

1. Shah, S., Bhatti, M.K.L.: Crisis of Electrical Energy in Pakistan and Future guideline for Policy makers. *International Journal of Basic & Applied Sciences IJBAS/IJENS* 9(9), 1–17 (2009)
2. Haq, D.N.U.: Energy Crisis in Pakistan. In: Hussain, K. (ed.) *IPRI Factfile* (2008)
3. Jin, L.: Report and Recommendation of the President to the Board of Directors. In: *Proposed Loan Islamic Republic of Pakistan: KESC Postprivatization Rehabilitation, Upgrade, and Expansion*, Asian Development Bank (2007)
4. Shokooh, D.F., Shokooh, S.: Intelligent load shedding need for a fast and optimal Solution. In: *IEEE PCIC Europe*. IEEE, Switzerland (2005)
5. Schönberger, J., Round, S., Duke, R.: Autonomous Load Shedding in a Nanogrid using DC Bus Signalling. In: *IEEE Industrial Electronics, IECON 2006, Paris* (2006)
6. Kersting, W.H.: *Distribution System Modeling and Analysis*. CRC Press, New Mexico (2006)
7. Fievet, J.P.: The Use of Programmable Logic Controllers in Paper Mill Load Shed Systems. *TAPPI Journal* 80(3), 105–109 (1997)
8. *Operating Procedures During Generating Capacity Deficiencies Causing Declining System Frequency Or Separation*, N.A.E.R.C.s (NERC), Mid America Interpool Network (1997)
9. Nagpal, M., Moshref, A., Shukri, Z., Vijayan, J., Chan, D., Henville, C.: Dynamic Simulations Optimize Application of an Underfrequency Load Shedding Scheme. In: *Western Protective Relay Conference* (1997)
10. Johnson, B.: Switchgear - single busbar or double busbar? *Distribution*, 32–36 (2008)
11. Cohn, N.: *Load shedding apparatus*, U.S.o.A.P.a.T. Office. Leeds and Northrup Company, Philadelphia (1972)
12. Ameli, M.T., Moslehpour, S., Golvazadat, M.: Determining the Spinning Reserve In Power Systems By Corrected Recursive PJM Method. In: *IAJC-IJME International Conference*, USA (2008)
13. Prada, J.F.: *The Value of Reliability in Power Systems - Pricing Operating Reserves - Department of Electrical Engineering and Computer Science*. Massachusetts Institute of Technology, USA (June 1999)
14. Chebbi, S., Bouchoucha, C., Annabi, M.: Electric energy management by adaptive load shedding. *ICGST International Journal on Automatic Control and Systems Engineering*, *ACSE* 5(3), 17–23 (2005)
15. Howe, W., Majewski, T.S., Kruse, G.A.: Method of load shedding to reduce the total power consumption of a load control system. *United States Patent Application*, US (2009)
16. Guilfoyle, D., Connolly, E.: *SCADA systems for electricity distribution control*. *Power Technology Int.*, 169–172 (1994)

JAM: Mitigating Jellyfish Attacks in Wireless Ad Hoc Networks

Fahad Samad^{1,3}, Qassem Abu Ahmed¹, Asadullah Shaikh^{2,3}, and Abdul Aziz³

¹ RWTH Aachen University, Germany
samad@i4.de,

qassemabuaahmed@gmail.com

² Kulliyyah of Information and Communication Technology,
International Islamic University, Malaysia
asadullah.shaikh@live.iium.edu.my

³ Institute of Business and Technology, Pakistan
abdul.aziz@biztekian.com

Abstract. In recent years, wireless ad hoc networks (WANETs) have become very popular due to their wide range of applications and their ability to be deployed under normal and harsh conditions while supporting high data rates. Although many intrusion detection and trust-based systems have been developed to protect ad hoc networks against misbehaviors such as rushing attacks, query-flood attacks, and selfishness of nodes, these defense mechanisms are still not able to detect protocol compliant attacks called *Jellyfish* (JF) attacks. They target *closed-loop* flows such as TCP that are responsive to network conditions like delay and packet losses and can easily partition the network. In this paper, we introduce a security scheme called JAM (Jellyfish Attacks Mitigator) which can be used to detect and mitigate Jellyfish attacks in ad hoc networks.

Keywords: Wireless Ad hoc Networks, Security, Denial of Service, and Jellyfish Attacks.

1 Introduction

Significant progress has been made in securing ad hoc networks by developing secure routing protocols [1,2] that ensure different security concepts such as authentication and data integrity. Moreover, intrusion detection and trust-based systems [3,4,5,6,7,8] have been developed to protect WANETs against misbehaviors such as rushing attack, query-flood attacks, and selfish behaviors. Yet, most of the defense mechanisms are not able to detect a set of protocol compliant attacks called *jellyfish* (JF) attacks [9].

Similar to a jellyfish which is difficult to be detected until after the sting, jellyfish attacks in ad hoc networks are also hard to detect because they conform to all existing protocol specifications. Jellyfish attackers (JF nodes) can severely reduce the goodput of all traversing closed-loop flows to near zero by periodically dropping a small fraction of packets (*JFPeriodicDroppingAttack*), reordering

them (*JFReorderAttack*), or delaying them (*JFDelayAttack*). A JF attack can severely degrade the performance of a network by preventing long-range communication and thus partitioning the network. For further details about the types of jellyfish attacks, please refer to the work of Aad et al. [9] or the appendix section. In this paper, we present a scheme called JAM [10] to mitigate jellyfish attacks. This scheme detects and circumvents malicious nodes and thus successfully establish routes free from malicious nodes.

2 Existing Schemes

Nadeem and Howarth [3] introduce an *anomaly-based intrusion detection system* (ABIDS). They introduce an ABIDS based on chi-square for intrusion detection. However, this technique relies on a Centralized Entity (CE) to detect anomalies which is not practical in WANETs due to the distributed nature of it. Pirzada and McDonald [5] present a *trust-based mechanism* (TBM) for establishing and managing trust in pure ad-hoc networks where no CE exists and the nodes are not required to be pre-configured. The main drawback of their approach is that the detected malicious nodes are not penalized and isolated from the network. Zouridaki *et al.* [7] introduce robust cooperative trust establishment schemes in Mobile Ad hoc Networks (MANETs) called *E-Hermes*. The scheme can successfully but slowly identify malicious nodes. Moreover, the destination must acknowledge (ACK) each packet and intermediate nodes must set timers. They incur a large overhead by sending a *message authentication code* (MAC) for each intermediate node on a route to assure packets' integrity. De Rango and Marano [6] improve the usage of a well-known secure AODV routing protocol (SAODV) [1] in terms of reducing the number of applied signatures and their verification by intermediate nodes in order to achieve a longer network life.

All the above mentioned trust models are not suitable for detecting jellyfish attacks due to the nature of TCP flows that are responsive to network conditions such as delay and packet loss. A JF node attacks TCP flows for a short time to force them to enter the slow-start state, during which only one segment is sent and the RTO is too high. In such cases, the above mentioned TBMs fail because they would not penalize a node that drops only one packet every few seconds.

3 Proposed Detection Model

There are some notations which have been used to describe our model. Some of the commonly used notations are formulated in [Table 1](#). In our proposed model, a general wireless ad-hoc network is considered. MAC layer acknowledgments are sent by a destination node to notify the source that the sent frame has been successfully received. When a MAC ACK is not received, the source has to resend the unacknowledged frame. Moreover, nodes are considered to operate in promiscuous mode as well. Additionally, a secure AODV protocol such as SAODV for authentication and message integrity is supposed to be working. As we consider intermediate nodes to be attackers, source and destination nodes are assumed to be trusted.

Table 1. Notations used in JAM

Symbol	Definition
$RREQ$	Route request packet
$RREP$	Route reply packet
$RERR$	Route error packet
RTO	Retransmission timeout
CHP	Catalyst helper packets
GPT_{low}^1	Threshold goodput of a flow lesser than which CHPs are sent
T_h^1	Threshold RTO value of a TCP connection above which CHPs are sent
T_h^2	An RTO value greater than T_h^1
T_{gt}	Time period in which average goodput of a flow is observed
T_{pd}	Observing nodes check for JF attacks after every T_{pd} seconds
T_{chp}^w	Duration for which no CHPs are sent on a route after RREQ message
MIN_INVS	Minimum Threshold for repeatedly detected drop intervals
NUM_FWD	Threshold number of evidences between specific intervals
Q_{max}	Maximum queues managed by observer nodes to log packet forwarding actions and reception time
E_{TH}	Threshold value of overall evidences required to be collected
t_{ex}	The catalyst-helper packets (CHPs) are sent periodically after $t_{ex} + \delta t$ seconds

3.1 Detecting Jellyfish Attacks

The main difficulty in detecting JF attacks consists of the non-continuous misbehavior of attackers. That is, an attacker quickly forces all victim TCP flows to enter the slow-start state so that a few packets will be sent over long periods. This makes it difficult for observing nodes to distinguish between malicious behaviors (packet dropping, reordering, and delaying) and benign behaviors due to network events such as congestion and route change. Therefore, in our proposed model, the TCP protocol is modified so that when it faces a very low goodput or high RTO values, it starts sending packets called *catalyst-helper packets* (CHPs) in a constant ratio to check if a congestion is still there or not. This avoids long waiting times if there is no longer network congestion and allows observing nodes to detect misbehaviors by attackers and hence those nodes can be isolated.

To identify packets in the network, they are supplied with cumulative sequence numbers (SEQs) in clear text. That is, when the routing agent receives a segment from layer 4, the SEQ field of the packet is incremented by one. Moreover, each new flow is supplied with a unique id number (*flow id*). This allows observing nodes to identify packets by 3-tuple values (IP address, flow id, SEQ) and to reduce the amount of bytes needed to store information about each observed packet by only storing these 3-tuple values. Moreover, observing nodes are easily able to detect JFreorder attacks by comparing the SEQs of outgoing packets only.

In order to detect JFperiodic attacks, observing nodes store the reception time of each packet at observed nodes. A packet that is not forwarded within a specific period is considered as dropped. Observing nodes also collect a set of distances between two successive observed drop intervals to emulate the malicious periodic drop interval. When many forwarded packets are observed, the set of offsets relative to the set of distances is determined and the biggest gap is computed.

When the found gap contains several drop intervals within it, a JFperiodic attack is detected. The accuracy of detection improves with an increase in the number of forwarded packets considered. The next subsections will describe the detection scheme of JFperiodic and JFreorder attacks in detail. The detection of JFdelay attacks is beyond the scope of this paper.

Modification of TCP Protocol. TCP congestion control has two main limitations during the slow-start state. First, the nodes back-off exponentially. Second, only one segment is sent between two successive retransmission timeouts (congestion window $cwnd = 1$). For instance, in severe cases it sends one segment and waits for 32 seconds, it then sends another segment and waits for 64 seconds, and then the connection terminates. Backing off exponentially and waiting for longer periods is not necessary in most cases. Moreover, sending a few segments during back off time does not bring the whole network down (unless the whole network is congested). Furthermore, when a relay node in a WANET is congested for a long time, it is likely that a link-breakage event would occur and a router error message RERR is sent to the source node. Therefore, there is a need to modify the TCP protocol to get rid of the above mentioned limitations of the protocol. Yet, the modification should not be in the core functionality of TCP in order to make it adaptable to the existing, wide-spread TCP variants.

We denote the last sent segment with the lowest sequence number that is not yet acknowledged by a catalyst-helper packet (CHP). Sending one CHP during back off time can avoid long waiting times. When this CHP is acknowledged, the RTO is reset to the minimal RTO and the congestion window is doubled. If the congested relay node is freed or another route is established, then the TCP flow resumes sending of the packets.

As depicted in [Figure 1](#), the TCP protocol is modified to send CHPs periodically with a small variation of every $t_{ex} + \delta t$ seconds in the following cases:

- As long as the RTO value of a TCP connection is greater than a threshold value T_h^1 and there exists an established path to the destination.
- The average goodput (in *Kbps*) during the last T_{gt} seconds (GPT_{gt}) is too low, that is, less than a threshold value GPT_{low} .

Moreover, if the RTO value is higher than a threshold value $T_h^2 > T_h^1$, which means that it is high enough to indicate a severe congestion/attack, the source node will initiate the route discovery procedure by sending a route request (RREQ) packet towards the destination node. Additionally, the sending time T_{RQ}^s is stored and no other CHPs on the same route will be sent for T_{chp}^w seconds. High values of T_h^1 and T_{gt} slow down the detection speed of malicious nodes while small values result in sending unnecessary CHPs which increases the congestion in the network if there is no attack. If the RTO is too high, then it is very likely that the route to the destination contains a congested node. Therefore, the source node will try to establish another route by initiating the route discovery procedure. The modification can be incorporated in existing TCP protocols via a patch.

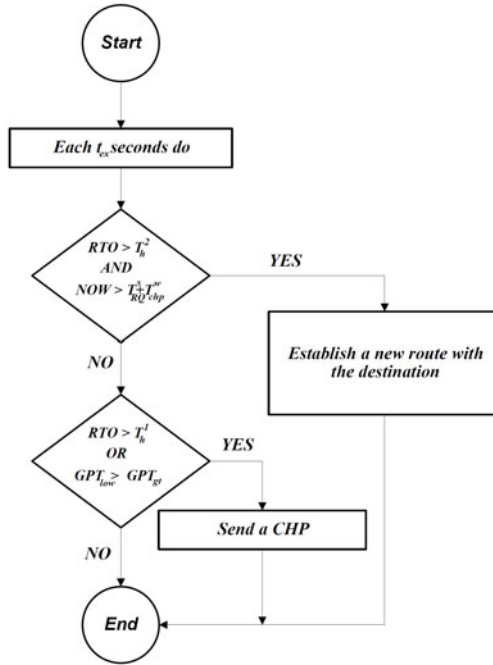


Fig. 1. TCP modification. NOW = current time.

We illustrate the effect of TCP-modification with an example. Consider [Figure 2](#) that describes an experiment conducted on a three-node chain with one relay node and one TCP connection. The AODV routing protocol and the IEEE 802.11 MAC protocol at 11 Mb/sec are used. To achieve the null (zero) goodput, the malicious node (relay node) drops all received packets for 22.5 mili-seconds after every 250 mili-seconds and forwards the rest. The JFperiodic attack starts from the 10-th second and the simulation duration is 100 seconds. The values of the modified TCP parameters are: $t_{ex} = 1sec$, $T_h^1 = 3sec$, $T_{gt} = 5sec$, $GPT_{low} = 10Kbps$, and $T_{chp}^w = 5sec$.

When no CHPs are sent, the attacker achieves a successful attack and brings the goodput of the victim flow to null (red line in the figure). All the retransmitted segments have been dropped by the attacker and the RTO timer doubles each time when a retransmission timeout occurs. The second graph (green line) describes the goodput when only one CHP is sent. At 15 sec, when the RTO is equal to 4, the sender sends a CHP which is successfully acknowledged. This causes the RTO value to be reset to the minimal RTO value (0.2 sec) and the congestion window to be doubled. The attack forces the TCP agent to have small RTO- and congestion window values which saves longer waiting time and thus results in a goodput of 50 Kbps. This is equal to 20% of the peak value. This allows nodes to detect attackers by observing a persistent dropping/reordering patterns. During the simulation, only one CHP is sent which incurs a very small overhead.

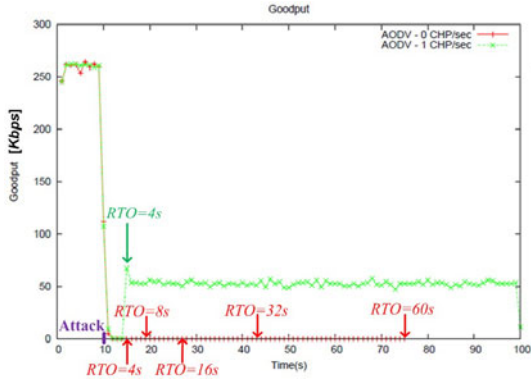


Fig. 2. Impact of sending CHPs on Goodput

In case of severe JFperiodic and JFreorder attacks, the sender needs to send more CHPs per second to accelerate the detection and isolation processes and thus establishes a new route free from malicious nodes.

TCP modification on client side is only a means to help network nodes to detect malicious nodes.

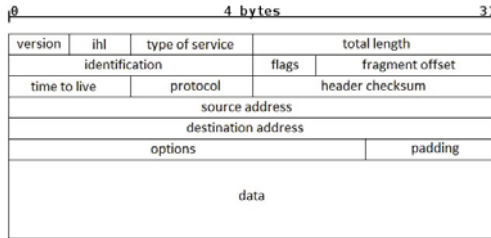


Fig. 3. Structure of the IP Header

Additional Information for IP Packets. [Figure 3](#) describes the structure of the IP header. Segments that are received by the network layer from the TCP agent are supplied with cumulative 16-bit sequence numbers (SEQs) starting from a random number. Moreover, each flow is identified with a unique 16-bit number (*flow id*). A 3-tuple value (IP address, flow id, SEQ) is used to identify IP packets in the network. The uniqueness is guaranteed because no two nodes exist that share the same IP. Each new flow gets a unique flow id by the network layer. Moreover, the flow id and the SEQs are sent in clear text to allow network nodes to identify the packets. Flow ids and SEQs can be incorporated in IP packets by exploiting the option field of IP packets.

Additional Information for Link Layer Acknowledgments. As the name implies, link layer ACKs are small frames that contain only link layer information. That is, observing nodes would not be able to detect when and which

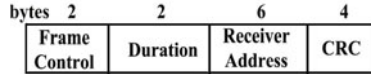


Fig. 4. IEEE 802.11 MAC ACK

packet an observed node has received. Moreover, in some MAC protocols such as the famous IEEE 802.11 MAC protocol, it is not possible for observing nodes to know the originator of a link layer ACK due to the missing ACK-sender address as shown in [Figure 4](#)

Therefore, link layer ACKs are modified to include the following information:

- MAC address of the acknowledging node,
- Source address of the acknowledged packet,
- Flow id of the acknowledged packet, and
- SEQ field of the acknowledged packet.

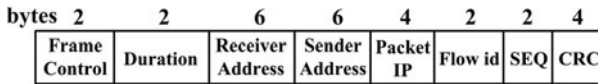


Fig. 5. Modified IEEE 802.11 MAC ACK

After modification, IEEE 802.11 ACKs would look as shown in [Figure 5](#). In this way, each packet’s reception and forwarding can be detected and identified by all one-hop nodes. We illustrate it here with an example. As shown in [Figure 6](#), nodes *A*, *C*, *D*, and *E* are located within the transmission range of node *B*. When *B* receives a packet from node *A* (step 1), *B* sends a link layer ACK to node *A* (step 2). Nodes *C* and *E* can identify the packet received by *B* and store the reception time. In step 3, node *B* forwards the packet to node *C*. Nodes *A*, *D*, and *E* can see the forwarding action of the same packet. If node *B* is a JF attacker, it will be detected and isolated simultaneously by all of its one-hop neighbors. When *B* tries to establish a new route through it by forwarding route request/reply (RREQ/RREP) packets, one-hop neighbors will refuse to process them by dropping them.

One advantage of the new IP and MAC ACK formats is the reduction of the amount of buffer space needed by observing nodes to store information about observed packets. Observing nodes in traditional trust based systems [\[4,5,6,7,8\]](#) store each observed received packet for *t* seconds. If the observed node does not forward the packet within *t* seconds, then the packet is considered dropped. If for example 500 packets of size 500 bytes are observed within $t = 2sec$, the maximal amount of buffer space needed is then 250 Kbytes, whereas the amount of buffer space needed in our scheme is very small. For example, an observing node needs to store the IP, flow id, and the first seen SEQ of a flow only once and then stores the SEQ offsets of observed packets relative to the first seen

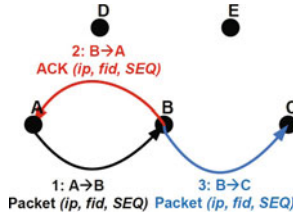


Fig. 6. Detecting actions of nodes

SEQ. However, a question arises that how would node *E* identify that node *B* has received a packet if the packet identification- and the MAC sender-fields are unknown? Another problem arises if nodes collect *second-hand-information* (recommendations) about each other: How to detect spurious recommendations?

3.2 Detecting Jellyfish Periodic Dropping Attack

The difficulty in detecting JFperiodic attacks is in differentiating between malicious dropping and dropping due to network events such as congestion. We see this problem from another aspect. If packets are dropped in periodic intervals, then no packets are forwarded in these intervals and all packet forwarding actions occur in other periodic intervals as shown in Figure 7.



Fig. 7. A JFperiodic Attack

The detection scheme exploits two features. First, packet reception time is independent of the receiver, that is, a node cannot control when to receive packets. Second, packet forwarding actions occur periodically in constant intervals.

The first feature is routing protocol dependent. When a small number of packet retransmission-attempts fail, a link-breakage error occurs and a RERR packet is sent towards source nodes, which is not desired by JF attackers. The second feature is used to distinguish between malicious packet dropping and packet dropping due to network events.

(i) Logging Actions of Neighbors

Each node in the network keeps track of its neighbors' actions on information packets. Recall that packets are identified by a 3-tuple value (IP address, flow id, SEQ). We define the possible actions that can be performed on a packet with a specific SEQ number as follows:

- NOT_SEEN: Packet has not been observed by an observing node (default value).
- RECEIVED: Observed node has received the packet, but has not yet forwarded it and the observer has started a RECEIVE_TIMEOUT timer.
- DROPPED: Packet had been received by an observed node and no forwarding action has been observed by the observer till the RECEIVE_TIMEOUT expires.
- FORWARDED: Observed node has forwarded the packet within RECEIVE_TIMEOUT seconds.

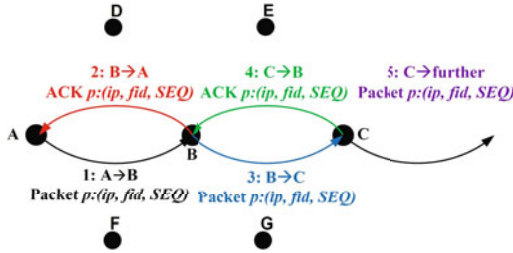


Fig. 8. An Example of Logging of Actions

Logging neighbors’ actions is illustrated in an example in [Figure 8](#). Consider that $A \rightarrow B$ means sent from node A to B , $B \rightarrow C$ means sent from node B to C , and so on. Let all nodes be relay nodes and direct neighbors of each other. Furthermore, we denote the action performed by node o on packet p and seen by node n by $act_o^n(p)$. Consider only the updating of node B ’s actions by nodes D , E , F , and G . Moreover, assume that node D has seen action 2, node E has only seen action 3, node F has only seen action 4, and node G has only seen action 5. When node D observes action 2, it sets $act_B^D(p) = \text{RECEIVED}$ and after RECEIVE_TIMEOUT seconds it sets $act_B^D(p) = \text{DROPPED}$. When node E observes action 3, it sets $act_B^E(p) = \text{FORWARDED}$. When node F observes action 4, it sets $act_B^F(p) = \text{FORWARDED}$. When node G observes action 5, it sets $act_B^G(p) = \text{FORWARDED}$.

As mentioned earlier, we only concentrate on JF attacks that target the whole network. Therefore, each observing node n manages a queue Q_o^n for all flows that traverse an observed neighbor o . Queue Q_o^n contains the logged actions together with the reception time of each logged packet (monotonically increasing) that has been observed until RECEIVE_TIMEOUT expires. Moreover, Q_o^n has a maximum size of Q_{max} , which plays an important role in the speed of detecting malicious nodes and it will be discussed in the next subsections. An entry of the queue Q_o^n consists of the following tuple:

Reception time of packet p $action \in \{DROP, FWD\}$

(ii) **Collecting Candidate Periodic Intervals.** Congestions and thus packet dropping actions are inevitable in WANETs. Therefore, JFperiodic attackers might also drop packets during the forwarding phase due to congestion. This makes it harder for observing nodes to detect constant periodic intervals that consist of pure packet forwarding and pure packet dropping subintervals as shown in [Figure 7](#). We transform the queue Q_o^n into a list of intervals denoted by *ltr* that consists of alternating *pure* drop- and forward-intervals. That is, each two successive equal actions belong to the same interval. Both of the successive equal actions are either in drop or in forward intervals. Each interval x has the following parameters:

- *x.stime*: start time of interval x ,
- *x.etime*: end time of interval x ,
- *x.middle*: middle time of interval x .

The set of candidate periodic intervals (*DISTANCES*) is then collected. For each drop interval x in *ltr* and for each drop interval y in *ltr* which is close to x , i.e. $|y.stime - x.stime| < T_{inv}$, where T_{inv} is a threshold value that expresses the distance between the intervals x and y , the differences between the start-, middle- and the end times of x and y are inserted into *DISTANCES*. The flow chart in [Figure 9](#) illustrates how the set *DISTANCES* is formed. For small values of T_{inv} (T_{inv} is smaller than the periodic drop interval length), it is very likely that the JFperiodic attack is not detected, while high values of T_{inv} may lead to unnecessary computational overhead.

(iii) **Detection Mechanism**

The detection mechanism is based on collecting *FORWARDED* actions, denoted by *evidences*. The more evidences are collected, the more accurate will be the detection of JFperiodic attacks. The detection mechanism is run for each *distance* in *DISTANCES*.

When the number of evidences is greater than a threshold value E_{TH} , the following steps are carried out:

- (a) The time axis starting from the oldest action in Q_o^n till the most recent action in Q_o^n is divided into intervals of length *distance* ([Figure 10 a](#)).
- (b) A new empty interval of length *distance* is created, denoted by *INV*.
- (c) The offset of each evidence relative to the start time of its interval is computed ([Figure 10 b](#)).
- (d) Each computed offset is then added to *INV* ([Figure 10 c](#)).
- (e) The maximum gap g_1 between two successive evidences in *INV* is determined.
- (f) Let g_2 be the difference between *distance*+the lowest offset in *INV* and the highest offset in *INV*. The maximum gap g is then equal to the maximum between g_1 and g_2 .

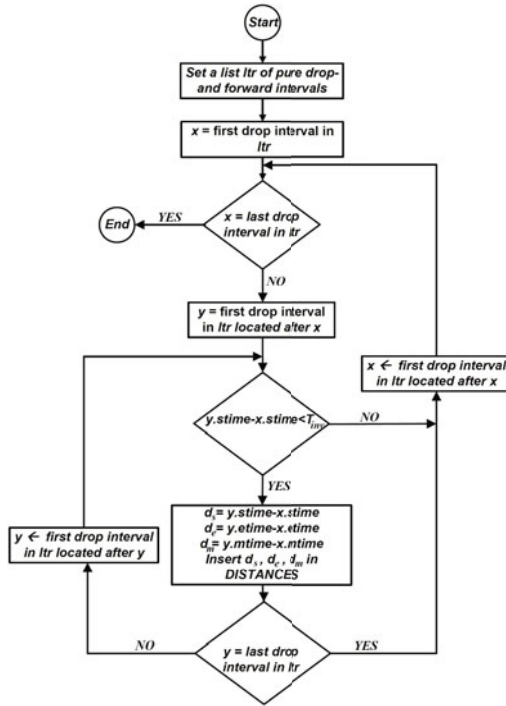


Fig. 9. Setting value of *DISTANCES*

(g) Let *num* be the number of drop intervals in *ltr* that are smaller than the gap *g* and are really located inside the found gap (offsets compared). If *num* is greater than a threshold value *MIN_NUM*, then a JFperiodic attack is detected.

The higher the E_{TH} , the more accurate the detection scheme. If the observed node *o* is benign, then the evidences in *INV* will be distributed throughout the whole interval and the maximum gap *g* will be very small so that it will not contain any drop intervals. If node *o* is malicious, the value of *g* will be high enough to include several pure drop intervals within it. Empirical results show that when $E_{TH} > 300 \cdot distance$, there will be no false positives. This means that there will be no benign nodes that are detected as JFperiodic attackers. Lower values might consider one or two benign nodes as attackers.

Q_{max} , the maximum size of Q_o^n , plays an important role in the detection speed of JFperiodic attackers. High values of Q_{max} achieve more accuracy in the detection mechanism. On the other hand, the detection speed gets slower because the queue Q_o^n would contain old actions that have been observed before the attack has started. These actions will be considered

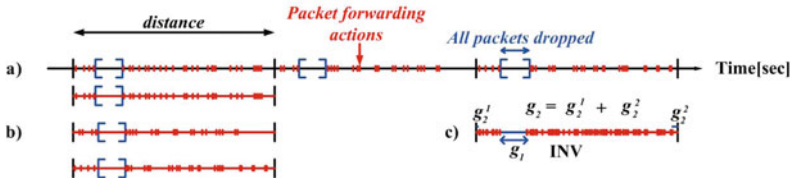


Fig. 10. Detecting JFperiodic Attacks

in the detection algorithm and will therefore result in smaller values of gap g and num . Hence, the probability to detect the attacks gets lower.

3.3 Detecting Jellyfish Reorder Attack

Including flow ids and cumulative SEQ numbers in IP packets makes the detection of JF reorder attacks very easy. This is because observing nodes can detect persistent reordering of packets by comparing the SEQ numbers of outgoing packets (of the same flow). If an observed node sends packets with SEQ number lower than the maximum sent one, a misbehavior is detected. If misbehaviors continue for at least $T_{reorder}$ seconds, a JF reorder attack is detected. If a victim flow suffers from a very low goodput, it starts sending CHPs and the attacker continues reordering packets and thus the attack will be detected by one-hop neighbors. Packet reordering events in WANETs are rare, short-lived, and occur due to network events such as route changes [9]. Threshold time $T_{reorder}$ must be longer than the duration of packet reordering due to these network events.

4 Conclusion

In this research paper a mitigation scheme to detect jellyfish attacks has been introduced. Future work includes the development of a new security scheme to detect and isolate colluding nodes, to enable source nodes to detect jellyfish nodes, and to exclude them from being part of new routes.

References

1. Zapata, M.G.: Secure ad hoc on-demand distance vector (saodv) routing. INTERNET-DRAFT draft-guerreromanet-saodv-06 (September 2006)
2. Kargl, et al.: Secure dynamic source routing. In: Hawaii International Conference on System Sciences, vol. 9, p. 320c (2005)
3. Nadeem, A., Howarth, M.: Adaptive intrusion detection & prevention of denial of service attacks in manets. In: Proceedings of the Int. Conf. on Wireless Comm. and Mobile Computing: Connecting the World Wirelessly, IWCMC 2009, pp. 926–930 (2009)
4. Boukerche, et al.: An adaptive computational trust model for mobile ad hoc networks. In: Proceedings of Int. Conf. on Wireless Comm. and Mobile Computing: Connecting the World Wirelessly, IWCMC 2009, pp. 191–195 (2009)

5. Pirzada, A., McDonald, C.: Trust establishment in pure ad-hoc networks. *Wireless Personal Communications* 37, 139–168 (2006)
6. De Rango, F., Marano, S.: Trust-based saodv protocol with intrusion detection and incentive cooperation in manet. In: *Proceedings of the 2009 International Conference on Wireless Communications and Mobile Computing: Connecting the World Wirelessly, IWCMC 2009*, pp. 1443–1448. ACM (2009)
7. Zouridaki, C., Mark, B.L.: Robust cooperative trust establishment for manets. In: *Proceedings of the Fourth ACM Workshop on Security of ad Hoc and Sensor Networks, SASN 2006*, pp. 23–34. ACM (2006)
8. Jiang, et al.: A scalable and robust approach to collaboration enforcement in mobile ad-hoc networks. *Communication and Networks* 9(1), 56–66 (2007)
9. Aad, et al.: Impact of denial of service attacks on ad hoc networks. *IEEE/ACM Trans. Netw.* 16, 791–802 (2008)
10. Samad, F.: *Securing Wireless Mesh Networks - A Three Dimensional Perspective*. PhD thesis, RWTH Aachen University, Germany (2011)

Aggregating Node Level Risk Assessment in Grids Using an R-out-of-N Model

Asif Sangrasi¹, Karim Djemame¹, and Imran Ali Jokhio²

¹School of Computing,
University of Leeds,
Leeds, UK

{scas, scskd}@leeds.ac.uk

²Department of Software Engineering,

Mehran University of Engineering and Technology Jamshoro, Sindh. Pakistan

Imran.jokhio@faculty.muet.edu.pk

Abstract. Risk assessment in Grids aims to improve the confidence level between the Resource Provider and End User to agree to a Service Level Agreement [SLA]. Risk assessment in Grids complements SLAs, which provide some improvement over the best effort approach. The existing efforts in risk assessment in Grids are at the granularity level of nodes or machines. We introduce Risk assessment aggregation at the node level based on R-out-of-N model. The experimental results show that R-out-of-N model provides more detailed options regarding the Risk value for selected R nodes against a total of N nodes.

Keywords: Risk Assessment, Grid Computing, Replaceable resources, Aggregation, R-out-of-N model.

1 Introduction

Grid technologies are based on a three-layered system made up of computation/data, information and knowledge layers [1]. A Grid can be defined by the three point checklist presented in [2].

Service Level Agreements (SLAs) improve upon the traditional best effort approaches [3]. However these improvements are limited by the risk involved in acceptance of an SLA between an End User and the Resource Provider. The new parameter of risk brings new prospects and options for both the Resource Provider and End User. These options get materialized by the introduction of risk along with the price and penalty in the SLA structure. This adds to the trust level between the End User and the Resource Provider. The Resource provider provides the End User with some value of Probability Failure (PoF) which in an ideal situation should not be over or underestimated. This PoF value provides the customer the option of checking the level of reliability of the Resource Provider [4, 5].

Risk for a scenario is defined as the product of the probabilities associated with each scenario and the consequences or the measure of the damage [6,7]. The risk in

this work is expressed by PoF. Risk Assessment in Grid computing have been introduced in [4, 8]. These efforts of Risk Assessment deal with risk at node level only and do not consider the type of the Grid Resources i.e. repairable or replaceable. Similarly, these efforts do not aggregate risk values from component to node level contrary to this work and [9]. In this work, we extend the work in [9] and use an R-out-of-N model instead of the parallel model. The usage of an R-out-of-N model allows selecting the aggregated risk valuation for R out of N nodes. In this way we improve on the static approach of the parallel model.

The contributions of this work are:

- a Risk Aggregation model at the node level to aggregate risk valuation of multiple nodes to a single value, with experimentation to demonstrate the usage of R-out-of-N model for aggregation of risk
- comparison with parallel model and a discussion of pros and cons of the proposed model against the existing.

The rest of this paper is structured as follows. Related work is presented in section two. Section three provides the details of R-out-of-N model for aggregation of risk value. The discussion of the experimentation conducted and the experimental results are available in section four. In, section five we compare the proposed aggregation model with the parallel model. Conclusion and future work are elucidated in section six.

2 Related Work

The concept of Risk Assessment in Grid computing was introduced by the AssessGrid project at two layers, i.e. Resource Provider and the broker [4]. The Risk modelling at the Resource Provider, related to this work, was carried out with both probabilistic and possibilistic approaches. The Risk Assessment at Resource Provider level in AssessGrid is achieved by Bayesian based model, to provide risk assessment values at node level. This approach is aimed at node level however it is in the same context as this work and [9]. The possibilistic modelling in the Assessgrid at Resource level is based on the work of Zadeh [10]. The work in Assessgrid at the broker level was aimed to introduce a Broker to negotiate and communicate on behalf of the End User with the Resource Provider and to select the appropriate Resource Provider among many [11, 12]. The work in the broker layer in Assessgrid is out of focus of this work. The risk modelling in AssessGrid is aimed at the node level and does not account for risk information at the component level. Moreover, Risk models in AssessGrid do not consider the nature of the Grid Failure data.

Risk Assessment in Grids is addressed directly in [8] and other indirect approaches in the similar context are available in [13-21].

A Grid availability model has been proposed in [13] to demonstrate that the performance of Grids is affected by the Grid failures. However the model fails short of proposing a risk assessment model at any layer. A notion of assessing risk on the basis of trust relationships with the actors is introduced in [14]. Performance implications of failures in Grids are addressed in [15] by providing a general failure framework. Raju et al. assess and evaluate various reliability models and select

Weibull distribution as the best fit model in [16], however their work is limited by lack of aggregation required at component and node levels as targeted by this paper. An effort to improve reliability of production grids by proposing a stochastic model is presented in [17]. By extracting Grid trace logs the stochastic model improves the job resubmission strategy [17]. A Markov Chain based risk managing approach is introduced in [18] to deal with risks of imperfect mechanisms, yet this approach fails short of addressing risk modelling in Grids based on Grid failure data. A study on disk failure patterns and characteristics of consumer-grade disk drives is available in [19], yet this study does not provide any mechanisms to estimate the risk of failure of disks or any other components. However, none of these works address the issue of Risk Assessment in Grids at the component level such as CPU, disk, memory, software, interconnect etcetera nor considers the type of the Grid failure data as replaceable or repairable.

This work extends the work in [9] in which a Probabilistic Risk Assessment model was proposed. The probabilistic model was based on the series model to aggregate the risk values from individual components to node level while a parallel model aggregates the risk values from single node to multiple nodes. In this paper we propose an R-out-of-N model to be utilized instead of the parallel model to aggregate the risk assessment values from single node to multiple node level.

3 R-out-of-N Model

There are a number of reliability structures/models that can be used to aggregate the PoF of multiple subsystems (nodes in this case) ranging from series model to R-out-of-N model. The series model is one of the structures that can be utilized to aggregate the PoF values of a number of elements and to have a combined PoF for all. However this model assumes that if one of the subsystems under consideration fails, the system fails. As this is not the case in this scenario as a result of which we do not utilize this model. Contrary to series model, it is assumed in the parallel model that the system fails when all the subsystems fail. Again, as in the current scenario an SLA may fail before all the components fail as result of which the parallel model has some limitations when utilized in current case, in fact the selected model is compared with the parallel model. Due to the limitations of the previous two models an R-out-of-N model was utilized in this scenario. An R-out-of-N model operates for the scenarios where R out of N nodes are in working condition. This model may be used to predict the probability of success/failure of number R nodes among a total of N nodes. The R-out-of-N model provides the flexibility with respect to the selection of multiple nodes and the aggregated PoF values for those nodes [22-24].

The following equation is used to predict the probability that R units will be functional out of N [23].

$$B(r; n) = \binom{n}{r} p^r q^{n-r} \quad (1)$$

Where p is the probability of success of exactly R-out-of-N nodes and q is the probability of failure of exactly R-out-of-N nodes. The probability of success of at least R-out-of-N nodes is given by [23]

$$P_s = \sum_{r=k}^n B(r; n) \tag{2}$$

For scenarios where N nodes are not identical, a Poisson binomial approximation [2] can be utilized. This binomial approximation holds for $p \leq 0.05$ and $n \geq 20$ for low reliability region and $q \leq 0.05$ and $n \geq 20$ for high reliability region. The average values of of Probability of Success (PoS) and PoF (\bar{p}, \bar{q}) are defined by [23]

$$\bar{p} = \frac{1}{n} \sum_{j=1}^n p_j \tag{3}$$

$$\bar{q} = \frac{1}{n} \sum_{j=1}^n q_j \tag{4}$$

The PoF of N-R or fewer nodes in the high reliability region represented by $Rh(t)$ is assessed by [23]

$$Rh(t) = \sum_{k=0}^{n-r} \frac{(n\bar{q})^k e^{-n\bar{q}}}{k!} \tag{5}$$

The PoF of N-R or fewer nodes in the low reliability region represented by $Rl(t)$ is assessed by [23]

$$Rl(t) = \sum_{k=r}^n \frac{(n\bar{p})^k e^{-n\bar{p}}}{k!} \tag{6}$$

4 Experimentation Results and Discussion

The experimental results obtained using the series model [9] are shown in Figure 1 where $C_i N_j$ denotes cluster i and node j respectively. The series model was used to aggregate the PoF values of individual components such as CPU, disk, memory, software, etcetera to node level as shown for six individual nodes in Figure 1.

The Grid Failure data [25] for p and q was only partially available for a number of selected nodes i.e. six nodes shown in Figure 1. The assumption of R-out-of-N model is to have at least 20 nodes. Consequently p and q values of the remainder of the 14 nodes were generated by considering these values as uniformly distributed pseudorandom numbers shown in Figure 2. The values of p and q were generated between the two extremes of available nodes that are the minimum and maximum values. The assumptions of this model only remain true for $t \leq 10$ minutes and $t \geq 100000$ for the available Grid failure data set.

The aggregated PoF using parallel model is shown in Figure 3. The parallel model aggregates the PoF values from individual nodes (20 node values in this scenario) to a single aggregated value at the given time t in future.

For R-out-of-N model, values of p and q were averaged to single value of \bar{p} and \bar{q} using the equations 3 and 4. The aggregated PoF of the nodes taking R out of N nodes was calculated using equations 5 and 6, the results are shown in Figure 4. The R-out-of-N model similar to parallel model aggregates the risk values for multiple nodes to a combined single value. As shown in results the R-out-f-N model beside aggregation of PoF for node values, also provides the PoF values for a selected number of nodes among a set of N nodes.

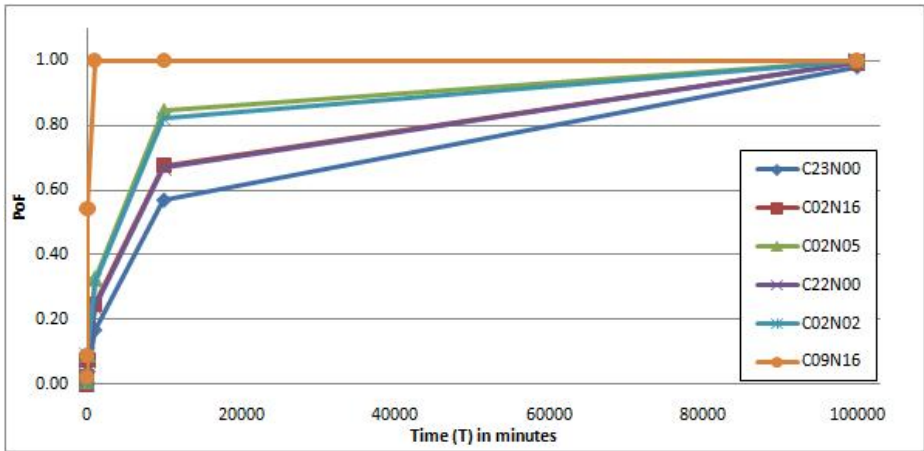


Fig. 1. PoF/q value of the individual nodes estimated using the Series Model

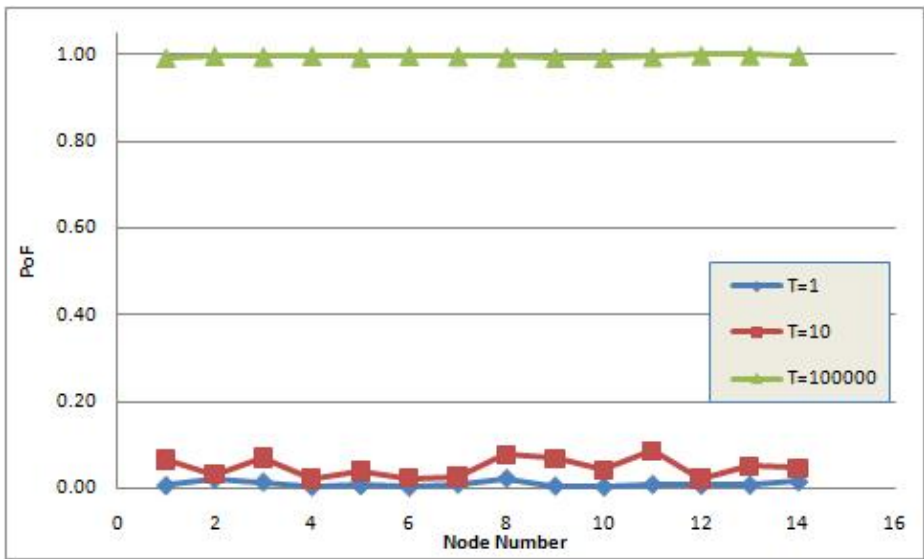


Fig. 2. PoF/q value of the randomly generated nodes

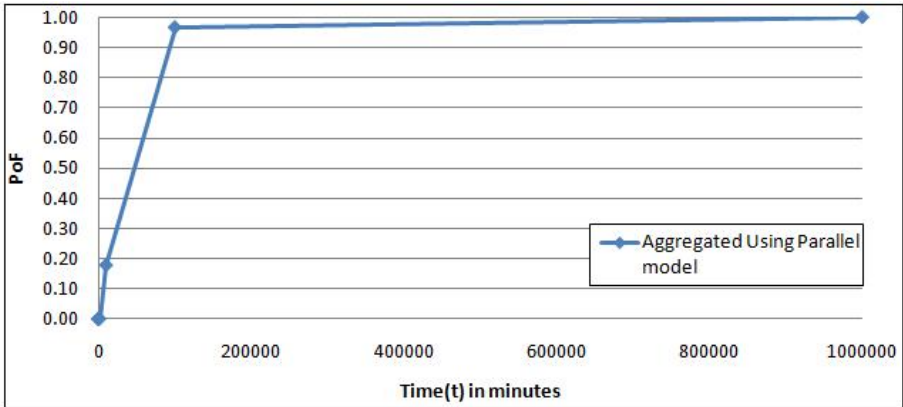


Fig. 3. Aggregated PoF using Parallel model

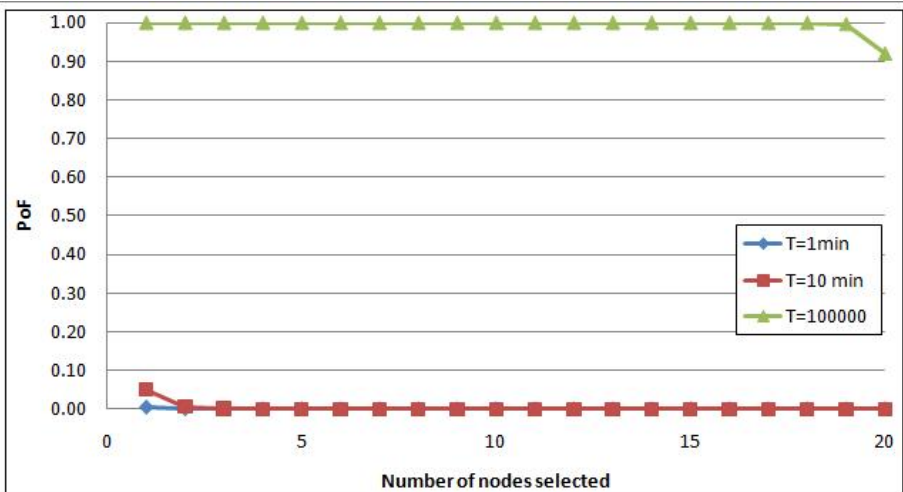


Fig. 4. PoF of selected nodes against the time (t) in minutes

5 Comparison of R-out-of-N Model with the Parallel Model

The usage of R-out-of-N model for this scenario has its pros and cons. The R-out-of-N model provides some advantages over the parallel model, as it provides the PoF of the R selected nodes out of N total nodes. As shown in figure 4, the PoF values for any selected number of nodes are provided. However, the R-out-of-N model has the following limitations in the current scenario.

- Usage of the dummy values of q to keep up with the assumption of availability of at least 20 nodes.
- The limitation of provision of PoF values only for very small or very large values of t and missing on the values of t in between as shown in figure 4 where PoF valuation is provided for $t=1$, 10 and $t=10000$ but not for the values of time in between.

The main advantage of R-out-of-N over the parallel model is the flexibility of calculation of PoF with any number of nodes selected out of a total of n nodes as evident in Figure 4 for the current scenario. This method of aggregation of PoF works better than the parallel model only when all the above given limitations are considered.

6 Conclusion and Future Work

The proposed R-out-of-N model for aggregation of risk values from single node to multiple nodes improves upon the parallel model. The parallel model aggregates the risk on assumption that an SLA fails when all the nodes fail. However the R-out-of-N model provides the risk estimations for any number of chosen nodes and estimates the risk for those failures. The major drawback of R-out-of-N model is that it is only applicable to very high or low values of time in current scenario. In future, this work can be extended towards aggregating risk values at the cluster level subject to the availability of Grid failure data.

References

1. De Roure, D., Baker, M.A., Jennings, N.R.: The evolution of the grid. In: *Grid Computing: Making the Global Infrastructure a Reality*, pp. 65–100 (2003)
2. Foster, I.: What is the grid? - a three point checklist. *GRIDtoday* 1(6) (July 2002)
3. Djemame, K., Padgett, J., Gourlay, I., Armstrong, D.: Brokering of risk-aware service level agreements in grids. *Concurrency and Computation: Practice and Experience* 23, 1558–1582 (2011)
4. Djemame, K., Gourlay, I., Padgett, J., Birkenheuer, G., Hovestadt, M., Kao, O., Voss, K.: Introducing risk management into the grid. In: *Second IEEE International Conference on e-Science and Grid Computing, E-Science 2006*, p. 28 (2006)
5. Hovestadt, M., Kao, O., Voss, K.: The first step of introducing risk management for pre-possessing slas. In: *IEEE International Conference on Services Computing, SCC 2006*, pp. 36–43 (2006)
6. Modarres, M.: *Risk Analysis in Engineering: Techniques, Tools, and Trends*, 1st edn. CRC (2006)
7. Kaplan, S., Garrick: On the quantitative definition of risk. *Risk Analysis* 1(1), 11–27 (1981)
8. Alsoghayer, R., Djemame, K.: Probabilistic risk assessment for resource provision in grids. In: *Proceedings of the 25th UK PEW*, pp. 99–110 (July 2009)

9. Sangrasi, A., Djemame, K.: Component level risk assessment in grids: A probabilistic risk model and experimentation. In: Proceedings of the 5th IEEE International Conference on Digital Ecosystems and Technologies Conference (DEST), pp. 68–75 (May 2011)
10. Zadeh, L.A.: Fuzzy Set as a Basis for a Theory of Possibility. *Fuzzy Sets and Systems* 1, 3–28 (1978)
11. Carlsson, C., Fullér, R.: Risk Assessment of SLAs in Grid Computing with Predictive Probabilistic and Possibilistic Models. In: Greco, S., Pereira, R.A.M., Squillante, M., Yager, R.R., Kacprzyk, J. (eds.) *Preferences and Decisions. Studies in Fuzziness and Soft Computing*, vol. 257, pp. 11–29. Springer, Heidelberg (2010)
12. Gourlay, I., Djemame, K., Padgett, J.: Reliability and risk in grid resource brokering. In: 2nd IEEE International Conference on Digital Ecosystems and Technologies, Phitsanulok, Thailand (2008)
13. Iosup, A., Jan, M., Sonmez, O., Epema, D.H.J.: On the dynamic resource availability in grids. In: 2007 8th IEEE/ACM International Conference on Grid Computing, pp. 26–33 (2007)
14. Asnar, Y., Giorgini, P., Massacci, F., Zannone, N.: From trust to dependability through risk analysis. In: Proceedings of the The Second International Conference on Availability, Reliability and Security, pp. 19–26. IEEE Computer Society, Washington, DC, USA (2007)
15. Zhang, Y., Squillante, M.S., Sivasubramaniam, A., Sahoo, R.K.: Performance Implications of Failures in Large-Scale Cluster Scheduling. In: Feitelson, D.G., Rudolph, L., Schwiegelshohn, U. (eds.) *JSSPP 2004. LNCS*, vol. 3277, pp. 233–252. Springer, Heidelberg (2005)
16. Raju, N., Gottumukkala, Liu, Y., Leangsuksun, C.B., Nassar, R., Scott, S.L.: eliability analysis of HPC clusters. In: Proceedings of the High Availability and Performance Computing Workshop (2006)
17. Lingrand, D., Montagnat, J., Martyniak, J., Colling, D.: Optimization of Jobs Submission on the EGEE Production Grid: Modeling Faults Using Workload. *Journal of Grid Computing* 8(2), 305–321 (2010)
18. Krautsevich, L., Lazouski, A., Martinelli, F., Yautsiukhin, A.: Risk-Aware Usage Decision Making in Highly Dynamic Systems. In: International Conference on Internet Monitoring and Protection, pp. 29–34 (2010)
19. Pinheiro, E., Weber, W.-D., Barroso, L.A.: Failure trends in large disk drive populations. In: Proceedings of the 5th USENIX Conference on File and Storage Technologies (February 2007)
20. Nieuwenhuijs, A., Luijff, E., Klaver, M.: Modeling Dependencies In Critical Infrastructures. In: Papa, M., Sheno, S. (eds.) *Critical Infrastructure Protection II. IFIP*, vol. 290, ch. 15, pp. 205–213. Springer, Boston (2009)
21. Schroeder, B., Gibson, G.A.: A large-scale study of failures in high-performance computingsystems. In: *DSN 2006 Conference Proceedings, Philadelphia* (2006)
22. Martz, H.F., Ray: Bayesian reliability analysis. *Wiley series in probability and statistics*. John Wiley and Sons (1982)
23. Shooman, M.L.: *Reliability of Computer Systems and Networks: Fault Tolerance, Analysis, and Design*. Wiley-Interscience Publication (2002)
24. Siewiorek, D.P., Swarz, R.S.: *Reliable Computer Systems: Design and Evaluation*. A K Peters/CRC Press (1998)
25. Los Alamos National Laboratories,
<http://institute.lanl.gov/data/lanldata.shtml>

Hybrid Ant Bee Colony Algorithm for Volcano Temperature Prediction

Habib Shah, Rozaida Ghazali, and Nazri Mohd Nawi

Faculty of Computer Science and Information Technology
Universiti Tun Hussein Onn Malaysia (UTHM)
Parit Raja, 86400 Batu Pahat, Johor, Malaysia
Habibshah.uthm@gmail.com,
{rozaida,nazri}@uthm.edu.my

Abstract. A social insect's techniques become more focus by researchers because of its nature behavior processing and by training neural networks through agents. Chief among them are Swarm Intelligence (SI), Ant Colony Optimization (ACO), and recently Artificial Bee Colony algorithm, which produced easy way for solving combinatorial problems and for training NNs. These social based techniques mostly used for finding optimal weight values in NNs learning. Usually, NNs trained by a standard and well known algorithm called Backpropagation (BP) have difficulties such as trapping in local minima, slow convergence or might fail sometimes. For recovering the above cracks the population or social insects based algorithms used for training NNs for minimizing network output error. Here, the hybrid of nature behavior agents' ant and bees combine's techniques used for training ANNs. The simulation result of a hybrid algorithm compared with, ABC and BP training algorithms. From the experimental results, the proposed Hybrid Ant Bee Colony (HABC) algorithm did improve the classification accuracy for prediction of a volcano time-series data.

Keywords: Swarm Intelligence, Ant Colony Optimization, Artificial Bee Colony, Hybrid Ant Bee Colony Algorithm, Back propagation.

1 Introduction

Neural Networks (NNs) a model of the biological neuron is the most important and suitable mathematical and scientific tool for solving a different combinatorial difficulty such as linear and non linear modeling, prediction, forecasting and classification [1-3]. It has powerful, flexible applications that have been successfully used in various applications such as statistical, biological, medical, industrial, mathematical, and software engineering. [4-6]. ANN learned their training techniques by parallel processing. NNs are capable of achieving many scientific research applications by providing optimal network architecture, activation function, input pre processing and optimal weight values.

Recently three NNs models, an ANN, radial-basis function, and recurrent Neural Networks (RNN) are used for the categorical prediction of seismic events occurring [7].

The probabilistic neural network can be used for prediction of earthquake magnitude but it does not yield a good result for prediction of magnitude greater than 7.5 [8]. The RNN technique can be used for prediction of the location and time of occurrence, but it is limited from 6.0 to M 7.5 for southern California earthquake [10].

ANN has applications in large range areas of human interests such as function approximation, process optimization, system identification, image processing, time series prediction, and intelligent control [9-14]. It can be trained by different training algorithms such as: BP, Improved BP algorithm, Evolutionary Algorithms (EA), Swarm Intelligence (SI), Differential Evolution (DE), and Hybrid Bee Ant Colony [15-23]. However, a BP learning algorithm has some difficulties; especially, it's getting trapped in local minima, where it can affect the NNs performance [24].

In order to overcome the drawbacks of standard BP, many algorithms used, which are based on mathematical approach, local and global optimization population techniques have been proposed for training the ANN, such as: Particle Swarm Optimization (PSO), ACO, (ABC-LM), ABC-MLP, HABC, Hybrid Bee Ant Colony (HBAC), Simulated Annealing (SA) and Tabu Search (TS)[14-24]. Recently population-based and Evolutionary algorithms are having reliable performance on training NNs [18].

In this study, the hybrid of two populations based algorithms; ABC and ACO HABC are proposed for training NNs for recovering the BP gap. These algorithms have recently been successfully applied in optimization problems and for training NNs [25]. The experimentation test is done by a volcano time-series data while the result compared with different approaches such as ABC and BP algorithms.

The rest paper is organized as follows: Related works given in Section 2. A brief review on ANN and BP training is given in Section 3. Section 4 contains on swarm intelligence briefing with subsection ABC and ACO algorithms. The proposed HABC algorithm is detailed in Section 5. Section 6 contains the simulation result with discussion. Finally, the paper concludes in Section 7.

2 Related Works

Volcanoes are the most impressive natural phenomena among seismic events, and people are captivated by their nature beauty as well as by their forceful eruptions. They exhibit a wide variety of eruption styles ranging from effusive eruptions typically resulting in lava flows or lava fountains, over medium sized explosive eruptions, to large eruptions with eruption columns of several tens of kilometers in height. Besides earthquakes, floods and storms, the volcanic eruptions present the largest natural hazards, and compared to earthquakes, floods and storms, they can even influence the earth's climate [26].

In this respect, NNs provides a quick and flexible approach for data integration and model development. To date, there have been a number of research advancements taken place in the area of NN's applications. Among them are automatic classifications of seismic signals at Mt. Vesuvius volcano, Italy and at Soufriere Hills volcano Montserrat [10, 28]. NNs are information processing paradigms that are

inspired by the way in which human brain processes information. NNs are very useful when the underlying problem is not clearly understood. Their applications do not require a priori knowledge about the system being modeled. Furthermore, they save data-storage requirements, since it is not required to keep all past data in the memory.

In this research, volcano time-series data are used for prediction task using the HABC training algorithm. The most important parameter of volcano eruption is the temperature is used here for simulation experiment. The data were obtained from the <http://www.climatedata.info/Forcing/Forcing/volcanoes.html>.

3 Artificial Neural Networks

ANNs are the most interested and understandable used in many tasks such as mathematical problems, statistical modeling by using different background of various data types. The accuracy makes this particular use of NNs as attractive to scientist analysts in various areas a different task as prediction, image processing, and other desired combinatorial task.

MLP is a universal approximate and mathematical model that contains a set of processing elements known as artificial neurons [11]. The network which is also known as feed forward neural network was introduced in 1957 to solve a non-linear XOR, and was then successfully applied to different combinatorial problems [16]. The basic building of MLP is constructed by neurons, which have some categories as input, hidden and output layers, as shown in Figure 1. The weight values between input and hidden nodes and between hidden and output nodes are randomly initialized. The network is highly used and tested on a different job. Figure 1 shows the basic architecture of Multilayer Perceptron [3].

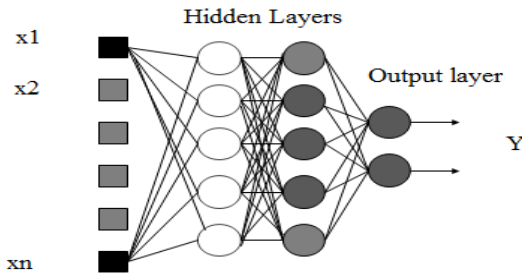


Fig. 1. Multilayer Perceptron Model

The output value of the MLP can be obtained by the following formula:

$$Y = f_i \left(\sum_{j=1}^n w_{ij} \cdot x_j + b_i \right) \tag{1}$$

Where Y is the output of the node x is the j_{th} input to the node, w is the connection weight between the input node and output node, b_i is the threshold (or bias) of the

node, and f_j is the node transfer function. Usually, the node transfer function is a non-linear function such as: a sigmoid function, a Gaussian functions. Network error function E will be minimized as

$$E(w(t)) = \frac{1}{n} \sum_{j=1}^n \sum_{k=1}^k (d_k - o_j) \quad (2)$$

Where $E(w(t))$ is the error at the t_{th} iteration; $w(t)$ is the weight in the connections at the t_{th} iteration; j shows training set, d_k is the desired output; o_j is the actual value of the k_{th} output node; k is the number of output nodes; and n is the no of patterns.

3.1 Backpropagation (BP) Learning Algorithms

BP is currently the most widely and well known used algorithm for training MLP. It was developed by Rumelhart [3]. The BP is a gradient descent method in which gradient of the error is calculated with respect to the weight's values for a given input by propagating the error backwards from output layer to hidden layer and further to input layer continuously. This step by step mathematical procedure adjusts the weights according to the error function. So, the adjustment of weights which decrease the error function is considered to be the optimal solution of the problem. In the input layer only inputs propagate through weights and passing through hidden layers and get output by some local information. For the BP error, each hidden unit is responsible for some part of the error.

Although the BP algorithm is a powerful technique applied to classification, combinatorial problems and for training MLP. However, as the problem complexity increases, the performance of BP falls off rapidly because gradient search techniques tend to get trapped at local minima. When the nearly global minima are well hidden among the local minima, BP can end up bouncing between local minima, especially for those non-linearly separable pattern classification problems or complex function approximation problem [24]. A second shortcoming is that the convergence of the algorithm is very sensitive to the initial value. So, it often converges to an inferior solution and gets trapped in a long training time.

4 Swarm Intelligence (SI)

Since the last two decades, SI has been the focus of many researches because of its unique behaviour inherent from the swarm insects [23, 28]. Bonabeau has defined the SI as "any attempt to design algorithm or distributed problem-solving devices inspired by the collective behaviour of nature insect colonies and other animal societies". He mainly focused on the behaviour of social insects alone such as termites, bees, wasps, and different ant species. However, swarms can be considered as any collection of interacting agents or individuals. Ants are individual agents of ACO [25].

4.1 Ant Colony Optimization (ACO)

ACO is a meta-heuristic procedure for the solution of a combinatorial optimization and discrete problems that has been inspired by the social insect's foraging behaviour

of real ant decision developed in 1990s [20]. Real ants are capable of finding Food Source (FS) by a short way through exploiting pheromone information, because ants leave pheromone on the ground, and have a probabilistic preference for trajectory with larger quantity of pheromone. Ants appear at a critical point in which they have to choose to get food, whether to turn right or left. Initially, they have no information about which is the best way for getting the FS.

Ants moves from the nest to the FS blindly for discovering the shortest path. The above behaviour of real ants has inspired ACO, an algorithm in which a set of artificial ants cooperate to the solution of a problem by sharing information. When searching for food, ants initially explore the area surrounding their nest in a random manner. As soon as an ant finds FS, it evaluates the quantity and the quality of the food and carries some of it back to the nest. The following is the ACO pseudo code.

```

Initialize Trail
Do While (Stopping Criteria Not Satisfied) - Cycle Loop
Do Until (Each Ant Completes a Tour) - Tour Loop
Local Trail Update
End Do
Analyze Tours
Global Trail Update
End Do
    
```

The parameters considered here are those that affect directly or indirectly the computation of the probability in formula:

$$P_k(r, s) = \begin{cases} \frac{[\tau(r, s)][\eta(r, s)]^\beta}{\sum_{u \in j_k(r)} [\tau(r, u)][\eta(r, u)]^\beta} & \text{if } s \in j_k(r) \\ 0 & \text{otherwise} \end{cases} \tag{3}$$

Where $s \in j_k(r)$ is the feasible Neighborhood of node r .

The following formula used for global updating rule: Once all ants have built their complete tours, pheromone is updated on all edges as follows:

$$\tau(r, s) \leftarrow (1 - \rho) \cdot \tau(r, s) + \sum_{k=1}^m \Delta \tau_k(r, s) \tag{4}$$

$\Delta \tau_k(r, s)$ is the amount of pheromone ant k puts on the coupling (i, j)

$$\Delta \tau_k(r, s) = \begin{cases} \frac{1}{L_k} & \text{if } (r, s) \in \text{tour done by ant } k. \\ 0 & \text{otherwise,} \end{cases} \tag{5}$$

Where m shows the number of ants, Q : a constant related to the quantity of a trail laid by ants as trail evaporation.

4.2 Artificial Bee Colony Algorithm (ABC)

ABC was proposed for optimization, classification, and NNs problem solution based on the intelligent foraging behaviour of honey bee [23]. The three bees determine the objects of problems by sharing information to other's bees. The employed bees use multidirectional search space for FS with initialization of the area. They get news and all possibilities to find FS and solution space. Sharing of information with onlooker bees is performed by employed bees. Onlooker bees: Onlooker bees evaluate the nectar quantity obtained by employed bees and choose a FS depending on the probability values calculated using the fitness values. Onlooker bees watch the dance of hive bees and select the best FS according to the probability proportional to the quality of that FS. Scout bees: Scout bees select the FS randomly without experience. If the nectar quantity of a FS is higher than that of the old source in their memory, they memorise the new position and forget the previous position. Whenever employed bees get a FS and use the FS very well again, they become scout bees to find a new FS by memorizing the best path. The detailed of ABC algorithm is shown as:

1. Initialize the population of solution's X_i where $i=1 \dots SN$
2. Evaluate the population
3. Cycle=1
4. Repeat from step 2 to step 13
5. Produce new solution v_{ij} in the neighbourhood of x_{ij} for the employed bees as

$$v_{ij} = x_{ij} + \Phi_{ij}(x_{ij} - x_{kj}) \tag{6}$$

Where k is a solution in the neighbourhood of i , Φ is a random value between $[-1, 1]$.

6. Apply the Greedy Selection process for the onlookers between x_i and v_i .
7. Calculate the p_i for the solutions x_i by means of their fitness values by using eq (7).

$$P_i = \frac{fit_i}{\sum_{k=1}^{SN} fit_n} \tag{7}$$

Calculate of fitness values

$$fit_i = \begin{cases} \frac{1}{1 + f_i} & f_i \geq 0 \\ 1 + abs(f_i) & f_i < 0 \end{cases} \tag{8}$$

8. Normalize p_i values into $[0, 1]$
9. Produce the new solutions v_i for the onlookers from the solutions x_i , selected depending on P_i , and evaluate them.

Apply the Greedy Selection process for the onlookers between x_i and v_i

10. Determine the abandoned solution (source), if exists, replace it with a new randomly produced solution x_i for the scout using the following equation.

$$v_{ij} = x_{ij} + \Phi_{ij}(x_{ij} - x_{kj}) \quad (9)$$

11. Memories the best FS position (solution) achieved so far.
12. Cycle=cycle+1
13. Until the cycle= Maximum Cycle Number (MCN)

5 Hybrid Ant Bee Colony (HABC) Algorithm

ABC and ACO were proposed for optimization, classification, and ANN problem solution based on the intelligent foraging behavior of honey bee and ant swarms [21, 23-25]. The ABC algorithm has a strong ability to find the global optimistic results optimal weight's values by bee's agents. It is successfully trained NNs for classification and prediction task. HABC combines the ACO properties in the ABC algorithm which may accelerate the evolving speed of ANNs and improve the classification precision of the well-trained networks. The hybrid algorithm is easily understandable, using an ABC algorithm to search the optimal combination of all the network parameters, and ACO used for selection best FS to find the accurate value of each parameter. HABC algorithm provides a solution in an organized form by dividing the agents into different tasks such as, employed bee, onlooker ant and scout bees. The detailed pseudo code of HABC algorithm is shown as follows:

1. Load colony size and food Number

$$FN = \frac{SN}{2} \quad (10)$$

King Bee {

If

$$FN = SN \% 2 = 0 \quad (11)$$

Then

$$FN = \frac{SN + 1}{2} \quad (12)$$

2. Initialize of solutions x_i
3. Evaluate the fitness of the population
4. Cycle =1
5. Repeat
6. Produce a new solution v_i by using equation

$$v_{ij} = x_{ij} + \Phi_{ij}(x_{ij} - x_{kj}) \quad (13)$$

Calculate τ_i

$$\tau_{(i)} = \begin{cases} \tau \geq 0 & \text{for } \frac{Q}{1 + f_i} \\ \tau < 0 & 1 + \text{abs}(f_i) \end{cases} \quad (14)$$

$$Q = \frac{1 + FN}{\sum_{i=1}^{SN} (E + O)} \quad (15)$$

Apply greedy selection process

7. Calculate the probability values $P_{(i)}$ for the solution x_i by

$$P(i) = \frac{(0.09) * \tau(i)}{\sum_{1 \leq j \leq m} \tau(j)} \quad (16)$$

8. FOR each onlooker ant {

Select a solution x_i depending on P_i

Produce new solution v_i

9. Calculate the value τ_i by eq (14)

10. Apply greedy selection process}

11. Continue ABC from step 9 to 13.

Where Q , E and O shows numbers of Queen, Employed and Onlookers ant respectively, x_i represents a solution is the fitness solution o , v_i indicates a neighbour solution of x_i , and P_i value of x_i . Also τ represents the fitness solution of trial i which is not improved and j represents the improved solution. In the algorithm, first half of the colony consists of employed ant, and the second half constitutes the onlooker ant. The Scout bee will be deciding the best values between onlookers and employed ant. In HABC algorithm, the position of a FS represents a possible solution to the optimization problem, and the nectar total of a FS corresponds to the fitness solution of the associated solution by King Bee. The King Bee initialized the colony size for employed and onlooker's ant. After initialization, the population of the positions (solutions) is subjected to repeated cycles, $C = 1, 2, \dots$ Maximum Cycle Number (MCN), of the search processes of the employed, onlooker and Scout Bee. An employed ant produces a modification on the position in her memory depending on the local information (visual information) and tests the nectar total (accurate solution) of the new source. The King Bee will gather employed and onlooker ant for decision of fitness solution. After all employed ant around complete the search process; they combine the nectar information of the FS and their position information with the onlooker ant on the food's area. An onlooker ant evaluates the nectar amount taken from all employed ant and chooses a FS with a probability related to its nectar quantity. The onlooker ant chooses a FS depending on the probability value associated with that FS, p_i , calculated by the eq (16). The King Bee initialized the colony size for bee. The FS will be divided in same quantity. King's bee will update

the FS for equal division on employed and onlookers' bee. The number of FS equals the half of the colony size and after division on employed and onlooker ant the will start searching for finding optimal FS. The information sharing with onlooker ant is performed by employed. An employed ant produces a modification on the source position in her memory and discovers a new FS position. Provided that the nectar quantity of the new source is higher than that of the previous source, the employed ant memorizes the new source position and forgets the old one. The onlooker ants evaluate the nectar quantity obtained by employed ants and choose a FS depending on the probability values. For this purpose, a fitness-based selection technique can be used. Onlooker ants watch the dance of hive ants and select the best FS according to the probability proportional to the quality of that FS.

6 Simulation Results and Discussion

In order to evaluate the performance of the HABC using volcano time-series data scheme for prediction, simulation experiments performed on a 1.66 GHz Core 2 Duo Intel Workstation with 2 GB RAM using Matlab 2010a software. The volcano temperature is used for the simulation. The comparison of standard BP-MLP, HABC and ABC algorithms are discussed based on the simulation results. The set of data contains about 1000 records are divided into two data sets 70% for training, 30% for testing. The learning rate (LR) and momentum (MOM) are set to 0.6 and 0.5 respectively. It should have to be noted that the ranges of weights are different for both experimentation as [1,-1], [10,-10] for BP, ABC and HABC. Furthermore, the minimum value of average of MSE selected for testing. The stopping criteria minimum error is set to 0.0001 BP-MLP while ABC and HABC stopped on MCN.

During the experimentation, five trials were performed for training. Each case, run was started with a same number of input parameters and with random foods and Area. The sigmoid function is used as activation function for network output. During the simulation, when the number of inputs, hidden and output nodes of the NNs and running time varies, the performance of training algorithms were stable, which is important for the designation of NNs in the current state. There is no specific convention for the decision of the number of hidden nodes. Here, we collect 2-2-1 network structure for BP, ABC and HABC.

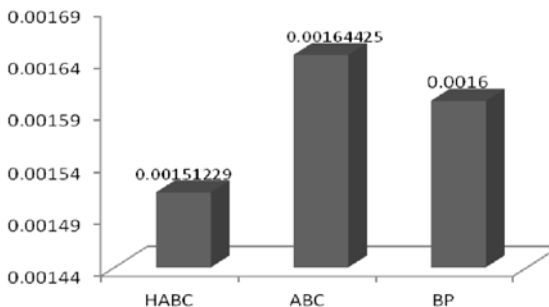


Fig. 2. Average MSE of Training HABC, ABC and BP

Finally, average of mean square errors (MSE), normalized MSE, Signal Noise Ratio, and CPU Time, are calculated for the above algorithms. Simulation results show the effectiveness and the efficiency of HABC algorithm. The comparison simulation of different network structure is presented in following figures.

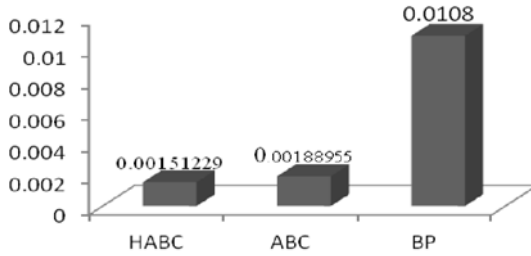


Fig. 3. Average MSE of Testing HABC, ABC and BP

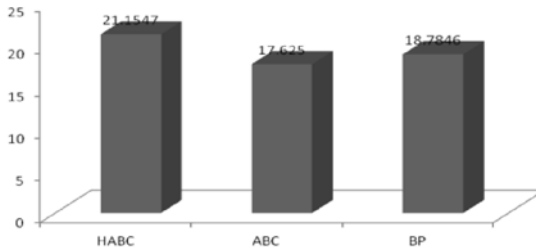


Fig. 4. Max SNR of HABC, ABC and BP algorithms

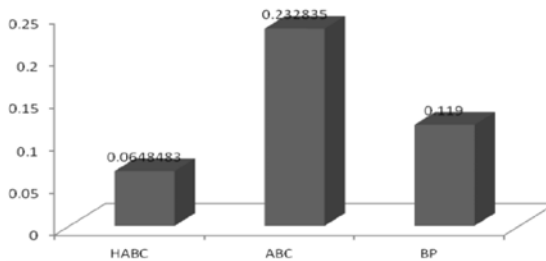


Fig. 5. Average of Normalized MSE for HABC, ABC and BP

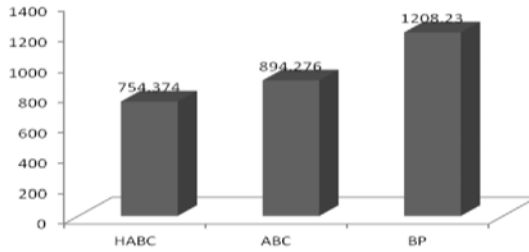


Fig. 6. CPU time for simulation of HABC, ABC and BP

In Fig 2 the average of five runs Mean Square Error is presented of HABC, BP and ABC training algorithms. The MSE of HABC is less as compared to ABC and BP for MCN 500 using volcano time series data. The testing results of the proposed HABC with BP and ABC are given in Fig 3, where the BP and ABC algorithm average MSE is greater than HABC. The SNR is shown in Fig 4, where the HABC algorithm shows higher than BP and ABC. The average of five NMSE of above algorithms is given in Fig 5. The CPU time of these algorithms with 500 MCN and five times running time are shown in Fig 6. The efficiency of HABC on the bases of MSE, NMSE, and CPU time shows outstanding performance than standard BP and ABC algorithms, especially in MSE for training and MSE for testing shows the best results for proposed HABC algorithm. Furthermore the SNR result shows the quality of the proposed approach.

7 Conclusion

The HABC algorithm merges the properties of the two nature swarm's ACO and ABC algorithm successfully, which are exploration and exploitation. The best possible weight values prove the high performance of the training MLP for time-series data prediction tasks using HABC algorithm. HABC has the great skill of searching global optimum solution. The optimum weights set of the algorithm may speed up the training process and improve the prediction accuracy. The above simulation results show that the proposed HABC algorithm can outstandingly learn the time-series data, which further extends the quality of the given approach with lower prediction error.

Acknowledgment. The authors would like to thank University Tun Hussein Onn Malaysia (UTHM) and Ministry of High Education (MOHE) for supporting this research under the FRGS.

References

1. Romano, Michele, A.U., et al.: Artificial neural network for tsunami forecasting. *Journal of Asian Earth Sciences* 36, 29–37 (2009)
2. Ghazali, R., Hussain, A.J., Liatsis, P.: Dynamic Ridge Polynomial Neural Network: Forecasting the univariate non-stationary and stationary trading signals. *Expert Systems with Applications* 38(4), 3765–3776 (2011)

3. Rumelhart, D.E., McClelland, J.L.: And the PDP Research Group, Parallel Distributed Processing: Explorations in the Microstructure of Cognition, vol. 1, 2. MIT Press, Cambridge (1986)
4. Osamu, F.: Statistical estimation of the number of hidden units for feedforward neural networks. *Neural Networks* 11(5), 851–859 (1998)
5. Shokri, A., Hatami, T., et al.: Near critical carbon dioxide extraction of Anise (*Pimpinella Anisum* L.) seed: Mathematical and artificial neural network modeling. *The Journal of Supercritical Fluids* 58(1), 49–57 (2011)
6. Thwin, M.M.T., Quah, T.-S.: Application of neural networks for software quality prediction using object-oriented metrics. *Journal of Systems and Software* 76(2), 147–156 (2005)
7. Taylor, S.R., Denny, M.D., Vergino, E.S., Glaser, R.E.: Regional discrimination between NTS explosions and earthquakes. *B. Seismol. Soc. Am.* 79, 1142–1176 (1989)
8. Adeli, H., Panakkat, A.: A probabilistic neural network for earthquake magnitude prediction. *Earthquake Engineering* 22, 1018–1024 (2009) ISBN- 0893-6080
9. Connor, J., Atlas, L.: Recurrent Neural Networks and Time Series Prediction. In: IEEE International Joint Conference on Neural Networks, New York, USA, pp. I 301–I 306.
10. Scarpetta, S., Giudicepietro, F., Ezin, E. C., Petrosino, S., Del Pezzo, E., Martini, M., and Marinaro, M.: Automatic Classification of seismic signals at Mt. Vesuvius Volcano, Italy using Neural Networks. *B. Seismol. Soc. Am.*, 95, 185–196, (2005)
11. Hornik, K., Stinchcombe, M., White, H.: Multilayer feedforward networks are universal approximators. *Neural Networks* 2(5), 359–366 (1989)
12. Cass, R., Radl, B.: Adaptive process optimization using functional-link networks and evolutionary algorithm. *Control Engineering Practice* 4(11), 1579–1584 (1996)
13. Gail, A. C.: Network models for pattern recognition and associative memory. *Neural Networks* 2(4), 243–257 (1989)
14. Tyan, C.-Y., Wang, P.P.: An application on intelligent control using neural network and fuzzy logic. *Neurocomputing* 12(4), 345–363 (1996)
15. Shah, H., Ghazali, R., Nawi, N.M.: Using Artificial Bee Colony Algorithm for MLP Training on Earthquake Time Series Data Prediction. *Journal of Computing* 3(6), 135–142 (2011)
16. Rosenblatt, F.: A Probabilistic Model for Information Storage and Organization in the Brain, vol. 65, pp. 386–408. Cornell Aeronautical Laboratory (1958)
17. Bonabeau, E., Dorigo, M., Theraulaz, G.: *Swarm Intelligence: From Natural to Artificial Systems*. Oxford University Press, NY (1999)
18. Yao, X.: Evolutionary artificial neural networks. *International Journal of Neural Systems* 4(3), 203–222 (1993)
19. Ilonen, J., Kamarainen, J.-K., et al.: Evolution Training Algorithm for Feed-Forward Neural Networks. *Neural Processing Letters* 17(1), 93–105 (2003)
20. Mendes, R., Cortez, P., Rocha, M., Neves, J.: Particle swarm for feedforward neural network training. In: Proceedings of the International Joint Conference on Neural Networks, vol. 2, pp. 1895–1899 (2002)
21. Dorigo, M., Di Caro, G., Corne, D., Dorigo, M., Glover, F.: The ant colony optimization meta-heuristic. *New Ideas in Optimization*, 11–32 (1999)
22. Ozturk, C., Karaboga, D.: Hybrid Artificial Bee Colony algorithm for neural network training. In: 2011 IEEE Congress on Evolutionary Computation, CEC 2011 (2011)
23. Karaboga, D., Akay, B., Ozturk, C.: Artificial Bee Colony (ABC) Optimization Algorithm for Training Feed-Forward Neural Networks. In: Torra, V., Narukawa, Y., Yoshida, Y. (eds.) MDAI 2007. LNCS (LNAI), vol. 4617, pp. 318–329. Springer, Heidelberg (2007)

24. Gori, M., Tesi, A.: On the problem of local minima in back-propagation. *IEEE Trans. Pattern Anal. Mach. Intell.* 14(1), 76–86 (1992)
25. Dorigo, M., Stützle, T.: *Ant Colony Optimization*. MIT Press (2004)
26. Schneider, S.H., Easterling, W.E., Mearns, L.O.: Adaptation: Sensitivity to natural variability, agent assumptions and dynamic climate changes. *Climatic Change* 45, 203–221 (2000)
27. Tiira, T.: Detecting tele-seismic events using artificial neural networks. *Comput. Geosci.* 25, 929–939 (1999)
28. Chau, K.W.: Particle swarm optimization training algorithm for A NNs in stage prediction of Shing Mun River. *Journal of Hydrology*, 363–367 (2006)

Building Wireless Sensor Networks Application Using Sun SPOTs

Asadullah Shaikh^{1,2}, Naveed Anjum³, Fahad Samad², and Asadullah Shah¹

¹ Kulliyyah of Information and Communication Technology,
International Islamic University, Malaysia

asadullah.shaikh@live.iium.edu.my, asadullah@kict.iium.edu.my

² Institute of Business and Technology, Pakistan
{asadullah,fahad.samad}@biztekian.com

³ University of Southern Denmark, Denmark
yoursanjum@gmail.com

Abstract. Wireless Sensor and Mobile ad-hoc Networks are characterized by their highly dynamic, multi-hop, and infrastructure-less nature. In this dynamic environment, different nodes offering different services may enter and leave the network at any time. Efficient and timely service discovery is a requirement for good utilization of shared resources in this kind of network. Service discovery is not a new problem. Many academic and industrial researchers have proposed numerous solutions (protocol/middleware) of service discovery for both wired and wireless networks. The wireless sensor networks have several characteristics that set them apart from the traditional wired networks. Hence, classical service discovery protocols in sensor networks are not applicable. This paper presents a service oriented architecture for autonomous wireless sensor networks that provide various services at different levels.

1 Introduction

During the past decade, the speed and reliability of communication over wireless network has increased rapidly. Due to this increase, distributed computing is now seen as an adaptable and economical way to enhance computing power and share information. Recent advances in both the hardware and the software have allowed for the emergence of purely distributed computing, in which each entity can be either client or server. One area of great interest in distributed systems is wireless ad-hoc network that allows collaboration in real time. Wireless ad-hoc networks are formed by a set of hosts that communicate with each other over a wireless channel. Each node has the ability to communicate directly with another node (or several of them) in its physical neighborhood. They may operate in a self-organized and decentralized manner. This allows to develop a dynamic network infrastructure which makes these networks extremely

cost effective. Ad-hoc wireless networks can be used for many applications such as the sensor-based system and the systems that are dynamically deployed for sudden incidents. Wireless sensor networks consisting of individual sensor nodes distributed over a given area are used to monitor some physical phenomenon (temperature, humidity) in the environment. The importance of such networks is increasing rapidly with advances in technology that result in smaller, cheaper, and power-efficient devices. As a result, wireless sensor networks (WSN) have become increasingly common in everyday applications. A fixed network structure was required in the past for computers to collaborate. However due to advances in wireless computing, network structures can now exercise significant flexibility. Still, the limited capability in terms of memory capacity and processor speed imposes difficulties upon wireless networking. Wireless sensor networks and its applications have many uses in everyday human life ranging from health care and logistics, through agriculture, forestry, civil and construction engineering, to surveillance and military applications. The sensors applications are growing ever larger in size and complexity. As sensor technology improves and the demand for new applications grows, most of the currently deployed sensor network systems will need to evolve over time. Currently, most of the sensor network applications are being developed in the low level languages such as nesC and C at the system level. This traditional low level approach cannot support to develop larger, scalable, and flexible sensor applications. Higher level software methodologies are needed to meet the scalability, flexibility, and portability requirements of modern sensor network systems. The computer networks are basically about using services; multiple users (clients) regardless of their location may use a single service. Hence, the networks connect the users and services. In distributed systems, clients use static service locations to discover services before using them. Moreover, manually configured network addresses pointing to services are sufficient. Wireless Sensor and Mobile ad-hoc Networks are characterized by their highly dynamic, multi-hop, and infrastructure-less nature. In this dynamic environment, different nodes, offering different services, may enter and leave the network at any time. Efficient and timely service discovery [1,2,3] is a requirement for good utilization of shared resources in these kind of networks.

The remainder of this paper focuses on a service oriented architecture for autonomous wireless sensor networks that provide various services at different levels. Section 2 describes the problem addressed in this paper. Section 3 focuses on the architectural design along with proposed solution while Section 4 explores the implementation environment. In Section 5, related work is presented. Finally, Section 6 provides the conclusion.

1.1 Problem Statement

Service discovery is not a new problem. Many academic and industrial researchers have proposed numerous solutions (protocol/middleware) of service discovery for both wired and wireless networks. The traditional view of service discovery within local area network is different from the scenarios in wireless ad-hoc networks. The wireless ad-hoc networks have several characteristics, as described

above, that set them apart from the traditional wired networks. Due to these differences, the classical service discovery protocols are not directly applicable to wireless networks.

1.2 Aims and Objectives

The aim of this paper is to present a service oriented architecture [4] which will handle autonomous sensors networks in which all entities of a network collaborate with each other through a suitable protocol. Furthermore, we design and implement a service discovery prototype for wireless sensor networks which allows sensors to take part in the service oriented environment where all nodes at work offer different services at different levels (different attributes). The design goal can be divided into following:

- Request/Reply base service discovery architecture which will handle autonomous sensors network in which entities/nodes (Sun SPOT [5]) will leave or join at any time.
- A protocol which allows Plug and Play sensor node (Sensor Integration)
- A scalable and dynamic wireless sensor network architecture which allows autonomous system administration of sensor nodes and easy sensor data flow management with nodes (Discovery/Routing).
- An architecture in which sensor nodes act as clients or service provider (services) or both.

2 Problem Evaluation

Nowadays there are many uses for wireless sensor networks in almost every field. As the sensor devices become cheaper and more powerful, we can now expect the number of possible applications for wireless sensor networks to grow. The wireless sensor systems need to evolve over time to support new needs and functionality due to changes in requirements or improvements in sensor technology. Throughout all these changes, the sensor network must maintain an acceptable level of operation, since in some cases human lives may depend on it. Wireless sensor networks must be reliable, scalable, and flexible to change. It is interesting that still the sensor applications are mainly written at a low level, which means at or near the system layer, where providing a scalable, flexible framework is extremely difficult. Low-level application design tends to overlook proper modularization, making development of complex application code very difficult. These types of applications also tend to bind the system functionality to the current set of resources. When resources or requirements change, engineers must spend extra time, man-power, and money to keep the system up-to-date. Given the wide spread use of traditional networking technologies, it may be surprising how challenging even simple tasks become in the domain of the wireless sensors networks. Nowadays, an application level developer expects certain services to be provided by the operating system or by network protocols. However, due to

the resource constraints of sensor nodes neither of these can be taken for guaranteed. Problems arise mainly from developing applications comparatively closer to the hardware on one side and the need for distributed algorithms in wireless sensor networks on the other. Implementing the service discovery architecture as an abstraction layer is widely accepted as a solution to this problem. The key to success is to provide the application level developer with a programming abstraction that empowers him to directly formulate the crucial parts of his application in a way that naturally maps to the wireless sensor network platform. In general, the service discovery in wireless ad-hoc environment is a difficult task. Nevertheless, it is a crucial feature for the usability of wireless ad-hoc networks. The service discovery allows devices to automatically locate network services with their attributes and to advertise their own capabilities to the rest of the network. To enable service discovery within wireless ad-hoc networks we face many challenges like enabling the resource-constrained wireless devices to discover services dynamically and enabling the service discovery in large wireless ad-hoc networks. In the simplest case, the service discovery mechanism needs to work without any configuration, management or administration. There are different scenarios where the service discovery protocol is being used in the wireless network environment. We would like to include a discussion on a few of these scenarios.

- Scenario 1: Imagine that you find yourself in a taxi cab without your wallet. Fortunately, you have a JINI technology enabled mobile phone, and your mobile service provider uses JINI technology to deliver network-based services tailored to your community. On your phone screen, you see a service for the City Taxi Cab Company, so you download the electronic payment application to authorize payment of your taxi cab fare. The cab company's payment system instantly recognizes the transaction and sends a receipt to the printer in the taxi. You take the receipt and you are on your way.
- Scenario 2: Consider an intelligent, on-line overhead projector with a library client. After identification to the system, the user may select a set of electronically stored charts or other document(s) for viewing. Rather than bringing foils to a meeting, the user accesses them through the LAN server in the library.
- Scenario 3: Consider an insurance salesman who visits a client's office. He wants to brief new products and their options to the client which are stored in his Windows CE Handheld PC. Since his Handheld PC has wireless network and supports UPnP, it automatically discovers and uses an Ethernet connected printer there without any network configuration and setup. He can print whatever in his Handheld PC or from computers in his main office and promote the new products.

Scenario 1 is a JINI demo scenario developed by Sun Microsystems and scenario 2 is a Salutation scenario by IBM. The last one is a UPnP scenario by Microsoft. At a glance, they seem to talk about the same stories: mobile devices, zero-configuration [6] and impromptu community enabled by service discovery protocols, and cooperation of the proximity network. Even though they work

in the same way, these three service discovery protocols have different origins, underlying technologies, flavors, and audiences. Since they see the problem at different angles and take different approaches to it. It is a fact that not all the service discovery architectures (protocols) provide the optimal solution. They all have some advantages and disadvantages. Especially for the ad hoc wireless infrastructure, it is very hard to come with the optimal solution due to the dynamic nature of the nodes. There are some challenges and requirements which hinder the development of service discovery architecture.

3 Architectural Design

We have concluded some capabilities of Sun SPOT on which we have developed our protocol. Every Sun SPOT can act as a mesh router which means that it forwards (relay) the packets toward the other Sun SPOT(s), which it receive. The Sun SPOT(s) use the AODV algorithm to determine the best route when the communications between them are routed over more than one hop. To maintain the route, every Sun SPOT use routing policies which can be enabled through the RoutingPolicyManager. The Sun SPOT(s) can also have the capability to broadcast the datagram packet. So we have approached our architecture design with higher-level programming methodologies on application layer with support from network layer's (AODV protocol) capabilities of Sun SPOT. We sum up with a directory-less architecture which is a suitable architecture for the resources constrained devices such as sensor nodes. To enable reliable service allocation, we apply the JINI lease mechanism in our architecture according to which a service is requested for a time period and then granted for negotiated period between the service user and the provider. In the following section, we propose our service discovery architecture.

3.1 Proposed Solution

We have proposed a directory-less architecture which is based on the pull-model (query the environment when service is required) service discovery approach. In our architecture, each participating node has the capabilities to store its own local services, deliver these services to other nodes, query the network for available services offered by others, and use the services it discovers in the network. The discovery process (we will call it service lookup process) is simple as the client node (requester) broadcasts the request to search for the service and waits a reply from any service provider. If a provider node (service provider) is found, then the provider issues a reply back to the client. The reply includes the id of the service provider, which is used for subsequent communication between the client and the provider. In case the service provider is not found, no reply is received by the client. The underlying network layer is responsible for routing the information within the network. The nodes in the network automatically transmit any received packets so that it is relayed to the entire network, including the nodes that are out of range of the original requester. Note that there are maximum

preset numbers of nodes which are traversed (time to live-TTL). When a node receives a request from the client during the service lookup phase, it checks the availability of the requested service within itself. Depending on the availability of service, the node issues a reply to the client. After a successful service lookup phase, further communication between the client and the provider is initiated by the client. It sends the lease and service binding request to the provider for the requested service. The lease request contains the provider's id so the node which receives the lease request matches the provider id with its own id and takes the necessary action in the form of lease reply. The provider sends the lease reply along with the service binding to the client. After the successful service binding phase, the client will have the service until the lease time expires. When the lease expires, the current communication session will end. Because the nodes are mobile, it is also likely that many link breakages along a route occur during the lifetime of that route. The underlying network protocol is also responsible to maintain a route for as long as the communication is active.

4 Implementation Environment

The prototype implementation is done in Java language. There are two reasons to select Java. First, we have used the Sun SPOT as sensor device and it is a Java embedded platform, more specifically Connected Limited Device Configuration (CDLC) of Java Micro Edition (J2ME) platform with the MIDP-1.0 (Mobile Information Device Profile) profile. Second, the Java language provides the feature like modularity, reusability, extendibility, and robustness for developing applications. We have used the NetBeans IDE as the development environment, since the NetBeans IDE is the default environment for developing the applications for the Sun SPOTs. Indeed, the choice of IDE is arbitrary as long as it supports ANT scripts. We utilize UML notations to explain the implementation of the architecture. The necessary implementation is discussed further in this section. All the experiments are done using the Sun SPOTs and having them all in the same room, placed a few feet away from each other. The behavior could be different in different environments. The implementation consists of the following Java packages:

- The XML parser `org.xmlpull.v1` and `org.kxml2.io` packages contain the XML parser [...] which we used to read the XML files.
- The service `org.sunspotworld.service` package contains the classes which model services used in the system.
- The service framework `org.sunspotworld` package implementations of the main service discovery architecture and its functionality.

As we have used the pre-developed XML parser, we will not provide the detailed implementation of it.

4.1 Services

Service is the abstract base class for all the services. It defines the basic functionality of the service. Any service which needs to be activated must inherit from

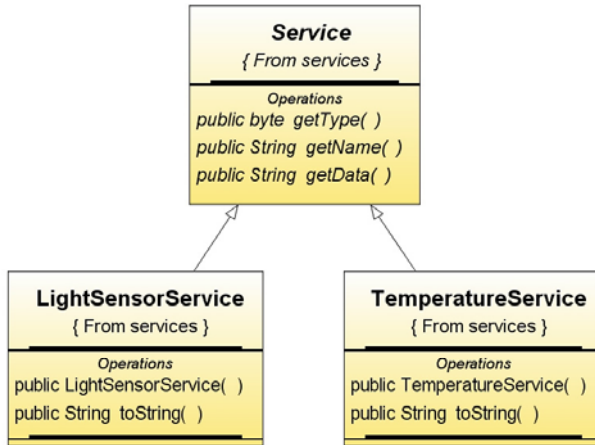


Fig. 1. UML Class Diagram of Service

this class. As shown in the UML class diagram in figure 1, the `LightSensorService` and `TemperatureService` classes are inherited from `Service`. These classes implement the actual functionality of the service e.g. activation and collection of data etc.

4.2 Framework Overview

Here is a brief overview of all the classes which implement the `Service` framework:

- `StartServiceMain` is the Midlet class and it starts the application.
- `SpotParticipant` models the spot itself.
- `ServiceReader` reads the service types defined in the XML file.
- `ServiceLoader` takes the service type codes and instantiates `Service` objects for each of them.
- `ServiceRequest` is a wrapper around the actual `Service` defining some additional info (e.g. lease time, interval).
- `Packet` wraps the data which we are sending between the spots. It is the message (packet).
- `PacketTypes` is an interface which just defines the different types of packets. We have five types of packet defined as:
 - `LOOKUP_PACKET` is sent by a client when a new service is required.
 - `LOOKUP_REPLY_PACKET` is sent by the service provider as a reply of `LOOKUP_PACKET` packet.
 - `LEASE_REQUEST_PACKET` is sent by the client as a reply of `LOOKUP_REPLY_PACKET` asking for the service data and lease time for that service.
 - `LEASE_REPLY_PACKET` is sent by the service provider with service data and for a particular lease time.

- LEASE_EXPIRED_PACKET sends by the service provider when the lease time is expired.
- PacketSender is responsible for the sending of packets.
- PacketReceiver is responsible for the receiving of packets.
- Persistent is an interface which is implemented by every class which is sent between the spots (in our case the class Packet) and has methods to persist and load an object.
- PacketHandler performs the necessary action based upon the message (packet) that spot has received. It is responsible for processing the messages and acting upon them (e.g. sending a reply). It contains two inner classes:
 - ServiceHandler starts a separate thread where it sends data to the spot which has requested the service. It terminates when the lease time expires.
 - TimeoutTimer is used to determine if a connection to a spot has been lost.

4.3 Working Procedure

When we start the application, it runs both at the service provider and the service requester which means that a Sun SPOT can both offer and request services. The application has two concurrent behaviors as Service Provider and Service Requester. The UML class diagram in figure 2 shows the structure of the classes.

Service Provider. The class SpotParticipant has the objects PacketReceiver and PacketSender. It uses the ServiceRequest and Service classes to implement the list of either the requested services or the offered services. The PacketReceiver and PacketSender classes use to communicate with other Sun SPOT(s). These classes communicate by sending and receiving data wrapped in Packet object. Packets are handled in the SpotParticipant class using the PacketHandler class.

Service Requester (Client). As a service provider, the SpotParticipant models the Sun SPOT node as the service provider. After this, it reads the XML file for the offered services, initiates the services, and loads them into internal list of offered services. The ServiceLoader class is responsible to load the services. It has a loadservice method which instantiates the service objects. Now service provider is ready and waits for any client for requested services.

Communication Protocol. This is a common functionality for the service requester (client) and the service provider. PacketSender and PacketReceiver are responsible for interaction within the communication protocol. PacketReceiver runs in a separate thread and is constantly listening for new messages. The PacketSender always broadcasts the packet along with the particular port while the PacketReceiver uses the server connection to receive the packet. When a packet is received, the PacketReceiver checks the receiver id of the packet and compares it to the id of the SpotParticipant which owns the receiver. If they are identical, it passes the packet to the SpotParticipant, otherwise it is dropped. If the sender id is an empty string (i.e. a receiver is not specified) the packet was meant as a broadcast message and it will be accepted by all the receivers.

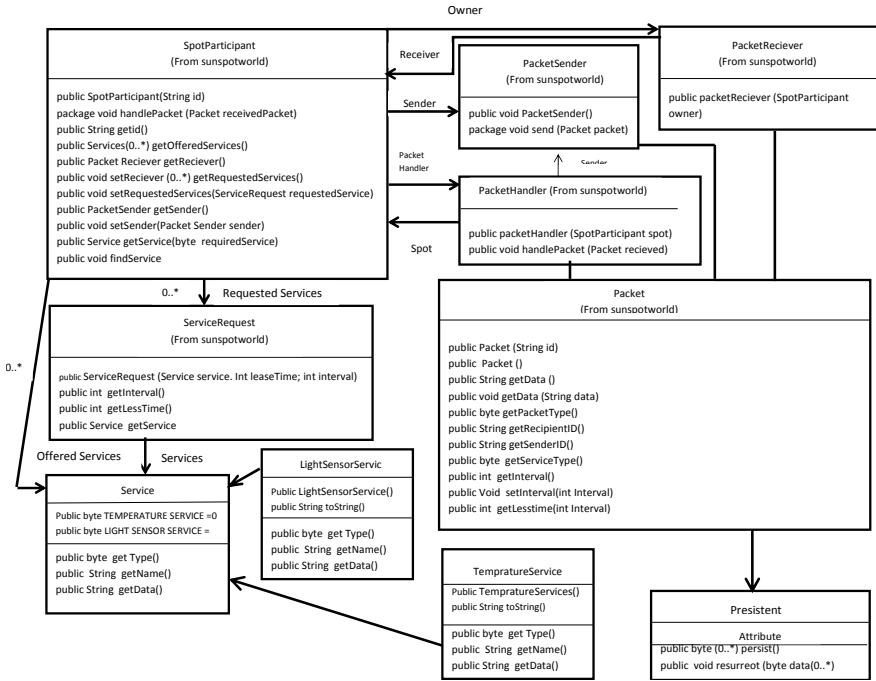


Fig. 2. UML Class Diagram of Service

Packet Handling. The packet handling is done by PacketHandler class. When any kind of packet arrives as defines by the PacketTypes interface, this class reads that packet and takes the necessary action based upon the information in that packet. For example, on the arrival of a lookup packet, it replies with a lookup reply packet. The lease is also handled by this class. It is handled by the ServiceHandler which is an inner class of PacketHandler. The ServiceHandler sends a lease expired packet to client when lease is expired. Additionally, the inner class TimeoutTimer of PacketHandler class is responsible to take care of the connection lost between the client and service provider. When the PacketHandler receives the LOOKUP_REPLY_PACKET packet, it starts a timer countdown and puts this communication session into the active services list of the client. The timeout time of the timer is set to the interval of the service request plus 10 seconds. Every time it receives a LEASE_REPLY_PACKET packet, it resets the timer. If the timer reaches 0 it is assumed that connection has been lost and the session is removed from the list of active services. It means that if it receives any data from that session after this, it will discard that data. Packet loss (i.e., the loss of LEASE_REPLY_PACKET packets) is also handled by the PacketHandler. The service provider sends a sequence number every time it sends a LEASE_REPLY_PACKET packet and the client checks that sequence number to see if any packets have been lost.

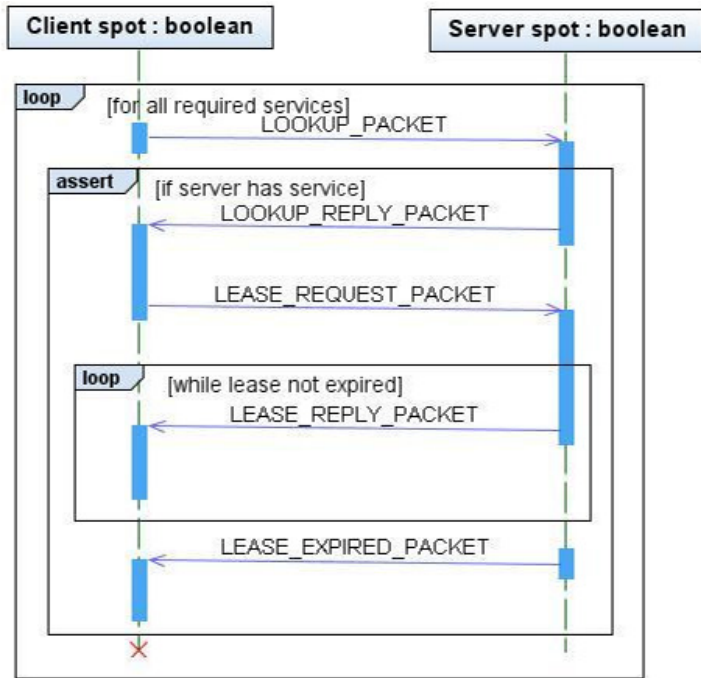


Fig. 3. Sequence Diagram

Communication Flow. To explain how the application works, we assume that a service provider is already running and a client needs the service. The client broadcasts the lookup packet which contains the packet type and service(s) and waits for reply from any service provider. When any running service provider receives this lookup packet, it checks the requested service(s) in offered service list. If it has the requested service(s), it replies back to client with the lookup reply packet with service(s) and its own address. When client gets this packet then it sends the lease request packet to the service provider in which the client asks for the service for the particular time period. As a reply, the service provider sends the requested services according to the lease time. When the lease expires, the service provider sends the lease expired packet to the client and stops sending the data. Figure 3 shows a sequence diagram (using UML notation) which illustrates the flow of communication between the client and the service provider.

In case of a connection loss between client and service provider, the client will wait for additional 10 seconds after the time interval set for the LEASE_REPLY_PACKET packet has passed. The lease (which is with the server) will still be active and the server will still send data over. The data will however be disregarded by the client if it should receive it at some later point.

Output. The output of the application can be obtained on the computer screen if we attach the client node with computer. But in case of field area where no computer is available, the output can be observed through the Sun SPOT(s) led lights. The blue led light moving from led 1 to led 8 demonstrates packet sending and red led light moving from led 1 to led 8 shows the packet receiving. The blinking green led light expresses the service offered in case of a service provider.

5 Related Work

As a whole, analyzing, evaluating, and categorizing service discovery solutions is a difficult task. Solutions are complex due to large number of responsibilities and diverse design approaches. This section serves as a standardized way of decomposing service discovery solutions and categorizes previous work in the area.

The existing service discovery architectures can be divided into two main categories: directory-less architecture and directory-based architecture. A directory is an entity that stores the information about services available in the network so as to enable service discovery and invocation. In the directory-less architecture, nodes do not distribute their service descriptions onto other nodes in the network. A device interested in a special service typically sends its search message to all reachable nodes. If one or more of these nodes can satisfy the request, a response is sent back to the requester.

Konark [7] is a middleware architecture which is designed specifically for the discovery and delivery of services in multi-hop ad hoc networks. It supports both "push and pull" models for the service discovery mechanism, with a cache in all devices. It defines an XML based service description language similar to Web Services Description Language (WSDL) with regard to service description. Konark uses multicast to advertise and discover services and allows for service delivery by running a lightweight HTTP server on every node that hosts services. Every node maintains a service registry, where it stores information about its own services and also about services that other nodes provide. This registry is actually a tree-structure with a number of levels that represent service classification.

PDP [8] is a distributed service discovery protocol designed for ad hoc networks. PDP takes into account inherent limitations of embedded devices such as power-constrained batteries and processing capabilities in such a way that the protocol reduces the number of messages sent through the network. PDP gives priority to the replies of the less-constrained devices by allowing the others to abort their answers. It also does away with the need of a central server and it is a fully distributed protocol that merges characteristics of both pull and push solutions. In PDP, devices maintain a cache of services previously announced, that is also used for the answers. All the messages are broadcast, and all devices cooperate by coordinating their replies and sharing the information in their caches. PDP takes into account different needs of the applications which allows to further reduce the power consumption.

6 Conclusion

Service discovery is not a new problem. Many academic and industrial researchers have proposed numerous solutions (protocol/middleware) of service discovery for both wired and wireless networks. We have proposed the Service Oriented Architecture (SOA) which will handle autonomous sensors networks in which all entities of a network collaborate with each other through a suitable protocol. Furthermore, we designed and implemented a service discovery prototype for wireless sensor networks which allows sensors to take part in the service oriented environment where all nodes of the network offer different services at different levels (different attributes).

References

1. Seok, O., et al.: An integrated approach for efficient routing and service discovery in mobile ad hoc networks. In: Second IEEE Consumer Communications and Networking Conference, CCNC 2005, pp. 184–189 (2005)
2. Lu, Y.: An Adaptive Middleware to Overcome Service Discovery Heterogeneity in Mobile Ad Hoc Environments. *IEEE Distributed Systems Online*, 1–1
3. Artail, H., Mershad, K.W., Hamze, H.: DSDM: A Distributed Service Discovery Model for Manets. *IEEE Transactions on Parallel and Distributed Systems*, 1224–1236
4. Bachara, P., Zielinski, K.: SOA-Compliant Programming Model for Intelligent Sensor Networks – SCA-Based Solution. In: 12th International Symposium on Symbolic and Numeric Algorithms for Scientific Computing (SYNASC), pp. 471–478 (2010)
5. Smith, R.B.: SPOTWorld and the Sun SPOT,” *Information Processing in Sensor Networks*, IPSN 2007, pp. 565–566, 25-27 (2007)
6. Zero Configuration Networking (Zeroconf) (last checked on January 07, 2012), <http://www.zeroconf.org/>
7. Helal, S., Desai, N., Verma, V., Lee, C.: Konark - A Service Discovery and Delivery Protocol for Ad-hoc Networks. In: *Proceedings of the Third IEEE Conference on Wireless Communication Networks (WCNC)*, New Orleans (2003)
8. Campo, C., Munoz, M., Perea, J.C., Martin, A., Garcia-Rubio, C.: PDP and GSDL: service discovery middleware to support spontaneous interactions in pervasive systems. In: *Proceedings of the 3rd Int’l Conf. on Pervasive Computing and Communications Workshops* (2005)

Study of Arduino for Creative and Interactive Artwork Installations

An Open Source Software Knowledge for Creativeness

Murtaza Hussain Shaikh*

Norwegian University of Science & Technology (NTNU), 7448 - Trondheim, Norway
Murtazahussainshaikh@gmail.com

Abstract. The Arts and Software are often thought as two parallel fields but with the growth of the information technology, the gap between these two fields is rather decreasing. The present existing majority of the tools are focused for the commercial business settings such as software development but the scope of the field can be increased to the other fields such as education and serving people in different fields such as Artists. The Artists are in search of open source software tools which can enhance their creative ability and at the same time want to collaborate with others to increase their knowledge on the tool. The creativity is difficult to measure as we have to consider the way the tool is enhancing the creative knowledge of the user using the tool. The creativity can also be based upon understanding the relations between different phenomena governing the tool such as Artist, Artwork, Visitor and Software. The ArTe conceptual model is based upon these principles, so the tools are evaluated based upon the ArTe conceptual model.

Keywords: Arduino, Artist, Artwork, Creativity, Collaboration, Conceptual Framework, Interactivity, Evaluation, Technology.

1 Introduction

As the computer science field has grown to be ubiquitous part of human's life, the need for making software and hardware support to fit to the needs of the users is constantly increasing. The issue closely connected with this phenomenon is creativity. Nearly every activity is involved with the creativity. Creativity occurs when somebody produces work which is useful, generative and influential [1]. While creativity is involved with every work yet it is difficult to access the creativity as creativity differs from person to person. The creative work from one person may seem to be general work from others point of view. The historical and Psychological attributes are also important to define the creativity.

The emergence of the digital media and computational tools has opened the doors for creativity. The cutting edge in the digital arts and role of new technologies can be

* Member, IEEE.

explored for the possible creativity [2, 3]. This gives an opportunity to involve arts with technologies to make creative works. There are other factors which influence the creative work, one such factor is the interactivity. The interactivity defines that artist; artwork and user have a role to play in order to give shape to the output of an interactive artwork [4]. The information technology have been influencing in shaping the creative artworks from 1960's. There is an intersection of Arts and Software interests which attracts the people from different backgrounds to work together for creative Artworks [5]. The tools available these days are very well suited to fulfill the needs of people from different background. There are many open source software and hardware tools available explicitly for creative works, such as Cohen's AARON, Arduino, Audacity, GIMP, Ink-space and Tux Paint etc. These are the open source tools explicitly developed by taking creativity of the user into consideration.

This paper is organized as; the first section introduces purpose of the paper and its areas of focus. The second section presents problem statement. The third section presents the Arts and Technology; this explains the relation between arts and technology and also introduces the concepts such as digital arts. In fourth section, this article presents the associated creativity and constraints. In fifth section, this article would discuss about the various categories to define the creative tool, this section also highlights the tools related to those category. The collaboration can be an estimate to know the creativity of the tool so the governing factors involved in the collaboration between the tools is discussed using ArTe. Finally, the last section there is a conclusion concerned to the creativity and scope for improvements.

2 Problem Statement

An information system is any combination of information technology and people's activities using that technology to support operations, management, and decision-making [6]. The scope of the information system is pervasive; it extends to needs of people in different sectors apart from the commercial business setting as illustrated in figure 1.



Fig. 1. Illustration of typical business setting of software development company [9]

One of the fields which information system can support is the arts. The artists can enhance their creativity by using the technology; however there are other factors which influence the creativity such as the interaction, cooperation and openness of the processes influencing the creative Artworks [7]. The tools available these days are practically more oriented towards the commercial business settings involving software product development as illustrated in figure 1, rather than increasing the creativity. The main focus of this paper is to “*understand the artistic creative process could be integrated with software & multimedia technologies using open source tools*”.

3 Arts and Technology

In recent years, artists are exploring possibilities to extend arts with the computation [8]. The role of information technology is increasing in creating the artworks. The creativity also plays an important role in choosing the right technologies for the artwork. There are various aspects associated with the interactive artworks and relations among those elements are important to analyze the interactivity of the artwork. The aspects are Artists, Artwork, Technologies and participants. The relation between these factors can be studied using the ArTe conceptual framework as illustrated in the figure 2. The focus on sharing, cooperation and openness is central in the artwork project, particularly with regards to technology. In order to truly integrate the field of Arts and Technology, one has to understand the relation between Arts and Technology. There exist many forms of arts however one of them which is closer to the technology is the digital arts. In order to truly integrate the field of Arts and Technology, one has to understand the relation between Arts and Technology. There exist many forms of arts however one of them which is closer to the technology is the digital arts.

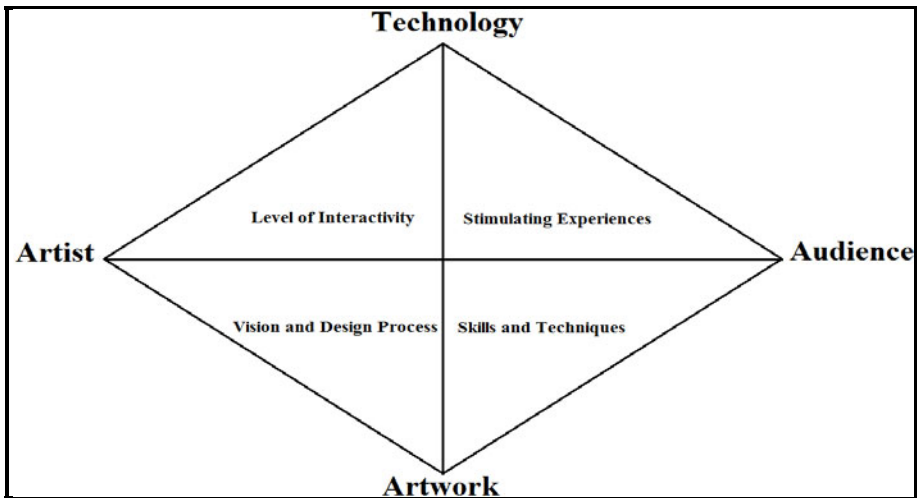


Fig. 2. The ArTe conceptual framework [9]

3.1 What Is Digital Art?

Digital art is a form of contemporary art, making distinctive works using the computer technology [11]. This art emerged in the 1970s but came into the limelight after growth in the technology like computers, software's, video devices, sound mixers and digital cameras. The process of digital art has been associated with various names computer art and multimedia art but the digital art is placed itself under the broad category of Media Arts.

There are different forms of digital arts such as Algorithmic art, Art game, Art software, Computer art, Computer art scene, Computer generated music, Computer graphics, Computer music, Cyber arts, Demo scene, Digital morphogenesis, Digital painting, Digital photography, Digital poetry, Dynamic Painting, Electronic art, Electronic music, Evolutionary art, Movie special effects, Fractal art, Generative art, Immersion (virtual reality), Interactive film, Machinima, Motion graphics, Multimedia, Music visualization, New Media Art, New Media Photo manipulation, Pixel art, Software art, Systems art, Traditional art, Video art, Video game art, Video game design, Video poetry and Virtual arts [12, 10]. The figure 3 illustrates the various technologies and hardware components associated with the different digital art works.



Fig. 3. Associated hardware with various forms of digital arts [10]

3.2 Creativity and Constraints Surpass

Creativity can be characterized as a process towards achieving an outcome recognized as innovative [13]. The creativity is often bound by the constraints, the true innovation happens, when the constraints and challenges are surpassed [14]. The following are the constraints in the path of creativity.

a) Changing Perspectives: The perspectives of the people varies as the creative work from one person may not be creative to other person, it can be general work from his/her perspective. The main challenge is to overcome this barrier and produce the work with

outstanding creativity. The outstanding creative work is any work which has stood test of time and recognized by people beyond the specialist community [15].

b) Expertise in Tool: The other challenge faced by the artists is the need to become expert with the tool in order to produce creative work. The tools such as image editing, modeling tools requires the user to have good understanding of the various functionalities of the tools and Programming knowledge in order to increase the horizons of their creativity.

c) Possible Selection of Tools: The choice of the tool depends mainly on the creativity of the artist. The creativity often depends on the selection of the tools for making the creative artwork. However, there can be some factors which will prevent the artist using the tools such as not meeting the full requirements of the project or lack of tool expertise.

4 Categories of Creative Support Tools

The tools supporting the creative works can be classified broadly into seven types namely Autonomous creative tools, Creative activity tools, Domain-specific tools with creativity scaffolding, Domain-specific tools with limited or no scaffolding, Domain-independent process support tools, Computer-supported collaborative work (CSCW) tools and Research tools [16].

4.1 Autonomous Creative Tools

The tools which facilitate the user to produce create works little or no input from the user. These kinds of tools are explicitly created to transform the thoughts of the user into creative form of work [16]. For example, Harold Cohen's computer system, AARON is one of these kinds.



Fig. 4. The generated output from the Cohen's AARON [15]

Cohen's artistic knowledge in drawings and paintings is captured using the program and then it creates the new work itself. This process generates automatically the output based on the programming in AARON [15].

4.2 Creative Activity Tools

These are the tools which aid the user to produce creative works [16]. The tools such as Mind Map and Free Mind are tools in this category. The figure 5, illustrates the output generated using the Free Mind tool. Free Mind is an open source tool developed using Java for increasing the productivity. The main function is to keep track of the various tasks involved in the project; this helps to get an overview on all the tasks involved in the concerned project [17].

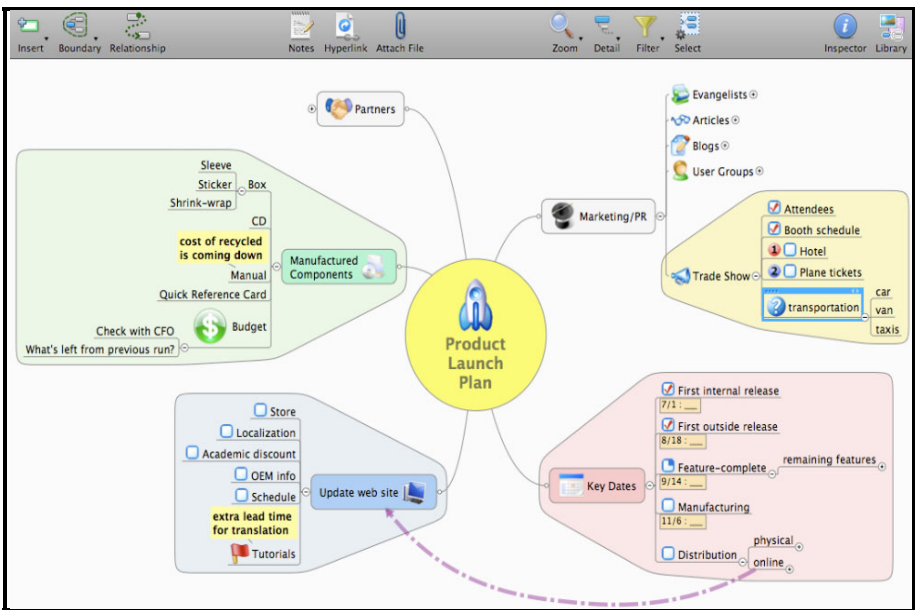


Fig. 5. The generated output from Free Mind

4.3 Domain-Specific Tools with Creativity Scaffolding

These are the tools specifically designed for the domain where the tool is going to be used. This gives the user flexibility to create and manipulate domain related data with ease and at the same time reduce the time needed to create the work [16]. The Master Writer is the tool in this category. The following figure 6 illustrates the output generated from the Master Writer [18]. This tool is useful for the people involved with the music especially song writers. The Master Writer provided the users with phrases, parts of speech, dictionary, thesaurus, and rhymes for composing a song [18]. This helps the people involved with the domain of music and at the same time reduces the time to compose a song.



Fig. 6. The generated output from the Master Writer

4.4 Domain-Specific Tools with Limited or No Scaffolding

These are the tools which allow the user to work at higher abstraction levels with no or little scaffolding [16]. The tools such as GIMP (GNU Image Manipulation Program) fall into this category. GIMP as illustrated in the figure 7, is an open source platform for image manipulations [19]. This tool allows the user to work with the images at higher abstraction levels such as photo retouching without paying attention to the fine details such as pixels etc. [19].

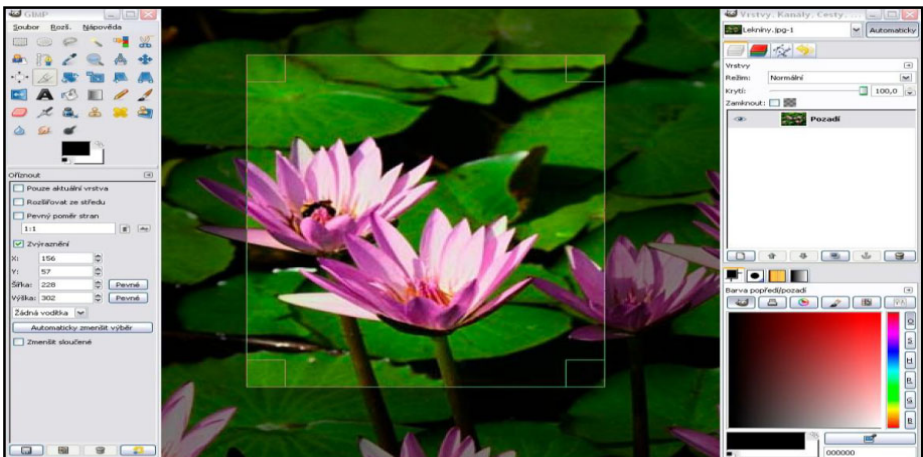


Fig. 7. Illustrates the crop function in the GIMP

4.5 Domain-Independent Process Support Tools

Domain-independent process support tools are the tools which support the process of creative works without any scaffolding towards creation or editing any image [16]. The creative work often demands evaluating the work, the tools such as versioning systems (SVN, CVS etc) helps the user to check the alternative possibilities for the creative works without losing the data [16].

4.6 Computer-Supported Collaborative Work Tools

The CSCW tools allow the user to produce creative work using shared collaboration between multiple users [16]. The collaboration becomes a need for a project involving multiple participants. The tools such as shared documents, shared editors, and shared spreadsheets are some examples of this category.

4.7 Research Tools

The research tools help the user in the process of researching and improving the knowledge by disseminating the works previously done in the field [16, 19]. The search engines and the citation tracking tools fall into this category which helps in the process of researching.

5 Evaluating Creative Support Tools

The creativity support tool can be truly tested by considering the impact level of tool on the creative thought process. The assessment has to be based upon various criteria's such as efficiency of the tool, cognitive support and other subjective assessments [16]. The creativity can also be based upon understanding the relations between different phenomena governing the tool such as Artist, Artwork, Visitor and Software. The ArTe conceptual model is based upon these principles, so the tools are evaluated based upon the ArTe conceptual model as illustrated in figure 2. The ArTe conceptual model can be applied to these creative support tools to understand the collaboration between the various phenomena associated with tools for achieving the creative works. The following table illustrates the collaboration between the various phenomena mentioned in ArTe applied to the tools stated in each category.

So the collaboration between the tools can be accessed by understanding the relations between these phenomena as mentioned in the above table. Thereby the creativity involved with the tool can be estimated based upon understanding these relations between the various phenomena.

Table 1. The Application of ArTe phenomena to creative tools

S.no	Tools / Phenomena	Artist	Artwork	Visitor	Software
1	Autonomous creative tools.	_____	Creative figures and drawings in Cohen`s AARON	Person Viewing the figure.	AARON
2	Creative Activity tools.	Person designing the tasks in Free-mind.	Free-mind output depicting the tree of tasks in project.	Person creating map, other persons involved with the project.	Free-mind
3	Domain specific-tools with creativity scaffolding.	User	Song composition.	Anyone listening to composed song.	Master writer
4	Domain specific-tools with limited / no scaffolding.	User of GIMP, viewing the GIMP output.	GIMP output file such as increased brightness, sharpness of image etc.	Person viewing image.	GIMP
5	Domain-independent process support tools.	User	Versions of some file system.	Person who has access to the file.	CVS, SVN
6	Computer supported collaborated work (CSCW) tools.	User who has access to shared files.	Shared documents, files, spread sheet etc.	Any person who has access to the shared file.	For example Google Docs.
7	Research tools	Person who is searching or has registered for checking the citing.	Search results, new citing etc.	_____	Google, Msn Search engines etc.

6 Conclusion

The collaboration between the Arts and Software field has been improving these days but however there is more scope for improvement. In order to improve the collaboration between the both fields for producing more creative works, the perspective of the Information systems has to be changed to orient towards the non commercial settings such as education and community informatics etc. The open source increases the horizons of creative thought process as users can use the tool and can change the binaries of the software to suit to their needs. This facilitates growth of open source community which can engage audience from different fields and share the knowledge for producing creative works. This will also help in making creative projects using collaboration between people from different fields.

Acknowledgement. I am thankful to all working staff of Omega Verkstad at Gamle Electro building, Norwegian University of Science and Technology (NTNU) for providing me the essential requirements for this paper. Lastly, I especially want to thank my mother for all the financial support to study in (NTNU). With her prayer's it could not be possible have a wonderful academic career.

References

1. Csikszentmihalyi, M.: *Creativity: Flow and Psychology of invention*. HarperCollins, New York (1996)
2. Boden, M.A.: *The Creative Mind: Myths and Mechanisms*. Weidenfeld and Nicolson, London (1997)
3. Edmonds, E.A., Weakleya, A., Knott, R., Pauletto, S.: *The studio as laboratory: Combining creative practice and digital technology research*. *Int. J. Human-Computer Studies* 63, 452–481 (2005)
4. Willis, K.D.D.: *User authorship and creativity within interactivity*. In: *Proceedings of the 14th Annual ACM International Conference on Multimedia (MULTIMEDIA 2006)*, pp. 731–735. ACM, New York (2006), <http://doi.acm.org/10.1145/1180639.1180796>
5. Giunchiglia, E., Maratea, M., Tacchella, A., Zambonin, D.: *Evaluating Search Heuristics and Optimization Techniques in Propositional Satisfiability*. In: Goré, R.P., Leitsch, A., Nipkow, T. (eds.) *IJCAR 2001*. LNCS (LNAI), vol. 2083, pp. 347–363. Springer, Heidelberg (2001)
6. Berezin, S., Campos, S., Clarke, E.M.: *Compositional reasoning in model checking*. In: de Roever, W.-P., Langmaack, H., Pnueli, A. (eds.) *COMPOS 1997*. LNCS, vol. 1536, pp. 81–102. Springer, Heidelberg (1998)
7. Ahmed, S.U., Jaccheri, L.: *SM'kadmi- Arts and Technology: Sonic Onyx: Case Study of an Interactive Artwork*. Springer, Heidelberg (2010)
8. Letizia, J.: *ArTe conceptual framework*, *Art and Technology*, <http://www.artentnu.com> (last accessed on October 23, 2010)
9. *Electronic Publication: Indtech Info Solutions Pvt. Ltd., Offshore Development*, <http://www.indtechinfo.com/offshoreddevelopment.aspxwww.artentnu.com> (last accessed on November 26, 2010)
10. Cimatti, A., Clarke, E.M., Giunchiglia, F., Roveri, M.: *NUSMV: a new symbolic model checker*. *International Journal on Software Tools for Technology Transfer (STTT)* 2(4) (March 2000)
11. Farooq, U., Carroll, J.M.: *Supporting creativity in distributed scientific communities*. In: *Proceedings of the 2005 International ACM SIGGROUP Conference on Supporting Group Work (GROUP 2005)*, pp. 217–226. ACM, New York (2005), <http://doi.acm.org/10.1145/1099203.1099242>
12. Audemard, G., Bertoli, P.G., Cimatti, A., Kornilowicz, A., Sebastiani, R.: *A SAT Based Approach for Solving Formulas over Boolean and Linear Mathematical Propositions*. In: Voronkov, A. (ed.) *CADE 2002*. LNCS (LNAI), vol. 2392, pp. 195–210. Springer, Heidelberg (2002)
13. Ernest Brants, T.: *Tnt - a statistical part- of-speech tagger*. In: *Proceedings of the 6th Conference on Applied Natural Language Processing, ANLP. ACL (2000)*
14. Terry, M.: *Open Source as a Test Bed for Evaluating Creativity Support Tools*. In: *Proceedings of the NSF Creative IT workshop at Arizona State University, USA (2007)*

15. Weill, P.: MIT Center for Information Systems Research. In: Director, as Presented at the Sixth e-Business Conference, Barcelona, Spain (March 27, 2007)
16. Giachetti, R.E.: Design of Enterprise Systems, Theory, Architecture, and Methods. CRC Press, Boca Raton (2010)
17. Resnick, M.: Sowing the Seeds for a More Creative Society. In: Learning and Leading with Technology. International Society for Technology in Education, Norway (2007)
18. Borälöv, A.: A Fully Automated Approach for Proving Safety Properties in Interlocking Software Using Automatic Theorem-Proving. In: Gnesi, S., Latella, D. (eds.) Proc. of the Second International ERCIM FMICS, Pisa, Italy (July 2006)
19. Ranjan, R.K., Aziz, A., Plessier, B., Pixley, C., Brayton, R.K.: Efficient BDD algorithms for FSM synthesis and verification. In: Proc. IEEE/ACM International Workshop on Logic Synthesis, Lake Tahoe, NV (May 1999)

Developing and Managing SLAs for Business Applications in Information Systems

Aijaz Soomro* and William Song

University of Durham, Durham, DH1 3LE, UK
{a.a.soomro,w.w.song}@dur.ac.uk

Abstract. Use of Service Level Agreements (SLAs) is crucial for a business organization to provide the value added goods and services to customers to achieve the business goals successfully. Efficient structural representation and management of SLAs can solve the problems of quality of service evaluation during service development and deployment. Existing specifications and structures for SLAs do not fully formalize and support for different automatic and dynamic behavioural aspects needed within the Business Organizations for SLAs. We address the issues on how to formalize and document the structures of SLAs for better utilization and improved results in various business domains. Our main focus is on the contents and processes of SLAs during service discovery, service delivery and scheduling of the services effectively and efficiently.

Keywords: SLA, QoS, Scheduling, SOA, Web Services.

1 Introduction

Every business organization requires faster and cheaper IT support, to align the IT services with corresponding Business Services. Within today's business IT infrastructures, the Service-Oriented Architecture (SOA) gives a new model for creating distributed applications. In SOA, web services are distributed building blocks which present well-defined interfaces that process and deliver messages for communications among them. The use of service based approaches supports in building cross organizational applications. A business with various systems and applications on different platforms can take an advantage from the SOA to build a loosely coupled integrated solution that implements unified workflows [1].

"Web Services" is an emerging technology that provides a systematic and extensible framework for application-to-application interaction built on the top of the existing web protocols, such as Extensible Markup Language (XML) standards [2]. Web Services are the most accepted invocation of the Service Oriented Architecture (SOA) [3]. All the content of a web service and service metadata is transmitted using XML. Due to the use of XML all hindrances caused by programming language dependencies and system dependencies are removed [4]. The core standards that are used in web services are Universal Description, Discovery and Integration (UDDI), Web Services Description Language (WSDL) and Simple Object Access Protocol (SOAP).

* Corresponding author.

It is noticed from the structural description of the Web Service standards, that these standards are mainly developed, and are particularly suitable, for service providers to describe and publish their services. But, there is less support for service consumers to search for web services, and some manual efforts are needed by the service consumers to describe their requirements, demands, and expectations on services.

In order to achieve a satisfactory level of the services being offered, the commitments and assurances of services are implemented and assured through the use of newly developed mechanism which is called Service Level Agreements (SLAs), which establish an agreeable contract between the service users and the service providers by stating the expectations and obligations explicitly between the two parties i.e. the service provider and the service consumer [5].

The existing SLA structures such as WSLA [6], WS-Agreement [7] and SLAng [8] are all focused on the technical aspects of services and do not cover the business aspects of the services. These should focus on non-functional terms of the services which are important to build the business relationship with the customers and providing the distinguished features between service providers and customers.

E-Businesses have the need to integrate their business processes and software applications with web services over the Internet. To offer the Quality of Service (QoS) over the Internet is a challenge because of its unpredictable and dynamic nature. To determine the Quality of Service of a service provider it is essential to supervise the Service Level Agreements created between the service provider and service consumer.

In order to better structure the SLAs, we discuss an overview of the SLA components described by different authors in section 2, then we extract and classify the most useful components from their domains. We will also compare different approaches expressing the necessary steps of the SLA life cycle. The comparative analysis on different phases of the SLA lifecycle motivates the selection of the necessary phases for our proposed work. After structuring the SLA terms and the Lifecycle Phases of SLAs, the Quality of Service termed by different authors will be compared in Table 1, and we will also propose an algorithm to schedule the services and service level agreements for better utilization of SLAs for web services in the SOA based applications.

The rest of the paper is organized as follows. Section 2 discusses the related work and the background. Section 3 discusses a real world scenario example, basic formal notations, dependencies between the components of SLAs, dependency graphs of components. Section 4 presents the framework model of proposed approach. Section 5 considers about the evaluation requirements and section 6 concludes the paper with future work directions.

2 Related Work

2.1 Service Level Agreement Components

It is a legal requirement for any business to have some formal contracts for the services they offer to their customers. A SLA is an agreed upon statement of the expectations and obligations that exist in a business relationship between the user and the service provider. It is a formalized representation of commitments in the form of a SLA

document which is required when the information is collected and SLA evaluations are to be automated [9].

A Service Level Agreement is a contract which is related with the guarantees of a web service. A SLA defines the level of service formally. SLAs describe the common understandings about services, priorities, responsibilities, guarantees, level of service availability, performance, and operation. A SLA is a formally negotiated agreement between two parties. A SLA between a service provider and its customers will assure customers that they can get the same service for which they are paying and it will obligate the service provider to obey its service promises [10]. The service guarantees are about what transactions need to be executed and how well they should be executed.

There are many SLA structures defined by various industries and academia, but to the best of our knowledge none of the structures is completely well defined. We have summarized the set of properties of SLAs from [6,7,10] given below:

SLA Purpose, Scope, Validity period, Restrictions, Penalties, Optional services, Exclusions and Administration [10]. Service Consumer, Service Provider, Agreement, Agreement (Template, Terms, Initiator, Responder, Creation, Context, Creation Constraints, Offer, Acceptance, Rejection), Business value and expiration [7]. Service Object, SLA Parameter, Metric, Measurement Directive, Function, Obligation, Action Guarantee [6]. Guarantee / Guarantee Terms [6,7]. Parties/Agreement Parties, Service Level Objectives (SLO) described by [6,7,10].

2.2 The Service Level Agreement Lifecycle

The structuring and management of SLAs is a kind of business process. It has formal lifecycle steps. Therefore the management of the SLAs needs to be interlaced between the different phases following a formal SLA lifecycle. By considering the SLA lifecycles from [6,11,12,13] we refine the different SLA lifecycle phases into the following sequence:

Define or develop Service, feedback [12]. Execution and decommission [13], enforce penalties [11]. Measurement, reporting, corrective management actions and SLA Deployment [6]. Discover service provider [11,13]. Negotiations [6,13]. Assessment [12,13]. Monitor [11,12]. Define/Develop SLA [11,12,13]. Terminate [11,13,6]. SLA Establishment/Preparation/Formation [6,11,12,13].

2.3 Quality of Service

Quality of service (QoS) is a key element for distinguishing the different services provided by different providers. The term “quality of service” is used for expressing non-functional requirements. The functional requirements describe a function of a software system or its components. A function is defined as a number of inputs, the behaviour, and outputs. The quality of service describes how well the system performs its operations.

The various quality of service terms have been used by different researchers in different kinds of domains. The W3C working group [14] summarized the definition of terms for quality of service and its metrics according to web service requirements. There are two groups of terms i.e. Performance and Security defined by W3C, while the other

Table 1. Quality of Service Terms

Performance	Dependability	Security	Domain specific Terms
Throughput	Availability	Authentication	Mobile Signal Quality
Response Time	Accessibility	Authorization	Mobile Contract Price
Latency	Accuracy	Accountability	Mobile Contract Length
Execution Time	Reliability	Confidentiality	Mob Term1,
Transaction Time	Capacity	Traceability	Mob Term2,
	Scalability	Auditability	Mob Term3,
	Exception Handling (Stability)	Non-Repudiation	etc.
	Robustness (Flexibility)	Encryption	
	Integrity (Data and Transaction)		

terms have been classified under the category of dependability [16, 15]. Since web services are so different in nature, it is impractical to describe all QoS metrics for all of the domains in a single model. Therefore, the fourth group, “application-specific metrics”, is created for the metrics that are specific to a certain domain [17]. Table 1 lists all four groups separately. We further elaborate Domain Specific terms in section 3 with the help of representation of terms by considering an example from the real world scenario.

3 Proposed Approach

Due to the limitations in the existing SLA research work, we propose our approach based on a real world scenario example. Then we construct the expressions for representing the objects or components used into the scenario. Last, we represent the dependencies between the components or items and we develop algorithms for scheduling the SLAs for Quality of Service Assessment purpose.

3.1 An Example from Real World Scenario

On average, most of the consumers or clients require more than one service at a time and they prefer to get multiple services from the same provider using a single package or service contract. While the service providers also look for those customers whom they can offer multiple services in either one or combined packages. It is a very common business strategy of every company or service provider to provide the more flexible and good service or service products to their clients for creating the market place for them. As a result it allows them to gain more clients. But the companies can gain more clients only if they assure their quality of service, while the quality of service is directly dependent on the service promises and service guarantees. Therefore the service promises should be formally described by Service Level Agreements.

Here we illustrate an example of a communication service provider in Fig.1, which offers different services such as 1) Mobile Phone, 2) Broadband, 3) Landline Telephone and 4) TV Channels.

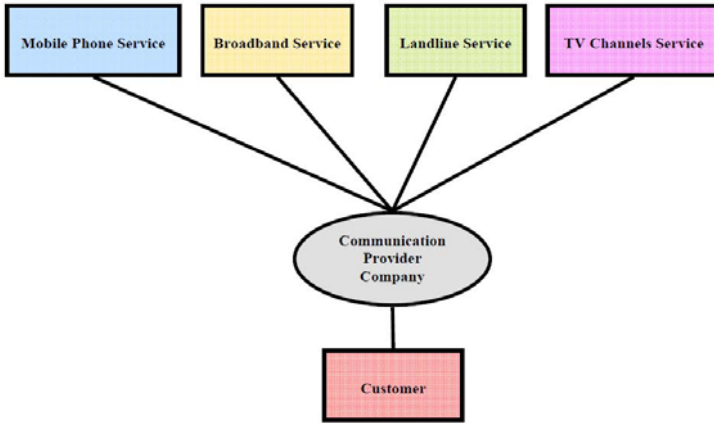


Fig. 1. Communication Services Provider

Our work illustrates how SLAs can be created for these services, how to represent the dependencies between services, their SLAs, their attributes and values, which can form SLAs based on individual services or the combination of services. We also represent the arrangement of these terms, and finally we schedule those SLAs based on the Quality of Service.

3.2 Basic Concept Elements

While section 3.1 gives a pictorial representation of a real world scenario focusing on services from a communication provider, in this section we define each component of the real world scenario with its formal description terms. Starting from a service or a set of services provided by one or more organizations, we consider each organization has one or more SLAs. One SLA can be composed of other SLAs . In the following we formally define these terms for the purpose of building up a set of formal relationship between services, SLAs , elements of SLAs, their dependencies and their scheduling in order to better utilize them in more formalized way. Some important definitions of the whole scenario terms are discussed below:

Definition (Provider): The Provider of the services is defined as:

$$P = \{P_1, P_2, \dots, P_n\},$$

where P denotes the set of n individual P_i Service Providers, and $1 \leq i \leq n$.

Definition (Consumer): The Consumer of the services is defined as:

$$C = \{C_1, C_2, \dots, C_n\},$$

where C denotes the set of n individual C_i Service Consumers, and $1 \leq i \leq n$.

Definition (Service): Each Provider offers a service or number of services defined as:

$$S = \{S_1, S_2, \dots, S_n\},$$

where S denotes the set of n individual S_i Services, and $1 \leq i \leq n$.

Definition (SLA): Each Service has one or more SLAs, and the set of SLAs can be represented as :

$$SLA = \{SLA_1, SLA_2, \dots, SLA_n\},$$

where SLA denotes the set of n individual SLA_i Service Level Agreements, and $1 \leq i \leq n$.

Definition (Composite SLA): A set of individual SLAs to form a composite SLA represented by :

$$CSLA = \{CSLA_1, CSLA_2, \dots, CSLA_n\},$$

where $CSLA$ denotes the set of n individual $CSLA_i$, and $1 \leq i \leq n$.

Definition (SLA Terms): Each individual SLA or Composite SLA has the set of Terms represented by :

$$T = \{T_1, T_2, \dots, T_n\},$$

where T denotes the set of n individual T_i SLA Terms, and $1 \leq i \leq n$.

Definition (SLA Parties): Each SLA is made between two or more parties and a set of SLA Parties can be represented by:

$$SP = \{SP_1, SP_2, \dots, SP_n\},$$

where SP denotes the set of n individual SP_i SLA Parties, and $1 \leq i \leq n$.

Definition(Performance Metrics): A set of Performance Metrics is represented by:

$$PM = \{PM_1, PM_2, \dots, PM_n\},$$

where PM denotes the set of n individual PM_i Performance Metrics, and $1 \leq i \leq n$.

Definition (SLA Penalties): The set of SLA Penalties is represented by :

$$PEN = \{PEN_1, PEN_2, \dots, PEN_n\},$$

where PEN denotes the set of n individual PEN_i SLA Penalties, and $1 \leq i \leq n$.

3.3 Basic SLA Structure

In this section we give a concrete SLA template based on the above mentioned real world scenario example in Table 2, which describes the set of SLA terms and its actual values.

Table 2. Concrete SLA Template

SLA Terms	Values
Purpose	A Communication Provider Service Contract
Service Description	Mobile Talk Time Minutes
Agreement	A 12 Month Contract for Mobile Pay Monthly Contract
Parties-Service Provider	The Provider "Orange Mobile"
Parties-Service Consumer	A customer "Mr. James"
Agreement Initiator	Mr. Kevin the "Sales Representative"
Validity Period	12 Months, Starting from January 2011.
Scope	Orange Network & T-Mobile Network
Restrictions	Only National Calls Allowed
Expiration	January 2012
Agreement Term1(Package Price)	£10 Per Month ,
Agreement Term1(Package Type)	Silver (500 Minutes Per Month)
Guarantee Term1(Coverage)	More than 90% Coverage all over the country.
Exclusion	0800 Numbers Not Inclusive
Penalty(on Provider)	If coverage Less than 90%, then 50% money Back to account.
Penalty (On Consumer)	If payment not received every 1st of Month then contract will be terminated, and Penalty amount will be payable by the consumer.

3.4 Dependencies and Graph Illustrations

In business organizations or related scenarios there exist lots of dependencies in the business processes. The service providers work on individual basis but they mostly depend on other service providers to utilize and integrate their own and borrowed services. A service itself can be dependent on other services either within the same organization or the services borrowed from the other organizations. The Service Level Agreements can be created based on the existing SLAs having the dependency between them. The terms of one SLA can also be dependent on other terms of the same SLA or from the other SLA used for the services by the same or different service providers. We define the dependencies by an operator symbol (\sim) in the following cases:

(a) Provider Dependency: It is possible that one Provider may be dependent on other provider. Therefore we represent this dependency as : P_i is the i^{th} Provider , and it can depend on the $i+1$ th, or $i-1$ th service provider.

$$P_i \sim P_{i+1} \text{ or } P_i \sim P_{i-1}$$

This type of dependency is drawn in a two dimensional dependency graph. In the first case the providers are divided into two classes i.e. one class is P_i and another class is P_j in Fig.2(a). It is possible that any of the P_i Providers can be dependent on any other provider from the P_j Providers or vice versa. In the second case the dependency of the companies between the same group P_i with respect to the particular level of dependency (low, medium or high) is shown in Fig.2(b).

(b) Service Dependency: Let S_{i+1} the service provided by the P_1 provider and S_{j+2} by the service provider P_2 . If S_{i+1} of P_1 is depending on S_{j+2} of P_2 then we represent this dependency as follows:

$$S_{i+1}P_1 \sim S_{j+2}P_2$$

We represent this dependency of services in Fig.2 (c), where on one dimension we use one Provider P_1 with service names from S_i to S_{i+n} , on the other dimension we represent the other provider P_2 with service names from S_j to S_{j+n} .

(c) SLA Dependency: Consider the example from section 3.1, Suppose two additional contracts of Broadband (SLA_2) and Landline (SLA_3) are created for an existing customer who already has a mobile contract (SLA_{i+1}). We represent this dependency of new $SLAs$ based on the existing SLA as below:

$$(SLA_2 \ \& \ SLA_3) \sim SLA_{i+1}$$

Fig.2(d) shows the dependency of SLA_{i+1} on SLA_2 and SLA_3 .

(d) Terms Dependency: Consider the example of Terms dependency from Table 1 (SLA template). We use different term values such as : $T1=Service \ Number$, $T2=Provider \ Name$, $T3=Service \ Price$, $T4=Service \ Penalties$, $T5=Total \ Number \ of \ Talk \ Time \ Minutes$ (Sliver). Here we formalize two kinds of dependencies of the terms: direct dependency and indirect or inverse dependency, which are discussed below.

1. If the price of the contract is increased, then more minutes of mobile are given to the customer. This is referred to as direct dependency. This Direct Proportional Dependency is represented as : $T3 (Service \ Price) \sim T5 (Total \ Number \ of \ Free \ Minutes)$. If $T3$ is increased then $T5$ will be increased.

2. In the inverse situation, with a contract type of mobile “pay as you go” from the mobile services, if the consumer will use more number of minutes then the charges per minute will be cheaper. In other words, if the use of minutes is less, then the price per minute will be high and customer will not get discount. This Inverse Proportional Dependency is represented as : $(T3 \sim 1/T5)$. If $T3$ is increased then $T5$ is decreased, while if $T5$ is increased then $T3$ is decreased.

The graph illustration of $T3$ Term directly proportional on $T5$ is represented in Fig.2(e) and the inversely proportional dependency is shown in Fig.2(f).

4 Framework Model

The proposed model diagram represented in Fig.3, is an extension to the Service Oriented Architecture (SOA) model. Since the existing SOA framework does not contain the built-in mechanism for Quality of Service and Service Level Agreement management, we propose a SLA structure and management framework model which lies between the service providers and service consumers. This framework can work as trusted third party component on behalf of providers and consumers for evaluating the quality of service for different service providers.

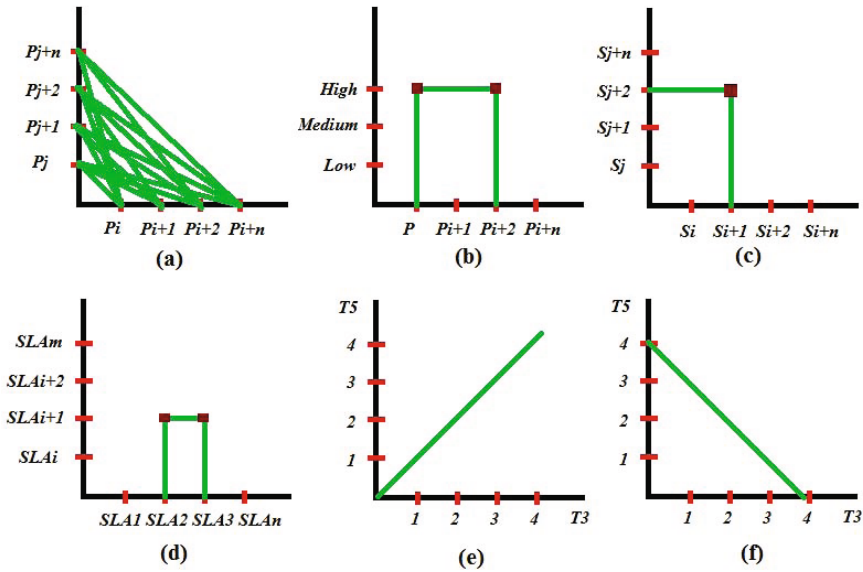


Fig. 2. Dependency Graphs

4.1 Components of the Framework Model

The proposed framework model incorporates our proposed approach to the formalism of SLA terms , QoS classification terms, and Scheduling Algorithm. It has components which are discussed briefly below:

Client Interface: The role of this component is to create a bridge for communication between the client and the proposed SLA Management Framework. Since the customers are not aware of all the technical aspects of Services and SLAs, the *Client Interface* provides the communication path for the clients in the form of messages passed to and from the Proposed Framework.

Service Provider Interface: The Service Providers are not experts of the Web Service at the technical levels, they are only professionals in their business activities. This component provides a way of communication between the providers of the services with the clients, Service Registries and the Proposed Framework components in order to achieve the business goals easily.

Service Repository: In addition to the basic use of the SOA approach (UDDI), this component stores more details about the service descriptions which are required for mapping and searching SLA templates with the associated services.

Templates Manager: This component stores all the formalized SLA templates which have been generalized from different existing approaches for multi-domains. This manager contains static templates and has capabilities to generate dynamic SLAs based on the changing requirements during Negotiation.

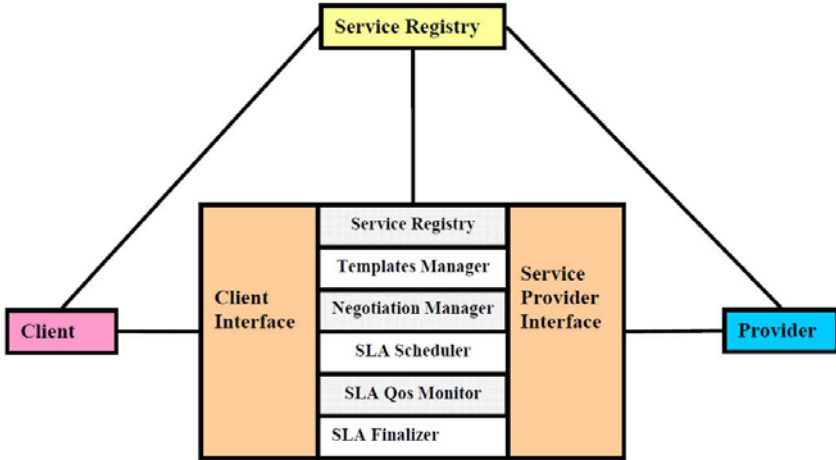


Fig. 3. Proposed Framework Model Diagram

Negotiation Manager: At the time of any change in SLA goals, the SLA document must be re-negotiated among the parties for adaptation in order to reach a mutual agreement. This component is responsible for such collaboration activities.

SLA Scheduler: This component is responsible for initiating and scheduling all the phases of the SLAs lifecycle including development, negotiation, execution, monitoring and termination steps.

SLA Monitor: The SLA monitor is responsible for storing the states of SLAs, and calculating the QoS values of different states of SLAs. In this component the SLA parameters are computed and compared against the guarantee terms defined in SLA in order to determine the quality of service being delivered.

SLA Finalizer: In this component the termination of the SLA contracts is performed either due to the contract expiration or violation of the contract, and compensation or penalties being enforced are triggered.

5 Evaluation

The assessment of the proposed study involves the two degrees of evaluation. The first is the assessment of the proposed framework model for structuring and managing the Service Level Agreements and the corresponding components as well as the substantial acceptance of the framework model. For the first evaluation requirement, the three criteria are considered: *adaptability*-to what extent the proposed framework model is able to accommodate the requirements of the selection and scheduling of SLAs and Services based on Quality of Service; *scalability*-at what scale this model is capable to process the requirements and services; and *flexibility*-how the framework model is able to couple to or decouple from the SLA components or terms when they are required or discarded according to domain specific needs.

For the second evaluation requirement, spotlighting on the components of the framework model and their interactions, the success of the framework model lies on the criteria for SLA Templates, Negotiation Manager, Scheduler, QoS Monitor, SLA Finalizer and the interconnection between the components. The SLA formal descriptions require matching of the user needs with service descriptions. The formation of the SLA templates should properly fulfil the contract requirements. The key issues can arise with the differences between the formal representation of the user requirements and service or SLA expressions. The Quality of Service as second major issue requires an establishment of effective formal descriptions for quality assessment. Thirdly, the selection and scheduling of the services and SLAs can give better decisions and effective managed plans for service provisions.

6 Conclusion

We have compared the existing approaches used for the SLA Lifecycles, Terminologies, Quality of Service terms and scheduling strategies. We have proposed the formal representation of the key components for SLAs, QoS Terms and Scheduling Algorithms. Finally we have proposed a framework model to accommodate these formal representations for SLAs, QoS and Scheduling Algorithms, which we believe to contribute to the progress of SOA applications having SLAs and QoS based scheduling aspects. Our next step of the research is to enhance the theoretical aspects of the proposed framework model and evaluation criteria to support the development of the model and its applications successfully.

References

1. Hasan, J., Duran, M.: *Expert Service-Oriented Architecture in C# 2005*, 2nd edn. Apress, Berkely (2006)
2. Curbera, F., Duftler, M.J., Khalaf, R., Nagy, W., Mukhi, N., Weerawarana, S.: *IEEE Internet Computing: Spotlight - Unraveling the Web Services Web: An Introduction to SOAP, WSDL, and UDDI*. *IEEE Distributed Systems Online* 3(4) (2002)
3. Cardoso, J.: *Semantic Web Services: Theory, Tools, and Applications*. University of Madeira, Portugal (2007)
4. Shaikh, A., Memon, M., Memon, N., Mibahuddin, M.: *The Role of Service Oriented Architecture in Telemedicine Healthcare System*. In: *International Conference on Complex, Intelligent and Software Intensive Systems*, Copyright 2009. IEEE (2009)
5. Padgett, J., Djemame, K., Dew, P.: *Grid service level agreements combining resource reservation and predictive run-time adaptation*. In: Cox, S.J., Walker, D.W. (eds.) *4th UK e-Science All Hands Meeting (AHM 2005) EPSRC* (2005)
6. Keller, A., Ludwig, H.: *The WSLA framework: specifying and monitoring service level agreements for web services*. *Network and Systems Management Special Limitation on E-Business Management* 11(1), 57–81 (2003)
7. Andrieux, A., Czajkowski, K., Dan, A., Keahey, K., Ludwig, H., Nakata, T., Pruyne, J., Rofrano, J., Tuecke, S., Xu, M.: *Web Services Agreement Specification (WSAgreement)*. In: *OGF proposed recommendation, GFD.107* (2007)
8. Lamanna, D.D., Skene, J., Emmerich, W.: *SLAng: A Language for Defining Service Level Agreements*. In: *FTDCS*, p. 100 (2003)

9. Padgett, J., Djemame, K., Dew, P.M.: Grid-Based SLA Management. In: EGC European Grid Conference, pp. 1076–1085 (2005)
10. Jin, L.-J., Machiraju, V., Sahai, A.: Analysis on service level agreement of web services. Technical Report HPL-2002-180, HP Laboratories, Palo Alto, CA (June 2002)
11. Sun Microsystems Internet Data Center Group (2002)
12. Xu, K., Zhang, X., Song, M., Song, J.: Research on SLA management model in service operation support system. In: 5th International Conference on Wireless Communications, Networking and Mobile Computing. IEEE (2009)
13. Telemanagement (TM) Forum. SLA Handbook Solution Suite V2.0, (2008), <http://www.tmforum.org/DocumentLibrary/SLAHandbookSolution/2035/Home.html>
14. W3C Working Group (2003), QoS for Web Services: Requirements and Possible Approaches, <http://www.w3c.or.kr/kr-office/TR/2003/ws-qos/> (retrieved from April 21, 2011)
15. Avizienis, A., Laprie, J., Randell, B.: Fundamental concepts of dependability. Technical Report N01145, LAASCNRS (2001)
16. Truong, H.L., Samborski, R., Fahringer, T.: Towards a Framework for Monitoring and Analyzing QoS Metrics of Grid Services. In: 2nd IEEE International Conference on e-Science and Grid Computing, December 4-6, IEEE Computer Society Press, Amsterdam (2006)
17. Wang, Y., Vassileva, J.: Toward Trust and Reputation Based Web Service Selection: A Survey. International Transactions on Systems Science and Applications 3(2), 118–132 (2007)

Image Retrieval Based on Color and Texture Feature Using Artificial Neural Network

Sajjad Hussain^{1,*}, Manzoor Hashmani¹, Muhammad Moinuddin¹,
Mikio Yoshida², and Hidenori Kanjo²

¹Faculty of Engineering, Sciences and Technology, IQRA University, Karachi, Pakistan
{enr.sajjadrizvi,mhashmani,mmoin73}@yahoo.com

²Broad Band Research Corporation, Osaka, Japan
{yos,hi_kanjo}@bbr.jp

Abstract. Content-based image retrieval CBIR is a technique that helps in searching a user desired information from a huge set of image files and interpret user intentions for the desired information. The retrieval of information is based on features of image like colour, shape, texture, annotation etc. Many of the existing methods focus on the feature extraction and to bridge up the gap between low level features and high level semantics. In this paper we propose a supervised machine learning (SML) using artificial neural network (ANN) and singular value decomposition (SVD) for image retrieval. Specifically we use back propagation algorithm (multilayer perceptron) (MLP) for training and testing our proposed model. Experimental results show that by changing parameters of feature vector back propagation method can have 62% precision instead of 49% as claimed by in Hyoung Ku LEE, Suk In Yoo [1].

Keywords: Colour based image retrieval, back propagation algorithm, artificial neural network based image retrieval, multilayer perceptron (MLP).

1 Introduction

Previously the information was primarily text based. But with the rapid growth in the field of computer network and low cost permanent storage media, the shapes of information become more interactive. The people are accessing more multimedia files than the past. In past, images, videos and audio files were only used for the entertainment purpose but nowadays these are the major source of information. Because of intense dependency on multimedia files for information searching, to obtain a desired result is a major problem as the search engine searches within the text associated with the multimedia files, instead of the contents of information. Intelligent and optimized text searching has already matured but there is a gigantic space available for the intelligent and optimized Contents Based Image Retrieval (CBIR).

* Corresponding author.

In this age of information technology we are intensively depending on the visual information and its contents as well as with the rapid growth of human computer interaction (HCI). This information requires new methods to archive and access multimedia information. While conventional databases allow for textual searches on metadata only[2]. In applications like medical image management, multimedia libraries, document archives, art collections, geographical information systems, law enforcement agencies, education, websites are surrounded by rich and un-optimized text description that may provide just contextual hints or semantic information about the contents. But the optimization cannot be achieved with this rich text description because most of the text is not relevant with the contents information. Moreover, the traditional keyword-based approaches require an enormous amount of human effort for manual annotation. In multimedia applications, comparisons often are not based on exact match, but rather based on similarity comparison. Therefore, there is an essential need of optimized and intelligent retrieval.

The commercial image search engines available as on date are: QBIC, VisualSeek, Virage, Netra, PicSOM, FIRE, AltaVista, etc. Region-Based Image Retrieval (RBIR) is a promising extension of CBIR [3]. Almost all the CBIR systems designed so far widely use features like color, shape and texture [4].

In this paper, we propose a Neural Network-based Image Retrieval System (NNIRS) specifically Back Propagation (BP) for training and testing. Initially all the training images are converted into feature vector (FV) containing color and texture feature. FV vector of each image is recorded in feature vector table (FVT) that is used for training and adjusting the weights of neural network. After off-line training, the weights of neural network testing data set are applied to the adjusted weight of ANN in order to retrieve most similar images.

The organization of the paper is as follows: Introduction is in Section 1, Section 2 describes the previous work related to (CBIR). Section 3 highlights the importance of using neural networks for CBIR. Overview of the Back Propagation algorithm is presented in Section 4. Section 5 outlines the various steps involved in the feature extraction while the structure of the neural network classifier is discussed in Section 6. Section 7 presents the simulation results. Finally, concluding remarks are given in Section 8.

2 Related Work

The evolution of contents based image retrieval has started from late 1970s. Till early 2000 majority of work was focused on improving the efficiency of image retrieval and the understanding of user intentions.

In 1996, Greg Pass Ramin Zabih [5] presented. histogram refinement method. Histogram refinement splits the pixels in a given bucket into several classes, based upon some local property. Within a given bucket, only pixels in the same class are compared. He described a split histogram called a colour coherence vector (CCV), which partitions each histogram bucket based on spatial coherence. In CCV approach

gap between high level concept and low level features and subjectivity of human perception was not handled effectively.

In 1997 Chad Carson, Serge Belongie, Hayit Greenspan, and Jitendra Malik [6] presented a new image representation which provides a transformation from the raw pixel data to a small set of localized coherent combine regions in colour and texture space. Like in CCV[5] is don't handle gap between high level concept and low level features subjectivity of human perception and also required image segmentation that make it computationally inefficient.

In 2000 Stefano Berretti, Alberto Del Bimbo, and Pietro Pala, [7] proposed retrieval by shape similarity using local descriptors and effective indexing. In this approach the system is intensive depend on domain knowledge and still subjectivity of human perception was given with the least weightage.

Again in 2000 Constantin Vertan, Nozha Boujemaa [8] focused on the possible embedding of the uncertainty and fuzziness regarding the colors of an image into histogram type descriptors. He embedded fuzzy logic system (FLS) in CBIR but the experimental result shows that the average precision of result was just about 57 to 58 % which is insufficient for major applications.

In 2001 Yixin Chen James Z Wang [9] proposed a soft computing approach, unified feature matching (UFM), which greatly increases the robustness of the retrieval system against segmentation related uncertainties. In the retrieval system, an image is represented by a set of segmented regions each of which is characterized by a fuzzy feature (fuzzy set) reflecting color, texture, and shape properties. It is a scheme of measuring the similarity between two images based on their fuzzified region representations. Experiment results demonstrate improved accuracy, robustness, and high speed. This approach is relatively better than previous one but there is still one deficiency that STML and optimization issue are still unattended.

In 2001 Ju Han and Kai- Kuang Ma,[10] presented a new colour histogram representation, called fuzzy color histogram (FCH). It is based on considering the color similarity of each pixel's colour associated to all the histogram bins through fuzzy-set membership function. The proposed FCH is further exploited in the application of image indexing and retrieval.

In 2003 Minakshi Banerjee and Malay K. Kundu [11] presented a robust technique for extracting edge map of an image which is followed by computation of global feature (like fuzzy compactness) using gray level as well as shape information of the edge map. Unlike other existing techniques it does not require pre segmentation for the computation of features. This algorithm is also computationally attractive as it computes different features with limited number of selected pixels. They concluded that fuzzy compactness provides a fairly good tool for indexing and be able to retrieve similar images from a heterogeneous database. In this model still the optimization and machine learning factor were missing.

Yuhang Wang, Fillia Makedon, James Ford, Li Shen Dina Goldin [12] in 2004 proposed a novel framework for automatic metadata generation based on fuzzy k- NN classification. Preliminary experiments showed very good annotation accuracy

(92% - 98% on synthetic images and 82% - 93% on real images) with only 4-5 training images. However, the system sometimes assigns a small value (less than 0.1) when zero is obviously the correct value.

In 2004 Raghu Krishnapuram, Swarup Medasani, Sung Hwan Jung, Young-Sik Choi, and Rajesh Balasubramaniam [13] discussed how fuzzy set theory can be effectively used for this purpose and describe an image retrieval system called FIRST (Fuzzy Image Retrieval SysTem). But the system is limited to the define set of images. It does not have adaptive feature and significance of optimization is still unattended.

S. Kulkarni, B. Verma¹, P. Sharma and H. Selvaraj [14] proposed a neuro-fuzzy technique for content based image retrieval in 2005. The technique is based on fuzzy interpretation of natural language, neural network learning and searching algorithms. Firstly, fuzzy logic is developed to interpret natural expressions such as mostly, many and few. Secondly, a neural network is designed to learn the meaning of mostly red, many red and few red. This approach is a beginning of intelligent CBIR system. However, the proposed model is not capable to handle object shapes and micro images like medical reports and ANN were design to learn queries not the dataset.

In 2001 Hyoung Ku LEE, Suk In Yoo [1] apply ANN specifically Radial basis function (RBF) on colour and wavelet coefficient although he achieve precision of 81.45% but with the same feature he got precision of 49% using MLP back propagation algorithm.

3 ANNIRS (Artificial Neural Network Based Image Retrieval System): Components and Structure

In this section, we first explain the architecture of the proposed approach, the ANNIRS, and then give explanation of the components of the system. Fig.1. shows the main components of the ANNIRS and the control flow among them.

The proposed approach is primarily divided into two sectors; one is training and the other is testing. First training images will be entered to an image database along with their desired output in order to have supervised learning then after extracting the color and texture feature it forms a FV and each training image has a FV and set of all FVs as recorded in description matrix table (DMT). These description vectors are provided to MLP whose weights are adjusted via back propagation (BP) algorithm [17]. The MLP architecture is used for the ANN because it is a well known fact that the MLP is a universal function approximator and it is found to be very efficient pattern classifier [17]. On the other hand a query / testing image is first converted into a feature vector and after manipulating it with the adjusted weight it gives the predicted output.

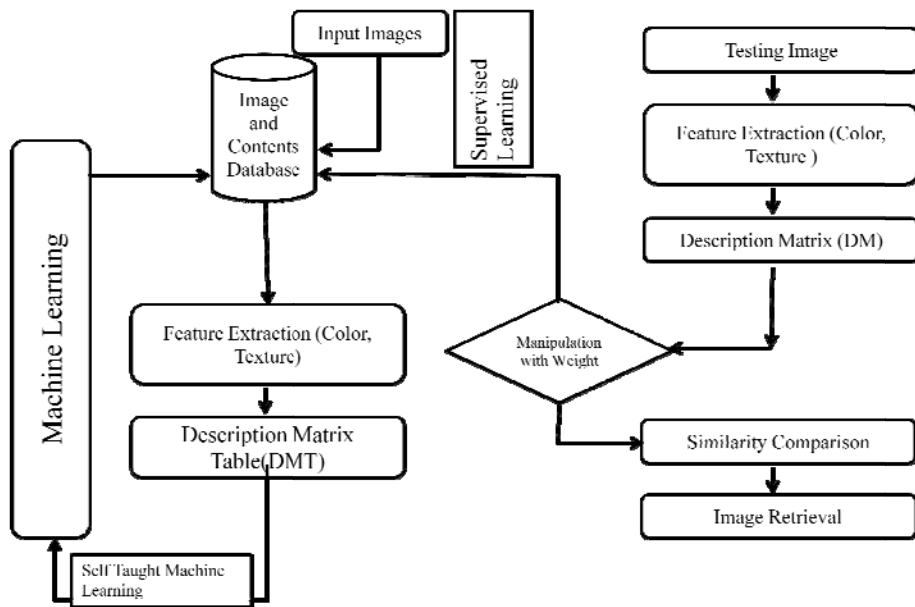


Fig. 1. Flow chart of proposed model

4 Back Propagation Algorithm

The Back Propagation (BP) algorithm involves two phases in training of patterns: a forward-propagation phase followed by a backward-propagation phase. In the first phase, the input signals are sent through the layers of the ANN. In each layer, there are computational units called neurons where a nonlinear activation function is used for the transformation of the incoming signals. Each neuron of one layer is connected with all the neurons of the next layer via link weights. In this way, the output is calculated. In the backward-propagation phase, the error is calculated by comparing the output with the desired target. This error is then used to update the weights of each link via some adaptive optimization rule. The most commonly used objective function for adaptive optimization rule is the mean-square error (MSE) which can be defined as:

$$MSE(n) = \sum_{j=1}^N (d_j(n) - y_j(n))^2 = \sum_{j=1}^N e_j^2(n) \quad (1)$$

Where $e_j(n)$ is the error between the output of the j th neuron ($y_j(n)$) and the corresponding desired response ($d_j(n)$) and N is the number of output nodes. For the modified BP algorithm, the weight associated with the i th neuron of the $(l-1)$ th layer to the j th neuron of the l th layer is updated as follows [17]:

$$w_{ji}^{(l)}(n+1) = \underbrace{w_{ji}^{(l)}(n)}_{\text{New weights}} + \underbrace{\mu(n)}_{\text{Old weights}} \underbrace{\delta_j^{(l)}(n)}_{\text{Local gradient}} y_i^{(l-1)}(n) \tag{2}$$

where μ is the learning rate and $\delta_j^{(l)}(n)$ is called local gradient associated with the j th neuron for the l th layer and can be computed according to

$$\delta_j^{(l)}(n) = \begin{cases} (d_j(n) - y_j^{(l)}(n))\phi'_j(v_j^{(l)}(n)), & \text{output layer,} \\ \phi'_j(v_j^{(l)}(n))\sum_k \delta_k^{(l+1)}(n)w_{kj}^{(l+1)}(n), & \text{hidden layer.} \end{cases} \tag{3}$$

5 Feature Extraction

5.1 The Color Feature

Color is the most prominent feature of an image. Retrieving images by color information is the most direct way among various image descriptors [15]. Here we measure the mean values and the standard deviation of the pixel colors as the color feature of an image. Every image in the database can be represented using three primaries of a color space. The most common color space is RGB. Thus, each pixel of a color image is represented by a vector.

$$Pi = \begin{bmatrix} Ri \\ Gi \\ Bi \end{bmatrix} \tag{4}$$

$$\mu = \frac{1}{M} \sum_{i=1}^M Pi \tag{5}$$

$$\sigma = \left[\frac{1}{M-1} \sum_{i=1}^M (Pi - \mu)^2 \right]^{1/2} \tag{6}$$

5.2 The Texture Feature

Texture is an important image feature that has been used for characterization of images. In this paper, the entropy is used to capture texture information in an image and is defined as follows.[15]

$$Entropy (E) = -\sum_i \sum_j C(i, j) \log C(i, j) \tag{7}$$

5.3 Feature Vector

In color based image retrieval, first the feature vector is constructed containing mean and standard deviation of RGB color and entropy of image as a texture feature.

Feature vector = [mean_red mean_green mean_blue std_red std_green std_blue entropy]

Each image in a database has a corresponding feature vector that server as image descriptor. All feature vectors are recorded in Feature Vector Table (FVT). FVT table have the ability to evolve for new input images for database.

6 The Structure of the Neural Network Classifier

ANN learning algorithm, the multi-layer perceptron is the most widely used algorithm. It is the generalized least mean square (LMS) rule, and it uses the Gradient Search method to minimize the average difference between the output and the target value on the ANN[16]. In proposed approach we used 15379 inputs with 40 input neuron and one hidden layer and one output layer with single output. Number of inputs can be reduced by SVD that causes reduction in sum of errors. We use $\tanh()$ and $\text{purelin}()$ as activation functions as output values are greater than 1. Training samples are 360 images while testing samples are 35 images.

7 Experimental Results

To study the retrieval precision of image retrieval system we implemented a prototype model on MATLAB with the following steps.

- Step 1: First we read training images from database and then transform it into matrix
- Step 2: Each matrix of the image has $M \times N \times 3$ dimension where M is the horizontal resolution, that is, 256 and N shows the vertical resolution, that is, 256 and 3 is the RGB plane. We separate each plane and then find the mean and standard deviation of each plane. After normalization we concatenate it with entropy of the image. Each feature vector contains color and texture feature.
- Step 3: Array of matrices are provided to the back propagation algorithm with 40 neurons at hidden layer.
- Step 4: Back propagation algorithm adjusts the weight of neurons. Fig.3. shows the actual output and Fig.4. shows the training output.
- Step 5: Sum of errors between actual output and output from neural network is calculated for each epoch. Results are shown in Fig.2.
- Step 6 Fig.5. shows the testing result.
- Step 7 Because of the large number of input parameters that is 15739, parameter performance of neural network is compromised. SVD is used for factorizing image. By using SVD sum of errors reduces against less number of epochs. Results are shown in Fig.6.

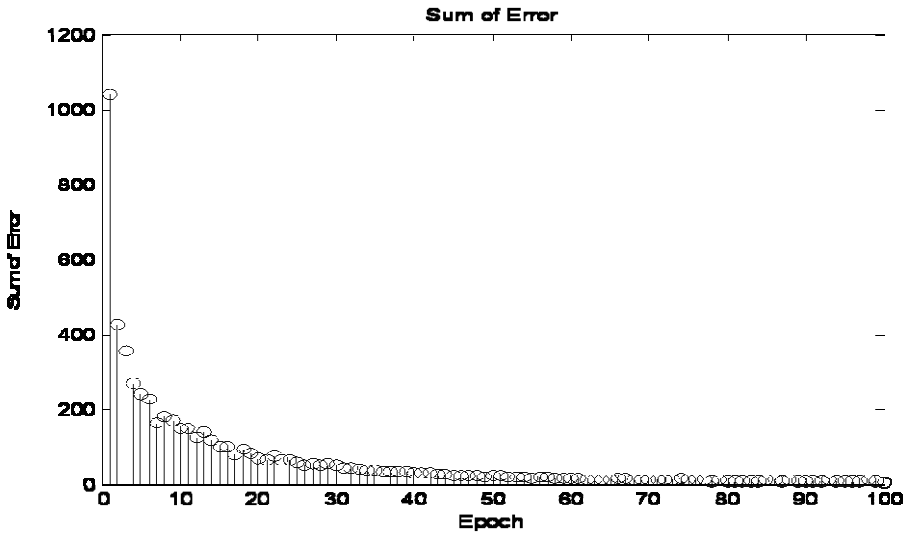


Fig. 2. Sum of error in training for 100 epoch

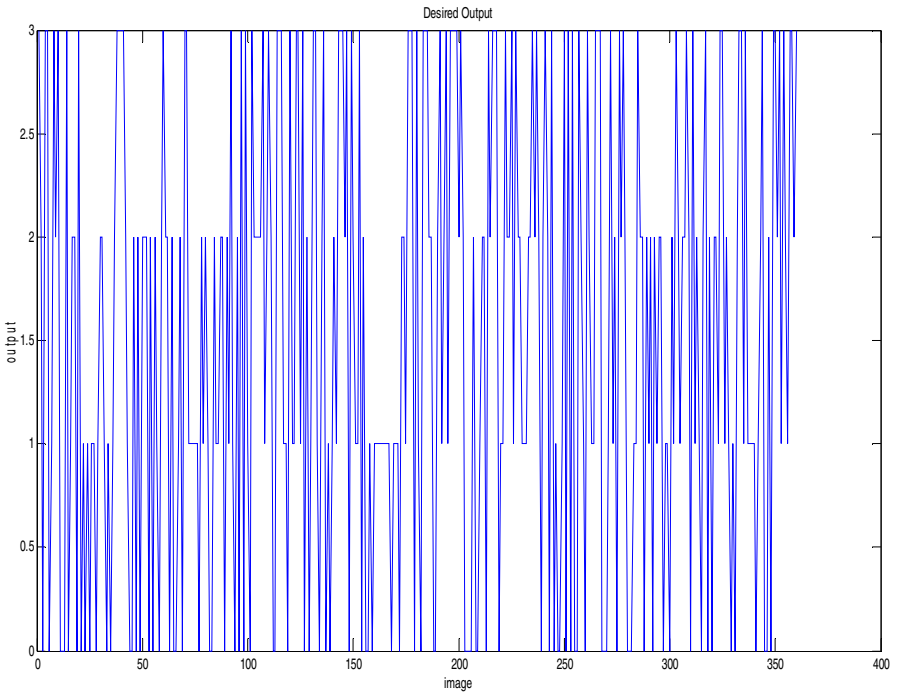


Fig. 3. Training, actual output

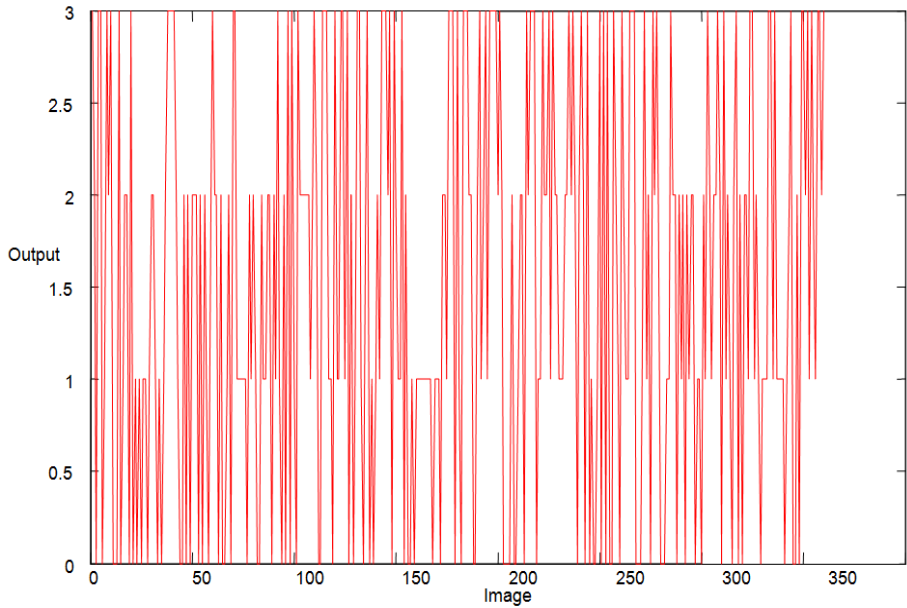


Fig. 4. Training, training output

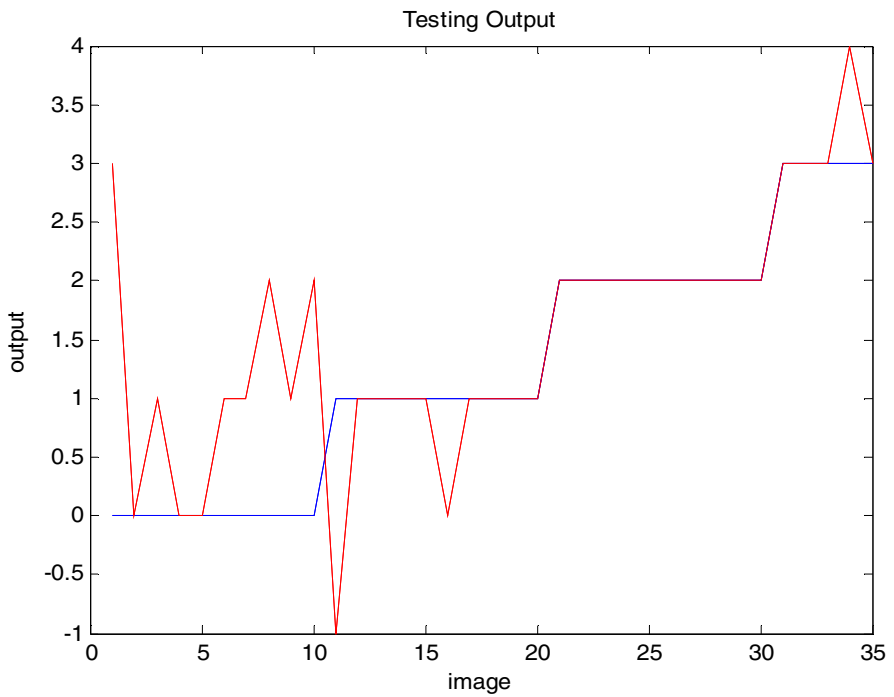


Fig. 5. Testing, Blue shows actual output and red shows trained output

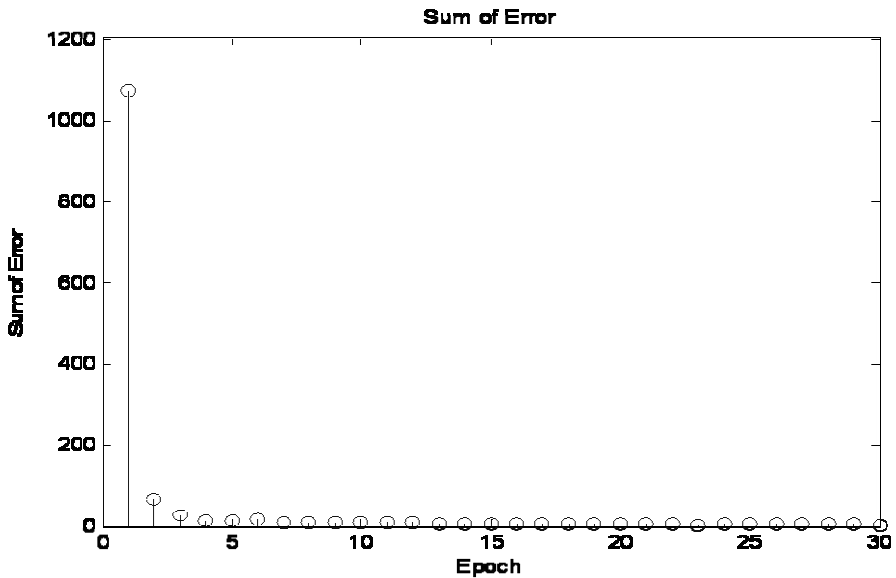


Fig. 6. Sum of error after using SVD

8 Conclusion

In this paper we propose a neural network based image retrieval system. MLP experimental results prove that by changing feature vector the precision of the system could be improved as claimed by Hyoung Ku LEE, Suk In Yoo [1]. We propose to change the feature vector as described in the paper to improve efficiency of retrieval. Experimental results show that our proposed system has improved the efficiency of retrieval by 13% (62% by our system against 49% by [1]).

Acknowledgment. We would like to thank Dr. Nadeem Qazi for his kind guidance and support.

References

1. Lee, H.K., Yoo, S.I.: Intelligent image retrieval using neural network. *IEICE Trans. Inf. & Syst.* E84-D(12) (2001)
2. Singhai, N., Shandilya, S.K.: A Survey On: Content Based Image Retrieval Systems. *International Journal of Computer Applications* (July 2010)
3. Chen, Y., Wang, J.Z.: Looking Beyond Region Boundaries. In: *Multimedia Content-Based Indexing and Retrieval Workshop, INRIA* (2001)
4. Nandagopalan, S., Adiga, B.S., Deepak, N.: A Universal Model for Content-Based Image Retrieval. *World Academy of Science, Engineering and Technology* 46 (2008)

5. Pass, G., Zabih, R.: Histogram refinement for content based image retrieval. In: WACV 1996 (1996)
6. Carson, C., Belongie, S., Greenspan, H., Malik, J.: Region Based Image Querying. This Work is Supported by an NSF Digital Library Grant (IRI 94-11334). IEEE (1997)
7. Berretti, S., Del Bimbo, A., Pala, P.: Retrieval by Shape Similarity with Perceptual Distance and Effective Indexing. IEEE Transactions on Multimedia
8. Vertan, C., Boujemaa, N.: Embedding Fuzzy Logic in Content Based Image Retrieval. In: 19th International Conference of the North American Issue Date on Fuzzy Information Processing Society, NAFIPS 2000, pp. 85–89 (2000)
9. Chen, Y., Wang, J.Z.: Looking Beyond Region Boundaries. In: Multimedia Content-Based Indexing and Retrieval Workshop, INRIA (2001)
10. Han, J., Ma, K.-K.: Fuzzy Color Histogram and Its Use in Color Image Retrieval. IEEE (2002)
11. Banerjee, M., Kundu, M.K.: Edge based features for content based image retrieval. Journal of Pattern Recognition Society Pattern Recognition 36, 2649–2661 (2003)
12. Wang, Y., Makedon, F., Ford, J., Shen, L., Goldin, D.: Generating Fuzzy Semantic Metadata Describing Spatial Relations from Images using the R-Histogram. In: JCDL 2004, June 7-11 (2004)
13. Krishnapuram, R., Medasani, S., Jung, S.-H., Choi, Y.-S., Balasubramaniam, R.: Content-Based Image Retrieval Based on a Fuzzy Approach. IEEE Transactions on Knowledge and Data Engineering 16(10) (October 2004)
14. Kulkarni, S., Verma, B., Sharma, P., Selvaraj, H.: Content Based Image Retrieval using a Neuro-Fuzzy Technique (2005)
15. Lai, C.-C., Chen, Y.-C.: Color Image Retrieval Based on Interactive Genetic Algorithm
16. Park, S.B., Lee, J.W., Kim, S.K.: Content-based image classification using a neural network. Pattern Recognition Letters 25 (2004)
17. Haykin, S.: Neural Networks: A Comprehensive Foundation, 2nd edn. Prentice Hall (1998)

An Objective Based Classification of Aggregation Techniques for Wireless Sensor Networks

Qurat-ul-Ain I. Tariq¹, Saneeha Ahmed¹, and Huma Zia²

¹ Department of Computer and Information Systems Engineering,
NED University of Engineering and Technology, Karachi, Pakistan
{qinayat, saneeha}@neduet.edu.pk

² Electronics and Computer Science Department,
University of Southampton, UK
hz2g11@ecs.soton.ac.uk

Abstract. Wireless Sensor Networks have gained immense popularity in recent years due to their ever increasing capabilities and wide range of critical applications. A huge body of research efforts has been dedicated to find ways to utilize limited resources of these sensor nodes in an efficient manner. One of the common ways to minimize energy consumption has been aggregation of input data. We note that every aggregation technique has an improvement objective to achieve with respect to the output it produces. Each technique is designed to achieve some target e.g. reduce data size, minimize transmission energy, enhance accuracy etc. This paper presents a comprehensive survey of aggregation techniques that can be used in distributed manner to improve lifetime and energy conservation of wireless sensor networks. Main contribution of this work is proposal of a novel classification of such techniques based on the type of improvement they offer when applied to WSNs. Due to the existence of a myriad of definitions of aggregation, we first review the meaning of term aggregation that can be applied to WSN. The concept is then associated with the proposed classes. Each class of techniques is divided into a number of subclasses and a brief literature review of related work in WSN for each of these is also presented.

Keywords: Aggregation, wireless sensor networks, data fusion, energy conservation.

1 Introduction

Wireless Sensor Networks (WSNs) are adhoc networks comprising of resource constrained nodes, mostly of small size and low cost, with sensing and communication capabilities. The nodes collect sensor readings and communicate them to sink, mostly outside network, also known as Base Station (BS), via neighbouring nodes. BS processes the data to get conclusions about the state of sensed environment. WSN has been identified as one of the most important technologies of 21st century and has gained popularity due to their applications in social, environmental, military, medical, disaster relief, search and rescue domains.

The nature of WSN applications requires nodes to be small and cheap which sets limitations on the available resources and capacity of these nodes. However, irrespective of resource constraints the nodes are bound to handle and transmit large amount of sensed data. Hence, a number of optimization techniques are used to minimize energy consumption, improve bandwidth utilization and increase throughput.

Aggregation is one of the common methods used to improve network lifetime in WSNs. Aggregation is a term that has been defined in literature in a number of ways, sometimes synonymously with (data or sensor) fusion. Van Renesse [1] describes aggregation as "... programmable composition of the raw data into less voluminous refined data...". Hence, aggregated result is aimed to be smaller in size and carries more relevance. Another definition found in the literature states aggregation as a process of combining data from different sources to eliminate redundancy [2]. Data fusion is a related concept that is frequently taken in similar contexts. It is defined as the combination of data from multiple sensors to achieve improved accuracy and inferences [3]. However, some researchers choose for a more generic connotation. This definition calls for the output information of fusion process to be better in 'quality' [4] or 'some sense' [5]. The criteria of betterment may be qualitative or quantitative.

We share this generic view and define aggregation as a process which, when applied on a set of data, results in an output that is an improved representation of input. The improvements are suggested to be in the form of accuracy, completeness, relevance, reliability, energy conservation, efficiency etc. In sensor networks, the input may comprise of data sensed by one sensor, collected over a period, also called *temporal aggregation*, or from a number of sensors (of same or different dimensionalities), also called *spatial aggregation*.

The efficiency of aggregation depends on a number of factors including location of sources in the network, number of sources, network density, aggregation function, routing protocol and network load. The greatest gains in performance are achieved when sources are closer to each other but far from sink [6]. However, aggregation also brings in some tradeoffs. It needs to allow adequate number of readings to be accumulated which may result in delay at intermediate nodes. Also, the prepared abridged version of data evidently lacks precision. However, careful selection of aggregation method suitable for the concerned application may help improve system performance in terms of congestion control, data accuracy and robustness.

We note that the discovery of need of aggregation in WSN has led researchers to propose various ways of exploiting this useful technique ranging from the simplest functions of average, min, sum etc. to more sophisticated Bayesian inference and Kalman filtering. Aggregation can be performed at sink having energy and computational resources in abundance. However, in-network data (sensor) fusion is found to be more effective in saving battery power by allowing partial aggregation at the nodes en route. The contribution of this work is two-fold. It provides a literature survey of aggregation techniques that have been proposed to be used in WSN to improve certain factors. Secondly, it proposes classification of methods in this large body of work in a novel manner. The classification criterion that we have chosen has been inferred from the very definition of the term aggregation. We believe that the

spirit of any aggregation technique is in the way it ‘improves the output’, hence, a good measure for categorizing the techniques. We study the ways in which quality can be improved in WSN domain and the techniques that are used to achieve this, grouping them according to the mentioned criterion.

The rest of the paper is structured in the following manner. Section 2 provides a brief overview of literature and the motivation behind this work. We introduce the classification hierarchy in section 3 with details of techniques available in each class. Section 4 concludes the paper.

2 Motivation and Related Work

There are only a handful of papers available in literature that provide consolidated review on aggregation techniques in WSN. A survey of protocols in WSN using aggregation and their impact on data latency, accuracy and energy consumption is presented in [7]. However, it does not emphasize on the computation (aggregation technique) that each node performs on the data before it is sent out. Other papers also survey the routing protocols and couple aggregation with network structure and its formation [8]. The work of [9] and [10] were found to be the closest to the ideas presented here. However, [9] groups the techniques in only two ways: 1) lossy and lossless, 2) duplicate sensitive and duplicate insensitive. Review presented in [10] is rather comprehensive but follows a different definition as it considers fusion as a broader version of aggregation and limits aggregation to summarization techniques only.

A body of research in literature has been dedicated to data centric routing protocols that employ services of an aggregator to transport data to sink in an efficient manner. One of the earliest proposals, also known as Directed Diffusion[11], is a query-based scheme and uses aggregation to reduce sensor data size while propagation to the requester. TAG[12] and COUGAR[13] use tree structure rooted at the Base station. Each node in the tree partially aggregates the data before forwarding to its parent node. Significant amount of work has also been carried out to explore heterogeneity in these schemes suggesting that aggregation should be performed by only selected nodes to better utilize network resources [14].

All the above mentioned protocols discuss the underlying routing infrastructure and suggest that any simple aggregation technique can be utilized e.g. sum, average etc. to provide the proof of concept. This work is focused on the aggregation functions applied on the sensed/received data. We consider aggregator as a separate process at each node working on top of routing protocol. It receives input from the routing layer, processes it for improvement and hands it back to the layer. A range of candidate algorithms to be executed by the aggregator are discussed below.

3 Classification

We present a classification of aggregation functions with respect to the purpose of their design focusing on in-network aggregation techniques only. We note that

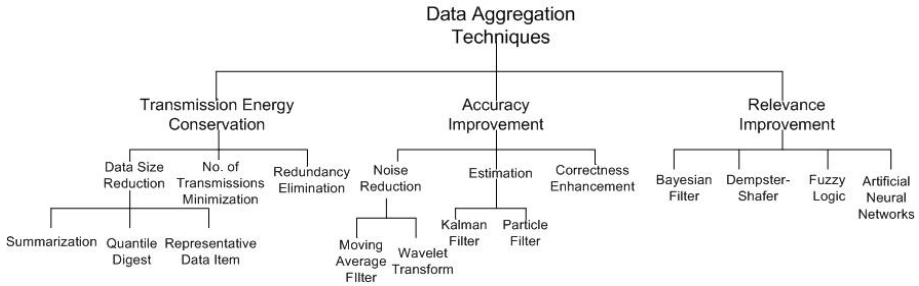


Fig. 1. Classification Hierarchy of Aggregation Techniques

various aggregation techniques are developed to achieve specific objectives e.g. reducing data size, improving reliability, confidence of the information, minimizing transmission energy etc. Classification hierarchy is shown in figure 2. Definition of each class with brief overview of how it has been used in WSN is given in the subsections below. Note that data size reduction is a by-product of most of these functions.

3.1 Transmission Energy Conservation

We know that transmitting 1 bit consumes as much energy as processing about 1,000 instructions [15]. This class encompasses algorithms that process sensed data to save transmission power. These techniques combine data to produce output that requires lesser energy for onward transmission. We divide this class in three sub-classes.

Data Size Reduction

This class represents a set of techniques that are particularly useful when the goal is to have the size of aggregated data, approximately equal to a single un-aggregated value. The following different types of methods are commonly used in WSN.

Summarization Techniques: Algorithms under this class attempt to find one single quantity extracted from the entire set of sensor readings. Most common functions such as average, min, max and count fall under this category. A sophisticated algorithm to calculate simple average using partial sum and count values has been demonstrated in [16] for query-based systems. Similarly, an algorithm for reporting only the most frequently occurring items is proposed in [17]. Another work uses weighted average to merge data from proximate groups [18].

Quantile Digest : Quantile is the division of ordered data into some equal sized data subsets. Q-Digest dynamically partitions the data set aiming to have partitions of almost same size. An algorithm for calculating quantile, specially median, of values reported by multiple sensors in a distributed manner while keeping errors within a certain bound, has been described in [19]. A node is placed in q-digest:

- i. If its count is not greater than n/k ; and
- ii. If sum of counts of the node, its parent and siblings is greater than n/k .

Where n is the total number of readings and k is a compression factor. This work is an extension of [20] that used histograms for estimation of median and other quartiles.

Representative Data Items: This technique is used to find a relatively small number of parameters or variables that represent an entire class of data items. We restrict ourselves to two common methods of this subclass due to space limitations.

Principle component analysis is a statistical technique used to convert a large set of highly correlated observations into a smaller set of uncorrelated values called principle components. This approach is used in [21] to find a small number of readings that represent large data sets in an accurate manner. Moreover, it has been demonstrated that good approximation of sensor measurements can be obtained by relying on few principle components [22].

Pattern coding is used when sensor readings can be grouped into classes and assigned concise codes. Sensors send these codes instead of actual readings to higher level aggregator (parent or CH) and achieve reduced transmission size [23]. CH may suppress duplicate codes and second phase may involve retrieving actual data values, if required.

Number of Transmissions Minimization

This class of algorithms repackages the received set data into one packet to avoid multiple transmissions without information loss. The scheme attempts to reduce packet's header overhead only. It has been shown that energy saving is more effective for small payload size [24]. It is mostly employed when either the network is not heavily overloaded or when higher granularity of data is required at sink. [25] demonstrates the use of aggregation by concatenation to solve consensus in WSN.

Redundancy Elimination

This class of algorithms exploits the simple fact that data sensed by nodes in close proximity is highly correlated. The simplest form of this technique is duplicate suppression[6], [23], [18] where only one copy among the duplicates received from multiple sensors is forwarded to higher level node. Data redundancy has serious impact on correctness of information in protocols which use duplicate sensitive functions like count, sum, average for computation of final result. OPAG[26] uses multi-path routing for reliable dissemination but prevents data from being aggregated more than once by letting each node choose its aggregator and pad the message with aggregator ID. This ensures that only the nominated nodes aggregate the encapsulated data whereas others will merely forward the redundant copies.

3.2 Accuracy Improvement

Algorithms in this class deal with data with the objective that the aggregate data has lesser impurities and higher precision. Aggregators analyse the data set, look for

associations and/or anomalies, relate it with the history and produce data that has better accuracy. This class is divided into three sub-classes given below.

Noise Reduction

Algorithms in WSNs process data that is prone to distortions and noise due to hardware transient faults and deployment in rough environments. Hence, noise removal techniques are applied to pre-process the sensed data before it can be used any further. These are temporal aggregation techniques that work on some predefined bounds to remove noise or unwanted spiky values in sensor readings. Two types of noise reduction techniques were found to be commonly used in WSN.

Moving Average Filter: It is a relatively simple technique to remove noise from digital signal streams in time domain. Simple arithmetic mean of a number (window size) of last sensor readings is calculated to produce each point in the output signal. This technique is demonstrated to effectively filter unwanted signal from the observations of magnetic, acoustic and thermal sensors in [27]. To ensure realistic filtering, the threshold is adjusted over time with respect to maximum signal strength of the observation.

Wavelet Transforms: Wavelets provide resolution at particular time and frequency, which makes them suitable for wireless sensor networks. Signals can be easily categorized by observing their behavior e.g. discontinuities or peaks. A number of variations with advanced features like compression [28], multi-resolution features for reproduction of signal [29], fast computation of coefficients [30] etc. have been used in WSN to smoothen input data streams.

Estimation

Estimation theory is about approximating unknown parameters based on the measured data. It uses law of probability to compute state of various field properties e.g. temperature, humidity, target location, object velocity etc. Improvement in accuracy is dependent on the knowledge of noise and probability distribution of the measured data. This section discusses two estimation methods commonly used in WSN known as Kalman Filtering and Particle Filtering. These techniques have been widely used in WSN for applications like aerospace and marine navigation, target tracking and target localization.

Kalman Filter: It is a mathematical model used to estimate the state of a process with minimal mean of the squared error. It works in two steps: prediction of current state (based on previous state estimate and its covariance) and updating estimate of current state (based on first step prediction and new measurement). Kalman filtering is well-suited to the resource constrained WSN as it does not rely on the entire history of information.

Kalman filters have been effectively used to predict data routes in mobile sensor networks by choosing paths with high delivery probability based on favorable

movement patterns and available resources [31]. A move from the centralized approach was proposed in [32] for WSN applications like tracking target [33] and reaching consensus [34]. This involved decomposing the filter into a number of distributed filters and associating them with consensus filters to get better estimates by incorporating readings of neighboring nodes.

In unreliable communication channels, effect of communication delays and data loss cannot be ignored. Kalman filter has been used in such scenarios to calculate threshold on the arrival rate readings, catering for affected intermittent arrivals [35].

Particle Filter: It is a nonlinear filter that performs estimation using sequential Monte Carlo methods to approximate probability density function of target state. The main idea is to represent the required posterior density functions by a set of random samples (particles) with associated weights and to compute estimates based on these. The filter outperforms traditional Kalman filter due to its ability to incorporate Non-Gaussian noise and detect targets with variable levels of intensity.

Distributed particle filter (PF) has been used to track moving target in [36] and [37] while keeping communication overhead to minimum. Advancements have also been proposed to cater for multi-modal sensor data [38], simultaneous detection and tracking of mobile target [39] and to compensate for the imperfect nature of the communication channel between sensors and fusion center [40].

Correctness/Reliability Enhancement

WSN nodes often find their applications in harsh and vulnerable conditions where nodes are susceptible to failures and sensed data may suffer transmission losses, inconsistencies and errors. This necessitates incorporation of a mechanism which can identify and discard spurious values to improve correctness of results. Specialized aggregation methods are designed that involves rounds of communication between neighboring nodes for sharing their observations to reach consensus on detection of the event of interest [41-43]. Each node makes use of spatial redundancy present in the network and updates its decision based on majority votes. As can be easily imagined, such techniques conserve less energy when higher accuracy is needed. Similar trend can be observed for aggregation latency.

Another type of algorithms in this class attempts to improve reliability by using trust model. Each node assigns trust rating to its neighbours on the basis of past records and accordingly decides to consider/ignore neighbour's observations [44].

3.3 Relevance Improvement (Inference)

This class of algorithms process data to draw some conclusion about system state based on some known and true set of parameter readings. These techniques build better understanding of the event/situation under observation and conjecture its state based on correlated low level data collected from the network. The result is of more relevance to the employing application and helps decide upon necessary actions. The methods discussed here are more complex than most of the previous classes. They are widely used in WSNs for target tracking, localization and event detection applications. We discuss four mechanisms in this class below.

Bayesian Filtering

It is the process of making inferences about a hypothesis from some evidence (in the form of measured data) using famous Bayes' probability model. An interesting WSN application of this technique is detection of faulty measurements using estimate of sensors' true reading given the neighbours' readings[45]. It has also been used to conserve energy by allowing a subset of nodes to sleep [46]. The missing data is then inferred at sink from the observed data of 'awake' nodes and prior probability distribution of the field being sensed. A multi-sensor fusion scheme using Bayesian inference for target detection is proposed in [47], wherein target's position and velocity is conjectured by combining multiple sensors' observations and prior information of target's position

Dempster-Shafer Inference

The Dempster-Shafer method is known as the theory of belief functions. Unlike Bayesian method, it does not need probabilities to be assigned to unknown propositions a priori. Degree of belief is obtained by combining available evidence from different sources. Dempster-Shafer Inference method has been used in [48] to achieve better battlefield picture fusing uncertain information in Airborne Sensor Networks. Each sensor gives a list of target types with different confidence levels which are then fused to classify the target types. Another application has been demonstrated in [49] to detect real-time events. Evidence of a sub event is reported in both temporal and spatial spectrum. Aggregator uses confidence function to calculate degree of belief which is incorporated in the final decision at sink. Furthermore, it has also been used to analyze data traffic for detection of failed aggregator nodes [50]. Greater decay in traffic indicates failure and activates topology rebuilding.

Fuzzy Logic

Fuzzy logic has been used for inference when the inputs are impure or conventional boolean solutions cannot be applied. Such inputs are fuzzified using a certain membership function. The outputs of these functions are supplied to an inference engine, which then generates fuzzified output, based on some output membership function. Generally, it is left to the application to obtain crisp output if required.

Due to the complexity of fuzzy engine, majority of the work available in literature performs inference task at the sink [51]. However, greater benefits can be achieved if the engine is implemented in a distributed manner over the nodes. A relevant example uses cluster heads to host inference engine to fuse collected data and identify the event [52]. Fuzzy logic is often used in conjunction with Artificial Neural Networks.

Artificial Neural Networks

Artificial Neural Networks (ANN) are used to extract patterns and detect trends that are too complex to be noticed by either humans or conventional computing techniques. Massive parallelism of very simple basic units called neurons, analogous

to the large number of sensors, has gained attention of scientists working on WSNs. The network is divided into connected layers of neurons, each producing outputs based on weighted sum of inputs and bias. Error at the final output is used to dynamically adjust interconnection weights.

Initial training is needed for supervised ANNs and is mostly performed at the sink after which the weights and thresholds of each layer are sent to the corresponding nodes. Aggregation scheme of [53] uses CHs as both hidden and output layer neurons whereas cluster members serve as input layer neurons. The task of CHs is to send the data that represents features of the sensed raw data to the sink, thereby reducing number of transmissions and removing redundant information.

ANN can easily be used to fuse multi-sensor data and can be extended with fuzzy and/or wavelet layers to perform more complex computations. For example, a 12 layered fuzzy NN to fuse four dimensional sensor readings for deducing fire emergency can be found in [54]. Similarly, In [55] a sensor net has been proposed that identifies intrusions using an unsupervised ANN based on fuzzy adaptive resonance theory (ART). Wavelets are also used here for preprocessing data.

4 Conclusion

Aggregation has been increasingly used in WSNs as an effective way of improving network lifetime. In-network aggregation is particularly used in data centric protocols due to evidence of significant gains in energy conservation. It covers a multitude of algorithms varying in complexity and level of operation ranging from simple summarization techniques to complex inference mechanisms. The survey presented in this paper indicates that selection of a technique is majorly influenced by the concerned WSN application domain and specification of the problem for which the WSN is deployed. We believe that the classification of these techniques with respect to type of improvements they offer will assist this selection. This is an on-going work and preparation of a more comprehensive classification in the form of a journal paper is underway.

References

1. Van Renesse, R.: The importance of aggregation. In: Dignum, F.P.M., Cortés, U. (eds.) AMEC 2000. LNCS (LNAI), vol. 2584, pp. 87–92. Springer, Heidelberg (2001)
2. Kalpakis, K., Dasgupta, K., Namjoshi, P.: Efficient algorithms for maximum lifetime data gathering and aggregation in wireless sensor networks. *Computer Networks* 42(6), 697–716 (2003)
3. Hall, D.L., Llinas, J.: An introduction to multisensor data fusion. *Proceedings of the IEEE* 85(1), 6–23 (1997)
4. Wald, L.: Some terms of reference in data fusion. *IEEE Transactions on Geoscience and Remote Sensing* 37(3), 1190–1193 (1999)
5. Dasarathy, B.V.: Information fusion-what, where, why, when, and how? *Information Fusion* 2(2), 75–76 (2001)

6. Krishnamachari, L., Estrin, D., Wicker, S.: The impact of data aggregation in wireless sensor networks. In: Proceedings of 22nd Intl. Conf. on Distributed Computing Systems Workshops. IEEE (2002)
7. Rajagopalan, R., Varshney, P.K.: Data-aggregation techniques in sensor networks: a survey. IEEE Communication Surveys & Tutorials 8(4), 48–63 (2006)
8. Laukik Chitnis, A.D., Ranka, S.: Aggregation Methods for Large Scale Sensor Networks. ACM (2006)
9. Fasolo, E., et al.: In-network aggregation techniques for wireless sensor networks: a survey. IEEE Wireless Comm. 14(2), 70–87 (2007)
10. Nakamura, E.F., Loureiro, A.A.F., Frery, A.C.: Information fusion for wireless sensor networks: Methods, models, and classifications. ACM Computing Surveys (CSUR) 39(3), 9-es (2007)
11. Intanagonwiwat, C., et al.: Directed diffusion for wireless sensor networking. IEEE/ACM Transactions on Networking 11(1), 2–16 (2003)
12. Madden, S., et al.: Tag: a tiny aggregation service for ad-hoc sensor networks. ACM SIGOPS Operating Systems Review 36(SI), 131–146 (2002)
13. Yao, Y., Gehrke, J.: The cougar approach to in-network query processing in sensor networks. SIGMOD Record 31(3), 9–18 (2002)
14. Vivek Mhatre, C.R.: Design guidelines for wireless sensor networks: communication, clustering and aggregation. Ad Hoc Networks Journal 02, 45–63 (2004)
15. Ammar, K., Nascimento, M.A.: Histogram and Other Aggregate Queries in Wireless Sensor Networks, 2011, Dept. of Computing Science. University of Alberta. Canada, TR-11-03 (February 2011)
16. Hellerstein, J., et al.: Beyond average: Toward sophisticated sensing with queries. Springer, Heidelberg (2003)
17. Manjhi, A., Nath, S., Gibbons, P.B.: Tributaries and deltas: efficient and robust aggregation in sensor network streams. In: Proc. of the ACM SIGMOD International Conference on Management of Data. ACM (2005)
18. Khedo, K., Doornik, R., Aucharuz, S.: READA: Redundancy Elimination for Accurate Data Aggregation in Wireless Sensor Networks Open Access. Elsevier Computer Networks 38(4), 393–422
19. Shrivastava, N., et al.: Medians and beyond: new aggregation techniques for sensor networks. ACM (2004)
20. Greenwald, M.B., Khanna, S.: Power-conserving computation of order-statistics over sensor networks. ACM (2004)
21. Masiero, R., et al.: Data acquisition through joint compressive sensing and principal component analysis. IEEE (2009)
22. Le Borgne, Y., Bontempi, G.: Unsupervised and supervised compression with principal component analysis in wireless sensor networks. In: 13th ACM International Conference on Knowledge Discovery and Data Mining, pp. 94–103. ACM Press, NY (2007)
23. Cam, H., et al.: Energy-efficient secure pattern based data aggregation for wireless sensor networks. Computer Comm. 29(4), 446–455 (2006)
24. He, T., Bium, B.M., Stankovic, J.A., Abdelzaher, T.: AIDA: Adaptive Application Independent Data Aggregation in Wireless Sensor Networks. ACM Transactions on Embedded Computing System
25. Köpke, A., Karl, H., Wolisz, A.: Consensus in WSN—Identifying critical protocol mechanisms. In: GI/ITG Fachgespräch Drahtlose Sensornetze, p. 39. Universität Karlsruhe, Karlsruhe, (TH)(February 2004)

26. Chen, Z., Shin, K.G.: OPAG: Opportunistic data aggregation in wireless sensor networks. In: Real-Time Syst Symp. IEEE, Barcelona (2008)
27. Gu, L., et al.: Lightweight detection and classification for wireless sensor networks in realistic environments (2005)
28. Sheybani, E.: Dimensionality Reduction and Noise Removal in Wireless Sensor Networks. In: 4th IFIP International Conference on New Technologies, Mobility and Security (NTMS). IEEE (2011)
29. Kulakov, A., Davcev, D., Trajkovski, G.: Application of wavelet neural-networks in wireless sensor networks. Software Engineering, Artificial Intelligence, Networking and Parallel/Distr. Computing (2005)
30. Ciancio, A., Ortega, A.: A distributed wavelet compression algorithm for wireless multihop sensor networks using lifting. In: Proceedings of Acoustics, Speech, and Signal Processing (ICASSP 2005). IEEE (2005)
31. Mascolo, C., Musolesi, M.: SCAR: context-aware adaptive routing in delay tolerant mobile sensor networks. In: Proceedings of the 2006 International Conference on Wireless Communications and Mobile Computing. ACM (2006)
32. Olfati-Saber, R.: Distributed Kalman filtering and sensor fusion in sensor networks. Networked Embedded Sensing and Control, 157–167 (2006)
33. Olfati-Saber, R., Sandell, N.F.: Distributed tracking in sensor networks with limited sensing range. In: American Control Conference. IEEE, Seattle (2008)
34. Spanos, D.P., Olfati-Saber, R., Murray, R.M.: Approximate distributed Kalman filtering in sensor networks with quantifiable performance. In: 2005 Fourth International Symposium on Information Processing in Sensor Networks (IPSN). IEEE Press (2005)
35. Sinopoli, B., et al.: Kalman filtering with intermittent observations. IEEE Transactions on Automatic Control 49(9), 1453–1464 (2004)
36. Djuric, P.M., Vemula, M., Bugallo, M.F.: Tracking with particle filtering in tertiary wireless sensor networks. IEEE (2005)
37. Coates, M.: Distributed particle filters for sensor networks. ACM (2004)
38. Wong, Y., et al.: Collaborative data fusion tracking in sensor networks using monte carlo methods. IEEE (2004)
39. Ahmed, N., et al.: Detection and tracking using wireless sensor networks. In: Proceedings of the 5th International Conference on Embedded Networked Sensor Systems. ACM (2007)
40. Ozdemir, O., Niu, R., Varshney, P.K.: Tracking in wireless sensor networks using particle filtering: Physical layer considerations. IEEE Transactions on Signal Processing 57(5), 1987–1999 (2009)
41. Swaszek, P.F., Willett, P.: Parley as an approach to distributed detection. IEEE Transactions on Aerospace and Electronic Systems 31(1), 447–457 (1995)
42. Quek, T.Q.S., Dardari, D., Win, M.Z.: Energy efficiency of dense wireless sensor networks: To cooperate or not to cooperate. IEEE Journal on Selected Areas in Communications 25(2), 459–470 (2007)
43. Van Dyck, R.E.: Detection performance in self-organized wireless sensor networks. IEEE (2002)
44. Probst, M.J., Kasera, S.K.: Statistical trust establishment in wireless sensor networks. IEEE (2007)
45. Krishnamachari, B., Iyengar, S.: Distributed bayesian algorithms for fault-tolerant event region detection in wireless sensor networks. IEEE Transactions on Computers 53(3), 241–250 (2004)

46. Hartl, G., Li, B.: infer: A Bayesian inference approach towards energy efficient data collection in dense sensor networks. *IEEE* (2005)
47. Cou, C., et al.: Multi-sensor data fusion using Bayesian programming: An automotive application. In: *IEEE/RSJ International Conference on Intelligent Robots and Systems*. *IEEE* (2002)
48. Yu, B., et al.: Uncertain information fusion for force aggregation and classification in airborne sensor networks. In: *AAAI 2004 Workshop on Sensor Networks*. *AAAI Press* (2004)
49. Li, S., et al.: Event detection services using data service middleware in distributed sensor networks. *Telecom Systems* 26(2), 351–368 (2004)
50. Nakamura, E.F., et al.: Using information fusion to assist data dissemination in wireless sensor networks. *Telecommunication Systems* 30(1), 237–254 (2005)
51. Su, W., Bougiouklis, T.C.: Data fusion algorithms in cluster-based wireless sensor networks using fuzzy logic theory. In: *ICCOM 2007 Proceedings of the 11th Conference on 11th WSEAS International Conference on Communications*. *WSEAS* (2007)
52. Manjunatha, P., Verma, A., Srividya, A.: Multi-Sensor Data Fusion in Cluster based Wireless Sensor Networks Using Fuzzy Logic Method. In: *Industrial and Information Systems, ICIIS 2008*. *IEEE* (2008)
53. Sun, L.Y., Cai, W., Huang, X.X.: Data aggregation scheme using neural networks in wireless sensor networks. In: *2010 2nd International Conference on Future Computer and Communication (ICFCC)*. *IEEE* (2010)
54. Sung, W.T., et al.: Multi-sensors data fusion for precise measurement based on ZigBee WSN via fuzzy control. In: *2010 International Symposium on Computer Communication Control and Automation (3CA)*. *IEEE* (2010)
55. Li, Y.Y., Parker, L.E.: Intruder detection using a wireless sensor network with an intelligent mobile robot response. In: *Southeastcon*. *IEEE* (2008)

A New Data Compression Technique Using an Evolutionary Programming Approach

Fahad Ullah¹ and Khawaja M. Yahya²

¹Department of Computer Systems Engineering University of Engg. and Technology Peshawar, PK

fahadullah@nwfpuet.edu.pk

²Department of Electrical Engineering University of Engineering and Technology Peshawar, PK

yahyakm@yahoo.com

Abstract. Data compression is a necessary technique required in various scenarios these days from data communication to data storage. Text is an important form of data used ubiquitously in different communications and in computer world. This paper presents a novel data compression technique that uses an evolutionary programming approach for the compression process. Text is used as the experimental data in this research. By using evolution, the best compression method(s) are chosen in order to achieve maximum compression accuracy. For different experiments, the compression extent is measured and also the results are compared with the compression methods, individually. The results reveal the commendable performance of the system and the effect of evolution on the overall compression.

Keywords: evolutionary programming, genetic algorithms, textual compression, compression ratio.

1 Introduction

Text has been an import form of data used in data communication as well as data storage. Although vivid media such as pictures and video are dominating over internet yet, textual data is still needed in various situations and scenarios. For instance, email, instant messaging, e-books and many other amenities that are part of the internet and communication world all heavily rely on the textual data. Compression or to be more precise, data compression is a technique that is applied on a particular form of untouched data in order to compress the data. Because the compressed data occupy less space hence higher the extent of compression, better is overall performance of the system that can either be some database or some communication system. Data compression can either be lossy or lossless. In picture and video, lossy compression is permissible for the reason that the information can still be obtained from those media. In contrast, textual compression has to be lossless because any loss in text after decompression will, at worse, make it useless. The most widely used criterion to measure the extent of compression is called compression ratio and it is given by:

$$\text{Compression Ratio} = \frac{\text{Compressed Data}}{\text{Uncompressed Data}}$$

A number of techniques have been deployed for text compression in past. C.Y. Teng et al. proposed an improved version of Bugajski-Russo N-gram algorithm. They showed substantial improvements in results in contrast to other contemporary algorithms of the same complexity [1]. F.S. Awan et al. presented Length Index Preserving Transform (LIFT), a lossless dictionary based transformation. The transformation could then be used with the source text in order to improve the overall compression rate of a text compression algorithm [2]. W. Sun et al. presented a dictionary based fast lossless text transformation algorithm that they called StarNT. Based on the algorithm, they developed a compression utility called StarZip which had improved results in compression in contrast to its contemporary applications [3]. L. Robert et al. proposed a reversible transformation technique in order to produce minimum bytes of intermediate data when the transformation was applied on the actual source text [4]. F. Ullah et al. used steganographic approach to text compression by hiding textual data in an image that could also work as a key and hence achieved compression with confidentiality [5].

Evolutionary algorithms such as Genetic Programming (GP) [6] and Cartesian Genetic Programming (CGP) [7] etc. are recently developed concepts that tend to mimic the concepts of natural evolution. By using artificial evolution, those algorithms have been successful in solving various problems with much higher accuracy in the results obtained. Evolutionary algorithms and other bio-inspired techniques such as Artificial Neural Network (ANN) have been used many times for data compression in the past. J. Schmidhuber et al. used sequential ANNs in combination with statistical coding techniques to achieve compression in some text files. By using their model, the compression ratio was better than other compression algorithms they used for comparison [8]. V. Aysha presented a parallel genetic algorithm compression model for scanned documents. Their algorithm had better results both in terms of compression ratio and execution time [9]. A. Kattan [10] et al. proposed GP-ZIP, a genetic programming based data compression utility. In their research, they made GP to select optimal compression algorithm in a number of standard compression algorithms for a particular chunk of data. They later introduced GP-ZIP* [11] and GP-ZIP3 [12] with many modifications and improvements.

This research is very closely based on work in [10] but it rather uses a different approach. In this paper an evolutionary algorithm is proposed that borrows features from both GP and CGP. In the compression process text is used as the experimental data because of the higher redundancy that textual data possess, the compression ratio is much prominent as compared to other forms of data such as images or video. Different standard data compression algorithms are used and selected based on the evolution process. The results obtained are compared with the individual standard compression models.

Section 2 of the paper presents the evolutionary algorithm in details. Section 3 details the experimental setup with both compression and decompression modules. Section 4 of the paper elaborates on the simulation and results. Finally the research is concluded in Section 5.

2 Proposed Model

Fig. 1 summarizes the genotype formation in the proposed evolutionary algorithm. The algorithm contains nodes just like CGP but instead of implementing simple functions, the nodes implements complete algorithms. The number of nodes in the system, as fig. 1 suggests, must equals the number of inputs to the system. C_1 through C_n are the inputs to the network and the different algorithms are represented by letters, for instance A, B, C, and so on. The genotype formation block generates the final genotype as shown in the figure. The genotype contains ordered pairs of the node function that it is implementing and also the system input that is connected to the particular node. The algorithm follows the following steps:

1. Form the parent genotype by randomly developing the genotype; assign a random function (algorithm) to the node and connect it with an input from the given list of system inputs.
2. Start the mutation process. In mutation, take the parent genotype and produce λ number of offspring based on the mutation rate set by the user. (The $1 + \lambda$ strategy for offspring is the same as it is used in CGP. The functions (algorithms) and the inputs to the node are changed randomly in the mutation process.)
3. In the mutation process, only choose the algorithm the node is implementing in a random way. For mutation in inputs, swap the inputs of two nodes with each other in a random fashion. This resembles crossing-over in GP.
4. Continue the mutation process and select the best among the parent and the offspring based on their fitness. (The fitness can be any error criterion set by the user and in this research, it is the compression ratio.)
5. Stop the evolution process if some break condition is reached i.e. a specific number of generations or the desired value of fitness.

The phenotype in this case is just the architectural representation of the genotype and fig. 1 itself contains the image of the phenotype. However, unlike CGP, there is no junk node formation in this case because as mentioned before, the number of inputs must be the same as the number of nodes in the network. Figure 2 represents the steps involved in the evolution process.

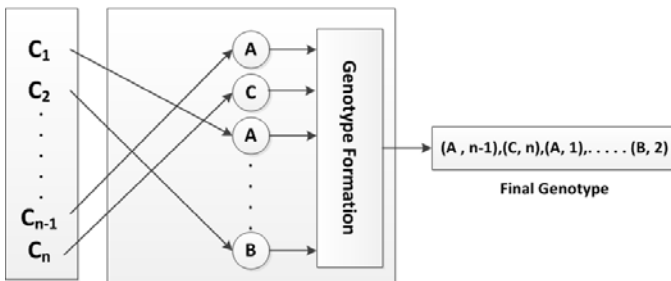


Fig. 1. Genotype formation using the evolutionary model

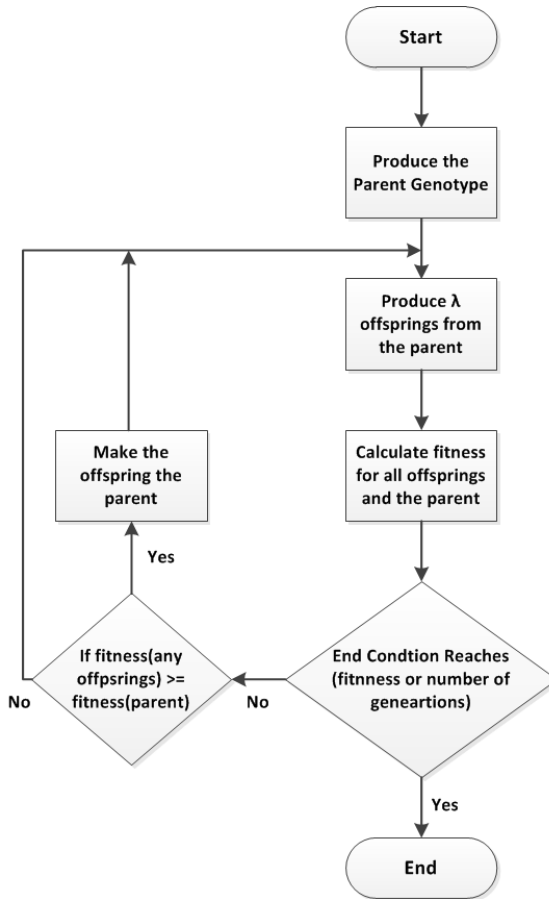


Fig. 2. The evolution process

3 Experimental Setup

The experimental setup is based on the two essential parts of a data compression model; the compression module and the decompression module. A communication model is considered in which data is compressed by the compression model and sent over the channel where it is received by the decompression model and hence decompressed. Before the model is implemented, the evolutionary algorithm model is trained on a set of textual data. After the training has been completed, the testing dataset is used in order to test the system in various scenarios.

3.1 Compression Module

Compression module is the principle part of the system. Based on the compression ratio, the system is trained until the desired results are obtained. Fig. 3 summarizes the compression module.

The data is in the form of text and it is read from the system and fed to the compression model. The compression model uses the evolutionary algorithm based model for the compression purpose. The compression model converts the input text into a number of chunks based on the user requirements. The number of nodes in the system equals the number of chunks of the textual data. Finally the system start evolution based on different parameters like mutation rate, number of offspring and the number—and types—of functions (compression algorithms) as set by the user. After the data has been compressed, the output containing the compressed data as well as the genotype is sent across the channel. The genotype must be sent with the data as the decompression module will require it for the decompression process.

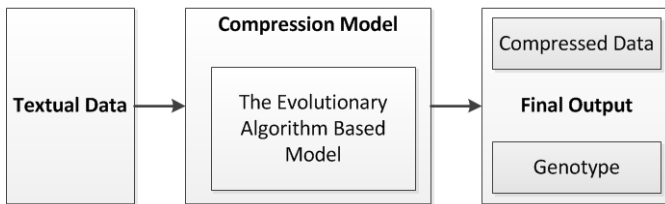


Fig. 3. The Compression Module

3.2 Decompression Module

The decompression module receives the compressed data over the channel. The data received is decompressed and the actual textual data is obtained. Fig. 4 depicts the decompression module in details.

The received data has both the compressed data as well as the genotype. The genotype will act as a key for the decompression process. The received data is forwarded to the decompression model where decompressing functions—or the corresponding algorithms that were used in compression process—are used on the compressed data. The “Key” in the Decompression model uses the genotype in order to decompress the data in a lossless and an accurate way. The final output represents the actual data after the decompression process.

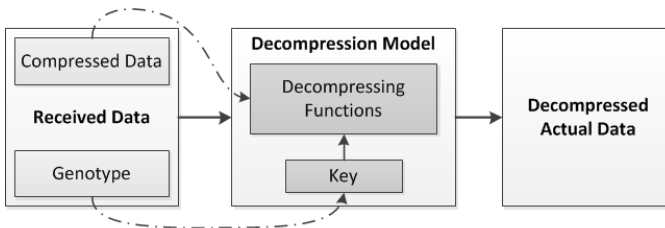


Fig. 4. The Decompression Module

4 Simulation and Results

MATLAB was used for simulation purpose. The textual data was based on Alexander Pope's "Eloisa to Abelard" [13] in such a way that different portions of the poem were copied in a repetitive manner into a same text file. For testing purpose, the same text source was used yet with different portions copied numerous times into the file. The mutation rate set in the simulation process was 10%. In $1 + \lambda$ offspring generation strategy, λ was set to 3. The functions or the compression algorithms used were Huffman coding [14], Running Length Encoding (RLE) [15] and Lempel-Ziv-Welch (LZW) algorithm [16]. For different number of chunks the results were analyzed. Table 1 and 2 summarize the training and testing results respectively.

Table 1. Training Results

S/N	Number of Chunks	Uncompressed Size	Compressed Size	Compression Ratio
1	4	17,568 bytes	5207 bytes	0.296
2	6	17,568 bytes	6049 bytes	0.344
3	8	17,568 bytes	5248 bytes	0.298
4	12	17,568 bytes	5823 bytes	0.331

Table 2. Testing Results

S/N	Number of Chunks	Uncompressed Size	Compressed Size	Compression Ratio
1	4	20,674 bytes	6161 bytes	0.298
2	6	20,674 bytes	7049 bytes	0.341
3	8	20,674 bytes	6098 bytes	0.295
4	12	20,674 bytes	7008 bytes	0.339

Both table 1 and table 2 show the results in terms of the compression ratio for different number of chunks into which the textual data is divided. The number of chunks also shows the number of nodes that the system contains. Fig. 5 gives the depiction of both training and testing results in the form of their respective curves for different number of nodes or chunks. Because the proposed system uses lossless textual compression algorithms, the decompression accuracy is 100 percent, that is, the text is retrieved in the decompression module in a lossless manner.

In table 3 below, a comparison has been made in terms of compression ratio. The proposed compression model is compared with the individual compression algorithms. As obvious from the table, the proposed model has overall better compression ratio in contrast to the compression algorithms that it is using for the text compression. Note that this algorithm itself hasn't been compared with other methods such as [8] or [10]. That is because this research tends to test the compression efficiency of the algorithm by selecting the fittest combination from a number of other compression algorithms.

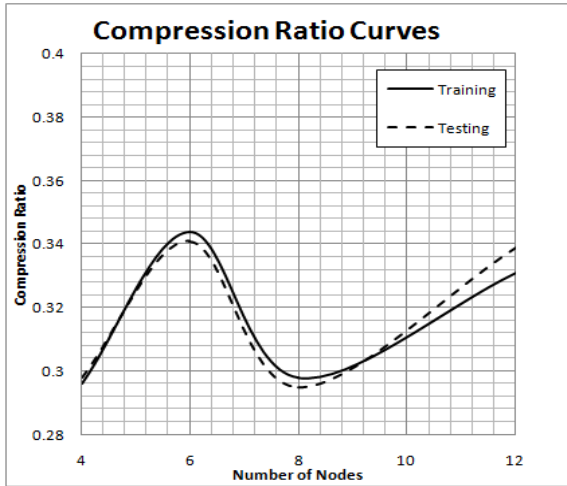


Fig. 5. Compression ratio curves for both training and testing results

Table 3. Comparison Table

S/N	Algorithm	Uncompressed Size	Compressed Size	Compression Ratio
1	Proposed	17,568 bytes	5207 bytes	0.296
2	Huffman [14]	17,568 bytes	13431 bytes	0.764
3	RLE [15]	17,568 bytes	7278 bytes	0.414
4	LZW [16]	17,568 bytes	9857 bytes	0.561

5 Conclusion

In this paper, a novel evolutionary algorithm was presented for textual data compression. The algorithm employed in this research had characteristics borrowed from both GP and CGP. The evolutionary text algorithm used different data compression algorithms—such as LZW, Huffman Coding and RLE—as functions implemented by the nodes it contained. For compression purpose, textual data was selected and a data communication based experimental model was presented. The textual compression using the novel evolutionary algorithm was simulated for different number of scenarios. In contrast to the different compression algorithms that the evolutionary compression model used, the results obtained in terms of compression ratio were measurably better and were as low as 0.295 for a particular case.

References

1. Teng, C.Y., Neuhoff, D.L.: An improved hierarchical lossless text compression algorithm. In: Proceedings of Data Compression Conference, pp. 292–301 (March 1995)
2. Awan, F.S., Mukherjee, A.: LIPT: a lossless text transform to improve compression. In: International Conference on Information Technology, pp. 452–460 (April 2001)
3. Sun, W., Zhang, N., Mukherjee, A.: Dictionary-based fast transform for text compression. In: ITCC 2003, pp. 176–182 (April 2003)
4. Robert, L., Nadarajan, R.: Simple lossless preprocessing algorithms for text compression. IET Software, 37–45
5. Ullah, F., Naveed, M., Babar, M.I., Iqbal, F.: Novel Use of Steganography for Both Confidentiality and Compression. International Journal of Engineering and Technology 2(4), 361–366 (2010)
6. Koza, J.R.: Genetic Programming: A Paradigm for Genetically Breeding Populations of Computer Programs to Solve Problems, Stanford University Computer Science Department technical report STAN-CS-90-1314 (June 1990)
7. Miller, J.F., Thomson, P.: Cartesian Genetic Programming. In: Poli, R., Banzhaf, W., Langdon, W.B., Miller, J., Nordin, P., Fogarty, T.C. (eds.) EuroGP 2000. LNCS, vol. 1802, pp. 121–132. Springer, Heidelberg (2000)
8. Schmidhuber, J., Heil, S.: Sequential Neural Text Compression. IEEE Transactions on Neural Networks 7(1), 142–146 (1996)
9. Aysha, V., Balakrishnan, K., Sundar, S.B.: Parallel Genetic Algorithm for Document Image Compression Optimization. In: International Conference on Electronics and Information Engineering, p. 483 (August 2010)
10. Kattan, A., Poli, R.: Evolutionary Lossless Compression with GP-ZIP. In: IEEE Congress on Computational Intelligence, pp. 2468–2472 (June 2008)
11. Kattan, A., Poli, R.: Evolutionary Lossless Compression with GP-ZIP*. In: 10th International Conference on Genetic and Evolutionary Computation (2008)
12. Kattan, A., Poli, R.: Evolutionary Synthesis of Lossless Compression Algorithms with GP-ZIP3. IEEE Congress on Evolutionary Computation, 1–8 (July 2010)
13. Pope, A.: “Eloisa to Aberald Text Source”,
<http://www.monadnock.net/poems/eloisa.html>
14. Huffman, D.A.: A method for the Construction of Minimum-Redundancy Codes. In: Proceedings of the I.R.E, pp. 1098–1102 (September 1952)
15. Golomb, S.W.: Run-Length Encoding. IEEE Transaction on Information Theory IT-12, 399–401 (1966)
16. Ziv, J., Lempel, A.: Compression of Individual Sequences via Variable-Rate Coding. IEEE Transactions on Information Theory (September 1978)

Evaluation of Dc/Dc Buck Converter Controlled by LMS (Least Mean Square) Algorithm for Different Values of Load Capacitor

Farooq Kifayat Ullah

Department of Computer Systems Engineering, University of Engineering and Technology,
Peshawar Campus, KPK, Pakistan
fkul08@gmail.com

Abstract. The performance of Dc/Dc Buck converter controlled by LMS algorithm has been evaluated for different values of capacitive load. A power converter, driven by an adaptive controller, can operate satisfactorily under unfavorable conditions of a range of uncertainty in component values. The controller used is capable of handling unknown disturbance due to its adaptive nature.

Keywords: Dc to Dc converter, Adaptive Control, Least Mean Square Methods.

1 Introduction

Power converters are widely used in many electronic devices. In many applications, it is probable that there occurs some uncertainties in the values of power train components and this change can lead to variations in value of power supplied to the appliance. Therefore, it is desirable that a power converter should have got the capability to tolerate such uncertainties along with catering the needs of acceptable loop dynamics. A power converter, driven by an adaptive controller, can operate satisfactorily under unfavorable conditions of a range of uncertainty in component values. Adaptive controllers are preferred over closed loop controller because the former are cheaper and give optimal performance even when parameters of power train might vary with time and temperature [1].

Digital control of power converters has several benefits like; optimal number of passive components, programming of system parameters and easy maintenance. Schemes, based on adaptive control, like system identification employed for offline control of a plant and auto tuned PID in dc-dc converters have already been used. [2,3]. There have been plenty of online adaptive controllers which employ system identification to recognize the plant parameters but those methods end up in computational complexity, hence expensive. Another option with lower complexity and not so good regulation comes with auto-tuning a PID during a tuning phase [3]. However, these techniques are not good enough to give optimal regulation in case of some random disturbance. This fact indicates that a good controller acting online should be impervious to disturbances.

The given adaptive controller is capable of handling these issues. Process identification describes the loop dynamics whilst the disturbances are taken into consideration. The association of process characterization with linear prediction is helpful here to design a controller which is worthy of doing two tasks; controller and process identifier. The implementation incorporates adaptive algorithm in a sleek manner and is self compensating [1]. The performance of adaptive controller has not been previously tested for reactive loads and this work analyzes the performance of the adaptive controller when reactive loads are applied at the output.

2 Background

2.1 Adaptive Algorithm

Conventional techniques of controlling buck converters used for regulation are unable to cope with issues of unknown disturbances. An adaptive controller based can address such issues which utilizes process identification to characterize the loop, taking the characteristics of disturbances in to account. The relationship between process characterization and linear prediction makes controller perform two actions viz. controller and process identifier which in turn solves the certainty equivalence problem and the identification can be run with continuously [1]. This concept has been implemented using adaptive LMS (Least Mean Square) algorithm by running it's functional blocks.

2.2 Graph Theory

The relationship between Kirchoff's laws (of current and voltage) and graph theory applied on electrical networks is exploited here to model the buck converter circuit into a suitable form. This mechanism is useful to end up with minimum handmade calculations and easy script implementation in some computer program like MATLAB [4]. An electrical network is transformed into the corresponding graph and selection of tree branches and links is made based on the maximal index criterion. Cut set and cycle matrices are obtained from the graph which are then used to form system equations in a prescribed manner. It is easy to form state space model of the system to be used for evaluation from these equations.

2.3 Modeling Methodology

The state space description of a system gives a set of coupled first order differential equations comprising of internal variables called *states*, together with a set of algebraic equations which combine state variables with output variables. These equations are put together in matrices to form a compact representation. This representation is then used here to simulate the system in MATLAB. The formal equations of state space are given by equations 1 and 2.

$$x' = Ax + Bu \tag{1}$$

$$y = Cx + Du \tag{2}$$

3 Modeling and Simulation

3.1 Deriving the State Space Model of the Buck Converter Using Graph Theory

The equivalent circuit model of a Buck Converter in the On State with capacitive load C_L is drawn in Fig.1. The chosen model is based on the BMR450 DC to DC converter manufactured by Ericsson.

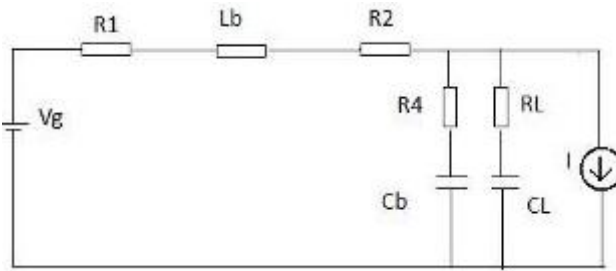


Fig. 1. Equivalent Circuit of Buck Converter in the On-Phase with Capacitive Load

In Fig. 1 load current is modeled as a current source ‘I’, R1 is the switch resistance, R2 is inductor resistance and R4 is ESR (Equivalent Series Resistance) for buck capacitor. Similarly, R1 is ESR for load capacitor. The circuit of Fig. 1 is redrawn in graphical form in Fig. 2.

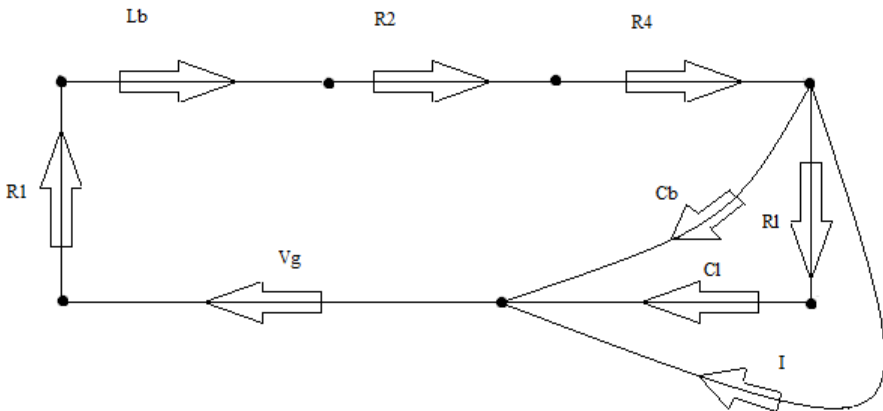


Fig. 2. On-Phase graph with chosen Span Tree

The tree branches have been shown by solid lines and links are given by dotted lines with arrows on each for direction. Each element has been labeled with its function name. This graph was used to derive the cut set matrix and cycle matrix. From this information, system equations were formed as given in equation 3.

$$\begin{bmatrix} i_u \\ i_c \\ i_{cl} \\ i_{R1} \\ i_{R2} \\ i_{R4} \\ u_{Rl} \\ u_L \\ u_l \end{bmatrix} = \begin{bmatrix} 0 & 0 & 0 & 0 & 0 & 0 & 0 & 1 & 0 \\ 0 & 0 & 0 & 0 & 0 & 0 & -1 & 1 & -1 \\ 0 & 0 & 0 & 0 & 0 & 0 & 0 & 1 & 0 \\ 0 & 0 & 0 & 0 & 0 & 0 & 0 & 0 & 1 \\ 0 & 0 & 0 & 0 & 0 & 0 & 0 & 0 & 1 \\ 0 & 0 & 0 & 0 & 0 & 0 & -1 & 1 & -1 \\ 0 & 1 & -1 & 0 & 0 & 1 & 0 & 0 & 0 \\ -1 & -1 & 0 & -1 & -1 & -1 & 0 & 0 & 0 \\ 0 & 1 & 0 & 0 & 0 & 1 & 0 & 0 & 0 \end{bmatrix} * \begin{bmatrix} u_u \\ u_c \\ u_{cl} \\ u_{R1} \\ u_{R2} \\ u_{R4} \\ u_{Rl} \\ i_L \\ i_l \end{bmatrix} \tag{3}$$

These equation were used to formulate state space model of the system as it is shown below.

The states taken are Vc (buck capacitor voltage), Vcl (load capacitor voltage) and il (buck inductor current). The corresponding state equations are:

$$i_c = C_b \frac{dv_c}{dt} = -2i_l + i_l \tag{4}$$

This implies that:

$$\dot{V}_c = \frac{1}{C_b}(i_l - 2I) \tag{5}$$

And from load capacitor current equation

$$\dot{V}_{cl} = \frac{1}{C_b} \tag{6}$$

And , buck inductor voltage gives the following

$$\dot{i}_l = \frac{1}{L}(-V_c - V_g + 2 I R_4 - i_L(R_1 + R_2 + R_4)) \tag{7}$$

The state space equations are formed as given here.

$$\dot{X} = Ax + Bu \tag{8}$$

$$\frac{d}{dt} \begin{pmatrix} V_c \\ V_{cl} \\ i_L \end{pmatrix} = \begin{bmatrix} 0 & 0 & \frac{1}{C_b} \\ 0 & 0 & 0 \\ -\frac{1}{L_b} & 0 & -(\frac{R_1+R_2+R_4}{C_b}) \end{bmatrix} + \begin{bmatrix} 0 & -\frac{2}{C_b} \\ 0 & \frac{1}{C_L} \\ -\frac{1}{L_b} & 2R_4 \end{bmatrix} * \begin{bmatrix} u_u \\ i_l \end{bmatrix} \tag{9}$$

$$Y = Cx + Du \tag{10}$$

$$V_o = [1 \quad 0 \quad R_4] * \begin{bmatrix} V_c \\ V_{cl} \\ i_L \end{bmatrix} + [0 \quad -R_4] * \begin{bmatrix} u_u \\ i_l \end{bmatrix} \tag{11}$$

3.2 State Space Averaged Model

To analyze the buck converter we can take the On state space equations and Off state space equations and find the time averaged model based on the duty cycle. Duty cycle is the duration of time the power supply is connected across the circuit. And is denote by d .

$$A_{dc} = A_{on}d + A_{off}(1 - d) \tag{12}$$

$$A_{on} = \begin{bmatrix} 0 & 0 & \frac{1}{Cb} \\ 0 & 0 & 0 \\ -\frac{1}{Lb} & 0 & -\frac{R+R_L+R_4}{Lb} \end{bmatrix} \tag{13}$$

$$A_{off} = \begin{bmatrix} 0 & 0 & 1/Cb \\ 0 & 0 & 0 \\ -1/Lb & 0 & -(R + R_L + R_4)/Lb \end{bmatrix} \tag{14}$$

$$d=0.5, 1-d=0.5$$

$$A_{dc} = A_{on} = A_{off} \tag{15}$$

$$B_{dc} = B_{on}d + B_{off}(1 - d) \tag{16}$$

where

$$B_{on} = \begin{bmatrix} 0 & -2/Cb \\ 0 & 1/C_L \\ -1/Lb & -2R_4/Lb \end{bmatrix} \text{ and } B_{off} = \begin{bmatrix} 0 & -2/C \\ 0 & 1/C_L \\ 0 & -2R_4/L \end{bmatrix}.$$

This means

$$B_{dc} = \begin{bmatrix} 0 & -2/Cb \\ 0 & -1/C_L \\ 1/2Lb & -2R_4/L \end{bmatrix}$$

As $C_{dc}=C_{on}d + C_{off}(1 - d)$ and $C_{on}=C_{off}$ this means

$$C_{dc}=C_{on}$$

$$C_{dc}=[1 \ 0 \ R_4]$$

Similarly $D_{dc}=D_{on}=D_{off}=[0 \ -R_4]$

These matrices can be used for calculation of the operating point since at the operating point

$\dot{x}=0$, where x is the state vector

$$x=A_{dc} \bar{X} + B_{dc} \bar{U}=0 \tag{17}$$

This implies

$$\bar{X} = A_{dc}^{-1}B_{dc}\bar{U} \tag{18}$$

Inserting values of the parameters for the BMR450 circuit with $C_L=470e-6$ Farad and $R_L=100e-3$ Ohm. We get,

$$\bar{X} = [0.001 \ 0 \ 1]^T \tag{19}$$

$$\bar{U} = [10 \ 0.5]^T \tag{20}$$

$$Y=C_{dc}.\bar{X}+D_{dc}\bar{U} = -(C_{dc}A_{dc}^{-1}B_{dc} -D_{dc}).\bar{U} =0.0035 \tag{21}$$

3.3 Linearization of the Operating Point

The small signal model which incorporates the duty cycle in the input vector is obtained as followsThe control and disturbance signals are placed in the input vector , where \hat{u} is the new input vector.

$$\hat{u}=\begin{bmatrix} u \\ d \end{bmatrix} \tag{22}$$

The linearized small signal state space equations are given by

$$\hat{\dot{x}} = \hat{A} \hat{x} + \hat{B} \hat{u}$$

$$\hat{y} = \hat{C} \hat{x} + \hat{D} \hat{u}$$

It should be noted and $\hat{u}(t)$ that x, \hat{u} are functions of time but for convenience we ignore writing them explicitly as $x(t)$

$$f(x,\hat{u})=\dot{x}=[d. A_{on} + (1-d)A_{off}]. x + [d. B_{on}+(1-d)B_{off}] \hat{u}$$

$$g(x,\hat{u})=y=[d. C + (1-d)C_{off}]. x + [d. D_{on}+(1-d)D_{off}] \hat{u}$$

$$\hat{A}=\frac{\sigma f}{\sigma x} \Big|_{x=\bar{X}, \hat{u}=\bar{U}} = d. A_{on} + (1-d)A_{off} \Big|_{x=\bar{X}, \hat{u}=\bar{U}} = A_{dc}$$

$$\hat{B}=\frac{\sigma f}{\sigma \hat{u}} \Big|_{x=\bar{X}, \hat{u}=\bar{U}} = d \begin{bmatrix} \frac{\sigma f}{\sigma u} & \frac{\sigma f}{\sigma d} \end{bmatrix} \Big|_{x=\bar{X}, \hat{u}=\bar{U}} = [B_{dc} \ B_{\hat{d}}]$$

$$B_{\hat{d}} = \frac{\sigma f}{\sigma d} = (A_{on} - A_{off})X + (B_{on} - B_{off})U$$

$\hat{A}, \hat{B}, \hat{C}, \hat{D}$ are the linearized state space parameters. This model can be transformed in to the frequency domain using traditional control theory tools.

3.4 Sampling of the System

As the controller used is a digital controller where as the plant or buck converter is a continuous system so we have to sample the output and feed it to the digital controller which is a predictor in conjunction with an adaptive gain element which varies the duty cycle according to the variation of the output and the predictor.

Another way to analyze the circuit is to Digitize the state space equations by sampling them.and working in the Z domain.

Assuming a piecewise constant input signal over the sampling interval ,T ie

$$\begin{aligned}
 u(t) &= u(nT) \\
 x(nT+T) &= Fx(nT) + Gu(nT) \\
 y(nT) &= C'X(nT) + D'u(nT)
 \end{aligned}$$

where the F,G matrices are given by $F=e^{A'T}$ and $G=\int_0^T e^{A'T} \dot{B}dt$.

4 Results and Conclusion

The simulation results for an uncontrolled buck converter subjected to Capacitive load is presented in Fig.3. A buck converter with PD controller and LMS applied with capacitor value 470 μF in Fig. 4 and 10 mF in Fig. 5.

The plots of Fig. 3, Fig. 4 and Fig. 5 show that the Adaptive controller works well for variation in Active load. It is observed that the adaptive controller shows lower steady state errors that the PD controller. In [1] a first order adaptive controller was successfully used to control a buck converter with resistive loads. These results show the transient performance of the adaptive controller will degenerate as active loads are applied across it as the plant becomes a second order system. Future work can involve using system identification to identify the load and using the resulting knowledge to adapt the controller for better transient performance.

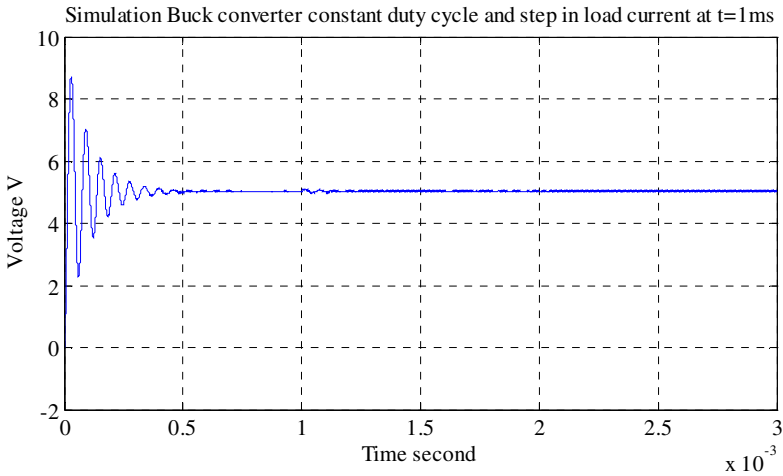


Fig. 3. An uncontrolled DC to DC Buck Converter with load current of 1 Ampere drawn after 1millisecond of operation

In Fig. 4 the output from PD controller is plotted in Top plot and the output of Adaptive controller is plotted in the bottom plot. The PD controller is used to initialize the Adaptive controller in the simulator to provide a soft start. It has been observed that the Adaptive filter is simulated just as well without the soft start.

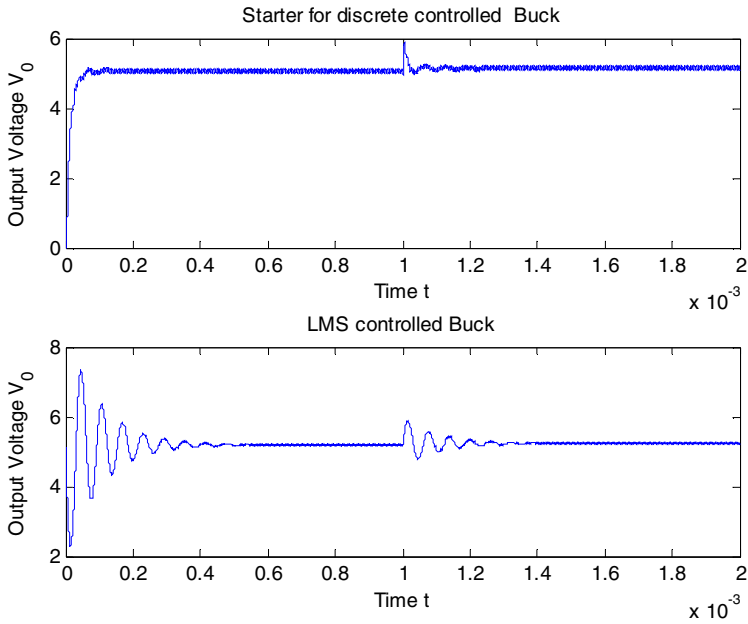


Fig. 4. Adaptive control of Buck Converter with 470 microFarad capacitive load connected at the output

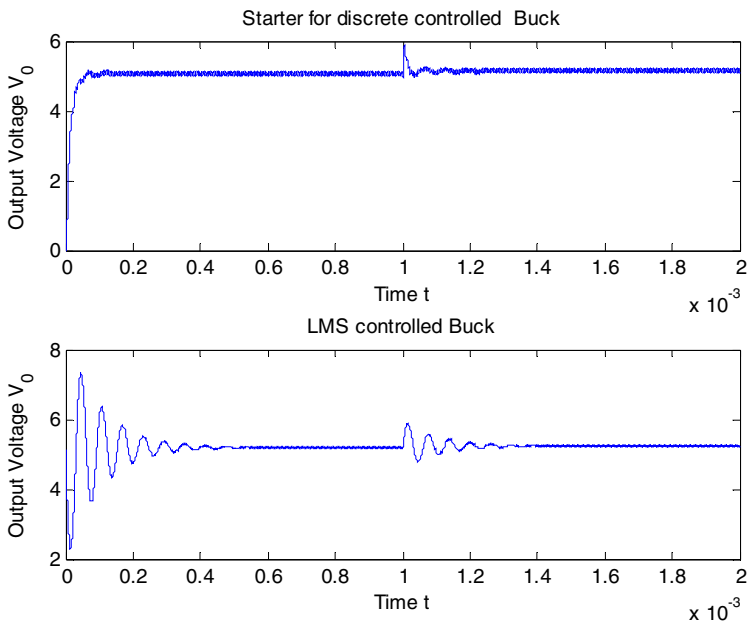


Fig. 5. Simulation for Buck Converter with 10 milliFarad applied at the output

References

1. Kelly, A., Rinne, K.: A self-compensating adaptive digital regulator for switching converters based on linear Prediction. In: IEEE APEC 2006, pp. 712–718. IEEE (2006)
2. Miao, B., Zane, R., Maksimovic, D.: Automated Digital Controller Design for Switching converters. In: Power Electronics Specialist Conference 2005, Recife Brazil (2005)
3. Stefanutti, W., Matavelli, P., Saggini, S., Ghioni, M.: Auto Tuning of Digitally controlled Buck Converters based on Relay Feedback. In: Power Electronics Specialist Conference 2005, Recife Brazil (2005)
4. West, D.B.: Introduction to Graph Theory. Prentice Hall, New York (2001)

Exploiting Multi View Video for Maximizing Lifetime of Wireless Video Sensor Networks

Saima Zareen, Khalid Iqbal, Almas Anjum, and Shoaib A. Khan

Department of Computer Engineering College of Electrical & Mechanical Engineering
National University of Sciences and Technology, Pakistan
saim03f@gmail.com, ksqibal64@hotmail.com,
almasanjum@yahoo.com, shoabak@ceme.nust.edu.pk

Abstract. Wireless Sensor Networks have attained extensive interest since the last few decades. Especially Wireless Multimedia sensor networks are being used in surveillances, health, traffic monitoring and entertainment where these sensors are deployed at different views for capturing the finer details of a given region. With their extensive use and benefits, they have many issues such as battery life, storage capacity, and bandwidth consumption. The aim of the research paper is to study the existing spatial correlation models in multi view videos and propose an approach which reduces battery consumption by minimizing the compression time of video frames based on the specific correlation model. This paper discusses the novel OPI model that is designed on the basis of correlation between sensor nodes. Experimental results have been derived using OPI model and the results depict that by using this approach, compression time of processed video frames is reduced as compared to the compression time of originally frames.

Keywords: Wireless sensor Networks (WSN), Overlapping Part Identifier (OPI), Wireless Multimedia WM, Field of View (FOV), Distributed Source Coding (DSC).

1 Introduction

These days, multimedia applications are much demanding when it comes to quick receiving, and transmission of detailed information with the high quality. Wireless Sensor networks serve as the most fulfilling demands of such applications. Wireless sensor networks contain devices, which have sensors capable of sensing change in events [1]. There are different categories of wireless sensors based on their applications. For example, video sensors had been designed to capture audio visual information. These video sensors are deployed to serve different purposes, such as surveillance [2, 4], monitoring health [3], control and monitor industrial processes [1].

Studies [5, 11] have shown that wireless mobile devices have limited power which is consumed during video capturing, pre-processing for encoding and transmitting or receiving information. Sensors have limited battery and their life largely depends on

the amount of available battery power [11]. Here sensors used in the studies are cameras that are directional and have a specific field of view. Using sensors for complex calculations is like ending its energy making sensor unable to accomplish the desired process or task. Hence methods should be adopted to ensure that the applications being used are not too complex (with respect to power consumption) when used with the sensors for multimedia processing.

2 Background and Motivation

Research work is being carried out in multi-view video processing, so that sensors resources can utilized be efficiently. Issues like camera calibration, local video processing, video encoding, its transmission and reception and storage often arise that hinders successful processing of multi-view videos. Researchers have contributed their part in addressing the solution of the issues mentioned above. Based on camera calibration techniques [6, 7], camera's intrinsic and extrinsic parameters can be estimated, i.e., the location of the camera, its field of view and distance of camera from the object.

Distributed Source Coding (DSC) [16], brought a revolution to the multi view video coding. It encodes the correlated source independently but decodes them jointly. Many approaches have been proposed for multi view video coding such as [13], in which authors introduced temporal side information along with homographic based inter-view side information. Low power consumption techniques like Prism [14], shifted computational intensive tasks such as motion compensated search from the encoder to the decoder. Junaid et al, in [15], have shown that PRISM is more power consuming than wyner ziv coding. DSC based techniques [16], generate side information based on temporal correlation. Spatial correlation can be considered for static video frames and can be decoded using DSC by generating side information based on spatial correlation rather than temporal correlation. If the side information is generated by considering both the temporal and spatial correlation, quality of video can be improved greatly. Considering these points in mind, the focus is made towards spatial correlation in multi view videos for wireless sensor networks. Different spatial correlation techniques have been proposed [8, 9, and 10] to minimize bandwidth, power consumption and communication overhead.

In a study [8], author proposed a model that calculated correlation between two sensors based upon the overlapping field of view of camera. Field of view of sensor node involves four parameters i.e. (R, α, P, V) [8]. Where R is the radius, α is the angle of view, P is the location of visual sensor and V is the direction of sensor. According to [8] an object is covered by the sensor node if the distance of object from the sensor is within the range of Radius R of a sensor's field of view. Based upon the correlation matrix calculated, it categorises the sensors into cooperative teams and partitioned the image by sensing the task across other camera, this reduces the workload at a single sensor. The model assumes a virtual sensor between two sensors and then calculates partial image points to be transmitted by each sensor node.

The assumption of virtual sensor node requires its position between the actual sensors, which is difficult to calculate.

In [9], Joseph C et al, proposed a model to exploit inter and intra sensor correlation for distributed sensors, keeping in view the power limited sensors. The model optimises the smallest overlapping region between the sensors to reduce the power consumption. Sensors communicate with the base station for getting information about the number of pixels to be transmitted by the individual sensor and number of pixels to be discarded for a certain region. However what will happen if the communication between sensor and base station fails. Also the model is complex and proposes to calculate non overlapping region based on intersection of overlapping fields of view, but does not give details of how to achieve it. Instead, it can be a better solution that each sensor be given the information of its neighbouring sensors and reduce the communication between the sensors among themselves [10]. This way, possibility of failure of communication between two sensors cannot affect the sensors encoding and transmission of other sensors in the network. In [10], authors have proposed a framework for calculating the spatial correlation among different sensors deployed at a certain region. Based on that correlation model, it selects sensors for transmitting the video within a certain disparity limit. This correlation technique is simple in calculations and gives accurate results having minimum constraints, therefore OPI model is proposed for the identification of overlapping part between the images and removing that overlapping part from the camera frames by using the spatial correlation technique [10].

1. We have used a correlation function to exploit the multi-view video for wireless sensor networks.
2. We propose a model for identifying the overlapping area between the sensors, and removing the overlapping part from the video frames called edited frames to be encoded.
3. We have used the “lossy compression” technique to compress the original and edited frames separately and measured the compression time.

The remainder of this paper is organised as follows, problem to be studied is described in Section 2. In Section 3 the model to exploit the multi view correlation is proposed. Section 4 results are discussed, and in Section 5 conclusion and future work are discussed.

3 Problem Statement

Consider a set $A=\{C1,C2,C3,C4,\dots,Cn\}$ of visual sensors deployed at a region ,these sensors capture the images as $\{Y1,Y2,Y3,Y4,\dots,Yn\}$. The correlation among these sensors can be calculated by using correlation function of [10]. How correlation model can be exploited in order to reduce the compression/encoding time of video frames processed by individual sensors?

3.1 Choosing a Spatial Correlation Model

We study different correlation [8, 9, 10], based techniques in multi view sensors. Considering the set $A = \{C1, C2, C3, C4, \dots, Cn\}$ of cameras and choosing the correlation technique that is based on simple calculations.

3.2 Overlapping Part Identifying Model

Multi view videos contain redundant information in their frames and encoding this redundant information causes resource consumption, which can be minimized, if redundant information within a frame is identified and removed.

3.3 Applying Compression to Calculate Encoding Time

Different compression techniques have been introduced, a general purpose lossy compression model is used from [12], and encoding time is calculated using that compression model.

4 Mathematical Model for Identification of Overlapping Part and Its Removal

The system model for OPI is derived from [10], in which rui dai et al have proposed visual sensor configuration for calculating correlation among camera sensors. OPI is using the correlation model of [10], that is why system model for OPI is based on the system model discussed in [10].

4.1 Sensing Model

Consider a set of cameras calibrated to capture multiple views of the object, placed at the origin. Cameras have sensing direction θ with x axis. Each Camera has its location represented by two coordinates x and y with its angle of view α as in Fig. 1.

A camera field of view can be calculated based upon its location P, focal length F, and radius R. When multiple cameras are deployed at a specific area of interest, the sensing direction θ of cameras can be calculated by camera calibration techniques [6, 7]. Cameras capture frames that contain redundant information and their FOVs overlap. It is very useful, if degree of correlation between the cameras is calculated and their FOV overlapping is identified. This helps in reducing encoding time and can reduce bandwidth consumption.

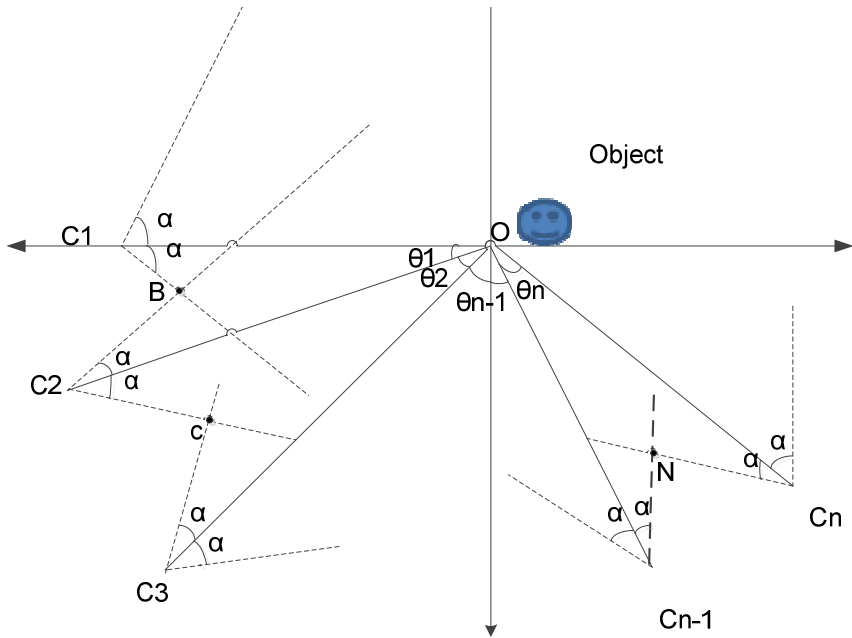


Fig. 1. System Model

In order to calculate spatial correlation between any two arbitrary cameras, such as camera_i and camera_j, a spatial correlation technique is used. In which [10], a pinhole camera model is assumed, which selects the reference points of the scene. Then coordinate transformation is applied to find out where these reference points lie in the coordinate system of a particular camera. The model proposed in [10], showed that if two cameras are perpendicular to each other then, there is no correlation. Using this correlation model, correlation among the cameras is calculated. With this correlation value, identify the overlapping part of FOVs between the cameras and the point from where the overlapping begins.

4.2 Overlapping Point Calculation

Consider the case of two cameras, camera 1 and camera 2, redraw the model for two cameras as shown in Fig. 2.

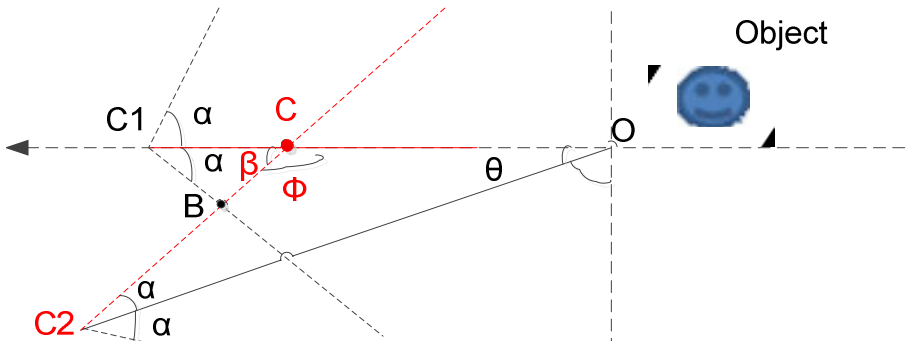


Fig. 2. Camera 1 and Camera 2 Model

Additional point such as C and angles such as β and ϕ are also shown. The angles of view of both cameras intersect at a point B as shown in the Fig. 2. It is the point B where the cameras overlap each other. To calculate point B following steps are proposed:

4.3 Calculate Angles

We cannot calculate the point B directly using a single triangle C1C2B, for this we will divide the system model of Fig. 2 into different triangles to find the unknowns i.e. B, C, β and ϕ are unknown. C1, C2, O, α and θ can be calculated using calibration methods discussed in [5,6]. First we will consider a triangle OCC2 as shown in Fig. 3 to calculate angle ϕ , the triangle theorem for sum of interior angles of a triangle is used which states that sum of interior angles of a triangle is 180. So according to triangle OCC2, $\alpha + \phi + \theta = 180$. Knowing the values of α and θ , we can calculate ϕ .

Find the Intersection Point. To find the intersection point B as shown in Fig. 5, consider the following scenario:

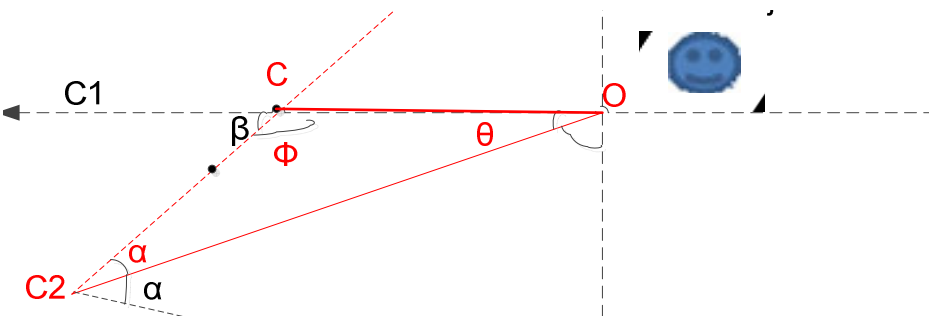


Fig. 3. Camera 1 and Camera 2 Model

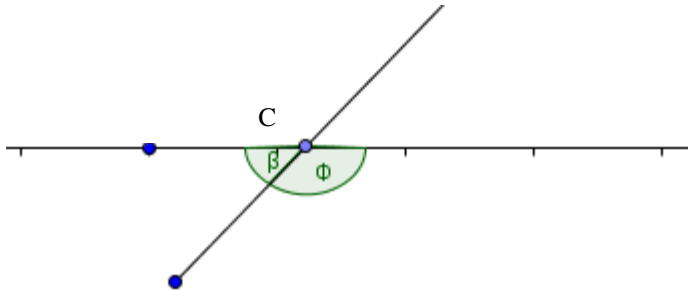


Fig. 4. Intersection of Camera1 and Camera2 with the plane

Step 1.

- i. C1 and C2 intersect the Plane at C, as shown in Fig.3.It is the intermediate point, which will help in calculating point B.
- ii. Calculate the angle β as shown in Fig. 4, using the value of ϕ .
 $\beta = 180 - \phi$.
- iii. Calculate the line of equations of both C1 and C2 intersecting at the point C.
Equation of line from C1 to C:

$y - y_1 = m_1(x - x_1)$ where $m_1 = \tan(\theta)$, as C lies on the same plane of C1.

$$y = y_1 + m_1(x - x_1) \quad (1)$$

Equation of line from C2 to C:

$y - y_2 = m_2(x - x_2)$ where $m_2 = \tan(\beta)$, as C1 intersects plane with the angle β .

$$y = y_2 + m_2(x - x_2) \quad (2)$$

- iv. Using substitution method Solve (1) and (2), to calculate x

$$x = (y_1 - y_2 + m_2 x_2 - m_1 x_1) / (m_2 - m_1) \quad (3)$$

Value of x can be substituted in (1) or (2) for calculating value of y. Point C(x_c, y_c) has been calculated. $x_c = x, y_c = y$

Step 2.

Now calculate intersection point B between FOVs of two cameras, by considering lines from C to B and C1 to B as shown in Fig 5.

- i. Calculate the equations of both lines CB and C1B with their angles of inclination α and β respectively using Step 1.
- ii. Solve the equations to calculate x and y, this way required point of overlapping B(x, y) has been calculated.

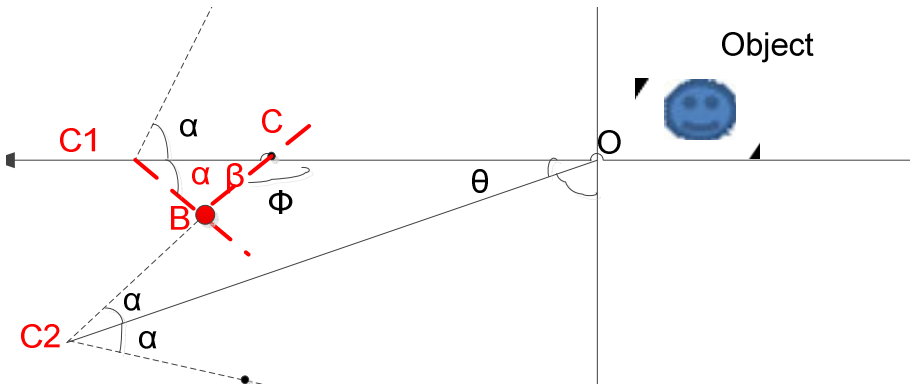


Fig. 5. Intersection of Camera1 and Camera2 FOVs

The above mathematical model can be generalized by selecting any camera_i and camera_j, by using the same sequence of above steps.

4.4 Methodology to Extract Overlapping Part from the Image

Calculate the correlation between cameras and find overlapping region between the camera frames. This overlapping region is identified in a triangular shape as shown in Fig.6. Therefore, overlapping region has three points that are required to be calculated. Using the above model starting point B of overlapping region is calculated and its remaining two points are assumed till the end of the frame as shown by P1 and P2 in the Fig.6. Centre of the frame is calculated and then point B is mapped in the frame. Starting from point B, extend using the α_i , α_j till the end of the frame. The end points P1 and P2 can be calculated with help of α_i and α_j using equation of straight line.

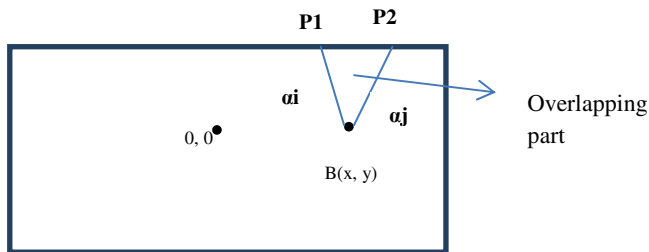


Fig. 6. Overlapping area in frame

5 Results

Camera 1 is placed to take picture of the object along the x-axis.it is the camera 1 calibration .Then Camera is rotated with θ to take the pictures, with following

different values of θ from the camera 1, $\theta = \{-15^\circ, -30^\circ, -45^\circ, -60^\circ, -75^\circ, -90^\circ, 105^\circ, 120^\circ, 135^\circ\}$. The proposed model is implemented in Matlab and points of intersection of FOVs of one camera with other cameras in network are calculated. Implementing the proposed methodology in Matlab, overlapping part is extracted within the frame. Advantage of this approach is that every node will process frames at its end, communication between sensors requires only four parameters (α , P, V, and R) from other sensor to be known for applying the OPI model. Compression technique based on discrete cosine Transform is applied over the frames and their timings of compression are calculated. Results of proposed technique are compared with the compression time of original frame of a camera. Plot in Fig.8 show the compression time of original frame C1 and remaining frames C2, C3, C4, C5, C6, C7, C8, C9 and C10, these frames are obtained by removing overlapping part from the frames of camera1 on the basis of correlation with other cameras. Fig. 9 shows the compression time of original frame (C2) and remaining frames of camera2 (C3, C4, C5, C6, C7, C8, C9 and C10).Original frame of camera 2 i.e. C2 takes time longer to compress than its remaining frame (C3, C4, C5, C6, C7, C8, C9 and C10) .Based upon the correlation values of camera 5 and camera 6,there is a small increase in compression time of remaining frame i.e. C8 ,because correlation between camera 2 and camera 8 is minimum as shown by Fig. 7.

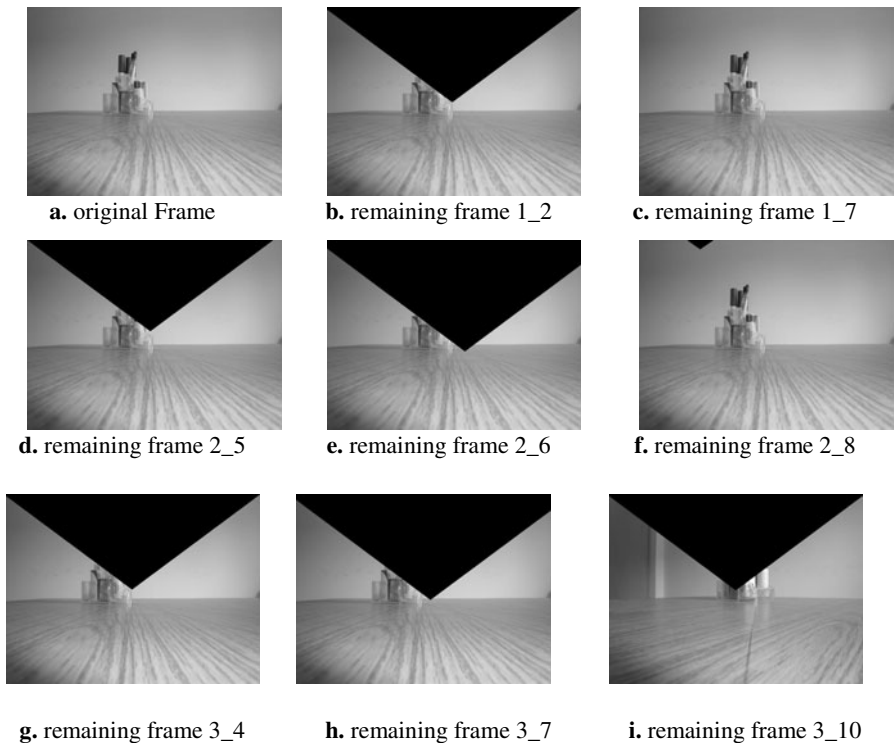


Fig. 7. Original Frames and Extracted Frames

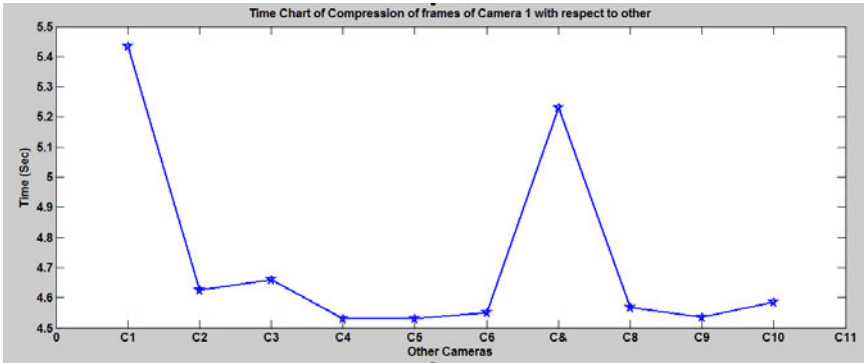


Fig. 8. Compression time of Camera 1 w.r.t other cameras

Fig.10 shows the compression timings of original frame (C3) of camera 3 and its remaining frames (C4, C5, C6, C7, C8, C9 and C10), that are obtained by applying OPI model. With the increase in correlation value between camera 3 and camera 4, compression time of remaining frame C4 is decreased as compared to original image of C3 camera 3. With the slight decrease in correlation value between camera 3 and camera 10, there is increase in compression time of the remaining frame C10. Above results show that, higher the degree of overlapping between the cameras the smaller is the compression time. If degree of overlapping is small, the larger is compression time of frames.

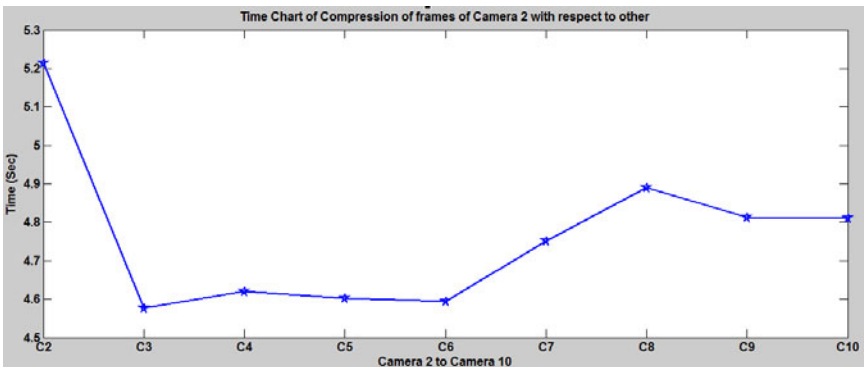


Fig. 9. Compression time of Camera 2 w.r.t other cameras

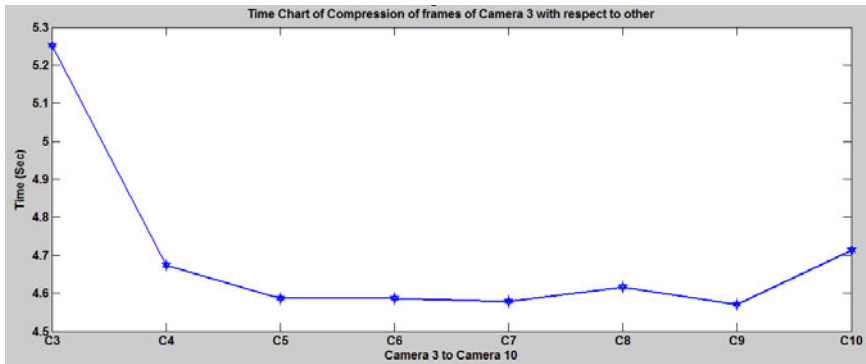


Fig. 10. Compression time of Camera 3 w.r.t other cameras

6 Conclusion and Future Improvements

Correlation in multi view sensors can be exploited based on the spatial correlation of video frames. Proposed model shows that, by identifying the overlapping point and extracting that overlapping part from the original frame, encoding time of frames can be minimized by keeping the minimum communication overhead between the sensors. The technique is simple in calculations and if we want to calculate the energy consumed by this technique at the encoder, it will be less than the total energy of encoding, transmitting and receiving a complete frame at the sensor, another benefit of approach is that, bandwidth consumption can be reduced. The Future work will include studying the distributed source coding techniques which exploits temporal correlation only and to incorporate the proposed model while decoding at the sink node. Decoding the correlated sources based on the spatial correlation needs to be investigated, according to DSC where side information is generated based on temporal correlation. It will be a better approach, if spatial correlation is considered along with temporal correlation in DSC and the technique can save the battery consumption.

References

1. What is Wireless Sensor Network,
<http://zone.ni.com/devzone/cda/tut/p/id/8707>
2. Akyildiz, I.F., Melodia, T., Chowdhury, K.R.: Wireless Multimedia Sensor Networks: Applications and Testbeds. Proceedings of the IEEE 96, 1588–1605 (2008)
3. Hu, F., Kumar, S.: Multimedia Query with QoS Considerations in Wireless Sensor Networks for Telemedicine. In: Proceedings of International Conference on Internet Multimedia Management Systems (SPIE IT), vol. 5242, pp. 217–227 (2003)
4. Soro, S., Heinzelman, W.: A survey of Visual Sensor networks. Advances in Multimedia, vol. 2009, Article ID 640386, 21 pages (2009)
5. Sklavos, N., Toulou, K.: A System Level Analysis of Power Consumption and Optimizations in 3G Mobile Devices, pp. 217–227 (2007)

6. Liu, X., Kulkarni, P., Shenoy, P., Ganesan, D.: Snapshot: A Self-Calibration Protocol for Camera Sensor Networks: Broadband Communications, Networks and Systems, pp. 1–10 (2006)
7. Mehta, V., Sheng, W.: Distributed Calibration of a Camera Sensor Network. In: Proceedings of the 2008 IEEE International Conference on Robotics and Biomimetics, pp. 1974–1979 (2009)
8. Mat, H., Liut, Y.: Correlation Based Video Processing in Video Sensor Networks. In: International Conference on Wireless Networks, Communications and Mobile Computing, vol. 2, pp. 987–992 (2005)
9. Dagher, J.C., Marcellin, M.W., Neifeld, M.A.: A Method for Coordinating the Distributed Transmission of Imagery. *IEEE Transactions on Image Processing* 15(7), 1705–1717 (2006)
10. Dai, R., Akyildiz, I.F.: A Spatial Correlation Model for Visual Information in Wireless Multimedia Sensor Networks. *IEEE Transactions on Multimedia* 11(6), 1148–1159 (2009)
11. Vijayakumar, P., Ravichadran, V.: Wireless Sensor Network Issues-An Overview. *International Journal of Wireless Networks and Communications* 1(1), 17–28 (2009)
12. Lossycompression, <http://www.mathworks.com/matlabcentral/fileexchange/31776-image-compression-based-on-dct>
13. Dufaux, F., Ouaret, M., Ebrahimi, T.: Recent Advances In Multi-View Distributed Video Coding. In: Proceedings of SPIE, vol. 6579 657902, pp. 1–11 (2007)
14. Puri, R., Majumdar, A., Ramchandran, K.: PRISM: A Video Coding Paradigm With Motion Estimation at the Decoder. *IEEE Transactions on Image Processing* 16(10), 2436–2447 (2007)
15. Ahmad, J.J., Khan, H.A., Khayam, S.A.: Energy Efficient Video Compression for Wireless Sensor Networks. In: 43rd Annual Conference on Information Sciences and Systems, pp. 629–634 (2009)
16. Xiong, Z., Liveris, A.D., Cheng, S.: Distributed Source Coding for Sensor Networks. In: Haykin, S., Liu, K.J.R. (eds.) *Handbook on Array Processing and Sensor Networks*. Wiley (2009)

Author Index

- Aamir, Muhammad 1
Abbas, Syed Muzahir 10, 20
Abbasi, M. Ali Babar 20
Abrar, Shafayat 62, 240
Abu Ahmed, Qassem 432
Ahmad, Jamil 176
Ahmed, Adeel 31
Ahmed, Anil 385
Ahmed, Saneeha 512
Ahmed, Syed Hassan 43
Ahsan, Affan 188
Akhtar, Pervez 52
Alam, Mahmood 295
Alhassani, Abdullah 305
Ali, Ahmad 373
Ali, Anum 62
Ali, Syed Muhammad Usman 295
Ali, Syed Saad Azhar 284
Ali, Zeeshan 81
Amin, Imran 349, 421
Amin, Noorul 92
Amir, Samreen 101
Anjum, Almas 541
Anjum, Naveed 466
Ansari, Muhammad Adil 122
Anthony, Richard 228
Anwar, Hirra 110
Arain, Muhammad Asif 122
Arshad, Junaid 132
Asif, Muhammad 101
Awan, Haroon Tariq 20
Azeem, Muhammad Mansoor 144
Aziz, Abdul 432
Aziz, Arshad 361
- Babar, Inayatullah 272
Bajwa, Imran Sarwar 164, 314, 326
Beckett, Paul 305
Bhalerao, Dipashree M. 154
Bhutto, Zuhaiuddin 284
Bouk, Safdar Hussain 43
- Choi, Tae-Sun 222
Chowdhry, Bhawani Shankar 1, 101
Chowdhry, Bhibekshan 101
Crespi, Noel 200
- Djemame, Karim 445
Dobbie, Gillian 314, 326
- Ghazali, Rozaida 453
- Hameed, Kashif 164
Hameed, Sarmad 421
Hameed, Sumira 385
Haroon, Farah 397
Hashmani, Manzoor 501
Hashmi, Muhammad Adnan 176
Hassan, Moezul 421
Haun, Michael 200
Hoene, Christian 200
Hultmann Ayala, Helon Vicente 122
Hussain, Bilal 188
Hussain, M. 73
Hussain, M. Ayyaz 222
Hussain, Mutawarra 373
Hussain, Sajjad 501
Hyder, Mansoor 200
- Ibrahim, Abdelmuttlib 92
Iftikhar, Aksam 373
Inayat, Irum 210
Inayat, Zubaria 210
Iqbal, Jamshed 144
Iqbal, Khalid 541
Iwao, Sasase 43
- Jaffar, M. Arfan 222
Jalil, Abdul 373
Javaid, Nadeem 43
Jokhio, Imran Ali 132, 445
- Kaleem, Muhammad 222
Kanho, Hidenori 501
Kausar, Rakshanada 385
Khalid, Omer 228
Khalid, Syed Safwan 240
Khan, Arsalan Hameed 261
Khan, Laiq 249

- Khan, Muhammad Umair 249
 Khan, Sajid Ali 73
 Khan, Salman Hameed 261
 Khan, Shahid Ahmed 10
 Khan, Shahryar 272
 Khan, Shoaib A. 541
 Khan, Zeashan Hameed 261

 Laghari, Khalil ur Rehman 200
 Latif, Kashif 361

 Madsen, Ole Brun 154
 Mahar, Faizullah 284
 Mahboob, Athar 361
 Mahmood, Faraz 295
 Mahmood, Farhan 188
 Mehmood, Amjad 43
 Memon, Tayab D. 305
 Mirza, Ashab 397
 Mohamadi, Moslem 338
 Moinuddin, Muhammad 501

 Naeem, Muhammad Asif 164, 314, 326
 Naveed, Nawazish 73
 Nawi, Nazri Mohd 453
 Nazir, Muhammad 73
 Nizamuddin 92
 Noor, Muhammad Asim 210

 Parveen, Abida 10
 Parvin, Hamid 338
 Parvin, Sajad 338
 Pathan, Dur Muhammad 81
 Petridis, Miltos 228
 Poncela, Javier 1
 Prasad, Ramjee 154

 Qamar, Shahid 249

 Rafique, Sabaina 20
 Rajper, Samina 349
 Rao, M. Muzaffar 361
 Rathore, Saima 373
 Rehan, Ahmed 261
 Rezaei, Zahra 338
 Riaz, Faisal 385
 Riaz, M. Tahir 154
 Riaz, Naveed 73

 Rizvi, Syed Ali Asad 397
 Rizwan, M. 20

 Sahar, Syeda Nida 409
 Sakrani, Hira 421
 Saleem, Ilyas 10
 Saleem, Khalid 31
 Samad, Abdul 144
 Samad, Fahad 432, 466
 Sanaullah, M. 222
 Sangrasi, Asif 445
 Shafi, Imran 176, 385
 Shah, Asadullah 466
 Shah, Habib 453
 Shah, Mahmood 132
 Shah, Syed Ismail 176
 Shahid, Saleem 20
 Shaikh, Abdul Wahid 349
 Shaikh, Asadullah 432, 466
 Shaikh, Faisal Karim 409
 Shaikh, Murtaza Hussain 478
 Shaikh, Zubair A. 349
 Shibli, Muhammad Awais 110
 Sohail, Muhammad 261
 Song, William 489
 Soomro, Aijaz 489
 Sunder, Sham 397

 Talha, Ahmad 188
 Tariq, Qurat-ul-Ain I. 512
 Tariq Butt, Tooba 421
 Toivanen, Pekka 144

 Ullah, Fahad 524
 Ullah, Farooq Kifayat 532
 Uqaili, Muhammad Aslam 1
 Usman, Muhammad 188

 Weber, Gerald 314, 326
 Willander, Magnus 295

 Yahya, Khawaja M. 524
 Yasin, Muhammad 52
 Yoshida, Mikio 501

 Zahra, Hijab 10
 Zareen, Saima 541
 Zia, Huma 512